Mathematical Problems in Engineering

Advances in Mathematical Modeling of Flow Problems with Fractional Derivatives

Lead Guest Editor: Muhammad Shoaib Anwar
Guest Editors: Waqar Azeem Khan and Muhammad Irfan

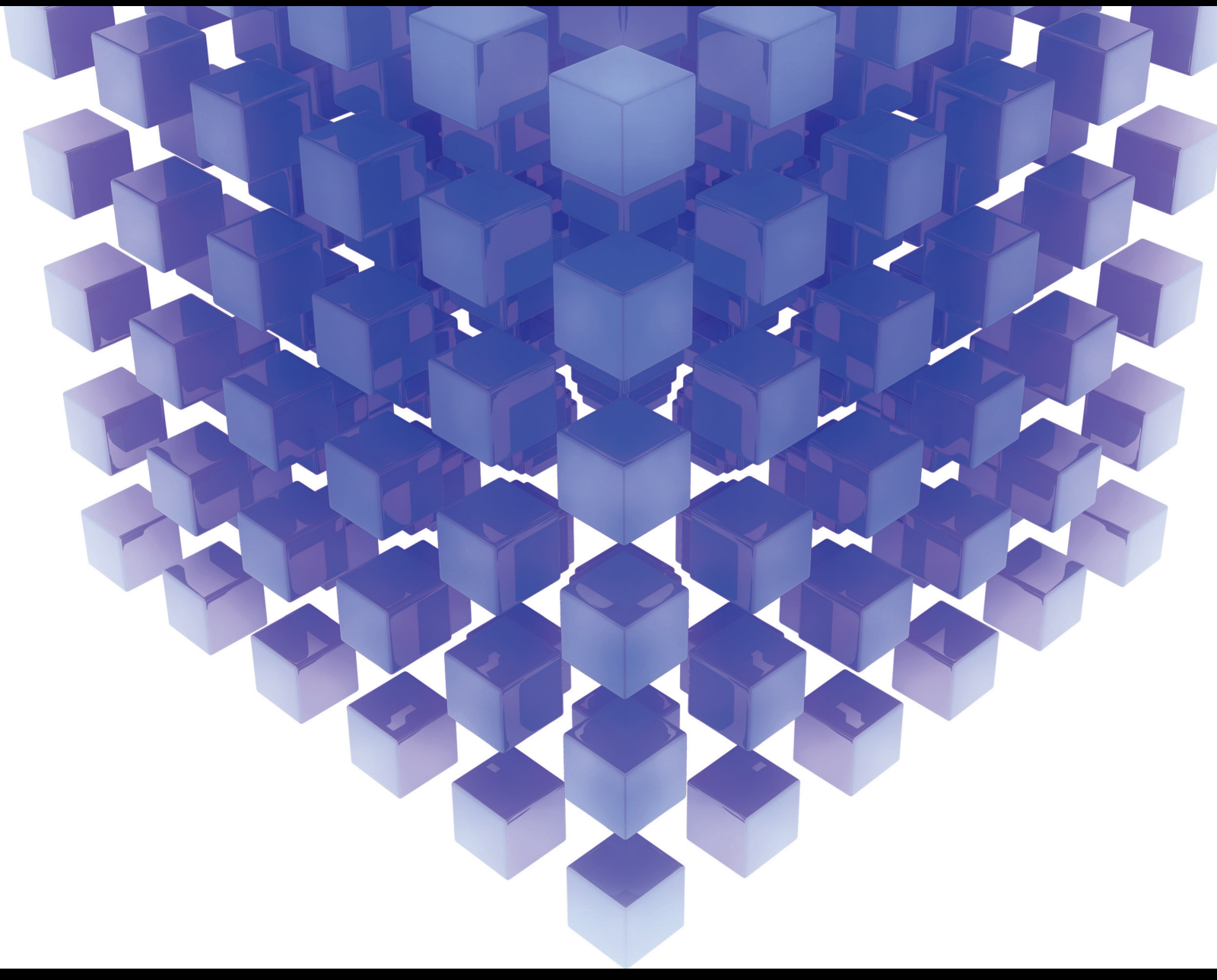

Advances in Mathematical Modeling of Flow Problems with Fractional Derivatives

Mathematical Problems in Engineering

Advances in Mathematical Modeling of Flow Problems with Fractional Derivatives

Lead Guest Editor: Muhammad Shoaib Anwar
Guest Editors: Waqar Azeem Khan and Muhammad Irfan

Chief Editor

Academic Editors

Contents

Hindawi
Mathematical Problems in Engineering
Volume 2022, Article ID 7980267, 10 pages
https://doi.org/10.1155/2022/7980267

Research Article

Unsteady MHD Williamson Fluid Flow with the Effect of Bioconvection over Permeable Stretching Sheet

Muhammad Imran Asjad,[1] **Muhammad Zahid**,[1] **Bagh Ali**,[2] **and Fahd Jarad**[3,4,5]

[1]*Department of Mathematics, University of Management and Technology, Lahore 54770, Pakistan*
[2]*Department of Applied Mathematics, Northwestern Polytechnical University, Xi'an 710072, China*
[3]*Department of Mathematics, Cankaya University, 06790 Etimesgut, Ankara, Turkey*
[4]*Department of Mathematics, King Abdulaziz University, Saudi Arabia*
[5]*Department of Medical Research, China Medical University Hospital, China Medical University, Taichung, Taiwan*

Correspondence should be addressed to Fahd Jarad; fahd@cankaya.edu.tr

Received 20 October 2021; Revised 15 August 2022; Accepted 15 September 2022; Published 3 October 2022

Academic Editor: Muhammad Irfan

The unsteady flow of Williamson fluid with the effect of bioconvection in the heat and mass transfer occurring over a stretching sheet is investigated. A uniform magnetic field, thermal radiation, thermal dissipation, and chemical reactions are taken into account as additional effects. The physical problem is formulated in the form of a system of partial differential equations and solved numerically. For this purpose, similarity functions are involved to transmute these equations into corresponding ordinary differential equations. After that, the Runge-Kutta method with shooting technique is employed to evaluate the desired findings with the utilization of a MATLAB script. As a result, the effects of various physical parameters on the velocity, temperature, and nanoparticle concentration profiles as well as on the skin friction coefficient and rate of heat transfer are discussed with the aid of graphs and tables. The parameters of Brownian motion and thermophoresis are responsible for the rise in temperature and bioconvection Rayleigh number diminishes the velocity field. This study on nanofluid bioconvection has been directly applied in the pharmaceutical industry, microfluidic technology, microbial improved oil recovery, modelling oil and gas-bearing sedimentary basins, and many other fields. Further, to check the accuracy and validation of the present results, satisfactory concurrence is observed with the existing literature.

1. Introduction

The complicated and fast processes in heavy machinery and small gadgets have created a serious problem of thermal imbalance. Various extraneous techniques, such as fins and fans, have been employed, but their utility is limited due to their large size. In 1995, Choi and Eastman [1] introduced nano-sized particles mixed in the fluid called nanofluid, which has more capacity for heat transfer as compared to fluid without nano-sized particles. Nanofluid has attained impressive consideration because of its huge applications in the fields of technology and engineering. Das et al. [2] discuss recent and future applications of fluids containing nano-sized particles. Turkyilmazoglu and Pop [3] examined the thermal and mass transportation influences on some natural convection streams of unsteady MHD nanofluids with the effect of radiation taken into account. Khan et al. [4] used the shooting method analyzed flow features of Williamson nanofluid influenced by variable viscosity depending on temperature and Lorentz force past an inclined nonlinear extending surface and also via graphically discussed the variable viscosity, mixed convection, Brownian motion, Lewis number, Prandtl number, Sherwood number, and Nusselt number. Sui et al. [5] introduced the Cattaneo-Christov model with double diffusion to analyze the significance of slip velocity, Brownian motion, thermophoresis, mass, thermal transportation, and variable viscosity in the stream of Maxwell upper convected

nanofluid over an extending surface using HAM. Izadi et al. [6] investigated the numerically thermogravitational convection of micropolar MHD nanofluid having thermal radiation and a magnetic field past a porous chamber in the presence of an elliptical heated cylinder.

Aman et al. [7] investigated the effects of a magnetic field, heat transfer, and slip conditions on the flow of MHD incompressible and viscous fluid through a converging/diverging medium. Hsiao [8] described the flow property of a 2-D electrically conducting micropolar nanofluid past an extending permeable surface with the magnetic field, mass, thermal transportation, viscous dissipation, and MHD effects taken into account. The significance of chemical reaction, heat source, viscous dissipation, thermal radiation, suction, and magnetic field on mixed convection flow of hydromagnetic Casson nanofluid through a nonlinear extending porous medium has been discussed by Ibrahim et al. [9]. Fatunmbi et al. [10] examined the reactive stream of micropolar MHD fluid through a permeable extending sheet having effects on concentration and thermal slip boundary conditions. Hayat et al. [11] studied the flow features of third-grade electrically conducting MHD nanofluid over a stretching sheet in the presence of activation energy, chemical reaction, convective boundary, and magnetic field effects. Mousavi et al. [12] described a novel combination of theoretical and experimental models that provides dual solutions for Casson hybrid nanofluid flow caused by a stretching/shrinking sheet. Jabbarpour et al. [13] investigated the issue of stable general three-dimensional magnetohydrodynamics stagnation-point boundary layer flow via an impermeable wavy circular cylinder using an aluminum-copper/water hybrid nanofluid as the working fluid and boundary conditions of velocity slip and temperature jump. Izady et al. [14] scrutinized the development of the Falkner-Skan problem is the flow of an aqueous Fe2O3-CuO/water hybrid nanofluid across a permeable stretching/shrinking wedge.

Hayat et al. [15] described the impact of second-grade magnetized nanofluid and the characteristics of mass and heat transfer due to stretching sheets using convective boundary conditions. Goud et al. [16] examined stagnation-point magnetohydrodynamics flow past an extending surface because of a slip boundary and thermal radiation. Srinivasulu and Goud [17] calculated mass and thermal transport in a Williamson nanofluid stream past a stretching surface with convective boundary and magnetic field effects. Khan and Nadeem [18] scrutinized the rotating stream of Maxwell nanofluid with activation energy and double diffusion through stretching sheets influenced by centrifugal, thermophoresis, and Coriolis forces.

Bioconvection describes the phenomenon in which living microorganisms denser than water swim upward in suspensions. These microorganisms pileup in the layer of the upper surface and, because of this pileup, the lower surface becomes less dense than the upper surface and the distribution of density becomes unstable due to the microorganisms falling into it, and phenomena of bioconvection occur. Bioconvection has applications in biological systems and biotechnology, such as purifying cultures, enzyme biosensors, and separating dead and living cells [19]. Raees et al. [20] examined the unsteady stream of bioconvection-mixed nanofluid containing gyrostatic motile microorganisms through a horizontal channel. Siddiqa et al. [21] numerically studied the bioconvection flow of nanofluid having mass and thermal transportation along with gyrotactic microorganisms through a curved vertical cone.

Abbasi et al. [22] introduced the bioconvection stream of viscoelastic nanofluid because of gyrotactic microorganisms past a rotating extending disc having zero-mass flux and convective boundary condition and also described the relatable parameters' influences on velocity, temperature, local density, Sherwood number, and Nusselt number in detail. Chu et al. [23] developed the Buongiorno model to analyze the stream of 2-D MHD bioconvection third-grade fluid along an extending sheet with the significance of motile microorganisms, activation energy, thermophoresis diffusion, Brownian motion, chemical reaction, and magnetic field taken into account. Henda et al. [24] examined the magnetized bioconvection flow of third-grade fluid past an extending cylinder with thermal radiation, activation energy, and a heat source. The effects of thermophoresis and Brownian motion are also discussed. Khan et al. [25] applied the numerical method bpv4c to a scrutinized stream of viscous bioconvection nanofluid through multiple geometries with heat flux, cross-diffusion, and Cattaneo-Christov, as well as Brownian motion, thermophoresis diffusion, and concentration gradients.

Because of its importance in engineering and industrial processes, non-Newtonian fluids compel researchers to investigate the phenomena of mass and heat transport. Shampoos, jelly, sugar, honey, human blood, pulps, and other non-Newtonian fluids are examples. Williamson fluid is also a category of the fluid model that is pseudo-plastic. Pseudo-plastic fluids have applications in the engineering and industrial fields, such as food processing, blood cells, photographic films, and inkjet printing. Li et al. [26] examined the combined effects of MHD and magnetic field on the stream of Williamson nanofluid through exponentially extending permeable sheets with heat generation/absorption. Hamid [27] investigated the influence of Brownian motion and thermophoresis on Williamson MHD nanofluid flow through a wedge using the zero-mass flux and convective boundary. Rasool et al. [28] scrutinized the Buongiorno model to discuss the flow behavior of reactive Williamson MHD nanofluid because of Brownian motion and thermophoresis over a nonlinear permeable sheet. Kumar et al. [29] introduced viscous dissipation, thermal radiation nonlinearly, joule heating, and magnetic field to analyze the stream of Williamson nanofluid past an extending sheet influenced by chemical reactions. Shateyi and Muzara [30] analyzed a thorough and detailed study of the incompressible conductive Williamson nanofluid on the extending permeable sheet. Ali et al. [31] investigated the effects of thermal diffusion, thermal radiation, and MHD on the time-dependent flow of a Maxwell nanofluid past an extending geometry using FEM.

Sindhu and Atangana [32] discussed the framework to model the efficiency and functionality lifespan of electronic

equipment with reliability analysis. Rehman et al. [33] discussed time-censored data and statistical inference for the Burr type X distribution in an accelerated life testing design using a geometric process. Shafiq et al. [34] simulated an effective statistical distribution to examine COVID-19 death rates in Canada and the Netherlands. Sindhu et al. [35] studied modelling of COVID-19 data using an exponentiated transformation of the Gumbel Type-II distribution. Shafiq et al. [36] scrutinized artificial neural network optimization of Darcy-Forchheimer squeezing flow in a nonlinear stratified fluid under convective conditions. Shafiq et al. [37] studied numerical and artificial neural network models to estimate unsteady hydromagnetic Williamson fluid flow on a radiative surface.

In most of the previous studies, the bioconvection of an unsteady Williamson nanofluid was rarely studied. The key aim of the current work is to examine the behavior of bioconvection impacts on Williamson MHD nanofluid transportation over an extending permeable sheet with the insertion of gyrotactic auto-motile organisms to avoid possible settling of nano entities. This investigation is relevant to high-temperature nanomaterial processing technology. Actually, common base fluids bear low thermal conductivity and thus, lose their practical importance. Nanoparticles may improve thermal transport in emerging sophisticated heat exchanger electronics. Bioconvection is presumed to inhibit the sedimentation of nano entities. The connotation of such meaningful attributes can be a useful extension and the results can be utilized for the desired effective thermal transportation in the heat exchanger of various technological processes.

2. Problem Formulation

Here we consider the flow of non-Newtonian Williamson nanofluids on the wall of sheet stretches with velocity $\widetilde{U_w} = cx/(1-at)$ along the x-axis and y-axis taken to be normal,

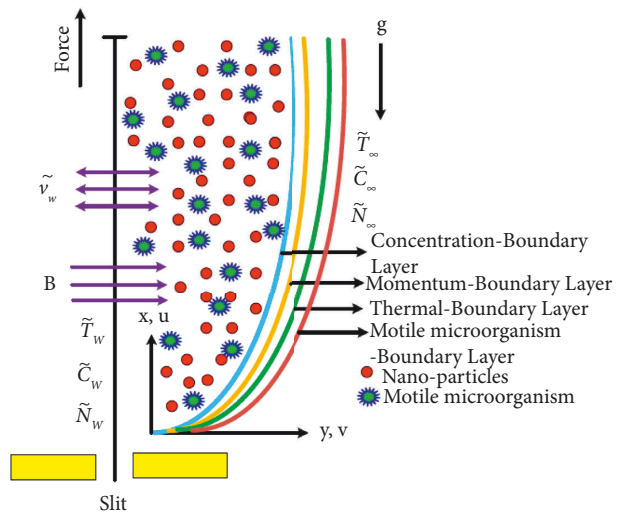

Figure 1: Geometry of the problem [38].

where $c>0$ is the rate of stretching along the x-axis. $\vec{B} = (0, B_0, 0)$ denotes the magnetic field applied to the flow region and acts in the y-direction. A mild diffusion of microorganisms and nanoparticles is set in the non-Newtonian base fluid. Thermal radiation is considered and bioconvection takes place because of microorganism's movement as shown in Figure 1 [38]. The fluid velocity component for two dimensional flow is $\tilde{u}, \tilde{v}$ the temperature is $\tilde{T}$, nanoparticle concentration is $\tilde{C}$, and microorganisms density is $\tilde{N}$. The appropriate governing equations are given [30, 31, 39].

Continuity equation:

$$\frac{\partial \tilde{u}}{\partial x} + \frac{\partial \tilde{v}}{\partial y} = 0. \tag{1}$$

Momentum equation:

$$\frac{\partial \tilde{u}}{\partial t} + \tilde{u}\frac{\partial \tilde{u}}{\partial x} + \tilde{v}\frac{\partial \tilde{u}}{\partial y} = \vartheta\frac{\partial^2 \tilde{u}}{\partial y^2} + 2\vartheta\Gamma\frac{\partial \tilde{u}}{\partial y}\frac{\partial^2 \tilde{u}}{\partial y^2} - \frac{\sigma}{\rho}\left(B_0^2\tilde{u}\right) + \frac{1}{\rho}\left[g\beta\rho\left(1-\widetilde{C_\infty}\right)\left(\tilde{T}-\widetilde{T_\infty}\right) - g\left(\rho_p-\rho_f\right)\left(\tilde{C}-\widetilde{C_\infty}\right) - g\gamma\left(\tilde{N}-\widetilde{N_\infty}\right)\right]. \tag{2}$$

Heat equation

$$\frac{\partial \tilde{T}}{\partial t} + \tilde{u}\frac{\partial \tilde{T}}{\partial x} + \tilde{v}\frac{\partial \tilde{T}}{\partial y} = \frac{K}{\rho C_p}\frac{\partial^2 \tilde{T}}{\partial y^2} + \frac{\mu}{\rho C_p}\left(\frac{\partial \tilde{u}}{\partial y}\right)^2 + \frac{\mu\Gamma}{\rho C_p}\left(\frac{\partial \tilde{u}}{\partial y}\right)^3 + \frac{\sigma}{\rho C_p}\left(\beta_0\tilde{u}\right)^2 - \frac{1}{\rho C_p}\frac{\partial q_r}{\partial y} + \tau\left(D_B\frac{\partial \tilde{T}}{\partial y}\frac{\partial \tilde{C}}{\partial y} + \frac{D_T}{\widetilde{T_\infty}}\left(\frac{\partial \tilde{T}}{\partial y}\right)^2\right). \tag{3}$$

Concentration equation

$$\frac{\partial \tilde{C}}{\partial t} + \tilde{u}\frac{\partial \tilde{C}}{\partial x} + \tilde{v}\frac{\partial \tilde{C}}{\partial y} = D\frac{\partial^2 \tilde{C}}{\partial y^2} - K_r\left(\tilde{C}-\tilde{C}_\infty\right) + \frac{D_T}{\widetilde{T_\infty}}\frac{\partial^2 \tilde{T}}{\partial y^2}. \tag{4}$$

Bioconvection equation

$$\frac{\partial \tilde{N}}{\partial t} + \tilde{u}\frac{\partial \tilde{N}}{\partial x} + \tilde{v}\frac{\partial \tilde{N}}{\partial y} + dW_c\left(\frac{\tilde{N}}{\nabla\tilde{C}}\frac{\partial \tilde{C}}{\partial y}\right) = D_n\frac{\partial^2 \tilde{N}}{\partial y^2}, \tag{5}$$

with the boundary conditions

$$\begin{aligned}
&\widetilde{u}(x,0) = \widetilde{U}_w,\\
&\widetilde{v}(x,0) = \widetilde{V}_w,\\
&\widetilde{T}(x,0) = \widetilde{T}_w,\\
&\widetilde{C}(x,0) = \widetilde{C}_w,\\
&\widetilde{N}(x,0) = \widetilde{N}_w,\\
&\widetilde{u} \longrightarrow 0,\ \widetilde{T} \longrightarrow \widetilde{T}_\infty,\ \widetilde{C} \longrightarrow \widetilde{C}_\infty,\\
&\widetilde{N} \longrightarrow \widetilde{N}_\infty,\ \text{as} y \longrightarrow \infty,\\
&\widetilde{T}_w(x,t) = \widetilde{T}_\infty + \frac{cx}{2\vartheta(1-at)^2}\widetilde{T}_0,\\
&\widetilde{C}_w(x,t) = \widetilde{C}_\infty + \frac{cx}{2\vartheta(1-at)^2}\widetilde{C}_0,\\
&\widetilde{N}_w(x,t) = \widetilde{N}_\infty + \frac{cx}{2\vartheta(1-at)^2}\widetilde{N}_0,
\end{aligned} \tag{6}$$

where $\widetilde{c} \geqslant 0$. $\widetilde{T}_0\,(0 \leqslant \widetilde{T}_0 \leqslant \widetilde{T}_w)$, $\widetilde{C}_0\,(0 \leqslant \widetilde{C}_0 \leqslant \widetilde{C}_w)$, and $\widetilde{N}_0\,(0 \leqslant \widetilde{N}_0 \leqslant \widetilde{N}_w)$ are the reference temperature, concentration, and bioconvection, respectively.

Roseland approximations [30],

$$q_r = \frac{4o^*}{3k_1}\frac{\partial \widetilde{T}^4}{\partial y}, \tag{7}$$

where σ^* is the Stefan-Boltzmann constant and k_1 is the mean absorption coefficient. Applying Taylor's series, we have $\widetilde{T}^4 \simeq 4\widetilde{T}_\infty^3\widetilde{T} - 3\widetilde{T}_\infty^4$, where $\widetilde{T}_\infty$, is the ambient temperature and the energy (3) becomes

$$\begin{aligned}
\frac{\partial \widetilde{T}}{\partial t} + \widetilde{u}\frac{\partial \widetilde{T}}{\partial x} + \widetilde{v}\frac{\partial \widetilde{T}}{\partial y} &= \frac{1}{\rho C_p}\left(\frac{16\sigma^*\widetilde{T}_\infty^3}{3k_1} + K\right)\frac{\partial^2 \widetilde{T}}{\partial y^2}\\
&+ \frac{\mu}{\rho C_p}\left(\frac{\partial \widetilde{u}}{\partial y}\right)^2 + \frac{\mu\Gamma}{\rho C_p}\left(\frac{\partial \widetilde{u}}{\partial y}\right)^3 + \frac{\sigma}{\rho C_p}(\beta_0\widetilde{u})^2.
\end{aligned} \tag{8}$$

Consider the following similarity transformation [30, 39]:

$$\begin{aligned}
\eta &= \sqrt{\frac{\widetilde{U}_w}{x\vartheta}}y,\\
\psi &= \sqrt{\vartheta x\widetilde{U}_w}f(\eta),\\
\theta(\eta) &= \frac{\widetilde{T} - \widetilde{T}_\infty}{\widetilde{T}_w - \widetilde{T}_\infty},\\
\phi(\eta) &= \frac{\widetilde{C} - \widetilde{C}_\infty}{\widetilde{C}_w - \widetilde{C}_\infty},\\
\chi(\eta) &= \frac{\widetilde{N} - \widetilde{N}_\infty}{\widetilde{N}_w - \widetilde{N}_\infty}.
\end{aligned} \tag{9}$$

With the velocity components given by $\widetilde{u} = \partial\psi/\partial y$ and $\widetilde{v} = -\partial\psi/\partial x$ where ψ is the stream function.

Dimensionless momentum equation:

$$\begin{aligned}
&(1 + 2We f'')f''' + ff'' - (f')^2 - S\left(f' + \frac{\eta}{2}f''\right)\\
&- M^2(f') + \lambda(\theta - Nr\phi - Rb\chi) = 0.
\end{aligned} \tag{10}$$

Dimensionless energy equation:

$$\begin{aligned}
&\frac{1}{\Pr}\left(1 + \frac{4R}{3}\right)\theta'' + f\theta' - \frac{S\eta}{2}\theta' - (2S + f')\theta\\
&+ Ec\left((f'')^2 + We(f'')^3\right) + M^2 Ec(f')^2\\
&+ Nb\theta'\phi' + Nt(\theta')^2 = 0.
\end{aligned} \tag{11}$$

Dimensionless concentration equation:

$$\frac{1}{Sc}\phi'' + \left(f - \frac{S\eta}{2}\right)\phi' + (2S - f' - \gamma)\phi = 0. \tag{12}$$

Dimensionless bioconvection equation

$$\chi'' + Lb\Pr f\chi' - Lb\Pr f'\chi - Pe\sigma\phi'' + \chi\phi'' + \chi'\phi' = 0. \tag{13}$$

The corresponding boundary conditions becomes

$$\begin{aligned}
&f(0) = f_w,\\
&f'(0) = 1,\\
&\phi(0) = 1,\\
&\chi(0) = 1,\\
&f'(\infty) \longrightarrow 0,\ f''(\infty) \longrightarrow 0,\ \theta(\infty) \longrightarrow 0,\\
&\phi(\infty) \longrightarrow 0,\ \chi(\infty) \longrightarrow 0.
\end{aligned} \tag{14}$$

The flow characteristics which are of engineering significance are the skin friction coefficient, the local Nusselt number, and the Sherwood number, which are defined, respectively:

$$\begin{aligned}
C_f &= \frac{\tau_w}{\rho U_w^2},\\
Nu_x &= \frac{xq_w}{K\left(\widetilde{T_w} - \widetilde{T_\infty}\right)},\\
Sh_x &= \frac{xj_w}{k_\infty\left(\widetilde{C_w} - \widetilde{C_\infty}\right)}.
\end{aligned} \tag{15}$$

Upon applying the necessary expressions for τ_w, q_w, and j_w, we get the following:

Table 1: Comparison of $C_f \mathrm{Re}_x^{(1/2)}$ (skin friction coefficient) - $f''(0)$ with variation of magnetic parameter M when f_w, λ, Nr, Rb, We, $S = 0$.

M	Ali et al. [31] using FEM	Our results using R-K
0.0	1.0000080	1.0000084
0.2	1.0954458	1.0954460
0.5	1.2247446	1.2247449
1.0	1.4142132	1.4142136
1.2	1.4832393	1.4832397
1.5	1.5811384	1.5811388
2.0	1.7320504	1.7320508

Table 2: Comparison of $Nu_x \mathrm{Re}_x^{-(1/2)}$ (Nusselt number) $-\theta'(0)$ values for Prandtl number Pr and other parameter f_w, λ, Nr, Rb,S, Ec, Nb, Nt,R, We,M, $\delta_2 = 0$.

Pr	Mabood and Shateyi, [40] using FDM	Ali et al. [31] using FEM	Our results using R-K
0.72	0.8088	0.8086339299	0.808834203980
1.00	1.0000	1.0000080213	1.000008368634
3.00	1.9237	1.9236777221	1.923678653470
10.00	3.7207	3.7206681683	3.720671163991
100.00		12.294051659	12.294081083857

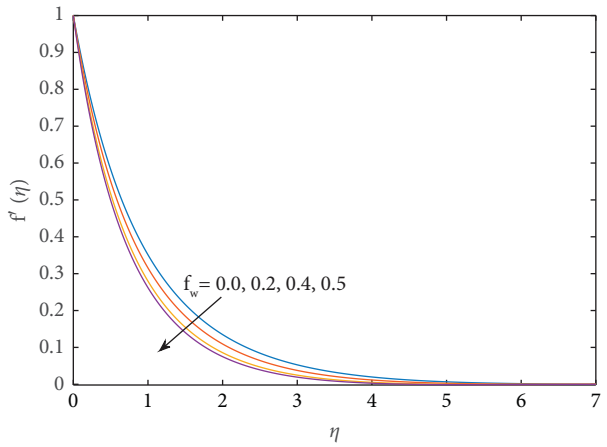

Figure 2: Influence of f_w on f' where $M = 0.5, S = 0.5, R\ d = 1.0, \mathrm{Pr} = 1.1, Nb = 0.1, Nt = 0.1, Le = 1, Nr = 0.3, Rb = 0.1, We = 0.1, pe = 1.0$.

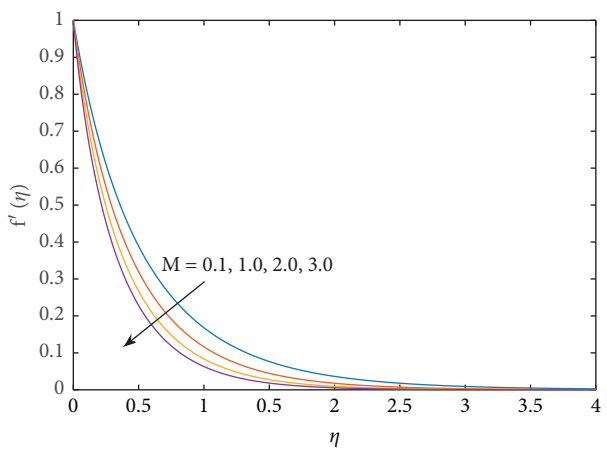

Figure 3: Influence of M on f' where $f_w = 0.5, S = 0.5, R\ d = 1.0, \mathrm{Pr} = 1.1, Nb = 0.1, Nt = 0.1, Le = 1, Nr = 0.3, Rb = 0.1, We = 0.1, pe = 1.0$.

$$C_f = \mathrm{Re}_x^{-1/2}\left[f''(0) + We f'^2(0)\right],$$
$$Nu_x = -\mathrm{Re}_x^{1/2}\left(1 + \frac{4R}{3}\right)\theta'(0), \tag{16}$$
$$Sh_x = -\mathrm{Re}_x^{1/2}\phi'(0).$$

The basic discretization methods are FDM (finite difference method), FVM (finite difference method), and FEM (finite element method). However, the computational cost and time of these methods are much higher for the determination of the unknowns, but the Runge-Kutta method is cost-effective and efficient. The Runge-Kutta method is widely used to solve ordinary differential equations. Runge-Kutta (R-K) methods with shooting techniques have been widely utilized for the solution of flow problems. This method with the shooting technique is a powerful scheme for solving ODEs. In short, the Runge-Kutta method solves the boundary value problems adequately, rapidly, and precisely. Thus, the relative simplicity and low computational cost have made this numeric scheme widely applied in the nonlinear analysis of applied science.

3. Results and Discussion

The physical meanings of the final nondimensional formulation of time-dependent MHD flow of Williamson nanofluid due to the stretch of a horizontal sheet in the presence of bioconvection and chemical reaction along the boundary constraints are solved numerically as described in the above segment. It is because inherent nonlinearity and coupling make the boundary value problem difficult to yield an exact solution. The pertinent parameters are varied in an appropriate range to reveal their influence on dependent variables for the concentration of nanoparticles, fluid temperature, microorganism distribution, and fluid velocity.

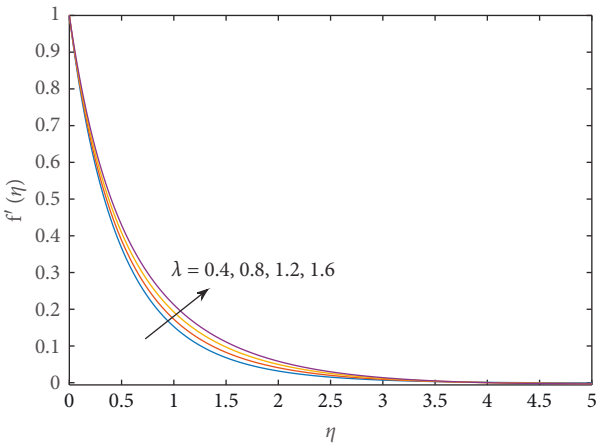

Figure 4: Influence of λ on $f\prime$ where $M = 0.5$, $f_w = 0.5$, $S = 0.5, R\,d = 1.0, \mathrm{Pr} = 1.1, Nb = 0.1,\ Nt = 0.1, Le = 1, Nr = 0.3, Rb = 0.1, We = 0.1, pe = 1.0$.

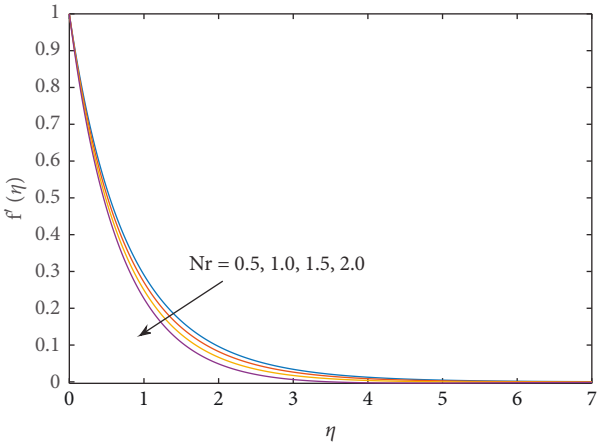

Figure 5: Influence of Nr on $f\prime$ where $M = 0.5$, $f_w = 0.5, S = 0.5$, $R\,d = 1.0, \mathrm{Pr} = 1.1, Nb = 0.1, Nt = 0.1, Le = 1, Rb = 0.1, We = 0.1$, $pe = 1.0$.

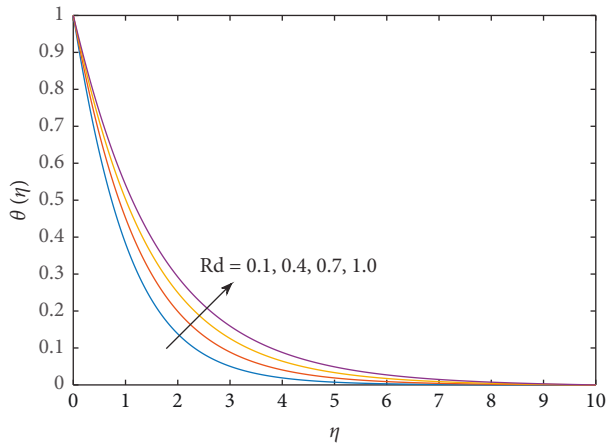

Figure 6: Influence of Rd on θ where $M = 0.5$, $f_w = 0.5, S = 0.5$, $\mathrm{Pr} = 1.1$, $Nb = 0.1$, $Nt = 0.1, Le = 1, Rb = 0.1, We = 0.1$, $pe = 1.0$.

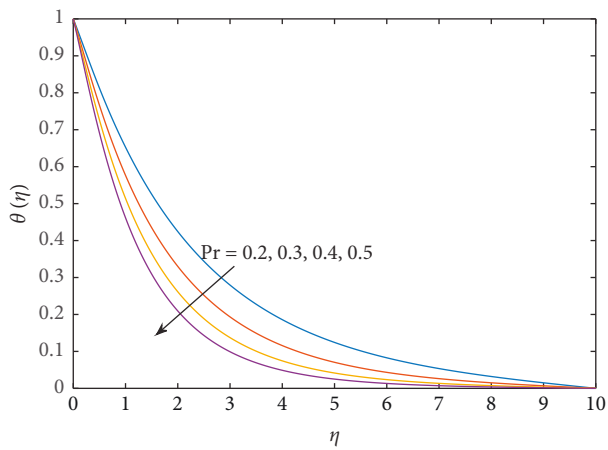

Figure 7: Influence of Pr on θ where $M = 0.5$, $f_w = 0.5, S = 0.5$, $Nb = 0.1, Nt = 0.1, Le = 1, Rb = 0.1, We = 0.1$, $pe = 1.0$.

To ensure the validation of the numeric procedure, current results are compared with those in the existing literature as limiting cases. The comparative output for skin friction factor $-f''(0)$ is shown in Table 1. For the present case and those of Ali et al. [31]. Table 2 contains present results for Nusselt number $-\theta'(0)$ when compared with Fazle and Shateyi [40] and Ali et al. [31]. A comparison of the results as depicted in these tables indicates acceptable agreement to validate this numeric procedure.

The velocity plot in Figure 2 depicts the slowing velocity of the fluid as the mass suction attributed with f_w is increased. From Figure 3, the impact of magnetic parameter M on the Williamson nanofluid velocity function is observed. The velocity of the flow seems to be reduced significantly when $M(0.1 \le M \le 0.3)$ is increased. The opposing force, known as the Lorentz force, inhibits the flow.

As shown in Figure 4, increasing the mixed convection parameter λ causes the flow velocity to increase to $f'(\eta)$. The sketches of velocity $f'(\eta)$ as drawn in Figure 5 indicate the slowing pattern of the flow for buoyancy ratio parameter Nr. $(\tilde{T}_w - \tilde{T}_\infty)$ is the reciprocal of the buoyancy ratio parameter. In the boundary layer regime, buoyancy effects are decreased to better display the flow.

The progressive value of the radiation parameter Rd causes a significant increase in the temperature field $\theta(\eta)$ in Figure 6. The greater Rd means a strong radiation mode of heat transfer which helps to raise the temperature.

Because the Prandtl number is inversely proportional to thermal diffusivity, a higher value decreases the degree of temperature $\theta(\eta)$ as shown in Figure 7. Significant rising behavior of $\theta(\eta)$ is observed in Figures 8 and 9 with increased values of Brownian motion parameter Nb and thermophoresis parameter Nt. The fast random motion of nanoparticles characterized by larger Nb is responsible for enhanced heat transfer to raise $\theta(\eta)$. Similarly, the higher Nt means a greater thermophoretic effect, which moves the nanoparticles from the hotter regime to the colder one and increases the thermal distribution.

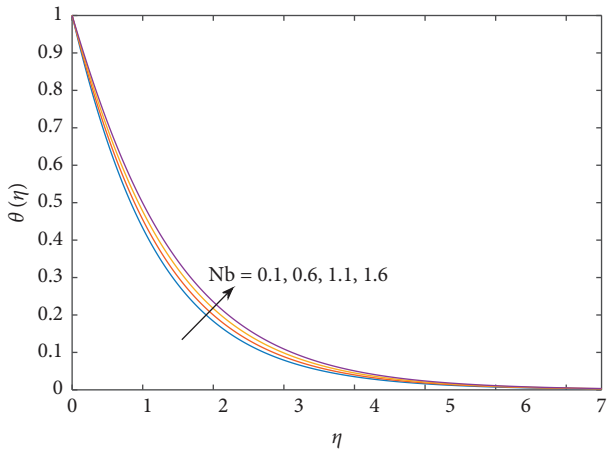

Figure 8: Influence of Nb on θ where $M = 0.5$, $f_w = 0.5$, $S = 0.5$, $Nt = 0.1$, $Le = 1$, Pr $= 1.1$, $Rb = 0.1$, $We = 0.1$, $pe = 1.0$.

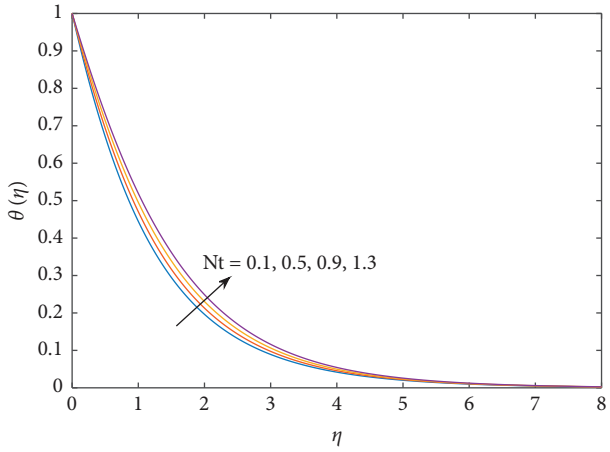

Figure 9: Influence of Nt on θ where $M = 0.5$, $f_w = 0.5$, $S = 0.5$, $Nb = 0.1$, $Le = 1$, Pr $= 1.1$, $Rb = 0.1$, $We = 0.1$, $pe = 1.0$.

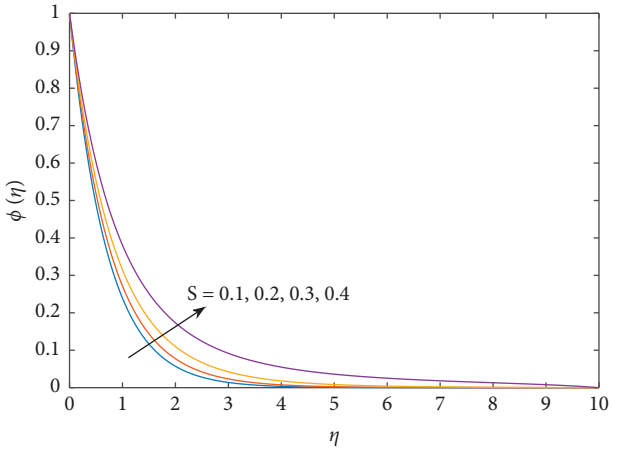

Figure 10: Influence of S on ϕ where $M = 0.5$, $f_w = 0.5$, $Nb = 0.1$, $Nt = 0.1$, $Le = 1$, Pr $= 1.1$, $Rb = 0.1$, $We = 0.1$, $pe = 1.0$.

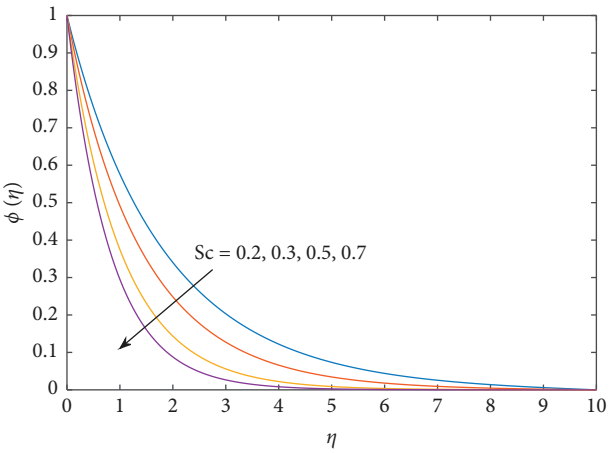

Figure 11: Influence of Sc on ϕ where $M = 0.5$, $f_w = 0.5$, $Nb = 0.1$, $Nt = 0.1$, $Le = 1$, Pr $= 1.1$, $Rb = 0.1$, $We = 0.1$, $pe = 1.0$.

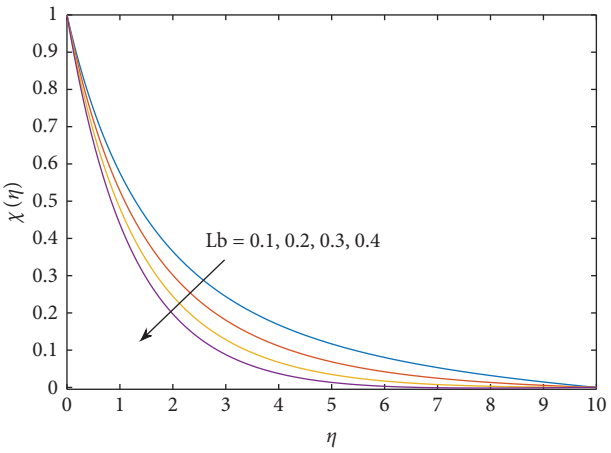

Figure 12: Influence of Lb on χ where $M = 0.5$, $f_w = 0.5$, $Nb = 0.1$, $Nt = 0.1$, $Le = 1$, Pr $= 1.1$, $Rb = 0.1$, $We = 0.1$, $pe = 1.0$.

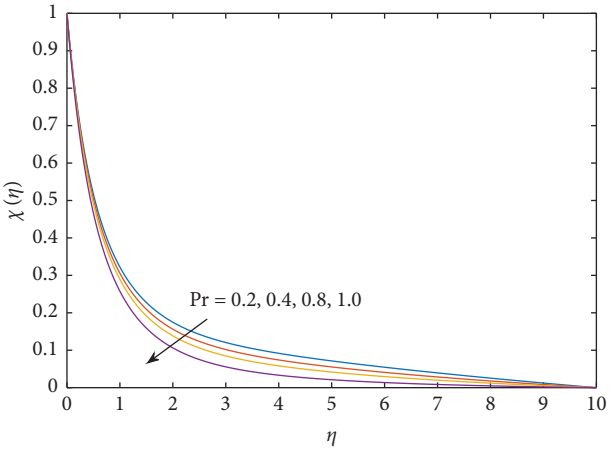

Figure 13: Influence of Pr on χ where $M = 0.5$, $f_w = 0.5$, $Nb = 0.1$, $Nt = 0.1$, $Le = 1$, $Rb = 0.1$, $We = 0.1$, $pe = 1.0$.

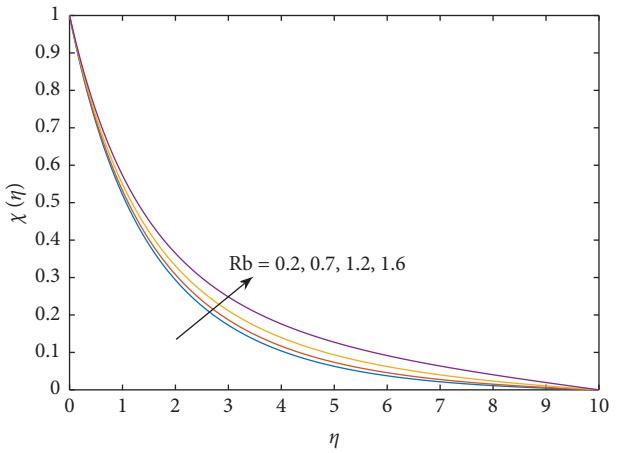

Figure 14: Influence of Rb on χ where $M = 0.5, f_w = 0.5, Nb = 0.1, Nt = 0.1, Le = 1, \Pr = 1.1, We = 0.1, pe = 1.0$.

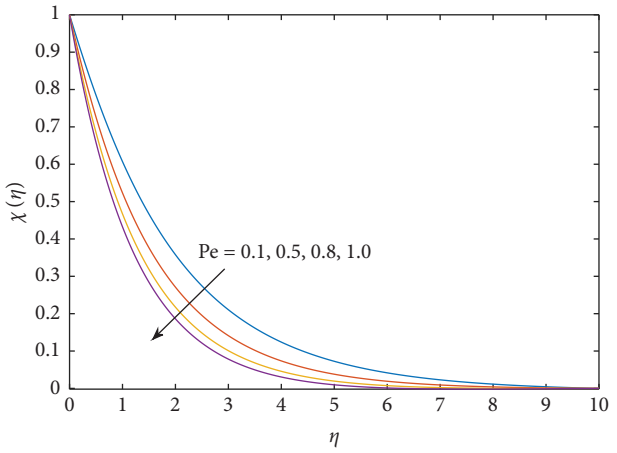

Figure 15: Influence of Pe on χ where $M = 0.5, f_w = 0.5, Nb = 0.1, Nt = 0.1, Le = 1, \Pr = 1.1, Rb = 0.1, We = 0.1$.

In Figure 10 shows the rising behavior of concentration $\phi(\eta)$ indirect relation to the unsteady parameter S. Figure 11 displays the decrement in $\phi(\eta)$ due to the larger value of Schmidt number Sc. The larger Schmidt number means less mass diffusivity to decrease $\phi(\eta)$. From Figure 12, the significant reduction of microorganisms' distribution function $\chi(\eta)$ is attained against improved inputs of bioconvection Lewis number Lb, which is reciprocal to the mass diffusivity of microorganisms. As seems from Figure 13, Prandtl number Pr causes the microorganism's distribution to decline. The bioconvection Rayleigh Rb is responsible for giving a direct increment to $\chi(\eta)$ as demonstrated in Figure 14. As it seems in Figure 15, the larger values of the Peclet number Pe cause the microorganism's distribution to decline.

4. Conclusions

Theoretical and numeric analysis for the magnetohydrodynamics of Williamson nanofluid owing to sudden stretching in a horizontal sheet has been presented in this communication. On the physical field, namely, velocity, temperature, concentration, and microorganism distribution, the effects of the emerging parameters are enumerated. Significant outcomes are summarised as follows:

(i) The velocity, temperature, concentration, and bioconvection parameters are boosted with λ, Rb, Nb, and Nt.

(ii) The velocity, temperature, concentration, and bioconvection parameters reduce with Nr, Lb, and Pe.

(iii) The conclusion of nanoparticles characterized by parameters Nb and Nt shows an increment in the temperature profile. Also, the parameters due to bioconvection have a significant influence on the flow of fluid.

(iv) Further, a study can be carried out with an increment in volume fraction and a non-Newtonian base flow of fluid.

(v) Validation of significant findings and results is debated in Section 3. In the results, satisfactory concurrence is observed when compared with existing literature.

Nomenclature

$S = a/c$:	Unsteadiness parameter
$f_w = v_0/\sqrt{c\vartheta}$:	Suction/injection parameter
$M^2 = \sigma B_0^3(1-at)/\rho a$:	Magnetic parameter
$R = 4\sigma^* \widetilde{T}_\infty^3/kK$:	Thermal radiation parameter
$Sc = \vartheta/D$:	Schmidt number
$Lb = \alpha/D_n$:	Bioconvection lewis number
$Pe = dW_c/D_n$:	Peclet number
$\sigma = \widetilde{N_\infty}/\widetilde{N_w} - \widetilde{N_\infty}$:	Bioconvection parameter
$\Pr = \mu c_p/K$:	Prandtl number
$\gamma = K_r(1-at)/c$:	Chemical reaction parameter
$Ec = \widetilde{U}_w^2/c_p(\widetilde{T}_w - \widetilde{T}_0)$:	Eckert number
$We = \Gamma\widetilde{U}_w\sqrt{c/\vartheta(1-at)}$:	Weissenberg number
$\lambda = (1-\widetilde{C}_\infty)\beta g(\widetilde{T}_w - \widetilde{T}_\infty)2l/U_w^2$:	Mixed convection parameter
$Nr = (\rho_p - \rho_f)(\widetilde{C_w} - \widetilde{C_\infty})/\beta(1 - \widetilde{C_\infty})\rho(\widetilde{T_w} - \widetilde{T_\infty})$	Buoyancy ratio parameter
:	
$Rb = (\rho_m - \rho_f)(\widetilde{N}_w - \widetilde{N}_\infty)/\beta(1-\widetilde{C_\infty})\rho(\widetilde{T}_w - \widetilde{T}_\infty)$	Rayleigh number of bioconvection
:	
$Nt = \tau D_T(\widetilde{T_w} - \widetilde{T_\infty})/\rho\widetilde{T_\infty}$:	Thermophoresis diffusion
$Nb = \tau D_B(\widetilde{C_w} - \widetilde{C_\infty})/\rho$:	Brownian factor
Re:	Reynold's number
$\widetilde{T}$:	Fluid temperature
$\widetilde{T}_w$:	Wall temperature
$\widetilde{T}_\infty$:	

T_∞: Temperature far away from the plate
u: Velocity component along x direction
μ: Dynamic viscosity
ν: Kinematic viscosity.

Data Availability

The data used to support this study are included within this article.

Conflicts of Interest

The authors state that there are no conflicts of interests reported in this work.

Authors' Contributions

All authors contributed equally and significantly to the writing of this paper. All authors read and approved the manuscript.

Acknowledgments

The authors are significantly appreciative and indebted to the University of Management and Technology, Lahore, Pakistan, for enabling and supporting the study effort. The authors extend their appreciation to the Department of Mathematics, Cankaya University, 06790 Etimesgut, Ankara, Turkey.

References

[1] S. U. Choi and J. A. Eastman, "Enhancing thermal conductivity of fluids with nanoparticles," Technical Reports Series, ANL/MSD/CP-84938; CONF-951135-29, Argonne National Lab, IL (United States), 1995.

[2] S. K. Das, S. U. Choi, W. Yu, and T. Pradeep, *Nanofluids: Science and Technology*, John Wiley & Sons, Hoboken, New Jersey, United States, 2007.

[3] M. Turkyilmazoglu and I. Pop, "Heat and mass transfer of unsteady natural convection flow of some nanofluids past a vertical infinite flat plate with radiation effect," *International Journal of Heat and Mass Transfer*, vol. 59, pp. 167–171, 2013.

[4] M. Khan, M. Malik, T. Salahuddin, and A. Hussian, "Heat and mass transfer of Williamson nanofluid flow yield by an inclined lorentz force over a nonlinear stretching sheet," *Results in Physics*, vol. 8, pp. 862–868, 2018.

[5] J. Sui, L. Zheng, and X. Zhang, "Boundary layer heat and mass transfer with cattaneo–christov double-diffusion in upper-convected Maxwell nanofluid past a stretching sheet with slip velocity," *International Journal of Thermal Sciences*, vol. 104, pp. 461–468, 2016.

[6] M. Izadi, M. A. Sheremet, S. Mehryan, I. Pop, H. F. Öztop, and N. Abu-Hamdeh, "MHD thermogravitational convection and thermal radiation of a micropolar nanoliquid in a porous chamber," *International Communications in Heat and Mass Transfer*, vol. 110, Article ID 104409, 2020.

[7] F. Aman, A. Ishak, and I. Pop, "Magnetohydrodynamic stagnation-point flow towards a stretching/shrinking sheet with slip effects," *International Communications in Heat and Mass Transfer*, vol. 47, pp. 68–72, 2013.

[8] K.-L. Hsiao, "Micropolar nanofluid flow with mhd and viscous dissipation effects towards a stretching sheet with multimedia feature," *International Journal of Heat and Mass Transfer*, vol. 112, pp. 983–990, 2017.

[9] S. Ibrahim, G. Lorenzini, P. Vijaya Kumar, and C. Raju, "Influence of chemical reaction and heat source on dissipative mhd mixed convection flow of a casson nanofluid over a nonlinear permeable stretching sheet," *International Journal of Heat and Mass Transfer*, vol. 111, pp. 346–355, 2017.

[10] E. O. Fatunmbi, H. A. Ogunseye, and P. Sibanda, "Magnetohydrodynamic micropolar fluid flow in a porous medium with multiple slip conditions," *International Communications in Heat and Mass Transfer*, vol. 115, Article ID 104577, 2020.

[11] T. Hayat, R. Riaz, A. Aziz, and A. Alsaedi, "Influence of arrhenius activation energy in mhd flow of third grade nanofluid over a nonlinear stretching surface with convective heat and mass conditions," *Physica A: Statistical Mechanics and Its Applications*, vol. 549, Article ID 124006, 2020.

[12] S. M. Mousavi, M. N. Rostami, M. Yousefi, S. Dinarvand, I. Pop, and M. A. Sheremet, "Dual solutions for casson hybrid nanofluid flow due to a stretching/shrinking sheet: a new combination of theoretical and experimental models," *Chinese Journal of Physics*, vol. 71, pp. 574–588, 2021.

[13] B. Jabbaripour, M. N. Rostami, S. Dinarvand, and I. Pop, "Aqueous aluminium–copper hybrid nanofluid flow past a sinusoidal cylinder considering three-dimensional magnetic field and slip boundary condition," *Proceedings of the Institution of Mechanical Engineers - Part E: Journal of Process Mechanical Engineering*, Article ID 095440892110464, 2021.

[14] M. Izady, S. Dinarvand, I. Pop, and A. J. Chamkha, "Flow of aqueous fe2o3–cuo hybrid nanofluid over a permeable stretching/shrinking wedge: a development on falkner–skan problem," *Chinese Journal of Physics*, vol. 74, pp. 406–420, 2021.

[15] T. Hayat, W. A. Khan, S. Z. Abbas, S. Nadeem, and S. Ahmad, "Impact of induced magnetic field on second-grade nanofluid flow past a convectively heated stretching sheet," *Applied Nanoscience*, vol. 10, no. 8, pp. 3001–3009, 2020.

[16] B. S. Goud, "Thermal radiation influences on mhd stagnation point stream over a stretching sheet with slip boundary conditions," *International Journal of Thermofluid Science and Technology*, vol. 7, no. 2, 2020.

[17] T. Srinivasulu and B. S. Goud, "Effect of inclined magnetic field on flow, heat and mass transfer of williamson nanofluid over a stretching sheet," *Case Studies in Thermal Engineering*, vol. 23, Article ID 100819, 2021.

[18] M. N. Khan and S. Nadeem, "A comparative study between linear and exponential stretching sheet with double stratification of a rotating Maxwell nanofluid flow," *Surfaces and Interfaces*, vol. 22, Article ID 100886, 2021.

[19] A. M. Spormann, "Unusual swimming behavior of a magnetotactic bacterium," *FEMS Microbiology Letters*, vol. 45, no. 1, pp. 37–45, 1987.

[20] A. Raees, H. Xu, and S.-J. Liao, "Unsteady mixed nano-bioconvection flow in a horizontal channel with its upper plate expanding or contracting," *International Journal of Heat and Mass Transfer*, vol. 86, pp. 174–182, 2015.

[21] S. Siddiqa, N. Begum, N. Begum, S. Saleem, M. Hossain, and R. S. Reddy Gorla, "Numerical solutions of nanofluid bioconvection due to gyrotactic microorganisms along a vertical wavy cone," *International Journal of Heat and Mass Transfer*, vol. 101, pp. 608–613, 2016.

[22] A. Abbasi, F. Mabood, W. Farooq, and M. Batool, "Bio-convective flow of viscoelastic nanofluid over a convective rotating stretching disk," *International Communications in Heat and Mass Transfer*, vol. 119, Article ID 104921, 2020.

[23] Y.-M. Chu, M. I. Khan, N. B. Khan et al., "Significance of activation energy, bio-convection and magnetohydrodynamic in flow of third grade fluid (non-Newtonian) towards stretched surface: a buongiorno model analysis," *International Communications in Heat and Mass Transfer*, vol. 118, Article ID 104893, 2020.

[24] M. B. Henda, H. Waqas, M. Hussain et al., "Applications of activation energy along with thermal and exponential space-based heat source in bioconvection assessment of magnetized third grade nanofluid over stretched cylinder/sheet," *Case Studies in Thermal Engineering*, vol. 26, Article ID 101043, 2021.

[25] S. A. Khan, H. Waqas, S. M. R. S. Naqvi, M. Alghamdi, and Q. Al-Mdallal, "Cattaneo-christov Double Diffusions Theories with Bio-Convection in Nanofluid Flow to Enhance the Efficiency of Nanoparticles Diffusion," *Case Studies In Thermal Engineering*, vol. 26, Article ID 101017, 2021.

[26] Y.-X. Li, M. H. Alshbool, Y.-P. Lv, I. Khan, M. Riaz Khan, and A. Issakhov, "Heat and mass transfer in mhd williamson nanofluid flow over an exponentially porous stretching surface," *Case Studies in Thermal Engineering*, vol. 26, Article ID 100975, 2021.

[27] A. Hamid, "Existence of dual solutions for wedge flow of magneto-williamson nanofluid: a revised model," *Alexandria Engineering Journal*, vol. 59, no. 3, pp. 1525–1537, 2020.

[28] G. Rasool, T. Zhang, A. J. Chamkha, A. Shafiq, I. Tlili, and G. Shahzadi, "Entropy generation and consequences of binary chemical reaction on mhd Darcy–forchheimer williamson nanofluid flow over non-linearly stretching surface," *Entropy*, vol. 22, no. 1, p. 18, 2019.

[29] A. Kumar, R. Tripathi, R. Singh, and V. Chaurasiya, "Simultaneous effects of nonlinear thermal radiation and joule heating on the flow of williamson nanofluid with entropy generation," *Physica A: Statistical Mechanics and Its Applications*, vol. 551, Article ID 123972, 2020.

[30] S. Shateyi and H. Muzara, "On the numerical analysis of unsteady mhd boundary layer flow of williamson fluid over a stretching sheet and heat and mass transfers," *Computation*, vol. 8, no. 2, p. 55, 2020.

[31] B. Ali, Y. Nie, S. A. Khan, M. T. Sadiq, and M. Tariq, "Finite element simulation of multiple slip effects on mhd unsteady Maxwell nanofluid flow over a permeable stretching sheet with radiation and thermo-diffusion in the presence of chemical reaction," *Processes*, vol. 7, no. 9, p. 628, 2019.

[32] T. N. Sindhu and A. Atangana, "Reliability analysis incorporating exponentiated inverse weibull distribution and inverse power law," *Quality and Reliability Engineering International*, vol. 37, no. 6, pp. 2399–2422, 2021.

[33] A. Rahman, T. N. Sindhu, S. A. Lone, and M. Kamal, "Statistical inference for burr type x distribution using geometric process in accelerated life testing design for time censored data," *Pakistan Journal of Statistics and Operation Research*, vol. 16, no. 3, pp. 577–586, 2020.

[34] A. Shafiq, S. Lone, T. N. Sindhu, Y. El Khatib, Q. M. Al-Mdallal, and T. Muhammad, "A new modified kies fréchet distribution: applications of mortality rate of covid-19," *Results in Physics*, vol. 28, Article ID 104638, 2021.

[35] T. N. Sindhu, A. Shafiq, and Q. M. Al-Mdallal, "Exponentiated transformation of gumbel type-ii distribution for modeling covid-19 data," *Alexandria Engineering Journal*, vol. 60, no. 1, pp. 671–689, 2021.

[36] A. Shafiq, A. B. Çolak, T. N. Sindhu, Q. M. Al-Mdallal, and T. Abdeljawad, "Estimation of unsteady hydromagnetic williamson fluid flow in a radiative surface through numerical and artificial neural network modeling," *Scientific Reports*, vol. 11, no. 1, Article ID 14521, 2021.

[37] A. Shafiq, A. B. Çolak, T. N. Sindhu, and T. Muhammad, "Optimization of Darcy-forchheimer squeezing flow in nonlinear stratified fluid under convective conditions with artificial neural network," *Heat Transfer Research*, vol. 53, no. 3, pp. 67–89, 2022.

[38] M. I. Asjad, M. Zahid, F. Jarad, and A. M. Alsharif, "Bio-convection flow of mhd viscous nanofluid in the presence of chemical reaction and activation energy," *Mathematical Problems in Engineering*, vol. 2022, Article ID 1707894, 9 pages, 2022.

[39] F. Wang, M. I. Asjad, S. U. Rehman et al., "Mhd williamson nanofluid flow over a slender elastic sheet of irregular thickness in the presence of bioconvection," *Nanomaterials*, vol. 11, no. 9, Article ID 2297, 2021.

[40] F. Mabood and S. Shateyi, "Multiple slip effects on mhd unsteady flow heat and mass transfer impinging on permeable stretching sheet with radiation," *Modelling and Simulation in Engineering*, vol. 2019, Article ID 3052790, 11 pages, 2019.

Hindawi
Mathematical Problems in Engineering
Volume 2022, Article ID 8461613, 9 pages
https://doi.org/10.1155/2022/8461613

Research Article

Chemically Reactive Flow and Energy Transport Phenomenon considering Variable Conductivity on Maxwell Fluid: A Numerical Simulation

Muavia Mansoor,[1] Yasir Nawaz,[2] Bilal Ahmad,[1] and Muhammad Irfan[3]

[1]*Department of Mathematics, University of Wah, Wah Cant, Pakistan*
[2]*Department of Mathematics, Air University, Islamabad, Pakistan*
[3]*Department of Mathematical Sciences, Federal Urdu University of Arts Science and Technology, Islamabad, Pakistan*

Correspondence should be addressed to Muhammad Irfan; mirfan@math.qau.edu.pk

Received 21 December 2021; Revised 6 April 2022; Accepted 20 April 2022; Published 19 May 2022

Academic Editor: A. M. Bastos Pereira

The present involvement is the theoretical use of the thermal extrusion structure accompanying with the various industrial progressions. The problem is composed by exploiting the MHD aspect on flow of Maxwell fluid. The properties of chemically reactive flow of magneto Maxwell fluid with effects of viscous dissipation over stretching sheet in stagnation region are elaborated here. The governing equations of phenomena are given in set of partial differential equations, and further these equations are reduced to set of ordinary differential equations using similarity transformations. MATLAB built in solver bvp4c is employed to solve obtained nonlinear boundary value problem. The solver uses the 4^{th} and 5^{th} order discretization scheme, and the outcomes in the form of velocity, temperature, and concentration profiles with variations of magnetic parameter, Maxwell parameter, heat generation parameter, Eckert number, Prandtl number, Schmidt number and reaction rate parameter are deliberated through graphs.

1. Introduction

During the last few decades, some of the researchers took great interest in the non-Newtonian fluid flow due to its practical applications. Their research accelerated due to the involvement of its applications in several chemical engineering processes, life sciences, and petroleum industries. Some important industrial fluids such as polymers, fossil fuels, pulps, food, and molten plastics show non-Newtonian fluids. The flow characteristics of both types of fluids (Newtonian and non-Newtonian) are explained in the form of constitutive equations. It is important to examine the flow behavior using these fluids and their several applications. A single equation is not capable of defining all the properties of non-Newtonian fluids and to overcome this deficiency, researchers have proposed different fluid models. The simplest models as discussed by researchers involve power law and grade fluid models. There is a major drawback of these simple models: the results obtained by these models are not compatible with flows. It is not able to guess the effects of elasticity. However, there is a special type of viscoelastic fluid called Maxwell fluid which explains the viscosity and elastic behavior of fluid which gains the attention of researchers. Aliakbar et al. [1] analyses its effect by considering the flow in applied magnetic fields with thermal radiation effects. Hayat and Qasim [2] extended their research by considering the same fluid with Joule heating effect. Shafiq and Khalique [3] examine upper convected Maxwell flow of stretching surface by using the Lie group methodology.

Stagnation point is the point during the fluid flow where the fluid velocity becomes zero. A conventional flow problem involved in the application of fluid mechanics is the two-dimensional flow near a stagnation point. Hiemenz [4] was the first to propose the work on stagnation point.

Homann [5] extended this work for an axisymmetric flow. Mahapatra and Gupta [6] investigated the effects of heat transfer during the stagnation point flow over the stretching surface, whereas its effects over shrinking sheet were analysed by Wang [7]. Mansur et al. [8] considered Buongiorno's model and analysed the effects of stagnation flow in nanofluids. Slip effects of the boundary layer flow near a stagnation point in the presence of magnetic field was discussed by Aman et al. [9]. Bachok and Ishak [10] considered the flow over nonlinearly stretching sheet and proposed a similarity solution for his model. Carbon nanotubes with single- and multiwalls influencing magnetohydrodynamic stagnation point nanofluid flow over variable thicker surfaces with concave and convex effects was studied by Shafiq et al. [11]. Considerable attention and a good amount of literature have been generated on this problem.

Viscous dissipation is a process in which the viscosity of fluid plays a significant role as it stores some amount of the kinetic energy of fluid particles during motion to its thermal energy and this process is an irreversible process. Brickman [12] primarily considered the effects of viscous dissipation. In his pioneer work, he considered the Newtonian fluid flow in a straight circular tube and proposed the result that the special effects were formed in the close region. Chand and Jat [13] considered the electrically conducting fluid and analysed thermal radiation effects together with viscous dissipation when the fluid is taken through a porous medium. Kishan and Deepa [14] considered the permeable sheet and drawn the numerical results of increasing the temperature of fluid due to the presence of viscous dissipation effects during the flow of micropolar fluid near the stagnation point. The effects of viscous dissipation and variable viscosity on moving vertical porous plate were reported by Singh [15]. Malik et al. [16] considered the Sisko fluid model for analyzing the effects contributed by viscous dissipation during the flow over a stretching cylinder. Shafiq et al. [17] studied the effects of viscous dissipation and Joule heating on Williamson fluid over stretching surface.

The major applications of the chemical reaction involved in chemical engineering processes are fibrous insulation, atmospheric flows, etc. Hayat et al. [18] discussed the impact on velocity and concentration of chemical species during the flow of upper [17] convective Maxwell fluid and used HAM to obtain the results of the proposed model. Bhattacharyya and Layek [19] reported the effects of chemical reaction by considering the electrically conducting fluid in a magnetic field over a vertical porous sheet and considered the same effects along with stagnation point in [20]. For more detail about this, see [21–23].

Keeping in view of the literature, the main aim of this study is to propose a model for the flow of Maxwell fluid over a stretching surface with combined effects of stagnation point and viscous dissipation in the presence of chemical species. The investigation will perform numerically with the help of computational software MATLAB. Possible flow patterns will also be drawn to visualize the flow behavior.

2. Problem Formulation

Consider the laminar incompressible, two-dimensional stagnation point flow of Maxwell fluid over a stretched plate. Let the plate be stretched with velocity $U_w = ax$ and $U_e = bx$ be the velocity at free stream. It is assumed that the x-axis$x$ – axis be taken along the plate and y-axis$y$ – axis be taken perpendicular to the plate and the motion of the flow is considered towards positive x-axis. x – axis. A magnetic field of constant strength B_0 is acting perpendicular to the plate. Let u and v be the horizontal and vertical components of velocity along x and y direction, respectively, T be temperature, and C be the concentration of the fluid. The geometry of this problem can be seen in Figure 1.

Under the boundary layer approximation and considering the effects of temperature-based thermal conductivity, viscous dissipation, heat generation, and chemical reaction, the governing Maxwell equations are expressed by [2, 3, 18]

$$\frac{\partial u}{\partial x} + \frac{\partial u}{\partial y} = 0, \tag{1}$$

$$u\frac{\partial u}{\partial x} + v\frac{\partial u}{\partial y} + \lambda_1\left(u^2\frac{\partial^2 u}{\partial x^2} + v^2\frac{\partial^2 u}{\partial y^2} + 2uv\frac{\partial^2 u}{\partial x\,\partial y}\right) = U_e\frac{dU_e}{dx} + v\frac{\partial^2 u}{\partial y^2} - \frac{\sigma {B_0}^2}{\rho}\left(u - U_e + \lambda_1 v\frac{\partial u}{\partial y}\right), \tag{2}$$

$$u\frac{\partial T}{\partial x} + v\frac{\partial T}{\partial y} = \frac{1}{\rho C_p}\frac{\partial}{\partial y}\left(k(T)\frac{\partial T}{\partial y}\right) + \frac{\mu}{\rho C_P}\left(\frac{\partial u}{\partial y}\right)^2 + \frac{Q_0}{\rho C_p}(T - T_\infty), \tag{3}$$

$$u\frac{\partial C}{\partial x} + v\frac{\partial C}{\partial y} = D\frac{\partial^2 C}{\partial y^2} - k_1(C - C_\infty). \tag{4}$$

Subject to the boundary conditions

$$\left.\begin{aligned} u = U_w, \quad v = 0,\ T = T_w,\ C = C_w \text{ at } y = 0 \\ u = U_e, \quad T = T_\infty,\ C = C_\infty \text{ at } y \longrightarrow \infty \end{aligned}\right\}, \tag{5}$$

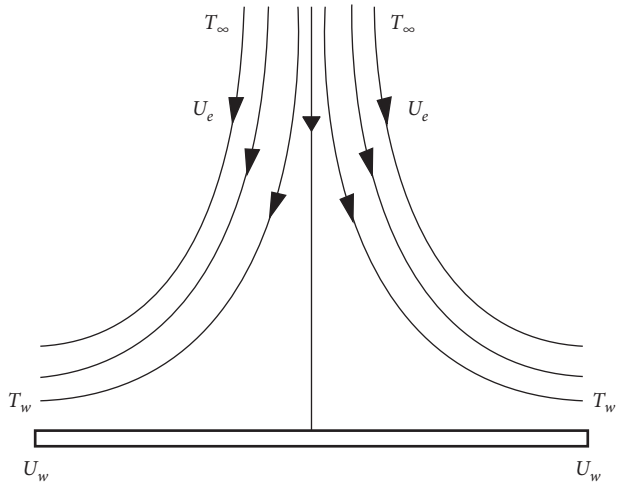

Figure 1: Geometry of the problem.

where $k(T) = k_\infty(1 - \epsilon\theta)$ is the variable conductivity, ν is the kinematic viscosity, σ is the electrical conductivity, λ_1 is the relaxation time, ρ is the fluid density, and k_1 is the reaction rate.

2.1. Transformation of the Governing System of Equations. By using nondimensional variables,

$$\eta = \sqrt{\frac{U_e}{\nu x}}y,$$

$$u = U_e f'(\eta),$$

$$v = -\sqrt{\frac{\nu U_e}{x}}f(\eta), \tag{6}$$

$$\theta = \frac{T - T_\infty}{T_w - T_\infty},$$

$$\varphi = \frac{C - C_\infty}{C_w - C_\infty}.$$

Continuity equation is identically satisfied, equations (2)–(4) can be written as follows:

$$f''' - \lambda f^2 f''' + f f'' + \lambda M^2 f f'' + 1 - f'^2 + M^2(1 - f') + 2\lambda f f' f'' = 0, \tag{7}$$

$$(1 - \epsilon\theta)\theta'' + pr\left(\delta\theta + Ec f''^2 + f\theta' - \frac{\theta'^2}{Pr}\right) = 0, \tag{8}$$

$$\varphi'' - Sc(\gamma\varphi - f\varphi\prime) = 0.$$

Subject to the boundary conditions,

$$\left.\begin{aligned} &f'(\eta) = \epsilon_1, \quad \theta(\eta) = 1, \ f(\eta) = 0, \ \varphi(\eta) = 1 \text{ at } \eta \longrightarrow 0 \\ &\theta(\eta) = 0, \quad f\prime(\eta) = 1, \ \varphi(\eta) = 0 \text{ at } \eta \longrightarrow \infty \end{aligned}\right\}, \tag{9}$$

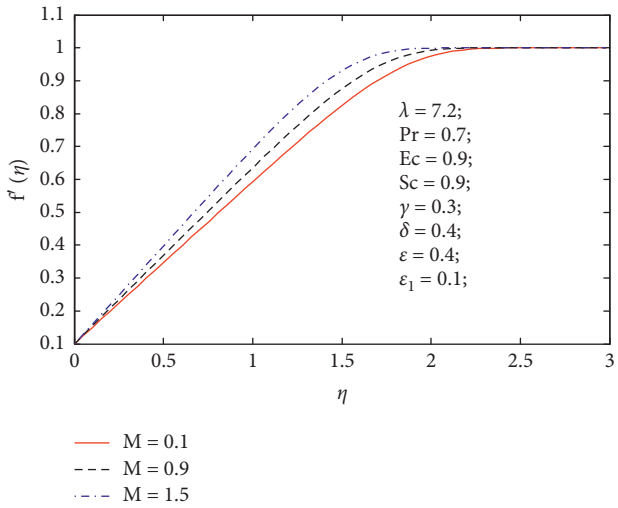

Figure 2: Velocity profile with variation of magnetic parameter M.

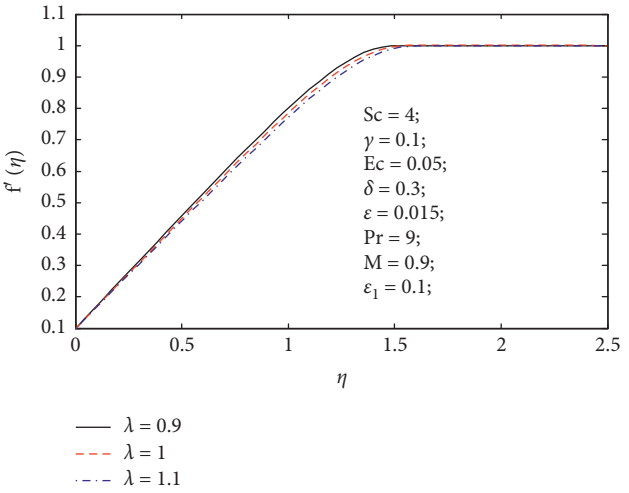

Figure 3: Velocity profile with variation of Maxwell parameterλ.

where $\lambda = a\lambda_1$ is the magnetic parameter, $M^2 = (\sigma B_0^2/\rho a)$ is the Maxwell parameter, $Pr = (C_p\mu_\infty/k_\infty)$ is the Prandtl number, $Sc = (\nu/D)$ is the Schmidt number, $\delta = (Q_0/a\rho C_p)$ is the heat absorption/generation parameter, $Ec = (U_e^2/C_p(T_w - T_\infty))$ is the Eckert number, and ϵ_1 is the ratio of stretching and free stream velocities.

3. Computational Procedure

Since the similarity method only gives the nondimensional equations which are further needed to be solved using some analytical or numerical method. In this section, the arise coupled nonlinear equations (2) to (4) together with boundary condition (5) are tackled numerically by MATLAB built in utility bvp4c. The MATLAB solver bvp4c solve scalar or system of differential equations using three-stage Lobatto IIIa formula. For giving the information of differential equations to the MATLAB solver, the conversion of the system of second- or higher-order differential equations into system of first-order ordinary differential equations is

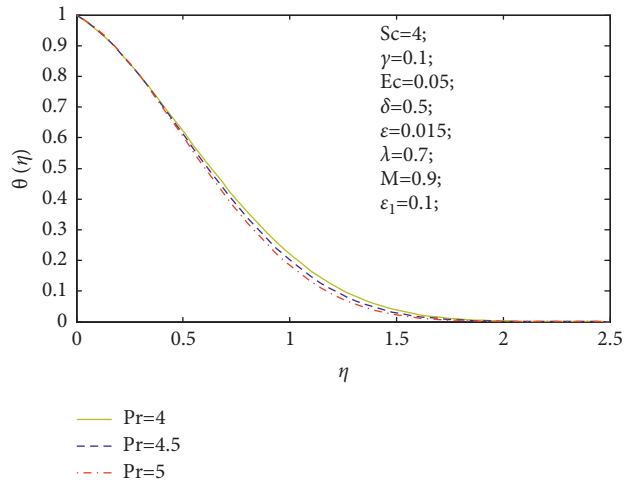

Figure 4: Temperature profile with variation of Prandtl numberPr.

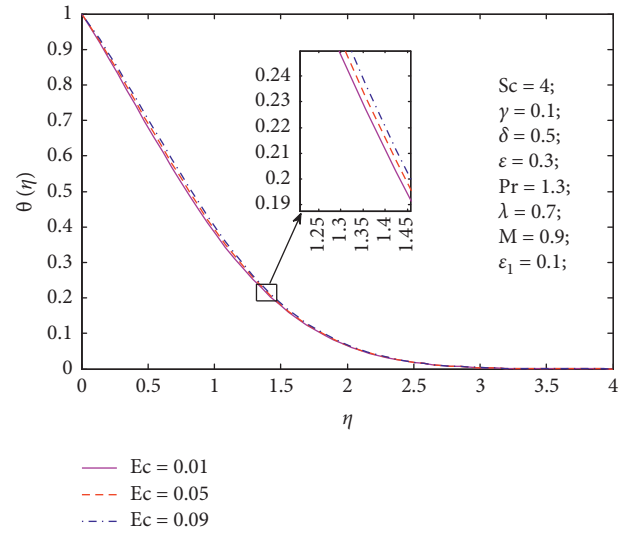

Figure 5: Temperature profile with variation of Eckert numberEc.

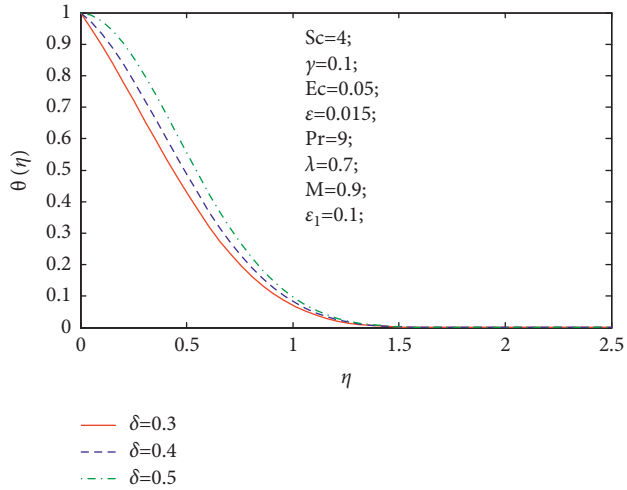

Figure 6: Temperature profile with variation of heat generation parameterδ.

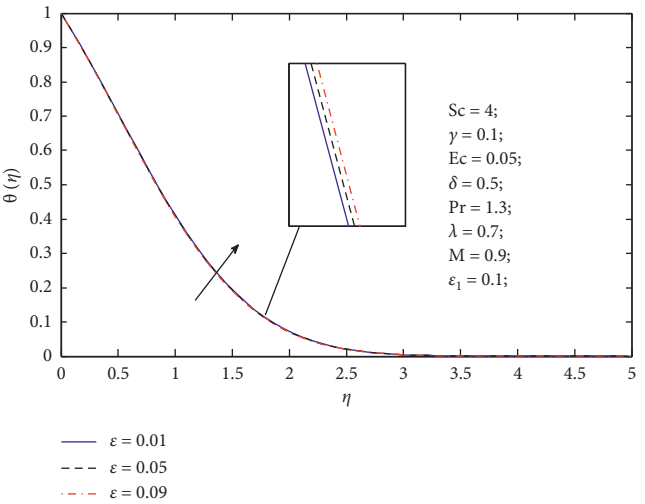

Figure 7: Temperature profile with variation of parameter ϵ.

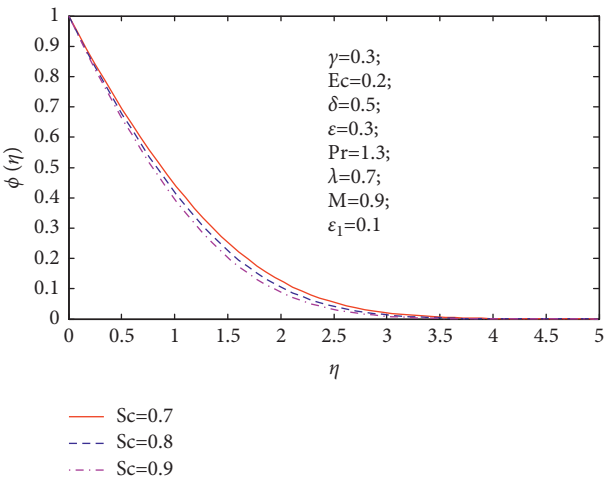

Figure 8: Concentration profile with variation of Schmidt number Sc.

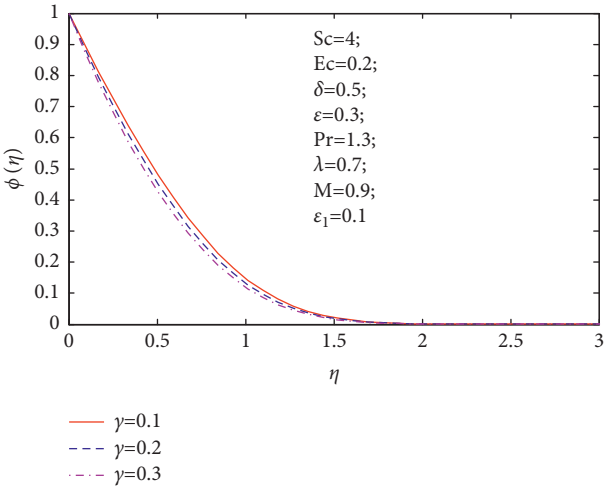

Figure 9: Concentration profile with variation of reaction rate parameter γ.

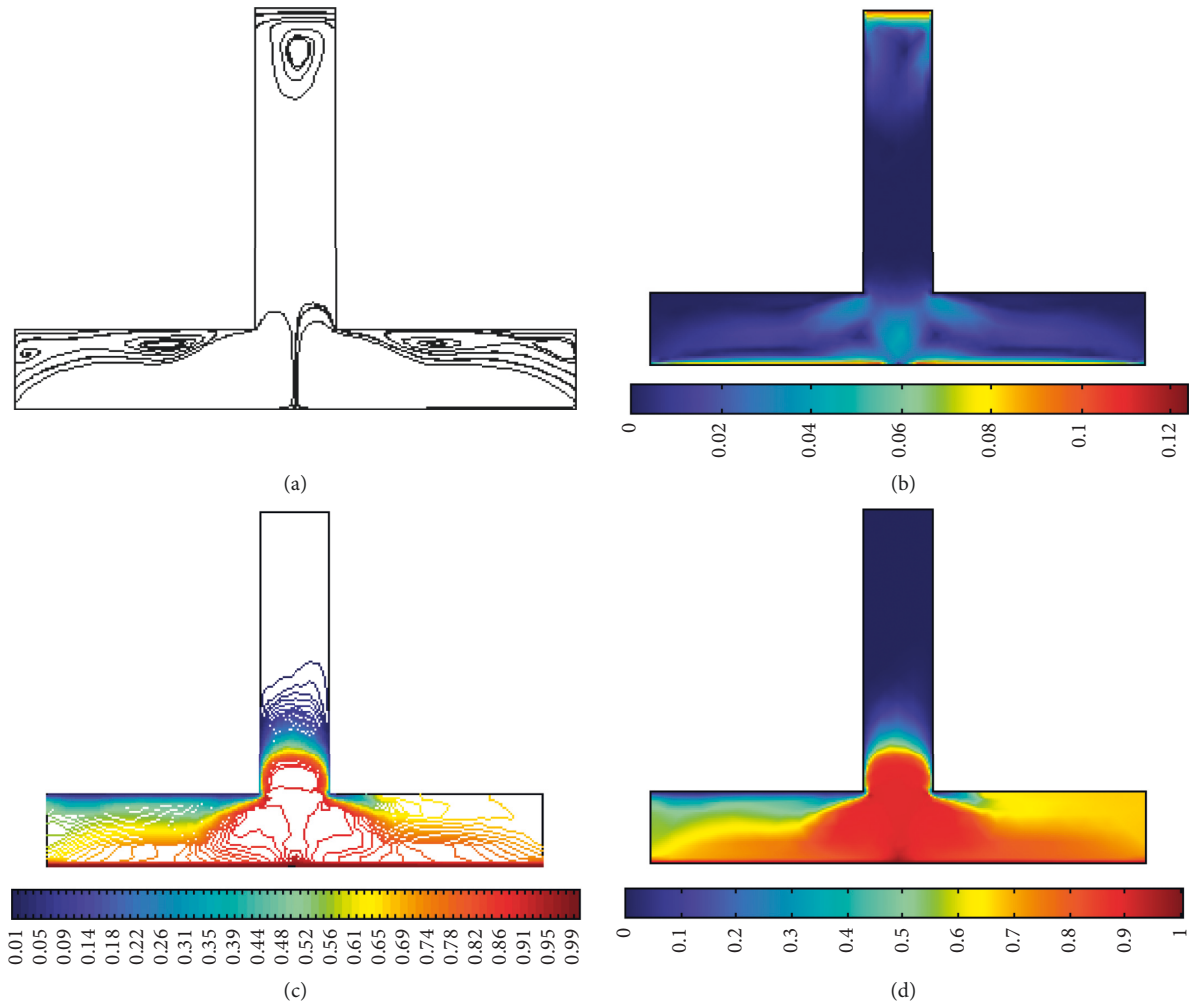

FIGURE 10: (a) Surface velocity plot. (b) Streamlines. (c) Temperature surface plot. (d) Isothermal contours using $U_e = 0.1$, $U_w = 0.1$ and $U_w = -0.1$ where $'+'\&'-'$ shows left and right translation respectively.

required. For this purpose, nonlinear equations are converted into first-order odes by invoking transformations in the following manners:

$$
\begin{aligned}
f' &= f_2,\\
f'' &= f_3,\\
f''' &= \frac{1}{\left(1-\lambda {f_1}^2\right)}\left(\left(1+\lambda M^2\right)f_1 f_3 + \left(1-f_2^2\right)\right.\\
&\quad \left. - M^2\left(f_2-1\right) + 2\lambda f_1 f_2 f_3\right),\\
\theta' &= f_5,\\
\theta'' &= \left(-\frac{pr}{a\left(1-\epsilon f_4\right)}\right)\left(\delta f_4 + Ec f_3^2 + a f_1 f_5 - \frac{a f_5^2}{Pr}\right),\\
\varphi' &= f_7,\\
\varphi'' &= Sc\left(\gamma f_6 - f f_7\right),
\end{aligned}
\tag{10}
$$

where $f = f_1$, $\theta = f_4$, and $\varphi = f_6$, and the boundary conditions can be specified by

$$
\left[f_{0,1}, f_{0,2} - \epsilon_1, f_{\text{inf},2} - 1, f_{0,4} - 1, f_{\text{inf},4}, f_{0,6} - 1, f_{\text{inf},6}\right]^t, \tag{11}
$$

where f_0 is used to describe the boundary condition for the left end point of the domain and f_{inf} is used to describe boundary conditions on the right end point of the domain for the equations (6)–(8) with boundary conditions (9).

4. Results and Discussions

The dimensionless sets of nonlinear ordinary differential equations have been solved by MATLAB solver bvp4c. This solver uses fourth and fifth order numerical method to solve given differential equations. It requires one set of initial guesses, to start the solving procedure. The set of first-order differential equations and set of boundary conditions are two of its inputs and the result can be seen through graphs. A one-dimension mesh may depend upon the user to choose grid points. Also, the mesh for initial conditions can be different from the mesh of the obtained solution.

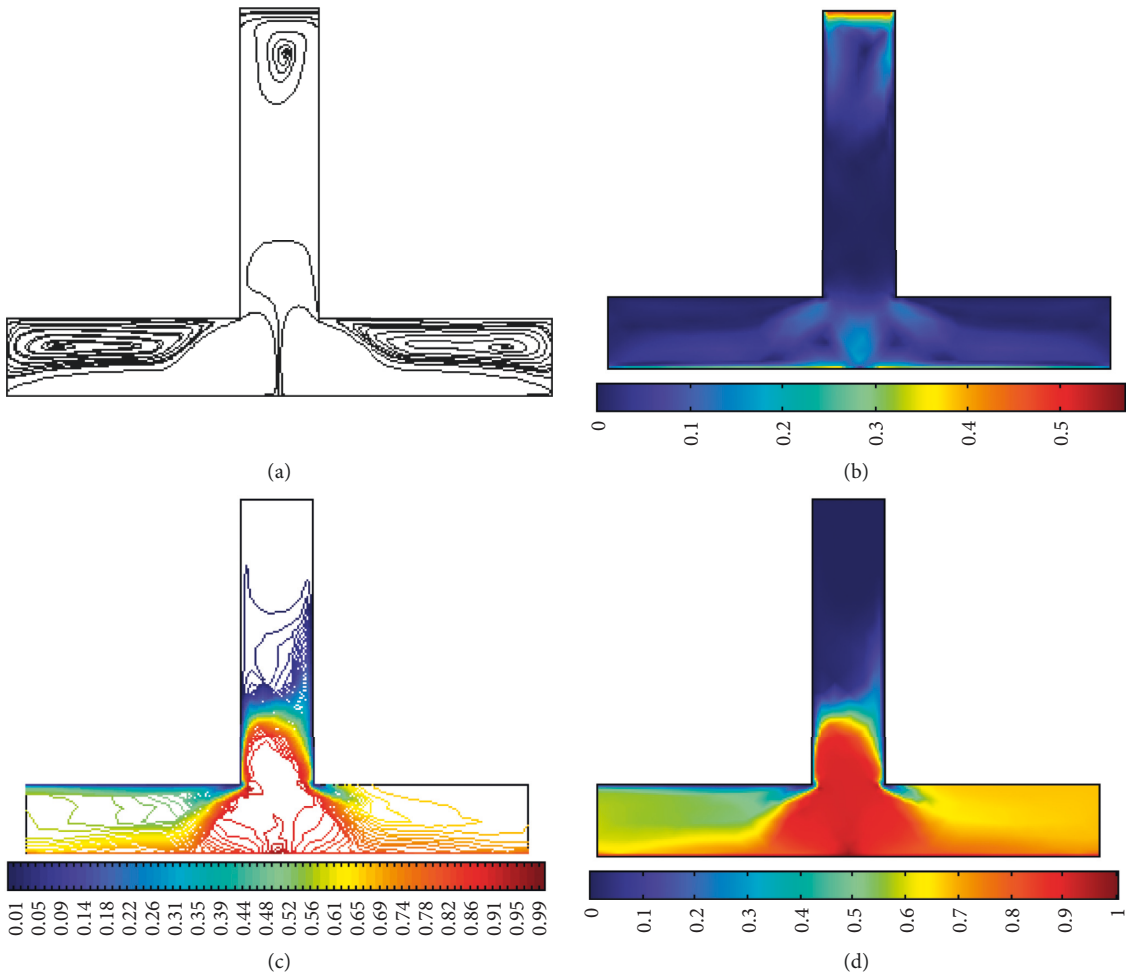

Figure 11: (a) Surface velocity plot (b) streamlines (c) temperature surface plot (d) Isothermal contours using $U_e = 0.5$, $U_w = 0.5$, and $U_w = -0.5$ where '+' and '−' shows left and right translation, respectively.

Figure 2 elucidates the impact of the magnetic parameter on velocity profile. The momentum boundary layer thickness decays by upraising the values of the magnetic parameter due to generation of the Lorentz force which is responsible for providing resistance to the velocity. Figure 3 elucidates the impact of Maxwell parameter on the velocity profile. The velocity de-escalates by raising the Maxwell parameter.

Figure 4 shows the impact of Prandtl number on temperature profile. The temperature de-escalates by enhancing the values of the Prandtl number. This happens due to decay of thermal diffusivity, and this decay is responsible for de-escalation of thermal conductivity and therefore the temperature of the fluid decreases. Figure 5 elucidates the impact of Eckert number on temperature profile. By looking at this Figure 5, it can be observed that the temperature is enhanced by upraising the values of the Eckert number. Figure 6 deliberates the impact of heat generation parameter on temperature profile. Temperature of the fluid escalates by enhancing the values of the heat generation parameter and this is happening due to an attached heat source that produces heat to the fluid and so the temperature of the fluid escalates. Figure 7 shows the impact of parameter ϵ on the temperature profile. By looking at Figure 7, it seems that the temperature enhanced by upraising the values of parameter ϵ. Physically, it describes the temperature gradients inside the material at the time of progress in addition to inside the materials. When ϵ increase, the magnitude of temperature also increases, which enhances the temperature field.

Figure 8 elucidates the behavior of concentration profile when Schmidt number varies. Figure 8 shows concentration decays by increasing the values of Schmidt number. The decrease of concentration is the consequence of using Fick's law because increasing values of the Schmidt number leads to slow down molecular flux and consequently molecular diffusion process becomes slow and so the concentration de-escalates. Figure 9 elucidates the impact of reaction rate parameter on concentration profile. From Figure 9, it can be observed that concentration decreases by upraising the values of reaction rate parameter.

Figures 10–12 are drawn using software which uses the finite element method to solve the partial differential equations. In these figures, variations of wall's velocity and free stream velocity are considered and found that the velocity of the fluid near to the plate is escalating by

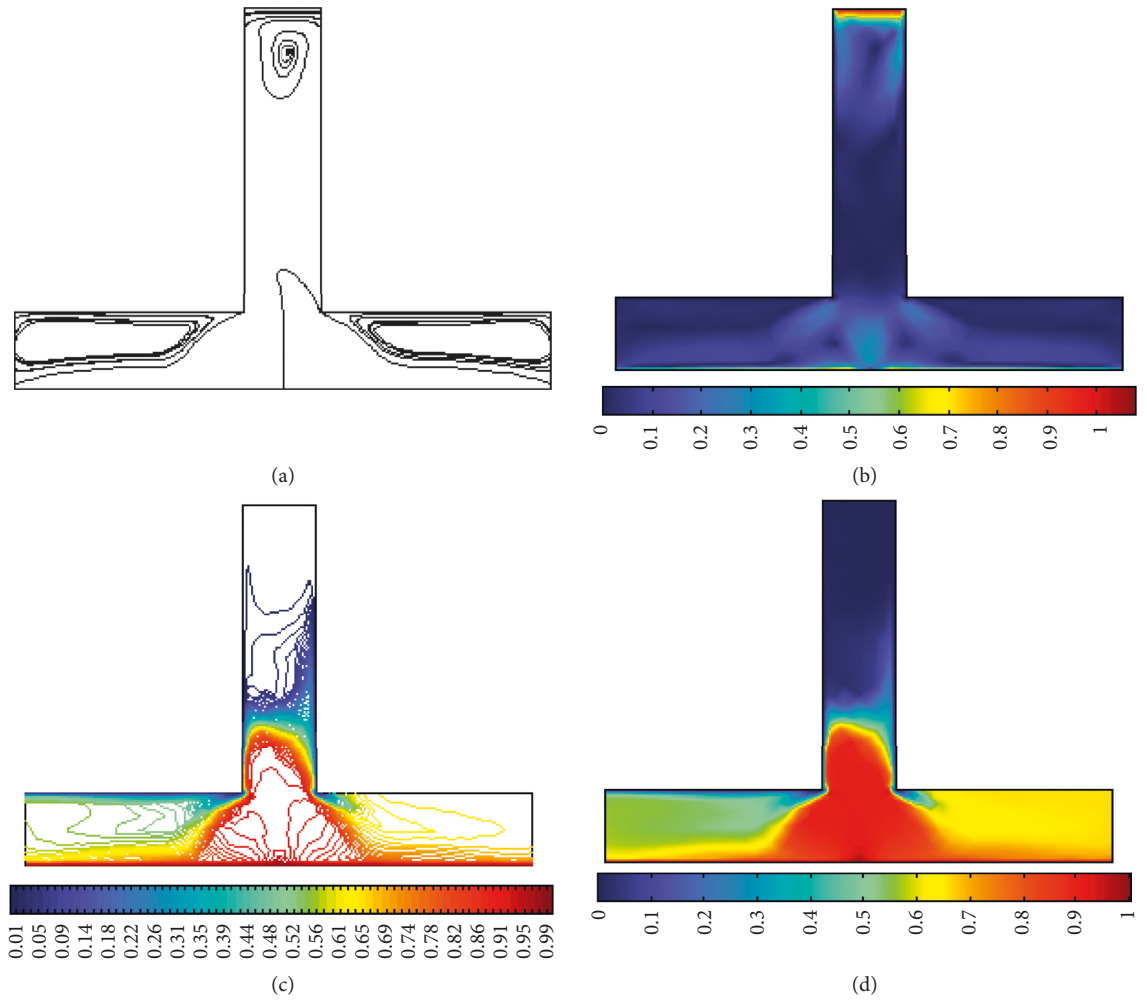

Figure 12: (a) Surface velocity plot. (b) Streamlines. (c) Temperature surface plot. (d) Isothermal contours using $U_e = 1$, $U_w = 1$, and $U_w = -1$ where $'+'$ and $'-'$ shows left and right translation, respectively.

Table 1: Numerical values of local Nusselt number and local Sherwood number with variation of parameters using $\epsilon_1 = 0.1$.

M	λ	Pr	Ec	Sc	γ	δ	ϵ	$-\theta'(0)$	$-\phi'(0)$
0.4	07	0.5	0.7	0.7	0.1	0.1	0.2	0.6118	0.5381
0.5	07	0.5	0.7	0.7	0.1	0.1	0.2	0.6113	0.5390
0.5	7.1	0.5	0.7	0.7	0.1	0.1	0.2	0.6113	0.5389
0.5	7.2	0.5	0.7	0.7	0.1	0.1	0.2	0.6114	0.5388
0.5	7.2	0.6	0.7	0.7	0.1	0.1	0.2	0.6080	0.5388
0.5	7.2	0.7	0.7	0.7	0.1	0.1	0.2	0.6045	0.5388
0.5	7.2	0.7	0.8	0.7	0.1	0.1	0.2	0.5722	0.5388
0.5	7.2	0.7	0.9	0.7	0.1	0.1	0.2	0.5404	0.5388
0.5	7.2	0.7	0.9	0.8	0.1	0.1	0.2	0.5404	0.5635
0.5	7.2	0.7	0.9	0.9	0.1	0.1	0.2	0.5404	0.5872
0.5	7.2	0.7	0.9	0.9	0.2	0.1	0.2	0.5404	0.6467
0.5	7.2	0.7	0.9	0.9	0.3	0.1	0.2	0.5404	0.7030
0.5	7.2	0.7	0.9	0.9	0.3	0.3	0.2	0.3663	0.7030
0.5	7.2	0.7	0.9	0.9	0.3	0.4	0.2	0.2725	0.7030
0.5	7.2	0.7	0.9	0.9	0.3	0.4	0.3	0.2581	0.7030
0.5	7.2	0.7	0.9	0.9	0.3	0.4	0.4	0.2351	0.7030

enhancing the velocity of wall and free stream velocity. The temperature also rises by upraising the velocity of wall and free stream velocity when varying the values from to 0.1 to 0.5, whereas the surface of temperature is approximately unchanged by increasing wall and free stream velocities from to 0.5 to 0.1.

Table 2: Comparison of the value of $-\theta'(0)$ for $M = \epsilon = \delta = \lambda = 0$ and $Ec = 0.3$.

Pr	[24]	[25]	Present
0.5	0.175815	0.176182	0.175812
1	0.299876	0.299877	0.299821
3	0.634113	0.634110	0.634119
5	0.870431	0.870427	0.870418
10	0.308613	0.308608	0.308631

Table 1 shows the numerical values for local Nusselt and local Sherwood numbers. From Table 1, it seems to be that the local Sherwood number escalates and de-escalates by growing values of magnetic parameter and Maxwell parameter, respectively. Local Nusselt number decays by the growth of the Prandtl number and Eckert number. Local Sherwood number increases by the rising Schmidt number. For validation and accuracy of our computations, Table 2 is presented in a limiting manner. Good agreement is achieved with the existing results.

5. Conclusion

The current study was comprised of mathematical model for two-dimensional, laminar, stagnation point flow of steady incompressible fluid with temperature-based thermal conductivity. This mathematical model was modified by using the similarity method and further governing system of equations are converted to set of ordinary differential equations (ODEs). MATLAB built in solver bvp4c has been implemented to solve set of ordinary differential equations. The major findings of this study are as follows:

(i) Velocity profile of the fluid was de-escalated by choosing larger values of the magnetic parameter.

(ii) Temperature profile was de-escalated by upraising the values of Prandtl number.

(iii) Concentration profile was decreased by upraising the values of Schmidt numbers.

Data Availability

There are no data available for this study.

Conflicts of Interest

The authors declare that they do not have any conflicts of interest.

References

[1] V. Aliakbar, A. Alizadeh-Pahlavan, and K. Sadeghy, "The influence of thermal radiation on MHD flow of Maxwellian fluids above stretching sheets," *Communications in Nonlinear Science and Numerical Simulation*, vol. 14, no. 3, pp. 779–794, 2009.

[2] T. Hayat and M. Qasim, "Influence of thermal radiation and Joule heating on MHD flow of a Maxwell fluid in the presence of thermophoresis," *International Journal of Heat and Mass Transfer*, vol. 53, no. 21-22, pp. 4780–4788, 2010.

[3] A. Shafiq and C. M. Khalique, "Lie group analysis of upper convected Maxwell fluid flow along stretching surface," *Alexandria Engineering Journal*, vol. 59, no. 4, pp. 2533–2541, 2020.

[4] K. Hiemenz, "Die Grenzschicht an einem in den gleichformigen Flussigkeitsstrom eingetauchten geraden Kreiszylinder," *Dinglers Polytech. J.*vol. 326, pp. 321–324, 1911.

[5] F. Homann, "Der Einfluß großer Zähigkeit bei der Strömung um den Zylinder und um die Kugel," *ZAMM - Zeitschrift für Angewandte Mathematik und Mechanik*, vol. 16, no. 3, pp. 153–164, 1936.

[6] T. R. Mahapatra and A. S. Gupta, "Heat transfer in stagnation-point flow towards a stretching sheet," *Heat and Mass Transfer*, vol. 38, no. 6, pp. 517–521, 2002.

[7] C. Y. Wang, "Stagnation flow towards a shrinking sheet," *International Journal of Non-linear Mechanics*, vol. 43, no. 5, pp. 377–382, 2008.

[8] S. Mansur, A. Ishak, and I. Pop, "Stagnation-point flow towards a stretching/shrinking sheet in a nanofluid using Buongiorno's model," *Proceedings of the Institution of Mechanical Engineers - Part E: Journal of Process Mechanical Engineering*, vol. 231, no. 2, pp. 172–180, 2017.

[9] F. Aman, A. Ishak, and I. Pop, "Magnetohydrodynamic stagnation-point flow towards a stretching/shrinking sheet with slip effects," *International Communications in Heat and Mass Transfer*, vol. 47, pp. 68–72, 2013.

[10] N. Bachok and A. Ishak, "Similarity solutions for the stagnation-point flow and heat transfer over a nonlinearly stretching/shrinking sheet," *Sains Malaysiana*, vol. 40, pp. 1297–1300, 2011.

[11] A. Shafiq, I. Khan, G. Rasool, E.-S. M. Sherif, and A. H. Sheikh, "Influence of single- and multi-wall carbon nanotubes on magnetohydrodynamic stagnation point nanofluid flow over variable thicker surface with concave and convex effects," *Mathematics*, vol. 8, no. 1, p. 104, 2020.

[12] H. C. Brinkman, "Heat effects in capillary flow I," *Applied Scientific Research*, vol. 2, no. 1, pp. 120–124, 1951.

[13] G. Chand and R. Jat, "Viscous dissipation and radiation effects on MHD flow and heat transfer over an unsteady stretching surface in a porous medium," *Thermal Energy and Power Engineering*, vol. 3, pp. 266–272, 2014.

[14] N. Kishan and G. Deepa, "Viscous dissipation effects on stagnation point flow and heat transfer of a micropolar fluid with uniform suction or blowing," *Advances in Applied Science Research*, vol. 3, pp. 430–439, 2012.

[15] P. Singh, "Viscous dissipation and variable viscosity effects on MHD boundary layer flow in porous medium past a moving vertical plate with suction," *International Journal of Engineering Science and Technology*, vol. 4, pp. 2647–2656, 2012.

[16] M. Y. Malik, A. Hussain, T. Salahuddin, and M. Awais, "Effects of viscous dissipation on MHD boundary layer flow of Sisko fluid over a stretching cylinder," *AIP Advances*, vol. 6, no. 3, Article ID 035009, 2016.

[17] A. Shafiq, M. M. Rashidi, Z. Hammouch, and I. Khan, "Analytical investigation of stagnation point flow of Williamson liquid with melting phenomenon," *Physica Scripta*, vol. 94, no. 3, Article ID 035204, 2019.

[18] T. Hayat, Z. Abbas, and N. Ali, "MHD flow and mass transfer of a upper-convected Maxwell fluid past a porous shrinking sheet with chemical reaction species," *Physics Letters A*, vol. 372, no. 26, pp. 4698–4704, 2008.

[19] K. Bhattacharyya and G. C. Layek, "Slip effect on diffusion of chemically reactive species in boundary layer flow over a vertical stretching sheet with suction or blowing," *Chemical*

Engineering Communications, vol. 198, no. 11, pp. 1354–1365, 2011.

[20] K. Bhattacharyya, S. Mukhopadhyay, and G. C. Layek, "Reactive solute transfer in magnetohydrodynamic boundary layer stagnation-point flow over a stretching sheet with suction/blowing," *Chemical Engineering Communications*, vol. 199, no. 3, pp. 368–383, 2012.

[21] T. Hayat, S. Qayyum, A. Alsaedi, and A. Shafiq, "Inclined magnetic field and heat source/sink aspects in flow of nanofluid with nonlinear thermal radiation," *International Journal of Heat and Mass Transfer*, vol. 103, pp. 99–107, 2016.

[22] A. Shafiq and T. N. Sindhu, "Statistical study of hydromagnetic boundary layer flow of Williamson fluid regarding a radiative surface," *Results in Physics*, vol. 7, pp. 3059–3067, 2017.

[23] T. N. Sindhu and A. Atangana, "Reliability analysis incorporating exponentiated inverse Weibull distribution and inverse power law," *Quality and Reliability Engineering International*, vol. 37, no. 6, pp. 2399–2422, 2021.

[24] E. Magyari and B. Keller, "Heat and mass transfer in the boundary layers on an exponentially stretching continuous surface," *Journal of Physics D: Applied Physics*, vol. 32, no. 5, pp. 577–585, 1999.

[25] M. Abd El-Aziz, "Viscous dissipation effect on mixed convection flow of a micropolar fluid over an exponentially stretching sheet," *Canadian Journal of Physics*, vol. 87, no. 4, pp. 359–368, 2009.

Hindawi
Mathematical Problems in Engineering
Volume 2022, Article ID 7067543, 14 pages
https://doi.org/10.1155/2022/7067543

Research Article

New Fractional Mercer–Ostrowski Type Inequalities with Respect to Monotone Function

Saad Ihsan Butt,[1] **Ammara Nosheen**,[2] **Jamshed Nasir**,[3] **Khuram Ali Khan**,[2] **and Rostin Matendo Mabela**[4]

[1]*COMSATS University Islamabad, Lahore Campus, Pakistan*
[2]*Department of Mathematics, University of Sargodha, Sargodha 40100, Pakistan*
[3]*Virtual University of Pakistan, Lahore Campus 54000, Pakistan*
[4]*Department of Maths and Computer Science, Faculty of Science, University of Kinshasa, Kinshasa, Democratic Republic of the Congo*

Correspondence should be addressed to Rostin Matendo Mabela; rostin.mabela@unikin.ac.cd

Received 22 December 2021; Accepted 9 April 2022; Published 18 May 2022

Academic Editor: Muhammad Irfan

This research focuses on Ostrowski type inequality in the form of classical Mercer inequality via ψ-Riemann–Liouville fractional integral (F-I) operators. Using the ψ-Riemann–Liouville F-I operator, we first develop and demonstrate a new generalized lemma for differentiable functions. Based on this lemma, we derive some fractional Mercer–Ostrowski type inequalities by using the convexity theory. These new findings extend and recapture previous published results. Finally, we presented applications of our work via the known special functions of real numbers such as q-digamma functions and Bessel function.

1. Introduction and Preliminaries

The well-known Ostrowski inequality, developed in 1938, established the following helpful and noteworthy integral inequality (see [1], page 468).

Suppose a mapping $\lambda: [a,b] \longrightarrow \mathfrak{R}$ is continuous on $[a,b]$ and differentiable on (a,b). If $|\lambda'(z)| \leq M$, for all $z \in [a,b]$, then, the following inequality holds:

$$\left|\lambda(z) - \frac{1}{b-a}\int_a^b \lambda(v)\mathrm{d}v\right| \leq M(b-a)\left[\frac{1}{4} + \frac{(z-(a+b)/2)^2}{(b-a)^2}\right]. \quad (1)$$

This finding is known as the Ostrowski inequality in the literature. Some generalizations, variations, and extensions of the Ostrowski inequality have been proposed in light of current findings and their related generalizations, variants, and extensions (see [2–4]).

This inequality yields an upper bound for the approximation of the integral average $1/(b-a)\int_a^b \lambda(v)\mathrm{d}v$ by the value of $\lambda(v)$ at the point $v \in [a,b]$.

In recent years, because of the widespread interest in the theory of inequalities, the theory of convex functions is now at the center of many studies. Convex functions are the topic of research in a number of disciplines due to their applicability in inequality theory [5–8] and defined as:

Definition 1. [5] A mapping $\lambda: \mathcal{J} \subset \mathfrak{R} \longrightarrow \mathfrak{R}$ is called to be convex on $\mathcal{J}$, if

$$\lambda((1-\zeta)y_1 + \zeta y_2) \leq (1-\zeta)\lambda(y_1) + \zeta\lambda(y_2), \quad (2)$$

holds for every $y_1, y_2 \in \mathcal{J}$ and $\zeta \in [0,1]$.

Kian and Moslehian used the Jensen–Mercer inequality and demonstrated the Hermite–Hadamard Mercer inequality in [9] as:

$$\lambda\left(a+b-\frac{y_1+y_2}{2}\right)\leq\frac{1}{y_2-y_1}\int_{y_1}^{y_2}\lambda(a+b-\zeta)\mathrm{d}\zeta$$
$$\leq\frac{\lambda(a+b-y_1)+\lambda(a+b-y_2)}{2}\leq\lambda(a)+\lambda(b)-\frac{\lambda(y_1)+\lambda(y_2)}{2}, \tag{3}$$

where λ is convex function on $[a,b]$.

The famous Jensen inequality, (see [5], Ch. 1) in the literature states that, if λ is convex function on the interval $[y_1,y_2]$, then

$$\lambda\left(\sum_{i=1}^{n}\sigma_i\ell_i\right)\leq\left(\sum_{i=1}^{n}\sigma_i\lambda(\ell_i)\right), \tag{4}$$

holds for all $\ell_i\in[y_1,y_2]$ and all $\sigma_i\in[0,1]$, $\sum_{i=1}^{n}\sigma_i=1$.

Jensen's inequality was modified by Mercer (see [10]) as

$$\lambda\left(y_1+y_2-\sum_{i=1}^{n}\sigma_i\ell_i\right)\leq\lambda(y_1)+\lambda(y_2)-\sum_{i=1}^{n}\sigma_i\lambda(\ell_i), \tag{5}$$

where λ is a convex function on $[y_1,y_2]$ holds for all $\ell_i\in[y_1,y_2]$ and

$$\sigma_i\in[0,1],\sum_{i=1}^{n}\sigma_i=1. \tag{6}$$

Jensen and Hermite–Hadamard type inequalities are the most dynamic inequalities pertaining convex functions. Jensen and its related inequalities are well-known and significant inequalities in mathematical analysis due to its diverse applications and useability in applied and information sciences. Some recent discoveries can be found in [11, 12].

Jensen-type Mercer's inequality is an effective inequality since it provides additional information with specific boundary constraints. The study of generalizations and improvements of Mercer's variants of Hermite–Hadamard type inequalities considering the variety of fractional integral (F-I) operators have been of great interest for researchers in recent years, as evidenced by a large amount of research on it (see [13–15]).

The fractional calculus has been extensively studied by many researchers from the last few decades to generalize, improve, and extend several classic inequalities in order to obtain new variants in different dimensions. There are not only global derivatives in so called fractional calculus (for example: Riemann–Liouville and Caputo), but also local fractional derivatives (Khalil and Almeida, among others) (see [16–18]).

Yue [19], in 2013, discovered new Ostrowski inequalities for fractional integral (F-I) operators along with its associated fractional inequalities. Later in 2014, Aljinović [20] first developed Montgomery identity for fractional integrals of one function with respect to another function and then derived generalized fractional Ostrowski inequality from it. In the same article, he also presented the associated Ostrowski fractional inequalities for fractional integrals of functions with first derivatives in L_p spaces and computed sharp bounds. In the same year, Yildirim and Kirtay [21] used the generalized Riemann–Liouville F-I to establish new variants for Ostrowski inequalities. Some recent development about weighted Ostrowski fractional inequalities can be observed in [22].

Vanterler da Costa Sousa and Capelas de Oliveira in [23] recently introduced the ψ-Hilfer fractional derivative with respect to another function. Also, they investigate some Gronwall inequalities and Cauchy–type problem using the newly introduced ψ-Hilfer operator.

Definition 2. ([24], p.3) Let $(y_1,y_2)(-\infty\leq y_1<y_2\leq\infty)$ be finite or infinite interval in $\mathfrak{R}$ and $\varrho>0$. Also, let ψ: $(y_1,y_2)\longrightarrow\mathfrak{R}_+$ be positive strictly increasing function possessing continuous derivative ψ' on (y_1,y_2). Then, left- and right-sided ψ-Riemann–Liouville F-I of a function λ with respect to another function ψ on $[y_1,y_2]$ can be given as

$$\left(I_{y_1+}^{\varrho;\psi}\right)\lambda(\ell)=\frac{1}{\Gamma(\varrho)}\int_{y_1}^{\ell}\psi'(\zeta)(\psi(\ell)-\psi(\zeta))^{\varrho-1}\lambda(\zeta)\mathrm{d}\zeta,\quad y_1<\ell, \tag{7}$$

and

$$\left(I_{y_2-}^{\varrho;\psi}\right)\lambda(\ell)=\frac{1}{\Gamma(\varrho)}\int_{\ell}^{y_2}\psi'(\zeta)(\psi(\zeta)-\psi(\ell))^{\varrho-1}\lambda(\zeta)\mathrm{d}\zeta,\quad \ell<y_2. \tag{8}$$

Remark 1. F-I operators elaborated in (7) and (8) yield several known F-I operators corresponding to various suitable selections of function ψ (see [25]), that are independently introduced by several authors with related results.

(i) By taking $\psi(y)=y$ as an identity function in (7) and (8), we get Riemann–Liouville F-I operators [24].

(ii) For $\psi(y)=y^{\varrho}/\varrho$, $\varrho>0$ in (7) and (8) produce Katugampola F-I operators defined by Chen and Katugampola in [26].

(iii) For $\psi(y)=y^{\tau+s}/\tau+s$, $\tau>0,s>0$ in (7) and (8) produce generalized conformable F-I operators defined by Khan and Khan in [27].

(iv) For $\psi(y)=(y-y_1)^s/s$, $s>0$, in (7), and $\psi(y)=-(y_2-y)^s/s$, $s>0$, in (8), one can get conformable F-I operators presented by Jarad et al. in [28].

The main good articles about Hermite–Hadamard inequalities involving ψ-Riemann–Liouville F-I operators are in references [29–31]. Some recent results about Hermite–Jensen–Mercer inequalities for ψ-Riemann–Liouville F-I operators can be seen in [14, 15].

The striking motive of this study is to develop generalized fractional equality for ψ-Riemann–Liouville F-I operators, which has a unique place among fractional integral operators, and to use this identity to generate some new Mercer–Ostrowski type inequalities for convex functions. The study also included applications of the findings, taking

into account several specific circumstances of the primary conclusions.

2. New Mercer–Ostrowski Type Inequalities

Throughout this portion, Mercer–Ostrowski inequalities for the ψ-Riemann–Liouville F-I operators are obtained for differentiable functions on (a,b). As a result, we present a novel identity pertaining ψ-Riemann–Liouville F-I operators, that will serve as an auxiliary equality to produce subsequent inequalities.

Lemma 1. *Consider λ: $[a,b] \subset (0,\infty) \longrightarrow \mathfrak{R}$ be a differentiable function and $\lambda' \in \mathscr{L}_1[a,b]$, with $b>a$. If ψ is a strictly increasing, positive monotone function on $(a,b]$ with continuous derivative ψ' on (a,b), then, for all $\varkappa, y_1, y_2, \nu \in [a,b]$ and $\varrho>0$, the following identity holds*

$$\begin{aligned}&\Xi_{\varrho,\psi}\lambda(y_1,y_2,\varkappa,\nu)\\&=\frac{1}{y_2-y_1}\int_{\psi^{-1}(\varkappa+a-\nu)}^{\psi^{-1}(\varkappa+a-y_1)}(\psi(\zeta)-(\varkappa+a-\nu))^{\varrho}\psi'(\zeta)(\lambda'\circ\psi)(\zeta)\mathrm{d}\zeta\\&+\frac{1}{y_2-y_1}\int_{\psi^{-1}(\varkappa+b-y_2)}^{\psi^{-1}(\varkappa+b-\nu)}((\varkappa+b-\nu)-\psi(\zeta))^{\varrho}\psi'(\zeta)(\lambda'\circ\psi)(\zeta)\mathrm{d}\zeta,\end{aligned}\tag{9}$$

where

$$\begin{aligned}\Xi_{\varrho,\psi}\lambda(y_1,y_2,\varkappa,\nu)&=\frac{(\nu-y_1)^{\varrho}}{y_2-y_1}\lambda(\varkappa+a-y_1)+\frac{(y_2-\nu)^{\varrho}}{y_2-y_1}\lambda(\varkappa+b-y_2)\\&-\frac{\Gamma(\varrho+1)}{y_2-y_1}\Big\{I^{\varrho;\psi}_{\psi^{-1}(\varkappa+a-y_1)^-}(\lambda^{\circ}\psi)\big(\psi^{-1}(\varkappa+a-\nu)\big)\\&+I^{\varrho;\psi}_{\psi^{-1}(\varkappa+b-y_2)^+}(\lambda^{\circ}\psi)\big(\psi^{-1}(\varkappa+b-\nu)\big)\Big\}.\end{aligned}\tag{10}$$

Proof. Let us start with

$$I_1:=\frac{\Gamma(\varrho+1)}{y_2-y_1}I^{\varrho;\psi}_{\psi^{-1}(\varkappa+a-y_1)^-}(\lambda^{\circ}\psi)\big(\psi^{-1}(\varkappa+a-\nu)\big),\tag{11}$$

$$\begin{aligned}&=\frac{\varrho}{y_2-y_1}\int_{\psi^{-1}(\varkappa+a-\nu)}^{\psi^{-1}(\varkappa+a-y_1)}(\psi(\zeta)-(\varkappa+a-\nu))^{\varrho-1}\psi'(\zeta)(\lambda^{\circ}\psi)(\zeta)\mathrm{d}\zeta\\&=\frac{1}{y_2-y_1}\int_{\psi^{-1}(\varkappa+a-\nu)}^{\psi^{-1}(\varkappa+a-y_1)}(\lambda^{\circ}\psi)(\zeta)d(\psi(\zeta)-(\varkappa+a-\nu))^{\varrho}d\zeta\\&=\frac{(\nu-y_1)^{\varrho}}{y_2-y_1}\lambda(\varkappa+a-y_1)\\&-\frac{1}{y_2-y_1}\int_{\psi^{-1}(\varkappa+a-\nu)}^{\psi^{-1}(\varkappa+a-y_1)}(\psi(\zeta)-(\varkappa+a-\nu))^{\varrho}\psi'(\zeta)(\lambda'\circ\psi)(\zeta)\mathrm{d}\zeta,\end{aligned}\tag{12}$$

and similarly, we get

$$\begin{aligned}I_2:&=\frac{\Gamma(\varrho+1)}{y_2-y_1}I^{\varrho;\psi}_{\psi^{-1}(\varkappa+b-y_2)^+}(\lambda^{\circ}\psi)\big(\psi^{-1}(\varkappa+b-\nu)\big)\\&=\frac{(y_2-\nu)^{\varrho}}{y_2-y_1}\lambda(\varkappa+b-y_2)\\&-\frac{1}{y_2-y_1}\int_{\psi^{-1}(\varkappa+b-y_2)}^{\psi^{-1}(\varkappa+b-\nu)}((\varkappa+b-\nu)-\psi(\zeta))^{\varrho}\psi'(\zeta)(\lambda'\circ\psi)(\zeta)\mathrm{d}\zeta.\end{aligned}\tag{13}$$

It follows from (11) and (13) that

$$\begin{aligned}&\frac{(\nu-y_1)^{\varrho}}{y_2-y_1}\lambda(\varkappa+a-y_1)+\frac{(y_2-\nu)^{\varrho}}{y_2-y_1}\lambda(\varkappa+b-y_2)-I_1-I_2\\&=\frac{1}{y_2-y_1}\int_{\psi^{-1}(\varkappa+a-\nu)}^{\psi^{-1}(\varkappa+a-y_1)}(\psi(\zeta)-(\varkappa+a-\nu))^{\varrho}\psi'(\zeta)(\lambda'\circ\psi)(\zeta)\mathrm{d}\zeta\\&+\frac{1}{y_2-y_1}\int_{\psi^{-1}(\varkappa+b-y_2)}^{\psi^{-1}(\varkappa+b-\nu)}((\varkappa+b-\nu)-\psi(\zeta))^{\varrho}\psi'(\zeta)(\lambda'\circ\psi)(\zeta)\mathrm{d}\zeta.\end{aligned}\tag{14}$$

By simplifying, we get the required result. □

Remark 2. Placing identity function $\psi(y)=y$ in (9), then, we get Lemma 2.1 given in [32].

Remark 3. If we set $\psi(y)=y$, $y_1=a$, $y_2=b$, and $\nu=\varkappa$ in (9), it reduces to Lemma 2 in [33].

Remark 4. Setting $\psi(y)=y$, $y_1=a$, $y_2=b$, $\nu=\varkappa$, and $\varrho=1$ in (9), it recaptures Lemma 1 proved in [2].

Theorem 1. *Under the assumptions of Lemma 1, if $|\lambda'|$ is convex function on $[a,b]$, then for all $\varrho>0$, the following inequality is valid.*

$$\begin{aligned}&\left|\Xi_{\varrho,\psi}\lambda(y_1,y_2,\varkappa,\nu)\right|\\&\le\frac{(\nu-y_1)^{\varrho+1}}{y_2-y_1}\left\{\frac{1}{\varrho+1}\big(|\lambda'(\varkappa)|+|\lambda'(a)|\big)-\left[\frac{1}{\varrho+2}|\lambda'(y_1)|+\frac{1}{(\varrho+1)(\varrho+2)}|\lambda'(\nu)|\right]\right\}\\&+\frac{(y_2-\nu)^{\varrho+1}}{y_2-y_1}\left\{\frac{1}{\varrho+1}\big(|\lambda'(\varkappa)|+|\lambda'(b)|\big)-\left[\frac{1}{\varrho+2}|\lambda'(y_2)|+\frac{1}{(\varrho+1)(\varrho+2)}|\lambda'(\nu)|\right]\right\}.\end{aligned}\tag{15}$$

Proof. By means of (9),

$$\Xi_{\varrho,\psi}\lambda(y_1,y_2,\varkappa,v)$$
$$=\frac{1}{y_2-y_1}\int_{\psi^{-1}(\varkappa+a-v)}^{\psi^{-1}(\varkappa+a-y_1)}(\psi(\zeta)-(\varkappa+a-v))^{\varrho}\psi'(\zeta)(\lambda'\circ\psi)(\zeta)\mathrm{d}\zeta$$
$$+\frac{1}{y_2-y_1}\int_{\psi^{-1}(\varkappa+b-y_2)}^{\psi^{-1}(\varkappa+b-v)}((\varkappa+b-v)-\psi(\zeta))^{\varrho}\psi'(\zeta)(\lambda'\circ\psi)(\zeta)\mathrm{d}\zeta. \tag{16}$$

Change of variables $s_1=\psi(\zeta)-(\varkappa+a-v)/v-y_1$ and $s_2=(\varkappa+b-v)-\psi(\zeta)/y_2-v$ and then $\zeta=s_1=s_2$ into the resulting equality, we get

$$\Xi_{\varrho,\psi}\lambda(y_1,y_2,\varkappa,v)$$
$$=\frac{(v-y_1)^{\varrho+1}}{y_2-y_1}\int_0^1\zeta^{\varrho}\left|\lambda'(\varkappa+a-[\zeta y_1+(1-\zeta)v])\right|\mathrm{d}\zeta$$
$$+\frac{(y_2-v)^{\varrho+1}}{y_2-y_1}\int_0^1\zeta^{\varrho}\left|\lambda'(\varkappa+b-[\zeta y_2+(1-\zeta)v])\right|\mathrm{d}\zeta. \tag{17}$$

Since $|\lambda'|$ is convex function on $[a,b]$, we obtain

$$\begin{aligned}\left|\Xi_{\varrho,\psi}\lambda(y_1,y_2,\varkappa,v)\right|&\le\frac{(v-y_1)^{\varrho+1}}{y_2-y_1}\int_0^1\zeta^{\varrho}\left|\lambda'(\varkappa+a-[\zeta y_1+(1-\zeta)v])\right|\mathrm{d}\zeta\\&+\frac{(y_2-v)^{\varrho+1}}{y_2-y_1}\int_0^1\zeta^{\varrho}\left|\lambda'(\varkappa+b-[\zeta y_2+(1-\zeta)v])\right|\mathrm{d}\zeta\\&\le\frac{(v-y_1)^{\varrho+1}}{y_2-y_1}\int_0^1\zeta^{\varrho}\left\{\left|\lambda'(\varkappa)\right|+\left|\lambda'(a)\right|-\left[\zeta\left|\lambda'(y_1)\right|+(1-\zeta)\left|\lambda'(v)\right|\right]\right\}\mathrm{d}\zeta\\&+\frac{(y_2-v)^{\varrho+1}}{y_2-y_1}\int_0^1\zeta^{\varrho}\left\{\left|\lambda'(\varkappa)\right|+\left|\lambda'(b)\right|-\left[\zeta\left|\lambda'(y_2)\right|+(1-\zeta)\left|\lambda'(v)\right|\right]\right\}\mathrm{d}\zeta\\&\le\frac{(v-y_1)^{\varrho+1}}{y_2-y_1}\left\{\frac{1}{\varrho+1}\left(\left|\lambda'(\varkappa)\right|+\left|\lambda'(a)\right|\right)-\left[\frac{1}{\varrho+2}\left|\lambda'(y_1)\right|+\frac{1}{(\varrho+1)(\varrho+2)}\left|\lambda'(v)\right|\right]\right\}\\&+\frac{(y_2-v)^{\varrho+1}}{y_2-y_1}\left\{\frac{1}{\varrho+1}\left(\left|\lambda'(\varkappa)\right|+\left|\lambda'(b)\right|\right)-\left[\frac{1}{\varrho+2}\left|\lambda'(y_2)\right|+\frac{1}{(\varrho+1)(\varrho+2)}\left|\lambda'(v)\right|\right]\right\}.\end{aligned} \tag{18}$$

Remark 5. If we set $\psi(y)=y$ in Theorem 1, one can get above inequality for Riemann–Liouville F-I operators given in Theorem 2.1 [32].

Remark 6. If we set $\psi(y)=y$, $y_1=a$, $y_2=b$, and $v=\varkappa$ in Theorem 1, it reduces to Theorem 7 in [33] that yields the same results with $s=1$.

Corollary 1. *If we set $\psi(y)=y$, $y_1=a, y_2=b$, and $v=\varkappa$ with $\varrho=1$ in Theorem 1, we get the following inequality*

$$\begin{aligned}&\left|\lambda(\varkappa)-\frac{1}{b-a}\int_a^b\lambda(\zeta)d\zeta\right|\\&\le\frac{(\varkappa-a)^2}{3(b-a)}\left\{\frac{1}{2}\left|\lambda'(a)\right|+\left|\lambda'(\varkappa)\right|\right\}+\frac{(b-\varkappa)^2}{3(b-a)}\left\{\frac{1}{2}\left|\lambda'(b)\right|+\left|\lambda'(\varkappa)\right|\right\}.\end{aligned} \tag{19}$$

□

Corollary 2. *If we set $\psi(y)=y$ and $\varrho=1$ in Theorem 1, we get the following Mercer–Ostrowski inequality:*

$$\begin{aligned}&\left|\left\{\frac{v-y_1}{y_2-y_1}\lambda(\varkappa+a-y_1)+\frac{y_2-v}{y_2-y_1}\lambda(\varkappa+b-y_2)\right\}-\frac{1}{y_2-y_1}\left\{\int_{\varkappa+a-v}^{\varkappa+a-y_1}\lambda(\zeta)d\zeta+\int_{\varkappa+b-y_2}^{\varkappa+b-v}\lambda(\zeta)\mathrm{d}\zeta\right\}\right|\\&\le\frac{(v-y_1)^2}{y_2-y_1}\left\{\frac{1}{2}\left(\left|\lambda'(\varkappa)\right|+\left|\lambda'(a)\right|\right)-\left[\frac{1}{3}\left|\lambda'(y_1)\right|+\frac{1}{6}\left|\lambda'(v)\right|\right]\right\}\\&+\frac{(y_2-v)^2}{y_2-y_1}\left\{\frac{1}{2}\left(\left|\lambda'(\varkappa)\right|+\left|\lambda'(b)\right|\right)-\left[\frac{1}{3}\left|\lambda'(y_2)\right|+\frac{1}{6}\left|\lambda'(v)\right|\right]\right\}.\end{aligned} \tag{20}$$

Corollary 3. *The following Mercer–Ostrowski inequality can be found in Theorem 1 with* $|\lambda'| \le M$

$$\left|\Xi_{\varrho,\psi}\lambda(y_1, y_2, \varkappa, v)\right| \le \frac{M}{(y_2 - y_1)(\varrho + 1)}\left\{(v - y_1)^{\varrho+1} + (y_2 - v)^{\varrho+1}\right\}. \tag{21}$$

Proof. The result can be obtained by using $|\lambda'(\varkappa + a - [\zeta y_1 + (1-\zeta)v])| \le M$ and $|\lambda'(\varkappa + b - [\zeta y_2 + (1-\zeta)v])| \le M$. □

Remark 7. If we set $\psi(y) = y$, $y_1 = a, y_2 = b$ and $v = \varkappa$ in Corollary 3, it reduces to Corollary 1 in [33].

Remark 8. If we set $\psi(y) = y$, $y_1 = a, y_2 = b$ and $v = \varkappa$ and $\varrho = 1$ in Corollary 3, it reduces to Theorem 2 in [2] that yields the same result with $s = 1$.

Theorem 2. *We assume that all the conditions of Lemma 1 hold. If* $|\lambda'|^q$ *is convex function on* $[a, b]$*, then, for all* $\varrho > 0$*, the following inequality*

$$\begin{aligned}
&\left|\Xi_{\varrho,\psi}\lambda(y_1, y_2, \varkappa, v)\right| \\
&\le \frac{(v - y_1)^{\varrho+1}}{y_2 - y_1}\left(\frac{1}{\varrho p + 1}\right)^{(1/p)}\left\{\left(|\lambda'(\varkappa)|^q + |\lambda'(a)|^q\right) - \frac{1}{2}\left[|\lambda'(y_1)|^q + |\lambda'(v)|^q\right]\right\}^{(1/q)} \\
&\quad + \frac{(y_2 - v)^{\varrho+1}}{y_2 - y_1}\left(\frac{1}{\varrho p + 1}\right)^{(1/p)}\left\{\left(|\lambda'(\varkappa)|^q + |\lambda'(b)|^q\right) - \frac{1}{2}\left[|\lambda'(y_2)|^q + |\lambda'(v)|^q\right]\right\}^{(1/q)},
\end{aligned} \tag{22}$$

holds, where $p, q > 1$ *are conjugate exponents.*

Proof. Applying classical Hölder integral inequality and the convexity of $|\lambda'|^q$ on the right side of (9), we get

$$\begin{aligned}
&\left|\Xi_{\varrho,\psi}\lambda(y_1, y_2, \varkappa, v)\right| \\
&\le \frac{(v - y_1)^{\varrho+1}}{y_2 - y_1}\int_0^1 \zeta^{\varrho}\left|\lambda'(\varkappa + a - [\zeta y_1 + (1-\zeta)v])\right|d\zeta \\
&\quad + \frac{(y_2 - v)^{\varrho+1}}{y_2 - y_1}\int_0^1 \zeta^{\varrho}\left|\lambda'(\varkappa + b - [\zeta y_2 + (1-\zeta)v])\right|d\zeta. \\
&\le \frac{(v - y_1)^{\varrho+1}}{y_2 - y_1}\left(\int_0^1 \zeta^{\varrho p}d\zeta\right)^{(1/p)}\left(\int_0^1 \left|\lambda'(\varkappa + a - [\zeta y_1 + (1-\zeta)v])\right|^q d\zeta\right)^{(1/q)} \\
&\quad + \frac{(y_2 - v)^{\varrho+1}}{y_2 - y_1}\left(\int_0^1 \zeta^{\varrho p}d\zeta\right)^{(1/p)}\left(\int_0^1 \left|\lambda'(\varkappa + b - [\zeta y_2 + (1-\zeta)v])\right|^q d\zeta\right)^{(1/q)} \\
&\le \frac{(v - y_1)^{\varrho+1}}{y_2 - y_1}\left(\int_0^1 \zeta^{\varrho p}d\zeta\right)^{(1/p)} \\
&\quad \times\left(\int_0^1 \left\{|\lambda'(\varkappa)|^q + |\lambda'(a)|^q - \left[\zeta|\lambda'(y_1)|^q + (1-\zeta)|\lambda'(v)|^q\right]\right\}d\zeta\right)^{(1/q)} \\
&\quad + \frac{(y_2 - v)^{\varrho+1}}{y_2 - y_1}\left(\int_0^1 \zeta^{\varrho p}d\zeta\right)^{(1/p)} \\
&\quad \times\left(\int_0^1 \left\{|\lambda'(\varkappa)|^q + |\lambda'(b)|^q - \left[\zeta|\lambda'(y_2)|^q + (1-\zeta)|\lambda'(v)|^q\right]\right\}d\zeta\right)^{(1/q)} \\
&\le \frac{(v - y_1)^{\varrho+1}}{y_2 - y_1}\left(\frac{1}{\varrho p + 1}\right)^{(1/p)}\left\{\left(|\lambda'(\varkappa)|^q + |\lambda'(a)|^q\right) - \frac{1}{2}\left[|\lambda'(y_1)|^q + |\lambda'(v)|^q\right]\right\}^{(1/q)} \\
&\quad + \frac{(y_2 - v)^{\varrho+1}}{y_2 - y_1}\left(\frac{1}{\varrho p + 1}\right)^{(1/p)}\left\{\left(|\lambda'(\varkappa)|^q + |\lambda'(b)|^q\right) - \frac{1}{2}\left[|\lambda'(y_2)|^q + |\lambda'(v)|^q\right]\right\}^{(1/q)}.
\end{aligned} \tag{23}$$

That finish the proof. □

Remark 9. If we set $\psi(y) = y$ in Theorem 2, it reduces to Theorem 2.2 in [32].

Remark 10. If we set $\psi(y) = y$, $y_1 = a$, $y_2 = b$, and $v = \varkappa$ in Theorem 2, it reduces to Theorem 8 in [33] that yields the same results with $s = 1$.

Corollary 4. *If we set $\psi(y) = y$, $y_1 = a$, $y_2 = b$, and $v = \varkappa$ with $\varrho = 1$ in Theorem 2, we have the following inequality:*

$$\begin{aligned}
&\left|\lambda(\varkappa) - \frac{1}{b-a}\int_a^b \lambda(\zeta)d\zeta\right| \le \frac{1}{2^{(1/q)}(b-a)}\left(\frac{1}{p+1}\right)^{(1/p)} \\
&\times\left[(\varkappa-a)^2\left\{\left|\lambda'(a)\right|^q + \left|\lambda'(\varkappa)\right|^q\right\}^{(1/q)}\right. \\
&\left.+ (b-\varkappa)^2\left\{\left|\lambda'(b)\right|^q + \left|\lambda'(\varkappa)\right|^q\right\}^{(1/q)}\right].
\end{aligned} \tag{24}$$

Corollary 5. *If we set $\psi(y) = y$ and $\varrho = 1$ in Theorem 2, we lead to following Mercer–Ostrowski inequality:*

$$\begin{aligned}
&\left|\left\{\frac{v-y_1}{y_2-y_1}\lambda(\varkappa+a-y_1) + \frac{y_2-v}{y_2-y_1}\lambda(\varkappa+b-y_2)\right\}\right. \\
&\left. - \frac{1}{y_2-y_1}\left\{\int_{\varkappa+a-v}^{\varkappa+a-y_1}\lambda(\zeta)d\zeta + \int_{\varkappa+b-y_2}^{\varkappa+b-v}\lambda(\zeta)\mathrm{d}\zeta\right\}\right| \\
&\le \frac{(v-y_1)^2}{y_2-y_1}\left(\frac{1}{p+1}\right)^{(1/p)}\left\{\left(\left|\lambda'(\varkappa)\right|^q + \left|\lambda'(a)\right|^q\right) - \frac{1}{2}\left[\left|\lambda'(y_1)\right|^q + \left|\lambda'(v)\right|^q\right]\right\}^{(1/q)} \\
&+ \frac{(y_2-v)^2}{y_2-y_1}\left(\frac{1}{p+1}\right)^{(1/p)}\left\{\left(\left|\lambda'(\varkappa)\right|^q + \left|\lambda'(b)\right|^q\right) - \frac{1}{2}\left[\left|\lambda'(y_2)\right|^q + \left|\lambda'(v)\right|^q\right]\right\}^{(1/q)}.
\end{aligned} \tag{25}$$

Corollary 6. *Let the function $|\lambda'|$ in Theorem 2 is assumed to be bounded that is $|\lambda'| \le M$, then the following result holds:*

$$\begin{aligned}
&\left|\Xi_{\varrho,\psi}\lambda(y_1, y_2, \varkappa, v)\right| \\
&\le \frac{M}{y_2-y_1}\left(\frac{1}{\varrho p+1}\right)^{\frac{1}{p}}\left\{(v-y_1)^{\varrho+1} + (y_2-v)^{\varrho+1}\right\}.
\end{aligned} \tag{26}$$

Proof. The result can be demonstrated by using $|\lambda'(\varkappa + a - [\zeta y_1 + (1-\zeta)v])| \le M$ and $|\lambda'(\varkappa + b - [\zeta y_2 + (1-\zeta)v])| \le M$. □

Remark 11. If we set $\psi(y) = y$, $y_1 = a$, $y_2 = b$, and $v = \varkappa$ in Corollary 6, it reduces to Corollary 2 in [33].

Remark 12. If we set $\psi(y) = y$, $y_1 = a$, $y_2 = b$, $v = \varkappa$ and $\varrho = 1$ in Corollary 6, it reduces to Theorem 3 in [2] that yields the same result with $s = 1$.

Theorem 3. *We assume that all the conditions of Lemma 1 hold. If $|\lambda'|^q$ is convex function on $[a, b]$, $q \ge 1$, then for all $\varrho > 0$, the following inequality*

$$\begin{aligned}
&\left|\Xi_{\varrho,\psi}\lambda(y_1, y_2, \varkappa, v)\right| \\
&\le \frac{(v-y_1)^{\varrho+1}}{y_2-y_1}\left(\frac{1}{\varrho+1}\right)^{1-(1/q)} \\
&\times\left\{\frac{1}{\varrho+1}\left(\left|\lambda'(\varkappa)\right|^q + \left|\lambda'(a)\right|^q\right) - \left[\frac{1}{\varrho+2}\left|\lambda'(y_1)\right|^q + \frac{1}{(\varrho+1)(\varrho+2)}\left|\lambda'(v)\right|^q\right]\right\}^{(1/q)} \\
&+ \frac{(y_2-v)^{\varrho+1}}{y_2-y_1}\left(\frac{1}{\varrho+1}\right)^{1-(1/q)} \\
&\times\left\{\frac{1}{\varrho+1}\left(\left|\lambda'(\varkappa)\right|^q + \left|\lambda'(b)\right|^q\right) - \left[\frac{1}{\varrho+2}\left|\lambda'(y_2)\right|^q + \frac{1}{(\varrho+1)(\varrho+2)}\left|\lambda'(v)\right|^q\right]\right\}^{(1/q)},
\end{aligned} \tag{27}$$

is valid.

Proof. Applying power-mean integral inequality and the convexity of $|\lambda'|^q$ on the right side of (9), we get

$$
\begin{aligned}
&\left|\Xi_{\varrho,\psi}\lambda(y_1,y_2,\varkappa,v)\right| \\
&\le \frac{(v-y_1)^{\varrho+1}}{y_2-y_1}\int_0^1 \zeta^{\varrho}\left|\lambda'\left(\varkappa+a-[\zeta y_1+(1-\zeta)v]\right)\right|\mathrm{d}\zeta \\
&\quad+\frac{(y_2-v)^{\varrho+1}}{y_2-y_1}\int_0^1 \zeta^{\varrho}\left|\lambda'\left(\varkappa+b-[\zeta y_2+(1-\zeta)v]\right)\right|\mathrm{d}\zeta \\
&\le \frac{(v-y_1)^{\varrho+1}}{y_2-y_1}\left(\int_0^1 \zeta^{\varrho}d\zeta\right)^{1-(1/q)}\left(\int_0^1 \zeta^{\varrho}\left|\lambda'\left(\varkappa+a-[\zeta y_1+(1-\zeta)v]\right)\right|^q\mathrm{d}\zeta\right)^{(1/q)} \\
&\quad+\frac{(y_2-v)^{\varrho+1}}{y_2-y_1}\left(\int_0^1 \zeta^{\varrho}d\zeta\right)^{1-(1/q)}\left(\int_0^1 \zeta^{\varrho}\left|\lambda'\left(\varkappa+b-[\zeta y_2+(1-\zeta)v]\right)\right|^q\mathrm{d}\zeta\right)^{(1/q)} \\
&\le \frac{(v-y_1)^{\varrho+1}}{y_2-y_1}\left(\int_0^1 \zeta^{\varrho}\mathrm{d}\zeta\right)^{1-(1/q)}\times\left(\int_0^1 \zeta^{\varrho}\left\{\left|\lambda'(\varkappa)\right|^q+\left|\lambda'(a)\right|^q-\left[\zeta\left|\lambda'(y_1)\right|^q+(1-\zeta)\left|\lambda'(v)\right|\right]\right\}^q\mathrm{d}\zeta\right)^{(1/q)} \\
&\quad+\frac{(y_2-v)^{\varrho+1}}{y_2-y_1}\left(\int_0^1 \zeta^{\varrho}\mathrm{d}\zeta\right)^{1-(1/q)} \\
&\quad\times\left(\int_0^1 \zeta^{\varrho}\left\{\left|\lambda'(\varkappa)\right|^q+\left|\lambda'(b)\right|^q-\left[\zeta\left|\lambda'(y_2)\right|^q+(1-\zeta)\left|\lambda'(v)\right|^q\right]\right\}\mathrm{d}\zeta\right)^{(1/q)} \\
&\le \frac{(v-y_1)^{\varrho+1}}{y_2-y_1}\left(\frac{1}{\varrho+1}\right)^{1-(1/q)} \\
&\quad\times\left\{\frac{1}{\varrho+1}\left(\left|\lambda'(\varkappa)\right|^q+\left|\lambda'(a)\right|^q\right)-\left[\frac{1}{\varrho+2}\left|\lambda'(y_1)\right|^q+\frac{1}{(\varrho+1)(\varrho+2)}\left|\lambda'(v)\right|^q\right]\right\}^{(1/q)} \\
&\quad+\frac{(y_2-v)^{\varrho+1}}{y_2-y_1}\left(\frac{1}{\varrho+1}\right)^{1-(1/q)} \\
&\quad\times\left\{\frac{1}{\varrho+1}\left(\left|\lambda'(\varkappa)\right|^q+\left|\lambda'(b)\right|^q\right)-\left[\frac{1}{\varrho+2}\left|\lambda'(y_2)\right|^q+\frac{1}{(\varrho+1)(\varrho+2)}\left|\lambda'(v)\right|^q\right]\right\}^{(1/q)}.
\end{aligned}
\tag{28}
$$

Which ends the proof. □

Remark 13. If we set $\psi(y)=y$ in Theorem 3, it reduces to Theorem 2.3 in [32].

Remark 14. If we set $\psi(y)=y$, $y_1=a$, $y_2=b$, and $v=\varkappa$ in Theorem 3, it reduces to Theorem 9 in [33] that yields the same results with $s=1$.

Corollary 7. *If we set $\psi(y)=y$, $y_1=a$, $y_2=b$, and $v=\varkappa$ with $\varrho=1$ in Theorem 3, we have the following inequality:*

$$
\begin{aligned}
&\left|\lambda(\varkappa)-\frac{1}{b-a}\int_a^b \lambda(\zeta)\mathrm{d}\zeta\right| \\
&\le \frac{1}{(b-a)}\left(\frac{1}{2}\right)^{1-(1/q)} \\
&\quad\times\frac{1}{3}\left[(\varkappa-a)^2\left\{\frac{1}{2}\left|\lambda'(a)\right|^q+\left|\lambda'(\varkappa)\right|^q\right\}^{(1/q)}\right. \\
&\quad\left.+(b-\varkappa)^2\left\{\frac{1}{2}\left|\lambda'(b)\right|^q+\left|\lambda'(\varkappa)\right|^q\right\}^{(1/q)}\right].
\end{aligned}
\tag{29}
$$

Corollary 8. *If we choose $\psi(y) = y$ and $\varrho = 1$ in Theorem 3, we have the following Mercer–Ostrowski inequality:*

$$\begin{aligned}
&\left|\left\{\frac{v-y_1}{y_2-y_1}\lambda(\varkappa+a-y_1)+\frac{y_2-v}{y_2-y_1}\lambda(\varkappa+b-y_2)\right\}-\frac{1}{y_2-y_1}\left\{\int_{\varkappa+a-v}^{\varkappa+a-y_1}\lambda(\zeta)d\zeta+\int_{\varkappa+b-y_2}^{\varkappa+b-v}\lambda(\zeta)\mathrm{d}\zeta\right\}\right| \\
&\le\frac{(v-y_1)^2}{y_2-y_1}\left(\frac{1}{2}\right)^{1-(1/q)}\left\{\frac{1}{2}\left(\left|\lambda'(x)\right|^q+\left|\lambda'(a)\right|^q\right)-\left[\frac{1}{3}\left|\lambda'(y_1)\right|^q+\frac{1}{6}\left|\lambda'(v)\right|^q\right]\right\}^{(1/q)} \\
&\quad+\frac{(y_2-v)^2}{y_2-y_1}\left(\frac{1}{2}\right)^{1-(1/q)}\left\{\frac{1}{2}\left(\left|\lambda'(\varkappa)\right|^q+\left|\lambda'(b)\right|^q\right)-\left[\frac{1}{3}\left|\lambda'(y_2)\right|^q+\frac{1}{6}\left|\lambda'(v)\right|^q\right]\right\}^{(1/q)}.
\end{aligned} \tag{30}$$

Corollary 9. *Assuming that $|\lambda'| \le M$, in Theorem 3, the following Mercer–Ostrowski inequality holds:*

$$\begin{aligned}
&\left|\Xi_{\varrho,\psi}\lambda(y_1,y_2,\varkappa,v)\right| \\
&\le\frac{M}{(y_2-y_1)(\varrho+1)}\left\{(v-y_1)^{\varrho+1}+(y_2-v)^{\varrho+1}\right\}.
\end{aligned} \tag{31}$$

Proof. Under the assumed conditions, we have $|\lambda'(\varkappa+a-[\zeta y_1+(1-\zeta)v])| \le M$ and $|\lambda'(\varkappa+b-[\zeta y_2+(1-\zeta)v])| \le M$. Thus, inequality (27) in Theorem 3 leads to inequality (31). □

Remark 15. If we set $\psi(y) = y$, $y_1 = a$, $y_2 = b$, and $v = \varkappa$ in Corollary 9, it reduces to Corollary 3 in [33].

Remark 16. If we set $\psi(y) = y$, $y_1 = a$, $y_2 = b$, $v = \varkappa$, and $\varrho = 1$ in Corollary 9, it reduces to Theorem 4 in [2] that yields the same result with $s = 1$.

Theorem 4. *We assume that all the assumptions of Lemma 1 holds. If $|\lambda'|^q$ is convex function on $[a,b]$, for all $\varrho > 0$, the following inequality*

$$\begin{aligned}
&\left|\Xi_{\varrho,\psi}\lambda(y_1,y_2,\varkappa,v)\right| \\
&\le\frac{(v-y_1)^{\varrho+1}}{y_2-y_1}\left\{\frac{1}{(\varrho p+1)p}+\frac{1}{q}\left(\left|\lambda'(\varkappa)\right|^q+\left|\lambda'(a)\right|^q-\frac{1}{2}\left[\left|\lambda'(y_1)\right|^q+\left|\lambda'(v)\right|\right]^q\right)\right\} \\
&\quad+\frac{(y_2-v)^{\varrho+1}}{y_2-y_1}\left\{\frac{1}{(\varrho p+1)p}+\frac{1}{q}\left(\left|\lambda'(\varkappa)\right|^q+\left|\lambda'(b)\right|^q-\frac{1}{2}\left[\left|\lambda'(y_2)\right|^q+\left|\lambda'(v)\right|\right]^q\right)\right\},
\end{aligned} \tag{32}$$

holds where $p, q > 1$ are conjugate exponents.

Proof. From (9), we obtain

$$\begin{aligned}
&\left|\Xi_{\varrho,\psi}\lambda(y_1,y_2,x,v)\right| \\
&\le\frac{(v-y_1)^{\varrho+1}}{y_2-y_1}\int_0^1\zeta^{\varrho}\left|\lambda'(\varkappa+a-[\zeta y_1+(1-\zeta)v])\right|\mathrm{d}\zeta \\
&\quad+\frac{(y_2-v)^{\varrho+1}}{y_2-y_1}\int_0^1\zeta^{\varrho}\left|\lambda'(\varkappa+b-[\zeta y_2+(1-\zeta)v])\right|\mathrm{d}\zeta.
\end{aligned} \tag{33}$$

Utilizing Young's inequality as

$$uv < \frac{1}{p}u^p+\frac{1}{q}v^q.$$

$$\begin{aligned}
&\left|\Xi_{\varrho,\psi}\lambda(y_1,y_2,\varkappa,v)\right| \\
&\le\frac{(v-y_1)^{\varrho+1}}{y_2-y_1}\left\{\frac{1}{p}\int_0^1\zeta^{\varrho p}d\zeta\right. \\
&\quad\left.+\frac{1}{q}\int_0^1\left|\lambda'(\varkappa+a-[\zeta y_1+(1-\zeta)v])\right|^q\mathrm{d}\zeta\right\} \\
&\quad+\frac{(y_2-v)^{\varrho+1}}{y_2-y_1}\left\{\frac{1}{p}\int_0^1\zeta^{\varrho p}d\zeta\right. \\
&\quad\left.+\frac{1}{q}\int_0^1\left|\lambda'(\varkappa+b-[\zeta y_2+(1-\zeta)v])\right|^q\mathrm{d}\zeta\right\}.
\end{aligned} \tag{34}$$

By the convexity of $|\lambda'|^q$, we have

$$\begin{aligned}\left|\Xi_{\varrho,\psi}\lambda(y_1,y_2,\varkappa,\nu)\right| &\le \frac{(\nu-y_1)^{\varrho+1}}{y_2-y_1}\\ &\times\left\{\frac{1}{p}\int_0^1\zeta^{\varrho p}d\zeta+\frac{1}{q}\int_0^1\left\{\left|\lambda'(\varkappa)\right|^q+\left|\lambda'(a)\right|^q-\left[\zeta\left|\lambda'(y_1)\right|^q+(1-\zeta)\left|\lambda'(\nu)\right|^q\right]\right\}\mathrm{d}\zeta\right\}\\ &+\frac{(y_2-\nu)^{\varrho+1}}{y_2-y_1}\\ &\times\left\{\frac{1}{p}\int_0^1\zeta^{\varrho p}\mathrm{d}\zeta+\frac{1}{q}\int_0^1\left\{\left|\lambda'(\varkappa)\right|^q+\left|\lambda'(b)\right|^q-\left[\zeta\left|\lambda'(y_2)\right|^q+(1-\zeta)\left|\lambda'(\nu)\right|^q\right]\right\}\mathrm{d}\zeta\right\}\\ &\le\frac{(\nu-y_1)^{\varrho+1}}{y_2-y_1}\left\{\frac{1}{(\varrho p+1)p}+\frac{1}{q}\left(\left|\lambda'(\varkappa)\right|^q+\left|\lambda'(a)\right|^q-\frac{1}{2}\left[\left|\lambda'(y_1)\right|^q+\left|\lambda'(\nu)\right|^q\right]\right)\right\}\\ &+\frac{(y_2-\nu)^{\varrho+1}}{y_2-y_1}\left\{\frac{1}{(\varrho p+1)p}+\frac{1}{q}\left(\left|\lambda'(\varkappa)\right|^q+\left|\lambda'(b)\right|^q-\frac{1}{2}\left[\left|\lambda'(y_2)\right|^q+\left|\lambda'(\nu)\right|^q\right]\right)\right\},\end{aligned}\tag{35}$$

and the proof is done. □

Remark 17. In Theorem 4, putting $\psi(y)=y$, then, one can get Mercer–Ostrowski inequality pertaining Riemann–Liouville F-I operators given in [32].

Corollary 10. *If we choose $\psi(y)=y$ and $\varrho=1$ in Theorem 4, the following Mercer–Ostrowski inequality holds:*

$$\begin{aligned}&\left|\left\{\frac{\nu-y_1}{y_2-y_1}\lambda(\varkappa+a-y_1)+\frac{y_2-\nu}{y_2-y_1}\lambda(\varkappa+b-y_2)\right\}-\frac{1}{y_2-y_1}\left\{\int_{\varkappa+a-\nu}^{\varkappa+a-y_1}\lambda(\zeta)d\zeta+\int_{\varkappa+b-y_2}^{\varkappa+b-\nu}\lambda(\zeta)\mathrm{d}\zeta\right\}\right|\\ &\le\frac{(\nu-y_1)^2}{y_2-y_1}\left\{\frac{1}{(p+1)p}+\frac{1}{q}\left(\left|\lambda'(\varkappa)\right|^q+\left|\lambda'(a)\right|^q-\frac{1}{2}\left[\left|\lambda'(y_1)\right|^q+\left|\lambda'(\nu)\right|\right]^q\right)\right\}\\ &+\frac{(y_2-\nu)^2}{y_2-y_1}\left\{\frac{1}{(p+1)p}+\frac{1}{q}\left(\left|\lambda'(\varkappa)\right|^q+\left|\lambda'(b)\right|^q-\frac{1}{2}\left[\left|\lambda'(y_2)\right|^q+\left|\lambda'(\nu)\right|^q\right]\right)\right\}.\end{aligned}\tag{36}$$

Corollary 11. *The following Mercer–Ostrowski inequality can be obtained from Theorem 4 by assuming $|\lambda'|\le M$:*

$$\begin{aligned}&\left|\Xi_{\varrho,\psi}\lambda(y_1,y_2,\varkappa,\nu)\right|\\ &\le\frac{1}{y_2-y_1}\left\{\frac{1}{(\varrho p+1)p}+\frac{1}{q}M^q\right\}\left[(\nu-y_1)^{\varrho+1}+(y_2-\nu)^{\varrho+1}\right].\end{aligned}\tag{37}$$

Theorem 5. *We assume that all the assumptions of Lemma 1 hold. If $|\lambda'|^q$ is concave function on $[a,b], q>1$, for all $\varrho>0$, the following inequality holds:*

$$\begin{aligned}&\left|\Xi_{\varrho,\psi}\lambda(y_1,y_2,\varkappa,\nu)\right|\\ &\le\left(\frac{1}{\varrho p+1}\right)^{\frac{1}{p}}\\ &\times\left\{\frac{(\nu-y_1)^{\varrho+1}}{y_2-y_1}\left|\lambda'\left(\varkappa+a-\frac{y_1+\nu}{2}\right)\right|\right.\\ &\left.+\frac{(y_2-\nu)^{\varrho+1}}{y_2-y_1}\left|\lambda'\left(\varkappa+b-\frac{y_2+\nu}{2}\right)\right|\right\},\end{aligned}\tag{38}$$

where $p,q>1$ are conjugate exponents.

Proof. From (9), by using the Hölder's inequality, we obtain

$$\begin{aligned}
&\left|\Xi_{\varrho,\psi}\lambda(y_1,y_2,\varkappa,v)\right| \\
&\le \frac{(v-y_1)^{\varrho+1}}{y_2-y_1}\int_0^1 \zeta^{\varrho}\left|\lambda'\left(\varkappa+a-[\zeta y_1+(1-\zeta)v]\right)\right|\mathrm{d}\zeta \\
&\quad+\frac{(y_2-v)^{\varrho+1}}{y_2-y_1}\int_0^1 \zeta^{\varrho}\left|\lambda'\left(\varkappa+b-[\zeta y_2+(1-\zeta)v]\right)\right|\mathrm{d}\zeta \\
&\le \frac{(v-y_1)^{\varrho+1}}{y_2-y_1}\left(\int_0^1 \zeta^{\varrho p}\mathrm{d}\zeta\right)^{(1/p)}\left(\int_0^1 \left|\lambda'\left(\varkappa+a-[\zeta y_1+(1-\zeta)v]\right)\right|^q\mathrm{d}\zeta\right)^{(1/q)} \\
&\quad+\frac{(y_2-v)^{\varrho+1}}{y_2-y_1}\left(\int_0^1 \zeta^{\varrho p}\mathrm{d}\zeta\right)^{(1/p)}\left(\int_0^1 \left|\lambda'\left(\varkappa+b-[\zeta y_2+(1-\zeta)v]\right)\right|^q\mathrm{d}\zeta\right)^{(1/q)}.
\end{aligned} \tag{39}$$

Since $|\lambda'|^q$ is concave mapping, therefore from (3), we obtain

$$\int_0^1 \left|\lambda'\left(\varkappa+a-[\zeta y_1+(1-\zeta)v]\right)\right|^q\mathrm{d}\zeta \le \left|\lambda'\left(\varkappa+a-\frac{y_1+v}{2}\right)\right|^q, \tag{40}$$

and

$$\int_0^1 \left|\lambda'\left(\varkappa+b-[\zeta y_2+(1-\zeta)v]\right)\right|^q\mathrm{d}\zeta \le \left|\lambda'\left(\varkappa+b-\frac{y_2+v}{2}\right)\right|^q. \tag{41}$$

By placing the inequalities (40) and (41) in (39), leads to (38). □

Remark 18. If we set $\psi(y)=y$ in Theorem 5, it reduces to Theorem 2.5 in [32].

Remark 19. If we set $\psi(y)=y$, $y_1=a$, $y_2=b$, $v=\varkappa$, and $\varrho=1$ in Theorem 5, it reduces to Theorem 5 in [2] that yields the same result with $s=1$.

Corollary 12. *If we choose $\psi(y)=y$ and $\varrho=1$ in Theorem 5, we deduce the Mercer–Ostrowski inequality as*

$$\begin{aligned}
&\left|\left\{\frac{v-y_1}{y_2-y_1}\lambda(\varkappa+a-y_1)+\frac{y_2-v}{y_2-y_1}\lambda(\varkappa+b-y_2)\right\}-\frac{1}{y_2-y_1}\left\{\int_{\varkappa+a-v}^{\varkappa+a-y_1}\lambda(\zeta)d\zeta+\int_{\varkappa+b-y_2}^{\varkappa+b-v}\lambda(\zeta)\mathrm{d}\zeta\right\}\right| \\
&\le\left(\frac{1}{p+1}\right)^{\frac{1}{p}}\left\{\frac{(v-y_1)^2}{y_2-y_1}\left|\lambda'\left(\varkappa+a-\frac{y_1+v}{2}\right)\right|+\frac{(y_2-v)^2}{y_2-y_1}\left|\lambda'\left(\varkappa+b-\frac{y_2+v}{2}\right)\right|\right\}.
\end{aligned} \tag{42}$$

3. Some Applications

3.1. Applications to Means. For two real numbers $0<\kappa_1<\kappa_2$, consider the following two important means:

The arithmetic mean:

$$A(\kappa_1,\kappa_2)=\frac{\kappa_1+\kappa_2}{2}. \tag{43}$$

The generalized logarithmic-mean:

$$L_m(\kappa_1,\kappa_2)=\left[\frac{\kappa_2^{m+1}-\kappa_1^{m+1}}{(m+1)(\kappa_2-\kappa_1)}\right]^{(1/m)};\quad m\in\mathfrak{R}\setminus\{-1,0\}. \tag{44}$$

Proposition 1. *Suppose $a,b>0$, then, we have the following inequality*

$$\begin{aligned}&\left|\left\{\frac{v-y_1}{y_2-y_1}(2A(\varkappa,a)-y_1)^n+\frac{y_2-v}{y_2-y_1}(2A(\varkappa,b)-y_2)^n\right\}\right.\\&\left.-\frac{1}{y_2-y_1}\{(v-y_1)L_m^m(\varkappa+a-y_1,\varkappa+a-v)+(v-y_2)L_m^m(\varkappa+b-v,\varkappa+a-y_2)\}\right|\\&\le\frac{n(v-y_1)^2}{y_2-y_1}\left(\frac{1}{2}\right)^{1-(1/q)}\left\{A\left(|\varkappa|^{(n-1)q},|a|^{(n-1)q}\right)-\left(\frac{1}{3}|y_1|^{(n-1)q}+\frac{1}{6}|v|^{(n-1)q}\right)\right\}^{(1/q)}\\&+\frac{n(y_2-v)^2}{y_2-y_1}\left(\frac{1}{2}\right)^{1-(1/q)}\left\{A\left(|\varkappa|^{(n-1)q},|b|^{(n-1)q}\right)-\left(\frac{1}{3}|y_2|^{(n-1)q}+\frac{1}{6}|v|^{(n-1)q}\right)\right\}^{(1/q)}.\end{aligned} \tag{45}$$

Proof. The result can be obtained immediately by taking into account Corollary 8 along with the convex function $\lambda(\varkappa)=\varkappa^n,\varkappa>0$. □

Proposition 2. *Suppose $a,b>0$, then, we have the following inequality:*

$$\begin{aligned}&\left|\left\{\frac{v-y_1}{y_2-y_1}(2A(\varkappa,a)-y_1)^n+\frac{y_2-v}{y_2-y_1}(2A(\varkappa,b)-y_2)^n\right\}\right.\\&\left.-\frac{1}{y_2-y_1}\{(v-y_1)L_m^m(\varkappa+a-y_1,\varkappa+a-v)+(v-y_2)L_m^m(\varkappa+b-v,\varkappa+a-y_2)\}\right|\\&\le\frac{(v-y_1)^2}{y_2-y_1}\left[\frac{1}{(p+1)p}+\frac{n}{q}\left\{2A\left(|\varkappa|^{(n-1)q},|a|^{(n-1)q}\right)-A\left(|y_1|^{(n-1)q},|v|^{(n-1)q}\right)\right\}\right]\\&+\frac{(y_2-v)^2}{y_2-y_1}\left[\frac{1}{(p+1)p}+\frac{n}{q}\left\{2A\left(|\varkappa|^{(n-1)q},|b|^{(n-1)q}\right)-A\left(|y_2|^{(n-1)q},|v|^{(n-1)q}\right)\right\}\right].\end{aligned} \tag{46}$$

Proof. The proof is the direct consequence of Corollary 10 by considering the convex function $\lambda(\varkappa)=\varkappa^n,\varkappa>0$. □

3.2. q-Digamma Function. The $\varphi_{\mathbf{q}}$-digamma function, which is described as the logarithmic derivative of the q-gamma function, is an essential function related to the q-gamma function (see [34]) given as

$$\begin{aligned}\varphi_{\mathbf{q}}&=-\ln(1-\mathrm{q})+\ln\mathrm{q}\sum_{k=0}^{\infty}\frac{\mathrm{q}^{k+\zeta}}{1-\mathrm{q}^{k+\zeta}}\\&=-\ln(1-\mathrm{q})+\ln\mathrm{q}\sum_{k=0}^{\infty}\frac{\mathrm{q}^{k\zeta}}{1-\mathrm{q}^{k\zeta}}.\end{aligned} \tag{47}$$

For $\mathrm{q}>1$ and $\zeta>0$, q-digamma function $\varphi_{\mathbf{q}}$ can be given as

$$\begin{aligned}\varphi_{\mathbf{q}}&=-\ln(\mathrm{q}-1)+\ln\mathrm{q}\left[\zeta-\frac{1}{2}-\sum_{k=0}^{\infty}\frac{\mathrm{q}^{-(k+\zeta)}}{1-\mathrm{q}^{-(k+\zeta)}}\right]\\&=-\ln(\mathrm{q}-1)+\ln\mathrm{q}\left[\zeta-\frac{1}{2}-\sum_{k=0}^{\infty}\frac{\mathrm{q}^{-k\zeta}}{1-\mathrm{q}^{-k\zeta}}\right].\end{aligned} \tag{48}$$

Proposition 3. *Assume that a and b are the real numbers such that $0<a<b$, $q>1$, $0<q<1$, and $q^{-1}=1-p^{-1}$. Then, the following inequality is valid:*

$$\begin{aligned}
&\left|\left\{\frac{v-y_1}{y_2-y_1}\varphi_{\mathbf{q}}(\varkappa+a-y_1)+\frac{y_2-v}{y_2-y_1}\varphi_{\mathbf{q}}(\varkappa+b-y_2)\right\}\right.\\
&\left.-\frac{1}{y_2-y_1}\left\{\int_{\varkappa+a-v}^{\varkappa+a-y_1}\varphi_{\mathbf{q}}(\zeta)\mathrm{d}\zeta+\int_{\varkappa+b-y_2}^{\varkappa+b-v}\varphi_{\mathbf{q}}(\zeta)\mathrm{d}\zeta\right\}\right|\\
&\le\frac{(v-y_1)^2}{y_2-y_1}\left(\frac{1}{2}\right)^{1-(1/q)}\left\{A\left(\left|\varphi_{\mathbf{q}}'(\varkappa)\right|^q,\left|\varphi_q'(a)\right|^q\right)-\left[\frac{1}{3}\left|\varphi_{\mathbf{q}}'(y_1)\right|^q+\frac{1}{6}\left|\varphi_{\mathbf{q}}'(v)\right|^q\right]\right\}^{(1/q)}\\
&\quad+\frac{(y_2-v)^2}{y_2-y_1}\left(\frac{1}{2}\right)^{1-(1/q)}\left\{A\left(\left|\varphi_{\mathbf{q}}'(\varkappa)\right|^q,\left|\varphi_{\mathbf{q}}'(b)\right|^q\right)-\left[\frac{1}{3}\left|\varphi_{\mathbf{q}}'(y_2)\right|^q+\frac{1}{6}\left|\varphi_{\mathbf{q}}'(v)\right|^q\right]\right\}^{(1/q)}.
\end{aligned}\tag{49}$$

Proof. The statement can be obtained by using Corollary 8 by considering $\lambda(\zeta)\longrightarrow\varphi_{\mathbf{q}}(\zeta)$. Since, $\varphi_{\mathbf{q}}'(\zeta)$ is a completely monotone function on $(0,\infty)$ for all $\zeta>0$, consequently, $\lambda'(\zeta):=\varphi_{\mathbf{q}}'(\zeta)$ is convex on the same interval $(0,\infty)$, (see [34]). □

3.3. Bounds Involving Modified Bessel Function. We know the first type of modified Bessel function $\mathfrak{B}_{\tau_1}$, which has the series interpretation (see [35], p.77)

$$\mathfrak{B}_{\tau_1}(\varkappa)=\sum_{n\ge0}\frac{(\varkappa/2)^{\tau_1+2n}}{n!\Gamma(\tau_1+n+1)},\tag{50}$$

where $\varkappa\in\mathfrak{R}$ and $\tau_1>-1$, while the second kind modified Bessel function $\hbar_{\tau_1}$ (see [35], p.78) is usually defined as

$$\phi_{\tau_1}(\varkappa)=\frac{\pi}{2}\frac{\mathfrak{B}_{-\tau_1}(\varkappa)-\mathfrak{B}_{\tau_1}(\varkappa)}{\sin\tau_1\pi}.\tag{51}$$

Consider the function $\Psi_{\tau_1}:\mathfrak{R}\longrightarrow[1,\infty)$ defined by

$$\Psi_{\tau_1}(\varkappa)=2^{\tau_1}\Gamma(\tau_1+1)\varkappa^{-\tau_1}\mathfrak{B}_{\tau_1}(\varkappa).\tag{52}$$

The first- and second-order derivative formula of $\Psi_{\tau_1}(\varkappa)$ is given as [35]:

$$\Psi_{\tau_1}'(\varkappa)=\frac{\varkappa}{2(\tau_1+1)}\Psi_{\tau_1+1}(\varkappa),\tag{53}$$

$$\Psi_{\tau_1}''(\varkappa)=\frac{\varkappa^2\Psi_{\tau_1+2}(\varkappa)}{4(\tau_1+1)(\tau_1+2)}+\frac{\Psi_{\tau_1+1}(\varkappa)}{2(\tau_1+1)}.\tag{54}$$

Proposition 4. *Suppose that* $\tau_1>-1$ *and* $0<a<b$, $q>1$. *Then, we have*

$$\begin{aligned}
&\left|\left\{\frac{v-y_1}{y_2-y_1}.\frac{\varkappa+a-y_1}{2(\tau_1+1)}.\Psi_{\tau_1+1}(\varkappa+a-y_1)+\frac{y_2-v}{y_2-y_1}.\frac{\varkappa+b-y_2}{2(\tau_1+1)}.\Psi_{\tau_1+1}(\varkappa+b-y_2)\right\}\right.\\
&\left.-\frac{1}{y_2-y_1}\left\{\left(\Psi_{\tau_1}(\varkappa+a-y_1)-\Psi_{\tau_1}(\varkappa+a-v)\right)+\left(\Psi_{\tau_1}(\varkappa+b-v)-\Psi_{\tau_1}(\varkappa+b-y_2)\right)\right\}\right|\\
&\le\frac{(v-y_1)^2}{y_2-y_1}\left\{\frac{1}{(p+1)p}\right.\\
&\quad+\frac{1}{q}\left(\left(\frac{\varkappa^2\Psi_{\tau_1+2}(\varkappa)}{4(\tau_1+1)(\tau_1+2)}+\frac{\Psi_{\tau_1+1}(\varkappa)}{2(\tau_1+1)}\right)^q+\left(\frac{a^2\Psi_{\tau_1+2}(a)}{4(\tau_1+1)(\tau_1+2)}+\frac{\Psi_{\tau_1+1}(a)}{2(\tau_1+1)}\right)\right)^q\\
&\quad\left.-\frac{1}{2}\left[\left(\frac{y_1^2\Psi_{\tau_1+2}(y_1)}{4(\tau_1+1)(\tau_1+2)}+\frac{\Psi_{\tau_1+1}(y_1)}{2(\tau_1+1)}\right)^q+\left(\frac{v^2\Psi_{\tau_1+2}(v)}{4(\tau_1+1)(\tau_1+2)}+\frac{\Psi_{\tau_1+1}(v)}{2(\tau_1+1)}\right)^q\right]\right\}\\
&\quad+\frac{(y_2-v)^2}{y_2-y_1}\left\{\frac{1}{(p+1)p}\right.\\
&\quad+\frac{1}{q}\left(\left(\frac{\varkappa^2\Psi_{\tau_1+2}(\varkappa)}{4(\tau_1+1)(\tau_1+2)}+\frac{\Psi_{\tau_1+1}(\varkappa)}{2(\tau_1+1)}\right)^q+\left(\frac{b^2\Psi_{\tau_1+2}(b)}{4(\tau_1+1)(\tau_1+2)}+\frac{\Psi_{\tau_1+1}(b)}{2(\tau_1+1)}\right)^q\right)\\
&\quad\left.-\frac{1}{2}\left[\left(\frac{y_2^2\Psi_{\tau_1+2}(y_2)}{4(\tau_1+1)(\tau_1+2)}+\frac{\Psi_{\tau_1+1}(y_2)}{2(\tau_1+1)}\right)^q+\left(\frac{v^2\Psi_{\tau_1+2}(v)}{4(\tau_1+1)(\tau_1+2)}+\frac{\Psi_{\tau_1+1}(v)}{2(\tau_1+1)}\right)^q\right]\right\}.
\end{aligned}\tag{55}$$

Proof. Substituting the mapping $\lambda \longrightarrow \Psi_{\tau_1}'$ to the inequality in Corollary 10. Note that all assumptions of Corollary 10 are satisfied (see [34]). Therefore, using the identities (53) and (54) gives required result. □

4. Conclusions

The objective of this study is to introduce the idea of new generalized fractional variants of Ostrowski inequality by employing Jensen–Mercer inequality for differentiable convex functions. The obtained results are intersting and generalized in a sense that by substituting identity function $\psi(y) = y$ and special value of $\varrho = 1$, we get connected to previously established results in the literature. Also, one can get variety of fractional Mercer–Ostrowski inequalities for different F-I operators by considering particular values of function ψ as mentioned in Remark 1. In addition, another motivating aspect of the study is that we try to give applications of means, q-digamma function, and Bessel function for Mercer–Ostrowski inequality in the similar passion as considered for Hermite–Hadamard type inequalities given in [8, 30]. Based on this study, researchers may contribute to the development of such results for twice differentiable functions.

Data Availability

No data are available.

Conflicts of Interest

The authors declare that they have no conflicts of interest.

References

[1] D. S. Mitrinovic, J. Pečarić, and A. M. Fink, *Inequalities Involving Functions and Their Integrals and Derivatives*, Vol. 53, Springer Science and Business Media, Berlin, Germany, 1991.

[2] M. Alomari, M. Darus, S. S. Dragomir, and P. Cerone, "Ostrowski type inequalities for functions whose derivatives are s-convex in the second sense," *Applied Mathematics Letters*, vol. 23, no. 9, pp. 1071–1076, 2010.

[3] S. S. Dragomir and T. M. Rassias, *Ostrowski Type Inequalities and Applications in Numerical Integration*, Kluwer Academic, Dordrecht, Netherlands, 2002.

[4] A. Ekinci, M. E. Ozdemir, and E. Set, "New integral inequalities of Ostrowski type for quasi-convex functions with applications," *Turkish Journal of Science*, vol. 5, no. 3, pp. 290–304, 2021.

[5] D. S. Mitrinović, J. E. Pečarić, and A. M. Fink, "Classical and New Inequalities in Analysis," *Mathematics and its Applications (East European Series)*, Vol. 61, Kluwer Academic Publishers Group, Dordrecht, Netherlands, 1993.

[6] Y. Qin, *Integral and Discrete Inequalities and Their Applications*, Springer International Publishing Switzerland, Birkhauser Basel, 2016.

[7] P. Agarwal, S. S. Dragomir, M. Jleli, and B. Samet, *Advances in Mathematical Inequalities and Applications*, Springer, Singapore, 2018.

[8] K. Mehrez and P. Agarwal, "New Hermite-Hadamard type integral inequalities for convex functions and their applications," *Journal of Computational and Applied Mathematics*, vol. 350, pp. 274–285, 2019.

[9] M. Kian and M. Moslehian, "Refinements of the operator Jensen-Mercer inequality," *The Electronic Journal of Linear Algebra*, vol. 26, 2013.

[10] A. M. Mercer, "A variant of Jensen's inequality," *Journal of Inequalities in Pure and Applied Mathematics*, vol. 4, Article ID 73, 2003.

[11] S. Khan, M. Adil Khan, S. I. Butt, and Y.-M. Chu, "A new bound for the Jensen gap pertaining twice differentiable functions with applications," *Advances in Difference Equations*, vol. 2020, no. 1, p. 333, 2020.

[12] S. I. Butt, M. Klaričić Bakula, Đ. Pečarić, and J. Pečarić, "Jensen-grüss inequality and its applications for the zipf-mandelbrot law," *Mathematical Methods in the Applied Sciences*, vol. 44, no. 2, pp. 1664–1673, 2021.

[13] H.-H. Chu, S. Rashid, Z. Hammouch, and Y. M. Chu, "New fractional estimates for Hermite-Hadamard-Mercer's type inequalities," *Alexandria Engineering Journal*, vol. 59, no. 5, pp. 3079–3089, 2020.

[14] S. I. Butt, A. Kashuri, M. Umar, A. Aslam, and W. Gao, "Hermite-Jensen-Mercer type inequalities via ψ-Riemann-Liouville k-fractional integrals," *AIMS Mathematics*, vol. 5, no. 5, Article ID 51935220, 2020.

[15] S. I. Butt, M. Umar, K. A. Khan, A. Kashuri, and H. Emadifar, "Fractional Hermite-Jensen-Mercer Integral Inequalities with Respect to Another Function and Application," *Complexity*, vol. 2021, Article ID 9260828, 30 pages, 2021.

[16] R. Khalil, M. Al Horani, A. Yousef, and M. Sababheh, "A new definition of fractional derivative," *Journal of Computational and Applied Mathematics*, vol. 264, pp. 65–70, 2014.

[17] P. O. Mohammed, H. Aydi, A. Kashuri, Y. S. Hamed, and K. M. Abualnaja, "Midpoint inequalities in fractional calculus defined using positive weighted symmetry function kernels," *Symmetry*, vol. 13, p. 550, 2021.

[18] H. Aydi, M. Jleli, and B. Samet, "On positive solutions for a fractional thermostat model with a convex-concave source term via $$\psi $$-Caputo fractional derivative," *Mediterranean Journal of Mathematics*, vol. 17, no. 1, p. 16, 2020.

[19] H. Yue, "Ostrowski inequality for fractional integrals and related fractional inequalities," *Transylvanian Journal of Mathematics and Mechanics*, vol. 5, pp. 85–89, 2013.

[20] A. A. Aljinović, "Montgomery identity and Ostrowski type inequalities for Riemann–Liouville fractional integral," *Journal of Mathematics*, vol. 2014, Article ID 503195, 6 pages, 2014.

[21] H. Yildirim and Z. Kirtay, "Ostrowski inequality for generalized fractional integral and related inequalities," *Malaya Journal of Matematik*, vol. 2, pp. 322–329, 2014.

[22] A. Kashuri, B. Meftah, P. O. Mohammed et al., "Fractional weighted ostrowski-type inequalities and their applications," *Symmetry*, vol. 13, no. 6, p. 968, 2021.

[23] J. Vanterler da Costa Sousa and E. Capelas de Oliveira, "A Gronwall inequality and the Cauchy-type problem by means of ψ-Hilfer operator," *Differential Equations & Applications*, vol. 11, no. 1, pp. 87–106, 2019.

[24] A. A. Kilbas, H. M. Srivastava, and J. J. Trujillo, *Theory and Applications of Fractional Differential Equations*, North-Holland, New York, NY, USA, 2006.

[25] G. Farid, "Study of a generalized Riemann-Liouville fractional integral via convex functions," *Communications Faculty Of Science University of Ankara Series A1Mathematics and Statistics*, vol. 69, no. 1, pp. 37–48, 2020.

[26] H. Chen and U. N. Katugampola, "Hermite-Hadamard and Hermite-Hadamard-Fejér type inequalities for generalized fractional integrals," *Journal of Mathematical Analysis and Applications*, vol. 446, no. 2, pp. 1274–1291, 2017.

[27] T. U. Khan and M. A. Khan, "Generalized conformable fractional operators," *Journal of Computational and Applied Mathematics*, vol. 346, pp. 378–389, 2019.

[28] F. Jarad, E. Ugurlu, T. Abdeljawad, and D. Baleanu, "On a new class of fractional operators," *Advances in Difference Equations*, vol. 2017, no. 1, pp. 1–16, 2017.

[29] K. Liu, J. Wang, and D. O'regan, "On the Hermite-Hadamard type inequality for Ψ-Riemann-Liouville fractional integrals via convex functions," *Journal of Inequalities and Applications*, vol. 2019, Article ID 27, 2019.

[30] P. O. Mohammed, "Hermite-Hadamard inequalities for Riemann-Liouville fractional integrals of a convex function with respect to a monotone function," *Mathematical Methods in the Applied Sciences*, vol. 44, no. 3, pp. 2314–2324, 2021.

[31] S. S. Dragomir, "Hermite-Hadamard type inequalities for generalized Riemann-Liouville fractional integrals of h -convex functions," *Mathematical Methods in the Applied Sciences*, vol. 44, no. 3, pp. 2364–2380, 2021.

[32] J. Nasir, S. I. Butt, S. Qaisar, E. Set, and A. O. Akdemir, "Some Mercer–Ostrowski type inequalities for differentiable convex functions via fractional integral operators,".

[33] E. Set, "New inequalities of Ostrowski type for mappings whose derivatives are s-convex in the second sense via fractional integrals," *Computers & Mathematics with Applications*, vol. 63, no. 7, pp. 1147–1154, 2012.

[34] S. Jain, K. Mehrez, D. Baleanu, and P. Agarwal, "Certain hermite-hadamard inequalities for logarithmically convex functions with applications," *Mathematics*, vol. 7, no. 2, p. 163, 2019.

[35] G. N. Watson, *A Treatise on the Theory of Bessel Functions*, Cambridge University Press, Cambridge, UK, 1995.

Hindawi
Mathematical Problems in Engineering
Volume 2022, Article ID 8280203, 11 pages
https://doi.org/10.1155/2022/8280203

Research Article

An Implementation of the Generalized Differential Transform Scheme for Simulating Impulsive Fractional Differential Equations

Zaid Odibat,[1] **Vedat Suat Erturk**,[2] **Pushpendra Kumar**,[3] **Abdellatif Ben Makhlouf**,[4] **and V. Govindaraj**[3]

[1]*School of Basic Sciences and Humanities, German Jordanian University, Amman 11180, Jordan*
[2]*Department of Mathematics, Faculty of Arts and Sciences, Ondokuz Mayis University, Samsun 55139, Turkey*
[3]*Department of Mathematics, National Institute of Technology Puducherry, Karaikal 609609, India*
[4]*Department of Mathematics, College of Science, Jouf University, P.O. Box: 2014, Sakaka, Saudi Arabia*

Correspondence should be addressed to Abdellatif Ben Makhlouf; abmakhlouf@ju.edu.sa

Received 8 October 2021; Revised 12 December 2021; Accepted 27 March 2022; Published 16 May 2022

Academic Editor: Muhammad Shoaib Anwar

In this research study, the generalized differential transform scheme has been applied to simulate impulsive differential equations with the noninteger order. One specific tool of the implemented scheme is that it converts the problems into a recurrence equation that finally leads easily to the solution of the considered problem. The validity and reliability of this method have successfully been accomplished by applying it to simulate the solution of some equations. It is shown that the considered method is very suitable and efficient for solving classes of fractional-order initial value problems for impulsive differential equations and might find wide applications.

1. Introduction

Present, impulsive differential equations are treated as a basic system to explore the structures of various phenomena that are subjected to unexpected variations in their states. Many evolution processes which are simulated in applied sciences are defined by differential equations with the impulse effect. The theory and applications addressing such problems have been reported [1–6]. Recently, some interesting solutions' existence results for impulsive differential equations have been explored largely; we suggest the reader to [7–11] and the papers therein.

Over the last few years, the applications of fractional derivatives are sharply increasing and a huge quantity of mathematical systems has been explored by using these operators in different regions of science and engineering [12–18]. In the theory of fractional calculus, we talk about the noninteger orders of differential operators. The fractional calculus is just a generalization of classical calculus and uses similar methods and features, but is more useful in the application field. The memory effects and hereditary natures of different types of processes and materials can be studied by fractional-order operators much more accurately. These operators involve the complete history of that function in the given domain or span, which we say memory effects. That is why fractional-order operators are the best fit to describe dynamical systems or various real-life problems. Also, the nonlocal characteristic is one of the beauties of fractional operators. This justifies that the future state of a model depends not only upon the present stage but also upon all past states. All features make the importance of noninteger order systems and that is why an active area of research.

Nowadays, impulsive fractional differential equations, as generalizations of impulsive classical differential equations, are applied to model various important dynamical phenomena containing evolutionary structures specified by abrupt variations of the position at particular instants. Some

recent developments in the stability, existence, and uniqueness of solutions for classes of impulsive fractional differential equations are investigated [19–27]. To date, a number of computational methods have been proposed to solve various types of noninteger order differential equations. Najafi and Allahviranloo [28] solved the linear and nonlinear fuzzy impulsive fractional differential equations by using the combination of reproducing kernel Hilbert space and fractional differential transform methods. A block-by-block numerical method is constructed for the impulsive fractional ordinary differential equations by carrying out a series of numerical examples in [29]. In [30], the Adomian decomposition method was applied to solve impulsive nonclassical type differential equations with the Caputo fractional operator. Very recently, a number of studies in the direction of efficiency and performance of various computational methods have been given by researchers [31–39]. In [40], authors have defined a novel fractional-order Lagrangian to study the motion of a beam on a nanowire. Some applications of noninteger order numerical methods in epidemiology and ecology can be seen [41, 42]. In the works presented in [20, 23, 26], we can observe a conflict between the obtained solutions for a particular impulsive fractional-order differential equation. In fact, they use different definitions for the Caputo fractional differential operators. However, to our knowledge, analytical or numerical techniques for solving impulsive fractional differential equations have not yet been sufficiently established. Therefore, the aim of this work is to implement the generalized differential transform scheme for analytically solving the initial value problem for the impulsive fractional differential equations:

$$\begin{cases} D_0^{\alpha} F(t) = f(t, F(t)), \quad \dfrac{t \in [0,T]}{\{t_1, t_2, \ldots, t_k\}}, \\ \Delta F(t_m) = F(t_m^+) - F(t_m^-) = I_m(F(t_m^-)), \quad m = 1, 2, \ldots, k, \\ F(0) = F_0, \end{cases} \tag{1}$$

where D_0^{α} is the Caputo fractional differential operator of order α with $0 < \alpha \leq 1$, described in Section 2, $f\colon [0,T] \times R \longrightarrow R$ is the appropriate continuous function, and $I_m\colon R \longrightarrow R$, t_m satisfying $0 = t_0 < t_1 < \cdots < t_k < t_{k+1} = T$ and $F_0 \in R$. The numbers t_m are called instants (or moments) of impulse, I_m shows the jump of the state t_m, and $F(t_m^+) = \lim_{h \longrightarrow 0+} F(t_m + h)$ and $F(t_m^-) = \lim_{h \longrightarrow 0-} F(t_m + h)$ specify the right and the left limits, respectively, of the state t_m.

2. Preliminaries and Notations

In this portion, first, we write few important definitions of fractional-order operators and generalized Taylor's formula. Next, we recall some relevant results which are applied in this research.

Definition 1. The Caputo fractional derivative operator of order α with $\alpha > 0$ is specified by

$$D_a^{\alpha} f(t) = J_a^{n-\alpha} D^n f(t), \tag{2}$$

where $n - 1 < \alpha \leq n, n \in N$, and D^n is the classical differential operator of order n and J^{μ} is the Riemann-Liouville fractional integral operator of order μ with $\mu > 0$.

Definition 2. The definition of Riemann-Liouville fractional integral operator of order μ with $\mu > 0$ is given by

$$J_a^{\mu} f(t) = \frac{1}{\Gamma(\mu)} \int_a^t (t - \tau)^{\mu - 1} f(\tau) d\tau, \quad t > a. \tag{3}$$

Brief discussion on the characteristics of the above given fractional derivative operators can be learned from [12–18].

It is worth mentioning that there are some differences between Caputo fractional differential operator D_a^{α}, given in Definition 1, and the usual integer differential operator D^n regarding the memory property. Caputo fractional operator of function f, $D_a^{\alpha} f(t)$, captures the complete history of the function f starting from $t = a$, while the classical derivative operator of the function f, $D^n f(t)$, only considers the nearby points. So, Caputo definition has long-term memory and long-span spatial interactions. In [43], the authors introduced the generalized Taylor's formula. This generalization is a derivation of a function as an infinite sum of terms that is simulated from the fractional derivative values of a function at a single point.

Theorem 1. *Assume that* $(D_a^{\alpha})^m f(t) \in C(a,b]$ *for* $m = 0, 1, \ldots, k+1$, *where* $0 < \alpha \leq 1$; *then, we have [43]*

$$f(x) = \sum_{i=0}^{k} \frac{(t-a)^{\alpha i}}{\Gamma(\alpha i + 1)} \left(\left(D_a^{\alpha}\right)^i f \right)(a+) + R_k^{\alpha}(t,a), \tag{4}$$

where

$$R_k^{\alpha}(t,a) = \frac{\left(\left(D_a^{\alpha}\right)^{1+k} f \right)(\xi)}{\Gamma((1+k)\alpha + 1)} (t-a)^{(1+k)\alpha}. \tag{5}$$

With $a \leq \xi \leq t$, for each $t \in (a,b]$, and D_a^{α} is the Caputo derivative operator of order α, with $(D_a^{\alpha})^k = D_a^{\alpha} \cdot D_a^{\alpha} \cdots D_a^{\alpha}$.

In some recent studies, number of results have been proposed to find the sufficient conditions regarding the solution existence for the Caputo-type IVPs for impulsive differential equations [20–22, 24, 25]. One of the most important results is given in the following theorem which establishes the connection between the IVP for the Caputo-type impulsive differential equation given in equation (1) and a class of integral equations.

Theorem 2. *Let* $0 < \alpha \leq 1$ *and* $f\colon [0,T] \times R \longrightarrow R$ *be Lebesgue measurable function with respect to* t *on* $[0,T]$. *A function* $x(t)$ *is a solution of IVP (1) if and only if* $x(t)$ *is a solution of the following integral equations [25]:*

$$x(t)=\begin{cases} x_0+\dfrac{1}{\Gamma(\alpha)}\displaystyle\int_0^t (t-\nu)f(\nu,x(\nu))\mathrm{d}\nu, & 0\le t\le t_1,\\ x_0+I_1\left(x\left(t_1^-\right)\right)+\dfrac{1}{\Gamma(\alpha)}\displaystyle\int_0^t (t-\nu)^{1-\alpha}f(\nu,x(\nu))\mathrm{d}\nu, & t_1<t\le t_2,\\ \vdots & \\ x_0+\displaystyle\sum_{i=1}^{m} I_i\left(x\left(t_i^-\right)\right)+\dfrac{1}{\Gamma(\alpha)}\displaystyle\int_0^t (t-\nu)^{1-\alpha}f(\nu,x(\nu))\mathrm{d}\nu, & t_m<t\le T. \end{cases} \tag{6}$$

3. Generalized Differential Transform Scheme

The differential transform method (DTM), proposed by Zhou [44] in 1986, was given for simulating ordinary and partial differential equations. This scheme produces approximations based on an iterative method for calculating power series solutions in the form of initial value constraints of differential equation. The scheme, which is well addressed in [45, 46], can be taken as an alternative method for constructing the solution as formal Taylor series without linearization, discretization, perturbation, or large computational work. More recently, for solving the noninteger order differential equations, the DTM was generalized by using generalized Taylor's formula ([47]) to calculate the solutions of such equations in the terms of fractional power series. The new extension, which is known as the generalized differential transform method (GDTM), gives a useful feature for getting fractional power series expansions for the solutions of nonlinear systems having nonclassical derivatives. For understanding of the learners, we give a review on the GDTM. We define the generalized differential transformation of the m^{th} derivative of the function $f(x)$ as follows [48]:

$$F_\alpha(m)=\frac{1}{\Gamma(\alpha m+1)}\left[\left(D_{x_0}^{\alpha}\right)f(x)\right]|_{x=x_0'}, \tag{7}$$

where $0<\alpha\le 1$, $(D_{x_0}^{\alpha})^m=D_{x_0}^{\alpha}\cdot D_{x_0}^{\alpha}\cdots D_{x_0}^{\alpha}$, ($m$-times), and the generalized differential inverse transform of $F_\alpha(m)$ is defined as

$$f(x)=\sum_{m=0}^{\infty}F_\alpha(m)(x-x_0)^{\alpha m}. \tag{8}$$

When we put (7) into (8), applying the generalized Taylor's formula, we receive

$$\begin{aligned}\sum_{m=0}^{\infty}F_\alpha(m)(x-x_0)^{\alpha m}&=\sum_{m=0}^{\infty}\frac{(x-x_0)^{\alpha m}}{\Gamma(\alpha m+1)}\left[\left(D_{x_0}^{\alpha}\right)^m f(x)\right]|_{x=x_0}\\&=f(x).\end{aligned} \tag{9}$$

So, (8) is the inverse transformation of the generalized differential transform (7). The GDTM consisting of the generalized differential transformation (7) and its inverse transform (8) has increased the applications of the DTM to fractional differential equations. The basic simulations done by generalized differential transformation can be learned from [48], and the mostly applicable characteristics are specified by the following theorems.

Theorem 3. *If $G_\alpha(k)$, $V_\alpha(k)$, and $W_\alpha(k)$ are the generalized differential transformations of the functions $g(x)$, $v(x)$, and $w(x)$, respectively, then [48]*

(i) If $g(x)=v(x)\mp w(x)$, then $G_\alpha(k)=V_\alpha(k)\mp W_\alpha(k)$;

(ii) If $g(x)=av(x)$, where $a\in R$, then $G_\alpha(k)=aV_\alpha(k)$;

(iii) If $g(x)=v(x)\cdot w(x)$, then $G_\alpha(k)=\sum_{l=0}^{k}V_\alpha(l)\cdot W_\alpha(k-l)$;

(iv) If $g(x)=D_{x_0}^{\alpha}v(x)$, then $G_\alpha(k)=(\Gamma(\alpha(k+1)+1)/\Gamma(\alpha k+1))V_\alpha(k+1)$;

(v) If $g(x)=(x-x_0)^{m\alpha}$, then $G_\alpha(k)=\delta(k-m)$, where $\delta(k)=\begin{cases}1, & k=0\\ 0, & k\ne 0\end{cases}$.

Theorem 4. *Suppose that $G_\alpha(n)$ and $V_\alpha(n)$ are the generalized differential transforms of the functions $g(x)$ and $v(x)$, simultaneously. Then, if $g(x)=D_{x_0}^{\beta}v(x)$, $m-1<\beta\le m$, where $D_{x_0}^{\alpha n}D_{x_0}^{\beta}v(x)=D_{x_0}^{\alpha n+\beta}v(x)$, for $n=0,1,2,\ldots$, then [48]*

$$G_\alpha(n)=\frac{\Gamma(\alpha n+1+\beta)}{\Gamma(\alpha n+1)}V_\alpha\left(\frac{n+\beta}{\alpha}\right). \tag{10}$$

4. GDTM for Impulsive Fractional Differential Equations

This section presents the applications of GDTM to solve IVP for the impulsive Caputo-type differential equations given in (1). The obtained piecewise continuous solutions of such IVPs demonstrate the performance and reliability of the method. Initially, one can verify that, using Definition 1 and Theorem 2, the solution of IVP (1) can be obtained as

$$y(t)=\begin{cases} y_1(t), & 0\le t\le t_1,\\ y_2(t), & t_1<t\le t_2,\\ \vdots & \\ y_{m+1}(t), & t_m<t\le T, \end{cases} \tag{11}$$

where the solution component $y_k(t)$ satisfies IVP:

$$D_0^{\alpha} y_k(t) = f\left(t, y_k(t)\right), \quad t > 0, \tag{12}$$

For $k = 1, 2, \ldots, m+1$, respect to the initial constraints,

$$\begin{cases} y_1(0) = y_0, \\ y_2(0) = y_0 + I_1\left(y\left(t_i^-\right)\right), \\ y_3(0) = y_0 + I_1\left(y\left(t_i^-\right)\right) + I_2\left(y\left(t_2^-\right)\right), \\ \vdots \\ y_{m+1}(0) = y_0 + \sum_{i=1}^{m} I_i\left(y\left(t_i^-\right)\right). \end{cases} \tag{13}$$

The main steps of the GDTM for simulating the nonclassical differential equations are as follows: first, we employ the generalized differential transformation, specified in (7), to IVP (1); then, the output is a recurrence relation. Second, simulating this relation by applying the inverse generalized differential transformation, given in (8), we get the solution component $y_j(t)$ of IVP (1) as

$$y_j(t) = \sum_{k=0}^{\infty} Y_j(k) \cdot t^{\alpha k}, \tag{14}$$

where $Y_j(k)$ stratifies the recurrence relation:

$$\frac{\Gamma((1+k)\alpha + 1)}{\Gamma(k\alpha + 1)} Y_j(1+k) = F\left(k, Y_j(k)\right), \tag{15}$$

where $Y_1(0) = y_0$, $Y_{j+1}(0) = y_0 + \sum_{i=1}^{j} I_i\left(y\left(t_i^-\right)\right)$, $j = 1, 2, \ldots, m$, and $F(k, Y_j(k))$ is the generalized differential transformation of the function $f(t, y_j(t))$. Now, by implementing the above analysis, piecewise continuous solutions of some illustrative IVPs for impulsive fractional-order differential equations are derived.

Furthermore, we will investigate the sufficient condition for the convergence of the series solution, given in (11). Based on these simulations, maximum absolute truncated error estimations for the solutions will also be addressed. Following the work presented in [49], we can establish the following results.

Theorem 5. *Let the solution of IVP (1) is obtained as given in (11), where the components $y_j(t)$ of the solution are evaluated as given in (14), and let $I_j = [t_{j-1}, t_j]$.*

(a) The series $\sum_{k=0}^{\infty} Y_j(k) \cdot t^{\alpha k}$, given in (14), converges if $\exists 0 < \gamma_j < 1$, such that $\|Y_j(k+1) \cdot t^{\alpha} / Y_j(k)\| < \gamma_j$, $\forall k \geq k_0$, for some $k_0 \in \mathbb{N}$ and $t \in I_j$, where $\|f(t)\| = \max_{t \in I_j} |f(t)|$, that is, the solution component $y_j(t)$ converges if $\lim_{k \longrightarrow \infty} |Y_j(k+1) / Y_j(k)| \cdot \max_{t \in I_j} t^{\alpha} < 1$.

(b) Let the series $\sum_{k=0}^{\infty} Y_j(k) \cdot t^{\alpha k}$ converges to the solution component $y_j(t)$. If the truncated series $\sum_{k=0}^{n} Y_j(k) \cdot t^{\alpha k}$ is considered as an approximation to the solutions $y_j(t)$, then the maximum absolute truncated error is calculated as $\|y_j(t) - \sum_{k=0}^{n} Y_j(k) \cdot t^{\alpha k}\| < \gamma_j^{n-n_0+1} / 1 - \gamma_j \max_{t \in I_j} |Y_j(n_0) \cdot t^{\alpha n_0}|$, for any $n_0 \geq 0$, where $Y_j(n_0) \neq 0$.

Another way, we derive, for each $i \geq k_0$ and $t \in I_j$, the parameters $\gamma_j(i)$ as

$$\gamma_j(i+1) = \begin{cases} \left\| \dfrac{Y_j(i+1) \cdot t^{\alpha}}{Y_j(i)} \right\|, & \left\| Y_j(i) \right\| \neq 0, \\ 0, & \left\| Y_j(i) \right\| = 0. \end{cases} \tag{16}$$

$i \in \mathbb{N} \cup \{0\}$; then, the series $\sum_{k=0}^{\infty} Y_j(k) \cdot t^{\alpha k}$ converges to an exact solution, $y_j(t)$, when $0 \leq \gamma_j(i) < 1$, $\forall i \geq k_0$.

To show the reliability, applicability, and performance of this scheme as an efficient tool in obtaining series solutions, some initial value problems for impulsive Caputo-type differential equations will be examined in the following examples.

Example 1. First, we recall the following IVP for the impulsive differential equation in the sense of Caputo derivative [50, 51]:

$$\begin{cases} D_0^{(1/4)} g(t) = t, \quad \dfrac{t \in (0, 2]}{\{1\}}, \\ g\left(1^+\right) = g\left(1^-\right) + 1, \\ g(0) = 0. \end{cases} \tag{17}$$

Using generalized differential transformation along with its properties, on both sides of (17), we get

$$G_j(k+1) = \frac{\Gamma(k/4 + 1)}{\Gamma(k/(4+5)/4)} \left[\delta(k-4)\right], \quad j = 1, 2, \tag{18}$$

where $G_1(0) = 0$ and $G_2(0) = 1$. Using the recurrence relation (18) and the transformed initial conditions, some initial components of the generalized differential transform solution for equation (17) can be written as follows:

$$\begin{aligned} G_1(0) &= G_1(1) \\ &= G_1(2) \\ &= G_1(3) \\ &= G_1(4) \\ &= 0, \\ G_1(5) &= \frac{1}{\Gamma(9/4)}, \\ G_2(0) &= 1, \\ G_2(1) &= G_2(2) \\ &= G_2(3) \\ &= G_2(4) \\ &= 0, \\ G_2(5) &= \frac{1}{\Gamma(9/4)}, \end{aligned} \tag{19}$$

where $G_1(k) = G_2(k) = 0$, for $k > 5$. So, the solution to the IVP for the impulsive Caputo-type differential equation given in (17) can be obtained as

$$g(t) = \begin{cases} \dfrac{16}{5\Gamma(1/4)} t^{(5/4)}, & 0 \le t \le 1, \\ \\ 1 + \dfrac{16}{5\Gamma(1/4)} t^{(5/4)}, & 1 < t \le 2, \end{cases} \tag{20}$$

which is the same solution of the initial value problem for the impulsive fractional differential (17) obtained in [50].

Example 2. We next adopt IVP for the impulsive Caputo-type differential equation:

$$\begin{cases} D_0^{\alpha} y(t) = 1 - y^2(t), & \dfrac{t \in (0,2]}{\{1\}}, \\ \\ y(1^+) = y(1^-) + 2, \\ \\ y(0) = 0, \end{cases} \tag{21}$$

where $0 < \alpha \le 1$. Using the generalized differential transformation to both sides of (21) and applying the features of the given transform, we obtain

$$Y_j(1+k) = \frac{\Gamma(k\alpha+1)}{\Gamma(\alpha(1+k)+1)} \left\{ \delta(k) - \sum_{l=0}^{k} Y_j(l) Y_j(k-l) \right\}, \quad j = 1, 2, \tag{22}$$

where $Y_1(0) = 0$ and $Y_2(0) = 1$. Using the recurrence relation (22) and the transformed initial conditions, the approximate solution to IVP for the impulsive equation given in equation (21) can be derived as

$$y(t) = \begin{cases} y_1(t), & 0 \le t \le 1, \\ y_2(t), & 1 < t \le 2. \end{cases} \tag{23}$$

Here,

$$\begin{aligned} y_1(t) &= \frac{1}{\Gamma(\alpha+1)} t^{\alpha} - \frac{1}{\Gamma(\alpha+1)^2} \frac{\Gamma(2\alpha+1)}{\Gamma(3\alpha+1)} t^{3\alpha} \\ &\quad + \frac{2}{\Gamma(\alpha+1)^3} \frac{\Gamma(2\alpha+1)}{\Gamma(3\alpha+1)} \frac{\Gamma(4\alpha+1)}{\Gamma(5\alpha+1)} t^{5\alpha} - \cdots, \\ y_2(t) &= 1. \end{aligned} \tag{24}$$

Since $Y_2(0) = 1$ and $Y_2(k) = 0$, for $k \ge 2$. The exact solution of the Caputo-type differential equation $D_0^{\alpha} y(t) = 1 - y^2(t)$ with respect to the initial constraint $y(0) = 0$ when $\alpha = 1$ is $y(t) = ((e^{2t} - 1)/(e^{2t} + 1))$. In Table 1, the obtained numerical solutions $\sum_{k=0}^{n} Y_1(k) \cdot t^{\alpha k}$, when $n = 21$, for the solution component $y_1(t)$ of the initial value problems given in (21), over the interval $0 < t < 1$, are compared with those obtained in [50] using the second kind Chebyshev wavelet scheme, the numerical solutions obtained in [51] using the double perturbation collocation method, and the exact solutions when $\alpha = 1$. It is clear from Table 1 that our approximate solutions are very close in favor with the exact solutions and are much accurate as compared to the solutions given in [50, 51]. Definitely, the accuracy of our approach can be dramatically improved by simulating further terms of $y_1(t)$.

Example 3. Now, we consider the following initial value impulsive Caputo-type differential equation:

$$\begin{cases} D_0^{\alpha} y(t) = -y(t) + 0.5 y^2(t) + 1, & \dfrac{t \in (0,2]}{\{1\}}, \\ \\ y(1^+) = y(1^-) + 1.25, \\ \\ y(0) = 0, \end{cases} \tag{25}$$

where $0 < \alpha \le 1$. Using the generalized differential transformation on both the sides of (25) with the characteristics of the generalized differential transformation, we obtain

$$Y_j(k+1) = \frac{\Gamma(\alpha k+1)}{\Gamma(\alpha(k+1)+1)} \left\{ -Y_j(k) + 0.5 \sum_{l=0}^{k} Y_j(l) Y_j(k-l) + \delta(k) \right\}, \quad j = 1, 2, \tag{26}$$

where $Y_1(0) = 0$ and $Y_2(0) = 1.25$. Applying the recurrence relation (27) and the transformed initial values, the approximate solution to the initial value impulsive fractional-order (25) can be derived by

$$y(t) = \begin{cases} y_1(t), & 0 \le t \le 1, \\ y_2(t), & 1 < t \le 2, \end{cases} \tag{27}$$

where

Table 1: Numerical outputs for equation (21) over $0 < t < 1$, when $\alpha = 1$.

t	Exact solution	Present method	Ref. [50]	Ref. [50]
0.1	0.099668	0.099668	0.099667	0.099694
0.2	0.197375	0.197375	0.197358	0.197437
0.3	0.291312	0.291313	0.291289	0.291345
0.4	0.379949	0.379949	0.379946	0.379928
0.5	0.462117	0.462117	0.462172	0.462074
0.6	0.537050	0.537050	0.537048	0.537033
0.7	0.604368	0.604368	0.604338	0.604397
0.8	0.664037	0.664037	0.664009	0.664082
0.9	0.716298	0.716300	0.716300	0.716314

$$y_1(t) = \frac{1}{\Gamma(\alpha+1)}t^{\alpha} - \frac{1}{\Gamma(2\alpha+1)}t^{2\alpha} + \frac{1}{\Gamma(3\alpha+1)}\left(1 + \frac{\Gamma(2\alpha+1)}{2\Gamma(\alpha+1)^2}\right)t^{3\alpha} + \cdots,$$

$$y_2(t) = 1.25 + \frac{17}{32}\frac{1}{\Gamma(\alpha+1)}t^{\alpha} + \frac{17}{128}\frac{1}{\Gamma(2\alpha+1)}t^{2\alpha} + \cdots. \tag{28}$$

In Figures 1 and 2, we compute $\gamma_1(i)$'s and $\gamma_2(i)$'s (defined in (16)), for different values of α, that correspond to the solution components $y_1(t)$ and $y_2(t)$, respectively, of (25) where x-axis shows the index i and y-axis shows the parameter γ_i. From Figures 1 and 2, since $\gamma_1(i) < 1$ and $\gamma_2(i) < 1$ for $i \geq 1$, we observe that the components $y_1(t)$ and $y_2(t)$ of the series solution converge to the exact solution for (25), at $\alpha = 1$, 0.90 and 0.80. Also, we conclude that $\gamma_1(i)$'s and $\gamma_2(i)$'s are not less than 1, if $\alpha = 0.7$, and so, the series solution components may diverge when $\alpha = 0.7$. In the same way, we can perform the numerical simulations to show that the nonclassical type power series solution of (25) may diverge at the fractional-order.

For big value of n, if the truncated series $\sum_{k=0}^{n} Y_1(k) \cdot t^{\alpha k}$ and $\sum_{k=0}^{n} Y_2(k) \cdot t^{\alpha k}$ are used as approximations to the exact solution components $y_1(t)$ and $y_2(t)$ over $0 < t \leq 1$ and $1 < t \leq 2$, respectively, according to Figures 1 and 2, the max. absolute truncation error can be estimated as

$$\left\| y_1(t) - \sum_{k=0}^{n} Y_1(k) \cdot t^{\alpha k} \right\| \leq \begin{cases} \dfrac{1}{1-0.6368}(0.6368)^n, & \alpha = 1, \\ \dfrac{1}{\Gamma(1.9)}\dfrac{1}{1-0.7659}(0.7659)^n, & \alpha = 0.9, \\ \dfrac{1}{\Gamma(1.8)}\dfrac{1}{1-0.9145}(0.9145)^n, & \alpha = 0.8, \end{cases} \tag{29}$$

and

$$\left\| y_2(t) - \sum_{k=0}^{n} Y_2(k) \cdot t^{\alpha k} \right\| \leq \begin{cases} \dfrac{1.25}{1-0.7545}(0.7545)^n, & \alpha = 1, \\ \dfrac{1.25}{1-0.8389}(0.8389)^n, & \alpha = 0.9, \\ \dfrac{1.25}{1-0.9257}(0.9257)^n, & \alpha = 0.8. \end{cases} \tag{30}$$

As a result, we can observe that the domain of convergence becomes large as the order of the fractional derivative increases. The performed numerical simulations justify that the series solutions of given impulsive fractional-order differential equation may diverge when the fractional derivative order is $\alpha \ll 1$.

Example 4. Finally, we adopt the initial value problem for the impulsive Caputo-type differential equation.

$$\begin{cases} D_0^{\beta} y(t) = -t - y - t^2 y^2 + \dfrac{\left(te^{-t} + t^2 e^{-3t}\right)}{y}, & \dfrac{t \in (0,3]}{\{1,2\}},\ 0 < \beta \leq 1, \\ y(1^+) = 1 + y(1^-), \\ y(2^+) = 1 + y(2^-), \\ y(0) = 1. \end{cases} \tag{31}$$

The exact solution of the system,

$$\begin{cases} D_0^{\beta} y(t) = -t - y - t^2 y^2 + \dfrac{\left(te^{-t} + t^2 e^{-3t}\right)}{y}, & t \in [0,1],\ 0 < \beta \leq 1, \\ y(0) = 1, \end{cases} \tag{32}$$

is given in [52, 53] by $y(t) = e^{-t}$ when $\beta = 1$. Using the characteristics of the generalized differential transformation of order α, (30) can be transformed to the following recurrence relation:

$$Y_j\left(\frac{k+\beta}{\alpha}\right) = \frac{\Gamma(\alpha k+1)}{\Gamma(\alpha k+\beta+1)}\left[-\delta\left(\frac{k-1}{\alpha}\right) - Y_j(k) - \sum_{k_2=0}^{k}\sum_{k_1=0}^{k_2}\delta\left(\frac{k_1-2}{\alpha}\right)Y_j(k_2-k_1)Y_j(k-k_2) + F(k)\right], \tag{33}$$

for $j = 1, 2, 3$, $F(k) = ([H(k) - \sum_{\lambda=0}^{k-1} F(\lambda)(k-\lambda)]/(0))$, $H(k) = P(k) + S(k)$, $P(k) = \sum_{p=0}^{k} E_1(p)\delta(k-p-(1/\alpha))$, and $S(k) = \sum_{p=0}^{k} E_2(p)\delta(k-p-(2/\alpha))$. Moreover, $E_1(k)$ and $E_2(k)$ represent the generalized transformations of e^{-t} and e^{-3t} that can be expressed, respectively, as follows:

$$E_1(k) = \begin{cases} \dfrac{(-1)^{\alpha k}}{(\alpha k)!}, & \alpha k \in \mathbb{Z}^+, \\ 0, & \alpha k \notin \mathbb{Z}^+, \end{cases} \qquad E_2(k) = \begin{cases} \dfrac{(-3)^{\alpha k}}{(\alpha k)!}, & \alpha k \in \mathbb{Z}^+, \\ 0, & \alpha k \notin \mathbb{Z}^+. \end{cases} \tag{34}$$

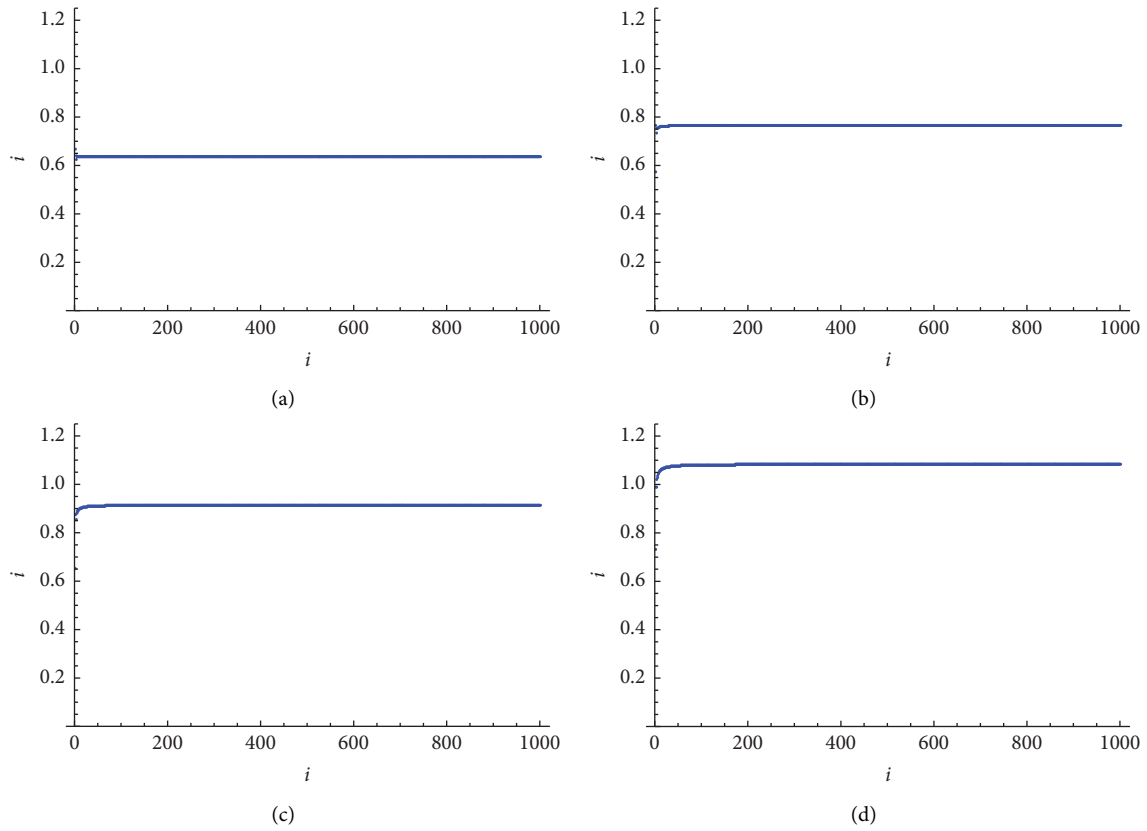

Figure 1: Numerical results of $\gamma_1(i)$'s for $y_1(t)$ of problem (26). (a) $\alpha = 1$. (b) $\alpha = 0.9$. (c) $\alpha = 0.8$. (d) $\alpha = 0.7$.

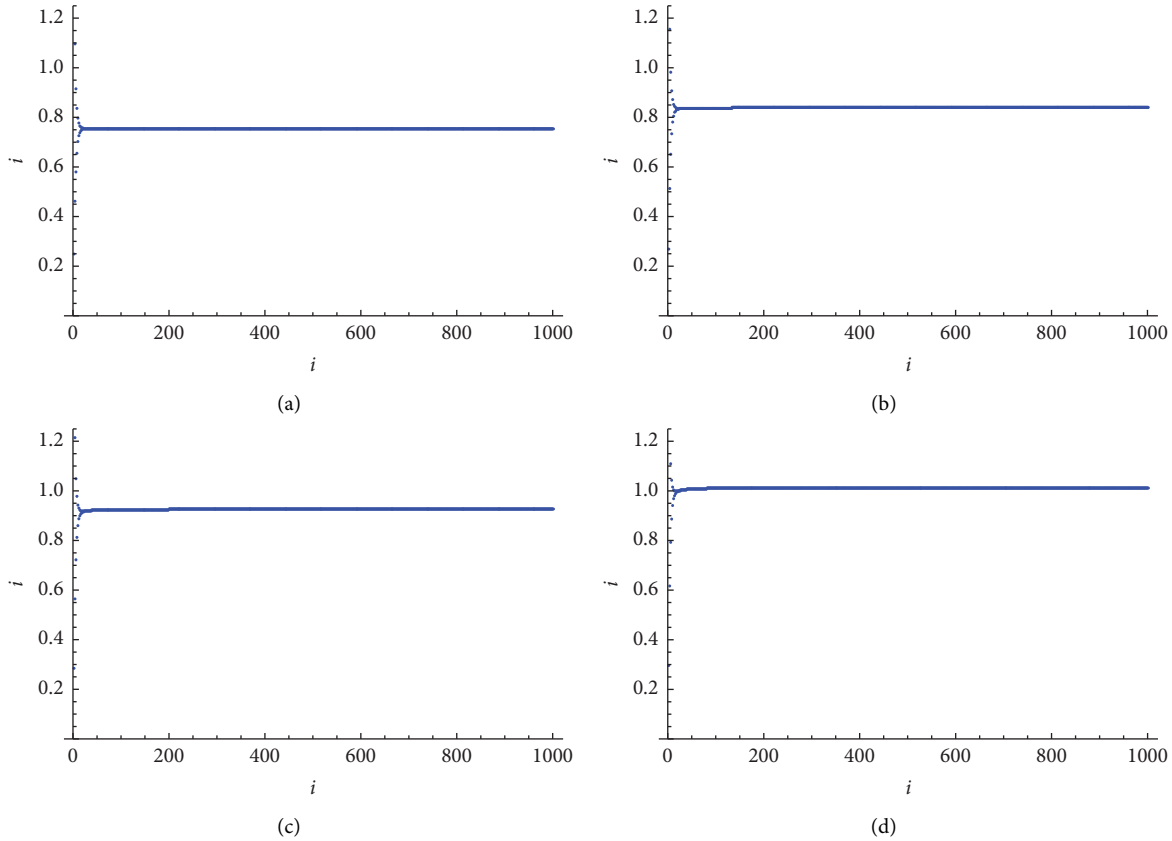

Figure 2: Numerical outputs of $\gamma_1(i)$'s for $y_2(t)$ of equation (26). (a) $\alpha = 1$. (b) $\alpha = 0.9$. (c) $\alpha = 0.8$. (d) $\alpha = 0.7$.

The initial condition and the jumps of the states of (30) are transformed as

$$\begin{aligned} &Y_1(0) = 1, Y_1(k) = 0, \quad \text{for } k = 1, 2, \ldots, \left(\frac{\beta}{\alpha - 1}\right), \\ &Y_2(0) = 2, Y_2(k) = 0, \quad \text{for } k = 1, 2, \ldots, \left(\frac{\beta}{\alpha - 1}\right), \\ &Y_3(0) = 3, Y_3(k) = 0, \quad \text{for } k = 1, 2, \ldots, \left(\frac{\beta}{\alpha - 1}\right). \end{aligned} \tag{35}$$

For $\beta = 0.8$, solving the recurrence relation (33) using the transformed conditions given in equation (35) up to $k = 18$, the approximate solution to IVP for the impulsive Caputo-type differential given in equation (31) can be derived as

$$y(t) = \begin{cases} y_1(t), & 0 \le t \le 1, \\ y_2(t), & 1 < t \le 2, \\ y_3(t), & 2 < t \le 3, \end{cases} \tag{36}$$

where

$$\begin{aligned} y_1(t) &= 1 - 1.0737t^{(4/5)} + 0.69948t^{(8/5)} - 0.33543t^{(12/5)} + 0.48426t^{(13/5)} \\ &\quad - 0.4261t^{(14/5)} + 0.12892t^{(16/5)} - 0.011358t^{(17/5)} + 0.90275t^{(18/5)} + \cdots, \\ y_2(t) &= 2 - 2.14734t^{(4/5)} + 1.39897t^{(8/5)} - 0.298242t^{9/5} - 0.670869t^{(12/5)} \\ &\quad + 0.376645t^{(13/5)} - 1.70424t^{(14/5)} + 0.257842t^{(16/5)} - 0.0550077t^{(17/5)} + \\ &\quad + 3.63717t^{(18/5)} + \cdots, \\ y_3(t) &= 3 - 3.22101t^{(4/5)} + 2.09845t^{(8/5)} - 0.397656t^{9/5} - 1.0063t^{(12/5)} + 0.340774t^{(13/5)} \\ &\quad - 3.83454t^{(14/5)} + 0.386763t^{(16/5)} - 0.0695575t^{(17/5)} + 8.14028t^{(18/5)} + \cdots. \end{aligned} \tag{37}$$

For $\beta = 0.85$, the approximate solutions $y_1(t)$, $y_2(t)$, and $y_3(t)$ can be evaluated as

$$\begin{aligned} y_1(t) &= 1 - 1.0575t^{(17/20)} + 0.64738t^{(17/10)} - 0.28464t^{(51/20)} + 0.44357t^{(27/10)} \\ &\quad - 0.40114t^{(57/20)} + 0.098657t^{(17/5)} + 0.0091578t^{(71/20)} + 0.81295t^{(37/10)} + \cdots, \\ y_2(t) &= 2 - 2.11503t^{(17/20)} + 1.29476t^{(17/10)} - 0.285815t^{(37/20)} - 0.569273t^{(51/20)} + 0.341673t^{(27/10)} \\ &\quad - 1.60458t^{(57/20)} + 0.197315t^{(17/5)} - 0.0355107t^{(71/20)} + 3.27489t^{(37/10)} + \cdots, \\ y_3(t) &= 3 - 3.17255t^{(17/20)} + 1.94214t^{(17/10)} - 0.381087t^{(37/20)} - 0.85391t^{(51/20)} \\ &\quad + 0.307706t^{(27/10)} - 3.610t^{(57/20)} + 0.295972t^{(17/5)} - 0.0504003t^{(71/20)} + 7.33025t^{(37/10)} + \cdots. \end{aligned} \tag{38}$$

While when $\beta = 1$, the approximate solutions $y_1(t)$, $y_2(t)$, and $y_3(t)$ can be evaluated as

$$\begin{aligned} y_1(t) &= 1 - t + \frac{t^2}{2} - \frac{t^3}{6} + \frac{t^4}{24} - \frac{t^5}{120} + \frac{t^6}{720} - \frac{t^7}{5040} + \frac{tx^8}{40320} - \frac{t^9}{362880} + \frac{t^{10}}{3628800} - \cdots, \\ y_2(t) &= 2 - 2t + 0.75\,t^2 - 1.41667t^3 + 2.11979\,t^4 - 1.54479\,t^5 + 1.59232\,t^6 \\ &\quad - 2.3723\,t^7 + 2.50693\,t^8 - 2.35509t^9 + 2.73001t^{10} - \cdots, \\ y_3(t) &= 3 - 3t + 1.16667t^2\_3.27778t^3 + 5.16204t^4 - 4.02253t^5 \\ &\quad + 5.04799t^6 + 8.22138t^7 + 9.0091t^8 - 9.70313t^9 + 13.3388t^{10} - \cdots. \end{aligned} \tag{39}$$

Table 2: Absolute errors for $y_1(t)$ over $0 < t < 1$, when $\beta = 1$, for equation (31).

t	Exact solution	$\lvert y_{\text{exact}} - y_{\text{Chebyshev}} \rvert$	$\lvert y_{\text{exact}} - y_{\text{Padé}} \rvert$	$\lvert y_{\text{exact}} - y_{\text{GDTM}} \rvert$
0.0	1.0000000000	0	0	0
0.1	0.9048374180	2×10^{-10}	1×10^{-10}	0×10^{-10}
0.2	0.8187307531	8×10^{-9}	8×10^{-9}	0×10^{-10}
0.3	0.7408182207	8×10^{-8}	8×10^{-8}	0×10^{-10}
0.4	0.6703200460	4×10^{-7}	4×10^{-7}	0×10^{-10}
0.5	0.6065306597	1×10^{-6}	1×10^{-6},	0×10^{-10}
0.6	0.5488116361	4×10^{-6}	4×10^{-6}	1×10^{-9}
0.7	0.4965853038	9×10^{-6}	9×10^{-6}	5×10^{-10}
0.8	0.4493289641	2×10^{-5}	2×10^{-5}	2×10^{-9}
0.9	0.4065696597	4×10^{-5}	4×10^{-5}	7×10^{-9}
1.0	0.3678794412	6×10^{-5}	6×10^{-5}	2×10^{-8}

Table 2 provides the exact solution and the absolute errors for the approximate solutions of $y_1(t)$, over $0 < t < 1$, obtained using the GDTM, Chebyshev method [52], and Padé approximation method [53] when $\beta = 1$. From Table 2, we can conclude that the absolute errors are so small, and the approximate solutions simulated from GDTM are so closed to the exact solutions. Here, the comparison is made in the first subinterval because, to our knowledge, techniques for solving IVPs for impulsive Caputo-type differential equations have not yet been sufficiently introduced.

5. Conclusion

In this research, the application and performance of the generalized differential transform scheme to simulate initial value problems for Caputo-type differential equations are addressed. The reliability of the given technique has been demonstrated through some illustrative examples, and the obtained results show perfect agreements with other methods over the first subinterval. The sufficient condition for convergence of the scheme is presented. The main property of the method, as shown in this study, is that it deforms the impulsive differential equations of fractional order into a set of recurrence equations which gives several successive approximations, and hence, the procedure is direct and straightforward. This work illustrates the flexibility of the method as a tool to solve the classes of nonlinear problems containing fractional derivatives, effectively, easily, and accurately.

Data Availability

No data were used to support this study.

Conflicts of Interest

The authors declare that they have no conflicts of interest.

References

[1] D. Baĭnov and P. Simeonov, "Pitman Monographs and Surveys in Pure and Applied Mathematics," *Impulsive differential equations: periodic solutions and applications*, Harlow: Longman Scientific and Technical, New York, NY, USA, 1993.

[2] I. M. Stamova and G. T. Stamov, "Lyapunov–Razumikhin method for impulsive functional differential equations and applications to the population dynamics," *Journal of Computational and Applied Mathematics*, vol. 130, no. 1-2, pp. 163–171, 2001.

[3] W. M. Haddad, V. S. Chellaboina, and S. G. Nersesov, *Impulsive and Hybrid Dynamical Systems: Stability, Dissipativity, and Control*, Princeton University Press, Princeton, NJ, USA, 2006.

[4] X. Liu, G. L. Zhang, and M. Z. Liu, "Analytic and numerical exponential asymptotic stability of nonlinear impulsive differential equations," *Applied Numerical Mathematics*, vol. 81, pp. 40–49, 2014.

[5] Z. Zhang and H. Liang, "Collocation methods for impulsive differential equations," *Applied Mathematics and Computation*, vol. 228, pp. 336–348, 2014.

[6] G.-L. Zhang, "High order Runge-Kutta methods for impulsive delay differential equations," *Applied Mathematics and Computation*, vol. 313, pp. 12–23, 2017.

[7] G. T. Stamov, "On the existence of almost periodic solutions for the impulsive Lasota-Wazewska model," *Applied Mathematics Letters*, vol. 22, no. 4, pp. 516–520, 2009.

[8] A. Huseynov, "Positive solutions of a nonlinear impulsive equation with periodic boundary conditions," *Applied Mathematics and Computation*, vol. 217, no. 1, pp. 247–259, 2010.

[9] X. Li, "Further analysis on uniform stability of impulsive infinite delay differential equations," *Applied Mathematics Letters*, vol. 25, no. 2, pp. 133–137, 2012.

[10] Q. Wang and M. Wang, "Existence of solution for impulsive differential equations with indefinite linear part," *Applied Mathematics Letters*, vol. 51, pp. 41–47, 2016.

[11] J. Wang, "Stability of noninstantaneous impulsive evolution equations," *Applied Mathematics Letters*, vol. 73, pp. 157–162, 2017.

[12] G. Samko, A. Kilbas, and O. Marichev, *Fractional Integrals and Derivatives: Theory and Applications*, Gordon & Breach, Amsterdam, Netherlands, 1993.

[13] Y. A. Rossikhin and M. V. Shitikova, "Applications of fractional calculus to dynamic problems of linear and nonlinear hereditary mechanics of solids," *Applied Mechanics Reviews*, vol. 50, no. 1, pp. 15–67, 1997.

[14] I. Podlubny, *Fractional Differential Equations*, Academic Press, New York, NY, USA, 1999.

[15] R. Hilfer, *Applications of Fractional Calculus in Physics*, World Scientific Publishing Company, Singapore, London, 2000.

[16] A. A. Kilbas, H. M. Srivastava, and J. J. Trujillo, *Theory and Applications of Fractional Differential Equations*, Elsevier, Amsterdam, Netherlands, 2006.

[17] C. P. Li and F. H. Zeng, *Numerical Method for Fractional Calculus*, Chapman and Hall/CRC, Boca Raton, FL, USA, 2015.

[18] C. Phang, A. Kanwal, and J. R. Loh, "New collocation scheme for solving fractional partial differential equations," *Hacettepe Journal of Mathematics and Statistics*, vol. 49, no. 3, pp. 1–19, 2019.

[19] M. Benchohra and F. Berhoun, "Impulsive fractional differential equations with variable times," *Computers & Mathematics with Applications*, vol. 59, no. 3, pp. 1245–1252, 2010.

[20] T. L. Guo and W. Jiang, "Impulsive fractional functional differential equations," *Computers & Mathematics with Applications*, vol. 64, no. 10, pp. 3414–3424, 2012.

[21] M. Fečkan, Y. Zhou, and J. Wang, "On the concept and existence of solution for impulsive fractional differential equations," *Communications in Nonlinear Science and Numerical Simulation*, vol. 17, no. 7, pp. 3050–3060, 2012.

[22] Z. Liu and X. Li, "Existence and uniqueness of solutions for the nonlinear impulsive fractional differential equations," *Communications in Nonlinear Science and Numerical Simulation*, vol. 18, no. 6, pp. 1362–1373, 2013.

[23] M. u. Rehman and P. W. Eloe, "Existence and uniqueness of solutions for impulsive fractional differential equations," *Applied Mathematics and Computation*, vol. 224, pp. 422–431, 2013.

[24] X. Zhang, "On the concept of general solution for impulsive differential equations of fractional-order q $\in$(1, 2)," *Applied Mathematics and Computation*, vol. 268, pp. 103–120, 2015.

[25] Y. Liu, "On piecewise continuous solutions of higher order impulsive fractional differential equations and applications," *Applied Mathematics and Computation*, vol. 287-288, pp. 38–49, 2016.

[26] J. Wang, M. Fečkan, and Y. Zhou, "A survey on impulsive fractional differential equations," *Fractional Calculus and Applied Analysis*, vol. 19, no. 4, pp. 806–831, 2016.

[27] Q. Chen, A. Debbouche, Z. Luo, and J. Wang, "Impulsive fractional differential equations with Riemann-Liouville derivative and iterative learning control," *Chaos, Solitons & Fractals*, vol. 102, pp. 111–118, 2017.

[28] N. Najafi and T. Allahviranloo, "Combining fractional differential transform method and reproducing kernel Hilbert space method to solve fuzzy impulsive fractional differential equations," *Computational and Applied Mathematics*, vol. 39, no. 2, p. 122, 2020.

[29] J. Cao, L. Chen, and Z. Wang, "A block-by-block method for the impulsive fractional ordinary differential equations," *Journal of Applied Analysis & Computation*, vol. 10, no. 3, pp. 853–874, 2020.

[30] F. Karimi, K. Sabzi, and M. Keshavarz, "Adomaian decomposition method for solving impulsive fractional differential equations," *Communications on Advanced Computational Science with Applications*, vol. 2017, no. 2, pp. 95–102, 2017.

[31] M. A. Zaky and A. S. Hendy, "Convergence analysis of an L1-continuous Galerkin method for nonlinear time-space fractional Schrödinger equations," *International Journal of Computer Mathematics*, vol. 98, no. 7, pp. 1420–1437, 2021.

[32] A. S. Hendy and M. A. Zaky, "Combined Galerkin spectral/finite difference method over graded meshes for the generalized nonlinear fractional Schrödinger equation," *Nonlinear Dynamics*, vol. 103, no. 3, pp. 2493–2507, 2021.

[33] R. M. Hafez, M. A. Zaky, and A. S. Hendy, "A novel spectral Galerkin/Petrov-Galerkin algorithm for the multi-dimensional space-time fractional advection-diffusion-reaction equations with nonsmooth solutions," *Mathematics and Computers in Simulation*, vol. 190, pp. 678–690, 2021.

[34] A. S. Hendy, M. A. Zaky, and R. H. De Staelen, "A general framework for the numerical analysis of high-order finite difference solvers for nonlinear multi-term time-space fractional partial differential equations with time delay," *Applied Numerical Mathematics*, vol. 169, pp. 108–121, 2021.

[35] M. A. Zaky, "An accurate spectral collocation method for nonlinear systems of fractional differential equations and related integral equations with nonsmooth solutions," *Applied Numerical Mathematics*, vol. 154, pp. 205–222, 2020.

[36] A. S. Hendy and M. A. Zaky, "Global consistency analysis of L1-Galerkin spectral schemes for coupled nonlinear space-time fractional Schrödinger equations," *Applied Numerical Mathematics*, vol. 156, pp. 276–302, 2020.

[37] M. A. Zaky, "Recovery of high order accuracy in Jacobi spectral collocation methods for fractional terminal value problems with non-smooth solutions," *Journal of Computational and Applied Mathematics*, vol. 357, pp. 103–122, 2019.

[38] P. Kumar, V. S. Erturk, and A. Kumar, "A new technique to solve generalized caputo type fractional differential equations with the example of computer virus model," *Journal of Mathematical Extension*, vol. 15, 2021.

[39] Z. Odibat, V. Suat Erturk, P. Kumar, and V. Govindaraj, "Dynamics of generalized Caputo type delay fractional differential equations using a modified Predictor-Corrector scheme," *Physica Scripta*, vol. 96, no. 12, Article ID 125213, 2021.

[40] V. S. Erturk, E. Godwe, D. Baleanu, P. Kumar, J. Asad, and A. Jajarmi, "Novel fractional-order Lagrangian to describe motion of beam on nanowire," *Acta Physica Polonica A*, vol. 140, no. 3, pp. 265–272, 2021.

[41] P. Kumar, V. S. Erturk, A. Yusuf, and S. Kumar, "Fractional time-delay mathematical modeling of Oncolytic Virotherapy," *Chaos, Solitons & Fractals*, vol. 150, Article ID 111123, 2021.

[42] P. Kumar, V. Suat Erturk, R. Banerjee, M. Yavuz, and V. Govindaraj, "Fractional modeling of plankton-oxygen dynamics under climate change by the application of a recent numerical algorithm," *Physica Scripta*, vol. 96, no. 12, Article ID 124044, 2021.

[43] Z. M. Odibat and N. T. Shawagfeh, "Generalized Taylor's formula," *Applied Mathematics and Computation*, vol. 186, no. 1, pp. 286–293, 2007.

[44] J. K. Zhou, *Differential Transformation and its Applications for Electrical Circuits*, Huazhong University Press, Wuhan, China, 1986, in Chinese.

[45] N. Bildik, A. Konuralp, F. Orakçı Bek, and S. Küçükarslan, "Solution of different type of the partial differential equation by differential transform method and Adomian's decomposition method," *Applied Mathematics and Computation*, vol. 172, no. 1, pp. 551–567, 2006.

[46] M. El-Shahed, "Application of differential transform method to non-linear oscillatory systems," *Communications in Nonlinear Science and Numerical Simulation*, vol. 13, no. 8, pp. 1714–1720, 2008.

[47] S. Momani, Z. Odibat, and V. S. Erturk, "Generalized differential transform method for solving a space- and time-fractional diffusion-wave equation," *Physics Letters A*, vol. 370, no. 5-6, pp. 379–387, 2007.

[48] Z. Odibat, S. Momani, and V. S. Erturk, "Generalized differential transform method: application to differential equations of fractional order," *Applied Mathematics and Computation*, vol. 197, no. 2, pp. 467–477, 2008.

[49] Z. M. Odibat, S. Kumar, N. Shawagfeh, A. Alsaedi, and T. Hayat, "A study on the convergence conditions of generalized differential transform method," *Mathematical Methods in the Applied Sciences*, vol. 40, no. 1, pp. 40–48, 2017.

[50] Y. Wang and Q. Fan, "The second kind Chebyshev wavelet method for solving fractional differential equations," *Applied Mathematics and Computation*, vol. 218, no. 17, pp. 8592–8601, 2012.

[51] O. A. Taiwo and M. O. Fesojaye, "Double perturbation collocation method for solving fractional Riccati differential equations," *International Journal of Cancer, Clinical Inventions and Experimental Oncology*, vol. 1, no. 1, pp. 1–18, 2015.

[52] M. Gülsu, Y. Öztürk, and M. Sezer, "On the solution of the Abel equation of the second kind by the shifted Chebyshev polynomials," *Applied Mathematics and Computation*, vol. 217, no. 9, pp. 4827–4833, 2011.

[53] C. Guler, "A new numerical algorithm for the Abel equation of the second kind," *International Journal of Computer Mathematics*, vol. 84, no. 1, pp. 109–119, 2007.

Hindawi
Mathematical Problems in Engineering
Volume 2022, Article ID 6948461, 13 pages
https://doi.org/10.1155/2022/6948461

Research Article

The Rayleigh–Stokes Problem for a Heated Generalized Second-Grade Fluid with Fractional Derivative: An Implicit Scheme via Riemann–Liouville Integral

Abdul Hamid Ganie,[1] Abdulkafi Mohammed Saeed,[2] Sadia Saeed,[3] and Umair Ali[3]

[1]*Basic Sciences Department, College of Science and Theoretical Studies, Saudi Electronic University, Abha Male 61421, Saudi Arabia*
[2]*Department of Mathematics, College of Science, Qassim University, Buraydah, Saudi Arabia*
[3]*Department of Applied and Statistics, Institute of Space Technology, Islamabad 44000, Pakistan*

Correspondence should be addressed to Umair Ali; umairkhanmath@gmail.com

Received 6 September 2021; Revised 29 January 2022; Accepted 1 March 2022; Published 5 May 2022

Academic Editor: Muhammad Irfan

The goal of this study is to use the fast algorithm to solve the Rayleigh–Stokes problem for heated generalized second-grade fluid (RSP-HGSGF) with Riemann–Liouville time fractional derivative using the fast algorithm. The modified implicit scheme, which is formulated by the Riemann–Liouville integral formula and applied to the fractional RSP-HGSGF, is proposed. Numerical experiments will be carried out to demonstrate that the scheme is simple to implement, and the results will reveal the best way to implement the suggested technique. The proposed scheme's stability and convergence will be examined using the Fourier series. The method is stable, and the approximation solution approaches the exact solution. A numerical demonstration will be provided to demonstrate the applicability and viability of the suggested strategy.

1. Introduction

The study and application of arbitrary-order derivatives and integrals are associated with fractional calculus. The use of fractional-order calculus in a variety of fields of science and engineering, including geometric phenomena, has sparked a lot of interest in this area [1]. The first discussion of fractional calculus took place between Leibniz and L'Hospital at the end of the seventeenth century [2]. The great mathematicians Erdelyi, Abel, Riemann, Laplace, Heaviside, Levy, Liouville, Riesz, Gunwald, Letnikov, and Fourier worked on it and had contributed [3]. Fractional-order integrals and derivatives play an important role in solving some chemical problems, and this field has been paid much attention since 1968. The most well-known book in the field of fractional calculus, originally written by Ross and Miller and Ross [4], Spanier and Oldham [5], Podlubny [6], and Samko et al. [7], explains the underlying theory of fractional calculus as well as its applications and solutions.

Many researchers have solved fractional-order problems using various methods. For example, Shivanian and Jafferabadi [8] used fractional derivatives to find the numerical solution for the RSP-HGSGF using spectral meshless radial point interpolation. The time-fractional derivative has been defined in the Riemann–Liouville sense. The Shape functions are created by using a point interpolation method and radial basis functions as basic functions. An efficient numerical approach for approximating RSP-HGSGF in a bounded domain is described by Liu et al. [9]. They investigated the proposed scheme's stability and convergence. To solve SFP-HGSGF, Wu [10] used a numerical approach. The stability, convergence, and consistency of the INAS for the SFP HGSGF have been investigated. RSPHGSGF was studied in a flow on a heated flat plate and within a heated edge by Shen et al. [11]. A viscoelastic fluid was described using the

fractional calculus technique in the constitutive relationship model. For the exact solution of the velocity and temperature fields, the Fourier transform on fractional-order Laplace operator is used. Yu et al. [12] used the Adomian decomposition method to solve the RSP-HGSGF. In general, without discretizing the problem, such series solutions converge quickly and the Adomian decomposition approach yields very precise numerical solutions. In this study, Chen et al. [13] presented two numerical methods for solving a two-dimensional variable-order subdiffusion anomalous problem. Their stability, convergence, and solvability were investigated using Fourier analysis. The numerical approximation for the Riemann–Liouville fractional-order derivative for the fractional SFP-HGSGF was studied by Yu et al. [14]. They used the implicit scheme with Riemann–Liouville fractional derivative to solve the direct and inverse problems. Lin and Jiang [15] devised a straightforward method for calculating the fractional derivative of an RSP-HGSG. They created the series of the exact solution to the problem using kernel theory and established the approximate solution of its fractional derivative using truncating series, which are uniformly convergent. Meanwhile, their method includes error estimation and stability analysis. Chen et al. [16] proposed the implicit and explicit techniques for solving the RSP-HGSGF of fractional order. The convergence, stability, and solvability of the problem have all been determined. In recent years, Chen et al. [17] discussed Stokes' initial challenge attention. The variable-order nonlinear RSP-HGSGF is investigated, and the fourth-order numerical technique is discussed. The Fourier approach is used to investigate the numerical scheme's theoretical analysis. Dehghan and Abbas Zadeh [18] developed a numerical solution for 2D fractional-order RSP-HGSGF on rectangular domains such as circular, L-shaped, and a unit square with circular holes. The RL principle is used to calculate the fractional derivatives. They used the Galerkin FEM to obtain a fully discrete scheme for the space direction by integrating the equation for the time variable. Finally, we compare the results of Galerkin FEM to those of other numerical techniques. The Rayleigh–Stokes problem for an edge in a generalized Oldroyd-B fluid was solved by Nikan and Avazzadeh et al. [19] using the radial basis function and fractional derivatives. The temporal derivative terms are discretized using the finite difference technique, while the spatial derivative terms are discretized using the local RBF-FD.

To maintain a constant number of nodes, they evaluate the distribution of data nodes within the local support area. The stability and convergence of the proposed method are also investigated. The RBF-FD results are compared to those of previous approaches on irregular domains, demonstrating the novel methodology's viability and efficiency. RSP-HGSGF flow was investigated by Zhai et al. [20] on a heated flat plate and within a heated edge. To describe such a viscoelastic fluid, a fractional calculus methodology was used in the constitutive relationship model. The velocity and temperature fields were solved in closed form using the Fourier transform and the fractional Laplace operator. Another study looked at the same model to describe a viscoelastic fluid [21, 22]. For the finite difference/finite element technique, Guan et al. [23] provided an enhanced version of a nonlinear source term with a fractional RSP. The backward difference formula and second-order Grünwald–Letnikov derivative are used to discretize the first-order time derivative. They use the Galerkin finite element approach to define a fully discrete strategy for the fractional RSP-HGSGF with a nonlinear source term in the space direction. A novel analytical technique is used to calculate the level of accuracy in the L2 norm in great detail. For the 2D modified anomalous fractional subdiffusion equation, Ali et al. [24] used a modified implicit difference approximation. The proposed scheme's convergence and stability are investigated using the Fourier series approach. It is shown that the scheme is unconditionally stable, and that the approximate solution converges to the exact solution. Bazhlekova et al. [25] investigated the RSP-HGSGF in time using the RL fractional derivative, and the problem was analysed in space using semidiscrete, continuous, and completely discrete formulations. Mohebbi et al. [26] compared the meshless approach to a fourth-order approximation for 2D fractional RSP and generated a completely discrete implicit scheme. Sun et al [27] contributed a review article on important fractional calculus information. They talked about the most important real-world applications as well as powerful mathematical tools. The numerical solution of a nonlinear fractional-order reaction-subdiffusion model was investigated by Nikan et al. [28]. For spatial discretization, they used the radial base function-finite difference method, and for time discretization, they used a weighted discrete scheme. They discussed theoretical analysis and tested two numerical examples for the computational efficiency of the proposed scheme, which yielded accurate results. In a separate study [29], the author proposed a meshless scheme for the fractional-order diffusion model. They eliminated the time derivative by integrating both sides of the proposed model and used local hybridization of cubic and radial basis functions for space derivatives. Nikan et al. [30] investigated the local hybrid kernel meshless approach for fractional-order model approximation. To approximate the time and space directions, they used the central difference approximation and Gaussian kernels, respectively. They verified the validity of the proposed method using numerical examples that are both accurate and efficient. Liu et al. [31] discussed the fractional dynamics modelled from the fractional-order PDEs. Fractional-order systems have importance in the field of electrochemistry, chaotic systems, biology etc. Ahmad et al. [32] formulated a new methodology named as variational iteration method I and successfully applied to a nonlinear model. They explained the compactness of the method and compared their results with the existed literature and found that the proposed method is more productive and reliable than others. Khan et al. [33] considered the numerical approach based on the collocation method for the inverse heat source problem and tasted the method both on regular and irregular domain. Different researchers discussed various numerical approaches for time and space fractional-order models in the research [27, 30, 34–38]. The goal of this research is to propose a new scheme for this model modified

implicit scheme for fractional-order RSP-HGSGF. It lowers the computational cost and allows for easy theoretical analysis using any method for the final scheme. In the procedure, the discretized form of the Riemann–Liouville integral operator is used to replace the Riemann–Liouville derivative with the first-order time derivative. The partial derivative with respect to time is then eliminated using backward difference approximation. Additionally, we use the Fourier series method to investigate the established method's stability and convergence criterion. Finally, numerical examples are presented and solved using the proposed method to verify the method's accuracy and feasibility. Maple 15 is used to code the numerical examples.

The following is how the rest of the paper is organized: The methodology of the proposed scheme is discussed in Section 2, followed by stability and convergence analysis in Sections 2.1 and 2.2. The numerical experiments and results are presented in Section 3 and discussed in Section 4. The conclusion is discussed in Section 5 of the report.

The aim of this study is to propose a modified implicit scheme for fractional RSP-HGSGF based on the formulated Riemann–Liouville integral operator. The partial derivative w.r.t. time is eliminated by backward difference approximation. Additionally, we investigate the stability and convergence criterion of the established method by the Fourier series method.

Here, we consider the following two-dimensional RSP-HGSGF with fractional derivative [22].

$$\frac{\partial Y(x,y,t)}{\partial t} = D_t^{1-\beta}\left(\frac{\partial^2 Y(x,y,t)}{\partial x^2} + \frac{\partial^2 Y(x,y,t)}{\partial y^2}\right) + \frac{\partial^2 Y(x,y,t)}{\partial x^2} + \frac{\partial^2 Y(x,y,t)}{\partial y^2} + H(x,y,t). \tag{1}$$

Initial and boundary conditions are as follows:

$$Y(x,y,t) = \varphi(x,y), \tag{2}$$

$$\begin{aligned} Y(0,y,t) &= \Omega_1(y,t), \mathrm{Y(L, y, t)} \\ &= \Omega_2(y,t), \\ Y(x,0,t) &= \Omega_3(y,t) Y(x,L,t) \\ &= \Omega_4(x,t), \\ 0 \le x, y \le L, 0 \le t \le T, \end{aligned} \tag{3}$$

where ${}_0D_t^{1-\beta} Y(x,y,t)$ represents the fractional-order Riemann–Liouville derivative of order $1-\beta$.

Lemma 1. *The β $(0\langle\beta\langle 1)$-order Riemann–Liouville fractional integral of the function $Y(x,y,t)$ on [0,T] can be defined in discretized form as*

$$I_0^{\beta} Y(x,y,t_m) = \frac{\tau^{\beta}}{\Gamma(\beta+1)} \sum_{j=0}^{m-1} d_j^{(\beta)} Y\left(x,y,t_{m-j}\right). \tag{4}$$

Lemma 2. *The coefficients constant $d_m^{(\beta)}$ $(m = 0, 1, 2, \ldots.)$ fulfils the following properties [29]:*

(i) $d_0^{\beta} = 1, \quad d_m^{\beta} \rangle 0, \ m = 0, 1, 2 \ldots$

(ii) $d_{m-1}^{\beta} \rangle d_m^{\beta}, \quad m = 1, 2 \ldots$

(iii) There exists a positive constant $C\rangle 0$, such that $\tau \le C d_m^{\beta} \tau^{\beta}, \quad m = 1, 2, \ldots$

(iv) $\sum_{j=0}^{m} d_j^{(\beta)} \tau^{\beta} = (m+1)^{\beta} \le T^{\beta}$

2. Methodology of the Proposed Scheme

The 2D RSP-HGSGF in equations (1)–(3) is solved by the modified implicit scheme. We utilized the Riemann–Liouville approximation for time-fractional and central difference for space derivative and partitioned the bounded domain into subintervals of lengths Δx and Δy. The space steps are $x_i = i\Delta x$, in the x-direction with $i = 1, \ldots, M_1 - 1$, $\Delta x = L/M_1$, and $y_j = j\Delta y$, in the y-direction with $j = 1, \ldots, \ M_2 - 1$, $\Delta y = L/M_2$. The time step is $t_m = m\tau$, $m = 1, \ldots, N$ where $\tau = T/N$. Let $Y_{i,j}^m$ be the numerical approximation to $Y(x_i, y_j, t_m)$; by applying (2) to (1), we obtain

$$\frac{\partial Y(x,y,t)}{\partial t} = \frac{\partial}{\partial t} I_0^{\beta}\left(\frac{\partial^2 Y(x,y,t)}{\partial x^2} + \frac{\partial^2 Y(x,y,t)}{\partial y^2}\right) + \frac{\partial^2 Y(x,y,t)}{\partial x^2} + \frac{\partial^2 Y(x,y,t)}{\partial y^2} + H(x,y,t). \tag{5}$$

Applying Lemma 1 and backward difference approximation w.r.t. time, we obtain

$$Y_{i,j}^m - Y_{i,j}^{m-1} = R_1 \sum_{j=o}^{m-1} d_j^{(\beta)}\left(\delta x^2 Y_{I,j}^{m-j} - \delta x^2 Y_{i,j}^{m-j-i}\right) + R_2 \sum_{j=o}^{m-1} d_j^{(\beta)}\left(\delta x^2 Y_{I,j}^{m-j} - \delta x^2 Y_{i,j}^{m-j-i}\right) + R_3\left(\frac{Y_{i,j}^m}{\Delta x^2}\right) + R_4\left(\frac{Y_{i,j}^m}{\Delta y^2}\right) + H(x, y, t), \tag{6}$$

where

$$R_1 = \frac{\tau^\beta}{\Gamma(\beta+1)\Delta x^2},$$
$$R_2 = \frac{\tau^\beta}{\Gamma(\beta+1)\Delta y^2},$$
$$R_3 = \frac{\tau}{\Delta x^2},$$
$$R_4 = \frac{\tau}{\Delta y^2}. \tag{7}$$

$$\delta x^2 Y_{i,j}^m = Y_{i+1,j}^m - 2Y_{i,j}^m + Y_{i-1,j}^m. \tag{8}$$

The simplified form of the proposed scheme for 2D RSP-HGSGF (1)-(3) and the conditions are as follows:

$$\begin{aligned} Y_{i,j}^m - Y_{i,j}^{m-1} = {} & R_1 \delta x^2 Y_{I,j}^m - R_1 d_{m-1}^{(\beta)} \delta x^2 Y_{I,j}^0 - R_1 \sum_{s=1}^{m-1} \left(d_{s-\beta}^{(\beta)} - d_s^{(\beta)} \right) \delta x^2 Y_{I,j}^{m-s} + R_2 \delta y^2 Y_{I,j}^m + R_2 \sum_{s=1}^{m-1} \left(d_{s-\beta}^{(\beta)} - d_s^{(\beta)} \right) \delta y^2 Y_{I,j}^{m-s} \\ & + R_3 \delta x^2 Y_{I,j}^m + R_4 \delta y^2 Y_{I,j}^m + \tau H_{i,j}^m, \end{aligned} \tag{9}$$

where $i = 1, 2, \ldots, M_1 - 1$, $j = 1, 2, \ldots, M_2 - 1$, and $m = 1, 2, \ldots, N - 1$.

$$\begin{aligned} Y_{I,j}^0 &= \Omega(x_i, y_j), \\ Y_{0,j}^m &= \Omega_1(y_j, t_m),\ Y_{i,0}^m = \Omega_2(x_i, t_m), \\ Y_{M_1,j}^m &= \Omega_3(y_j, t_m),\ Y_{i,M_2}^m = \Omega_4(x_i, t_m), \\ 0 &\le x, y \le L,\ 0 \le t \le T. \end{aligned} \tag{10}$$

2.1. Stability. We find the stability of the proposed scheme by Fourier technique. Let the approximate solution be $\Psi_{i,j}^m$ for (9); we have

$$\begin{aligned} \Psi_{i,j}^m - \Psi_{i,j}^{m-1} = {} & R_1 \left(\Psi_{i+1,j}^m - 2\Psi_{i,j}^m + \Psi_{i-1,j}^m \right) - R_1 d_{m-1}^{(\beta)} \left(\Psi_{i+1,j}^0 - 2\Psi_{i,j}^0 + \Psi_{i-1,j}^0 \right) - R_1 \sum_{s=1}^{m-1} \left(d_{s-1}^{(\beta)} - d_s^{(\beta)} \right) \left(\Psi_{i+1,j}^{m-s} - 2\Psi_{i,j}^{m-s} + \Psi_{i,j+1}^{m-s} \right) + \\ & R_2 \left(\Psi_{i,j}^{m-s} - 2\Psi_{i,j}^{m-s} + \Psi_{i,j-1}^{m-s} \right) + R_2 d_{m-1}^{(\beta)} \left(\Psi_{i,j+1}^0 - 2\Psi_{i,j}^0 + \Psi_{i,j-1}^0 \right) - R_2 \sum_{s=1}^{m-1} \left(d_{s-1}^{(\beta)} - d_s^{(\beta)} \right) \left(\Psi_{i,j+1}^{m-s} - 2\Psi_{i,j}^{m-s} + \Psi_{i,j-1}^{m-s} \right) \\ & + R_3 \left(\Psi_{i+1,j}^m - 2\Psi_{i,j}^m + \Psi_{i-1,j}^m \right) \\ & + R_4 \left(\Psi_{i,j+1}^m - 2\Psi_{i,j}^m + \Psi_{i,j-1}^m \right). \end{aligned} \tag{11}$$

Next, the error is defined as

$$\varphi_{i,j}^m = Y_{i,j}^m - \Psi_{i,j}^m. \tag{12}$$

where $\varphi_{i,j}^m$ satisfies (11) and

$$\begin{aligned} \varphi_{i,j}^m - \varphi_{i,j}^{m-1} = {} & R_1 \left(\varphi_{i+1,j}^m - 2\varphi_{i,j}^m + \varphi_{i-1,j}^m \right) - R_1 d_{m-1}^{(\beta)} \left(\varphi_{i+1,j}^0 - 2\varphi_{i,j}^0 + \varphi_{i-1,j}^0 \right) - R_1 \sum_{s=1}^{m-1} \left(d_{s-1}^{(\beta)} - d_s^{(\beta)} \right) \left(\varphi_{i+1,j}^{m-s} - 2\varphi_{i,j}^{m-s} + \varphi_{i,j+1}^{m-s} \right) \\ & + R_2 \left(\varphi_{i,j+1}^{m-s} - 2\varphi_{i,j}^{m-s} + \varphi_{i,j-1}^{m-s} \right) + R_2 d_{m-1}^{(\beta)} \left(\varphi_{i,j+1}^0 - 2\varphi_{i,j}^0 + \varphi_{i,j-1}^0 \right) - R_2 \sum_{s=1}^{m-1} \left(d_{s-1}^{(\beta)} - d_s^{(\beta)} \right) \left(\varphi_{i,j+1}^{m-s} - 2\varphi_{i,j}^{m-s} + \varphi_{i,j-1}^{m-s} \right) + \\ & R_3 \left(\varphi_{i+1,j}^m - 2\varphi_{i,j}^m + \varphi_{i-1,j}^m \right) + R_4 \left(\varphi_{i,j+1}^m - 2\varphi_{i,j}^m + \varphi_{i,j-1}^m \right). \end{aligned} \tag{13}$$

The error initial and boundary conditions are given as

$$\begin{aligned}\varphi_{0,j}^{m} &= \varphi_{M_1,j}^{m}\\ &= \varphi_{i,0}^{m}\\ &= \varphi_{i,M_2}^{m}\\ &= \varphi_{i,j}^{0}\\ &= 0.\end{aligned} \tag{14}$$

Define the following grid functions for $m = 1, 2 \ldots, N$:

$$\varphi^{m}(x,y) = \left\{ \begin{array}{c} \varphi_{i,j}^{m}, \text{ when } x_{i-\frac{\Delta x}{2}} < x \le x_{i+\frac{\Delta x}{2}},\ y_{j-\frac{\Delta y}{2}} < y \le y_{i+\frac{\Delta y}{2}},\\ 0, \text{when } 0 \le x \le \frac{\Delta x}{2} \text{ or } L - \frac{\Delta x}{2} \le x \le L,\\ 0, \text{when } 0 \le y \le \frac{\Delta y}{2} \text{ or } L - \frac{\Delta y}{2} \le y \le L. \end{array} \right\}. \tag{15}$$

Then, $\varphi^{m}(x,y)$ can be expanded in Fourier series such as

$$\varphi^{m}(x,y) = \sum_{l_1,l_2=-\alpha}^{\alpha} \mathrm{X}^{m}(l_1,l_2) e^{\sqrt[2]{-1}\pi\left(\frac{l_1 x}{L} + \frac{l_2 y}{L}\right)}, \tag{16}$$

where

$$\mathrm{X}^{m}(l_1,l_2) = \frac{1}{L}\int_0^L \int_0^L \varphi^{m}(x,y) e^{\sqrt[-2]{-1}\pi\left(\frac{l_1 x}{L} + \frac{l_2 y}{L}\right)} \mathrm{d}x\mathrm{d}y. \tag{17}$$

From the definition of l^2 norm and Parseval equality, we have

$$\left\|\varphi^{m}\right\|_{\alpha}^{2} = \sum_{i=1}^{M_1-1}\sum_{j=1}^{M_2-1} \Delta x \Delta y \left|\varphi_{i,j}^{m}\right|^2 = \sum_{l_1,l_2=-\alpha}^{\alpha} \left|\mathrm{X}^{m}(l_1,l_2)\right|^2. \tag{18}$$

Suppose that

$$\varphi_{i,j}^{m} = \mathrm{X}^{m} e^{\sqrt{-1}\left(\alpha_1 i\Delta x + \alpha_2 j\Delta y\right)}, \tag{19}$$

where $\alpha_1 = 2\pi l_1/L$ and $\alpha_2 = 2\pi l_2/L$, and substituting (19) in (13), we get $\mathrm{X}^{m} e^{\sqrt{-1}(\alpha_1 i\Delta x + \alpha_2 j\Delta y)} - \mathrm{X}^{m} e^{\sqrt{-1}(\alpha_1 i\Delta x + \alpha_2 j\Delta y)} = R_1 (\mathrm{X}^{m} e^{\sqrt{-1}(\alpha_1 (i+1)\Delta x + \alpha_2 j\Delta y)} - 2\mathrm{X}^{m} e^{\sqrt{-1}(\alpha_1 i\Delta x + \alpha_2 j\Delta y)} + \mathrm{X}^{m} e^{\sqrt{-1}(\alpha_1 (i-1)\Delta x + \alpha_2 j\Delta y)}) - R_1 d_{m-1}^{(\beta)} (\mathrm{X}^{0} e^{\sqrt{-1}(\alpha_1 (i+1)\Delta x + \alpha_2 j\Delta y)} - 2\mathrm{X}^{0} e^{\sqrt{-1}(\alpha_1 i\Delta x + \alpha_2 j\Delta y)} + \mathrm{X}^{0} e^{\sqrt{-1}(\alpha_1 (i-1)\Delta x + \alpha_2 j\Delta y)}) - R_1 \sum_{s=1}^{m-1} (d_{s-1}^{(\beta)} - d_{s}^{(\beta)}) (\mathrm{X}^{m-s} e^{\sqrt{-1}(\alpha_1 (i+1)\Delta x + \alpha_2 j\Delta y)} - 2\mathrm{X}^{m-s} e^{\sqrt{-1}(\alpha_1 i\Delta x + \alpha_2 j\Delta y)} + \mathrm{X}^{m-s} e^{\sqrt{-1}(\alpha_1 (i-1)\Delta x + \alpha_2 j\Delta y)}) + R_2 (\mathrm{X}^{m} e^{\sqrt{-1}(\alpha_1 i\Delta x + \alpha_2 (j+1)\Delta y)} - 2\mathrm{X}^{m} e^{\sqrt{-1}(\alpha_1 i\Delta x + \alpha_2 j\Delta y)} + \mathrm{X}^{m} e^{\sqrt{-1}(\alpha_1 i\Delta x + \alpha_2 (j-1)\Delta y)}) + R_2 d_{m-1}^{(\beta)} (\mathrm{X}^{0} e^{\sqrt{-1}(\alpha_1 i\Delta x + \alpha_2 j\Delta y)} - 2\mathrm{X}^{0} e^{\sqrt{-1}(\alpha_1 i\Delta x + \alpha_2 j\Delta y)} + \mathrm{X}^{0} e^{\sqrt{-1}(\alpha_1 i\Delta x + \alpha_2 j\Delta y)}) - R_2 \sum_{s=1}^{m-1} (d_{s-1}^{(\beta)} - d_{s}^{(\beta)}) (\mathrm{X}^{m-s} e^{\sqrt{-1}(\alpha_1 i\Delta x + \alpha_2 (j+1)\Delta y)} - 2\mathrm{X}^{m-s} e^{\sqrt{-1}(\alpha_1 i\Delta x + \alpha_2 j\Delta y)} + \mathrm{X}^{m-s} e^{\sqrt{-1}(\alpha_1 i\Delta x + \alpha_2 (j-1)\Delta y)}) + R_3 (\mathrm{X}^{m} e^{\sqrt{-1}(\alpha_1 (i+1)\Delta x + \alpha_2 j\Delta y)} - 2\mathrm{X}^{m} e^{\sqrt{-1}(\alpha_1 i\Delta x + \alpha_2 j\Delta y)} + \mathrm{X}^{m} e^{\sqrt{-1}(\alpha_1 (i-1)\Delta x + \alpha_2 j\Delta y)}) + R_4 (\mathrm{X}^{m} e^{\sqrt{-1}(\alpha_1 i\Delta x + \alpha_2 (j+1)\Delta y)} - 2\mathrm{X}^{m} e^{\sqrt{-1}(\alpha_1 i\Delta x + \alpha_2 j\Delta y)} + \mathrm{X}^{m} e^{\sqrt{-1}(\alpha_1 i\Delta x + \alpha_2 (j-1)\Delta y)})$.

After simplifying, we get

$$\begin{aligned}\mathrm{X}^{m}\left[1 + \nu_1 + \nu_2\right] &= \mathrm{X}^{m-1} + \mathrm{X}^{0} d_{m-1}^{(\beta)} \nu_1 + \nu_1 \sum_{s=1}^{m-1} \left(d_{s-1}^{(\beta)} - d_{s}^{(\beta)}\right) \mathrm{X}^{m-s},\\ \mathrm{X}^{m} &= \frac{\mathrm{X}^{m-1} + \mathrm{X}^{0} d_{m-1}^{(\beta)} \nu_1 + \nu_1 \sum_{s=1}^{m-1} \left(d_{s-1}^{(\beta)} - d_{s}^{(\beta)}\right) \mathrm{X}^{m-s}}{\left[1 + \nu_1 + \nu_2\right]},\end{aligned} \tag{20}$$

where $\nu_1 = [4R_1 \sin \alpha_1 \Delta x/2 + 4R_2 \sin \alpha_2 \Delta y/2]$ and $\nu_2 = [4R_3 \sin \alpha_1 \Delta x/2 + 4R_4 \sin \alpha_2 \Delta y/2]$.

Proposition 1. *If* X^{m} $(m = 1, 2, \ldots, N)$ *satisfies (20), then* $|\mathrm{X}^{m+1}| \le |\mathrm{X}^{0}|$.

Proof. By using mathematical induction, we take $m = 1$ in (20).

$$\mathrm{X}^{1} = \frac{\left(1 + d_{0}^{(\beta)} \nu_1\right) \mathrm{X}^{0}}{\left(1 + \nu_1 + \nu_2\right)}, \tag{21}$$

and as $\nu_1, \nu_2 \geq 0$, $b_0^{(\beta)} = 1$, then

$$\left|X^1\right| \leq \left|X^0\right|. \tag{22}$$

Now, assume that

$$\left|X^n\right| \leq \left|X^0\right|;\ n = 1, 2, \ldots, m-1, \tag{23}$$

and as $0 < \beta < 1$, from (20) and Lemma 2, we obtain

$$\begin{aligned}
\left|X^m\right| &\leq \frac{\left|X^{m-1}\right| + b_{m-1}^{(\beta)}\nu_1\left|X^0\right| + \nu_1\sum_{s=1}^{m-1}\left(d_{s-1}^{(\beta)} - d_s^{(\beta)}\right)X^{m-s}}{1+\nu_1+\nu_2}, \leq \frac{1 + d_{m-1}^{(\beta)}\nu_1 + \nu_1\sum_{s=1}^{m-1}\left(d_{s-1}^{(\beta)} - d_s^{(\beta)}\right)}{\left(1+\nu_1+\nu_2\right)}\left|X^0\right|, \\
&= \frac{1 + d_{m-1}^{(\beta)}\nu_1 + \nu_2\left(1 - d_{m-1}^{(\beta)}\right)}{\left(1+\nu_1+\nu_2\right)}\left|X^0\right|, \\
&= \frac{1+\nu_1}{1+\nu_1+\nu_2}X^0, \\
\left|X^m\right| &\leq \left|X^0\right|.
\end{aligned} \tag{24}$$

This completes the proof.

Based on the above proof, it can be summarized that the solution of (5) satisfies the following inequality:

$X^m{}_2 \leq X^0{}_2$.

And, we demonstrated that the proposed scheme is unconditionally stable. □

2.2. Convergence. Here, we use a similar method to examine the convergence of the scheme. Let $Y(x_i, y_j, t_m)$ represent the exact solution; then, the truncation error of the scheme is obtained as follows: from (3),

$$\begin{aligned}
T_{i,j}^m &= Y\left(x_i, y_j, t_m\right) - Y\left(x_i, y_j, t_{m-1}\right) - R_1\sum_{j=o}^{m-1} d_s^{(\beta)}\delta x^2\left(Y\left(x_i, y_j, t_{m-s}\right) - Y\left(x_i, y_j, t_{m-s-1}\right)\right), \\
&+ R_2\sum_{j=o}^{k-1} d_s^{(\beta)}\delta y^2\left(Y\left(x_i, y_j, t_{m-s}\right) - Y\left(x_i, y_j, t_{m-s-1}\right)\right) + R_3\delta x^2 Y\left(x_i, y_j, t_m\right) + R_4\delta y^2 Y\left(x_i, y_j, t_m\right) - \tau h\left(x_i, y_j, t_m\right).
\end{aligned} \tag{25}$$

From (1), we have

$$\begin{aligned}
T_{i,j}^m &= \frac{Y_{i,j}^m - Y_{i,j}^{m-1}}{\tau} - \frac{\partial Y\left(x_i, y_j, t_m\right)}{\partial t} + \left(\frac{\partial^2 Y\left(x_i, y_j, t_m\right)}{\partial x^2}\right) - R_1\sum_{s=0}^{m-1} d_s^{(\beta)}\delta x^2\left(Y_{i,j}^{m-s} - Y_{i,j}^{m-s-1}\right) + \left(\frac{\partial^2 Y\left(x_i, y_j, t_m\right)}{\partial y^2}\right) \\
&- R_2\sum_{s=0}^{m-1} b_s^{(\beta)}\delta y^2\left(Y_{i,j}^{m-s} - Y_{i,j}^{m-s-1}\right) + \left(\frac{\partial^2 Y\left(x_i, y_j, t_m\right)}{\partial x^2}\right) - R_3\delta x^2\left(Y_{i,j}^m\right) + \left(\frac{\partial^2 Y\left(x_i, y_j, t_m\right)}{\partial x^2}\right) - R_4\delta y^2\left(Y_{i,j}^m\right) \\
&= O(\tau + (\tau(\Delta x)) + \tau(\Delta y)).
\end{aligned} \tag{26}$$

Since $i, j, an\ d\ m$ are finite, there is a positive constant C_1, for all $i, j, an\ d\ m$, which then have

$$\left|T_{i,j}^m\right| \leq C_1(\tau + \tau(\Delta x)) + \tau(\Delta y)). \tag{27}$$

The error is defined as

$$\phi_{i,j}^m = Y\left(x_i, y_j, t_m\right) - Y_{i,j}^m. \tag{28}$$

From (25), we have

$$\begin{aligned}
Y(x_i, y_j, t_m) = {} & Y(x_i, y_j, t_{m-1}) + R_1\big(Y(x_i, y_j, t_m) - 2Y(x_i, y_j, t_m) + Y(x_i, y_j, t_m)\big) - \\
& R_1 d_{m-1}^{(\beta)}\big(\big(Y(x_{i+1}, y_j, t_0) - 2Y(x_i, y_j, t_0) + Y(x_{i-1}, y_j, t_0)\big) - \\
& R_1 \sum_{s=1}^{m-1} \big(d_{s-1}^{(\beta)} - d_s^{(\beta)}\big)\big(Y(x_{i+1}, y_j, t_{m-s}) - 2Y(x_i, y_j, t_{m-s}) - Y(x_{i-1}, y_j, t_{m-s})\big) \\
& + R_2\big(Y(x_i, y_{j+1}, t_m) - 2Y(x_i, y_j, t_m) + Y(x_i, y_{j-1}, t_m)\big) - \\
& R_2 d_{m-1}^{(\beta)}\big(\big(Y(x_i, y_{j+1}, t_m) - 2Y(x_i, y_j, t_m) + Y(x_i, y_{j-1}, t_m)\big) \\
& - R_2 \sum_{s=1}^{m-1} \big(d_{s-1}^{(\beta)} - d_s^{(\beta)}\big)\big(Y(x_i, y_{j+1}, t_{m-s}) - 2Y(x_i, y_j, t_{m-s}) + Y(x_i, y_{j-1}, t_{m-s})\big) \\
& + R_3\big(Y(x_{i+1}, y_{j+1}, t_m) - 2Y(x_i, y_{j+1}, t_m) + Y(x_{i-1}, y_{j+1}, t_m)\big) \\
& + R_4\big(Y(x_i, y_{j+1}, t_m) - 2Y(x_i, y_{j+1}, t_m) + Y(x_i, y_{j-1}, t_m)\big) + \tau h(x_i, y_j, t_m).
\end{aligned} \tag{29}$$

To obtain the error equation, subtract (29) from (5) to obtain

$$\begin{aligned}
\phi_{i,j}^m - \phi_{i,j}^{m-1} = {} & R_1\big(\phi_{i+1,j}^m - 2\phi_{i,j}^{m-1} + \phi_{i-1,j}^m\big) - R_1 d_{m-1}^{(\beta)}\big(\phi_{i+1,j}^m - 2\phi_{i,j}^{m-1} + \phi_{i-1,j}^m - R_1 \sum_{s=1}^{m-1}\big(d_{s-1}^{(\beta)} - d_s^{(\beta)}\big)\big(\phi_{i+1,j}^m - 2\phi_{i,j}^{m-1} + \phi_{i-1,j}^m\big) \\
& + R_2\big(\phi_{i,j}^m - 2\phi_{i,j}^{m-1} + \phi_{i,j}^m\big) - \\
& R_2 d_{m-1}^{(\beta)}\big(\phi_{i,j+1}^0 - 2\phi_{i,j}^0 + \phi_{i,j-1}^0\big) - R_2 \sum_{s=1}^{m-1}\big(d_{s-1}^{(\beta)} - d_s^{(\beta)}\big)\big(\phi_{i,j+1}^{m-s} 2 - \phi_{i,j}^{m-s} + \phi_{i,j-1}^{m-s}\big) + R_3\big(\phi_{i+1,j}^m - 2\phi_{i,j}^{m-1} + \phi_{i-1,j}^m\big) \\
& + R_4\big(\phi_{i,j+1}^{m-s} - 2\phi_{i,j}^{m-s} + \phi_{i,j-1}^{m-s}\big) + \tau T_{i,j}^m.
\end{aligned} \tag{30}$$

With error boundary conditions,

$$\phi_{0,j}^m = \phi_{M_1,j}^m = \phi_{0,j}^m = \phi_{i,M_2}^m = 0,\ m = 1, 2, \ldots, N. \tag{31}$$

And, the initial condition

$$\phi_{i,j}^0 = 0,\ i = 1, 2, \ldots, M_1 - 1,\ j = 1, 2, \ldots, M_2 - 1. \tag{32}$$

Next, we define the following grid functions for $m = 1, 2, \ldots, N$:

$$\phi^m(x, y) = \left\{ \begin{array}{c} \phi_{i,j}^m,\ \text{when } x_{i-\frac{\Delta x}{2}} < x \le x_{i+\frac{\Delta x}{2}},\ y_{j-\frac{\Delta y}{2}} < y \le y_{j+\frac{\Delta y}{2}}, \\ 0,\ \text{when } 0 \le x \le \frac{\Delta x}{2} \text{ or } L - \frac{\Delta x}{2} \le x \le L, \\ 0,\ \text{when} 0 \le y \le \frac{\Delta y}{2} \text{ or } L - \frac{\Delta y}{2} \le y \le L. \end{array} \right\}. \tag{33}$$

$$T^m(x,y)=\left\{\begin{array}{l} T_{i,j}^m,\ \text{when } x_{i-\frac{\Delta x}{2}}<x\le x_{i+\frac{\Delta x}{2}},\ y_{j-\frac{\Delta y}{2}}<y\le y_{j+\frac{\Delta y}{2}},\\ 0,\ \text{when } 0\le x\le \frac{\Delta x}{2}\ or\ L-\frac{\Delta x}{2}\le x\le L,\\ 0,\ \text{when } 0\le y\le \frac{\Delta y}{2}\ or\ L-\frac{\Delta y}{2}\le y\le L. \end{array}\right\}. \tag{34}$$

Here, the $\phi^m(x,y)\ an\ d\,T^m(x,y)$ can be expanded in Fourier series such as

$$\phi^m(x,y)=\sum_{l_1,l_2=-\alpha}^{\alpha}\zeta^m(l_1,l_2)e^{2\sqrt{-1}\pi\left(l_1x/L+l_2y/L\right)},\ m=1,2,\ldots,N,$$

$$T^m(x,y)=\sum_{l_1,l_2=-\alpha}^{\alpha}\varphi^m(l_1,l_2)e^{2\sqrt{-1}\pi\left(l_1x/L+l_2y/L\right)},\ m=1,2,\ldots,N, \tag{35}$$

where

$$\zeta^m(l_1,l_2)=\frac{1}{L}\int_0^L\int_0^L\phi^m(x,y)e^{2\sqrt{-1}\pi\left(\frac{l_1x}{L}+\frac{l_2y}{L}\right)}\mathrm{d}x\mathrm{d}y, \tag{36}$$

$$\varphi^m(l_1,l_2)=\frac{1}{L}\int_0^L\int_0^L\phi^m(x,y)e^{2\sqrt{-1}\pi\left(l_1x/L+l_2y/L\right)}\mathrm{d}x\mathrm{d}y. \tag{37}$$

From the definition of l^2 norm and the Parseval equality, we have

$$\left\|\phi^m\right\|_{l^2}^2=\sum_{i=1}^{M_1-1}\sum_{j=1}^{M_2-1}\Delta x\Delta y\left|e_{i,j}^m\right|=\sum_{l_1,l_2=-\alpha}^{\alpha}\left|\rho^m(l_1,l_2)\right|^2, \tag{38}$$

$$T^{m2}_{l^2}=\sum_{i=1}^{M_1-1}\sum_{j=1}^{M_2-1}\Delta x\Delta y\left|e_{i,j}^m\right|=\sum_{l_1,l_2=-\alpha}^{\alpha}\left|\varphi^m(l_1,l_2)\right|^2. \tag{39}$$

Based on the previous equations, suppose that

$$\varphi_i^m=\zeta^m e^{\sqrt{-1}\left(\alpha_1 i\Delta x+\alpha_2 i\Delta y\right)}, \tag{40}$$

$$T_i^m=\varphi^m e^{\sqrt{-1}\left(\alpha_1 i\Delta x+\alpha_2 i\Delta y\right)}. \tag{41}$$

Respectively, we have $\alpha_1=2\pi l_1/L$ and $\alpha_2=2\pi l_2/L$; substitute (40) and (41) into (30) and we get$\zeta^m e^{\sqrt{-1}(\alpha_1 i\Delta x+\alpha_2 j\Delta y)}-\zeta^m e^{\sqrt{-1}(\alpha_1 i\Delta x+\alpha_2 j\Delta y)}=R_1(\zeta^m e^{\sqrt{-1}(\alpha_1(i+1)\Delta x+\alpha_2 j\Delta y)}-2\zeta^m e^{\sqrt{-1}(\alpha_1 i\Delta x+\alpha_2 j\Delta y)}+\zeta^m e^{\sqrt{-1}(\alpha_1(i-1)\Delta x+\alpha_2 j\Delta y)})-R_1 d_{m-1}^{(\beta)}(\zeta^m e^{\sqrt{-1}(\alpha_1(i+1)\Delta x+\alpha_2 j\Delta y)}-2\zeta^m e^{\sqrt{-1}(\alpha_1 i\Delta x+\alpha_2 j\Delta y)}+\zeta^m e^{\sqrt{-1}(\alpha_1(i-1)\Delta x+\alpha_2 j\Delta y)})-R_1\sum_{s=1}^{m-1}(d_{s-1}^{(\beta)}-d_s^{(\beta)})(\zeta^m e^{\sqrt{-1}(\alpha_1(i+1)\Delta x+\alpha_2 j\Delta y)}-2\zeta^m e^{\sqrt{-1}(\alpha_1 i\Delta x+\alpha_2 j\Delta y)}+\zeta^m e^{\sqrt{-1}(\alpha_1(i-1)\Delta x+\alpha_2 j\Delta y)})+R_2(\zeta^m e^{\sqrt{-1}(\alpha_1 i\Delta x+\alpha_2(j+1)\Delta y)}-2\zeta^m e^{\sqrt{-1}(\alpha_1 i\Delta x+\alpha_2 j\Delta y)}+\zeta^m e^{\sqrt{-1}(\alpha_1 i\Delta x+\alpha_2(j-1)\Delta y)})+R_2 d_{m-1}^{(\beta)}(\zeta^m e^{\sqrt{-1}(\alpha_1 i\Delta x+\alpha_2 j\Delta y)}-2\zeta^m e^{\sqrt{-1}(\alpha_1 i\Delta x+\alpha_2 j\Delta y)}+\zeta^m e^{\sqrt{-1}(\alpha_1 i\Delta x+\alpha_2 j\Delta y)})-R_2\sum_{s=1}^{m-1}(d_{s-1}^{(\beta)}-d_s^{(\beta)})(\zeta^m e^{\sqrt{-1}(\alpha_1 i\Delta x+\alpha_2(j+1)\Delta y)}-2\zeta^m e^{\sqrt{-1}(\alpha_1 i\Delta x+\alpha_2 j\Delta y)}+\zeta^m e^{\sqrt{-1}(\alpha_1 i\Delta x+\alpha_2(j-1)\Delta y)})+R_3(\zeta^m e^{\sqrt{-1}(\alpha_1(i+1)\Delta x+\alpha_2 j\Delta y)}-2\zeta^m e^{\sqrt{-1}(\alpha_1 i\Delta x+\alpha_2 j\Delta y)}+\zeta^m e^{\sqrt{-1}(\alpha_1(i-1)\Delta x+\alpha_2 j\Delta y)})+R_4(\zeta^m e^{\sqrt{-1}(\alpha_1 i\Delta x+\alpha_2(j+1)\Delta y)}-2\zeta^m e^{\sqrt{-1}(\alpha_1 i\Delta x+\alpha_2 j\Delta y)}+\zeta^m e^{\sqrt{-1}(\alpha_1 i\Delta x+\alpha_2(j-1)\Delta y)})+\tau(\varphi^m e^{\sqrt{-1}(\alpha_1 i\Delta x+\alpha_2 j\Delta y)})$,

Simplifying the previous equation, we obtain

$$\zeta^m=\frac{\zeta^{m-1}+\zeta^0 b_{m-1}^{(\beta)}\nu_1+\nu_1\sum_{s=1}^{m-1}\left(d_{s-1}^{(\beta)}-d_s^{(\beta)}\right)\zeta^{m-s}}{\left[1+\nu_1+\nu_2\right]}, \tag{42}$$

where

$$\begin{aligned}\nu_1&=4R_1\sin\frac{\alpha_1\Delta x}{2}+4R_2\sin\frac{\alpha_2\Delta y}{2}\Big],\\ \nu_2&=4R_3\sin\frac{\alpha_1\Delta x}{2}+4R_4\sin\frac{\alpha_2\Delta y}{2}\Big].\end{aligned} \tag{43}$$

Proposition 2. *Let $\zeta^m(m=1,2,\ldots,N)$ be the solution of (42); then, there is a positive constant C_2 so that*

$$|\zeta^m|\le C_2 m\tau|\varphi^1|.$$

Proof. From $\phi^0=0$ and (36), we have

$$\zeta^o=\zeta^o(l_1,l_2)=0. \tag{44}$$

From (37) and (39), then there is a positive constant C_2, such that

$$\left|\varphi^m\right|\le C_2\left|\varphi^1(l_1,l_2)\right|. \tag{45}$$

Using mathematical induction, for $m=1$, then from (42) and (44), we obtain

$$\zeta^1=1/1+\nu_1+\nu_2\left(\tau\varphi^1\right). \tag{46}$$

Since $\nu_1,\nu_2\ge 0$, from (45), we get

$$\left|\zeta^1\right|\le\tau\left|\varphi^1\right|\le C_2\tau\left|\varphi^1\right|. \tag{47}$$

Now, suppose that

$$\left|\zeta^m\right|\le C_2 m\tau\left|\varphi^1\right|,\ n=1,2,\ldots,m-1. \tag{48}$$

As $0<\beta<1$, $\nu_1,\nu_2\ge 0$.

From (41) and (44) and Lemma 2, we have

$$
\begin{aligned}
\left|\zeta^m\right| &= \frac{|\zeta|^{m-1} + \nu_1 \sum_{s=1}^{m-1}\left(d_{s-1}^{\beta} - d_s^{\beta}\right)|\zeta|^{m-s} + \tau|\varphi|^m}{\left(1+\nu_1+\nu_2\right)},\\
\left|\zeta^m\right| &= \frac{C_2(m-1)\tau|\varphi|^1 + \nu_1 \sum_{s=1}^{m-1}\left(d_{s-1}^{\beta} - d_s^{\beta}\right)C_2(m-s)\tau|\varphi|^1 + C_2\tau|\varphi|^1}{\left(1+\nu_1+\nu_2\right)},\\
&\le \left[\frac{(m-1) + \nu_1(m-1)\sum_{s=1}^{m-1}\left(b_{s-1}^{\beta} - b_s^{\beta}\right) + 1}{\left(1+\nu_1+\nu_2\right)}\right]C_2\tau|\varphi|^1,\\
&= \left[\frac{m + \nu_1(m-1)\sum_{s=1}^{m-1}\left(b_{s-1}^{\beta} - b_s^{\beta}\right) + 1}{\left(1+\nu_1+\nu_2\right)}\right]C_2\tau|\varphi|^1,\\
&= \left[\frac{m + \nu_1(m-1) + \left(1 - b_{m-1}^{(\beta)}\right)}{\left(1+\nu_1+\nu_2\right)}\right]C_2\tau|\varphi|^1,\\
&\le mC_2\tau\left|\varphi^1\right|.
\end{aligned}
\tag{49}
$$

The proof is completed via the induction method. □

Theorem 1. *The modified implicit difference scheme l^2 is convergent, and the order of convergence is $O(\tau + \tau(\Delta x)^2 + \tau(\Delta y)^2)$.*

Proof: From (27) and (39), we obtain

$$
\begin{aligned}
T^k &\le \sqrt{M_x\Delta x}\sqrt{M_y\Delta y}\,C_1\left(\tau + \tau(\Delta x)^2 + \tau(\Delta y)^2\right) = LC_1\left(\tau + \tau(\Delta x)^2 + \tau(\Delta y)^2\right)\\
\varphi^k{}_{l^2} &\le kC_2\tau T^1 \le C_1C_2k\tau L\left(\tau + \tau\left(\Delta x^2\right) + \tau\left(\Delta y^2\right)\right).
\end{aligned}
\tag{50}
$$

As $k\tau \le T$, thus

$$
\varphi^k{}_{l^2} \le C_1C_2k\tau L\left(\tau + \tau\left(\Delta x^2\right) + \tau\left(\Delta y^2\right)\right), \tag{51}
$$

where $C = C_1C_2TL$. □

3. Numerical Experiment

Example 1. Consider the following two-dimensional Rayleigh–Stokes problem for heated generalized second-grade fluid with the fractional derivative [22]:

$$
\frac{\partial Y(x,y,t)}{\partial t} = {}_0D_t^{1-\beta}\left(\frac{\partial^2 Y(x,y,t)}{\partial x^2} + \frac{\partial Y(x,y,t)}{\partial y^2}\right) + \frac{\partial^2 Y(x,y,t)}{\partial x^2} + \frac{\partial^2 Y(x,y,t)}{\partial y^2} + h(x,y,t), 0 \le \beta \le 1,\ 0 \le t \le T, \tag{52}
$$

with initial and boundary conditions

$$
\begin{aligned}
Y(x,y,0) &= 0,\ 0 \le x,\ y \le 1,\\
Y(0,y,t) &= e^y t^{1+\beta},\ Y(1,y,t)\\
&= e^{1+y}t^{1+\beta},\\
Y(x,0,t)) &= e^x t^{1+\beta},\ Y(x,1,t)\\
&= e^{1+x}t^{1+\beta},\ 0 \le t \le T.
\end{aligned}
\tag{53}
$$

Here, $h(x,y,t) = ((1+\beta)t^{\beta} - 2\Gamma(2+\beta)/\Gamma(1+2\beta)t^{2\beta} - 2t^{1+\beta})e^{x+y}$ and the exact solution of (52) is given by

$$
Y(x,y,t) = e^{x+y}t^{1+\beta}. \tag{54}
$$

The error between the numerical solution and exact solution is defined as follows:

$$
E_{\infty} = \max_{0\le i,j\le M, 0\le m\le N}\left|Y\left(x_i,y_j,t_m\right) - Y_{i,j}^m\right|. \tag{55}
$$

And, the rate of convergence for space variable can be defined as

$$
= -\text{order} = \log_2\left(\frac{\left\|E_{\infty}(16\tau,\ 2\Delta x)\right\|}{\left\|E_{\infty}(\tau,\ \Delta x)\right\|}\right). \tag{56}
$$

Table 1: The error table for different values at $\tau, \Delta x, \Delta y$, and γ.

τ	$\Delta x = \Delta y$	$\gamma = 0.5$	$\gamma = 0.6$	$\gamma = 0.7$	$\gamma = 0.8$	$\gamma = 0.9$
1/4	1/2	$2.180E-2$	$1.316E-2$	$1.601E-2$	$1.889E-2$	$2.481E-2$
1/16	1/4	$4.573E-3$	$5.267E-3$	$5.934E-3$	$6.606E-2$	$7.312E-2$
1/64	1/8	$1.330E-3$	$1.484E-3$	$1.634E-3$	$1.789E-3$	$1.958E-3$
1/128	1/10	$7.701E-4$	$8.426E-4$	$9.141E-4$	$9.898E-4$	$1.073E-4$

Table 2: The error table for different values at $\tau, \Delta x, \Delta y$, and γ.

$\tau = \Delta x = \Delta y$	$\gamma = 0.35$	$\gamma = 0.65$	$\gamma = 0.85$
1/2	$7.9899E-3$	$2.4671E-2$	$3.8181E-2$
¼	$4.5383E-3$	$1.4258E-2$	$2.1050E-2$
1/6	$3.3873E-3$	$9.9350E-3$	$1.4272E-2$
1/8	$2.8140E-3$	$7.7703E-3$	$1.0965E-2$
1/10	$2.4289E-3$	$6.3977E-3$	$8.9159E-3$

Table 3: The error table for different values at $\tau, \Delta x, \Delta y$, and γ.

τ	$\Delta x = \Delta y$	$\gamma = 0.5$	$\gamma = 0.6$	$\gamma = 0.7$	$\gamma = 0.8$	$\gamma = 0.9$
1/16	1/4	$5.0794E-3$	$5.9521E-3$	$6.7049E-3$	0.00746352	$8.2610E-3$
1/8	1/8	$1.4043E-3$	$1.6387E-3$	$8.5596E-3$	$1.0150E-3$	$1.8575E-3$
1/144	1/12	$6.2458E-4$	$6.8873E-4$	$7.5239E-4$	$8.1996E-4$	$8.9478E-4$

Table 4: The error table for different values at $\tau, \Delta x$, and Δy and at a fixed value of $\gamma = 0.25$.

N	$\Delta x = \Delta y = 1/5$	$\Delta x = \Delta y = 1/10$	$\Delta x = \Delta y = 1/15$	$\Delta x = \Delta y = 1/20$
20	$1.9274E-3$	$9.5392E-4$	$7.6704E-4$	$7.0147E-4$
40	$1.7467E-3$	$1.6060E-3$	$5.7985E-4$	$4.3020E-4$
60	$1.6504E-3$	$6.6854E-4$	$5.4537E-4$	$3.2953E-4$

The developed modified implicit scheme is applied to problems (52) to (54).

Tables 1–4 show the errors E_∞ for values of space step size $(\Delta x, \Delta y)$ and τ. Here, time step τ is defined by $\tau = T/N$.

Tables 1–4 indicate that, as we reduce the time and space step size τ and $(\Delta x, \Delta y)$, the error decreases for a fixed value of γ.This shows that the method converges to the exact solution.

Example 2. Consider the following Cable equation:

$$\frac{\partial Y(x,t)}{\partial t} = {}_0D_t^{1-\rho_1}\left(K\frac{\partial^2 Y(x,t)}{\partial x^2}\right) - \mu^2\,{}_0D_t^{1-\rho_2}Y(x,t) + 2\left(t + \frac{\pi^2 t^{1+\rho_1}}{\Gamma(2+\rho_1)} + \frac{t^{1+\rho_2}}{\Gamma(2+\rho_2)}\right)\sin(\pi x), \tag{57}$$

with initial and boundary conditions

$$\begin{aligned} &Y(x,0) = 0,\ 0 \le x \le L,\\ &Y(0,t) = t^2\sin(\pi x), \quad Y(L,t) = \beta_2(t),\ 0 < t \le T. \end{aligned} \tag{58}$$

The exact solution is $Y(x,t) = t^2\sin(\pi x)$.

4. Results and Discussion

A modified implicit scheme is developed and applied on RSP-HGSGF. Numerical example is given to support theoretical study. The error between the exact and numerical solution is calculated using different values of N and M. Also, at different values of γ, Tables 1–4 are created to show the comparison of the numerical scheme with the exact solution in terms of maximum error. In example 2, we solved the fractional-order Cable equation, and the numerical results are shown in Table 5 for various values of space and time step size. The values of ρ_1 and ρ_2 are also changed, and the obtained results are converging with reduced step sizes. Here, the error is calculated using Maple15 software with the increase in the number of space and time steps. Figures 1–3 are plotted for different values of M and N, and fractional order γ shows good agreement with the exact solution.

Table 5: Numerical results of example 2 of the proposed scheme for various values of ρ_1, ρ_2, N, and Δx.

Δx	N	$\rho_1, \rho_2 = 0.25$	$\rho_1, \rho_2 = 0.5$	$\rho_1, \rho_2 = 0.95$
1/10	40	$1.173E-2$	$8.131E-2$	$6.552E-3$
	80	$8.032E-3$	$6.452E-3$	$5.762E-3$
	110	$5.912E-3$	$5.528E-3$	$5.171E-3$
1/20	40	$8.146E-3$	$6.312E-3$	$3.272E-3$
	80	$4.537E-3$	$2.989E-3$	$2.409E-3$
	110	$2.428E-3$	$2.015E-3$	$9.146E-4$
1/40	40	$7.294E-3$	$3.781E-3$	$2.491E-3$
	80	$3.639E-3$	$2.173E-3$	$1.591E-3$
	110	$1.578E-3$	$1.257E-3$	$9.015E-4$

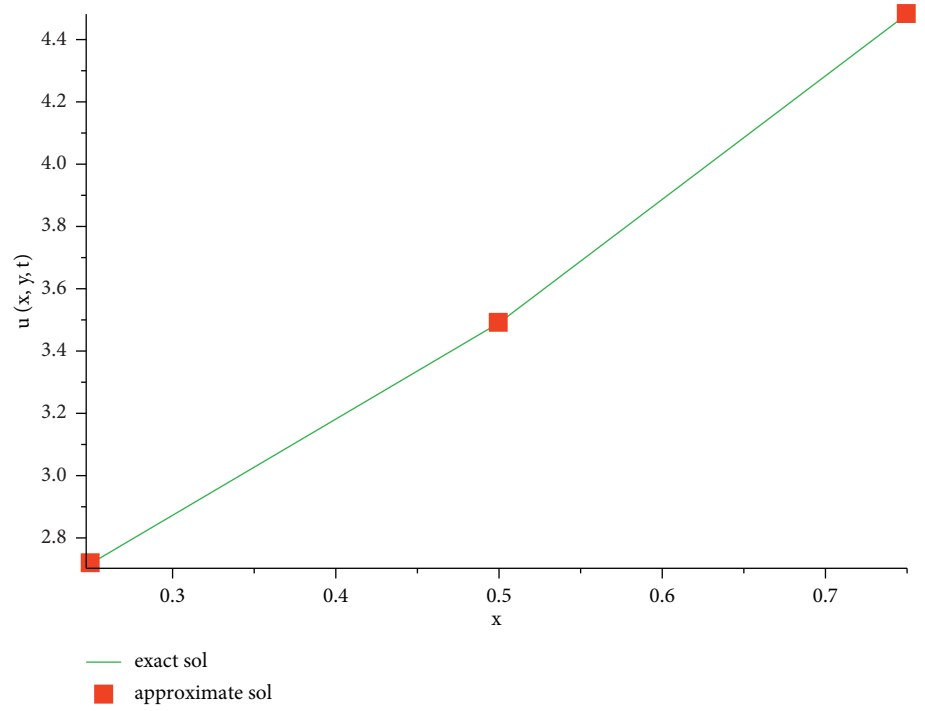

Figure 1: Comparing equations (52) and (54) at $M = 4$, $N = 2$, and $\gamma = 0.25$.

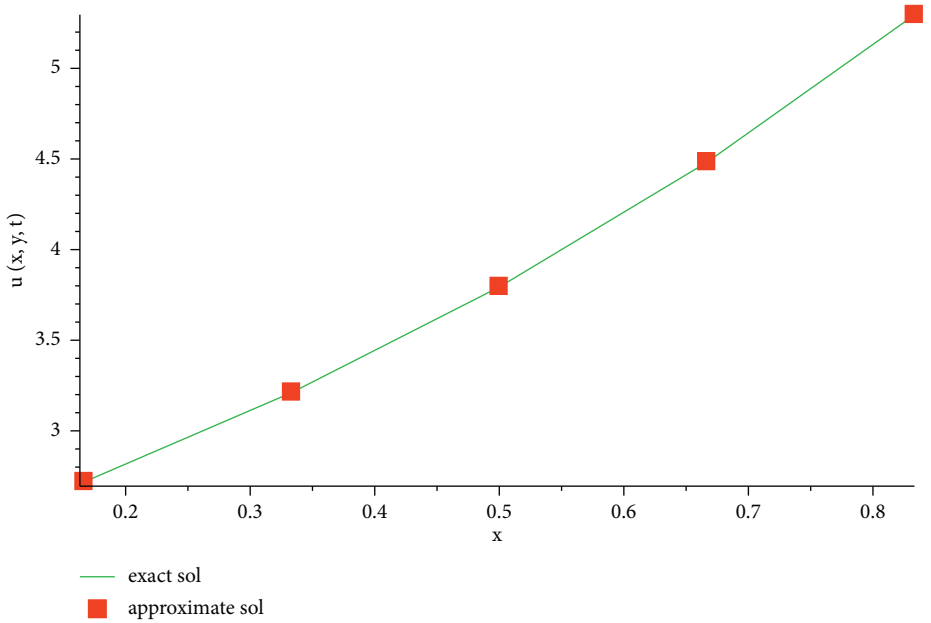

Figure 2: Comparing equations (52) and (54) at $M = 6$, $N = 6$, and $\gamma = 0.35$.

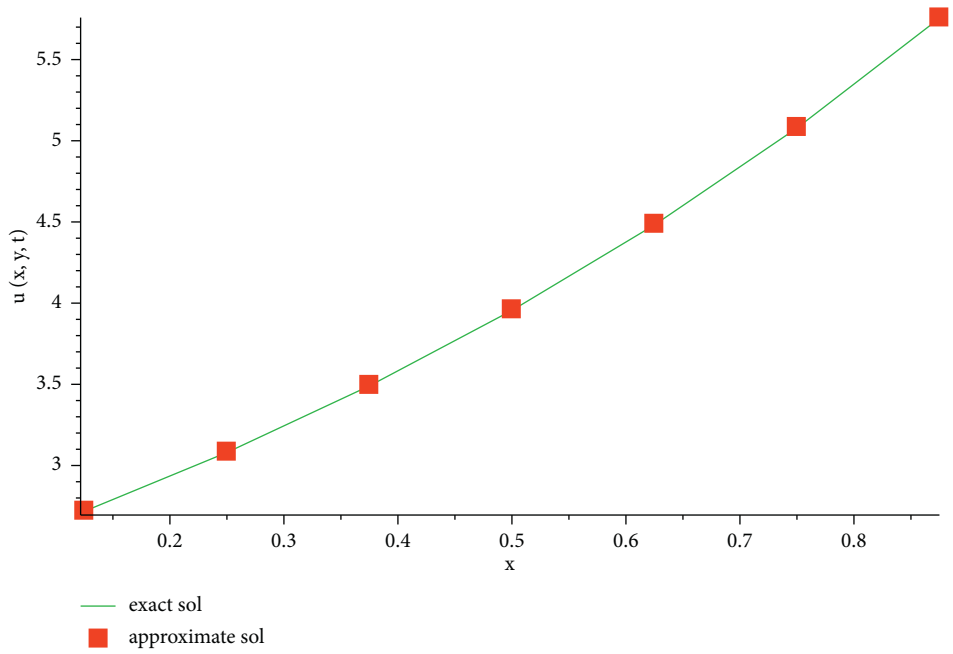

Figure 3: Comparing equations (52) and (54) at $M = 8$, $N = 8$, and $\gamma = 0.85$.

5. Conclusion

A modified implicit difference scheme is formulated for 2D RSP-HGSGF, and a derivative of fractional order has been described in this paper. The modified scheme has the improvement of low computational cost and can be easily applied. The Fourier technique has been used for the theoretical analysis stability, and convergence with order $(\tau + (\Delta x) + (\Delta y))$ is unconditionally stable and convergent. The numerical experiment for the 2D RSP-HGSGF and 1D Cable equation is conducted, which shows that the modified implicit scheme is easy to implement, and the results show good performance of the proposed schemes [39].

Abbreviations

RSP-	Rayleigh–Stokes problem for heated
HGSGF:	generalized second-grade fluid
SFP:	Stokes first problem
INAS:	Implicit numerical approximation scheme
RBF-FD:	Radial basis function finite difference
FEM:	Finite element method
2D:	Two-dimensional
RL:	Riemann–Liouville.

Data Availability

All the related materials have been cited in the paper.

Conflicts of Interest

The authors declare no conflicts of interest.

References

[1] U. Ali, A. Iqbal, M. Sohail, F. A. Abdullah, and Z. Khan, "Compact implicit difference approximation for time-fractional diffusion-wave equation," *Alexandria Engineering Journal*, vol. 61, no. 5, pp. 4119–4126, 2022.

[2] U. Ali, M. A. Khan, M. M. Khater, A. A. Mousa, and R. A. Attia, "A new numerical approach for solving 1D fractional diffusion-wave equation," *Journal of Function Spaces*, vol. 2021, Article ID 6638597, 2021.

[3] U. Ali, "Numerical Solutions for Two Dimensional Time-Fractional Differential Sub-diffusion Equation," Doctoral dissertation, Ph. D. Thesis, University Sains Malaysia, Penang, Malaysia, 2019.

[4] K. S. Miller and B. Ross, *An Introduction to the Fractional Calculus and Fractional Differential Equations*, John Wiley, New York, 1993.

[5] K. B. Oldham and J. Spanier, *Fractional Calculus*, Academic Press, New York and London, 1974.

[6] I. Podlubny, *Fractional Differential Equations*, Academic Press, New York, 1999.

[7] S. G. Samko, A. A. Kilbas, and O. I. Marichev, *Fractional Integrals and Derivaives, Theory and Applications*, Gordon and Breach Science Pub- lishers, USA, 1993.

[8] E. Shivanian and A. Jafarabadi, "Rayleigh-Stokes problem for a heated generalized second grade fluid with fractional derivatives: a stable scheme based on spectral meshless radial point interpolation," *Engineering with Computers*, vol. 34, no. 1, pp. 77–90, 2018.

[9] J. Liu, H. Li, and Y. Liu, "A new fully discrete finite difference/element ap- proximation for fractional cable equation," *J. Appl. Math. Comput.*, pp. 1–17, 2015.

[10] C. Wu, "Numerical solution for Stokes' first problem for a heated generalized second grade fluid with fractional derivative," *Applied Numerical Mathematics*, vol. 59, no. 10, pp. 2571–2583, 2009.

[11] F. Shen, W. Tan, Y. Zhao, and T. Masuoka, "The Rayleigh-Stokes problem for a heated generalized second grade fluid

with fractional derivative model," *Nonlinear Analysis: Real World Applications*, vol. 7, no. 5, pp. 1072–1080, 2006.

[12] B. Yu, X. Jiang, and H. Qi, "An inverse problem to estimate an unknown order of a Riemann-Liouville fractional derivative for a fractional Stokes' first problem for a heated generalized second grade fluid," *Acta Mechanica Sinica*, vol. 31, no. 2, pp. 153–161, 2015.

[13] C.-M. Chen, F. Liu, I. Turner, and V. Anh, "Numerical schemes and multivariate extrapolation of a two-dimensional anomalous sub-diffusion equation," *Numerical Algorithms*, vol. 54, no. 1, pp. 1–21, 2010.

[14] F. Liu, Q. Yang, and I. Turner, "Two new implicit numerical methods for the fractional cable equation," *Journal of Computational and Nonlinear Dynamics*, vol. 6, no. 1, 7 pages, 2014.

[15] B. Yu, X. Jiang, and H. Qi, "An inverse problem to estimate an unknown order of a Riemann-Liouville fractional derivative for a fractional Stocks' first problem for a heated generalized second grade fluid," *Acta Mechanica Sinica*, vol. 31, no. 2, pp. 153–161, 2015.

[16] C. M. Chen, F. Liu, V. Anh, and I. Turner, "Numerical methods for solving a two-dimensional variable-order anomalous subdiffusion equation," *Mathematics of Computation*, vol. 277, no. 81, pp. 345–366, 2011.

[17] M. C. Chen, F. Liu, I. Turner, and V. Anh, "Numerical methods with fourth-order spatial accuracy for variable-order nonlinear Stokes' first problem for a heated generalized second grade fluid," *Computers & Mathematics with Applications*, vol. 62, no. 3, pp. 971–986, 2013.

[18] M. Dehghan and M. Abbaszadeh, "A finite element method for the numerical solution of Rayleigh-Stokes problem for a heated generalized second grade fluid with fractional derivatives," *Engineering with Computers*, vol. 33, no. 3, pp. 587–605, 2017.

[19] O. Nikan and Z. Avazzadeh, "An improved localized radial basis-pseudospectral method for solving fractional reaction-subdiffusion problem," *Results in Physics*, vol. 23, Article ID 104048, 2021.

[20] S. Zhai, X. Feng, and Y. He, "An unconditionally stable compact ADI method for three-dimensional time-fractional convection-diffusion equationiffusion equation," *Journal of Computational Physics*, vol. 269, pp. 138–155, 2014.

[21] C. M. Chen, F. Liu, K. Burrage, and Y. Chen, "Numerical method of the variable-order Rayleigh-Stocks' problem for a heated generalized second grade fluid with fractional derivative," *IMA Journal of Applied Mathematics*, pp. 1–21, 2005.

[22] W. Chunhong, "Numerical solution for Stocks' first problem for a heated generalized second grade fluid with fractional derivative," *Applied Numerical Mathematics*, vol. 59, pp. 2571–2583, 2009.

[23] Z. Guan, X. Wang, and J. Ouyang, "An improved finite difference/finite element method for the fractional Rayleigh–Stokes problem with a nonlinear source term," *Journal of Applied Mathematics and Computing*, vol. 65, no. 1, pp. 451–479, 2021.

[24] U. Ali, F. A. Abdullah, and S. T. Mohyud-Din, "Modified implicit fractional difference scheme for 2D modified anomalous fractional sub-diffusion equation," *Advances in Difference Equations*, vol. 2017, no. 1, pp. 1–14, 2017.

[25] E. Bazhlekova, B. Jin, R. Lazarov, and Z. Zhou, "An analysis of the Rayleigh-Stokes problem for a generalized second-grade fluid," *Numerische Mathematik*, vol. 131, no. 1, pp. 1–31, 2015.

[26] A. Mohebbi, M. Abbaszadeh, and M. Dehghan, "Compact finite difference scheme and RBF meshless approach for solving 2D Rayleigh-Stokes problem for a heated generalized second grade fluid with fractional derivatives," *Computer Methods in Applied Mechanics and Engineering*, vol. 264, pp. 163–177, 2013.

[27] Z.-Z. Sun and X. Wu, "A fully discrete difference scheme for a diffusion-wave system," *Applied Numerical Mathematics*, vol. 56, no. 2, pp. 193–209, 2006.

[28] O. Nikan, Z. Avazzadeh, and J. A. T. Machado, "Numerical study of the nonlinear anomalous reaction-subdiffusion process arising in the electroanalytical chemistry," *Journal of Computational Science*, vol. 53, Article ID 101394, 2021.

[29] O. Nikan, Z. Avazzadeh, and J. T. Machado, "A local stabilized approach for approximating the modified time-fractional diffusion problem arising in heat and mass transfer," *Journal of Advanced Research*, vol. 32, 2021.

[30] O. Nikan, Z. Avazzadeh, and J. A. Tenreiro Machado, "Numerical investigation of fractional nonlinear sine-Gordon and Klein-Gordon models arising in relativistic quantum mechanics," *Engineering Analysis with Boundary Elements*, vol. 120, pp. 223–237, 2020.

[31] F. Liu, P. Zhuang, Q. Liu, M. Zheng, and V. V. Anh, "Fractional-order systems, numerical techniques, and applications: finite element and spectral methods for multiterm time-and time-space fractional dynamic systems and applications," *In Fractional Order Systems*, Academic Press, vol. 1, pp. 179–256, 2022.

[32] H. Ahmad, A. R. Seadawy, A. H. Ganie, S. Rashid, T. A. Khan, and H. Abu-Zinadah, "Approximate Numerical solutions for the nonlinear dispersive shallow water waves as the Fornberg–Whitham model equations," *Results in Physics*, vol. 22, Article ID 103907, 2021.

[33] M. N. Khan, I. Hussain, I. Ahmad, and H. Ahmad, "A local meshless method for the numerical solution of space-dependent inverse heat problems," *Mathematical Methods in the Applied Sciences*, vol. 44, no. 4, pp. 3066–3079, 2021.

[34] F. M. Salama, N. N. A. Hamid, N. N. A. Hamid, and N. H. M. Ali, "An efficient modified hybrid explicit group iterative method for the time-fractional diffusion equation in two space dimensions," *AIMS Mathematics*, vol. 7, no. 2, pp. 2370–2392, 2022.

[35] A. Ali and N. H. M. Ali, "On skewed grid point iterative method for solving 2D hyperbolic telegraph fractional differential equation," *Advances in Difference Equations*, vol. 2019, no. 1, pp. 1–29, 2019.

[36] S. Patnaik and F. Semperlotti, "A generalized fractional-order elastodynamic theory for non-local attenuating media," *Proceedings of the Royal Society A*, vol. 476, no. 2238, Article ID 20200200, 2020.

[37] S. Patnaik, M. Jokar, and F. Semperlotti, "Variable-order Approach to Nonlocal Elasticity: Theoretical Formulation, Order Identification via Deep Learning, and Applications," *Computational Mechanics*, pp. 1–32, 2021.

[38] W. Sumelka, "Fractional viscoelasticity," *Mechanics Research Communications*, vol. 56, pp. 31–36, 2014.

[39] O. Nikan and Z. Avazzadeh, "An improved localized radial basis-pseudospectral method for solving fractional reaction-subdiffusion problem," *Results in Physics*, vol. 23, Article ID 104048, 2021.

Hindawi
Mathematical Problems in Engineering
Volume 2022, Article ID 8208342, 11 pages
https://doi.org/10.1155/2022/8208342

Research Article

Energy Transport and Effectiveness of Thermo-Sloutal Time's Relaxation Theory in Carreau Fluid with Variable Mass Diffusivity

Muhammad Irfan,[1] **Muhammad Shoaib Anwar**,[2] **Humara Sardar**,[3] **Masood Khan**,[4] **and Waqar Azeem Khan**[5,6]

[1]*Department of Mathematical Sciences Federal Urdu University of Arts, Sciences & Technology, Islamabad 44000, Pakistan*
[2]*Department of Mathematics, University of Jhang, Jhang 35200, Pakistan*
[3]*Department of Mathematics, Rawalpindi Women University 6th Road, Satellite Town, Rawalpindi, Punjab 46300, Pakistan*
[4]*Department of Mathematics, Quaid-I-Azam University, Islamabad 44000, Pakistan*
[5]*Nonlinear Analysis and Applied Mathematics (NAAM) Research Group Department of Mathematics Faculty of Science King AbdulAziz University, Jeddah 21589, Saudi Arabia*
[6]*Department of Mathematics, Mohi-ud-Din Islamic University, Nerian Sharif, Islamabad, Azad Jammu & Kashmir 12010, Pakistan*

Correspondence should be addressed to Muhammad Irfan; muhammad.irfan@uow.edu.pk

Received 21 November 2021; Revised 27 February 2022; Accepted 8 March 2022; Published 18 April 2022

Academic Editor: Yong Aaron Tan

Two different frames' temperature creates thermal transport that gives advantage in energy fabrication in the power sector, burning in microscopic devices, and for remedy transport through heat transfer in materials. Here the article scrutinizes the transport of head utilizing the thermo-sloutal time's relaxation, and aspects of non-Fick's flux with variable conductivity and mass diffusivity in Carreau fluid have been elaborated. The magnetic aspect is also examined in a bidirectional stretched surface. The numerical procedure of ODEs via bvp4c method has been aimed at the solutions of influential parameters. The portrayal of influential factors is also presented. The intensifying behavior has been noted on concentration and temperature scattering when inconsistent thermal conductivity and variable mass diffusivity boost up. Furthermore, the temperature and concentration relaxation times are incorporated for the better understanding of the flow problem. The assessments of current article with former literature are also presented for the endorsement of outcomes.

1. Introduction

Throughout the past years, it has been noticed that many substances of industrial importance, particularly of multiphase behavior like polymeric melts, foams, emulsions, suspensions, dispersions, and slurries do not validate the Newtonian law of viscosity. In the literature, such fluids are named as, non-Newtonian liquids, nonlinear liquids, and rheological complex liquids. In non-Newtonian fluids [1–10], the apparent viscosity is not persistent and is a function of shear rate, and shear stress. In fact, under suitable conditions, the apparent viscosity of nonlinear materials is a function of kinematic history of fluid elements, flow geometry and shear rate. Non-Newtonian models come into play when major variations in the shear rate of fluid elements. Various rheological models had been considered to cater the behavior of non-Newtonian materials. In 1972, Carreau suggested the Carreau fluid model; for instance see Carreau [11] and Carreau et al. [12]. It remains with this physical model that the viscosity can be characterized for a boundless shear rates range. Carreau fluid viscosity is considered as a function of shear rate, infinite shear rate, relaxation time, power law index, and zero shear rates. Pantokratoras [13] elucidated a particular Carreau model with the help of controlling number "n." For, $0 < n < 1$, fluid behavior is considered as shear-thinning, shear-thickening

for $n > 1$, and for $n = 1$, Newtonian. So, the Carreau fluid acts as the classical Newtonian fluid at smaller values of shear rate and power law fluid at larger values of shear rate. Recently, Salahuddin [14] considered the numerical solutions of Carreau fluid flow and the flow was generated by the stretching cylinder. Transport mechanism in MHD nano-Carreau fluid flow with microorganism's gyrotactic flow was discussed by Elayarani et al. [15].

In literature, analysis of transport mechanisms in the Carreau fluid flow mainly considered classical Fourier equations for heat and mass distributions. Classical Fourier equations are parabolic equations that lead to a paradox of heat and mass flux, i.e. an initial contribution of energy and concentration delivers an immediate experience by a whole system. The paradox was addressed by Cattaneo [16] with the addition of relaxation time. Christov [17] contributed to the theory of Cattaneo with the introduction of Oldroyd, an upper-convected derivative in place of an unsteady rate of change. So in this article, instead of classical Fourier equations we have adopted the Cattaneo–Christov transport mechanism for standard Carreau fluid flow. Reddy and Kumar [18] analyzed the stream line study of heat transfer in micro-polar fluid flow above a melting boundary. Ibrahim and Gadisa [19] discussed the simulations for transfer of heat in convective Oldroyd-B fluid flow using Finite Element Method (FEM). Flow was generated by a stretching sheet with heat absorption. Utilizing the theory of Cattaneo-Christov numerous researchers have analyzed these aspects in diverse models [20–24].

Here disclose the properties of thermo-sloutal time's relaxation in 3D magneto Carreau fluid considering variable mass diffusivity and variable conductivity. The existent Carreau fluid model is proficient in describing the phenomena of shear thinning and shear thickening. The blood flow via tapered arteries with stenosis is the noteworthy application of Carreau fluid. Moreover, blood flow via tapered arteries with stenosis has fascinated the consideration of numerous researchers. Because flows via arteries pose grave healthiness threats and are a foremost reason of humanity and sickness in the technologically advanced domain. Reduction of an artery, or stenosis, can outcome from considerable plaque pledge, and possibly will reason a severe decline in blood flow. The plaques possibly will also be disrupted off into elements, or emboli, which might be lodged in an artery downstream. In intellectual arteries the threat of embolism is that the cracked spots are passed into the brain, frustrating neurological indications or a stroke. The impacts of numerous factors are examined graphically. Additionally, assessment tables via limiting sense with (bvp4c) and analytically (HAM) are reported.

2. Development of Physical Model

2.1. Rheological Models. The reported Carreau fluid model has the following Cauchy stress tensor (τ^*):

$$\tau^* = -pI + \mu(\dot{\gamma})A_1, \tag{1}$$

with

$$\mu(\dot{\gamma}) = (\mu_0 - \mu_\infty)\left[1 + (\Gamma\dot{\gamma})^2\right]^{n-1/2} + \mu_\infty, \text{and } \dot{\gamma} = \sqrt{\frac{1}{2}tr\left(A_1^2\right)}. \tag{2}$$

Now considering $\mu_\infty \ll \mu_0$ and $\mu_\infty = 0$, we have

$$\tau^* = -pI + \mu_0\left[1 + (\Gamma\dot{\gamma})^2\right]^{n-1/2}A_1. \tag{3}$$

The stress components are reported to be

$$\begin{aligned}
\tau^*_{xx} &= \mu_0\left[1 + (\Gamma\dot{\gamma})^2\right]^{n-1/2}\left(2\frac{\partial u}{\partial x}\right),\\
\tau^*_{yy} &= \mu_0\left[1 + (\Gamma\dot{\gamma})^2\right]^{n-1/2}\left(2\frac{\partial v}{\partial y}\right),\\
\tau^*_{zz} &= \mu_0\left[1 + (\Gamma\dot{\gamma})^2\right]^{n-1/2}\left(2\frac{\partial w}{\partial z}\right),\\
\tau^*_{xy} &= \tau^*_{yx} = \mu_0\left[1 + (\Gamma\dot{\gamma})^2\right]^{n-1/2}\left(\frac{\partial v}{\partial x} + \frac{\partial u}{\partial y}\right),\\
\tau^*_{xz} &= \tau^*_{zx} = \mu_0\left[1 + (\Gamma\dot{\gamma})^2\right]^{n-1/2}\left(\frac{\partial w}{\partial x} + \frac{\partial u}{\partial z}\right),\\
\tau^*_{yz} &= \tau^*_{zy} = \mu_0\left[1 + (\Gamma\dot{\gamma})^2\right]^{n-1/2}\left(\frac{\partial w}{\partial y} + \frac{\partial v}{\partial z}\right).
\end{aligned} \tag{4}$$

2.2. Problem Description. Here examine the characteristics of inconsistent thermal conductivity and variable diffusivity of mass in Carreau fluid flow to bidirectional stretched surface. Velocities of the fluid in x–and y–directions are reflected to be $u = ax$ and along the vertical direction $v = by$; where a, $b > 0$ and occurrence of flow exists in area $z > 0$ see Figure 1. The non-Fick's mass, and non-Fourier's heat fluxes scheme considering magnetic influence have been studied. These norm yields the following Carreau fluid equations [2, 3, 5]:

$$\frac{\partial u}{\partial x} + \frac{\partial v}{\partial y} + \frac{\partial w}{\partial z} = 0,$$

$$u\frac{\partial u}{\partial x} + v\frac{\partial u}{\partial y} + w\frac{\partial u}{\partial z} + \frac{\sigma B_0^2 u}{\rho_f} - \nu\frac{\partial^2 u}{\partial z^2}\left[1 + \Gamma^2\left(\frac{\partial u}{\partial z}\right)^2\right]^{\frac{n-1}{2}} + \nu\Gamma^2(n-1)\left[1 + \Gamma^2\left(\frac{\partial u}{\partial z}\right)^2\right]^{\frac{n-3}{2}}\left(\frac{\partial u}{\partial z}\right)^2\left(\frac{\partial^2 u}{\partial z^2}\right) = 0,$$

$$u\frac{\partial v}{\partial x}+v\frac{\partial v}{\partial y}+w\frac{\partial v}{\partial z}+\frac{\sigma B_0^2 v}{\rho_f}-\nu\frac{\partial^2 v}{\partial z^2}\left[1+\Gamma^2\left(\frac{\partial v}{\partial z}\right)^2\right]^{\frac{n-1}{2}}+\nu\Gamma^2(n-1)\left[1+\Gamma^2\left(\frac{\partial v}{\partial z}\right)^2\right]^{\frac{n-3}{2}}\left(\frac{\partial v}{\partial z}\right)^2\left(\frac{\partial^2 v}{\partial z^2}\right)=0,$$

$$u\frac{\partial T}{\partial x}+v\frac{\partial T}{\partial y}+w\frac{\partial T}{\partial z}-\frac{1}{(\rho c)_f}\frac{\partial}{\partial z}\left(K(T)\frac{\partial T}{\partial z}\right)+\Gamma_T\left[\begin{array}{l}u^2\dfrac{\partial^2 T}{\partial x^2}+2uv\dfrac{\partial^2 T}{\partial x\,\partial y}+u\dfrac{\partial u}{\partial x}\dfrac{\partial T}{\partial x}+u\dfrac{\partial v}{\partial x}\dfrac{\partial T}{\partial y}+u\dfrac{\partial w}{\partial x}\dfrac{\partial T}{\partial z}\\ +v^2\dfrac{\partial^2 T}{\partial y^2}+2vw\dfrac{\partial^2 T}{\partial y\,\partial z}+v\dfrac{\partial u}{\partial y}\dfrac{\partial T}{\partial x}+v\dfrac{\partial v}{\partial y}\dfrac{\partial T}{\partial y}+v\dfrac{\partial w}{\partial y}\dfrac{\partial T}{\partial z}\\ +w^2\dfrac{\partial^2 T}{\partial z^2}+2uw\dfrac{\partial^2 T}{\partial x\,\partial z}+w\dfrac{\partial u}{\partial z}\dfrac{\partial T}{\partial x}+w\dfrac{\partial v}{\partial z}\dfrac{\partial T}{\partial y}+w\dfrac{\partial w}{\partial z}\dfrac{\partial T}{\partial z}\end{array}\right]=0,$$

$$u\frac{\partial C}{\partial x}+v\frac{\partial C}{\partial y}+w\frac{\partial C}{\partial z}-\frac{\partial}{\partial z}\left(D(C)\frac{\partial C}{\partial z}\right)+\Gamma_C\left[\begin{array}{l}u^2\dfrac{\partial^2 C}{\partial x^2}+2uv\dfrac{\partial^2 C}{\partial x\,\partial y}+u\dfrac{\partial u}{\partial x}\dfrac{\partial C}{\partial x}+u\dfrac{\partial v}{\partial x}\dfrac{\partial C}{\partial y}+u\dfrac{\partial w}{\partial x}\dfrac{\partial C}{\partial z}\\ +v^2\dfrac{\partial^2 C}{\partial y^2}+2vw\dfrac{\partial^2 C}{\partial y\,\partial z}+v\dfrac{\partial u}{\partial y}\dfrac{\partial C}{\partial x}+v\dfrac{\partial v}{\partial y}\dfrac{\partial C}{\partial y}+v\dfrac{\partial w}{\partial y}\dfrac{\partial C}{\partial z}\\ +w^2\dfrac{\partial^2 C}{\partial z^2}+2uw\dfrac{\partial^2 C}{\partial x\,\partial z}+w\dfrac{\partial u}{\partial z}\dfrac{\partial C}{\partial x}+w\dfrac{\partial v}{\partial z}\dfrac{\partial C}{\partial y}+w\dfrac{\partial w}{\partial z}\dfrac{\partial C}{\partial z}\end{array}\right]=0,\tag{5}$$

$$U_w(x)=u=ax, V_w(y)=v=by, w=0, T=T_w, C=C_w \text{ at } z=0,$$

$$u\longrightarrow 0, v\longrightarrow 0, w\longrightarrow 0, T\longrightarrow T_\infty, C\longrightarrow C_\infty, \text{as} z\longrightarrow\infty.$$

The variable aspect of thermal conductivity $K(T)$ and mass diffusivity $D(C)$, respectively, elaborated as

$$K(T)=k_1\left(1+\varepsilon_1\frac{T-T_\infty}{\Delta T}\right),\quad D(C)=k_2\left(1+\varepsilon_2\frac{C-C_\infty}{\Delta C}\right).\tag{6}$$

2.3. Appropriate Transformations. Letting

$$u=axf'(\eta),\quad v=ayg'(\eta),\quad w=-\sqrt{a\nu}[f(\eta)+g(\eta)],\quad \theta(\eta)=\frac{T-T_\infty}{T_w-T_\infty},\quad \phi(\eta)=\frac{C-C_\infty}{C_w-C_\infty},\quad \eta=z\sqrt{\frac{a}{\nu}}.\tag{7}$$

(6) and (7) yield the following expressions:

$$f'''\left[1+We_1^2f''^2\right]^{n-3/2}\left[1+nWe_1^2f''^2\right]-f'^2+f''(f+g)+M^2f'=0.\tag{8}$$

$$g'''\left[1+We_2^2g''^2\right]^{n-3/2}\left[1+nWe_2^2g''^2\right]-g'^2+g''(f+g)+M^2g'=0.\tag{9}$$

$$(1+\varepsilon_1\theta)\theta''+\varepsilon_1\theta'^2+\Pr(f+g)\theta'-\Pr\delta_T\left[(f+g)(f'+g')\theta'+(f+g)^2\theta''\right]=0.\tag{10}$$

$$(1+\varepsilon_2\phi)\phi\prime'+\varepsilon_2\phi'^2+Sc(f+g)\phi\prime-Sc\delta_C\left[(f+g)(f'+g')\phi\prime+(f+g)^2\phi\prime'\right]=0.\tag{11}$$

$$f(0)=0,\quad g(0)=0,\quad f'(0)=1,\quad g'(0)=\alpha,\quad \theta(0)=1,\quad \phi(0)=1.\tag{12}$$

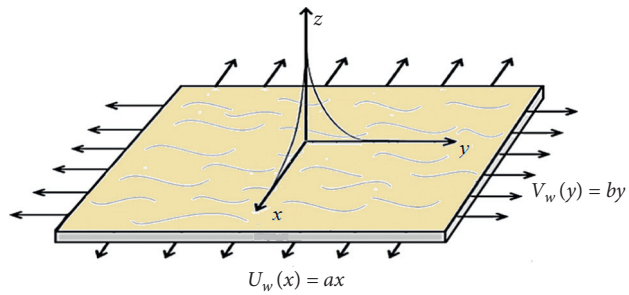

Figure 1: Flow configuration and coordinate system.

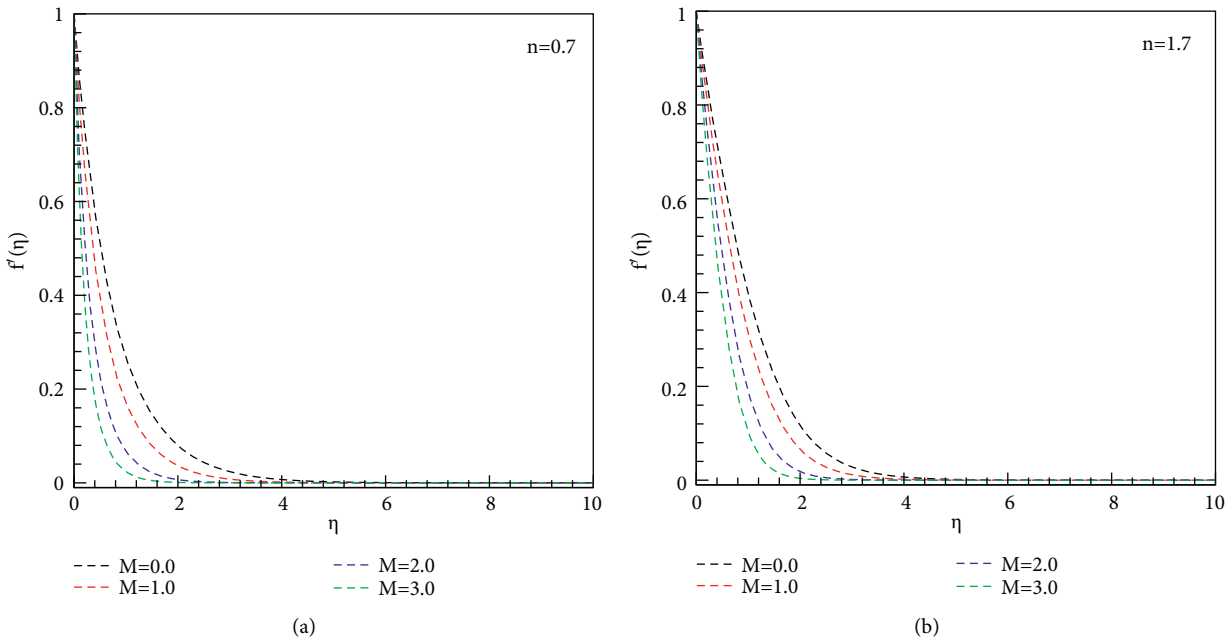

Figure 2: (a, b) Plot of η vs. $f'(\eta)$ for M.

$$f' \longrightarrow 0, \quad g' \longrightarrow 0, \quad \theta \longrightarrow 0, \quad \phi \longrightarrow 0, \quad as \quad \eta \longrightarrow \infty. \tag{13}$$

Here, $(We_1, We_2) = (\sqrt{\Gamma^2 a U_w^2/\nu}, \sqrt{\Gamma^2 a v_w^2/\nu})$ signify the local Weissenberg numbers, $M\,(= \sigma B_0^2/\rho_f a)$ magnetic field, $(\delta_T, \delta_C) = (a\Gamma_T, a\Gamma_C)$ thermal and concentration relaxation time factors, $\alpha\,(= b/a)$ ratio of stretching rates factor, and $Sc\,(= \nu/D)$ the Schmidt number and.

3. Physical Amounts

3.1. The Coefficients of Skin Friction C_{fx} and C_{fy}. The quantities of this interest are

$$C_{fx} = \frac{\tau_{xz}}{1/2\rho U_w^2} \quad \text{and} \quad C_{fy} = \frac{\tau_{yz}}{1/2\rho U_w^2}. \tag{14}$$

Dimensionless form of the above equation:

$$\frac{1}{2} C_{fx} \mathrm{Re}_x^{1/2} = f''(0)\left[1 + We_1^2 f''^2(0)\right]^{n-1/2},$$
$$\frac{1}{2}\left(\frac{U_w}{V_w}\right) C_{fy} \mathrm{Re}_x^{1/2} = g''(0)\left[1 + We_2^2 g''^2(0)\right]^{n-1/2}. \tag{15}$$

Here, $Re_x = ax^2/\nu$ stands for Reynolds number.

4. Numerical Approach (bvp4c)

The numerical procedure of ODEs via bvp4c method has been disclosed here by discretize procedure and we revise the equations (8)–(13) into first-order differential systems:

$$f = p_1, f' = p_2, f'' = p_3, f''' = p_3', g = p_4, g' = p_5, g'' = p_6, g''' = p_6', \theta = p_7, \theta' = p_8, \theta'' = p_8', \phi = p_9, \phi\prime = y_{10}, \phi'' = p_{10}',$$

$$p_3' = \frac{-(p_1 + p_4)p_3 + p_2^2 - M^2 p_2}{\Omega_1}; \quad \Omega_1 = \left(1 + nWe_1^2 p_3^2\right) * \left(1 + We_1^2 p_3^2\right)^{\frac{n-3}{2}},$$

$$p_6' = \frac{-(p_1 + p_4)p_6 + p_5^2 - M^2 p_5}{\Omega_2}; \quad \Omega_2 = \left(1 + nWe_2^2 p_6^2\right) * \left(1 + We_2^2 p_6^2\right)^{\frac{n-3}{2}} \tag{16}$$

$$p_8' = \frac{-\Pr(p_1 + p_4)p_8 - \varepsilon_1 p_8^2 + \Pr\delta_T[(p_1 + p_4)(p_2 + p_5)p_8]}{\Omega_3}; \Omega_3 = (1 + \varepsilon_1 p_7) - \Pr\delta_T(p_1 + p_4)^2,$$

$$p_{10}' = \frac{-Sc(p_1 + p_4)p_{10} + Sc\delta_C[(p_1 + p_4)(p_2 + p_5)p_{10}]}{\Omega_4}; \Omega_4 = (1 + \varepsilon_2 p_9) - Sc\delta_C(p_1 + p_4)^2,$$

$$p_1(0) = 0, p_2(0) = 1, p_2(\infty) = 0; p_4(0) = 0, p_5(0) = \alpha, p_5(\infty) = 0; p_7(0) = 1, p_7(\infty) = 0; p_9(0) = 1, p_9(\infty) = 0.$$

5. Analysis of Results

Here, variable aspects of mass diffusivity and thermal conductivity considering non-Fick's mass, and non-Fourier's heat and fluxes have been studied with magnetic properties. Here $\Gamma_T = \Gamma_C = 0.1, \varepsilon_1 = \varepsilon_2 = 0.4$, $M = \alpha = 0.5$, $\Pr = Sc = 1.5, We_1 = We_2 = 2.5$ have been stated fixed values excepting particular in graphs for $n = 0.7$ and $n = 1.7$.

5.1. Velocity $f\prime(\eta)$ for M. Figures 2(a) and 2(b) determine the performance of magnetic factor M on velocity component $f\prime(\eta)$. The higher M falloff the velocity component for both cases $(n = 0.7)$ and $(n = 1.7)$. Physically, higher magnetic field creates a body force named as Lorentz force, which faces the fluid gesture and, therefore, it diminishes the fluid independence of movement. Consequently, when magnetic flux growths, the retardation force rises and this struggle existing to the flow is accountable for diminishing the liquid velocity.

5.2. Temperature $\theta(\eta)$ for M, ε_1, Pr, and Γ_T. Figures 3(a), 3(b), 4(a), and 4(b) envision the plots of magnetic factor M and variable conductivity factor ε_1 on Carreau fluid temperature scattering. Here noted that $\theta(\eta)$ intensifies when M and ε_1 enhances. When M increases, the Carreau fluid temperature rises and similar performance is acknowledged for ε_1. When M intensify the Lorentz force improves which form additional struggle to the liquid motion to convert the energy into heat. This information reasons to the intensifying of $\theta(\eta)$. Significantly, $\theta(\eta)$ growths for augmenting values of ε_1 as a consequence of enormous heat transport amount from the sheet to the solid and as a result the $\theta(\eta)$ boosts up.

Figures 5(a), 5(b), 6(a), and 6(b) explore temperature of the Carreau fluid with the values of the Prandtl number Pr and the thermo relaxation factor Γ_T which falloff $\theta(\eta)$. The Carreau fluid temperature decays for larger Pr. As thermal diffusivity and Pr have differing relationship, this fact decays $\theta(\eta)$. When $\Pr \gg 1$, the momentum diffusivity controls the performance; however, $\Pr \ll 1$, the thermal diffusivity controls. Furthermore, Γ_T decline $\theta(\eta)$. Physically, the fluid material needs an extra interval for heat transportation to its neighboring fundamentals which improves the gradient of temperature. Hence, $\theta(\eta)$ decay for Γ_T.

5.3. Concentration $\phi(\eta)$ for Γ_C, ε_2, and Sc. The portrayals of Figures 7(a) and 7(b) along with Figures 8(a) and 8(b) scrutinize performance of mass relaxation factor Γ_C and mass diffusivity ε_2 concentration field. The field of concentration, $\phi(\eta)$ decays for Γ_C; but, enhances for ε_2. Here conflicting enactments have been noted for Γ_C and ε_2 for both values of $(n = 0.7)$ and $(n = 1.7)$. When Γ_C raised the concentration field falls. Physically, the mass relaxation time factor is high and liquid elements need much time to diffuse when Γ_C enhancing which display declining behavior of $\phi(\eta)$. The advanced mass diffusivity factor increases the mass diffusivity which causes the higher mass transportation. Therefore $\phi(\eta)$ intensifies. The performance of Schmith number Sc for the values of $(n = 0.7)$ and $(n = 1.7)$ has been examined in Figures 9(a) and 9(b) on concentration. The solute of Carreau fluid decays for intensifying Sc. Physically, Sc is the relation between mass and momentum diffusivities. When Sc upturned, the mass diffusivity falls off. Therefore, the concentration field declines.

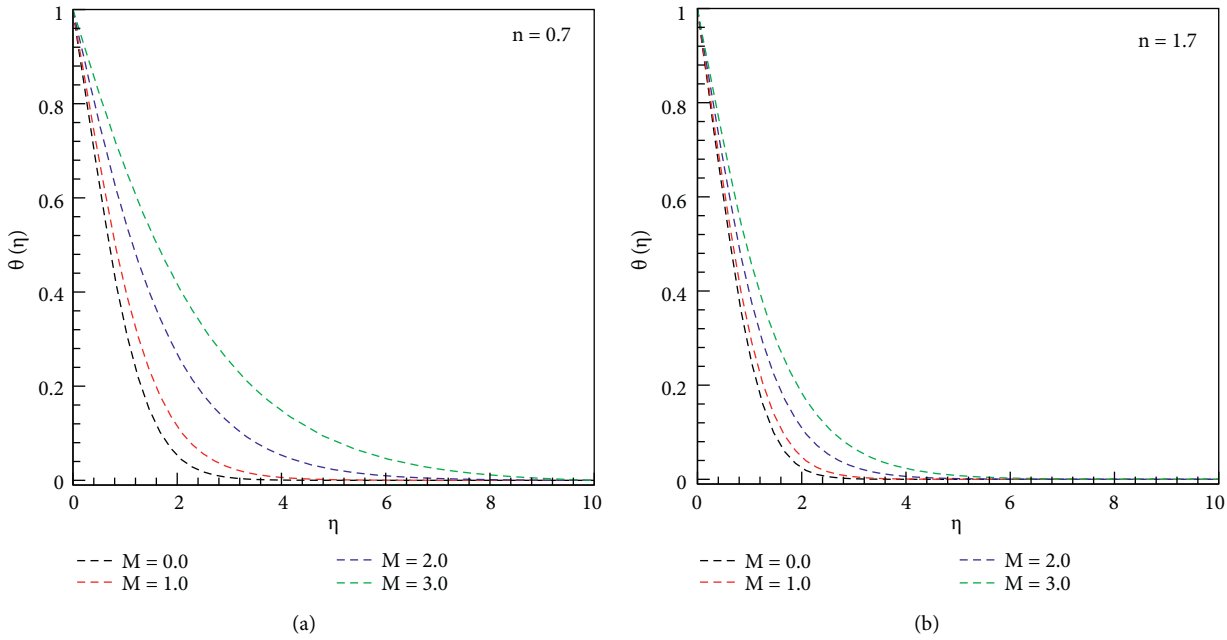

Figure 3: (a, b) Plot of η vs. $\theta(\eta)$ for M.

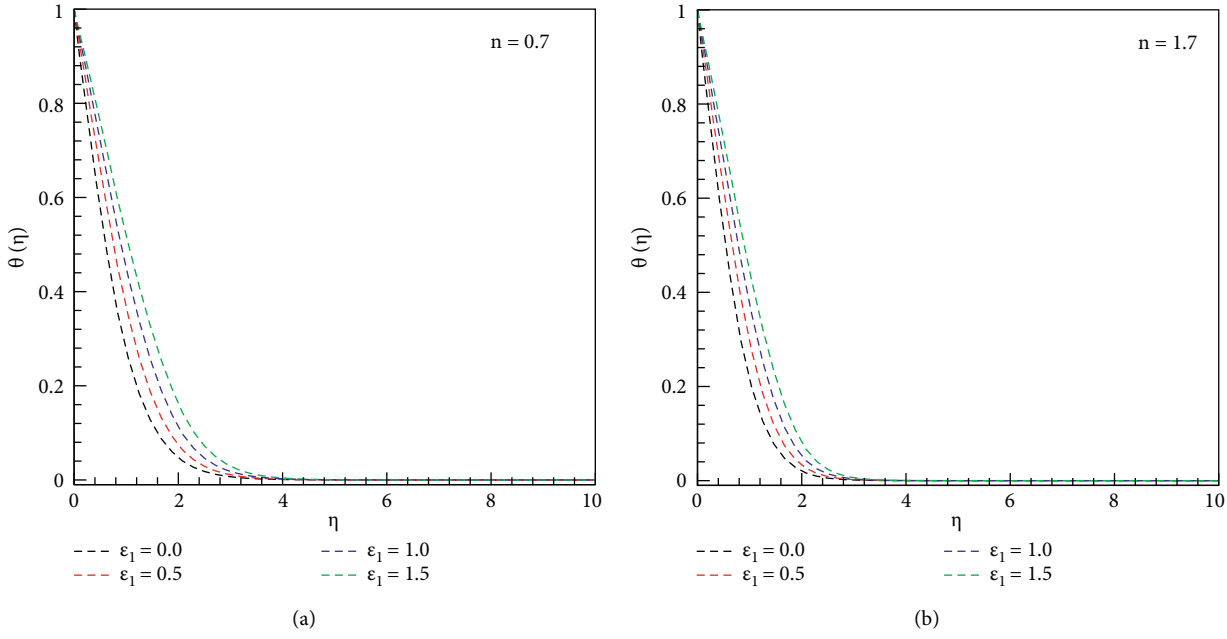

Figure 4: (a, b) Plot of η vs. $\theta(\eta)$ for ε_1.

5.4. Table of Skin Friction Coefficients. Table 1 structured for larger values of M *an d* α for $1/2C_{fx}Re_x^{1/2}$ and $1/2\,(U_w/V_w)C_{fy}Re_x^{1/2}$ for both instances $n = 0.7$ and $n = 1.7$. Here noted that the magnitude of $1/2C_{fx}Re_x^{1/2}$ and $1/2\,(U_w/V_w)C_{fy}Re_x^{1/2}$ increases when M *an d* α intensifies.

5.5. Comparison of bvp4c and HAM. Additionally, the HAM and bvp4c graphical comparisons for Newtonian case are reported in Figure 10 for $f\prime\,(\eta)$ *an d* $g\prime\,(\eta)$. Here, excellent portrayal are noted between both the methodologies.

To elaborate the comparison of $-\theta'\,(0)$ in limiting circumstances for diverse values of ε_1, Pr, and α, respectively, Tables 2 and 3 are acknowledged. These tables indicate a brilliant outcome associated with former literatures.

6. Closing Remarks

Here the essentials of thermo-sloutal time's relaxation in magnetite Carreau liquid with inconsistent aspects of mass diffusivity and thermal conductivity have been examined. The upcoming direction and significance of this model is

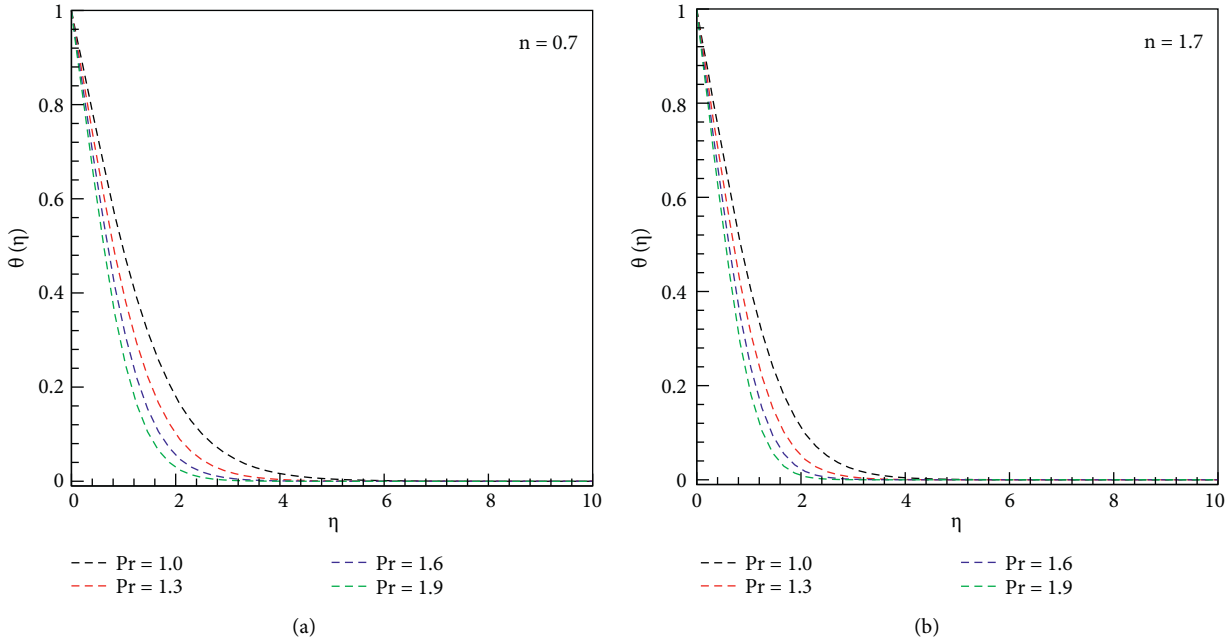

FIGURE 5: (a, b) Plot of η vs. $\theta(\eta)$ for Pr.

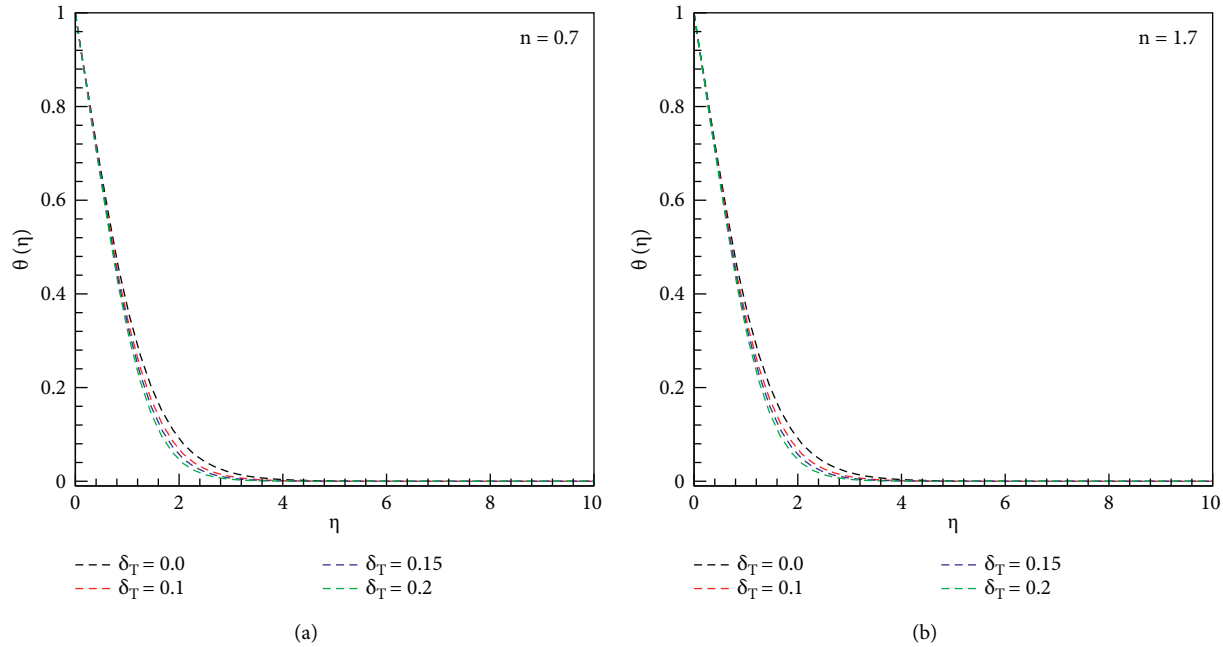

FIGURE 6: (a, b) Plot of η vs. $\theta(\eta)$ for δ_T.

that blood flow via tapered arteries with a stenosis is the essential use of Carreau fluid model because this model deals with the phenomena of shear thinning/thickening fluids. Furthermore, this model is extended for calculating the multiple solutions and also for curved surfaces. The salient particulars of this analysis are acknowledged as

(i) The magnetic factor M declined the velocity field.

(ii) The Carreau fluid temperature exaggerated for ε_1, however falloffs for δ_T.

(iii) The larger M the temperature field is improved for $n = 0.7 \, an \, d \, n = 1.7$.

(iv) Opposite influences were noted for $\Gamma_C \, an \, d \, \varepsilon_2$ on concentration scattering.

(v) Outstanding outcomes have been examined in limiting cases for $-\theta'(0)$.

(vi) The exceptional graphical depictions are plotted for comparisons of HAM and bvp4c of Carreau fluid model.

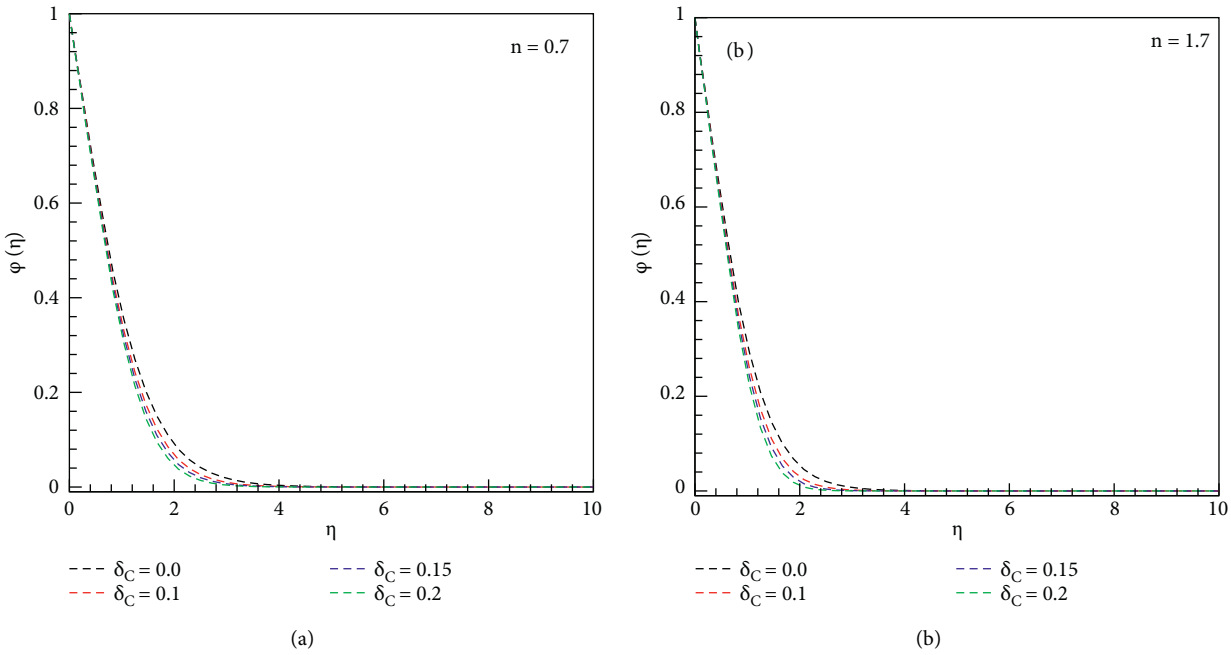

Figure 7: (a, b) Plot of η vs. $\phi(\eta)$ for δ_C.

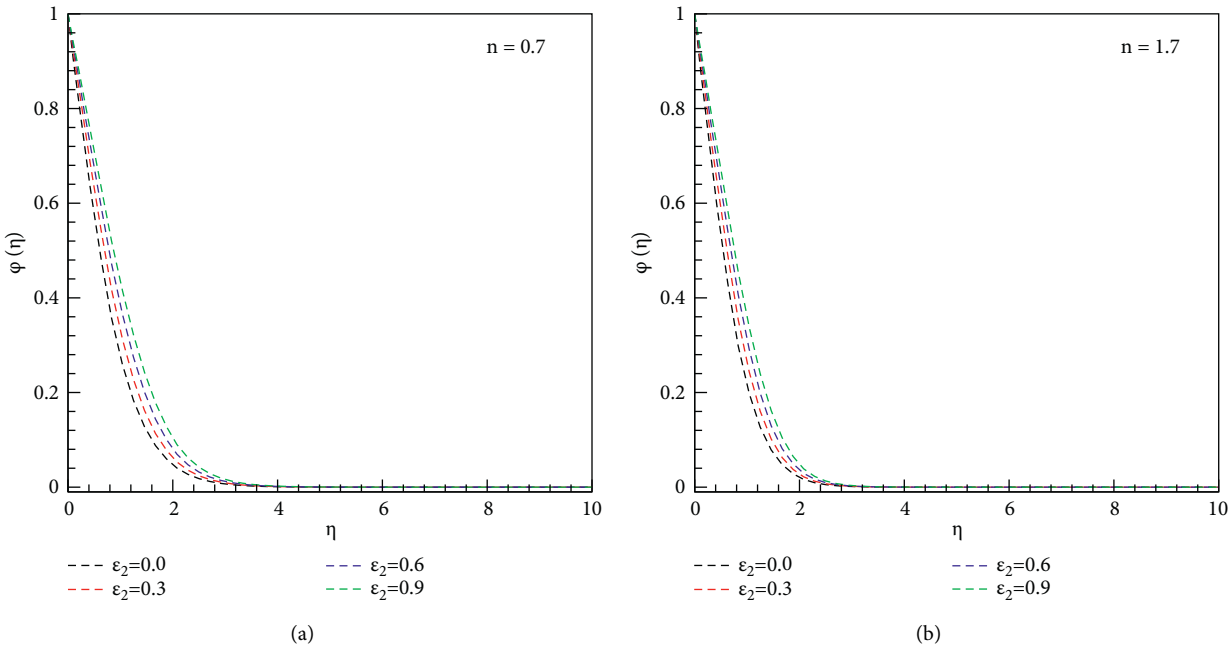

Figure 8: (a, b) Plot of η vs. $\phi(\eta)$ for ε_2.

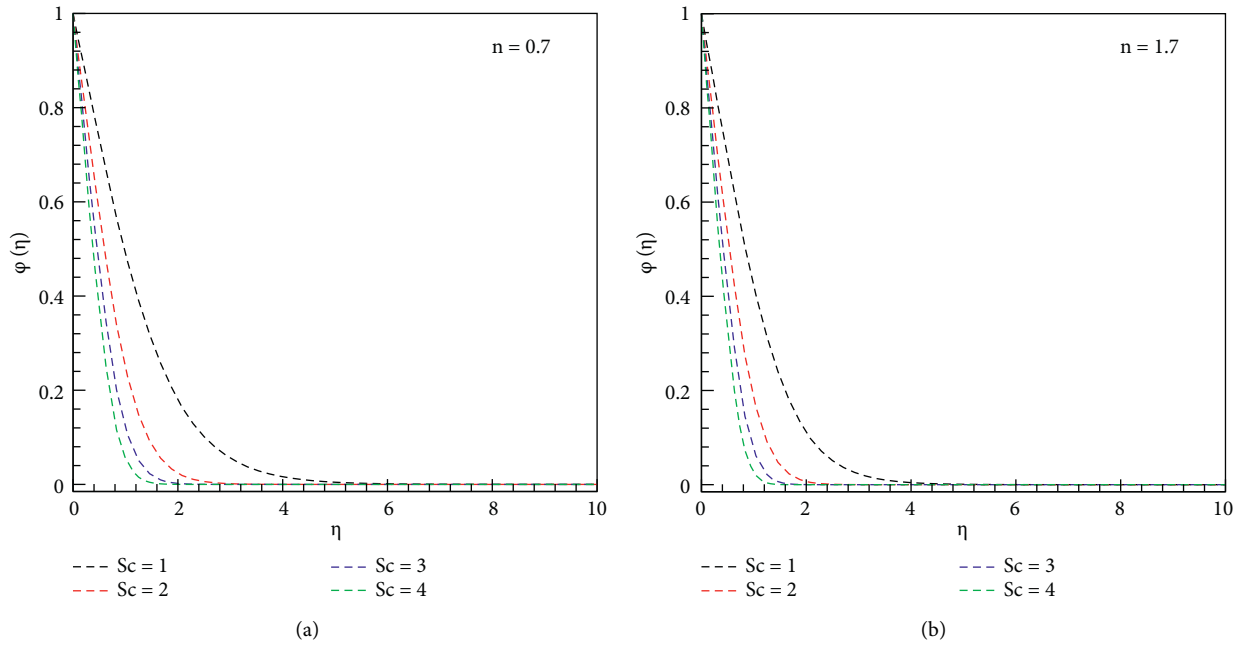

Figure 9: (a, b) Plot of η vs. $\phi(\eta)$ for Sc.

Table 1: Outcomes of skin friction coefficients when $We_1 = We_2 = 2.5$.

M	α	$1/2C_{fx}Re_x^{1/2}$		$1/2\,(U_w/V_w)C_{fy}Re_x^{1/2}$	
		$n = 0.7$	$n = 1.7$	$n = 0.7$	$n = 1.7$
0.5	0.5	−2.75267	−6.28875	−0.735299	−1.17469
1.0		−3.91194	−9.92461	−1.097060	−1.88793
1.5		−5.72221	−16.5755	−1.666760	−3.15998
0.5	0.7	−2.85709	−6.69579	−1.41209	−2.70100
	0.8	−2.90692	−6.90700	−1.86225	−3.87658
	0.9	−2.95537	−7.12294	−2.39147	−5.40309

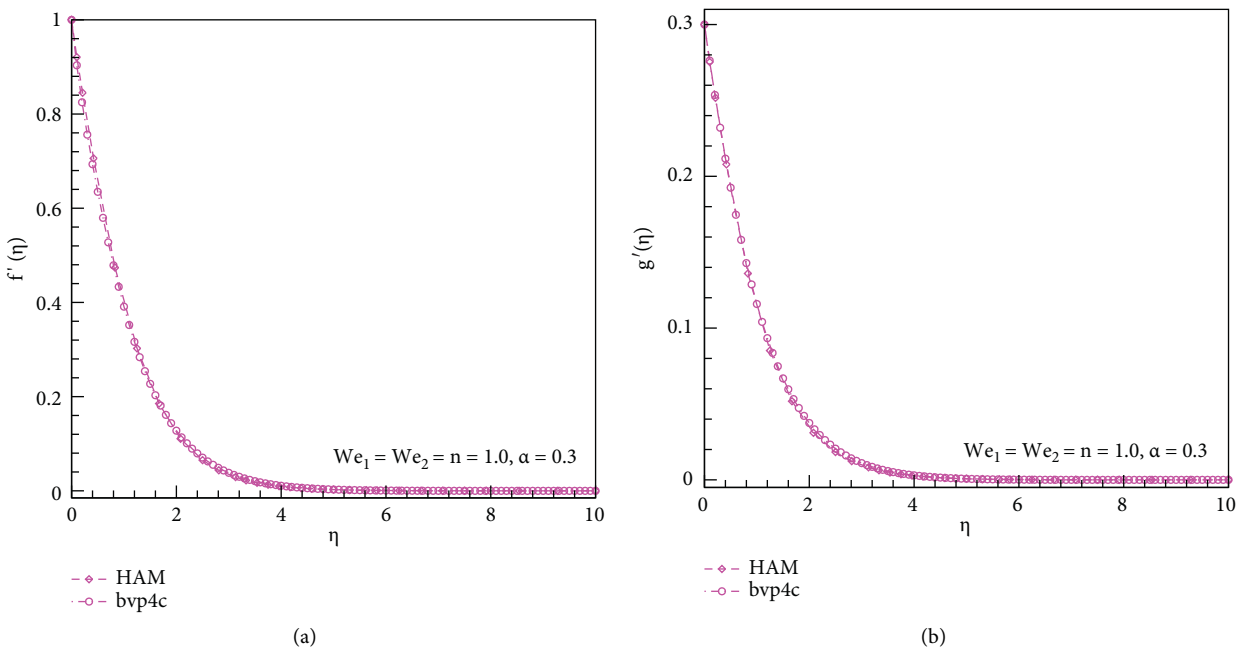

Figure 10: (a, b) Plot of η vs. $f'(\eta)\,and\,dg\prime(\eta)$ for HAM and bvp4c comparison.

Table 2: Outcomes of $-\theta'(0)$ for ε_1 and Pr when $We_1 = We_2 = \Gamma_T = \Gamma_C = \alpha = \varepsilon_2 = Sc = 0$ and $n = 1$ are fixed.

ε_1	Pr	$-\theta'(0)$	
		Ref. [25]	Present (bvp4c)
0.2	1.3	0.604568	0.60457302
0.3		0.569570	0.56957494
0.4		0.539040	0.53904539
0.2	1.5	0.664040	0.66404537
	1.7	0.719773	0.71978160
	2.0	0.797638	0.79765199

Table 3: Outcomes of $-\theta'(0)$ for α when $We_1 = We_2 = \Gamma_T = \Gamma_C = \varepsilon_1 = \varepsilon_2 = Sc = 0$ and $n = 1$ are fixed.

α	$-\theta'(0)$		
	Ref. [26]	Ref. [27]	Present (bvp4c)
0.25	0.665933	0.665939	0.6659332
0.50	0.735334	0.735336	0.7353329
0.75	0.796472	0.796472	0.7964718

Abbreviations

Γ: Material constant
n: Power law index
μ_0: Zero and infinity shear rate viscosities
p: Pressure
μ_∞: Infinity shear rate viscosities
γ: Shear rate
(u, v, w): Velocity components $[ms^{-1}]$
(x, y, z): Space coordinates $[ms^{-1}]$
$(\rho c)_f$: Heat capacity of fluid $[JK^{-1}.m^{-3}]$
ν: Kinematic viscosity $[m^2s^{-1}]$
T: Temperature of fluid $[K]$
C: Concentration of fluid $[K]$
$K(T)$: Variable thermal conductivity
$D(C)$: Variable mass diffusivity
k_1: Thermal conductivity of $(W/m.K)$ surrounding
k_2: Mass diffusivity of surrounding
T_∞: Ambient fluid temperature $[K]$
C_∞: Ambient fluid concentration $[K]$
T_w: Wall temperature $[K]$
C_w: Wall concentration $[K]$
δ_T: Thermal relaxation time
δ_C: Solutal relaxation time
C_{fx}, C_{fy}: Skin friction coefficients
τ_{xz}, τ_{yz}: Surface shear stresses
We_1, We_2: Local Weissenberg numbers
α: Ratio of stretching rates parameter
Γ_T, Γ_C: Thermal and concentration relaxation time factors
M: Magnetic factor
Pr: Prandtl number
ε_1: Thermal conductivity factor
Sc: Schmidt number
ε_2: Mass diffusivity factor
HAM: Homotopy analysis method
ODEs: Ordinary differential equations
tr: Trace of a tensor
PDEs: Partial differential equations
α: Ratio of stretching rates parameter.

Data Availability

This is the theoretical analysis, and no data are used in this study.

Conflicts of Interest

The authors declare that they have no conflicts of interest.

References

[1] J. Sui, L. Zheng, and X. Zhang, "Boundary layer heat and mass transfer with Cattaneo-Christov double-diffusion in upper-convected Maxwell nanofluid past a stretching sheet with slip velocity," *International Journal of Thermal Sciences*, vol. 104, pp. 461–468, 2016.

[2] L. Liu, L. Zheng, F. Liu, and X. Zhang, "Anomalous convection diffusion and wave coupling transport of cells on comb frame with fractional Cattaneo-Christov flux," *Communications in Nonlinear Science and Numerical Simulation*, vol. 38, pp. 45–58, 2016.

[3] M. Khan, M. Irfan, W. A. Khan, and A. S. Alshomrani, "A new modeling for 3D Carreau fluid flow considering nonlinear thermal radiation," *Results in Physics*, vol. 7, pp. 2692–2704, 2017.

[4] A. S. Dogonchi and D. D. Ganji, "Impact of Cattaneo-Christov heat flux on MHD nanofluid flow and heat transfer between parallel plates considering thermal radiation effect," *Journal of the Taiwan Institute of Chemical Engineers*, vol. 80, pp. 52–63, 2017.

[5] M. Irfan, M. Khan, and W. A. Khan, "On model for three-dimensional Carreau fluid flow with Cattaneo-Christov double diffusion and variable conductivity: A numerical approach," *Journal of the Brazilian Society of Mechanical Sciences and Engineering*, vol. 40, no. 12, 2018.

[6] N. Acharya, S. Maity, and P. K. Kundu, "Differential transformed approach of unsteady chemically reactive nanofluid flow over a bidirectional stretched surface in presence of magnetic field," *Heat Transfer*, vol. 49, no. 6, pp. 3917–3942, 2020.

[7] N. Acharya, R. Bag, and P. K. Kundu, "Unsteady bioconvective squeezing flow with higher-order chemical reaction and second-order slip effects," *Heat Transfer*, vol. 50, no. 6, pp. 5538–5562, 2021.

[8] M. Waqas, "Diffusion of stratification based chemically reactive Jeffrey liquid featuring mixed convection," *Surfaces and Interfaces*, vol. 23, Article ID 100783, 2021.

[9] N. Acharya, "Spectral quasi linearization simulation on the radiative nanofluid spraying over a permeable inclined spinning disk considering the existence of heat source/sink," *Applied Mathematics and Computation*, vol. 411, Article ID 126547, 2021.

[10] N. Acharya, H. Mondal, and P. K. Kundu, "Spectral approach to study the entropy generation of radiative mixed convective couple stress fluid flow over a permeable stretching cylinder," *Proceedings of the Institution of Mechanical Engineers - Part C: Journal of Mechanical Engineering Science*, vol. 235, no. 15, pp. 2692–2704, 2021.

[11] P. J. Carreau, "Rheological equations from molecular network theories," *Transactions of the Society of Rheology*, vol. 16, Article ID 99127, 1972.

[12] P. J. Carreau, D. D. Kee, and M. Daroux, "An analysis of the viscous behaviour of polymeric solutions," *Canadian Journal of Chemical Engineering*, vol. 57, no. 2, pp. 135–140, 1979.
[13] A. Pantokratoras, "Non-similar blasius and sakiadis flow of a non-Newtonian carreau fluid," *Journal of the Taiwan Institute of Chemical Engineers*, vol. 56, pp. 1–5, 2015.
[14] T. Salahuddin, "Carreau fluid model towards a stretching cylinder: Using Keller box and shooting method," *Ain Shams Engineering Journal*, vol. 11, no. 2, pp. 495–500, 2020.
[15] M. Elayarani, M. Shanmugapriya, and P. Senthil Kumar, "Intensification of heat and mass transfer process in MHD carreau nanofluid flow containing gyrotactic microorganisms," *Chemical Engineering and Processing - Process Intensification*, vol. 160, Article ID 108299, 2021.
[16] C. Cattaneo, "Sulla conduzione del calore," *Atti Semin Mat Fis Univ Modena Reggio Emilia*, vol. 3, pp. 83–101, 1948.
[17] C. I. Christov, "On frame indifferent formulation of the Maxwell-Cattaneo model of finite-speed heat conduction," *Mechanics Research Communications*, vol. 36, no. 4, pp. 481–486, 2009.
[18] M. G. Reddy and K. G. Kumar, "Cattaneo-Christov heat flux feature on carbon nanotubes filled with micropolar liquid over a melting surface: A stream line study," *International Communications in Heat and Mass Transfer*, vol. 122, Article ID 105142, 2021.
[19] W. Ibrahim and G. Gadisa, "Finite element solution of nonlinear convective flow of Oldroyd-B fluid with Cattaneo-Christov heat flux model over nonlinear stretching sheet with heat generation or absorption," *Propulsion and Power Research*, vol. 9, no. 3, pp. 304–315, 2020.
[20] N. Acharya, K. Das, and P. K. Kundu, "Cattaneo-Christov intensity of magnetised upper-convected Maxwell nanofluid flow over an inclined stretching sheet: A generalised Fourier and Fick's perspective," *International Journal of Mechanical Sciences*, vol. 130, pp. 167–173, 2017.
[21] D. Lu, M. Mohammad, M. Ramzan, M. Bilal, F. Howari, and M. Suleman, "MHD boundary layer flow of Carreau fluid over a convectively heated bidirectional sheet with non-Fourier heat flux and variable thermal conductivity," *Symmetry*, vol. 11, no. 5, p. 618, 2019.
[22] S. Sarojamma, R. V. Lakshmi, P. V. S. Narayana, and I. L. Animasaun, "Exploration of the significance of autocatalytic chemical reaction and Cattaneo-Christov heat flux on the dynamics of a micropolar fluid," *J. Appl. Comput. Mechanics*, vol. 6, pp. 77–89, 2020.
[23] Y. J. Lim, M. N. Zakaria, S. Mohamad Isa, N. A. Mohd Zin, A. Q. Mohamad, and S. Shafie, "VON Kármán Casson fluid flow with Navier's slip and cattaneo-christov heat flux," *Case Studies in Thermal Engineering*, vol. 28, Article ID 101666, 2021.
[24] P. S. Reddy and P. Sreedevi, "Effect of Cattaneo - christov heat flux on heat and mass transfer characteristics of Maxwell hybrid nanofluid flow over stretching/shrinking sheet," *Physica Scripta*, vol. 96, no. 12, Article ID 125237, 2021.
[25] W. A. Khan, M. Irfan, and M. Khan, "An improved heat conduction and mass diffusion models for rotating flow of an Oldroyd-B fluid," *Results in Physics*, vol. 7, pp. 3583–3589, 2017.
[26] I.-C. Liu and H. I. Andersson, "Heat transfer over a bidirectional stretching sheet with variable thermal conditions," *International Journal of Heat and Mass Transfer*, vol. 51, no. 15-16, pp. 4018–4024, 2008.
[27] A. Munir, A. Shahzad, and M. Khan, "Convective flow of Sisko fluid over a bidirectional stretching surface," *PLoS One*, vol. 10, no. 6, Article ID e0130342, 2015.

Hindawi
Mathematical Problems in Engineering
Volume 2022, Article ID 5746202, 11 pages
https://doi.org/10.1155/2022/5746202

Research Article

Generalization of Tangential Complexes of Weight Three and Their Connections with Grassmannian Complex

Sadaqat Hussain,[1] **Nasreen Kausar**,[2] **Sajida Kousar**,[3] **Parameshwari Kattel**,[4] **and Tahir Shahzad**[5]

[1]*Department Mathematics, University of Baltistan Skardu, Gilgit Baltistan, Skardu, Pakistan*
[2]*Department of Mathematics, Faculty of Arts and Sciences, Yildiz Technical University, Esenler 34210, Istanbul, Turkey*
[3]*Department of Mathematics and Statistics, International Islamic University Islamabad, Islamabad, Pakistan*
[4]*Department of Mathematics, Tri-Chandra Multiple Campus, Tribhuvan University, Kathmandu, Nepal*
[5]*Department of Basic Sciences and Humanities, University of Engineering and Technology, Lahore 54890, Pakistan*

Correspondence should be addressed to Parameshwari Kattel; parameshwari.kattel@trc.tu.edu.np

Received 3 November 2021; Revised 3 March 2022; Accepted 4 March 2022; Published 11 April 2022

Academic Editor: Ardashir Mohammadzadeh

Following earlier work by Gangl, Cathelineaue, and others, Siddiqui defined the Siegel's cross-ratio identity and Goncharov's triple ratios over the truncated polynomial ring $\mathbb{F}[\varepsilon]_\nu$. They used these constructions to introduce both dialogarithmic and trilogarithmic tangential complexes of first order. They proposed various maps to relate first-order tangent complex to the Grassmannian complex. Later, we extended all the notions related to dialogarithmic complexes to a general order n. Now, this study is aimed to generalize all of the constructions associated to trilogarithmic tangential complexes to higher orders. We also propose morphisms between the tangent to Goncharov's complex and Grassmannian subcomplex for general order. Moreover, we connect both of these complexes by demonstrating that the resulting diagrams are commutative. In this generalization process, the classical Newton's identities are used. The results reveal that the tangent group $TB_3^n(F)$ of a higher order and defining relations are feasible for all orders.

1. Introduction

Polylogarithms have been known for almost three centuries in various disciplines of mathematics such as Feynman integrals, volume functions of hyperbolic tetrahedrons, quantum field theory, and Dedikend Zeta functions. Since the last two decades, it became important after Bloch's work, in which he introduced a group (Bloch Group) and found connections of this group with algebraic K theory (see [1, 2]). Suslin introduced the well-known Grassmannian Complex and Bloch–Suslin complex (see [3, 4]). Later, Goncharov used geometric configurations in order to define the motivic complexes and to prove Zagier's conjecture on polylogarithms and special L values for weight 2 and 3 (see [4]). He also introduced the triple ratio together with Zagier by antisymmetrization of his own formula $f_2^{(3)}$. Moreover, he related the Grassmannian subcomplexes to his trilogarithmic motivic complexes by introducing several homomorphisms of the form $f_i^{(3)}$ (see [2, 5, 6]). Cathelineau studied variants (infinitesimal and tangential) of these motivic complexes and presented a tangent group $T\mathscr{B}_2(F)$ which is, in fact, a F vector space (see [7]). Siddiqui defined the tangent group $T\mathscr{B}_3(F)$ and its complexes for the first order. He used geometric configurations to construct cross-ratio, triple-ratio, and Siegel cross-ratio identity for dual numbers and then proposed various maps to relate Grassmannian complex and first-order tangent complex (see [8, 9]). He himself attempted to extend his constructions to the second-order tangent complex and gave some results for a special case.

Hussain and Siddiqui [10] discussed the tangent group and its associated complexes for the second order by

introducing second-order tangent group, denoted by $T\mathscr{B}_2^2(F)$. They extended cross-ratio, Goncharov's triple-ratio, and Siegel's cross-ratio identity of the first order to second order. They also proposed morphisms such as τ_{0,ε^2}^2 and τ_{1,ε^2}^2 for weight two and τ_{0,ε^2}^3, τ_{1,ε^2}^3, and τ_{2,ε^2}^3 for weight three, in order to connect the second-order tangential complex with the Grassmannian complex. Recently, the degree of the tangent group of weight 2 is generalized by introducing a group $T\mathscr{B}_2^n(F)$ [11]. This group is used to construct a generalized tangent complex:

$$T\mathscr{B}_2^n(\mathbb{F}) \xrightarrow{\partial_{\varepsilon^n}} \left(\mathbb{F}\otimes\overset{2}{\wedge}\mathbb{F}^\times\right)\oplus\left(\overset{3}{\wedge}\mathbb{F}\right). \tag{1}$$

This complex is further related to the Grassmannian complex by introducing maps π_{0,ε^n}^2 and π_{1,ε^n}^2. As the order of the tangent group is generalized only for weight two, it is still a matter of great concern and motivates to introduce and analyse higher order tangent groups of weight three which will eventually be used for the establishment of generalized tangent complexes of weight three. In this work, we construct higher order tangent to Goncharov's complexes and its associated algebraic constructions (cross ratio, Siegel's identity, triple ratio, etc.) of weight three and to obtain a generalized formula for the order $n \geq 3$. We also propose general formula for the maps which connect the trilogarithmic tangential complexes of order greater than two to the Grassmannian complexes. For this, we define nth-order tangent group $T\mathscr{B}_3^n(F)$ of weight 3 along with its functional equations. We define a map ∂_{ε^n} to construct the following tangent complex of general order:

$$T\mathscr{B}_3^n(\mathbb{F}) \xrightarrow{\partial_{\varepsilon^n}} \left(T\mathscr{B}_2^n(\mathbb{F})\otimes\mathbb{F}^\times\right)\oplus\left(\mathbb{F}\otimes\mathscr{B}_2(\mathbb{F})\right) \xrightarrow{\partial_{\varepsilon^n}} \left(\mathbb{F}\otimes\overset{2}{\wedge}\mathbb{F}^\times\right)\oplus\left(\overset{3}{\wedge}\mathbb{F}\right). \tag{2}$$

Our next goal is to connect the above complex to the well-known Grassmannian complex. This will be achieved through an inductive approach and using Newton–Girard identities (see Section 2.4). Using the results from Siddiqui [9], we will determine the coefficients of the cross-ratio and Siegel cross-ratio identity and determinants of order n. After these constructions, we will move to find morphisms of the connection π_{0,ε^n}^3, π_{1,ε^n}^3, and π_{2,ε^n}^3 so as to relate Grassmannian complex to Cathelineau's trilogarithmic complex. The consequence of this connection is the formation of diagram (D), and at the end, we prove that this diagram is commutative.

2. Materials and Methods

This section is devoted to give brief introduction to certain concepts and constructions related to this work. Many of the terms also found in [1, 4, 9, 10, 12, 13] can be consulted for more details.

2.1. Complex. Suppose that

$$A_i \xrightarrow{f_i} A_{(i-1)} \xrightarrow{f_{i-1}} \cdots \xrightarrow{f_0} A_0 \tag{3}$$

is a chain of abelian groups with corresponding maps f_k; then, such a chain is said to be a complex if

$$f_{(i-1)} \circ f_i = 0. \tag{4}$$

2.2. Grassmannian Complex. Let X be any nonempty set. Consider $C_m(X)$ be any free Abelian group generated by the elements of G/X^m, where G is a group which acts on X; then, we define a differential map $d\colon C_m(X) \longrightarrow C_{m-1}(X)$ as

$$d\colon (x_1,\ldots,x_m) \mapsto \sum_{i=0}^{m} (-1)^m (x_1,\ldots,\widehat{x}_i,\ldots,x_m). \tag{5}$$

Also, if we denote $C_m(n)$ to be a free Abelian group generated by the configurations of the elements of an n dimensional vector space V_n and $(x_i|x_1,\ldots,\widehat{x}_i,\ldots,x_m)$ be the projective configuration of the j^{th} component x_j along the i^{th} component x_i, where $i \neq j$, $j = 1,\ldots,m$, then we define a projective differential map $d'\colon C_{(m+1)}(n+1) \longrightarrow C_m(n)$ as

$$d'\colon (x_1,\ldots,x_m) \mapsto \sum_{i=0}^{m} (-1)^m (x_i|x_1,\ldots,\widehat{x}_i,\ldots,x_m). \tag{6}$$

By using these differential maps and free Abelian groups generated by configurations, we have a bicomplex of the form called Grassmannian bicomplex.

From this bicomplex, we can form many subcomplexes such as

$$C_{m+2}(n+2) \xrightarrow{d'} C_{m+1}(n+1) \xrightarrow{d'} C_m(n) \tag{7}$$

or

$$C_{m+2}(n) \xrightarrow{d} C_{m+1}(n) \xrightarrow{d} C_m(n). \tag{8}$$

These subcomplexes are known as Grassmannian complexes.

2.3. Tensor Product. Let A and B be two free Abelian groups ($\mathbb{Z}$—modules); then, the tensor product of A and B is denoted as $A\otimes B$ and defined as a free Abelian group with generators $a\otimes b$ for $a \in A$ and $b \in B$, satisfying the relations

$$\begin{aligned} (a_1+a_2)\otimes b &= a_1\otimes b + a_2\otimes b,\\ a\otimes(b_1+b_2) &= a\otimes b_1 + a\otimes b_2,\\ ra\otimes b &= r(a\otimes b) = a\otimes rb, \end{aligned} \tag{9}$$

where $a, a_1, a_2 \in A$, $b, b_1, b_2 \in B$, and $r \in F$.

2.4. Newton–Girard Identities. Girard introduced some identities which describe relationship between roots of a polynomial and its coefficients (see [14, 15]). Later, Newton generalized these identities and gave a recursive formula. Today these identities are known as Newton–Girard identities whose explanation is as follows. Suppose $f(y)$ is a polynomial like

$$g(y) = y^n + c_1 y^{n-1} + c_2 y^{n-2} + c_3 y^{n-3} + \ldots\ldots + c_{n-1}y + c_n, \tag{10}$$

with n of its roots $r_1, r_2, \ldots\ldots r_n$. We use the notation δ_k for the sum of the kth powers of roots as

$$\delta_k = r_1^k + r_2^k + \ldots\ldots + r_n^k, \tag{11}$$

where $k \in \mathbb{Z}^+$ and $\delta_k = 0$ for $k \rangle n$. And

$$\delta_k + c_1\delta_{k-1} + c_2\delta_{k-2} + s_3c_{k-3} + \ldots\ldots + c_{k-1}\delta_1 + kc_k = 0. \tag{12}$$

This identity allows us to deduce the relations:

$$\begin{aligned} \delta_1 + c_1 &= 0, \\ \delta_2 + c_1\delta_1 + 2c_2 &= 0, \\ \delta_3 + c_1\delta_2 + c_2\delta_1 + 3c_3 &= 0, \\ \delta_4 + c_1\delta_3 + c_2\delta_2 + c_3\delta_1 + 4c_4 &= 0. \end{aligned} \tag{13}$$

Now, considering the most generalized form of the polynomial,

$$f(y) = \sum_{i=0}^{n} t_i y^i. \tag{14}$$

And with the assumption that $t_k = 0$ for $k \langle 0$, we define δ_k, for $k \geqslant 0$, as

$$\delta_k = r_1^k + r_2^k + \ldots\ldots + r_n^k. \tag{15}$$

By interchanging "k" to "$(-k)$," we obtain

$$\delta_{-k} = r_1^{-k} + r_2^{-k} + \ldots\ldots + r_n^{-k}. \tag{16}$$

Finally, we can conclude the general form of Newton's identity as

$$t_j(n-j) + t_{j+1}\delta_{-1} + t_{j+2}\delta_{-2} + t_{j+3}\delta_{-3} + \ldots\ldots + t_n\delta_{j-n} = 0; \quad j \leqslant n. \tag{17}$$

Furthermore, we can deduct the following results:

$$\begin{aligned} M_1 &= \frac{t_1}{s}, \\ M_2 &= \frac{2t_2}{s} - \frac{t_1^2}{s^2}, \\ M_3 &= \frac{3t_3}{s} - \frac{3t_1t_2}{s^2} + \frac{t_1^3}{s^3}, \\ M_4 &= \frac{4t_4}{s} - \frac{4t_1t_3}{s^2} - \frac{2t_2^2}{s^2} + \frac{4t_1^2t_2}{s^3} - \frac{t_1^4}{s^4}. \end{aligned} \tag{18}$$

In general notation,

$$M_n = \frac{nt_n}{s} - \sum_{r=1}^{n-1} \frac{t_{n-r}}{s} M_r, \tag{19}$$

here we used $M_i = -\delta_{-k}$, $\forall i = 0, 1, 2, \ldots$ and $t_0 = s$.

When we consider the case $t_0 = 1 - s$, the above identities will become

$$\begin{aligned} N_1 &= \frac{-t_1}{s-1}, \\ N_2 &= \frac{-2t_2}{s-1} - \frac{t_1^2}{(s-1)^2}, \\ N_3 &= \frac{-3t_3}{s-1} - \frac{3t_1t_2}{(s-1)^2} - \frac{t_1^3}{(s-1)^3}, \\ N_4 &= \frac{-4t_4}{s-1} - \frac{4t_1t_3}{(s-1)^2} - \frac{2t_2^2}{(s-1)^2} - \frac{4t_1^2t_2}{(s-1)^3} - \frac{t_1^4}{(s-1)^4}. \end{aligned} \tag{20}$$

The general form will be

$$N_n = \frac{nt_n}{1-s} - \sum_{r=1}^{n-1} \frac{t_{n-r}}{1-s} N_r. \tag{21}$$

In [10], we have extended the idea of trilogarithmic tangent group up to the second order by proposing a group $T\mathscr{B}_3^2(\mathbb{F})$ and its complex. It is quite natural to think for the generalization of the degree of this group and other constructions (complexes, morphisms, cross ratio, etc.) related to this group. Let us define the following.

2.5. First-Order Tangent Group of Weight 3. A first-order tangent group, denoted by $T\mathscr{B}_2(F)$, is a $\mathbb{Z}$ module generated by the elements of the form $\langle s; s'] \in \mathscr{Z}[F[\varepsilon]_2]$, a quotient by the expression,

$$\langle s; s'] - \langle t; t'] + \left\langle \frac{t}{s}; \left(\frac{t}{s}\right)' \right] - \left\langle \frac{1-t}{1-s}; \left(\frac{1-t}{1-s}\right)' \right] + \left\langle \frac{s(1-t)}{t(1-s)}; \left(\frac{s(1-t)}{t(1-s)}\right)' \right], \tag{22}$$

where $s, t \neq 0, 1, s \neq t$, $\langle s; s'] = [s + s'\varepsilon] - [s]$; $(s, s' \in F)$,

$$\left(\frac{t}{s}\right)' = \frac{st' - s't}{s^2},$$
$$\left(\frac{1-t}{1-s}\right)' = \frac{(1-t)s' - (1-s)t'}{(1-s)^2}, \tag{23}$$

and

$$\left(\frac{s(1-t)}{t(1-s)}\right)' = \frac{t(1-t)s' - s(1-s)t'}{(t(1-s))^2}. \tag{24}$$

As the second order is discussed in [10], we define the third order directly.

2.6. Third-Order Tangent Group of Weight 3. We denote $T\mathscr{B}_3^3(\mathbb{F})$ to be the trilogarithmic tangent group of order three which is a $\mathbb{Z}$ module over the truncated polynomial ring $\mathbb{F}[\varepsilon]_4$ whose generators are the elements of the form $\langle s; t_1, t_2, t_3] \in \mathbb{Z}[\mathbb{F}[\varepsilon]_4]$, where $\langle s; t_1, t_2, t_3] = [s + t_1\varepsilon + t_2\varepsilon^2 + t_3\varepsilon^3] - [s]$, $(s, t_1, t_2, t_3 \in \mathbb{F})$ and quotient by the kernel of map

$$\partial\colon \mathbb{Z}[\mathbb{F}[\varepsilon]_4] \longrightarrow \left(T\mathscr{B}_2^3(\mathbb{F}) \otimes \mathbb{F}^\times\right) \oplus \left(\mathbb{F} \otimes \mathscr{B}_2(\mathbb{F})\right), \tag{25}$$

such that

$$\partial\left(\langle a; b_1, b_2, b_3]_2\right) = \langle s; t_1, t_2, t_3]_2^3 \otimes s + \left(\frac{3t_3}{s} - \frac{3t_1t_2}{s^2} + \frac{t_1^3}{s^3}\right) \otimes [s]_2, \tag{26}$$

where $\oplus$ and $\otimes$, respectively, represent the direct sum and tensor product of free Abelian groups or modules' tensor product of the free Abelian groups.

2.7. Generalized Tangent Group of Weight 3. Let the characteristic of the field $\mathbb{F}$ be zero and $\mathbb{F}[\varepsilon]_{n+1}$ represent the ring of truncated polynomials. We call $T\mathscr{B}_3^n(\mathbb{F})$ the tangent group of weight 3 and order n which can be defined as a $\mathbb{Z}$ module over $\mathbb{F}[\varepsilon]_{n+1}$ with generators of the form $\langle s; t_1, t_2, \ldots, t_n] \in \mathbb{Z}[\mathbb{F}[\varepsilon]_{n+}]$, where $\langle s; t_1, t_2, \ldots, t_n] = [s + t_1\varepsilon + t_2\varepsilon^2 + \cdots + t_n\varepsilon^n] - [s]$, $(s, t_1, t_2, \ldots, t_n \in \mathbb{F})$ and quotient by $\mathrm{Ker}\partial$:

$$\partial\colon \mathbb{Z}\left[\mathbb{F}[\varepsilon]_{n+1}\right] \longrightarrow \left(T\mathscr{B}_2^n(\mathbb{F}) \otimes \mathbb{F}^\times\right) \oplus \left(\mathbb{F} \otimes \mathscr{B}_2(\mathbb{F})\right), \tag{27}$$

where ∂ can be written as

$$\partial\left(\langle s; t_1, t_2, \ldots, t_n]_2\right) = \langle s; t_1, t_2, \ldots, t_n]_2^n \otimes s + M_n \otimes [s]_2. \tag{28}$$

The factor M_n is given in (8). For $n = 1, 2$, we obtain the groups $T\mathscr{B}_3(\mathbb{F})$ and $T\mathscr{B}_3^2(\mathbb{F})$. The former is defined in [9] and later is in [10]. By using the group $T\mathscr{B}_3^n(\mathbb{F})$, the following tangential complex can be obtained:

$$T\mathscr{B}_3^n(\mathbb{F}) \xrightarrow{\partial_{\varepsilon^n}} \left(T\mathscr{B}_2^n(\mathbb{F}) \otimes \mathbb{F}^\times\right) \oplus \left(\mathbb{F} \otimes \mathscr{B}_2(\mathbb{F})\right) \xrightarrow{\partial_{\varepsilon^n}} \left(\mathbb{F} \otimes \overset{2}{\wedge} \mathbb{F}^\times\right) \oplus \left(\overset{3}{\wedge} \mathbb{F}\right). \tag{29}$$

2.8. Triple Ratio. The triple ratio $r(u_0, \ldots, u_5)$ of six points is given in [12] as

$$r_3(u_0, \ldots, u_5) = \frac{(u_0u_1u_3)(u_1u_2u_4)(u_2u_0u_5)}{(u_0u_1u_4)(u_1u_2u_5)(u_2u_0u_3)}, \tag{30}$$

whose tangential version for $\nu = 2$ can be traced in [8, 10] as

$$r_{3,\varepsilon}(l_0^*, \ldots, l_5^*) = \frac{\{(l_0^*l_1^*l_3^*)(l_1^*l_2^*l_4^*)(l_2^*l_0^*l_5^*)\}_\varepsilon}{(l_0l_1l_4)(l_1l_2l_5)(l_2l_0l_3)} - \frac{(l_0l_1l_3)(l_1l_2l_4)(l_2l_0l_5)}{(l_0l_1l_4)(l_1l_2l_5)(l_2l_0l_3)} \frac{\{(l_0^*l_1^*l_4^*)(l_1^*l_2^*l_5^*)(l_2^*l_0^*l_3^*)\}_\varepsilon}{(l_0l_1l_4)(l_1l_2l_5)(l_2l_0l_3)}. \tag{31}$$

We extend this notion for $\nu = n + 1$ as

$$\begin{aligned} r_{3,\varepsilon^n}(u_0^*, \ldots, u_5^*)) = \mathrm{Alt}_6 \Bigg\{ & \frac{\{(u_0^*u_1^*u_3^*)(u_1^*u_2^*u_4^*)(u_2^*u_0^*u_5^*)\}_{\varepsilon^n}}{(u_0u_1u_4)(u_1u_2u_5)(u_2u_0u_3)} - r_{3,\varepsilon^{n-1}}(u_0^*, \ldots, u_5^*) \frac{\{(u_0^*u_1^*u_4^*)(u_1^*u_2^*u_5^*)(u_2^*u_0^*u_3^*)\}_\varepsilon}{(u_0u_1u_4)(u_1u_2u_5)(u_2u_0u_3)} \\ & - r_{3,\varepsilon^{n-2}}(u_0^*, \ldots, u_5^*) \frac{\{(u_0^*u_1^*u_4^*)(u_1^*u_2^*u_5^*)(u_2^*u_0^*u_3^*)\}_{\varepsilon^2}}{(u_0u_1u_4)(u_1u_2u_5)(u_2u_0u_3)} - \ldots - r_3(u_0, \ldots, u_5) \frac{\{(u_0^*u_1^*u_4^*)(u_1^*u_2^*u_5^*)(u_2^*u_0^*u_3^*)\}_{\varepsilon^n}}{(u_0u_1u_4)(u_1u_2u_5)(u_2u_0u_3)} \Bigg\}. \end{aligned} \tag{32}$$

3. Main Results and Discussion

3.1. Dilogarithmic Bicomplexes. In this section, we will connect the Grassmannian bicomplex to the tangent to the Bloch–Suslin complex. This connection can be displayed through the figure.

The maps π^3_{0,ε^n}, π^3_{1,ε^n}, π^3_{2,ε^n}, and ∂_{ε^n} are defined for $n = 1, 2$ in [9, 10], respectively. Here, we redefine these maps using Newton identities which will enable us to propose these maps for order " n." For this, we suppose the following notations. $\Delta(u_0^*, \ldots, \widehat{u}_i^*, \ldots, u_3^*)_{\varepsilon^j} = \lambda_{ij}$, $\Delta(u_0^*, \ldots, \widehat{u}_{i+1}^*, \ldots, u_3^*)_{\varepsilon^j} = \lambda_{(i+1)j}$, $\Delta(u_0^*, \ldots, \widehat{u}_{i+2}^*, \ldots, u_3^*)_{\varepsilon^j} = \lambda_{(i+2)j}$, and $\Delta(u_0^*, \ldots, \widehat{u}_{i+3}^*, \ldots, u_3^*)_{\varepsilon^j} = \lambda_{(i+3)j}$ for all $i = 0, 1, 2, 3$, $j = 0, 1, 2, 3, \ldots n$ with $\lambda_{i0} = \Delta(u_0, \ldots, \widehat{u}_i, \ldots, u_3)$ and $\lambda_{(i+1)0} = \Delta(u_0, \ldots, \widehat{u}_{i+1}, \ldots, u_3)$ $\lambda_{(i+2)0} = \Delta(u_0, \ldots, \widehat{u}_{i+2}, \ldots, u_3)$ $\lambda_{(i+3)0} = \Delta(u_0, \ldots, \widehat{u}_{i+3}, \ldots, u_3)$. Note that we write $\Delta(u^*)_{\varepsilon^0} = \Delta(u)$.

Newton's theorem associates a power sum P_{ij} function for every polynomial with coefficients λ_{ij} and gives the following relations (see Section 2.4):

$$\begin{aligned}
P_{i1} &= \frac{\lambda_{i1}}{\lambda_{i0}},\\
P_{i2} &= \frac{2\lambda_{i2}}{\lambda_{i0}} - \frac{\lambda_{i1}^2}{\lambda_{i0}^2},\\
P_{i3} &= \frac{3\lambda_{i3}}{\lambda_{i0}} - \frac{3\lambda_{i1}\lambda_{i2}}{\lambda_{i0}^2} + \frac{\lambda_{i1}^3}{\lambda_{i0}^3},\\
P_{i4} &= \frac{4\lambda_{i4}}{\lambda_{i0}} - \frac{4\lambda_{i1}\lambda_{i3}}{\lambda_{i0}^2} - \frac{2\lambda_{i2}^2}{\lambda_{i0}^2} + \frac{4\lambda_{i1}^2\lambda_{i2}}{\lambda_{i0}^3} - \frac{\lambda_{i1}^4}{\lambda_{i0}^4},
\end{aligned} \tag{33}$$

with the general term,

$$P_{in} = \frac{n\lambda_{in}}{\lambda_{i0}} - \sum_{r=1}^{n-1} \frac{\lambda_{i(n-r)}}{\lambda_{i0}} P_{ir}. \tag{34}$$

Above constructions enable us to rewrite the maps $\pi^3_{0,\varepsilon}$ and π^3_{0,ε^2} in a precise form as

$$\begin{aligned}
\pi^3_{0,\varepsilon}(u_0^*, \ldots, u_3^*) &= \sum_{i=0}^{3} (-1)^i \left(P_{i1} \otimes \frac{\lambda_{(i+1)0}}{\lambda_{(i+2)0}} \wedge \frac{\lambda_{(i+3)0}}{\lambda_{(i+2)0}} + \bigwedge_{\substack{k=0\\k\neq i}}^{3} P_{k1} \right), i \bmod 4,\\
\pi^3_{0,\varepsilon^2}(u_0^*, \ldots, u_3^*) &= \sum_{i=0}^{3} (-1)^i \left(P_{i2} \otimes \frac{\lambda_{(i+1)0}}{\lambda_{(i+2)0}} \wedge \frac{\lambda_{(i+3)0}}{\lambda_{(i+2)0}} + \bigwedge_{\substack{k=0\\k\neq i}}^{3} P_{k2} \right), i \bmod 4.
\end{aligned} \tag{35}$$

For $n = 3$, we propose

$$\pi^3_{0,\varepsilon^3}(u_0^*, \ldots, u_3^*) = \sum_{i=0}^{3} (-1)^i \left(P_{i3} \otimes \frac{\lambda_{(i+1)0}}{\lambda_{(i+2)0}} \wedge \frac{\lambda_{(i+3)0}}{\lambda_{(i+2)0}} + \bigwedge_{\substack{k=0\\k\neq i}}^{3} P_{k3} \right), i \bmod 4. \tag{36}$$

Using an inductive approach, one can write

$$\pi^3_{0,\varepsilon^n}(u_0^*,\dots,u_3^*)=\sum_{i=0}^{3}(-1)^i\left(P_{in}\otimes\frac{\lambda_{(i+1)0}}{\lambda_{(i+2)0}}\wedge\frac{\lambda_{(i+3)0}}{\lambda_{(i+2)0}}+\bigwedge_{\substack{k=0\\k\neq i}}^{3}P_{kn}\right),\ i \bmod 4. \tag{37}$$

Next, we move to describe $\pi^3_{1,\varepsilon^n}(u_0^*,\dots,u_3^*)$. We follow an inductive approach to generalize this map because already we have the definitions of $\pi^3_{1,\varepsilon^n}(u_0^*,\dots,u_3^*)$, for $n=1,2,3$ (see [8, 10]). There, we observe that the complexity of this map increases when its order become higher and higher. So, to overcome this situation, we introduce some notations as follows. Let $\Delta(u_0^*,\dots,\widehat{u}_i^*,\dots,\widehat{u}_j^*,\dots,u_4^*)_{\varepsilon^r}=\delta_{ijr}$ with $\Delta(u_0,\dots,\widehat{u}_i,\dots,\widehat{u}_j,\dots,u_4)=\delta_{ij0}$ and $r=0,\dots,n$; then, for a polynomial whose coefficients are δ_{ijr}, there should be an rth power sum say S_{ijr} satisfying the identities below:

$$\begin{aligned}
S_{ij1}&=\frac{\delta_{ij1}}{\delta_{ij0}},\\
S_{ij2}&=\frac{2\delta_{ij2}}{\delta_{ij0}}-\frac{\delta^2_{ij1}}{\delta^2_{ij0}},\\
S_{ij3}&=\frac{3\delta_{ij3}}{\delta_{ij0}}-\frac{3\delta_{ij1}\delta_{ij2}}{\delta^2_{ij0}}+\frac{\delta^3_{ij1}}{\delta^3_{ij0}},\\
S_{ij4}&=\frac{4\delta_{ij4}}{\delta_{ij0}}-\frac{4\delta_{ij1}\delta_{ij3}}{\delta^2_{ij0}}-\frac{2\delta^2_{ij2}}{\delta^2_{ij0}}+\frac{4\delta^2_{ij1}\delta_{ij2}}{\delta^3_{ij0}}-\frac{\delta^4_{ij1}}{\delta^4_{ij0}}.
\end{aligned} \tag{38}$$

And in general,

$$S_{ijn}=\frac{n\delta_{ijn}}{\delta_{ij0}}-\sum_{m=1}^{n-1}\frac{\delta_{ij(n-m)}}{\delta_{ij0}}S_{ijm}. \tag{39}$$

Again, we rewrite the maps $\pi^3_{1,\varepsilon}$ and π^3_{1,ε^2}, which are defined in [9, 10], respectively, in current settings as

$$\begin{aligned}
&\pi^3_{1,\varepsilon}(u_0^*,\dots,u_4^*)\\
&=-\frac{1}{3}\sum_{\substack{i,j=0\\j\neq i}}^{4}(-1)^i\Big(\big\langle r(u_i|u_0,\dots,\widehat{u}_i,\dots,u_4);r_\varepsilon(u_i^*|u_0^*,\dots,\widehat{u^*}_i,\dots,u_4^*)\big]_2\\
&\quad\otimes\prod_{i\neq j}\Delta(\widehat{u}_i,\widehat{u}_j)+(S_{ij1})\otimes[r(u_i|u_0,\dots,\widehat{u}_i,\dots,u_4)]_2\Big),\\
&\pi^3_{1,\varepsilon^2}(u_0^*,\dots,u_4^*)\\
&=-\frac{1}{3}\sum_{\substack{i,j=0\\j\neq i}}^{4}(-1)^i\Big(\big\langle r(u_i|u_0,\dots,\widehat{u}_i,\dots,u_4);r_\varepsilon(u_i^*|u_0^*,\dots,\widehat{u^*}_i,\dots,u_4^*),r_{\varepsilon^2}(u_i^*|u_0^*,\dots,\widehat{u^*}_i,\dots,u_4^*)\big]_2^2\\
&\quad\otimes\prod_{i\neq j}\Delta(\widehat{u}_i,\widehat{u}_j)+(S_{ij2})\otimes[r(u_i|l_0,\dots,\widehat{u}_i,\dots,l_4)]_2\Big).
\end{aligned} \tag{40}$$

For $n = 3$, we also propose

$$\begin{aligned}
&\pi^3_{1,\varepsilon^3}(u_0^*,\ldots,u_4^*)\\
&= -\frac{1}{3}\sum_{\substack{i,j=0\\ j\neq i}}^{4}(-1)^i\Bigg(\left\langle r(u_i|u_0,\ldots,\widehat{u}_i,\ldots,u_4); r_\varepsilon(u_i^*|u_0^*,\ldots,\widehat{u^*}_i,\ldots,u_4^*),\ldots,r_{\varepsilon^3}(u_i^*|u_0^*,\ldots,\widehat{u^*}_i,\ldots,u_4^*)\right]_2^3\\
&\otimes\prod_{i\neq j}\Delta(\widehat{u}_i,\widehat{u}_j)+(S_{ij3})\otimes[r(u_i|u_0,\ldots,\widehat{u}_i,\ldots,u_4)]_2\Bigg).
\end{aligned}\tag{41}$$

It is now easy to express π^3_{1,ε^n} as

$$\begin{aligned}
&\pi^3_{1,\varepsilon^n}(u_0^*,\ldots,u_4^*)\\
&= -\frac{1}{3}\sum_{\substack{i,j=0\\ j\neq i}}^{4}(-1)^i\Bigg(\left\langle r(u_i|u_0,\ldots,\widehat{u}_i,\ldots,u_4); r_\varepsilon(u_i^*|u_0^*,\ldots,\widehat{u^*}_i,\ldots,u_4^*),\ldots,r_{\varepsilon^n}(u_i^*|u_0^*,\ldots,\widehat{u^*}_i,\ldots,u_4^*)\right]_2^n\\
&\otimes\prod_{i\neq j}\Delta(\widehat{u}_i,\widehat{u}_j)+(S_{ijn})\otimes[r(u_i|u_0,\ldots,\widehat{u}_i,\ldots,u_4)]_2\Bigg).
\end{aligned}\tag{42}$$

The map π^3_{2,ε^n} can simply be defined as the triple ratio which is given in (17). For $\nu = 2, 3$, it is given in [8, 10] as

$$\begin{aligned}
\pi^3_{2,\varepsilon}(u_0^*,\ldots,u_5^*) &= \frac{2}{45}\mathrm{Alt}_6\left\langle r_3(u_0,\ldots,u_5); r_{3,\varepsilon}(u_0^*,\ldots,u_5^*)\right]_3,\\
\pi^3_{2,\varepsilon^2}(u_0^*,\ldots,u_5^*) &= \frac{2}{45}\mathrm{Alt}_6\left\langle r_3(u_0,\ldots,u_5); r_{3,\varepsilon}(u_0^*,\ldots,u_5^*), r_{3,\varepsilon^2}(u_0^*,\ldots,u_5^*)\right]_3.
\end{aligned}\tag{43}$$

And, for $n = 3$, we propose

$$\pi^3_{2,\varepsilon^3}(u_0^*,\ldots,u_5^*) = \frac{2}{45}\mathrm{Alt}_6\left\langle r_3(u_0,\ldots,u_5); r_{3,\varepsilon}(u_0^*,\ldots,u_5^*), r_{3,\varepsilon^2}(u_0^*,\ldots,u_5^*), r_{3,\varepsilon^3}(u_0^*,\ldots,u_5^*)\right]_3.\tag{44}$$

Therefore, in general, it may be

$$\pi^3_{2,\varepsilon^n}(u_0^*,\ldots,u_5^*) = \frac{2}{45}\mathrm{Alt}_6\langle r_3(u_0,\ldots,u_5); r_{3,\varepsilon}(u_0^*,\ldots,u_5^*), r_{3,\varepsilon^2}(u_0^*,\ldots,u_5^*),\ldots,r_{3,\varepsilon^n}(u_0^*,\ldots,u_5^*)\Big]_3. \tag{45}$$

The horizontal map ∂_{ε^n} of the diagram (D) works in two ways. First is when it sends the members of $T\mathscr{B}_3^n(F)$ to $(T\mathscr{B}_2^n(F)\otimes F^\times)\oplus(F\otimes\mathscr{B}_2(F))$ and second way is when it sends$_2$ elements of $(T\mathscr{B}_2^n(F)\otimes F^\times)\oplus(F\otimes\mathscr{B}_2(F))$ into $(F\otimes\overset{2}{\wedge}F^\times)\oplus(\overset{3}{\wedge}F)$. This map is defined in [9, 10], for $n=1,2$, as

$$\begin{aligned}
&\partial_\varepsilon(\langle s;t]_2\otimes c + x\otimes[y]_2)\\
&\quad=\frac{t}{s}\otimes(1-s)\wedge c-\frac{t}{(1-s)}\otimes s\wedge c + x\otimes(1-y)\wedge y+\frac{t}{s}\wedge\frac{t}{(1-s)}\wedge x,\\
&\partial_{\varepsilon^2}(\langle s;t_1,t_2]_2\otimes c + x\otimes[y]_2)\\
&\quad=\left(\frac{2t_2}{s}-\frac{t_1^2}{s^2}\right)\otimes(1-s)\wedge c-\left(\frac{2t_2}{(1-s)}+\frac{t_1^2}{(1-s)^2}\right)\otimes s\wedge c\\
&\qquad+x\otimes(1-y)\wedge y+\left(\frac{2t_2}{s}-\frac{t_1^2}{s^2}\right)\wedge\left(\frac{2t_2}{(1-s)}+\frac{t_1^2}{(1-s)^2}\right)\wedge x.
\end{aligned} \tag{46}$$

And, for $n=3$, we propose this map as

$$\begin{aligned}
&\partial_{\varepsilon^3}\left(\langle s;t_1,t_2,t]^3_{32}\otimes c + x\otimes[y]_2\right),\\
&\quad=\left(\frac{3t_3}{a}-\left(\frac{3t_1t_2}{s^2}-\frac{t_1^3}{s^3}\right)\right)\otimes(1-s)\wedge c-\left(\frac{3t_3}{1-s}-\left(\frac{3t_1t_2}{(1-s)^2}-\frac{t_1^3}{(1-s)^3}\right)\right)\otimes s\wedge c,\\
&\qquad+x\otimes(1-y)\wedge y+\left(\frac{3t_3}{s}-\left(\frac{3t_1t_2}{s^2}-\frac{t_1^3}{s^3}\right)\right)\wedge\left(\frac{3t_3}{1-s}-\left(\frac{3t_1t_2}{(1-s)^2}-\frac{t_1^3}{(1-s)^3}\right)\right)\wedge x.
\end{aligned} \tag{47}$$

We can make these definitions more precise using identities of Newton, i.e.,

$$\begin{aligned}
&\partial_{\varepsilon^2}(\langle s;t_1,t_2]_2\otimes c + a\otimes[b]_2)\\
&\quad=M_1\otimes(1-s)\wedge c-N_1\otimes s\wedge c+a\otimes(1-b)\wedge b+M_1\wedge N_1\wedge a,\\
&\partial_{\varepsilon^3}(\langle s;t_1,t_2,t_3]_2\otimes c + a\otimes[b]_2)\\
&\quad=M_3\otimes(1-s)\wedge c-N_3\otimes s\wedge c+a\otimes(1-b)\wedge b+M_3\wedge N_3\wedge a.
\end{aligned} \tag{48}$$

Therefore, we can write

$$\begin{aligned}
&\partial_{\varepsilon^n}(\langle s;t_1,t_2,\ldots,t_n]_2\otimes c + a\otimes[b]_2),\\
&\quad=M_n\otimes(1-s)\wedge c-N_n\otimes s\wedge c+a\otimes(1-b)\wedge b+M_n\wedge N_n\wedge a.
\end{aligned} \tag{49}$$

The map ∂_{ε^n} of right square of the diagram (D) has already been defined in [9, 10] for order 1 and 2 as

$$\begin{aligned}
\partial_\varepsilon(\langle s;t]_3) &= \langle s;t]_2\otimes s+\frac{t}{s}\otimes[s]_2,\\
\partial_{\varepsilon^2}\left(\langle s;t_1,t_2]^2_3\right) &= \langle s;t_1,t_2]^2_2\otimes s+\left(\frac{2t_2}{s}-\frac{t_1^2}{s^2}\right)\otimes[s]_2.
\end{aligned} \tag{50}$$

And, for order 3, we propose

$$\partial_{\varepsilon^3}\left(\left\langle s;t_1,t_2,t_3\right]_3^3\right)=\left\langle s;t_1,t_2,t_3\right]_2^3\otimes s+\left(\frac{3t_3}{s}-\left(\frac{3t_1t_2}{s^2}-\frac{t_1^3}{s^3}\right)\right)\otimes[s]_2. \tag{51}$$

If we consider a polynomial having coefficients t_i together with a kth power sum function T_k, then we can express the above maps in a precise form like

$$\begin{aligned}\partial_{\varepsilon}\left(\left\langle t_0;t_1\right]_3^2\right)&=\left\langle t_0;t_1\right]_2\otimes t_0+T_1\otimes[t_0]_2,\\ \partial_{\varepsilon^2}\left(\left\langle t_0;t_1,t_2\right]_3^2\right)&=\left\langle t_0;t_1,t_2\right]_2^2\otimes t_0+T_2\otimes[t_0]_2,\\ \partial_{\varepsilon^3}\left(\left\langle t_0;t_1,t_2,t_3\right]_3^3\right)&=\left\langle t_0;t_1,t_2,t_3\right]_2^3\otimes t_0+T_3\otimes[t_0]_2.\end{aligned} \tag{52}$$

Therefore,

$$\partial_{\varepsilon^n}\left(\left\langle t_0;t_1,t_2,t_3,\ldots,t_n\right]_3^n\right)=\left\langle t_0;t_1,t_2,t_3,\ldots,t_n\right]_2^n\otimes t_0+T_n\otimes[t_0]_2, \tag{53}$$

where $t_i=r_{3,\varepsilon^i}(u_0^*,\ldots,u_5^*), i=0,\ldots,n$, and

$$T_n=\frac{nt_n}{t}-\sum_{r=1}^{n-1}\frac{t_{n-r}}{t}T_r. \tag{54}$$

Theorem 1. *The right square of (D) commutes, that is,*

$$\partial_{\varepsilon^n}\circ\pi^3_{1,\varepsilon^n}=\pi^3_{0,\varepsilon^n}\circ d. \tag{55}$$

Proof. We split the map,

$$\pi^3_{0,\varepsilon^n}\colon C_4\left(\mathbb{A}^3_{\mathbb{F}[\varepsilon]_{n+1}}\right)\longrightarrow\left(\mathbb{F}\otimes\wedge^2\mathbb{F}^\times\right)\oplus\left(\wedge^3\mathbb{F}\right), \tag{56}$$

into the sum of two maps:

$$\phi_1^n\colon C_4\left(\mathbb{A}^3_{\mathbb{F}[\varepsilon]_{n+1}}\right)\longrightarrow\left(\mathbb{F}\otimes\wedge^2\mathbb{F}^\times\right) \tag{57}$$

and

$$\phi_2^n\colon C_4\left(\mathbb{A}^3_{\mathbb{F}[\varepsilon]_{n+1}}\right)\longrightarrow\left(\wedge^3\mathbb{F}\right). \tag{58}$$

Then, we write

$$\pi^3_{0,\varepsilon^n}=\phi_1^n+\phi_2^n. \tag{59}$$

The definitions of d and π^3_{0,ε^n} allow us to write

$$\begin{aligned}\phi_1^n\circ d(u_0^*,\ldots,u_4^*)&=\phi_1^n\left(\sum_{i=0}^{4}(-1)^i(u_0^*,\ldots,\widehat{u}_i^*,\ldots,u_4^*)\right)\\ &=\widetilde{\mathrm{Alt}}_{(01234)}\left(\sum_{i=0}^{3}(-1)^i\left(\frac{n\lambda_{in}}{\lambda_{i0}}-\sum_{r=1}^{n-1}\frac{\lambda_{i(n-r)}}{\lambda_{i0}}P_{ir}\right)\otimes\frac{\lambda_{(i+1)0}}{\lambda_{(i+2)0}}\wedge\frac{\lambda_{(i+3)0}}{\lambda_{(i+2)0}}\right),\\ \phi_2^n\circ d(u_0^*,\ldots,u_4^*)&=\phi_2^n\left(\sum_{i=0}^{4}(-1)^i(u_0^*,\ldots,\widehat{u}_i^*,\ldots,u_4^*)()\right)\\ &=\widetilde{\mathrm{Alt}}_{(01234)}\left(\sum_{i=0}^{3}(-1)^i\bigwedge_{\substack{k=0\\k\neq i}}^{3}\left(\frac{n\lambda_{kn}}{\lambda_{k0}}-\sum_{r=1}^{n-1}\frac{\lambda_{k(n-r)}}{\lambda_{k0}}P_{kr}\right)\right).\end{aligned} \tag{60}$$

The inner expression of (37) will gives us terms such as $(a_1)_{\varepsilon^n}/a_1\otimes b\wedge c$, $(a_1)_{\varepsilon^i}(a_2)_{\varepsilon^j}/a_1^2\otimes b\wedge c, i+j=n$, and $(a_1)_{\varepsilon^i}(a_2)_{\varepsilon^j}(a_3)_{\varepsilon^k}/a_1^3\otimes b\wedge c, i+j+k=n$. Moreover, the simplification process vanishes the terms with $x_\alpha\neq x_\beta\neq x_\gamma\ldots$ and remains only those terms whose $x_i's$ are the same. Next, we expand the outer sum and use some arithmetic to simplify the result. We can use the same algorithm on the other part $\phi_2^n\circ d(u_0^*,\ldots,u_4^*)$ and get the result in precise form and hence will get the value of $\pi^3_{0,\varepsilon^n}\circ d$. Next, we move to evaluate $\partial_{\varepsilon^n}\circ\pi^3_{1,\varepsilon^n}$. For this, we take $(u_0^*,\ldots,u_4^*)\in C_5(\mathbb{A}^3_{\mathbb{F}[\varepsilon]_{n+1}})$ so that

$$\begin{aligned}&\partial_{\varepsilon^n}\circ\pi^3_{1,\varepsilon^n}(u_0^*,\ldots,u_4^*),\\ &=\partial_{\varepsilon^n}\left(-\frac{1}{3}\sum_{\substack{i,j=0\\j\neq i}}^{4}(-1)^i\left(\left\langle a;b_1,b_2,\ldots,b_n\right]_2^n\otimes\prod_{i\neq j}\Delta\left(\widehat{u}_i,\widehat{u}_j\right)+\left(S_{ijn}\right)\otimes\left[r\left(u_i|u_0,\ldots,\widehat{u}_i,\ldots,u_4\right)_2\right]\right)\right),\end{aligned} \tag{61}$$

where $s = r(u_i|u_0,\ldots,\widehat{u}_i,\ldots,u_4)$, $t_1 = r_\varepsilon(u_i^*|u_0^*,\ldots,\widehat{u^*}_i,\ldots,u_4^*)$, $t_2 = r_{\varepsilon^2}(u_i^*|su_0^*,\ldots,\widehat{u^*}_i,\ldots,u_4^*)$, and $t_n = r_{\varepsilon^n}(u_i^*|u_0^*,\ldots,\widehat{u^*}_i,\ldots,u_4^*)$ and S_{ijn} is defined in (22). Using definition of ∂_{ε^n} and settings of (8) and (10), we can write as

$$
\begin{aligned}
&= -\frac{1}{3}\sum_{\substack{i,j=0\\ j\neq i}}^{4}(-1)^i\left\{\left(\frac{nt_n}{s}-\sum_{r=1}^{n-1}\frac{t_{n-r}}{s}M_r\right)\otimes(1-s)\wedge\prod_{i\neq j}\Delta\left(\widehat{u}_i,\widehat{u}_j\right)\right.\\
&-\left(\frac{nt_n}{1-s}-\sum_{r=1}^{n-1}\frac{t_{n-r}}{1-s}N_r\right)\otimes s\wedge\prod_{i\neq j}\Delta\left(\widehat{u}_i,\widehat{u}_j\right)+S_{ijn}\otimes(1-y)\wedge y\\
&\left.+\left(\frac{nb_n}{s}-\sum_{r=1}^{n-1}\frac{t_{n-r}}{s}M_r\right)\wedge\left(\frac{nt_n}{1-s}-\sum_{r=1}^{n-1}\frac{t_{n-r}}{1-s}N_r\right)\wedge S_{ijn}\right\},
\end{aligned}
\tag{62}
$$

where $y = [r(u_i|u_0,\ldots,\widehat{u}_i,\ldots,u_4)]_2$. This expression can further be transformed into a simpler form by using first the axioms of tensor and wedge product and then expanding through summation. This will give us a precise value of $\partial_{\varepsilon^n}\circ\pi^3_{1,\varepsilon^n}(u_0^*,\ldots,u_4^*)$ which will be exactly equal to the value $\pi^3_{1,\varepsilon^n}\circ d(u_0^*,\ldots,u_4^*)$. □

Theorem 2. *The left part of the diagram (D) commutes, that is,*

$$\partial_{\varepsilon^n}\circ\pi^3_{2,\varepsilon^n} = \pi^3_{1,\varepsilon^n}\circ d. \tag{63}$$

Proof. The maps π^3_{1,ε^n}, ∂_{ε^n}, and π^3_{2,ε^n} are explained in (25), (35), and (28), respectively. Taking $(u_0^*,\ldots,u_5^*)\in C_6(\mathbb{A}^3_{F[\varepsilon]_{n+1}})$ and applying (28), we have

$$
\begin{aligned}
&\partial_{\varepsilon^n}\circ\pi^3_{2,\varepsilon^n}(u_0^*,\ldots,u_5^*)\\
&\quad=\partial_{\varepsilon^n}\left(\frac{2}{45}\mathrm{Alt}_6\left\langle r_3(u_0,\ldots,u_5);r_{3,\varepsilon}(u_0^*,\ldots,u_5^*),r_{3,\varepsilon^2}(u_0^*,\ldots,u_5^*),\ldots,r_{3,\varepsilon^n}(u_0^*,\ldots,u_5^*)\right]_3^n\right).
\end{aligned}
\tag{64}
$$

Applying definition (35) and using (36), we obtain

$$
= \frac{2}{45}\mathrm{Alt}_6\left\{\left\langle c;c_1,c_2,\ldots,c_n\right]_2^n\otimes c+\left(\frac{nc_n}{c}-\sum_{r=1}^{n-1}\frac{c_{n-r}}{c}T_r\right)\otimes[c]_2\right\},
\tag{65}
$$

where $c_i = r_{3,\varepsilon^i}(u_0^*,\ldots,u_5^*), i = 0,1,2,\ldots,n$, and $T_1 = c_1/c$ Here, we can use the combinatorial techniques which are used in the proof of Theorem 5.6 of [9] and can write equation (42) as

$$
= \frac{1}{3}\mathrm{Alt}_6\left\{\left\langle c;c_1,c_2,\ldots,c_n\right]_2^n\otimes(u_0u_1u_3)+\left(\frac{n(u_0^*u_1^*u_3^*)_{\varepsilon^n}}{(l_0l_1l_3)}-\sum_{r=1}^{n-1}\frac{(u_0^*u_1^*u_3^*)_{\varepsilon^{n-r}}}{(u_0u_1u_3)}V_r\right)\otimes[c]_2\right\},
\tag{66}
$$

where V_r represents the rth sum of powers of the polynomial having coefficients $(u_0^*u_1^*u_3^*)_{\varepsilon^i}$ and $V_1 = (u_0^*u_1^*u_3^*)_\varepsilon/(u_0u_1u_3)$. To attain RHS, we express the map π^3_{1,ε^n} as an alternation sum:

$$
\begin{aligned}
\pi^3_{1,\varepsilon^n}(u_0^*,\ldots,u_5^*) = \frac{1}{3}\mathrm{Alt}_6\Big\{&\left\langle r(u_0|u_1u_2u_3u_4);r_\varepsilon(u_0^*|u_1^*u_2^*u_3^*u_4^*),\ldots,r_{\varepsilon^n}(u_0^*|u_1^*u_2^*u_3^*u_4^*)\right]_2^2\otimes(u_0u_1u_2)\\
&+\left(\frac{n(u_0^*u_1^*u_3^*)_{\varepsilon^n}}{(u_0u_1u_3)}-\sum_{r=1}^{n-1}\frac{(u_0^*u_1^*u_3^*)_{\varepsilon^{n-r}}}{(u_0u_1u_3)}V_r\right)\otimes[c]_2\Big\}.
\end{aligned}
\tag{67}
$$

Now, it becomes easy to attain the value of $\pi^3_{1,\varepsilon^n} \circ d(u_0^*, \ldots, u_5^*)$ with the help of (44). For this, we proceed by enforcing d and then applying π^3_{1,ε^n}. Now, we are going to follow the procedure of Theorem 5.6 of [8] which will provide us a result exactly the same as (43). □

4. Conclusion

Polylogarithmic groups have been studied by several renowned mathematicians such as Goncharove, Zagier, Bloch, Suslin, and Cathelineaue. A tangential version of these groups of weight two and three is studied by Siddiqui for the first order. Recently, the study of tangential groups of weight two and their associated maps are extended to a general order n. In this work, we have shown that the notions associated to trilogarithmic tangential groups $T\mathscr{B}^n_3(\mathbb{F})$ such as cross ratio, triple ratio, Siegel's identity and other relations are valid for higher orders. All these notions are being constructed for the trilogarithmic tangential groups of higher order. Using the groups $T\mathscr{B}^n_3(\mathbb{F})$ and a map ∂_{ε^n}, we formed the following complexes:

$$T\mathscr{B}^n_3(\mathbb{F}) \xrightarrow{\partial_{\varepsilon^n}} \left(T\mathscr{B}^n_2(\mathbb{F}) \otimes \mathbb{F}^\times\right) \oplus \left(\mathbb{F} \otimes \mathscr{B}_2(\mathbb{F})\right) \xrightarrow{\partial_{\varepsilon^n}} \left(\mathbb{F} \otimes \overset{2}{\wedge} \mathbb{F}^\times\right) \oplus \left(\overset{3}{\wedge} \mathbb{F}\right). \tag{68}$$

Moreover, we have proposed morphisms, π^3_{0,ε^n}, π^3_{1,ε^n}, and π^3_{2,ε^n} in order to connect Grassmannian complexes to the trilogarithmic tangential complexes for higher orders. This generalization process has been carried out with the help of Newton's identities. Lastly, we proved that the resulting diagrams of connectivity are commutative.

The above results motivate us to compute higher order tangent groups for weight $n \geq 4$ and use it to construct the higher order tangent to Goncharov's complex for weight 4 or even higher [16].

Data Availability

No data were used to support this study.

Conflicts of Interest

The authors declare that there were no conflicts of interest regarding the publication of this article.

Authors' Contributions

All authors contributed equally to the preparation of this manuscript.

References

[1] M. Khalid, M. Sultana, A. Iqbal, and J. Khan, "Geometry of tangential and configuration chain complexes for higher weights," *Punjab University Journal of Mathematics*, vol. 52, no. 2, pp. 29–55, 2020.

[2] M. Khalid, M. Sultana, A. Iqbal, and J. Khan, "Generalized geometry of tangential and affine configuration chain complexes," *Punjab University Journal of Mathematics*, vol. 53, no. 11, pp. 793–811, 2021.

[3] S. Hussain, Z. Hussain, S. Hussain, and R. Siddiqui, "Maps between tangential complexes for projective configurations," *Journal Of Mechanics Of Continua and Mathematical Sciences*, vol. 16, no. 7, pp. 146–157, 2021.

[4] M. Khalid, J. Khan, and A. Iqbal, "Generalized geometry of Goncharov and conguration complexes," *Turkish Journal of Mathematics*, vol. 42, pp. 1509–1527, 2018.

[5] M. Khalid, J. Khan, and A. Iqbal, "Extension of morphisms in geometry of chain complexes," *Punjab University Journal of Mathematics*, vol. 51, no. 1, pp. 29–49, 2019.

[6] M. Khalid, J. Khan, and A. Iqbal, "Generalization of higher order homomorphism in configuration complexes," *Punjab University Journal of Mathematics*, vol. 49, no. 2, pp. 37–49, 2017.

[7] J.-L. Cathelineau, "The tangent complex to the Bloch-Suslin complex," *Bulletin de la Société Mathématique de France*, vol. 135, no. 4, pp. 565–597, 2007.

[8] R. Siddiqui, "Infinitesimal and tangent to polylogarithmic complexes for higher weight," *AIMS Mathematics*, vol. 4, no. 4, pp. 1248–1257, 2019.

[9] R. Siddiqui, "Tangent to bloch-suslin and grassmannian complexes over the dual numbers," 2012, https://arxiv.org/abs/1205.4101.

[10] S. Hussain and R. Siddiqui, "Grassmannian complex and second order tangent complex," *Punjab University Journal of Mathematics*, vol. 48, no. 2, pp. 1353–1363, 2016.

[11] S. Hussain and R. Siddiqui, "Morphisms between grassmannian complex and higher order tangent complex," *Communications in Mathematics and Applications*, vol. 10, no. 3, pp. 509–518, 2019.

[12] A. B. Goncharov, "Geometry of configurations, polylogarithms, and motivic cohomology," *Advances in Mathematics*, vol. 114, no. 2, pp. 197–318, 1995.

[13] P. Elbaz-Vincent and H. Gangl, "On Poly(ana)logs I," *Compositio Mathematica*, vol. 130, no. 2, pp. 161–214, 2002.

[14] S. Bera and S. Mukherjee, "Generalized power sum and Newton-girard identities," *Graphs and Combinatorics*, vol. 36, no. 4, pp. 1–8, 2020.

[15] S. Chamberlin and A. Rafizadeh, "A generalized Newton-Girard formula for monomial symmetric polynomials," *Rocky Mountain Journal of Mathematics*, vol. 50, no. 3, 2020.

[16] S. Hussain and R. Siddiqui, "Projective configurations and variant of Cathelineau complex," *Journal of Prime Research in Mathematics*, vol. 6, pp. 1353–1363, 2016.

Hindawi
Mathematical Problems in Engineering
Volume 2022, Article ID 3390478, 18 pages
https://doi.org/10.1155/2022/3390478

Research Article

Heat Transfer in a Fractional Nanofluid Flow through a Permeable Medium

Muhammad Shoaib Anwar,[1] **Muhammad Irfan**,[2] **Majid Hussain**,[3] **Taseer Muhammad**,[4] **and Zakir Hussain**[5]

[1]*Department of Mathematics, University of Jhang, Gojra Road, Jhang 35200, Pakistan*
[2]*Department of Mathematics, University of WAH, Quaid Avenue, Wah Rawalpindi, Punjab 47040, Pakistan*
[3]*Department of Natural Sciences and Humanities, University of Engineering and Technology, Lahore 54890, Pakistan*
[4]*Department of Mathematics, College of Sciences, King Khalid University, Abha 61413, Saudi Arabia*
[5]*Department of Mathematics, University of Baltistan, Skardu, Pakistan*

Correspondence should be addressed to Muhammad Shoaib Anwar; shoaib_tts@yahoo.com

Received 19 October 2021; Revised 6 December 2021; Accepted 28 January 2022; Published 2 March 2022

Academic Editor: Ali Ahmadian

This study examines viscoelastic fractional nanofluid flow through Darcy medium. Memory characteristics due to elasticity are explored with noninteger time derivatives. The unsteady motion of MHD flow is modeled by nonlinear differential equations. Buoyancy forces are incorporated via convection parameters in the flow domain. Fractional relaxation time is considered to control the propagation speed of temperature. A finite difference, along with finite element, a numerical algorithm has been developed for the computation of governing flow equations. Friction coefficient, Sherwood numbers, and Nusselt numbers are computed for the noninteger derivative model. Simulations revealed that noninteger numbers have congruous behavior for concentration, temperature, and velocity fields. It is also noted that heat flux, δ_1, and mass flux, δ_2, numbers have contradictory effects on the friction coefficient. Various flows, particularly in polymer industries and electrospinning for the production of nanofibers, can be tackled in a comparable pattern.

1. Introduction

In this communication, we have described the transport of momentum, heat, and concentration with the help of mathematical relations. Mathematical relations are formulated with constitutive expressions that handle fluxes of the above-prescribed quantities [1]. Formulated equations, remained helpful to analyze the transport of heat, diffusion of chemical species, movement of geological flows, engineering applications, meteorology, material science, and medicines [2, 3]. Molecular contact and Brownian motion [1] characterized the conductivity, diffusivity, and viscosity for the nanofluid in the flow domain. Particularly, transfer of heat is an analog of mass transfer in the constitutive expressions for fluxes. Fick's law governs the diffusion in mass transport, and Fourier's law handles the conduction mechanism in heat transfer. Here we have considered the generalized Fourier and Fick laws to incorporate relaxation times. Transport phenomena in Newtonian and non-Newtonian flows can be seen in heat exchangers, thermal devices, granular insulation, fiber technology, nuclear repositories, fermentation processes, geothermal extractions, and the production of crude oil [4–11]. In the literature, the transfer of heat and mass is widely reported by distinguished researchers. For example, Salama et al. [12] discussed the solution of a flow problem through porous media with flux approximations. In this communication, the viscoelastic fluid model of second grade is analyzed for the transport mechanism with suspended nanoparticles. Viscoelastic second-grade fluid model exhibits differential type nature. For differential fluids, stress is expressed by an explicit velocity gradient. Differential models describe the fluids in

terms of their shear thickening and thinning effects, normal stress effects, thixotropy exhibition, and nonlinear behavior of creeping and yielding. Flow problems, which include polymer suspensions and slurries, in fiber handling can be discussed with a given mathematical model [13].

Governing flow equations with noninteger time derivatives have been proven for useful analysis of viscoelastic trends [14]. Nowadays, mathematical modeling with noninteger derivatives have gained importance in various branches of science. For example, valuable impact can be seen in fluid mechanics. Moreover, the influence of noninteger modeling is seen in viscoelasticity, control theory, and electrochemistry [15–17]. Advancements in fractional modeling are carried out with the passage of time and the inclusion of new fractional derivatives in the literature, for example, Yang's fractional derivative, Atangana–Baleanu derivatives, and Caputo derivatives [18, 19]. Both natural and artificial systems can be analyzed in a better way via noninteger time derivatives as they describe hereditary aspects of materials [20–24]. Simulations of anomalous nonlinear models can be used to approximate experimental data in a better way when compared to usual rheological models [25–30].

Porous medium flows occur in soil mechanics, ceramics, and industrial and mineral processing. The complexity of the flow problem is increased with the presence of a porous medium. This is mainly due to the interface between packing particles and fluid molecules. Darcy flow is analyzed by various researchers. Nonlinear Darcy flow is examined by Ervin et al. [31]. The Lorentz force shows a significant role in viscoelastic problems such as in MHD generators and control theory. Magnetic field impacts can be seen in porous medium flows that are encountered in metallurgical systems, extrusion and penetration practices, etc. The flow domain is greatly influenced by convection as a transport mechanism, is greatly changed by both buoyancy and gravitational forces. Convection's importance can be seen in boilers, nuclear reactors, and heat exchangers. Zhou and Liang [32] discussed convection in unsteady flow problems.

The industrial importance of nanofluids is significant in lightweight materials production, the breakdown of organic pollutants, and in the production of nanofibers [33, 34]. Here, under consideration, flow is unidirectional through a channel of infinite extent. By this configuration, fluid velocity and its gradient are orthogonal to each other, which may lead to the addition of a nonlinear convection term in the governing equations. These flows are mostly observed in the long narrow channels. Many microchannel flows are described by these solutions, their superposition, and by the small perturbation of these flows [35, 36]. Viscoelastic flows can also be used in electrospinning for nanofibers production. Nanofibers are formulated by an electric charged jet of polymer solution that is of viscoelastic nature. An increase of yield stress along with a viscoelastic jet causes a decrease in fluid elongation [37, 38]. The structure of nanoparticles is between atomic and bulk. The possibility of nano particles' inclusion is due to their strong interaction with base fluid. Inclusion of these particles effectively changes the characteristics of the base fluid. For instance, nanoparticle suspension increases the thermal conductivity of the base fluid. Wang and Zhang [39] analyzed heat transfer in nanofluid flow. With the passage of time, fractional nanofluid flows require more attention in literature. Solutions to fractional flow problems are usually discussed with integral transforms. But integral transforms are not helpful for solving nonlinear coupled fractional equations. Due to this, numerical solutions are proposed for flow problems(see [40–43]). In this article, we have tackled the problem with finite element and finite difference techniques to solve the described fractional flow configuration.

Particularly in this communication, we have considered modeling with noninteger derivatives of nanofluid flow. Due to this, we have achieved more control over the flow simulations with the help of fractional derivatives when compared with the classical mathematical flow models. Flux conditions are imposed at $y = 0$, while quadratic variations are observed at the fixed boundary. A Darcy flow medium is observed with an applied magnetic field to the flow domain. Moreover, here we have proposed a scheme with numerical discretization to obtain the stable results of the coupled nonlinear fractional equations. Space variable is discretized by finite element while time variable is discretized by finite difference scheme. The influence of the involved physical parameters is discussed appropriately. In Section 2, modeling with noninteger time derivatives is discussed. The flow field is approximated by the proposed scheme in Section 3. A numerical approximation of the flow problem is given in Section 4. Finally, key results are given in Section 5.

2. Mathematical Description

In this study, we considered heat transfer in the MHD flow of the nanoliquid with noninteger derivatives of time. Modeling with noninteger derivatives helps to achieve more control over the flow simulations when compared with the classical models that contain ordinary derivatives. A nanofluid is formed with nanoparticles and base liquid. The medium of fluid flowing is considered to be a Darcy porous medium. Moreover, Neumann boundary conditions are supposed to be in the heating domain. At the start, there is no movement in the medium. At that time, the whole configuration is at constant temperature θ_0 and concentration ϕ_0. With the passage of time, disturbance in the liquid is observed due to the lower domain. We consider the velocity field to be a function of y and t only. Then we consider

$$\mathbf{U} = u(y,t)\mathbf{e}_{\mathbf{x}}. \tag{1}$$

For the Cauchy stress tensor, Rivlin–Ericksen tensors, Darcy law and thermodynamic stability conditions of differential type second grade fluid (see [21] and references therein). The fractional formalism of thermal and concentration gradients can be seen in [45, 46].

Here is a brief description of the mathematical modeling. In order to formulate an energy equation with Caputo fractional derivative α including nanoparticles, consider the classical energy equation for incompressible fluid of the Buongiorno article (see [46]).

$$\rho_f c_f \frac{\partial \theta}{\partial t} = -\nabla \cdot \mathbf{q} + h_p \nabla \cdot \mathbf{J}_p, \tag{2}$$

where $\mathbf{q}$, $\mathbf{J}_p$ denote fluxes of energy and diffusion and for definition (see [46]). Temperature and concentration propagation of infinite order can be seen with $\mathbf{q}$, $\mathbf{J}_p$ in Buongiorno article (see [46]). We can overcome this situation with the introduction of fractional relaxation times using reference [45], so we define $\mathbf{q}$, $\mathbf{J}_p$ as

$$\left(1 + \frac{\tau_1^\alpha}{\Gamma(1+\alpha)} \frac{\partial^\alpha}{\partial t^\alpha}\right)\mathbf{q} = -k\nabla\theta + h_p\left(1 + \frac{\tau_1^\alpha}{\Gamma(1+\alpha)} \frac{\partial^\alpha}{\partial t^\alpha}\right)\mathbf{J}_p, \tag{3}$$

$$\left(1 + \frac{\tau_1^\alpha}{\Gamma(1+\alpha)} \frac{\partial^\alpha}{\partial t^\alpha}\right)\mathbf{J}_p = -\rho_p D_B \nabla\phi - \rho_p D_\theta \frac{\nabla\theta}{\theta_0}. \tag{4}$$

Now using (2) and (3) and $\nabla h_p = c_p \nabla\theta$ [46], we obtained

$$\rho_f c_f \left(1 + \frac{\tau_1^\alpha}{\Gamma(1+\alpha)} \frac{\partial^\alpha}{\partial t^\alpha}\right)\frac{\partial\theta}{\partial t} = k\nabla^2\theta + \rho_p c_p \left(1 + \frac{\tau_1^\alpha}{\Gamma(1+\alpha)} \frac{\partial^\alpha}{\partial t^\alpha}\right) \left(D_B \nabla\phi \cdot \nabla\theta + \frac{D_\theta}{\theta_0}\nabla\theta \cdot \nabla\theta\right). \tag{5}$$

Similarly using the equation of concentration in Buongiorno model [46], we get

$$\left(\frac{\partial}{\partial t} + \nabla \cdot \mathbf{U}\right)\phi = -\frac{1}{\rho_p}\nabla \cdot \mathbf{J}_p, \tag{6}$$

reduces to

$$\left(1 + \frac{\tau_2^\beta}{\Gamma(1+\beta)} \frac{\partial^\beta}{\partial t^\beta}\right)\frac{\partial\phi}{\partial t} = D_B\nabla^2\phi + \frac{D_\theta}{\theta_0}\nabla^2\theta. \tag{7}$$

Finally, governing present flow equations are

$$\nabla \cdot \mathbf{U} = 0, \tag{8}$$

$$\frac{d\mathbf{U}}{dt} = \frac{1}{\rho_f}(\nabla \cdot \mathbb{S} + \mathbf{r}) + \mathbf{b} + g\left[\beta_1(\theta - \theta_0) + \beta_2(\theta - \theta_0)^2\right], \tag{9}$$

$$\frac{d}{dt}\left(1 + \frac{\tau_1^\alpha}{\Gamma(1+\alpha)} \frac{\partial^\alpha}{\partial t^\alpha}\right)\theta = \alpha_3\frac{\partial^2\theta}{\partial y^2} + \tau\left(1 + \frac{\tau_1^\alpha}{\Gamma(1+\alpha)} \frac{\partial^\alpha}{\partial t^\alpha}\right)\left(D_B\frac{\partial\theta}{\partial y}\frac{\partial\phi}{\partial y} + \frac{D_\theta}{\theta_0}\left(\frac{\partial\theta}{\partial y}\right)^2\right), \tag{10}$$

$$\frac{d}{dt}\left(1 + \frac{\tau_2^\beta}{\Gamma(1+\beta)} \frac{\partial^\beta}{\partial t^\beta}\right)\phi = D_B\frac{\partial^2\phi}{\partial y^2} + \frac{D_\theta}{\theta_0}\frac{\partial^2\theta}{\partial y^2}, \tag{11}$$

where $\mathbb{S}$ stands for the Cauchy tensor of stress for fluid of second grade (see [21]), $\mathbf{r}$ is the Darcy resistance of porous medium (see [21]), and $\mathbf{b}$ denotes body force.

The pressure gradient is assumed to be negligible.

2.1. Governing Equations. The equations that modeled the flow problem along with their conditions are given here. Continuity (8) will reduce to identity with velocity given in (1). After some mathematical simplifications, modeled equations reduce to

$$\frac{\partial u}{\partial t} = \left(\nu + \frac{\alpha_1}{\rho_f}\frac{\partial}{\partial t}\right)\left[\frac{\partial^2 u}{\partial y^2}\right] - \frac{\psi}{K}\left(\nu + \frac{\alpha_1}{\rho_f}\frac{\partial}{\partial t}\right)u - \frac{\sigma B_0^2}{\rho_f}u + g\left[\beta_1(\theta - \theta_0) + \beta_2(\theta - \theta_0)^2\right], \tag{12}$$

$$\frac{\partial}{\partial t}\left(1 + \frac{\tau_1^\alpha}{\Gamma(1+\alpha)} \frac{\partial^\alpha}{\partial t^\alpha}\right)\theta = \alpha_3\frac{\partial^2\theta}{\partial y^2} + \tau\left(1 + \frac{\tau_1^\alpha}{\Gamma(1+\alpha)} \frac{\partial^\alpha}{\partial t^\alpha}\right)\left(D_B\frac{\partial\theta}{\partial y}\frac{\partial\phi}{\partial y} + \frac{D_\theta}{\theta_0}\left(\frac{\partial\theta}{\partial y}\right)^2\right), \tag{13}$$

$$\frac{\partial}{\partial t}\left(1 + \frac{\tau_2^\beta}{\Gamma(1+\beta)} \frac{\partial^\beta}{\partial t^\beta}\right)\phi = D_B\frac{\partial^2\phi}{\partial y^2} + \frac{D_\theta}{\theta_0}\frac{\partial^2\theta}{\partial y^2}. \tag{14}$$

2.1.1. Flow Problem Conditions. Here we are considering the flow in a channel separated by a distance L. At the start, the whole flow configuration is still with constant temperature θ_0 and constant concentration ϕ_0. Flow is generated by the movement of the domain at $y = 0$, while the pressure gradient is assumed to be zero in that case. For temperature and concentration, domain at $y = 0$ is connected to a source, and the change in temperature is also changing with time, while in the domain at $y = L$, only temperature changes with time. The case for concentration is similar. Flow conditions are given as

$$u(0,t) = A\frac{\nu^2}{L^4}t^2, u(L,t) = 0, \tag{15}$$

$$-k\left(\frac{\partial\theta}{\partial y}\right)_{y=0} = \frac{q_\theta\nu^2}{L^4}t^2 \text{and} \theta(L,t) = \theta_0\left(1+\frac{\nu^2}{L^4}t^2\right), t>0, \tag{16}$$

$$-D_B\left(\frac{\partial\phi}{\partial y}\right)_{y=0} = \frac{q_\phi\nu^2}{L^4}t^2 \text{and} \phi(L,t) = \phi_0\left(1+\frac{\nu^2}{L^4}t^2\right), t>0, \tag{17}$$

$$u(y,0) = 0, \theta(y,0) = \theta_0, \phi(y,0) = \phi_0 \text{and} \frac{\partial\theta}{\partial t}(y,0) = 0 = \frac{\partial\phi}{\partial t}(y,0), |y| \le L. \tag{18}$$

A complete description of the flow domain is identified via equations (12)–(18).

2.1.2. Skin Friction Coefficients. Friction among fluid and solid boundaries is of great importance in the analysis of flow domains bounded by solid boundaries. Coefficients of friction are mathematically defined as

$$\mathscr{C}_f := \frac{2\tau_w}{\rho A^2}, \tag{19}$$

where shear stress at the wall is

$$\tau_w = \left[\left(\mu + \alpha_1\frac{\partial}{\partial t}\right)\frac{\partial u}{\partial y}\right]_{y=0,L}. \tag{20}$$

2.1.3. Nusselt Numbers. Change of temperature at $y = 0$ and $y = L$ are determined by the dimensionless, Nusselt number. Present flow domain, Nusselt numbers are given as

$$Nu_1 = \frac{-L(\partial\theta/\partial y)_{y=L}}{\theta_{s_1} - \theta_0}, \tag{21}$$

where θ_{s_1} is constant temperature, at $y = L$. At $y = 0$, the Nusselt number is given by

$$Nu_2 = \frac{-L(\partial\theta/\partial y)_{y=0}}{\theta_{s_2} - \theta_0}, \tag{22}$$

here θ_{s_2} is the temperature, at $y = 0$.

2.1.4. Mass Transfer Nusselt Numbers. Change of concentration at $y = 0$ and $y = L$ is determined by mass transfer Nusselt, Sherwood numbers. The present flow domain and Sherwood numbers are given as

$$Sh_1 = \frac{-L(\partial\phi/\partial y)_{y=L}}{\phi_{s_1} - \phi_0}, \tag{23}$$

where ϕ_{s_1} is the constant concentration at $y = L$. At $y = 0$, the Sherwood number is given by

$$Sh_2 = \frac{-L(\partial\phi/\partial y)_{y=0}}{\phi_{s_2} - \phi_0}, \tag{24}$$

here ϕ_{s_2} is the concentration at $y = 0$.

2.1.5. Problem in Nondimensionalization. We have defined the following dimensionless quantities to make mathematical problem (12)–(18) as nondimensionalized.

$$\widehat{y} := \frac{y}{L}, \widehat{t} := \frac{\nu}{L^2}t\widehat{u} := \frac{u}{A}, \widehat{\theta} := \frac{\theta-\theta_0}{\theta_0}\widehat{\phi} := \frac{\phi-\phi_0}{\phi_0}. \tag{25}$$

Using, (25), with dimensionless quantities, the IBVP (12)–(18) considered as without hats

$$(1+\epsilon)\frac{\partial u}{\partial t} = \left(1+\gamma\frac{\partial}{\partial t}\right)\left[\frac{\partial^2 u}{\partial y^2}\right] - (\lambda + Ha)u + (\lambda_1 + \lambda_2\theta)\theta,$$

$$\Pr\frac{\partial}{\partial t}\left(1+\delta_3\frac{\partial^\alpha}{\partial t^\alpha}\right)\theta = \frac{\partial^2\theta}{\partial y^2} + \Pr\left(1+\delta_3\frac{\partial^\alpha}{\partial t^\alpha}\right)\left(Nb\frac{\partial\theta}{\partial y}\frac{\partial\phi}{\partial y} + Nt\left(\frac{\partial\theta}{\partial y}\right)^2\right), \tag{26}$$

$$Sc\frac{\partial}{\partial t}\left(1+\delta_4\frac{\partial^\beta}{\partial t^\beta}\right)\phi = \frac{\partial^2\phi}{\partial y^2} + \left(\frac{Nt}{Nb}\right)\frac{\partial^2\theta}{\partial y^2}, |y| < 1, t > 0,$$

and problem conditions are given by

$$\begin{cases} u(0,t) = t^2, u(1,t) = 0, \left(\dfrac{\partial\theta}{\partial y}\right)_{y=0} = -\delta_1 t^2, \left(\dfrac{\partial\phi}{\partial y}\right)_{y=0} = -\delta_2 t^2, \theta(1,t) = t^2 = \phi(1,t), \\ \\ u(y,0) = 0, \theta(y,0) = 0 = \dfrac{\partial\theta}{\partial t}(y,0) \text{and} \phi(y,0) = 0 = \dfrac{\partial\phi}{\partial t}(y,0). \end{cases} \tag{27}$$

Here dimensionless numbers are given as

$$\begin{aligned} &\epsilon := \frac{\phi\alpha_1}{\rho K}, \gamma := \frac{\alpha_1}{\rho L^2}, \lambda := \frac{\psi L^2}{K}, Ha := \frac{\sigma B_0^2 L^2}{\mu}, \Pr := \frac{\nu}{\alpha_3}, Sc := \frac{\nu}{D_B}, \\ &\lambda_1 := \frac{gL^2\beta_1\theta_0}{A\nu}, \lambda_2 := \frac{gL^2\beta_2\theta_0^2}{A\nu}, Nb := \frac{\tau\phi_0 D_B}{\nu}, \delta_1 := \frac{q_\theta L}{\theta_0 k}, \delta_2 := \frac{q_\phi L}{\phi_0 D_B}, \\ &Nt := \frac{\tau D_\theta}{\nu}, \delta_3 := \frac{\tau_1^\alpha \nu^\alpha}{\Gamma(1+\alpha)L^{2\alpha}}, \delta_4 := \frac{\tau_2^\beta \nu^\beta}{\Gamma(1+\beta)L^{2\beta}}. \end{aligned} \tag{28}$$

Moreover, the dimensionless coefficients of friction, Nusselt, and mass transfer Nusselt numbers are defined by

$$\begin{aligned} &\frac{ReC_f}{2} = \left[\left(1 + \gamma\frac{\partial}{\partial t}\right)\frac{\partial u}{\partial y}\right]_{y=0,1}, \\ &\frac{Nu_1}{Re} = -\left(\frac{\partial\theta}{\partial y}\right)_{y=1} \text{and} \frac{Nu_2}{Re^2} = \delta_1 t^2, \\ &\frac{Sh_1}{Re} = -\left(\frac{\partial\phi}{\partial y}\right)_{y=1} \text{and} \frac{Sh_2}{Re^2} = \delta_2 t^2. \end{aligned} \tag{29}$$

3. Numerical Discretization Scheme

Numerical discretization of the flow problems (26) and (27) is presented here. The finite difference scheme(FDS) is used to discretize the fractional time derivative as given by [15, 21, 43], while the derivative with respect to space variable is discretized with the finite element scheme(FES) proposed in [15, 21]. The well-posedness of the flow problem can be checked in appropriate spaces [43]. Precisely, we note no ill-posedness in the defined flow problem.

Functional spaces are incorporated in the discretization of the model (26) and (27).

We point out that $\mathscr{L}^2(\Omega)$, square-integrable space of functions on $\Omega = (0,1)$ along with $\mathscr{L}^2$, norm and inner space product. Further, $\mathscr{H}^p(\Omega)$ stands for the Sobolev space, with $p > 0$, $\mathscr{H}_0^p(\Omega)$ is defined as the closure of $\mathscr{C}_0^\infty(\overline{\Omega})$ in $\mathscr{H}^p(\Omega)$ and $\mathscr{C}_0^\infty(\overline{\Omega})$ represents infinite differentiable continuous functions, with proper compact support, in Ω [44]. Also, we use the space

$$\mathscr{H}_1^p(\Omega) = \left\{\mathbf{u} \in \mathscr{H}^p(\Omega) | \mathbf{u}|_{y=1} = 0\right\}, \tag{30}$$

with $\mathbb{L}^2(\Omega) = \mathscr{L}^2(\Omega) \times \mathscr{L}^2(\Omega) \times \mathscr{L}^2(\Omega)$ and $\mathbb{H}(\Omega) = \mathscr{H}_0^p(\Omega) \times \mathscr{H}_1^p(\Omega) \times \mathscr{H}_1^p(\Omega)$.

Let $\mathscr{L}^2(0,T;\mathscr{V}(\Omega))$: $[0,t_f] \longrightarrow \mathscr{V}$ equipped with

$$\begin{aligned} (u,v)_{\mathscr{L}^2\left(0,t_f;\mathscr{V}(\Omega)\right)} &:= \int_0^{t_f} (u,v)_{\mathscr{V}(\Omega)} dt \text{ and} \|u\|_{\mathscr{L}^2(0,T;\mathscr{V}(\Omega))} \\ &:= \left(\int_0^{t_f} \|u\|_{\mathscr{V}(\Omega)}^2 dt\right)^{1/2}. \end{aligned} \tag{31}$$

Furthermore, $\mathscr{C}^0([0,t_f];\mathscr{V}(\Omega))$ is the space of continuous functions u: $[0,t_f] \longrightarrow \mathscr{V}$ with

$$\|u\|_{\mathscr{C}^0\left(\left[0,t_f\right];\mathscr{V}(\Omega)\right)} := \max_{t\in\left[0,t_f\right]} \|u\|_{\mathscr{V}}. \tag{32}$$

Analogously, for $k \in \mathbb{N}$,

$$\mathscr{C}^k\left(\left[0,t_f\right];\mathscr{V}(\Omega)\right) := \left\{u \in \mathscr{C}^0\left(\left[0,t_f\right];\mathscr{V}(\Omega)\right)\partial_t^j u \in \mathscr{C}^0([0,T];\mathscr{V}(\Omega)), \forall j \le k: j \in \mathbb{N}\right\}. \tag{33}$$

and

$$\|u\|_{\mathscr{C}^k([0,t_f];\mathscr{V}(\Omega))} := \max_{j=0}^{k}\left(\left\|\partial_t^j u\right\|_{\mathscr{C}^0([0,t_f];\mathscr{V}(\Omega))}\right), \quad (34)$$

and also, we denote by $\mathbb{C}^k([0,t_f];\mathbb{V}(\Omega)) = [\mathscr{C}^k([0,t_f];\mathscr{V}(\Omega))]^3$.

3.1. Approximations using FDS. Fractional time derivative in (26) and (27) is discretized by FDS. The interval of time, $[0,t_f]$ is partitioned by time step $\tau := t_f/m$ so that $t_k := k\tau$, and $k = 0,1,2,\ldots,m$. Estimation of the derivative of time at some fixed, t_k, $0 < k < m$

$$\frac{\partial u}{\partial t}(y,t_k) \simeq \frac{u(y,t_{k+1}) - u(y,t_k)}{\tau}, t_k \le s \le t_{k+1}, \quad (35)$$

here, $k = 0$,

$$\frac{\partial u}{\partial t}(y,t_0) \simeq \frac{u(y,t_1) - u(y,t_0)}{\tau}. \quad (36)$$

Initial conditions of flow (27) give

$$u(y,t_1) \simeq 0 \text{ and } u(y,t_0) \simeq 0. \quad (37)$$

Fractional derivative of time, ∂_t^α $(0 < \alpha < 1)$, $0 \le k < m$, estimated with the Caputo derivative [43].

$$\partial_t^\alpha \phi(t) := \frac{1}{\Gamma(m-\alpha)} \int_0^t (t-\tau)^{m-\alpha-1} \frac{\partial^m}{\partial \tau^m} \phi(\tau) d\tau, \quad m-1 < \Re e\{\alpha\} < m, m \in \mathbb{N}, \quad (38)$$

and the Gamma function $\Gamma(\cdot)$ is given as

$$\Gamma(z) := \int_{\mathbb{R}} \xi^{z-1} e^{-\xi} d\xi, z \in \mathbb{C}, \Re\{z\} > 0. \quad (39)$$

Fractional derivative of time $\partial_t^\alpha \phi$ agrees with ordinary derivative $\partial_t^m \phi$ as $\alpha \longrightarrow m$, $m-1 < \alpha < m$, for an integer m. Also, we specify the following operators

$$\mathscr{L}_t^\alpha[\theta(\cdot)](t) := \left(\frac{\partial}{\partial t} + \delta_2 \frac{\partial^{(\alpha+1)}}{\partial t^{(\alpha+1)}}\right)[\theta(t)],$$
$$\mathscr{Q}_t^\alpha[\theta(\cdot)](t) := \left(1 + \delta_2 \frac{\partial^\alpha}{\partial t^\alpha}\right)[\theta(t)]. \quad (40)$$

Estimations with FDS of operators $\mathscr{L}_t^\alpha[\theta]$, $\mathscr{Q}_t^\alpha[\theta]$ can be taken as (please see [26])

$$\mathscr{L}_t^\alpha[\theta](t_{k+1}) = \left(\frac{\partial}{\partial t} + \delta_2 \frac{\partial^{\alpha+1}}{\partial t^{\alpha+1}}\right)[\theta](t_{k+1}),$$
$$\simeq \frac{\theta(t_{k+1}) - \theta(t_k)}{\tau} + C_\alpha[\theta(t_{k+1}) - 2\theta(t_k) + \theta(t_{k-1})] + C_\alpha(\psi_k^\alpha[\theta] - \psi_{k-1}^\alpha[\theta]), \quad (41)$$

and

$$\mathscr{Q}_t^\alpha[\theta](t_{k+1}) = \left(1 + \delta_2 \frac{\partial^\alpha}{\partial t^\alpha}\right)[\theta](t_{k+1}),$$
$$\simeq \theta(t_{k+1}) + \delta_2 C_\alpha[\theta(t_{k+1}) - \theta(t_k)] + \delta_2 C_\alpha \psi_k^\alpha[\theta], \quad (42)$$

with $c_\alpha = \tau^{-\alpha}/\Gamma(2-\alpha)$ and where $b_s^\alpha := (s+1)^{1-\alpha} - (s)^{1-\alpha}$, for $0 \le s \le m$, with

$$\psi_k^\alpha[\theta] := \sum_{s=1}^{k} b_s^\alpha[\theta(y,t_{k+1-s}) - \theta(y,t_{k-s})] \text{with} \psi_0^\alpha[\theta] := 0. \quad (43)$$

3.2. Approximations using FES. In this section, the FES discretization of space variables is discussed in detail. It can be achieved by the partition of domain $\Omega = [0,1]$ with n subdomains $\Omega_i = (y_i, y_{i+1})$ such that $i = 1,2,\ldots,n$, satisfying

$$\overline{\Omega} = \bigcup_{i=1}^{n} \overline{\Omega}_i \text{ and } \Omega_i \bigcap \Omega_j = \varnothing, \forall i \ne j. \quad (44)$$

The defined elements Ω_i of width h are constant, *i.e.*, $h := 2/n := y_{i+1} - y_i$. Considering subspace of finite dimension $\{\mathscr{V}_0^h(\Omega)\}_{h>0}$ of $\mathscr{H}_0^1(\Omega)$ and $\{\mathscr{V}_1^h(\Omega)\}_{h>0}$ of $\mathscr{H}_1^1(\Omega)$

$$\mathscr{V}_0^h(\Omega) := \{\phi \in \mathscr{H}_0^1(\Omega)\phi_{\Omega_i} \in P_r(\Omega_i), \forall i = 1,2,\ldots,n\},$$
$$\mathscr{V}_1^h(\Omega) := \{\phi \in \mathscr{H}_1^1(\Omega)\phi_{\Omega_i} \in P_r(\Omega_i), \forall i = 1,2,\ldots,n\}, \quad (45)$$

$P_r(\Omega_i)$ is the Lagrange polynomial space of degree less or equal to r over Ω_i with $i = 1,2,\ldots,n$. Also, we note that $\mathbb{V}^h(\Omega) = \mathscr{V}_0^h(\Omega) \times \mathscr{V}_1^h(\Omega) \times \mathscr{V}_1^h(\Omega)$.

The weak form of the flow model (26) and (27) can be taken as.

Weak form: We need to find $(u,\theta,\phi) \in \mathbb{C}^1([0,T];\mathbb{H}(\Omega))$ such that

$$\begin{cases} (1+\epsilon)\dfrac{\partial}{\partial t}(u,v)+\left(1+\gamma\dfrac{\partial}{\partial t}\right)\langle u,v\rangle+(\lambda+Ha)(u,v)-((\lambda_1+\lambda_2\theta)\theta,v)=0, \\ \Pr\mathscr{L}_t^{\alpha}(\theta,\zeta)+\langle\theta,\zeta\rangle-\Pr\mathbb{Q}_t^{\alpha}(\theta,\zeta)\left(Nb\left(\dfrac{\partial\theta}{\partial y}\dfrac{\partial\phi}{\partial y},\zeta\right)+Nt\left(\left(\dfrac{\partial\theta}{\partial y}\right)^2,\zeta\right)\right)=(-\delta_1 t,\zeta(0)), \\ Sc\mathscr{L}_t^{\beta}(\phi,\psi)+\langle\phi,\psi\rangle+\left(\dfrac{Nt}{Nb}\right)\langle\theta,\psi\rangle=(-\delta_1 t-\delta_2 t,\psi(0)), \\ u(y,0)=,\theta(y,0)=0=\dfrac{\partial\theta}{\partial t}(y,0),\text{and}\phi(y,0)=0=\dfrac{\partial\phi}{\partial t}(y,0), \end{cases} \tag{46}$$

for all $(v,\zeta,\psi)\in\mathbb{H}(\Omega)$.

Weak form (46) is used to incorporate, discrete weak form, at $t=t_k$, $0<k<m$

$$\begin{cases} \text{Find}(u_h(\cdot,t_{k+1}),\theta(\cdot,t_{k+1}),\phi(\cdot,t_{k+1}))\in\mathbb{V}^h(\Omega)\text{s.t.}\forall(v,\varsigma,\phi)\in\mathbb{V}^h(\Omega) \\ (1+\epsilon)\dfrac{\partial}{\partial t}(u_h(y,t_{k+1}),v)+\left(1+\gamma\dfrac{\partial}{\partial t}\right)\langle u_h((y,t_{k+1})),v\rangle+(\lambda+Ha)(u_h(y,t_{k+1}),v) \\ -((\lambda_1+\lambda_2\theta_h(y,t_{k+1}))\theta_h(y,t_{k+1}),v)=0, \\ \Pr\mathscr{L}_t^{\alpha}(\theta_h(y,t_{k+1}),\zeta)+\langle\theta_h(y,t_{k+1}),\zeta\rangle-\Pr Nb\mathbb{Q}_t^{\alpha}\left(\dfrac{\partial\theta_h(y,t_{k+1})}{\partial y}\dfrac{\partial\phi_h(y,t_{k+1})}{\partial y},\zeta\right) \\ -\Pr Nt\mathbb{Q}_t^{\alpha}\left(\left(\dfrac{\partial\theta_h(y,t_{k+1})}{\partial y}\right)^2,\zeta\right)=(-\delta_1 t,\zeta(0)), \\ Sc\mathscr{L}_t^{\beta}(\phi_h(y,t_{k+1}),\psi)+\langle\phi_h(y,t_{k+1}),\psi\rangle+\dfrac{Nt}{Nb}\langle\theta_h(y,t_{k+1}),\psi\rangle=(-\delta_1 t-\delta_2 t,\psi(0)), \\ u_h^0(y)=0,\theta_h^0(y)=0=\theta_h^1(y),\phi_h^0(y)=0=\phi_h^1(y), \end{cases} \tag{47}$$

where $u_h^0(\cdot)=u_h(\cdot,t_0)$, $\theta_h^1(\cdot)=\theta_h(\cdot,t_1)$, $\phi_h^1(\cdot)=\phi_h(\cdot,t_1)$, $\theta_h^0(\cdot)=\theta(\cdot,t_0)$, and $\phi_h^0(\cdot)=\phi(\cdot,t_0)$. The numerical solution (u_h,θ_h,ϕ_h) to (47) is given as

$$u_h(y,t_{k+1}) = \sum_{p=1}^{N_h} u_p(t_{k+1}) W_{0h}^p(y), y \in \overline{\Omega},$$
$$\theta_h(y,t_{k+1}) = \sum_{l=1}^{N_h} \theta_l(t_{k+1}) W_{1h}^l(y), y \in \overline{\Omega}, \quad (48)$$
$$\phi_h(y,t_{k+1}) = \sum_{l=1}^{N_h} \phi_l(t_{k+1}) W_{1h}^l(y), y \in \overline{\Omega},$$

where $\mathbf{W}_{0h} = \{W_{0h}^p | p = 1,2,\ldots,N_{0h}\}$ defines a basis, $\mathscr{V}_0^h(\Omega)$ along with $N_{0h} \coloneqq \dim(\mathscr{V}_0^h)$, $\mathbf{W}_{1h} = \{W_{1h}^l | l = 1,2,\ldots,N_{1h}\}$ forms a basis of $\mathscr{V}_1^h(\Omega)$ with $N_{1h} \coloneqq \dim(\mathscr{V}_1^h)$ and (u_p, θ_l, ϕ_l) are yet to be determined. Further, considering v as W_{0h}^q for various values of q as $q = 1,2,\ldots,N_{0h}$, ζ, and ψ, W_{1h}^m for various values of m as $m = 1,2,\ldots,N_{1h}$, consequently we obtain the following nonlinear algebraic system of equations:

$$\begin{cases} (1+\epsilon)\mathbb{A}_0^h \dfrac{d}{dt}[\mathbf{U}_h] + \tau\mathbb{B}_0^h\left(1+\gamma\dfrac{d}{dt}\right)[\mathbf{U}_h] + \tau(\lambda+Ha)\mathbb{M}_0^h\mathbf{U}_h + \tau\lambda_1\mathbb{M}_0^h\mathbf{\Theta}_h + \tau\lambda_2\Theta_h(t_k)\mathbb{M}_0^h\mathbf{\Theta}_h = 0, \\ \Pr\mathbb{A}_1^h\mathscr{L}_{k+1}^\alpha[\mathbf{\Theta}_h] + \tau\mathbb{B}_1^h\mathbf{\Theta}_h - \tau\Pr Nb\Phi_h(t_k)\mathscr{C}_1^h\mathbb{Q}_{k+1}^\alpha[\mathbf{\Theta}_h] - \tau\Pr Nt\theta_h(t_k)\mathscr{C}_1^h\mathbb{Q}_{k+1}^\alpha[\mathbf{\Theta}_h] = -\delta_1 t\mathbf{I}, \\ Sc\mathbb{A}_1^h\mathscr{L}_{k+1}^\beta[\mathbf{\Phi}_h] + \tau\mathbb{B}_1^h\mathbf{\Phi}_h + \tau\dfrac{Nt}{Nb}\mathbb{B}_1^h\mathbf{\Theta}_h = (-\delta_1 t - \delta_2 t)\mathbf{I}, \\ \mathbf{U}_h^0 = 0, \mathbf{\Theta}_h^0 = 0 = \mathbf{\Theta}_h^1, \mathbf{\Phi}_h^0 = 0 = \mathbf{\Phi}_h^1, \end{cases} \quad (49)$$

where for all $p,q = 1,2,\ldots,N_{0h}$ and $l,m = 1,2,\ldots,N_{1h}$.

$$\begin{aligned} &(\mathbf{U}_h)_p \coloneqq u_p, (\mathbf{\Theta}_h)_l \coloneqq \theta_l, (\mathbf{\Phi}_h)_l \coloneqq \phi_l, \\ &\left(\mathbb{A}_0^h\right)_{qp} \coloneqq \left(W_{0h}^p, W_{0h}^q\right), \left(\mathbb{B}_0^h\right)_{qp} \coloneqq \langle W_{0h}^p, W_{0h}^q\rangle, \left(\mathbb{M}_0^h\right)_{qp} \coloneqq \left(W_{0h}^p, W_{0h}^q\right), \\ &\left(\mathbb{A}_1^h\right)_{lm} \coloneqq \left(W_{1h}^l, W_{1h}^m\right), \left(\mathbb{B}_1^h\right)_{lm} \coloneqq \langle W_{1h}^l, W_{1h}^m\rangle, \left(\mathscr{C}_1^h\right)_{lm} \coloneqq \langle W_{1h}^l, W_{1h}^m\rangle (\mathbf{I})_m \coloneqq (1,0,0,\ldots,0)^\dagger. \end{aligned} \quad (50)$$

The system of algebraic equations, (50) has been computed by Newton's method. Linear Lagrange elements have been applied to get matrices in the defined system (50).

3.3. Convergence of Proposed Scheme. Here we have given the validation of the proposed numerical scheme so that one can confidently perform simulations of real scenarios. A comparison of numerical and theoretical error estimates is presented here. We postulate the proposed mathematical model will satisfy the given error estimates.

$$\begin{aligned} \|\zeta_h(t_k) - \zeta_{ex}(t_k)\|_{L_2(\Omega)} &\le D_1\left(h^{r+1} + \tau^\alpha\right), \\ \|\zeta_h(t_k) - \zeta_{ex}(t_k)\|_{H^1(\Omega)} &\le D_2\left(h^r + \tau^\alpha\right), \end{aligned} \quad (51)$$

here constants $D_1 > 0$ and $D_2 > 0$ are not dependent of h, step size, and τ (see [43]).

Theoretical and numerical error estimates are compared with the induction of source terms F_{fab1} in the momentum equation, F_{fab2} in the energy equation, and F_{fab3} in the concentration equation of model (26) to obtain an exact fabricated solution.

$$\begin{cases} (1+\epsilon)\dfrac{\partial u}{\partial t} = \left(1+\gamma\dfrac{\partial}{\partial t}\right)\left[\dfrac{\partial^2 u}{\partial y^2}\right] - (\lambda + Ha)u + (\lambda_1 + \lambda_2\theta)\theta + F_{\text{fab1}}(y,t), \\ \Pr\dfrac{\partial}{\partial t}\left(1+\delta_3\dfrac{\partial^\alpha}{\partial t^\alpha}\right)\theta = \dfrac{\partial^2\theta}{\partial y^2} + \Pr\left(1+\delta_3\dfrac{\partial^\alpha}{\partial t^\alpha}\right)\left(Nb\dfrac{\partial\theta}{\partial y}\dfrac{\partial\phi}{\partial y} + Nt\left(\dfrac{\partial\theta}{\partial y}\right)^2\right) + F_{\text{fab2}}(y,t), \\ Sc\dfrac{\partial}{\partial t}\left(1+\delta_4\dfrac{\partial^\beta}{\partial t^\beta}\right)\phi = \dfrac{\partial^2\phi}{\partial y^2} + \left(\dfrac{Nt}{Nb}\right)\dfrac{\partial^2\theta}{\partial y^2} + F_{\text{fab3}}(y,t), \end{cases} \tag{52}$$

with given conditions. The fabricated solutions completely satisfied the given equations, $u_{ex}(y,t)$, $\theta_{\text{ex}}(y,t)$, and $\phi_{\text{ex}}(y,t)$ along with conditions. For the validation of the proposed scheme, we have inserted F_{fab1}, F_{fab2}, and F_{fab3} in the system (50). Error curves have been plotted and they are shown in Figures 1(a), 1(b), and 2.

Errors are presented in norms on log scales of $H^1(\Omega)$ and $L_2(\Omega)$ for different values of h. The slopes of error curves are nearly equal to 2 in the case of $H^1(\Omega)$ and 3 in case of $L_2(\Omega)$. Theoretically, in 3.15 and 3.16, Lagrange polynomials are of degrees $r+1$ and r, respectively. In the proposed scheme we have incorporated a second-degree Lagrange polynomial, so exact values must be equal to 2 in case of $H^1(\Omega)$ and 3 in case of $L_2(\Omega)$. This shows the agreement between theoretical and numerical error estimates. So, the proposed scheme (50), is convergent and can efficiently handle real simulations of proposed model (26). The error estimates for velocity, temperature, and concentration are given in Tables 1 and 2.

4. Approximate Simulated Results

This section deals with the results of the velocity field, temperature field, and concentration of nanofluid with nonlinear convection and flux conditions using MATLAB R2017a. Brownian phenomena of motion and thermophoresis are analyzed while evaluating this study. Fluid is flowing through the Darcy porous medium. Flow and magnetic fields are orthogonal. The proposed algorithm is employed for numerical solutions of governing nonlinear fractional equations. Discretization of time and space variables is carried out by FDS and FES, respectively. We analyze the characteristics of physical numbers on flow field generation. Transfer of heat and mass are also discussed for various pertinent numbers. Variations of flow quantities with the variation of different nondimensional numbers help to understand the problem. Simulated results are seen over intervals of time [0, 2], and [0, $\sqrt{2}$]. Figure 3, is used for demonstration of velocity behavior with the variation of $0 < \alpha < 1$. It is observed that for higher values of α, velocity increases (see Figure 3(a)). However, this occurrence is hereditary in character and cannot be considered to be other variations of pertinent parameters.

Change in velocity with the variation of $0.1 \le Ha \le 3$, and $0.1 \le \gamma \le 0.8$ are plotted in Figure 3(b). The plot showed that a decrease in velocity is noted for higher values of Ha and opposite behavior is obtained for the viscoelastic parameter, γ. As Ha increases, Lorentz force decreases, which slows down fluid motion. As a result, velocity decreases for higher values of Ha. Porosity parameter $0 \le \lambda \le 7$ and convection number $0.1 \le \lambda_1 \le 3.5$ influence on the velocity, which is plotted in Figure 4. It is noted that velocity decreases for higher values of λ, while an opposite trend is noted for λ_1 in Figure 4(a). With the increase of λ, permeability decreases while porosity increases. So, the velocity profile decreases with the increase of λ. Force of inertia is inversely related to λ_1 and direct influence is given for buoyancy force. As $\lambda_1 > 0$, heat transfers from plates to fluid. So, $(\theta_{s_1} - \theta_0)$ and $(\theta_{s_2} - \theta_0)$ increase. Consequently, the increase in λ_1 increases buoyancy forces, $(\theta_{s_1} - \theta_0)$ and $(\theta_{s_2} - \theta_0)$. So, increase in fluid velocity is noted in this case.

Similar behavior of nonlinear convection number $0.1 \le \lambda_2 \le 6.5$ is noted in Figure 4(b). When there is convection, it is nonlinear in nature, so as noted, the same results are observed for the convection parameter λ_1. It is noted that an increase in the Darcy resistance number, $0.1 \le \epsilon \le 6.5$ reflects a decrease in velocity. This is because an increase in ϵ permeability decreases while porosity increases. Hence, a decrease in velocity with an increase in Darcy resistance number is noted.

Figure 5 is plotted to observe the temperature profile, for several values of α. Temperature profile, increases as α increases in Figure 5(a). Temperature profile behavior with the increase of pedesis number $0.1 \le Nb \le 4$, Schmidt parameter $0.1 \le Sc \le 4$ are observed via Figure 5(b). It is noted that temperature increases. as Sc, Nb increase. Momentum diffusivity enhances with the increase of Sc, which increases friction between different layers of the flow domain. As a result, an increase in temperature is seen with the increase of Sc. A decrease of temperature with the decrease of base fluid heat capacity is noted with an increase of Nb.

The influence of $0.1 \le \Pr \le 7$, Prandtl number, $0.1 \le Nt \le 4$ thermophoresis number, on temperature is plotted in Figure 6. With the increase of Nt, the temperature profile increases, while the opposite trend is observed in the case of Pr in Figure 6(a). With the increase of Nt, the heat capacity of the nanofluid decreases, as a result, the temperature profile increases, for higher values of Nt. With the increase of Pr, thermal diffusivity, decreases so temperature decreases with the increase of Pr. Figure 6(b) is plotted to show the influence of heat flux, $0.1 \le \delta_1 \le 0.8$ and mass flux, $0.1 \le \delta_2 \le 0.8$ numbers on temperature. It is noted

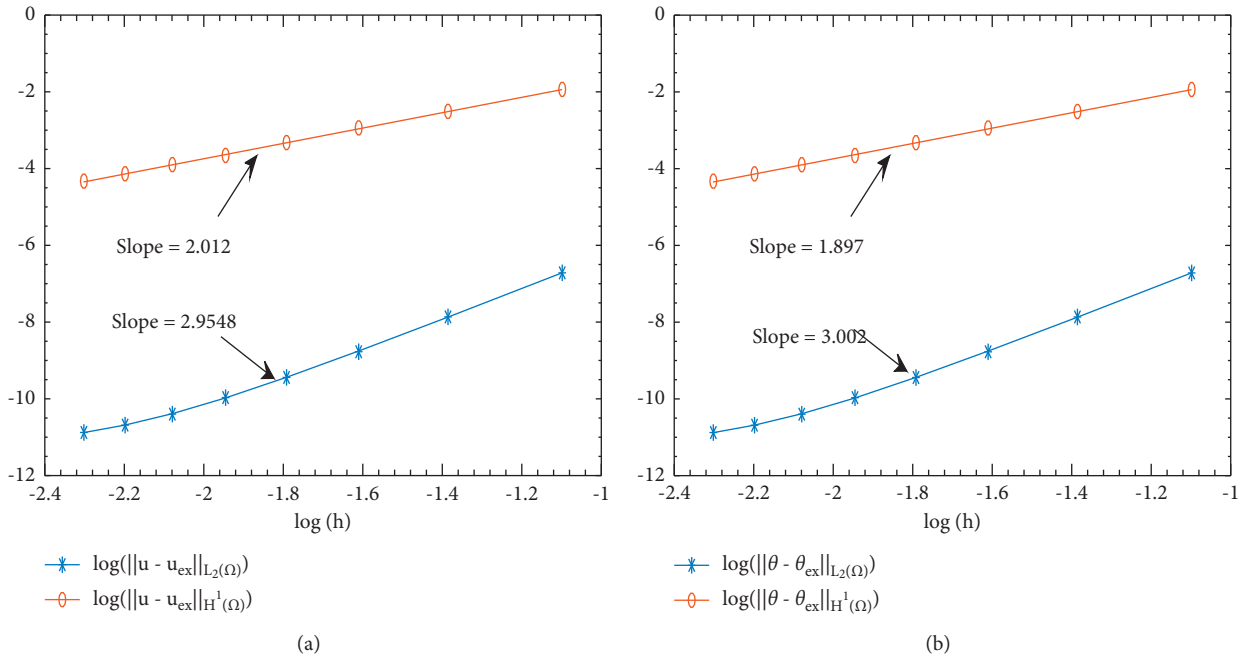

Figure 1: Error estimates for temperature and velocity. (a) Velocity H_1 and L_2 error curves. (b) Temperature H_1 and L_2 error curves.

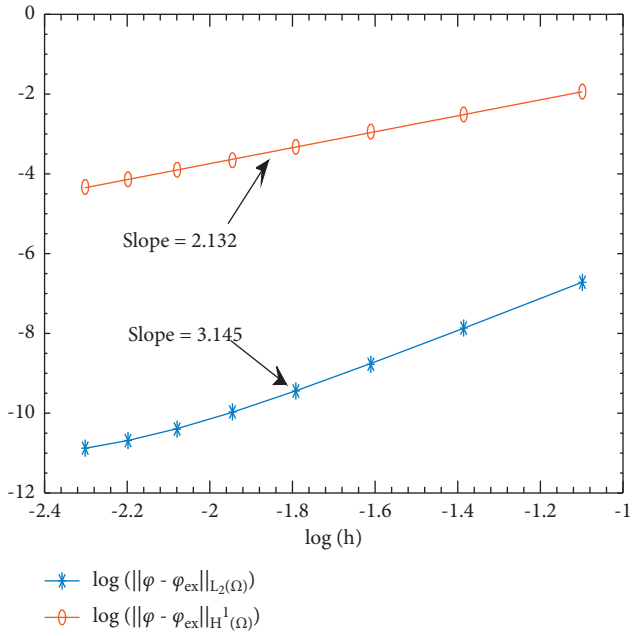

Figure 2: Concentration H_1 and L_2 error curves.

Table 1: Error estimates for velocity and temperature.

n	h	Error estimates of velocity		Error estimates of temperature	
		$\|u - u_{ex}\|_{L_2(\Omega)}$	$\|u - u_{ex}\|_{H^1(\Omega)}$	$\|\theta - \theta_{ex}\|_{L_2(\Omega)}$	$\|\theta - \theta_{ex}\|_{H^1(\Omega)}$
7	0.3000	2.5816528×10^{-5}	1.2760729×10^{-1}	1.211254×10^{-4}	1.4354533×10^{-1}
10	0.2360	1.7530926×10^{-5}	1.0335894×10^{-1}	3.809745×10^{-5}	8.0745776×10^{-2}
13	0.1807	1.2588759×10^{-5}	8.5420742×10^{-2}	1.584725×10^{-5}	5.1678524×10^{-2}
16	0.1728	9.5167115×10^{-6}	7.1777154×10^{-2}	7.961548×10^{-6}	3.5888249×10^{-2}
19	0.1529	7.5460756×10^{-6}	6.1157856×10^{-2}	4.640422×10^{-6}	2.6367821×10^{-2}
22	0.1502	6.2508125×10^{-6}	5.2734257×10^{-2}	3.080778×10^{-6}	2.0187853×10^{-2}
25	0.1456	5.3821874×10^{-6}	4.5938245×10^{-2}	2.2959072×10^{-6}	1.5949251×10^{-2}
28	0.1378	4.7890743×10^{-6}	4.0375489×10^{-2}	1.8817548×10^{-6}	1.2918457×10^{-2}

Table 2: Error estimates for concentration.

n	h	Error estimates of concentration	
		$\|u - u_{ex}\|_{L_2(\Omega)}$	$\|u - u_{ex}\|_{H^1(\Omega)}$
7	0.3000	3.6875492×10^{-4}	2.2760729×10^{-2}
10	0.2360	1.7254876×10^{-4}	1.0335894×10^{-2}
13	0.1807	1.4258149×10^{-4}	9.5124783×10^{-3}
16	0.1728	8.1568473×10^{-5}	8.2549678×10^{-3}
19	0.1529	6.4582167×10^{-5}	6.3548962×10^{-3}
22	0.1502	4.8723459×10^{-5}	5.7854216×10^{-3}
25	0.1456	3.1248753×10^{-5}	4.3698524×10^{-3}
28	0.1378	2.4529751×10^{-5}	3.9645871×10^{-3}

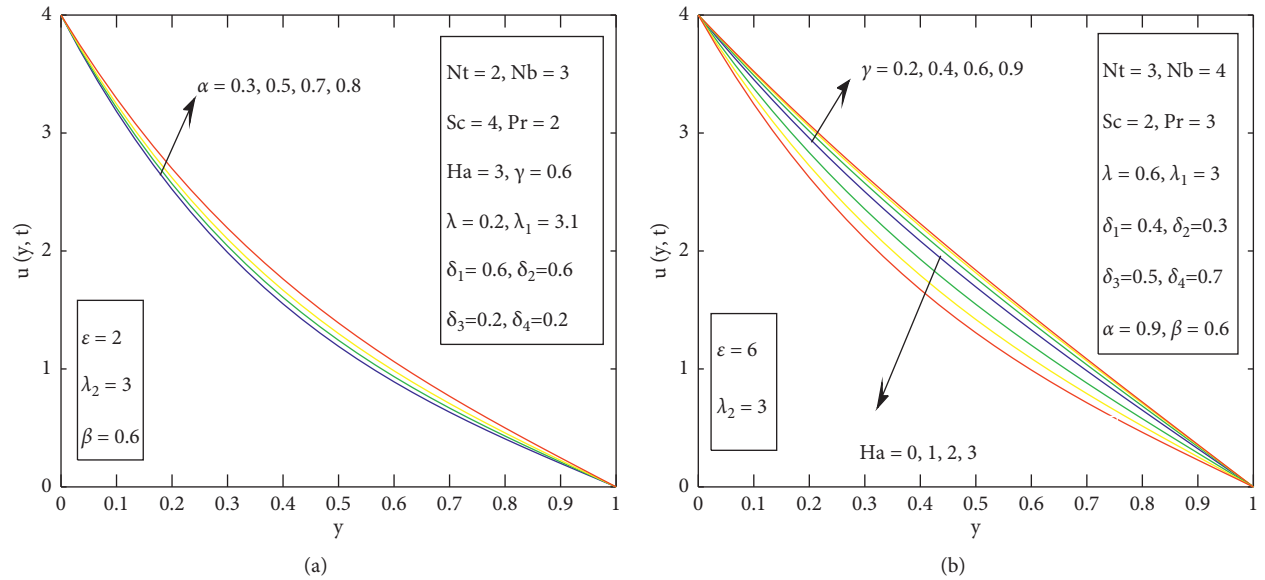

Figure 3: Influence of noninteger number, Hartmann number, and viscoelastic number on velocity. (a) Change in velocity with α. (b) Change in velocity with H_a and Υ.

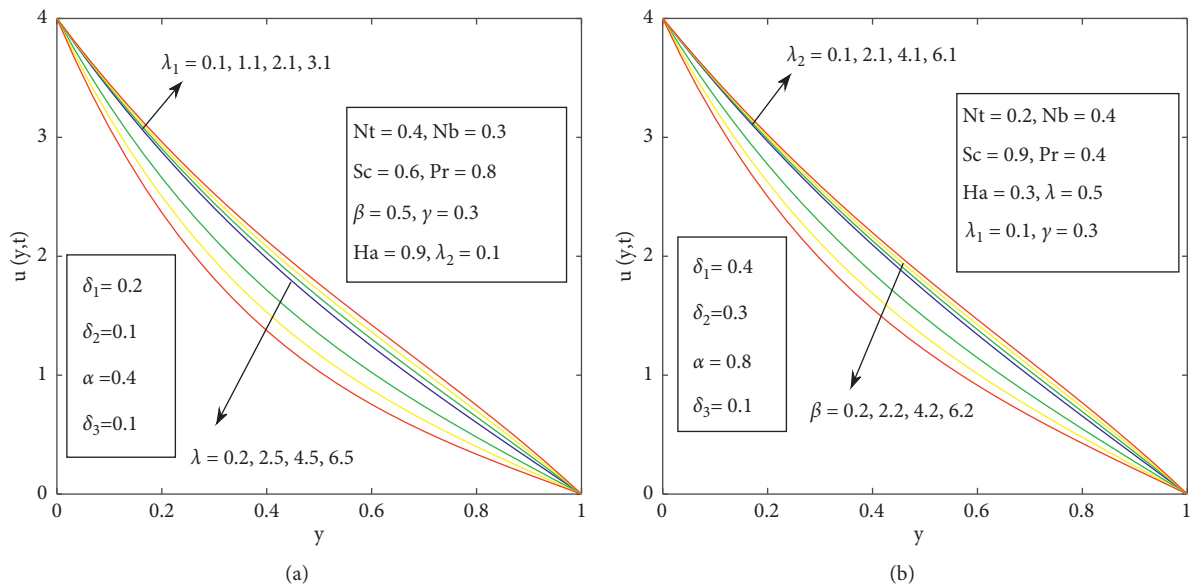

Figure 4: Influence of porosity, Darcy resistance, and convection numbers on velocity. (a) Change in velocity with λ and λ_1. (b) Change in velocity with λ_2 and ε.

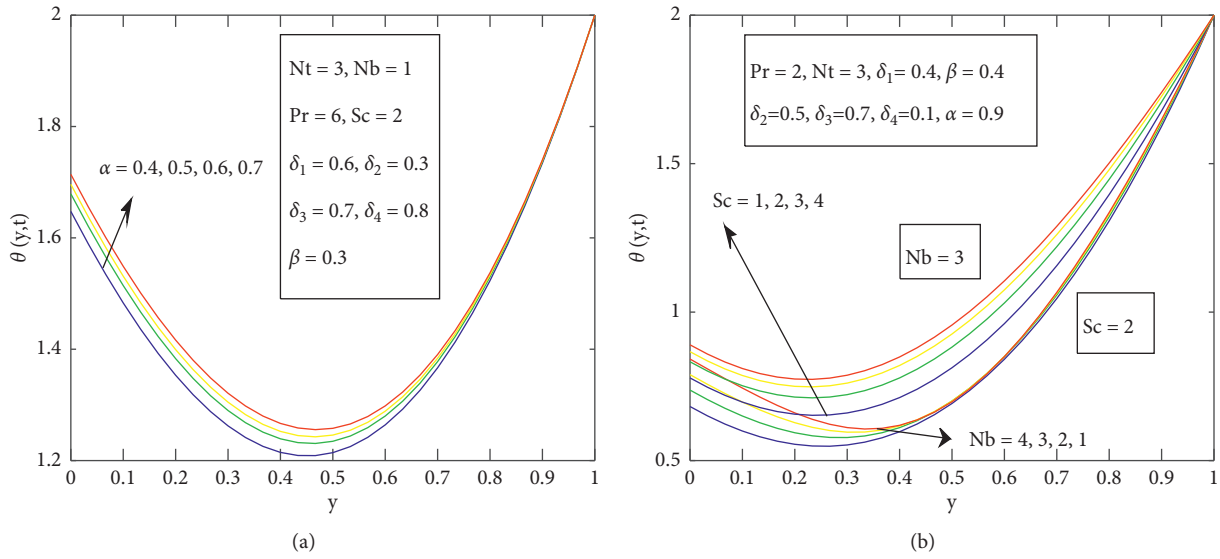

FIGURE 5: Influence of noninteger number, pedesis parameter, and Schmidt number on temperature. (a) Change in temperature with α. (b) Change in temperature with *Sc* and *Nb*.

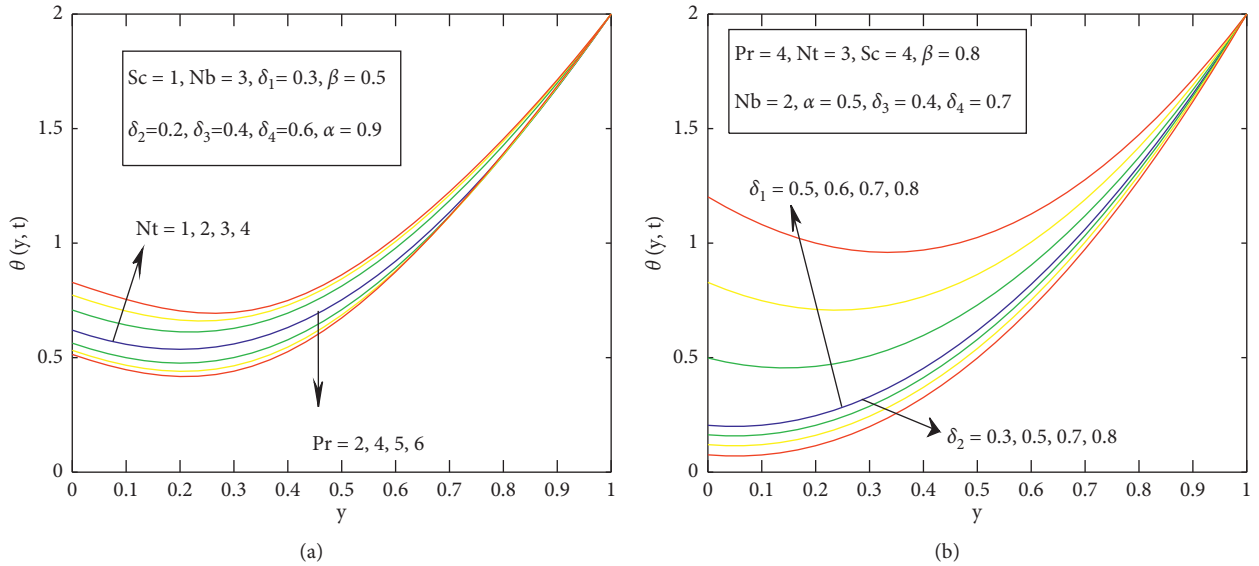

FIGURE 6: Influence of Prandtl number, heat and mass fluxes, and thermophoresis numbers on temperature. (a) Change in temperature with *Pr* and *Nt*. (b) Change in temperature with δ_1 and δ_2.

temperature increases for higher values of δ_1 while opposite trends are seen for the case of δ_2. With the increase of δ_1, thermal conductivity, the fluid decreases which decreases the heat passage rate through the base fluid, so temperature increases for higher values of δ_1.

Figure 7 is outlined to observe concentration change for various values of α. Concentration is at a higher level for higher values of α in Figure 7(a). Effects of thermophoresis, *Nt*, pedesis, *Nb* numbers on concentration are plotted in Figure 7(b). Concentration increases, for higher values of *Nt*, while the opposite behavior is noted for *Nb*. An increase in concentration, is because of an increase in the coefficient of thermophoretic diffusion.

The influence of Prandtl *Pr*, and Schmidt *Sc* numbers on concentration can be seen via Figure 8. Concentration increases for higher values of *Pr*, while the opposite behavior is noted in the case of *Sc* as shown in Figure 8(a). Momentum diffusivity increases for higher values of *Pr*, as a result, concentration is at a greater level for higher values of *Pr*. The viscosity of fluid increases, and the Brownian diffusion coefficient decreases for higher values of *Sc*. So, the concentration remains at a lower level for higher values of *Sc*. Figure 8(b) is outlined to observe the impact of heat flux δ_1, and mass flux δ_2 numbers on concentration. Concentration increases for higher values of δ_1 and δ_2. The rate of transfer of concentration decreases for higher values of δ_2. So, the

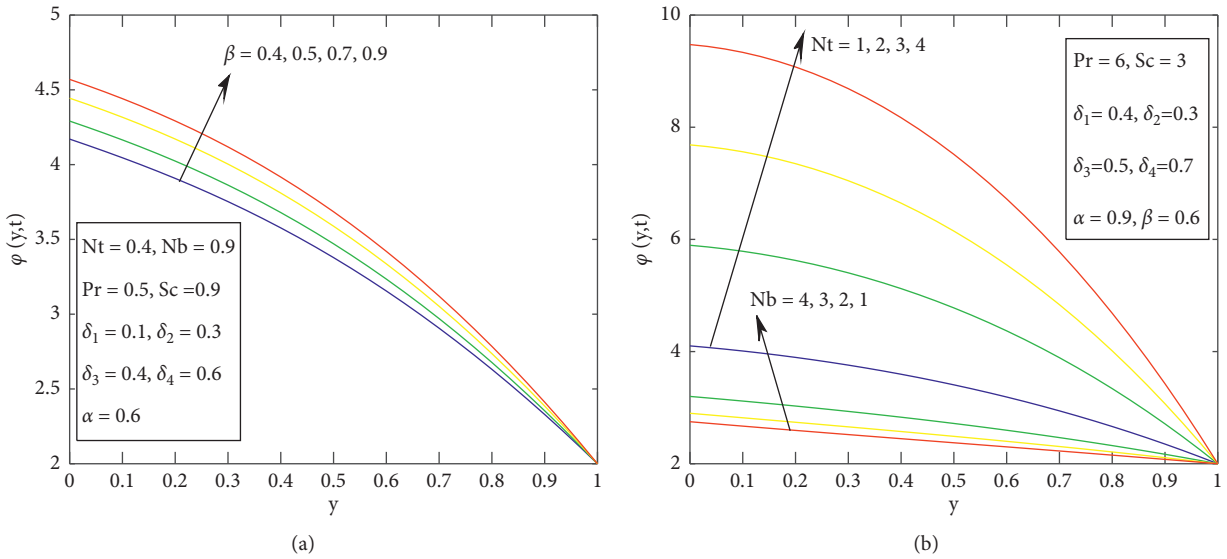

FIGURE 7: Influence of fractional number, thermophoresis, and pedesis numbers on concentration. (a) Change in concentration with α. (b) Change in concentration with Nt, and Nb.

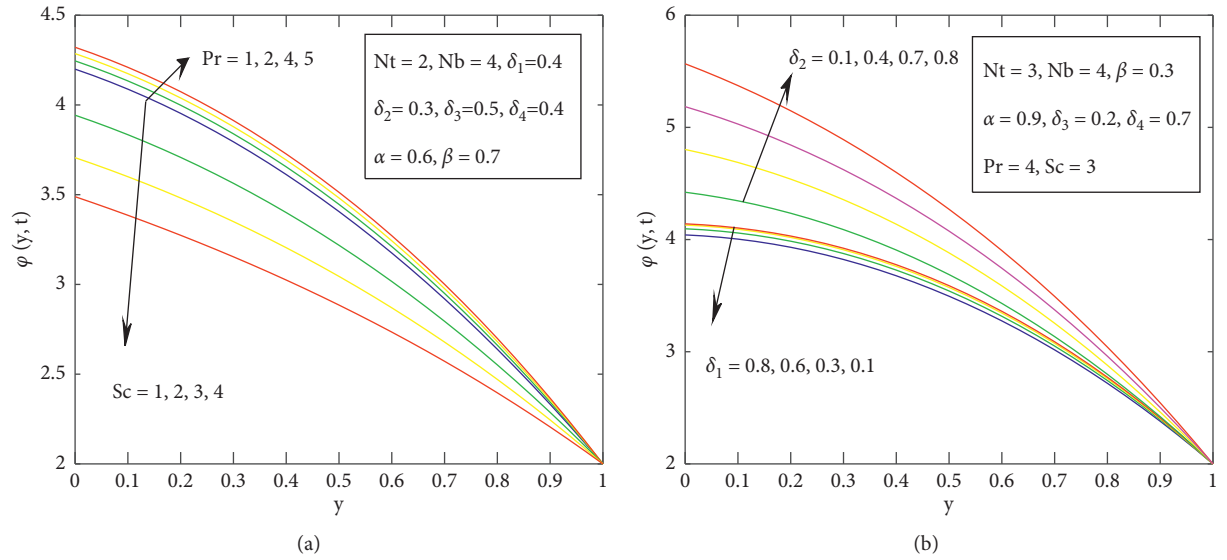

FIGURE 8: Influence of Prandtl number, heat and mass fluxes numbers, and Schmidt number on concentration. (a) Change in concentration with Pr, and Sc. (b) Change in concentration with δ_1, and δ_2.

concentration increases for higher values of δ_2. At the end Figures 9(a) and 9(b)–12(a) and 12(b) are plotted for time dependent velocity, temperature, and concentration profiles. These figures showed anomalous character of noninteger nanofluid.

Variations of skin friction with pertinent fractional model parameters are examined via Tables 3 and 4. Skin friction magnitude increases with the increase of α, β, λ, δ_2, Pr, and Ha , while it decreases with the increase of γ, λ_1, λ_2, δ_1, Sc, Nt, and Nb.

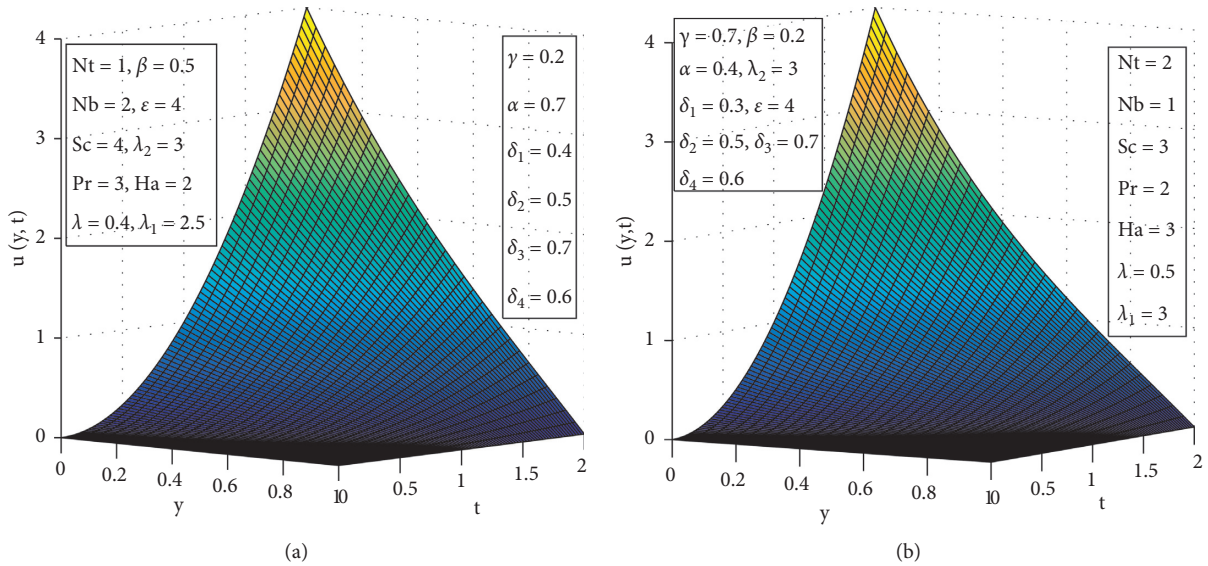

Figure 9: Unsteady velocity for various values of physical parameters over the interval $[0, 2]$.

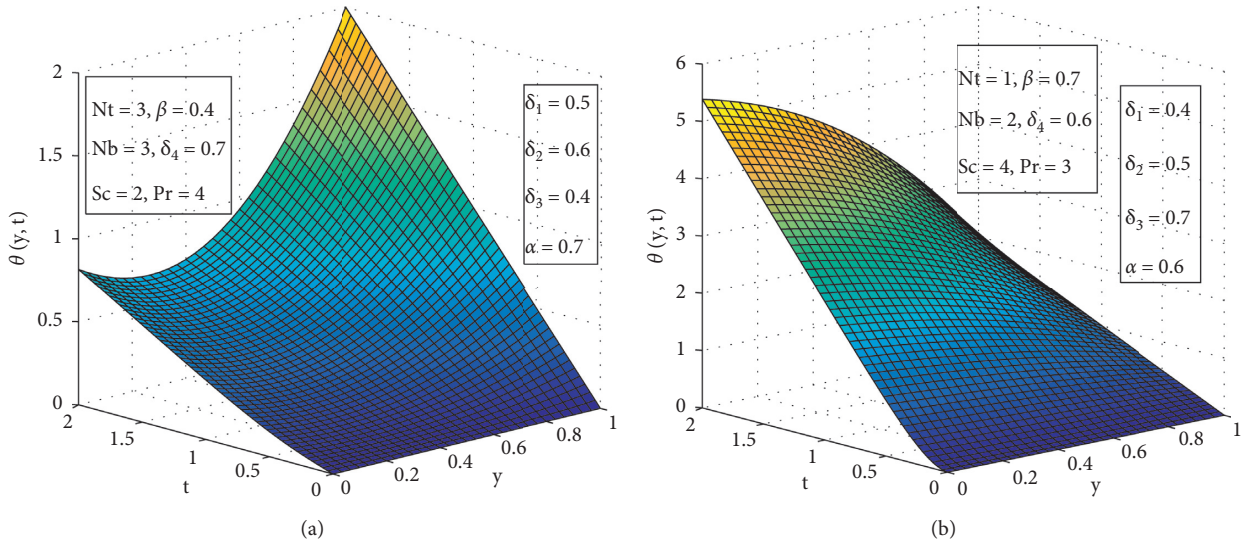

Figure 10: Unsteady temperature and concentration for various values of physical parameters over the interval $[0, \sqrt{2}]$.

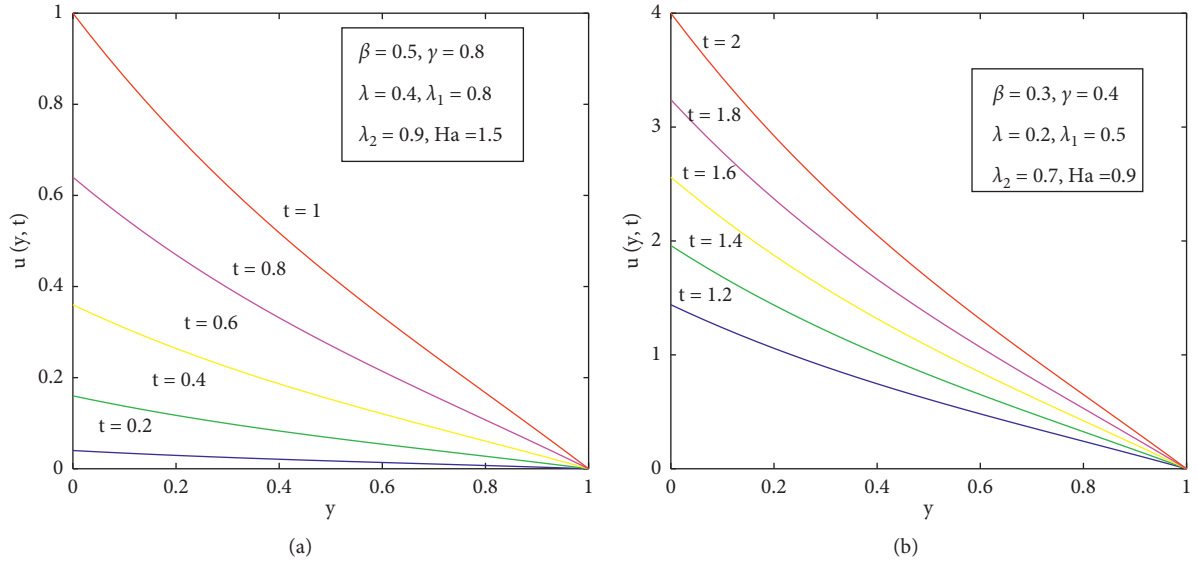

Figure 11: Velocity profiles for various final times for $Nt = 0.6$, $Sc = 0.5$, $Nb = 0.7$, $\delta_1 = 0.5$, $Pr = 0.8$, $\delta_2 = 0.3$, $\delta_3 = 0.1$, and $\delta_4 = 0.1$. (a) Variations of velocity profile when $\alpha = 0.5$. (b) Variations of velocity profile when $\alpha = 0.1$.

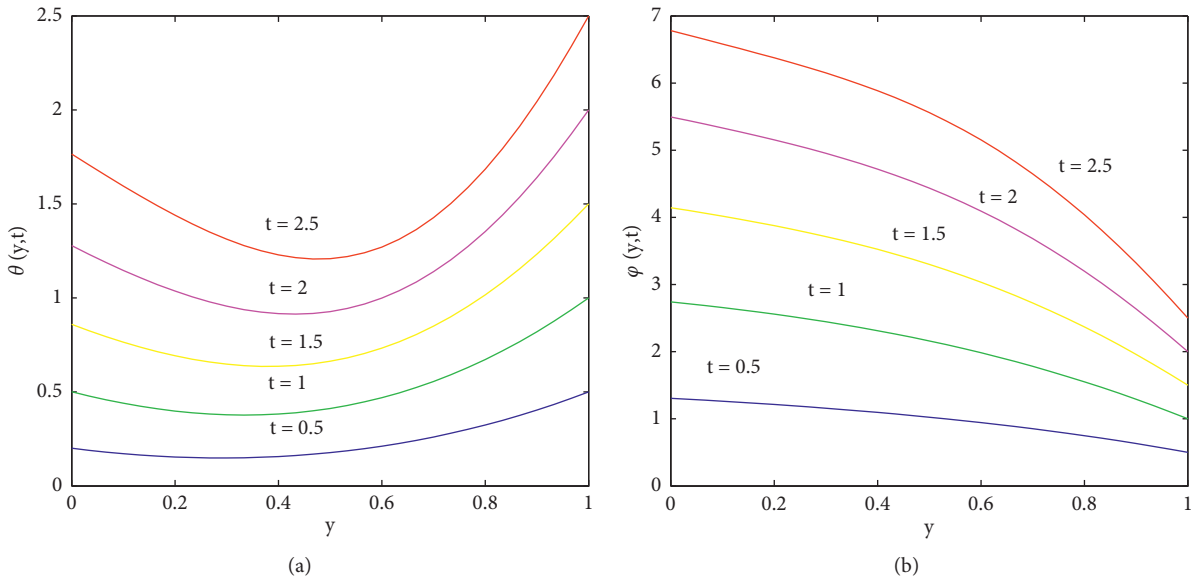

Figure 12: Temperature and concentration profiles for various final times for $Nt = 0.9$, $Sc = 0.3$, $Nb = 0.8$, $\delta_1 = 0.7$, $Pr = 1$, $\delta_2 = 0.8$, $\delta_3 = 0.1$ and $\delta_4 = 0.1$. (a) Variations of temperature profile when $\alpha = 0.7$. (b) Variations of temperature profile when $\beta = 0.7$.

Table 3: Influence of fractional flow numbers on the coefficient of friction at $(y, t) = (0, 0.1)$ for $Sc = 0.5$, $Nt = 0.3$, $Pr = 0.4$, $Nb = 0.4$, $\delta_1 = 0.4$, $\delta_2 = 0.6$, $\delta_3 = 0.01$, $\delta_4 = 0.01$, $\alpha = 0.5$, and $\beta = 0.5$.

ϵ	γ	λ	λ_1	λ_2	Ha	$\mathrm{Re}C_f/2$
0.1	0.2	0.1	0.2	0.1	0.2	−2.351733
0.2						−2.430800
0.3	0.2					−2.507821
	0.3					−2.305209
	0.4	0.1				−2.168051
		0.2				−2.177760
		0.3	0.2			−2.187445

Table 3: Continued.

ϵ	γ	λ	λ_1	λ_2	Ha	$\mathrm{Re}C_f/2$
			0.3			−2.133404
			0.4	0.1		−2.079362
				0.2		−2.078998
				0.3	0.2	−2.078633
					0.3	−2.088548
					0.4	−2.098437

Table 4: Influence of fractional flow numbers on the coefficient of friction at $(y,t) = (0, 0.1)$ for $\epsilon = 0.3$, $\beta = 0.3$, $\gamma = 0.4$, $\lambda = 0.1$, $Ha = 0.5$, $\delta_3 = 0.01$, $\delta_4 = 0.01$, $\lambda_1 = 0.5$, and $\lambda_2 = 0.7$.

α	δ_1	δ_2	Pr	Sc	Nt	Nb	$\mathrm{Re}C_f/2$
0.1	0.5	0.4	0.6	0.5	0.4	0.5	−0.314325
0.2							−0.567381
0.3	0.5						−0.936514
	0.6						−0.890553
	0.7	0.4					−0.844409
		0.5					−0.844564
		0.6	0.6				−0.844719
			0.7				−0.870374
			0.8	0.5			−0.892903
				0.6			−0.892822
				0.7	0.4		−0.892728
					0.5		−0.892449
					0.6	0.5	−0.892164
						0.6	−0.891937
						0.7	−0.891685

5. Conclusion

The flow of a nanofluid with a fractional derivative of time and nonlinear convection is studied in this communication. The fractional derivative of time is used to analyze the memory characteristics. Applications of Darcy porous medium can be encountered in numerous industries. Brownian motion effects are also considered while formulating the flow domain. A numerical algorithm is incorporated to estimate variations in the flow field. Flow is carried out by variable acceleration of the lower boundary. The flow direction and the applied magnetic field are orthogonal. Conditions for heat and mass gradients are considered at the bottom boundary, while quadratic variation is seen at the upper boundary. Enhancement in velocity is noted, for higher values of α, λ_1, γ, andλ_2, and opposite behavior is seen in case of λ, Ha, and β. Also, the enhancement of temperature profiles are observed for higher values of Nt, Nb, Sc, α, and δ_1, and opposite behavior is noted in case of Pr and δ_2. Concentration increases with the increase of α, Nt, Pr, δ_1, and δ_2, and decreasing behavior is observed for Nb and Sc. It is believed that fractional porous medium flows of nanofluids can be tackled with the current study. Flow, discussed in this communication, can be tackled in the manufacture of fiber and in geology. Moreover, the current study can be extended to Maxwell fluid flow. An analysis can also be performed to tackle nonlinear radiation effects in a fluid of differential type with fractional derivative.

Nomenclature

u: Velocity component
t: Time
ϕ: Fluid concentration
ϕ_0: Initial concentration
c_p: Nanoparticles specific heat
h_p: Nanoparticles enthalpy
α, β: Fractional derivatives
α_3: Thermal diffusivity
g: Gravitational acceleration
τ: Heat capacities ratio
σ: Electrical conductivity
ψ: Porosity
α_1: Second-grade fluid material parameter
k: Thermal conductivity
q_θ: Heat flux
ϵ: Darcy resistance parameter
λ: Porosity parameter
λ_1, λ_2: Convection parameters
Nt: Thermophoresis parameter
δ_1: Heat flux parameter
δ_3, δ_4: Relaxation time parameters
Pr: Prandtl parameter
y: Space coordinate
θ: Fluid temperature
θ_0: Initial temperature
c_f: Specific heat

ρ_f: Fluid density
ρ_p: Nanoparticles density
τ_1, τ_2: Relaxation times
D_B: Diffusion coefficient
D_θ: Thermophoretic coefficient
β_1, β_2: Thermal expansion coefficients
K: Permeability
B_0: Applied magnetic field
A: Dimensional constant
ν: Kinematic viscosity
q_ϕ: Concentration flux
γ: Viscoelastic parameter
λ: Magnetic parameter
Nb: Pedesis parameter
Nb: Pedesis parameter
δ_2: Mass flux parameter
Sc: Schmidt parameter
Re: Reynold parameter.

Data Availability

No data were used to support this study.

Conflicts of Interest

The authors declare that there are no conflicts of interest in this study.

Authors' Contributions

All authors contributed equally to the commenting, proofreading, and writing of this communication.

Acknowledgments

The authors extend their appreciation to the Deanship of Scientific Research at King Khalid University, Abha, Saudi Arabia, for funding this work through the research groups program under grant number RGP.2/20/43.

References

[1] J. Julyan and A. J. Hutchinson, "Conservation laws and conserved quantities of the governing equations for the laminar wake flow behind a small hump on a solid wall boundary," *International Journal of Non-linear Mechanics*, vol. 100, pp. 48–57, 2018.

[2] A. M. Megahed, M. G. Reddy, and W. Abbas, "Modeling of MHD fluid flow over an unsteady stretching sheet with thermal radiation, variable fluid properties and heat flux," *Mathematics and Computers in Simulation*, vol. 185, pp. 583–593, 2021.

[3] M. G. Reddy and S. A. Shehzad, "Molybdenum disulfide and magnesium oxide nanoparticle performance on micropolar cattaneo-christov heat flux model," *Applied Mathematics and Mechanics*, vol. 42, no. 4, pp. 541–552, 2021.

[4] A. M. Megahed and M. G. Reddy, "Numerical treatment for MHD viscoelastic fluid flow with variable fluid properties and viscous dissipation," *Indian Journal of Physics*, vol. 95, no. 4, pp. 673–679, 2021.

[5] M. G. Reddy, P. VIjayakumari, M. V. V. N. L. Sudharani, and K. G. Kumar, "Quadratic convective heat transport of casson nanoliquid over a contract cylinder: an unsteady case," *BioNanoScience*, vol. 10, no. 1, pp. 344–350, 2020.

[6] M. G. Reddy and K. G. Kumar, "Cattaneo-Christov heat flux feature on carbon nanotubes filled with micropolar liquid over a melting surface: a stream line study," *International Communications in Heat and Mass Transfer*, vol. 122, Article ID 105142, 2021.

[7] M. G. Reddy, N. K. R, B. C. Prasannakumara, N. G. Rudraswamy, and K. Ganesh Kumar, "Magnetohydrodynamic flow and heat transfer of a hybrid nanofluid over a rotating disk by considering Arrhenius energy," *Communications in Theoretical Physics*, vol. 73, no. 4, Article ID 045002, 2021.

[8] A. K. Verma, A. K. Gautam, K. Bhattacharyya, and I. Pop, "Entropy generation analysis of Falkner-Skan flow of Maxwell nanofluid in porous medium with temperature-dependent viscosity," *Pramana*, vol. 95, no. 2, Article ID 69, 2021.

[9] A. K. Pandey, S. Rajput, K. Bhattacharyya, and P. Sibanda, "Impact of metal oxide nanoparticles on unsteady stagnation point flow of the hybrid base fluid along a flat surface," *Pramana*, vol. 95, no. 1, Article ID 5, 2021.

[10] A. K. Verma, A. K. Gautam, K. Bhattacharyya, and R. P. Sharma, "Existence of boundary layer nanofluid flow through a divergent channel in porous medium with mass suction/injection," *Sādhanā*, vol. 46, no. 2, Article ID 98, 2021.

[11] A. K. Verma, A. K. Gautam, K. Bhattacharyya, A. Banerjee, and A. J. Chamkha, "Boundary layer flow of non-Newtonian Eyring-Powell nanofluid over a moving flat plate in Darcy porous medium with a parallel free-stream: multiple solutions and stability analysis," *Pramana*, vol. 95, no. 4, Article ID 173, 2021.

[12] A. Salama, S. Sun, and M. F. Wheeler, "Solving global problem by considering multitude of local problems: application to fluid flow in anisotropic porous media using the multipoint flux approximation," *Journal of Computational and Applied Mathematics*, vol. 267, pp. 117–130, 2014.

[13] A. Rasheed and M. S. Anwar, "Simulations of variable concentration aspects in a fractional nonlinear viscoelastic fluid flow," *Communications in Nonlinear Science and Numerical Simulation*, vol. 65, pp. 216–230, 2018.

[14] I. Podlubny, *Fractional Differential Equations*, Academic Press, New York, NY, USA, 1999.

[15] J. Sabatier, O. P. Agrawal, and J. A. Tenreiro Machado, *Advances in Fractional Calculus: Theoretical Developments and Applications in Physics and Engineering*, Sprin. Publish. Company, New York, NY, USA, 2007.

[16] Y. Liu, "Solvability of anti-periodic BVPs for impulsive fractional differential systems involving Caputo and Riemann–Liouville fractional derivatives," *International Journal of Nonlinear Sciences and Numerical Stimulation*, vol. 19, 2018.

[17] D. P. Ahokposi, A. Atangana, and D. P. Vermeulen, "Modelling groundwater fractal flow with fractional differentiation via Mittag-Leffler law," *The European Physical Journal Plus*, vol. 132, no. 4, Article ID 165, 2017.

[18] A. Atangana and D. Baleanu, "New fractional derivatives with nonlocal and non-singular kernel: theory and application to heat transfer model," *Thermal Science*, vol. 20, no. 2, pp. 763–769, 2016.

[19] K. Sayevand and K. Pichaghchi, "Analysis of nonlinear fractional KdV equation based on He's fractional derivative," *Nonlinear Sci. Lett. A*, vol. 7, pp. 77–85, 2016.

[20] M. Khan, S. Hyder Ali, and H. Qi, "On accelerated flows of a viscoelastic fluid with the fractional Burgers' model," *Nonlinear Analysis: Real World Applications*, vol. 10, no. 4, pp. 2286–2296, 2009.

[21] M. Shoaib Anwar and A. Rasheed, "Heat transfer at microscopic level in a MHD fractional inertial flow confined between non-isothermal boundaries," *The European Physical Journal Plus*, vol. 132, no. 7, Article ID 305, 2017.

[22] L. Wang and J. Wang, "Multiplicity results for degenerate fractional p-Laplacian problems with critical growth," *International Journal of Nonlinear Sciences and Numerical Stimulation*, vol. 19, no. 2, pp. 215–222, 2018.

[23] J. Zhao, L. Zheng, X. Zhang, and F. Liu, "Unsteady natural convection boundary layer heat transfer of fractional Maxwell viscoelastic fluid over a vertical plate," *International Journal of Heat and Mass Transfer*, vol. 97, pp. 760–766, 2016.

[24] X.-J. Yang, "General fractional calculus operators containing the generalized Mittag-Leffler functions applied to anomalous relaxation," *Thermal Science*, vol. 21, pp. S317–S326, 2017.

[25] N. Makris, G. F. Dargush, and M. C. Constantinou, "Dynamic analysis of generalized viscoelastic fluids," *Journal of Engineering Mechanics*, vol. 119, no. 8, pp. 1663–1679, 1993.

[26] M. S. Anwar and A. Rasheed, "Simulations of a fractional rate type nanofluid flow with non-integer Caputo time derivatives," *Computers & Mathematics with Applications*, vol. 74, no. 10, pp. 2485–2502, 2017.

[27] M. Mozafarifard, D. Toghraie, and H. Sobhani, "Numerical study of fast transient non-diffusive heat conduction in a porous medium composed of solid-glass spheres and air using fractional Cattaneo subdiffusion model," *International Communications in Heat and Mass Transfer*, vol. 122, Article ID 105192, 2021.

[28] M. S. Anwar, "Numerical study of transport phenomena in a nanofluid using fractional relaxation times in Buongiorno model," *Physica Scripta*, vol. 95, no. 3, Article ID 035211, 2020.

[29] S. E. Ahmed, "Caputo fractional convective flow in an inclined wavy vented cavity filled with a porous medium using Al2O3-Cu hybrid nanofluids," *International Communications in Heat and Mass Transfer*, vol. 116, Article ID 104690, 2020.

[30] M. S. Anwar, R. T. M. Ahmad, T. Shahzad, M. Irfan, and M. Z. Ashraf, "Electrified fractional nanofluid flow with suspended carbon nanotubes," *Computers & Mathematics with Applications*, vol. 80, no. 5, pp. 1375–1386, 2020.

[31] V. J. Ervin, H. Lee, and J. Ruiz-Ramírez, "Nonlinear Darcy fluid flow with deposition," *Journal of Computational and Applied Mathematics*, vol. 309, pp. 79–94, 2017.

[32] Z. Zhou and D. Liang, "The mass-preserving and modified-upwind splitting DDM scheme for time-dependent convection-diffusion equations," *Journal of Computational and Applied Mathematics*, vol. 317, pp. 247–273, 2017.

[33] N. S. Akbar, D. Tripathi, and Z. H. Khan, "Numerical investigation of Cattanneo-Christov heat flux in CNT suspended nanofluid flow over a stretching porous surface with suction and injection," *Discrete and Continuous Dynamical Systems-Series S*, vol. 11, pp. 595–606, 2018.

[34] A. Aziz, W. Jamshed, and W. Jamshed, "Unsteady MHD slip flow of non Newtonian power-law nanofluid over a moving surface with temperature dependent thermal conductivity," *Discrete & Continuous Dynamical Systems-S*, vol. 11, no. 4, pp. 617–630, 2018.

[35] B. J. Kirby, *Micro and Nanoscale Fluid Mechanics: Transport in Microfluidic Devices*, Cambridge Univ. Press, Cambridge, UK, 2010.

[36] M. Sheikholeslami and D. D. Ganji, "Nanofluid flow and heat transfer between parallel plates considering Brownian motion using DTM," *Computer Methods in Applied Mechanics and Engineering*, vol. 283, pp. 651–663, 2015.

[37] Y. Liu and Ji-H. He, "Bubble electrospinning for mass production of nanofibers," *International Journal of Nonlinear Sciences and Numerical Stimulation*, vol. 8, pp. 393–396, 2011.

[38] P. Valipour, H. Zaersabet, M. Hatami, A. Zolfagharian, and S. E. Ghasemi, "Numerical study on polymer nanofibers with electrically charged jet of viscoelastic fluid in electrospinning process," *Journal of Central South University*, vol. 24, no. 10, pp. 2275–2280, 2017.

[39] G. Wang and J. Zhang, "Thermal and power performance analysis for heat transfer applications of nanofluids in flows around cylinder," *Applied Thermal Engineering*, vol. 112, pp. 61–72, 2017.

[40] M. Waqas, M. I. Khan, T. Hayat, and A. Alsaedi, "Numerical simulation for magneto Carreau nanofluid model with thermal radiation: a revised model," *Computer Methods in Applied Mechanics and Engineering*, vol. 324, pp. 640–653, 2017.

[41] S. Nazari, R. Ellahi, M. M. Sarafraz, M. R. Safaei, A. Asgari, and O. A. Akbari, "Numerical study on mixed convection of a non-Newtonian nanofluid with porous media in a two lid-driven square cavity," *Journal of Thermal Analysis and Calorimetry*, vol. 140, no. 3, pp. 1121–1145, 2020.

[42] M. H. Heydari, H. L. Dastjerdi, and M. N. Ahmadabadi, "An efficient method for the numerical solution of a class of nonlinear fractional Fredholm integro-differential equations," *International Journal of Nonlinear Sciences and Numerical Stimulation*, vol. 19, 2018.

[43] Y. Lin and C. Xu, "Finite difference/spectral approximations for the time-fractional diffusion equation," *Journal of Computational Physics*, vol. 225, no. 2, pp. 1533–1552, 2007.

[44] R. A. Adams, *Sobolev Spaces*, Academic Press, New York, NY, USA, 1975.

[45] A. M. Abd El-Lateif and A. M. Abdel-Hameid, "Comment on "Solutions with special functions for time fractional free convection flow of Brinkman-type fluid" by F. Ali et al," *The European Physical Journal Plus*, vol. 132, no. 9, Article ID 407, 2017.

[46] J. Buongiorno, "Convective transport in nanofluids," *Journal of Heat Transfer*, vol. 128, no. 3, pp. 240–250, 2006.

Hindawi
Mathematical Problems in Engineering
Volume 2022, Article ID 7269033, 19 pages
https://doi.org/10.1155/2022/7269033

Research Article

Fejér–Pachpatte–Mercer-Type Inequalities for Harmonically Convex Functions Involving Exponential Function in Kernel

Saad Ihsan Butt,[1] **Saba Yousaf**,[1] **Khuram Ali Khan**,[2] **Rostin Matendo Mabela**,[3] **and Abdullah M. Alsharif**[4]

[1]*Department of Mathematics, COMSATS University Islamabad, Islamabad, Lahore Campus, Pakistan*
[2]*Department of Mathematics, University of Sargodha, Sargodha 40100, Pakistan*
[3]*Department of Maths and Computer Science, University of Kinshasa, Democratic Republic of the Congo*
[4]*Department of Mathematics and Statistics, College of Science, Taif University, P. O. Box 11099, Taif 21944, Saudi Arabia*

Correspondence should be addressed to Rostin Matendo Mabela; rostin.mabela@unikin.ac.cd

Received 17 October 2021; Accepted 14 December 2021; Published 2 March 2022

Academic Editor: Muhammad Shoaib Anwar

In the present study, fractional variants of Hermite–Hadamard, Hermite–Hadamard–Fejér, and Pachpatte inequalities are studied by employing Mercer concept. Firstly, new Hermite–Hadamard–Mercer-type inequalities are presented for harmonically convex functions involving fractional integral operators with exponential kernel. Then, weighted Hadamard–Fejér–Mercer-type inequalities involving exponential function as kernel are proved. Finally, Pachpatte–Mercer-type inequalities for products of harmonically convex functions via fractional integral operators with exponential kernel are constructed.

1. Introduction

Integral inequalities have been widely used in various sciences, including mathematical sciences, applied sciences, differential equations, and functional analysis. In the last two decades, these inequalities have gained attention from researchers. In most mathematical analysis areas, many types of integral inequalities are used. They are very important in approximation theory and numerical analysis, which estimate the error's approximation. Integral inequalities are useful tools in the study of different classes of differential equations and integral equations. They are today employed not only in mathematics but also in physics, computer science, and biology.

Convexity has several uses in business, medicine, industry, and art that have a significant impact on our daily lives. One of the most important applications of the convex function is the formulation of inequalities. Many equalities and inequalities have been defined for convex functions, but Jensen's inequality and the Hermite–Hadamard integral inequality are the most notable results [1–3]. The following notion of convex function plays a significant role in optimization theory and in other fields of sciences.

Definition 1. A function Ω: $I \subset \mathbb{R} \longrightarrow \mathbb{R}$ is called a convex function on I, if

$$\Omega\left(\eta \mathfrak{a}_1 + (1-\eta)\mathfrak{a}_2\right) \leq \eta\Omega\left(\mathfrak{a}_1\right) + (1-\eta)\Omega\left(\mathfrak{a}_2\right), \tag{1}$$

for all $\mathfrak{a}_1, \mathfrak{a}_2 \in I$ and $\eta \in [0,1]$, holds.

The following classical Jensen's inequality is defined as generalization of convex functions.

Theorem 1 (see [1]). *Suppose that Ω is a convex function on $[\mathfrak{a}_1, \mathfrak{a}_2]$; then,*

$$\Omega\left(\sum_{\ell=1}^{n} \eta_\ell \varkappa_\ell\right) \leq \sum_{\ell=1}^{n} \eta_\ell \Omega\left(\varkappa_\ell\right), \tag{2}$$

for all $\varkappa_\ell \in [\mathfrak{a}_1, \mathfrak{a}_2]$ and $\eta_\ell \in [0,1]$, where $\ell = 1, 2, \ldots, n$ with $\sum_{\ell=1}^{n} \eta_\ell = 1$.

Inequality (2) is a key to extract applications in information theory. It is very useful in computing optimal bounds for joint and conditional entropies and mutual information (for instance, see [4–6] and the references therein).

Hermite–Hadamard inequalities may be considered as a refinement of the concept of convexity, and it is simply inferred from Jensen's inequality as follows.

Theorem 2 (see [2]). *If Ω is a convex function on the interval $[\mathfrak{a}_1, \mathfrak{a}_2]$ with $\mathfrak{a}_1 < \mathfrak{a}_2$, then*

$$\Omega\left(\frac{\mathfrak{a}_1 + \mathfrak{a}_2}{2}\right) \leq \frac{1}{\mathfrak{a}_2 - \mathfrak{a}_1} \int_{\mathfrak{a}_1}^{\mathfrak{a}_2} \Omega(\varkappa) d\varkappa \leq \frac{\Omega(\mathfrak{a}_1) + \Omega(\mathfrak{a}_2)}{2}. \quad (3)$$

It has been applied in several branches such as finance, engineering, and science (see [2]). In recent years, Hermite–Hadamard inequalities for convex functions have gotten a lot of attention, and as a result, there have been a lot of refinements and generalizations.

In 2003, Mercer presented a variant of Jensen's inequality as follows.

Theorem 3 (see [7]). *Suppose that Ω is a convex function on the interval $[\theta_1, \theta_2]$; then,*

$$\Omega\left(\theta_1 + \theta_2 - \sum_{\ell=1}^{n} \eta_\ell \varkappa_\ell\right) \leq \Omega(\theta_1) + \Omega(\theta_2) - \sum_{\ell=1}^{n} \eta_\ell \Omega(\varkappa_\ell), \quad (4)$$

for all $\varkappa_\ell \in [\theta_1, \theta_2]$ and $\eta_\ell \in [0, 1]$, where $\ell = 1, 2, \ldots, n$ with $\sum_{\ell=1}^{n} \eta_\ell = 1$.

Over the years, the Jensen–Mercer inequality became a topic of foremost interest for many scholars as they have investigated and studied in various ways including bringing it to a higher dimension and acquiring it for convex operators along with its several refinements, operator variants for superquadratic functions, improvements, and many generalizations with applications in information theory (see [8–10]).

In [11], Íşcan gave the definition of harmonic convexity as follows.

Definition 2. A function $\Omega: I \subset \mathbb{R}\backslash\{0\} \longrightarrow \mathbb{R}$ is said to be harmonically convex on I, if

$$\Omega\left(\frac{\mathfrak{a}_1\mathfrak{a}_2}{\eta\mathfrak{a}_1 + (1-\eta)\mathfrak{a}_2}\right) \leq \eta\Omega(\mathfrak{a}_2) + (1-\eta)\Omega(\mathfrak{a}_1), \quad (5)$$

holds for all $\mathfrak{a}_1, \mathfrak{a}_2 \in I$ and $\eta \in [0, 1]$.

In [11], Íşcan for the first time introduced the Hermite–Hadamard inequality for harmonically convex function along with the following identity.

Theorem 4 (see [11]). *Suppose that $\Omega: I \subseteq (0, \infty) \longrightarrow \mathbb{R}$ is a harmonically convex function and $\mathfrak{a}_1, \mathfrak{a}_2 \in I$ with $\mathfrak{a}_1 < \mathfrak{a}_2$. If $\Omega \in L[\mathfrak{a}_1, \mathfrak{a}_2]$, then*

$$\Omega\left(\frac{2\mathfrak{a}_1\mathfrak{a}_2}{\mathfrak{a}_1 + \mathfrak{a}_2}\right) \leq \frac{\mathfrak{a}_1\mathfrak{a}_2}{\mathfrak{a}_2 - \mathfrak{a}_1} \int_{\mathfrak{a}_1}^{\mathfrak{a}_2} \frac{\Omega(\varkappa)}{\varkappa^2} d\varkappa \leq \frac{\Omega(\mathfrak{a}_1) + \Omega(\mathfrak{a}_2)}{2}. \quad (6)$$

Lemma 1 (see [11]). *If $\Omega: I \subseteq (0, \infty) \longrightarrow \mathbb{R}$ is a differentiable function on I^o and $\mathfrak{a}_1, \mathfrak{a}_2 \in I$ with $\mathfrak{a}_1 < \mathfrak{a}_2$ and $\Omega' \in L[\mathfrak{a}_1, \mathfrak{a}_2]$, then*

$$\begin{aligned} &\frac{\Omega(\mathfrak{a}_1) + \Omega(\mathfrak{a}_2)}{2} - \frac{\mathfrak{a}_1\mathfrak{a}_2}{\mathfrak{a}_2 - \mathfrak{a}_1} \int_{\mathfrak{a}_1}^{\mathfrak{a}_2} \frac{\Omega(\varkappa)}{\varkappa^2} d\varkappa \\ &= \frac{\mathfrak{a}_1\mathfrak{a}_2(\mathfrak{a}_2 - \mathfrak{a}_1)}{2} \int_0^1 \frac{1 - 2\eta}{(\eta\mathfrak{a}_2 + (1-\eta)\mathfrak{a}_1)^2} \Omega' \\ &\cdot \left(\frac{\mathfrak{a}_1\mathfrak{a}_2}{\eta\mathfrak{a}_2 + (1-\eta)\mathfrak{a}_1}\right) d\eta. \end{aligned} \quad (7)$$

The most prominent inequalities connected to the integral mean of a harmonically convex function are the Hermite–Hadamard inequalities or their weighted versions which are called Hermite–Hadamard–Fejér inequalities for harmonically convex functions. In [12], Chen and Wu established the Hermite–Hadamard–Fejér inequality for harmonically convex functions.

Theorem 5 (see [12]). *Let $\Omega: I \subseteq (0, \infty) \longrightarrow \mathbb{R}$ be a harmonically convex function and $\mathfrak{a}_1, \mathfrak{a}_2 \in I$ with $\mathfrak{a}_1 < \mathfrak{a}_2$. If $\Omega \in L[\mathfrak{a}_1, \mathfrak{a}_2]$ and $\omega: [\mathfrak{a}_1, \mathfrak{a}_2] \subseteq (0, \infty) \longrightarrow \mathbb{R}$ is non-negative, integrable, and harmonically symmetric with respect to $2\mathfrak{a}_1\mathfrak{a}_2/\mathfrak{a}_1 + \mathfrak{a}_2$, that is, $\omega(\varkappa) = \omega(1/(1/\mathfrak{a}_1) + (1/\mathfrak{a}_2) - (1/\varkappa))$, then*

$$\begin{aligned} \Omega\left(\frac{2\mathfrak{a}_1\mathfrak{a}_2}{\mathfrak{a}_1 + \mathfrak{a}_2}\right) \int_{\mathfrak{a}_1}^{\mathfrak{a}_2} \frac{\omega(\varkappa)}{\varkappa^2} d\varkappa &\leq \int_{\mathfrak{a}_1}^{\mathfrak{a}_2} \frac{\Omega(x)\omega(\varkappa)}{\varkappa^2} d\varkappa \\ &\leq \frac{\Omega(\mathfrak{a}_1) + \Omega(\mathfrak{a}_2)}{2} \int_{\mathfrak{a}_1}^{\mathfrak{a}_2} \frac{\omega(\varkappa)}{\varkappa^2} d\varkappa. \end{aligned} \quad (8)$$

In [13], Chen and Wu obtained two Hermite–Hadamard-type inequalities for products of harmonically convex functions as follows.

Theorem 6 (see [13]). *Let $\Omega, \omega: [\mathfrak{a}_1, \mathfrak{a}_2] \subseteq (0, \infty) \longrightarrow [0, \infty)$, $\mathfrak{a}_1, \mathfrak{a}_2 \in (0, \infty)$, be functions such that $\Omega, \omega, \Omega\omega \in L[\mathfrak{a}_1, \mathfrak{a}_2]$. If Ω and ω are harmonically convex on $[\mathfrak{a}_1, \mathfrak{a}_2]$, then*

$$\frac{\mathfrak{a}_1\mathfrak{a}_2}{\mathfrak{a}_2 - \mathfrak{a}_1} \int_{\mathfrak{a}_1}^{\mathfrak{a}_2} \frac{\Omega(\varkappa)\omega(\varkappa)}{\varkappa^2} d\varkappa \leq \frac{1}{3} M(\mathfrak{a}_1, \mathfrak{a}_2) + \frac{1}{6} N(\mathfrak{a}_1, \mathfrak{a}_2), \quad (9)$$

$$\begin{aligned} 2\Omega\left(\frac{2\mathfrak{a}_1\mathfrak{a}_2}{\mathfrak{a}_1 + \mathfrak{a}_2}\right)\omega\left(\frac{2\mathfrak{a}_1\mathfrak{a}_2}{\mathfrak{a}_1 + \mathfrak{a}_2}\right) &\leq \frac{\mathfrak{a}_1\mathfrak{a}_2}{\mathfrak{a}_2 - \mathfrak{a}_1} \int_{\mathfrak{a}_1}^{\mathfrak{a}_2} \frac{\Omega(\varkappa)\omega(\varkappa)}{\varkappa^2} d\varkappa \\ &+ \frac{1}{6} M(\mathfrak{a}_1, \mathfrak{a}_2) + \frac{1}{3} N(\mathfrak{a}_1, \mathfrak{a}_2), \end{aligned} \quad (10)$$

where $M(\mathfrak{a}_1, \mathfrak{a}_2) = \Omega(\mathfrak{a}_1)\omega(\mathfrak{a}_1) + \Omega(\mathfrak{a}_2)\omega(\mathfrak{a}_2)$ and $N(\mathfrak{a}_1, \mathfrak{a}_2) = \Omega(\mathfrak{a}_1)\omega(\mathfrak{a}_2) + \Omega(\mathfrak{a}_2)\omega(\mathfrak{a}_1)$.

Fractional calculus is an extension of classical calculus. Fractional calculus is now a well-known technique in engineering science, with wide range of applications in material modeling. A growing number of degree considerations have recently been given to fractional calculus and its numerous applications. Fractional integral/derivative operators are extremely important in the development of fractional calculus. Fractional differential equations and dynamical frameworks were established a few decades ago as key tools for exhibiting a variety of phenomena in various branches of pure and applied sciences. Many physical problems can be modeled using fractional differential equations, including heat equations, wave equations, Poisson equations, and Laplace equations, biological populations, fluid mechanics, thermodynamics, viscoelasticity, vibration, advection-diffusion, groundwater flow with memory, and signal processing [14, 15]. Several studies have shown that fractional operators can accurately explain complex long memory and multiscale phenomena in materials that are difficult to capture using standard mathematical methods including classical differential calculus. The significance of fractional calculus can be more understandable, and several works involving fractional calculus have been done.

Several well-known inequalities and related results can be generalized and extended via fractional integral operators (see [16–19] and the references therein).

Definition 3 (see [15]). Let $\Omega \in L[\mathfrak{a}_1, \mathfrak{a}_2]$. The Riemann–Liouville fractional integrals $J^{\alpha}_{\mathfrak{a}_1^+}\Omega$ and $J^{\alpha}_{\mathfrak{a}_2^-}\Omega$ of order $\alpha > 0$ with $\mathfrak{a}_1 \geq 0$ are defined by

$$J^{\alpha}_{\mathfrak{a}_1^+}\Omega(\varkappa) = \frac{1}{\Gamma(\alpha)}\int_{\mathfrak{a}_1}^{\varkappa}(\varkappa - u)^{\alpha-1}\Omega(u)\mathrm{d}u, \quad \varkappa > \mathfrak{a}_1,$$
$$J^{\alpha}_{\mathfrak{a}_2^-}\Omega(\varkappa) = \frac{1}{\Gamma(\alpha)}\int_{\varkappa}^{\mathfrak{a}_2}(u - \varkappa)^{\alpha-1}\Omega(u)\mathrm{d}u, \quad \varkappa < \mathfrak{a}_2, \tag{11}$$

respectively. Here, $\Gamma(\alpha)$ is the gamma function defined by $\Gamma(\alpha) = \int_0^{\infty} e^{-u}u^{\alpha-1}\mathrm{d}u$ and $J^0_{\mathfrak{a}_1^+}\Omega(\varkappa) = J^0_{\mathfrak{a}_2^-}\Omega(\varkappa) = \Omega(\varkappa)$.

In [20], Iscan and Wu for the first time introduced Hermite–Hadamard-type inequalities for harmonically convex functions for Riemann–Liouville fractional integral operators along with the following integral identity.

Theorem 7 (see [20]). *Let Ω: $[\mathfrak{a}_1, \mathfrak{a}_2] \subseteq (0, \infty) \longrightarrow \mathbb{R}$ be a function with $\mathfrak{a}_1 < \mathfrak{a}_2$ and $\Omega \in L[\mathfrak{a}_1, \mathfrak{a}_2]$. If Ω is a harmonically convex function, then*

$$\Omega\left(\frac{2\mathfrak{a}_1\mathfrak{a}_2}{\mathfrak{a}_1 + \mathfrak{a}_2}\right) \leq \frac{\Gamma(\alpha+1)}{2}\left(\frac{\mathfrak{a}_1\mathfrak{a}_2}{\mathfrak{a}_2 - \mathfrak{a}_1}\right)^{\alpha}\left[J^{\alpha}_{1/\mathfrak{a}_1^-}(\Omega\circ\mathfrak{g})\left(\frac{1}{\mathfrak{a}_2}\right) + I^{\alpha}_{1/\mathfrak{a}_2^+}(\Omega\circ\mathfrak{g})\left(\frac{1}{\mathfrak{a}_1}\right)\right] \leq \frac{\Omega(\mathfrak{a}_1) + \Omega(\mathfrak{a}_2)}{2}, \tag{12}$$

where $\mathfrak{g}(\mathfrak{u}) = 1/\mathfrak{u}$.

Lemma 2 (see [20]). *Suppose that Ω: $[\mathfrak{a}_1, \mathfrak{a}_2] \subseteq (0, \infty) \longrightarrow \mathbb{R}$ is a differentiable function on I^o and $\Omega' \in L[\mathfrak{a}_1, \mathfrak{a}_2]$; then,*

$$\begin{aligned}&\frac{\Omega(\mathfrak{a}_1) + \Omega(\mathfrak{a}_2)}{2} - \frac{\Gamma(\alpha+1)}{2}\left(\frac{\mathfrak{a}_1\mathfrak{a}_2}{\mathfrak{a}_2 - \mathfrak{a}_1}\right)^{\alpha}\left[J^{\alpha}_{1/\mathfrak{a}_1^-}(\Omega\circ\mathfrak{g})\left(\frac{1}{\mathfrak{a}_2}\right) + I^{\alpha}_{1/\mathfrak{a}_2^+}(\Omega\circ\mathfrak{g})\left(\frac{1}{\mathfrak{a}_1}\right)\right]\\ &= \frac{\mathfrak{a}_1\mathfrak{a}_2(\mathfrak{a}_2 - \mathfrak{a}_1)}{2}\int_0^1 \frac{[\eta^{\alpha} - (1-\eta)^{\alpha}]}{(\eta\mathfrak{a}_1 + (1-\eta)\mathfrak{a}_2)^2}\Omega'\left(\frac{\mathfrak{a}_1\mathfrak{a}_2}{\eta\mathfrak{a}_1 + (1-\eta)\mathfrak{a}_2}\right)\mathrm{d}\eta,\end{aligned} \tag{13}$$

where $\mathfrak{g}(\mathfrak{u}) = 1/\mathfrak{u}$.

In [21], İşcan and Kunt represented the Hermite–Hadamard–Fejér-type inequality for harmonically convex functions in Riemann–Liouville fractional integral forms as follows.

Theorem 8 (see [21]). *Let Ω: $I \subseteq (0, \infty) \longrightarrow \mathbb{R}$ be a harmonically convex function and $\mathfrak{a}_1, \mathfrak{a}_2 \in I$ with $\mathfrak{a}_1 < \mathfrak{a}_2$. If $\Omega \in L[\mathfrak{a}_1, \mathfrak{a}_2]$ and ω: $[\mathfrak{a}_1, \mathfrak{a}_2] \subseteq (0, \infty) \longrightarrow \mathbb{R}$ is nonnegative, integrable, and harmonically symmetric with respect to $2\mathfrak{a}_1\mathfrak{a}_2/\mathfrak{a}_1 + \mathfrak{a}_2$, that is, $\omega(\varkappa) = \omega(1/(1/\mathfrak{a}_1) + (1/\mathfrak{a}_2) - (1/\varkappa))$, then*

$$\begin{aligned}&\Omega\left(\frac{2\mathfrak{a}_1\mathfrak{a}_2}{\mathfrak{a}_1 + \mathfrak{a}_2}\right)\left[J^{\alpha}_{1/\mathfrak{a}_1^-}(\omega\circ\mathfrak{g})\left(\frac{1}{\mathfrak{a}_2}\right) + J^{\alpha}_{1/\mathfrak{a}_2^+}(\omega\circ\mathfrak{g})\left(\frac{1}{\mathfrak{a}_1}\right)\right]\\ &\leq \left[J^{\alpha}_{1/\mathfrak{a}_1^-}(\Omega\omega\circ\mathfrak{g})\left(\frac{1}{\mathfrak{a}_2}\right) + J^{\alpha}_{1/\mathfrak{a}_2^+}(\Omega\omega\circ\mathfrak{g})\left(\frac{1}{\mathfrak{a}_1}\right)\right]\\ &\leq \frac{\Omega(\mathfrak{a}_1) + \Omega(\mathfrak{a}_2)}{2}\left[J^{\alpha}_{1/\mathfrak{a}_1^-}(\omega\circ\mathfrak{g})\left(\frac{1}{\mathfrak{a}_2}\right) + J^{\alpha}_{1/\mathfrak{a}_2^+}(\omega\circ\mathfrak{g})\left(\frac{1}{\mathfrak{a}_1}\right)\right],\end{aligned} \tag{14}$$

where $\alpha > 0$ $\mathfrak{g}(\mathfrak{u}) = 1/\mathfrak{u}$, $u \in [1/\mathfrak{a}_2, 1/\mathfrak{a}_1]$.

The importance of Hadamard-type inequalities is due to their roles in various fields of modern mathematics such as numerical analysis, probability, mathematical analysis, and related fields [2, 22]. Many researchers generalize and extend their studies to Hermite–Hadamard, Hermite–Hadamard–Fejér, and Pachpatte-type inequalities involving fractional integrals for various classes of convex functions (see [20, 21, 23, 24] and the references therein).

Recently (from 2020 to 2021), some new kinds of fractional treatment of Hermite–Jensen–Mercer-type inequalities for a variety of fractional integral operators were presented in [25–27]. All these results were investigated for convex functions or s-convex functions, and many applications to special functions like Bessel and q-digamma functions were obtained.

Since there a is massive literature about the development of fractional Mercer integral inequalities involving convex functions but still there exist many gaps to be filled for fractional integral inequalities for other classes of convex functions. Therefore, the basic aim of this paper is to present three new Hadamard–Mercer-type inequalities for harmonically convex functions using fractional integral operators with exponential kernel. We also give fractional Mercer integral inequalities for product of two harmonically convex functions. We hope that the new techniques formulated in this paper are more energizing than the accessible one.

Ahmad et al. [23] gave the definition of two new fractional integral operators with an exponential kernel.

Definition 4. Let $\Omega \in L(\mathfrak{a}_1, \mathfrak{a}_2)$. The fractional integral operators $I^{\alpha}_{\mathfrak{a}_1}\Omega(\varkappa)$ and $I^{\alpha}_{\mathfrak{a}_2}\Omega(\varkappa)$ of order $\alpha \in (0,1)$ are, respectively, defined by

$$I^{\alpha}_{\mathfrak{a}_1}\Omega(\varkappa) = \frac{1}{\alpha}\int_{\mathfrak{a}_1}^{\varkappa} \exp\left(-\frac{1-\alpha}{\alpha}(\varkappa - u)\right)\Omega(u)\mathrm{d}u, \quad \varkappa > \mathfrak{a}_1,$$
$$I^{\alpha}_{\mathfrak{a}_2}\Omega(\varkappa) = \frac{1}{\alpha}\int_{\varkappa}^{\mathfrak{a}_2} \exp\left(-\frac{1-\alpha}{\alpha}(u - \varkappa)\right)\Omega(u)\mathrm{d}u, \quad \varkappa < \mathfrak{a}_2. \tag{15}$$

Remark 1. If $\alpha = 1$, then

$$\lim_{\alpha \longrightarrow 1} I^{\alpha}_{\mathfrak{a}_1}\Omega(\varkappa) = \int_{\mathfrak{a}_1}^{\varkappa}\Omega(u)\mathrm{d}u,$$
$$\lim_{\alpha \longrightarrow 1} I^{\alpha}_{\mathfrak{a}_2}\Omega(\varkappa) = \int_{\varkappa}^{\mathfrak{a}_2}\Omega(u)\mathrm{d}u. \tag{16}$$

For the convenience of expression, throughout the paper, we set

$$\rho = \frac{1-\alpha}{\alpha}\left(\frac{\mathfrak{a}_2 - \mathfrak{a}_1}{\mathfrak{a}_1\mathfrak{a}_2}\right). \tag{17}$$

2. Hermite–Hadamard–Mercer-Type Inequalities for Harmonically Convex Function

Theorem 9. *Suppose that Ω: $[\theta_1, \theta_2] \subseteq (0,\infty) \longrightarrow \mathbb{R}$ is a positive function with $0 \le \theta_1 < \theta_2$. If Ω is a harmonically convex function on $[\theta_1, \theta_2]$ and $\Omega \in L[\theta_1, \theta_2]$, then*

$$\Omega\left(\frac{1}{(1/\theta_1)+(1/\theta_2)-(\mathfrak{a}_1+\mathfrak{a}_2/2\mathfrak{a}_1\mathfrak{a}_2)}\right) \le \Omega(\theta_1)+\Omega(\theta_2) - \frac{1-\alpha}{2[1-\exp(-\rho)]}\left[I^{\alpha}_{1/\mathfrak{a}_1}(\Omega\circ\mathfrak{g})\left(\frac{1}{\mathfrak{a}_2}\right) + I^{\alpha}_{1/\mathfrak{a}_2}(\Omega\circ\mathfrak{g})\left(\frac{1}{\mathfrak{a}_1}\right)\right]$$
$$\le \Omega(\theta_1)+\Omega(\theta_2) - \Omega\left(\frac{2\mathfrak{a}_1\mathfrak{a}_2}{\mathfrak{a}_1+\mathfrak{a}_2}\right), \tag{18}$$

$$\Omega\left(\frac{1}{(1/\theta_1)+(1/\theta_2)-(\mathfrak{a}_1+\mathfrak{a}_2/2\mathfrak{a}_1\mathfrak{a}_2)}\right) \le \frac{1-\alpha}{2[1-\exp(-\rho)]}$$
$$\cdot\left[I^{\alpha}_{((1/\theta_1)+(1/\theta_2)-(1/\mathfrak{a}_1))}(\Omega\circ\mathfrak{g})\left(\frac{1}{\theta_1}+\frac{1}{\theta_2}-\frac{1}{\mathfrak{a}_2}\right)\right.$$
$$\left. + I^{\alpha}_{((1/\theta_1)+(1/\theta_2)-(1/\mathfrak{a}_2))}(\Omega\circ\mathfrak{g})\left(\frac{1}{\theta_1}+\frac{1}{\theta_2}-\frac{1}{\mathfrak{a}_1}\right)\right]$$
$$\le \frac{1}{2}\left[\Omega\left(\frac{1}{(1/\theta_1)+(1/\theta_2)-(1/\mathfrak{a}_1)}\right)+\Omega\left(\frac{1}{(1/\theta_1)+(1/\theta_2)-1/\mathfrak{a}_2}\right)\right]$$
$$\le \Omega(\theta_1)+\Omega(\theta_2) - \frac{\Omega(\mathfrak{a}_1)+\Omega(\mathfrak{a}_2)}{2}, \tag{19}$$

for all $\mathfrak{a}_1, \mathfrak{a}_2 \in [\theta_1, \theta_2]$, $\alpha > 0$, $\mathfrak{g}(\mathfrak{u}) = 1/\mathfrak{u}$, $u \in [1/\theta_2, 1/\theta_1]$ and ρ is defined in (17).

Proof. Using the Jensen–Mercer inequality for harmonically convex function, we have

$$\Omega\left(\frac{1}{(1/\theta_1)+(1/\theta_2)-(\overline{\mathfrak{a}_1}+\overline{\mathfrak{a}_2}/2\overline{\mathfrak{a}_1}\overline{\mathfrak{a}_1})}\right) \le \Omega(\theta_1)+\Omega(\theta_2) - \frac{\Omega(\overline{\mathfrak{a}_1})+\Omega(\overline{\mathfrak{a}_2})}{2}, \tag{20}$$

for all $\overline{\mathfrak{a}_1}$, $\overline{\mathfrak{a}_2} \in [\theta_1, \theta_2]$. By changing of the variables $\overline{\mathfrak{a}_1} = \mathfrak{a}_1\mathfrak{a}_2/\eta\mathfrak{a}_1 + (1-\eta)\mathfrak{a}_2$, $\overline{\mathfrak{a}_2} = \mathfrak{a}_1\mathfrak{a}_2/\eta\mathfrak{a}_2 + (1-\eta)\mathfrak{a}_1$ for all $\mathfrak{a}_1, \mathfrak{a}_2 \in [\theta_1, \theta_2]$ and $\eta \in [0,1]$ in (20), we obtain

$$\Omega\left(\frac{1}{(1/\theta_1)+(1/\theta_2)-(\mathfrak{a}_1+\mathfrak{a}_2/2\mathfrak{a}_1\mathfrak{a}_2)}\right) \le \Omega(\theta_1)+\Omega(\theta_2)-\frac{1}{2}\left[\Omega\left(\frac{\mathfrak{a}_1\mathfrak{a}_2}{\eta\mathfrak{a}_1+(1-\eta)\mathfrak{a}_2}\right)+\Omega\left(\frac{\mathfrak{a}_1\mathfrak{a}_2}{\eta\mathfrak{a}_2+(1-\eta)\mathfrak{a}_1}\right)\right]. \tag{21}$$

Multiplying by $\exp(-\rho\eta)$ on both sides of (21) and then integrating with respect to η over $[0,1]$, we have

$$\begin{aligned}
&\frac{[1-\exp(-\rho)]}{\rho}\Omega\left(\frac{1}{(1/\theta_1)+(1/\theta_2)-(\mathfrak{a}_1+\mathfrak{a}_2/2\mathfrak{a}_1\mathfrak{a}_2)}\right)\\
&\le\frac{[1-\exp(-\rho)]}{\rho}[\Omega(\mathfrak{a}_1)+\Omega(\mathfrak{a}_2)]-\frac{1}{2}\int_0^1\exp(-\rho\eta)\\
&\quad\cdot\left[\Omega\left(\frac{\mathfrak{a}_1\mathfrak{a}_2}{\eta\mathfrak{a}_1+(1-\eta)\mathfrak{a}_2}\right)+\Omega\left(\frac{\mathfrak{a}_1\mathfrak{a}_2}{\eta\mathfrak{a}_2+(1-\eta)\mathfrak{a}_1}\right)\right]d\eta\\
&=\frac{[1-\exp(-\rho)]}{\rho}[\Omega(\theta_1)+\Omega(\theta_2)]-\frac{\mathfrak{a}_1\mathfrak{a}_2}{2(\mathfrak{a}_2-\mathfrak{a}_1)}\left[\int_{1/\mathfrak{a}_2}^{1/\mathfrak{a}_1}\exp\left(-\frac{1-\alpha}{\alpha}\left(\frac{1}{\mathfrak{a}_1}-u\right)\right)\Omega\left(\frac{1}{u}\right)du\right.\\
&\quad\left.+\int_{1/\mathfrak{a}_2}^{1/\mathfrak{a}_1}\exp\left(-\frac{1-\alpha}{\alpha}\left(u-\frac{1}{\mathfrak{a}_2}\right)\right)\Omega\left(\frac{1}{u}\right)du\right]\\
&=\frac{[1-\exp(-\rho)]}{\rho}[\Omega(\theta_1)+\Omega(\theta_2)]-\frac{\alpha\mathfrak{a}_1\mathfrak{a}_2}{2(\mathfrak{a}_2-\mathfrak{a}_1)}\left[I^{\alpha}_{1/\mathfrak{a}_2}(\Omega\circ\mathfrak{g})\left(\frac{1}{\mathfrak{a}_1}\right)+I^{\alpha}_{1/\mathfrak{a}_1}(\Omega\circ\mathfrak{g})\left(\frac{1}{\mathfrak{a}_2}\right)\right].
\end{aligned} \tag{22}$$

Multiplying by $\rho/[1-\exp(-\rho)]$ on both sides of above equation and putting the value of ρ which is given in (17), we get

$$\Omega\left(\frac{1}{(1/\theta_1)+(1/\theta_2)-\mathfrak{a}_1+\mathfrak{a}_2/2\mathfrak{a}_1\mathfrak{a}_2}\right) \le \Omega(\theta_1)+\Omega(\theta_2)-\frac{1-\alpha}{2[1-\exp(-\rho)]}\left[I^{\alpha}_{1/\mathfrak{a}_1}(\Omega\circ\mathfrak{g})\left(\frac{1}{\mathfrak{a}_2}\right)+I^{\alpha}_{1/\mathfrak{a}_2}(\Omega\circ\mathfrak{g})\left(\frac{1}{\mathfrak{a}_1}\right)\right]. \tag{23}$$

Thus, the first inequality of (18) is proved. Now we prove the second inequality in (18); since Ω is a harmonically convex function, then, for $\eta \in [0,1]$, it yields

$$\begin{aligned}
\Omega\left(\frac{2\mathfrak{a}_1\mathfrak{a}_2}{\mathfrak{a}_1+\mathfrak{a}_2}\right)&=\Omega\left(\frac{2}{(\eta/\mathfrak{a}_1)+(1-\eta/\mathfrak{a}_2)+(1-\eta/\mathfrak{a}_1)+(\eta/\mathfrak{a}_2)}\right)\\
&\le\frac{1}{2}\left[\Omega\left(\frac{\mathfrak{a}_1\mathfrak{a}_2}{\eta\mathfrak{a}_2+(1-\eta)\mathfrak{a}_1}\right)+\Omega\left(\frac{\mathfrak{a}_1\mathfrak{a}_2}{\eta\mathfrak{a}_1+(1-\eta)\mathfrak{a}_2}\right)\right].
\end{aligned} \tag{24}$$

Multiplying by $\exp(-\rho\eta)$ on both sides of (24) and then integrating with respect to η over $[0,1]$, we have

$$\begin{aligned}
&\frac{[1-\exp(-\rho)]}{\rho}\Omega\left(\frac{2\mathfrak{a}_1\mathfrak{a}_2}{\mathfrak{a}_1+\mathfrak{a}_2}\right)\\
&\le\frac{1}{2}\left[\int_0^1\exp(-\rho\eta)\Omega\left(\frac{\mathfrak{a}_1\mathfrak{a}_2}{\eta\mathfrak{a}_2+(1-\eta)\mathfrak{a}_1}\right)\right.\\
&\quad\left.+\Omega\left(\frac{\mathfrak{a}_1\mathfrak{a}_2}{\eta\mathfrak{a}_1+(1-\eta)\mathfrak{a}_2}\right)d\eta\right]\\
&=\frac{\alpha\mathfrak{a}_1\mathfrak{a}_2}{2(\mathfrak{a}_2-\mathfrak{a}_1)}\left[I^{\alpha}_{1/\mathfrak{a}_1}(\Omega\circ\mathfrak{g})\left(\frac{1}{\mathfrak{a}_2}\right)+I^{\alpha}_{1/\mathfrak{a}_2}(\Omega\circ\mathfrak{g})\left(\frac{1}{\mathfrak{a}_1}\right)\right].
\end{aligned} \tag{25}$$

Then,

$$-\Omega\left(\frac{2\mathfrak{a}_1\mathfrak{a}_2}{\mathfrak{a}_1+\mathfrak{a}_2}\right) \geq -\frac{1-\alpha}{2[1-\exp(-\rho)]} \cdot \left[I^{\alpha}_{1/\mathfrak{a}_1}(\Omega\circ\mathfrak{g})\left(\frac{1}{\mathfrak{a}_2}\right)+I^{\alpha}_{1/\mathfrak{a}_2}(\Omega\circ\mathfrak{g})\left(\frac{1}{\mathfrak{a}_1}\right)\right]. \tag{26}$$

Adding $\Omega(\mathfrak{a}_1)+\Omega(\mathfrak{a}_2)$ to both sides of (26), we find the second inequality of (18).

Now, we prove inequality (19). Since Ω is a harmonically convex function, then, we have that for any $\mathfrak{a}_1, \mathfrak{a}_2 \in [\theta_1, \theta_2]$,

$$\begin{aligned}\Omega\left(\frac{2\mathfrak{a}_1\mathfrak{a}_2}{\mathfrak{a}_1+\mathfrak{a}_2}\right) &= \Omega\left(\frac{1}{1/2\left(\left(\eta/\mathfrak{a}_1\right)+\left(1-\eta/\mathfrak{a}_2\right)+\left(1-\eta/\mathfrak{a}_1\right)+\left(\eta/\mathfrak{a}_2\right)\right)}\right)\\ &\leq \frac{1}{2}\left[\Omega\left(\frac{1}{\left(\eta/\mathfrak{a}_1\right)+\left(1-\eta/\mathfrak{a}_2\right)}\right)+\Omega\left(\frac{1}{\left(1-\eta/\mathfrak{a}_1\right)+\left(\eta/\mathfrak{a}_2\right)}\right)\right]\\ &\leq \frac{\Omega(\mathfrak{a}_1)+\Omega(\mathfrak{a}_2)}{2}.\end{aligned} \tag{27}$$

Replacing $\mathfrak{a}_1$ and $\mathfrak{a}_2$ by $1/(1/\theta_1)+(1/\theta_2)-(1/\mathfrak{a}_1)$ and $1/(1/\theta_1)+(1/\theta_2)-(1/\mathfrak{a}_2)$, respectively, in (27), we get

$$\begin{aligned}\Omega\left(\frac{1}{(1/\theta_1)+(1/\theta_2)-\left(\mathfrak{a}_1+\mathfrak{a}_2/2\mathfrak{a}_1\mathfrak{a}_2\right)}\right) &\leq \frac{1}{2}\left[\Omega\left(\frac{1}{(1/\theta_1)+(1/\theta_2)-\left(\eta/\mathfrak{a}_1+1-\eta/\mathfrak{a}_2\right)}\right)+\Omega\left(\frac{1}{(1/\theta_1)+(1/\theta_2)-\left(1-\eta/\mathfrak{a}_1+\eta/\mathfrak{a}_2\right)}\right)\right]\\ &\leq \frac{1}{2}\left[\Omega\left(\frac{1}{(1/\theta_1)+(1/\theta_2)-(1/\mathfrak{a}_1)}\right)+\Omega\left(\frac{1}{(1/\theta_1)+(1/\theta_2)-(1/\mathfrak{a}_2)}\right)\right].\end{aligned} \tag{28}$$

Multiplying by $\exp(-\rho\eta)$ on both sides of (28) and then integrating with respect to η over $[0,1]$, we obtain

$$\begin{aligned}&\frac{[1-\exp(-\rho)]}{\rho}\Omega\left(\frac{1}{(1/\theta_1)+(1/\theta_2)-\left(\mathfrak{a}_1+\mathfrak{a}_2/2\mathfrak{a}_1\mathfrak{a}_2\right)}\right)\\ &\leq \frac{1}{2}\left[\int_0^1 \exp(-\rho\eta)\Omega\left(\frac{1}{(1/\theta_1)+(1/\theta_2)-\left(\eta/\mathfrak{a}_1+1-\eta/\mathfrak{a}_2\right)}\right)d\eta\right.\\ &\quad\left.+\int_0^1 \exp(-\rho\eta)\Omega\left(\frac{1}{(1/\theta_1)+(1/\theta_2)-\left(1-\eta/\mathfrak{a}_1+\eta/\mathfrak{a}_2\right)}\right)d\eta\right]\\ &\leq \frac{[1-\exp(-\rho)]}{2\rho}\left[\Omega\left(\frac{1}{(1/\theta_1)+(1/\theta_2)-(1/\mathfrak{a}_1)}\right)+\Omega\left(\frac{1}{(1/\theta_1)+(1/\theta_2)-(1/\mathfrak{a}_2)}\right)\right].\end{aligned} \tag{29}$$

It is obvious that

$$\begin{aligned}
&\frac{1}{2}\left[\int_0^1 \exp(-\rho\eta)\Omega\left(\frac{1}{1/\theta_1+1/\theta_2-((\eta/\mathfrak{a}_1)+(1-\eta/\mathfrak{a}_2))}\right)\mathrm{d}\eta+\int_0^1 \exp(-\rho\eta)\Omega\left(\frac{1}{1/\theta_1+1/\theta_2-(1-\eta/\mathfrak{a}_1+\eta/\mathfrak{a}_2)}\right)\mathrm{d}\eta\right]\\
&=\frac{\mathfrak{a}_1\mathfrak{a}_2}{2(\mathfrak{a}_2-\mathfrak{a}_1)}\left[\int_{(1/\theta_1)+(1/\theta_2)-(1/\mathfrak{a}_1)}^{(1/\theta_1)+(1/\theta_2)-(1/\mathfrak{a}_2)}\exp\left(-\frac{1-\alpha}{\alpha}\left(\left(\frac{1}{\theta_1}+\frac{1}{\theta_2}-\frac{1}{\mathfrak{a}_2}\right)-u\right)\right)\Omega\left(\frac{1}{u}\right)\mathrm{d}u\right.\\
&\quad\left.+\int_{(1/\theta_1)+(1/\theta_2)-(1/\mathfrak{a}_1)}^{(1/\theta_1)+(1/\theta_2)-(1/\mathfrak{a}_2)}\exp\left(-\frac{1-\alpha}{\alpha}\left(u-\left(\frac{1}{\theta_1}+\frac{1}{\theta_2}-\frac{1}{\mathfrak{a}_1}\right)\right)\right)\Omega\left(\frac{1}{u}\right)\mathrm{d}u\right]\\
&=\frac{\alpha\mathfrak{a}_1\mathfrak{a}_2}{2(\mathfrak{a}_2-\mathfrak{a}_1)}\left[I^{\alpha}_{((1/\theta_1)+(1/\theta_2)-(1/\mathfrak{a}_1))}(\Omega\circ\mathfrak{g})\left(\frac{1}{\theta_1}+\frac{1}{\theta_2}-\frac{1}{\mathfrak{a}_2}\right)+I^{\alpha}_{((1/\theta_1)+(1/\theta_2)-(1/\mathfrak{a}_2))}(\Omega\circ\mathfrak{g})\left(\frac{1}{\theta_1}+\frac{1}{\theta_2}-\frac{1}{\mathfrak{a}_1}\right)\right].
\end{aligned}\tag{30}$$

Using the Jensen–Mercer inequality for harmonically convex function, we conclude that

$$\begin{aligned}
&\Omega\left(\frac{1}{(1/\theta_1)+(1/\theta_2)-(\mathfrak{a}_1+\mathfrak{a}_2/2\mathfrak{a}_1\mathfrak{a}_2)}\right)\\
&\le\frac{1-\alpha}{2[1-\exp(-\rho)]}\left[I^{\alpha}_{((1/\theta_1)+(1/\theta_2)-(1/\mathfrak{a}_1))}(\Omega\circ\mathfrak{g})\left(\frac{1}{\theta_1}+\frac{1}{\theta_2}-\frac{1}{\mathfrak{a}_2}\right)+I^{\alpha}_{((1/\theta_1)+(1/\theta_2)-(1/\mathfrak{a}_2))}(\Omega\circ\mathfrak{g})\left(\frac{1}{\theta_1}+\frac{1}{\theta_2}-\frac{1}{\mathfrak{a}_1}\right)\right]\\
&\le\frac{1}{2}\left[\Omega\left(\frac{1}{1/\theta_1+1/\theta_1-1/\mathfrak{a}_1}\right)+\Omega\left(\frac{1}{1/\theta+1/\theta_1-1/\mathfrak{a}_2}\right)\right]\\
&\le\Omega(\theta_1)+\Omega(\theta_2)-\frac{\Omega(\mathfrak{a}_1)+\Omega(\mathfrak{a}_2)}{2}.
\end{aligned}\tag{31}$$

So, inequality (19) is proved. □

Remark 2. If we take $\mathfrak{a}_1=\theta_1$ and $\mathfrak{a}_2=\theta_2$ in Theorem 9, then we have Theorem 2.1 in [24].

Remark 3. For $\alpha\longrightarrow 1$, we have

$$\lim_{\alpha\longrightarrow 1}\frac{1-\alpha}{2[1-\exp(-\rho)]}=\frac{\mathfrak{a}_1\mathfrak{a}_2}{2(\mathfrak{a}_2-\mathfrak{a}_1)}.\tag{32}$$

Under the assumptions of Theorem 9 with $\alpha=1$, one has

$$\begin{aligned}
\Omega\left(\frac{1}{(1/\theta_1)+(1/\theta_2)-(\mathfrak{a}_1+\mathfrak{a}_2/2\mathfrak{a}_1\mathfrak{a}_2)}\right)&\le\Omega(\theta_1)+\Omega(\theta_2)-\int_0^1\Omega\left(\frac{\mathfrak{a}_1\mathfrak{a}_2}{\eta\mathfrak{a}_1+(1-\eta)\mathfrak{a}_2}\right)\mathrm{d}\eta\\
&\le\Omega(\theta_1)+\Omega(\theta_2)-\Omega\left(\frac{2\mathfrak{a}_1\mathfrak{a}_2}{\mathfrak{a}_1+\mathfrak{a}_2}\right),
\end{aligned}\tag{33}$$

$$\begin{aligned}
\Omega\left(\frac{1}{(1/\theta_1)+(1/\theta_2)-(\mathfrak{a}_1+\mathfrak{a}_2/2\mathfrak{a}_1\mathfrak{a}_2)}\right)&\le\frac{\mathfrak{a}_1\mathfrak{a}_2}{\mathfrak{a}_2-\mathfrak{a}_1}\int_{\mathfrak{a}_1}^{\mathfrak{a}_2}\frac{1}{\eta^2}\Omega\left(\frac{1}{(1/\theta_1)+(1/\theta_2)-(1/\eta)}\right)\mathrm{d}\eta\\
&\le\Omega(\theta_1)+\Omega(\theta_2)-\frac{\Omega(\mathfrak{a}_1)+\Omega(\mathfrak{a}_2)}{2},
\end{aligned}\tag{34}$$

for all $\mathfrak{a}_1,\ \mathfrak{a}_2\in[\theta_1,\theta_2]$. Inequalities (33) and (34) were proved by Baloch et al. in [28, Theorem 3.5] and [29, Theorem 2.1].

Remark 4. If $\alpha\longrightarrow 1$, $\mathfrak{a}_1=\theta_1$, and $\mathfrak{a}_2=\theta_2$ in Theorem 9, then we have Hermite–Hadamard inequality (6) for harmonically convex function which was proved by Işcan in [11].

Lemma 3. *Let $\Omega\colon [\theta_1,\theta_2]\subseteq(0,\infty)\longrightarrow\mathbb{R}$ be a differentiable function on (θ_1,θ_2) with $\theta_1<\theta_2$. If $\Omega'\in L[\theta_1,\theta_2]$, then*

$$\begin{aligned}
&\frac{1}{2}\left[\Omega\left(\frac{1}{(1/\theta_1)+(1/\theta_2)-(1/\mathfrak{a}_1)}\right)+\Omega\left(\frac{1}{(1/\theta_1)+(1/\theta_2)-(1/\mathfrak{a}_2)}\right)\right]-\frac{1-\alpha}{2[1-\exp(-\rho)]}\\
&\quad\cdot\left[I^{\alpha}\left(\frac{1}{\theta_1}+\frac{1}{\theta_2}-\frac{1}{\mathfrak{a}_2}\right)(\Omega^{\circ}\mathfrak{g})\left(\frac{1}{\theta_1}+\frac{1}{\theta_2}-\frac{1}{\mathfrak{a}_2}\right)+I^{\alpha}\left(\frac{1}{\theta_1}+\frac{1}{\theta_2}-\frac{1}{\mathfrak{a}_2}\right)(\Omega^{\circ}\mathfrak{g})\left(\frac{1}{\theta_1}+\frac{1}{\theta_2}-\frac{1}{\mathfrak{a}_1}\right)\right]\\
&=\frac{\mathfrak{a}_2-\mathfrak{a}_1}{2\mathfrak{a}_1\mathfrak{a}_2[1-\exp(-\rho)]}\left[\int_0^1\frac{\exp(-\rho(1-\eta))}{(1/\theta_1)+(1/\theta_2)-((\eta/\mathfrak{a}_1)+(1-\eta/\mathfrak{a}_2))^2}\Omega'\left(\frac{1}{(1/\theta_1)+(1/\theta_2)-((\eta/\mathfrak{a}_1)+(1-\eta/\mathfrak{a}_2))}\right)d\eta\right.\\
&\quad\left.-\int_0^1\frac{\exp(-\rho\eta)}{((1/\theta_1)+(1/\theta_2)-((\eta/\mathfrak{a}_1)+(1-\eta/\mathfrak{a}_2)))^2}\Omega'\left(\frac{1}{(1/\theta_1)+(1/\theta_2)-((\eta/\mathfrak{a}_1)+(1-\eta/\mathfrak{a}_2))}\right)d\eta\right],
\end{aligned}\tag{35}$$

for all $\mathfrak{a}_1,\mathfrak{a}_2\in[\theta_1,\theta_2]$, $\alpha>0$, and $\mathfrak{g}(\mathfrak{u})=1/\mathfrak{u}$, $u\in[1/\theta_2,1/\theta_1]$.

Proof. Let $A_\eta=1/\theta_1+1/\theta_2-(\eta/\mathfrak{a}_1+1-\eta/\mathfrak{a}_2)$. It suffices to note that

$$\begin{aligned}
&\frac{1}{2}\left[\Omega\left(\frac{1}{(1/\theta_1)+(1/\theta_2)-(1/\mathfrak{a}_1)}\right)+\Omega\left(\frac{1}{(1/\theta_1)+(1/\theta_2)-(1/\mathfrak{a}_2)}\right)\right]-\frac{1-\alpha}{2[1-\exp(-\rho)]}\\
&\quad\cdot\left[I^{\alpha}_{(1/\theta_1+1/\theta_1-1/\mathfrak{a}_1)}(\Omega\circ\mathfrak{g})\left(\frac{1}{\theta_1}+\frac{1}{\theta_2}-\frac{1}{\mathfrak{a}_2}\right)+I^{\alpha}_{(1/\theta_1+1/\theta_1-1/\mathfrak{a}_2)}(\Omega\circ\mathfrak{g})\left(\frac{1}{\theta_1}+\frac{1}{\theta_2}-\frac{1}{\mathfrak{a}_1}\right)\right]\\
&=\frac{\mathfrak{a}_2-\mathfrak{a}_1}{2\mathfrak{a}_1\mathfrak{a}_2[1-\exp(-\rho)]}\left[\int_0^1\frac{\exp(-\rho(1-\eta))}{A_\eta^2}\Omega'\left(\frac{1}{(1/\theta_1)+(1/\theta_2)-((\eta/\mathfrak{a}_1)+(1-\eta/\mathfrak{a}_2))}\right)d\eta\right.\\
&\quad\left.-\int_0^1\frac{\exp(-\rho\eta)}{A_\eta^2}\Omega'\left(\frac{1}{(1/\theta_1)+(1/\theta_2)-((\eta/\mathfrak{a}_1)+(1-\eta/\mathfrak{a}_2))}\right)d\eta\right]=I_1-I_2.
\end{aligned}\tag{36}$$

By integrating by part, we have

$$\begin{aligned}
I_1&=\frac{1}{2[1-\exp(-\rho)]}\left[\exp(-\rho(1-\eta))\Omega\left(\frac{1}{A_\eta}\right)\Big|_0^1-\rho\int_0^1\exp(-\rho\eta)\Omega\left(\frac{1}{A_\eta}\right)d\eta\right]\\
&=\frac{1}{2[1-\exp(-\rho)]}\left[\Omega\left(\frac{1}{(1/\theta_1)+(1/\theta_2)-(1/\mathfrak{a}_1)}\right)-\exp(-\rho)\Omega\left(\frac{1}{(1/\theta_1)+(1/\theta_2)-(1/\mathfrak{a}_2)}\right)\right.\\
&\quad\left.-\rho\left(\frac{\mathfrak{a}_1\mathfrak{a}_2}{\mathfrak{a}_2-\mathfrak{a}_1}\right)\int_{1/\theta_1+1/\theta_2-1/\mathfrak{a}_1}^{1/\theta_1+1/\theta_2-1/\mathfrak{a}_2}\exp\left(-\frac{1-\alpha}{\alpha}\left(u-\left(\frac{1}{\theta_1}+\frac{1}{\theta_2}-\frac{1}{\mathfrak{a}_1}\right)\right)\right)\Omega\left(\frac{1}{u}\right)du\right]\\
&=\frac{1}{2[1-\exp(-\rho)]}\left[\Omega\left(\frac{1}{(1/\theta_1)+(1/\theta_2)-(1/\mathfrak{a}_1)}\right)-\exp(-\rho)\Omega\left(\frac{1}{(1/\theta_1)+(1/\theta_2)-(1/\mathfrak{a}_2)}\right)\right.\\
&\quad\left.-\rho\left(\frac{\alpha\mathfrak{a}_1\mathfrak{a}_2}{\mathfrak{a}_2-\mathfrak{a}_1}\right)I^{\alpha}_{(1/\theta_1+1/\theta_2-1/\mathfrak{a}_2)}(\Omega\circ\mathfrak{g})\left(\frac{1}{\theta_1}+\frac{1}{\theta_2}-\frac{1}{\mathfrak{a}_1}\right)\right],
\end{aligned}\tag{37}$$

and similarly we get

$$
\begin{aligned}
I_2 &= \frac{1}{2[1-\exp(-\rho)]}\left[\exp(-\rho\eta)\Omega\left(\frac{1}{A_\eta}\right)\Big|_0^1 - (-\rho)\int_0^1 \exp(-\rho\eta)\Omega\left(\frac{1}{A_\eta}\right)\mathrm{d}\eta\right] \\
&= \frac{1}{2[1-\exp(-\rho)]}\left[\exp(-\rho)\Omega\left(\frac{1}{(1/\theta_1)+(1/\theta_1)-(1/\mathfrak{a}_1)}\right) - \Omega\left(\frac{1}{(1/\theta_1)+(1/\theta_2)-(1/\mathfrak{a}_2)}\right)\right. \\
&\quad \left. + \rho\left(\frac{\mathfrak{a}_1\mathfrak{a}_2}{\mathfrak{a}_2-\mathfrak{a}_1}\right)\int_{(1/\theta_1)+(1/\theta_1)-(1/\mathfrak{a}_1)}^{(1/\theta_1)+(1/\theta_1)-(1/\mathfrak{a}_2)} \exp\left(-\frac{1-\alpha}{\alpha}\left(\left(\frac{1}{\theta_1}+\frac{1}{\theta_2}-\frac{1}{\mathfrak{a}_2}\right)-u\right)\right)\Omega\left(\frac{1}{u}\right)\mathrm{d}u\right] \\
&= \frac{1}{2[1-\exp(-\rho)]}\left[\exp(-\rho)\Omega\left(\frac{1}{(1/\theta_1)+(1/\theta_2)-(1/\mathfrak{a}_1)}\right) - \Omega\left(\frac{1}{(1/\theta_1)+(1/\theta_2)-(1/\mathfrak{a}_2)}\right)\right. \\
&\quad \left. + \rho\left(\frac{\alpha\mathfrak{a}_1\mathfrak{a}_2}{\mathfrak{a}_2-\mathfrak{a}_1}\right) I^{\alpha}_{(1/\theta_1)+(1/\theta_1)-(1/\mathfrak{a}_1)}(\Omega\circ\mathfrak{g})\left(\frac{1}{\theta_1}+\frac{1}{\theta_2}-\frac{1}{\mathfrak{a}_2}\right)\right].
\end{aligned}
\tag{38}
$$

Using (37) and (40) in (36), we get equality (35). □

Remark 5. From Lemma 2 with $\alpha \longrightarrow 1$, $\mathfrak{a}_1 = \theta_1$, and $\mathfrak{a}_2 = \theta_2$, we indeed have Lemma 1 which was proved by Íşcan in [11].

Theorem 10. *If $\Omega: I = [\theta_1, \theta_2] \subseteq (0,\infty) \longrightarrow \mathbb{R}$ is a differentiable function on (θ_1, θ_2) with $\theta_1 < \theta_2$ and $\Omega' \in L[\theta_1, \theta_2]$. If $|\Omega'|$ is a harmonically convex on $[\theta_1, \theta_2]$, then*

$$
\begin{aligned}
&\left|\frac{1}{2}\left[\Omega\left(\frac{1}{(1/\theta_1)+(1/\theta_2)-(1/\mathfrak{a}_1)}\right)+\Omega\left(\frac{1}{(1/\theta_1)+(1/\theta_2)-(1/\mathfrak{a}_2)}\right)\right] - \frac{1-\alpha}{2[1-\exp(-\rho)]}\left[I^{\alpha}_{(1/\theta_1+1/\theta_2-1/\mathfrak{a}_1)}(\Omega\circ\mathfrak{g})\left(\frac{1}{\theta_1}+\frac{1}{\theta_2}-\frac{1}{\mathfrak{a}_2}\right)\right.\right. \\
&\quad \left.\left. + I^{\alpha}_{(1/\theta_1+1/\theta_2-1/\mathfrak{a}_2)}(\Omega\circ\mathfrak{g})\left(\frac{1}{\theta_1}+\frac{1}{\theta_2}-\frac{1}{\mathfrak{a}_1}\right)\right]\right| \\
&\le \frac{\mathfrak{a}_2-\mathfrak{a}_1}{2\mathfrak{a}_1\mathfrak{a}_2[1-\exp(-\rho)]}\int_0^{1/2}[\exp(-\rho\eta)-\exp(-\rho(1-\eta))]\left[\left(\frac{\eta}{\mu_1^2}+\frac{1-\eta}{\mu_2^2}\right)\left|\Omega'\left(\frac{1}{(1/\theta_1)+(1/\theta_2)-(1/\mathfrak{a}_1)}\right)\right|\right. \\
&\quad \left.+\left(\frac{1-\eta}{\mu_1^2}+\frac{\eta}{\mu_2^2}\right)\left|\Omega'\left(\frac{1}{(1/\theta_1)+(1/\theta_2)-(1/\mathfrak{a}_2)}\right)\right|\right]d\eta\,,
\end{aligned}
\tag{39}
$$

where

$$
\mu_1 = \frac{1}{\theta_1}+\frac{1}{\theta_2}-\left(\frac{\eta}{\mathfrak{a}_1}+\frac{1-\eta}{\mathfrak{a}_2}\right), \tag{40}
$$

$$
\mu_2 = \frac{1}{\theta_1}+\frac{1}{\theta_2}-\left(\frac{1-\eta}{\mathfrak{a}_1}+\frac{\eta}{\mathfrak{a}_2}\right), \tag{41}
$$

for all $\mathfrak{a}_1, \mathfrak{a}_2 \in [\theta_1, \theta_2]$, $\alpha > 0$, and $\mathfrak{g}(\mathfrak{u}) = 1/\mathfrak{u}$, $u \in [1/\theta_2, 1/\theta_1]$.

Proof. Since $|\Omega'|$ is a harmonically convex on $[\theta_1, \theta_2]$, using Lemma 2, we can obtain

$$\left|\frac{1}{2}\left[\Omega\left(\frac{1}{(1/\theta_1)+(1/\theta_2)-(1/\mathfrak{a}_1)}\right)+\Omega\left(\frac{1}{(1/\theta_1)+(1/\theta_2)-(1/\mathfrak{a}_2)}\right)\right]-\frac{1-\alpha}{2[1-\exp(-\rho)]}\left[I^{\alpha}_{(1/\theta_1+1/\theta_2-1/\mathfrak{a}_1)}(\Omega\circ\mathfrak{g})\left(\frac{1}{\theta_1}+\frac{1}{\theta_2}-\frac{1}{\mathfrak{a}_2}\right)\right.\right.$$

$$\left.\left.+I^{\alpha}_{(1/\theta_1+1/\theta_2-1/\mathfrak{a}_2)}(\Omega\circ\mathfrak{g})\left(\frac{1}{\theta_1}+\frac{1}{\theta_2}-\frac{1}{\mathfrak{a}_1}\right)\right]\right|$$

$$\leq\frac{\mathfrak{a}_2-\mathfrak{a}_1}{2\mathfrak{a}_1\mathfrak{a}_2[1-\exp(-\rho)]}\int_0^1\frac{|\exp(-\rho\eta)-\exp(-\rho(1-\eta))|}{\left((1/\theta_1)+(1/\theta_2)-\left((\eta/\mathfrak{a}_1)+(1-\eta/\mathfrak{a}_2)\right)\right)^2}\left|\Omega'\left(\frac{1}{(1/\theta_1)+(1/\theta_2)-\left((\eta/\mathfrak{a}_1)+(1-\eta/\mathfrak{a}_2)\right)}\right)\right|\mathrm{d}\eta$$

$$\leq\frac{\mathfrak{a}_2-\mathfrak{a}_1}{2\mathfrak{a}_1\mathfrak{a}_2[1-\exp(-\rho)]}\left[\int_0^{1/2}\frac{[\exp(-\rho\eta)-\exp(-\rho(1-\eta))]}{\left((1/\theta_1)+(1/\theta_2)-\left((\eta/\mathfrak{a}_1)+(1-\eta/\mathfrak{a}_2)\right)\right)^2}\left(\eta\left|\Omega'\left(\frac{1}{(1/\theta_1)+(1/\theta_2)-(1/\mathfrak{a}_1)}\right)\right|\right.\right.$$

$$\left.+(1-\eta)\left|\Omega'\left(\frac{1}{(1/\theta_1)+(1/\theta_2)-(1/\mathfrak{a}_2)}\right)\right|\right)\mathrm{d}\eta+\int_{1/2}^1\frac{[\exp(-\rho(1-\eta))-\exp(-\rho\eta)]}{\left((1/\theta_1)+(1/\theta_2)-\left((\eta/\mathfrak{a}_1)+(1-\eta/\mathfrak{a}_2)\right)\right)^2}$$

$$\cdot\left(\eta\left|\Omega'\left(\frac{1}{(1/\theta_1)+(1/\theta_2)-(1/\mathfrak{a}_1)}\right)\right|\right.$$

$$\left.\left.+(1-\eta)\left|\Omega'\left(\frac{1}{(1/\theta_1)+(1/\theta_2)-(1/\mathfrak{a}_2)}\right)\right|\right)\mathrm{d}\eta\right]\leq\frac{\mathfrak{a}_2-\mathfrak{a}_1}{2\mathfrak{a}_1\mathfrak{a}_2[1-\exp(-\rho)]}$$

$$\cdot\left[\int_0^{1/2}\frac{[\exp(-\rho\eta)-\exp(-\rho(1-\eta))]}{\left((1/\theta_1)+(1/\theta_2)-\left((\eta/\mathfrak{a}_1)+(1-\eta/\mathfrak{a}_2)\right)\right)^2}\left(\eta\left|\Omega'\left(\frac{1}{(1/\theta_1)+(1/\theta_2)-(1/\mathfrak{a}_1)}\right)\right|\right.\right.$$

$$\left.+(1-\eta)\left|\Omega'\left(\frac{1}{(1/\theta_1)+(1/\theta_2)-(1/\mathfrak{a}_2)}\right)\right|\right)\mathrm{d}\eta+\int_0^{1/2}\frac{[\exp(-\rho\eta)-\exp(-\rho(1-\eta))]}{\left((1/\theta_1)+(1/\theta_2)-\left((1-\eta/\mathfrak{a}_1)+(\eta/\mathfrak{a}_2)\right)\right)^2}$$

$$\cdot\left((1-\eta)\left|\Omega'\left(\frac{1}{(1/\theta_1)+(1/\theta_2)-(1/\mathfrak{a}_1)}\right)\right|\right.$$

$$\left.\left.+\eta\left|\Omega'\left(\frac{1}{(1/\theta_1)+(1/\theta_2)-(1/\mathfrak{a}_2)}\right)\right|\right)\mathrm{d}\eta\right]$$

$$=\frac{\mathfrak{a}_2-\mathfrak{a}_1}{2\mathfrak{a}_1\mathfrak{a}_2[1-\exp(-\rho)]}\int_0^{1/2}[\exp(-\rho\eta)-\exp(-\rho(1-\eta))]$$

$$\cdot\left[\left(\frac{\eta}{\mu_1^2}+\frac{1-\eta}{\mu_2^2}\right)\left|\Omega'\left(\frac{1}{(1/\theta_1)+(1/\theta_2)-(1/\mathfrak{a}_1)}\right)\right|+\left(\frac{1-\eta}{\mu_1^2}+\frac{\eta}{\mu_2^2}\right)\left|\Omega'\left(\frac{1}{(1/\theta_1)+(1/\theta_2)-(1/\mathfrak{a}_2)}\right)\right|\right]\mathrm{d}\eta\Bigg|. \tag{42}$$

This completes the proof. □

Remark 6. For $\alpha\longrightarrow 1$, we have

$$\lim_{\alpha\longrightarrow 1}\frac{1-\alpha}{2[1-\exp(-\rho)]}=\frac{\mathfrak{a}_1\mathfrak{a}_2}{2(\mathfrak{a}_2-\mathfrak{a}_1)},$$
$$\lim_{\alpha\longrightarrow 1}\frac{\exp(-\rho\eta)-\exp(-\rho(1-\eta))}{2[1-\exp(-\rho)]}=\frac{1-2\eta}{2}. \tag{43}$$

If $\alpha\longrightarrow 1$, $\mathfrak{a}_1=\theta_1$, and $\mathfrak{a}_2=\theta_2$ in Theorem 10, then we get Theorem 2.6 which was proved by İşcan in [11].

3. Fejér–Hadamard–Mercer-Type Inequality for Harmonically Convex Function

Theorem 11. *If $\Omega: I\subseteq(0,\infty)\longrightarrow\mathbb{R}$ is a harmonically convex function for $\theta_1,\theta_2\in I$ with $\theta_1<\theta_2$. such that If $\Omega\in L[\theta_1,\theta_2]$ and ω: $[\theta_1,\theta_2]\subseteq(0,\infty)\longrightarrow\mathbb{R}$ is nonnegative,*

integrable, and harmonically symmetric with respect to $2\theta_1\theta_2/\theta_1+\theta_2$, *that is,* $\omega(\varkappa)=\omega(1/(1/\theta_1)+(1/\theta_2)-(1/\varkappa))$, *then*

$$\begin{aligned}
&\Omega\left(\frac{1}{(1/\theta_1)+(1/\theta_2)-(\mathfrak{a}_1+\mathfrak{a}_2/2\mathfrak{a}_1\mathfrak{a}_2)}\right)\left[I^{\alpha}_{(1/\theta_1+1/\theta_2-1/\mathfrak{a}_1)}(\omega\circ\mathfrak{g})\left(\frac{1}{\theta_1}+\frac{1}{\theta_2}-\frac{1}{\mathfrak{a}_2}\right)+I^{\alpha}_{(1/\theta_1+1/\theta_2-1/\mathfrak{a}_2)}(\omega\circ\mathfrak{g})\left(\frac{1}{\theta_1}+\frac{1}{\theta_2}-\frac{1}{\mathfrak{a}_1}\right)\right]\\
&\quad\le\left[I^{\alpha}_{(1/\theta_1+1/\theta_2-1/\mathfrak{a}_1)}(\omega\circ\mathfrak{g})\left(\frac{1}{\theta_1}+\frac{1}{\theta_2}-\frac{1}{\mathfrak{a}_2}\right)+I^{\alpha}_{(1/\theta_1+1/\theta_2-1/\mathfrak{a}_2)}(\Omega\omega\circ\mathfrak{g})\left(\frac{1}{\theta_1}+\frac{1}{\theta_2}-\frac{1}{\mathfrak{a}_1}\right)\right]\\
&\quad\le\frac{1}{2}\left[\Omega\left(\frac{1}{(1/\theta_1)+(1/\theta_2)-(1/\mathfrak{a}_1)}\right)+\Omega\left(\frac{1}{(1/\theta_1)+(1/\theta_2)-(1/\mathfrak{a}_2)}\right)\right]\left[I^{\alpha}_{(1/\theta_1+1/\theta_2-1/\mathfrak{a}_1)}(\omega\circ\mathfrak{g})\left(\frac{1}{\theta_1}+\frac{1}{\theta_2}-\frac{1}{\mathfrak{a}_2}\right)\right.\\
&\qquad\left.+I^{\alpha}_{(1/\theta_1+1/\theta_2-1/\mathfrak{a}_2)}(\omega\circ\mathfrak{g})\left(\frac{1}{\theta_1}+\frac{1}{\theta_2}-\frac{1}{\mathfrak{a}_1}\right)\right],
\end{aligned}\tag{44}$$

for all $\mathfrak{a}_1,\mathfrak{a}_2\in[\theta_1,\theta_2]$, $\alpha>0$, *and* $\mathfrak{g}(\mathfrak{u})=1/\mathfrak{u}$, $u\in[1/\theta_2,1/\theta_1]$.

Proof. If Ω is a harmonically convex function on $[\theta_1,\theta_2]$, then for all $\mathfrak{a}_1,\mathfrak{a}_2\in[\theta_1,\theta_2]$,

$$\begin{aligned}
\Omega\left(\frac{2\mathfrak{a}_1\mathfrak{a}_2}{\mathfrak{a}_1+\mathfrak{a}_2}\right)&=\Omega\left(\frac{1}{1/2\left((\eta/\mathfrak{a}_1)+(1-\eta/\mathfrak{a}_2)+(1-\eta/\mathfrak{a}_1)+\eta/\mathfrak{a}_2\right)}\right)\\
&\le\frac{1}{2}\left[\Omega\left(\frac{1}{(\eta/\mathfrak{a}_1)+(1-\eta/\mathfrak{a}_2)}\right)+\Omega\left(\frac{1}{(1-\eta/\mathfrak{a}_1)+(\eta/\mathfrak{a}_2)}\right)\right]\le\frac{\Omega(\mathfrak{a}_1)+\Omega(\mathfrak{a}_2)}{2}.
\end{aligned}\tag{45}$$

Replacing $\mathfrak{a}_1$ and $\mathfrak{a}_2$ by $1/(1/\theta_1)+(1/\theta_2)-(1/\mathfrak{a}_1)$ and $1/(1/\theta_1)+(1/\theta_2)-(1/\mathfrak{a}_2)$, respectively, we get

$$\begin{aligned}
\Omega\left(\frac{1}{(1/\theta_1)+(1/\theta_2)-(\mathfrak{a}_1+\mathfrak{a}_2/2\mathfrak{a}_1\mathfrak{a}_2)}\right)&\le\frac{1}{2}\left[\Omega\left(\frac{1}{(1/\theta_1)+(1/\theta_2)-((\eta/\mathfrak{a}_1)+(1-\eta/\mathfrak{a}_2))}\right)\right.\\
&\left.+\Omega\left(\frac{1}{(1/\theta_1)+(1/\theta_2)-((1-\eta/\mathfrak{a}_1)+(\eta/\mathfrak{a}_2))}\right)\right]\\
&\le\left[\Omega\left(\frac{1}{(1/\theta_1)+(1/\theta_2)-(1/\mathfrak{a}_1)}\right)+\Omega\left(\frac{1}{(1/\theta_1)+(1/\theta_2)-(1/\mathfrak{a}_2)}\right)\right].
\end{aligned}\tag{46}$$

Multiplying by

$$\exp(-\rho\eta)\omega\left(\frac{1}{(1/\theta_1)+(1/\theta_2)-((1-\eta/\mathfrak{a}_1)+(\eta/\mathfrak{a}_2))}\right),\tag{47}$$

on both sides of (46) and then integrating with respect to η over $[0,1]$, we obtain

$$
\begin{aligned}
&2\Omega\left(\frac{1}{(1/\theta_1)+(1/\theta_2)-(\mathfrak{a}_1+\mathfrak{a}_2/2\mathfrak{a}_1\mathfrak{a}_2)}\right)\int_0^1 \exp(-\rho\eta)\omega\left(\frac{1}{(1/\theta_1)+(1/\theta_2)-((1-\eta/\mathfrak{a}_1)+(\eta/\mathfrak{a}_2))}\right)\mathrm{d}\eta\\
&\quad\le \int_0^1 \exp(-\rho\eta)\Omega\left(\frac{1}{(1/\theta_1)+(1/\theta_2)-((\eta/\mathfrak{a}_1)+(1-\eta/\mathfrak{a}_2))}\right)\omega\left(\frac{1}{(1/\theta_1)+(1/\theta_2)-((1-\eta/\mathfrak{a}_1)+(\eta/\mathfrak{a}_2))}\right)\mathrm{d}\eta\\
&\quad+\int_0^1 \exp(-\rho\eta)\Omega\left(\frac{1}{(1/\theta_1)+(1/\theta_2)-((1-\eta/\mathfrak{a}_1)+(\eta/\mathfrak{a}_2))}\right)\omega\left(\frac{1}{(1/\theta_1)+(1/\theta_2)-((1-\eta/\mathfrak{a}_1)+(\eta/\mathfrak{a}_2))}\right)\mathrm{d}\eta\\
&\quad\le\left[\Omega\left(\frac{1}{(1/\theta_1)+(1/\theta_2)-(1/\mathfrak{a}_1)}\right)+\Omega\left(\frac{1}{(1/\theta_1)+(1/\theta_2)-(1/\mathfrak{a}_2)}\right)\right]\int_0^1 \exp(-\rho\eta)\omega\left(\frac{1}{(1/\theta_1)+(1/\theta_2)-((1-\eta/\mathfrak{a}_1)+(\eta/\mathfrak{a}_2))}\right)\mathrm{d}\eta,
\end{aligned}
\tag{48}
$$

where

$$
\begin{aligned}
&\int_0^1 \exp(-\rho\eta)\Omega\left(\frac{1}{(1/\theta_1)+(1/\theta_2)-((\eta/\mathfrak{a}_1)+(1-\eta/\mathfrak{a}_2))}\right)\omega\left(\frac{1}{(1/\theta_1)+(1/\theta_2)-((1-\eta/\mathfrak{a}_1)+(\eta/\mathfrak{a}_2))}\right)\mathrm{d}\eta\\
&\quad+\int_0^1 \exp(-\rho\eta)\Omega\left(\frac{1}{(1/\theta_1)+(1/\theta_2)-((1-\eta/\mathfrak{a}_1)+(\eta/\mathfrak{a}_2))}\right)\omega\left(\frac{1}{(1/\theta_1)+(1/\theta_2)-((1-\eta/\mathfrak{a}_1)+(\eta/\mathfrak{a}_2))}\right)\mathrm{d}\eta\\
&=\frac{\mathfrak{a}_1\mathfrak{a}_2}{\mathfrak{a}_2-\mathfrak{a}_1}\left[\int_{1/\theta_1+1/\theta_2-1/\mathfrak{a}_1}^{1/\theta_1+1/\theta_2-1/\mathfrak{a}_2}\exp\left(-\frac{1-\alpha}{\alpha}\left(u-\left(\frac{1}{\theta_1}+\frac{1}{\theta_2}-\frac{1}{\mathfrak{a}_1}\right)\right)\right)\Omega\left(\frac{1}{((1/\theta_1)+(1/\theta_2)-(1/\mathfrak{a}_1))+((1/\theta_1)+(1/\theta_2)-(1/\mathfrak{a}_2))-u}\right)\right.\\
&\quad\left.\omega\left(\frac{1}{u}\right)\mathrm{d}u+\int_{1/\theta_1+1/\theta_2-1/\mathfrak{a}_1}^{1/\theta_1+1/\theta_2-1/\mathfrak{a}_2}\exp\left(-\frac{1-\alpha}{\alpha}\left(u-\left(\frac{1}{\theta_1}+\frac{1}{\theta_2}-\frac{1}{\mathfrak{a}_1}\right)\right)\right)\Omega\left(\frac{1}{u}\right)\omega\left(\frac{1}{u}\right)\mathrm{d}u\right]\\
&=\frac{\mathfrak{a}_1\mathfrak{a}_2}{\mathfrak{a}_2-\mathfrak{a}_1}\left[\int_{1/\theta_1+1/\theta_2-1/\mathfrak{a}_1}^{1/\theta_1+1/\theta_2-1/\mathfrak{a}_2}\exp\left(-\frac{1-\alpha}{\alpha}\left(\left(\frac{1}{\theta_1}+\frac{1}{\theta_2}-\frac{1}{\mathfrak{a}_2}\right)-u\right)\right)\Omega\left(\frac{1}{u}\right)\omega\right.\\
&\quad\cdot\left(\frac{1}{((1/\theta_1)+(1/\theta_2)-(1/\mathfrak{a}_1))+((1/\theta_1)+(1/\theta_2)-(1/\mathfrak{a}_2))-u}\right)\mathrm{d}u\\
&\quad\left.+\int_{1/\theta_1+1/\theta_2-1/\mathfrak{a}_1}^{1/\theta_1+1/\theta_2-1/\mathfrak{a}_2}\exp\left(-\frac{1-\alpha}{\alpha}\left(u-((1/\theta_1)+(1/\theta_2)-(1/\mathfrak{a}_1))\right)\right)\Omega\left(\frac{1}{u}\right)\omega\left(\frac{1}{u}\right)\mathrm{d}u\right]\\
&=\frac{\alpha\mathfrak{a}_1\mathfrak{a}_2}{\mathfrak{a}_2-\mathfrak{a}_1}\left[I^{\alpha}_{(1/\theta_1+1/\theta_2-1/\mathfrak{a}_1)}(\Omega\omega\circ\mathfrak{g})\left(\frac{1}{\theta_1}+\frac{1}{\theta_2}-\frac{1}{\mathfrak{a}_2}\right)+I^{\alpha}_{(1/\theta_1+1/\theta_2-1/\mathfrak{a}_2)}(\Omega\omega\circ\mathfrak{g})\left(\frac{1}{\theta_1}+\frac{1}{\theta_2}-\frac{1}{\mathfrak{a}_1}\right)\right].
\end{aligned}
\tag{49}
$$

That is,

$$
\begin{aligned}
&2\Omega\left(\frac{1}{(1/\theta_1)+(1/\theta_2)-(\mathfrak{a}_1+\mathfrak{a}_2/2\mathfrak{a}_1\mathfrak{a}_2)}\right)\int_0^1 \exp(-\rho\eta)\omega\left(\frac{1}{(1/\theta_1)+(1/\theta_2)-((1-\eta/\mathfrak{a}_1)+(\eta/\mathfrak{a}_2))}\right)\mathrm{d}\eta\\
&\quad\le\frac{\alpha\mathfrak{a}_1\mathfrak{a}_2}{\mathfrak{a}_2-\mathfrak{a}_1}\left[I^{\alpha}_{(1/\theta_1+1/\theta_2-1/\mathfrak{a}_1)}(\Omega\omega\circ\mathfrak{g})\left(\frac{1}{\theta_1}+\frac{1}{\theta_2}-\frac{1}{\mathfrak{a}_2}\right)+I^{\alpha}_{(1/\theta_1+1/\theta_2-1/\mathfrak{a}_2)}(\Omega\omega\circ\mathfrak{g})\left(\frac{1}{\theta_1}+\frac{1}{\theta_2}-\frac{1}{\mathfrak{a}_1}\right)\right]\\
&\quad\le\left[\Omega\left(\frac{1}{(1/\theta_1)+(1/\theta_2)-(1/\mathfrak{a}_1)}\right)+\Omega\left(\frac{1}{(1/\theta_1)+(1/\theta_2)-(1/\mathfrak{a}_2)}\right)\right]\int_0^1 \exp(-\rho\eta)\\
&\quad\cdot\omega\left(\frac{1}{(1/\theta_1)+(1/\theta_2)-((1-\eta/\mathfrak{a}_1)+(\eta/\mathfrak{a}_2))}\right)\mathrm{d}\eta.
\end{aligned}
\tag{50}
$$

Since ω is symmetric with respect to $2\theta_1\theta_2/\theta_1+\theta_2$, we have

$$\begin{aligned} &I^{\alpha}_{(1/\theta_1+1/\theta_2-1/\mathfrak{a}_2)}(\omega\circ\mathfrak{g})\left(\frac{1}{\theta_1}+\frac{1}{\theta_2}-\frac{1}{\mathfrak{a}_1}\right)\\ &\quad= I^{\alpha}_{(1/\theta_1+1/\theta_2-1/\mathfrak{a}_1)}(\omega\circ\mathfrak{g})\left(\frac{1}{\theta_1}+\frac{1}{\theta_2}-\frac{1}{\mathfrak{a}_2}\right)\\ &\quad= \frac{1}{2}\left[I^{\alpha}_{(1/\theta_1+1/\theta_2-1/\mathfrak{a}_1)}(\omega\circ\mathfrak{g})\left(\frac{1}{\theta_1}+\frac{1}{\theta_2}-\frac{1}{\mathfrak{a}_2}\right)+I^{\alpha}_{(1/\theta_1+1/\theta_2-1/\mathfrak{a}_2)}(\omega\circ\mathfrak{g})\left(\frac{1}{\theta_1}+\frac{1}{\theta_2}-\frac{1}{\mathfrak{a}_1}\right)\right]. \end{aligned} \tag{51}$$

Therefore, we have

$$\begin{aligned} &\Omega\left(\frac{1}{(1/\theta_1)+(1/\theta_2)-(\mathfrak{a}_1+\mathfrak{a}_2/2\mathfrak{a}_1\mathfrak{a}_2)}\right)\left[I^{\alpha}_{(1/\theta_1+1/\theta_2-1/\mathfrak{a}_1)}(\omega\circ\mathfrak{g})\left(\frac{1}{\theta_1}+\frac{1}{\theta_2}-\frac{1}{\mathfrak{a}_2}\right)+I^{\alpha}_{(1/\theta_1+1/\theta_2-1/\mathfrak{a}_2)}(\omega\circ\mathfrak{g})\left(\frac{1}{\theta_1}+\frac{1}{\theta_2}-\frac{1}{\mathfrak{a}_1}\right)\right]\\ &\le\left[I^{\alpha}_{(1/\theta_1+1/\theta_2-1/\mathfrak{a}_1)}(\Omega\omega\circ\mathfrak{g})\left(\frac{1}{\theta_1}+\frac{1}{\theta_2}-\frac{1}{\mathfrak{a}_2}\right)+I^{\alpha}_{(1/\theta_1+1/\theta_2-1/\mathfrak{a}_2)}(\Omega\omega\circ\mathfrak{g})\left(\frac{1}{\theta_1}+\frac{1}{\theta_2}-\frac{1}{\mathfrak{a}_1}\right)\right]\\ &\le\frac{1}{2}\left[\Omega\left(\frac{1}{(1/\theta_1)+(1/\theta_1)-(1/\mathfrak{a}_1)}\right)+\Omega\left(\frac{1}{(1/\theta_1)+(1/\theta_1)-(1/\mathfrak{a}_2)}\right)\right]\left[I^{\alpha}_{(1/\theta_1+1/\theta_2-1/\mathfrak{a}_1)}(\omega\circ\mathfrak{g})\left(\frac{1}{\theta_1}+\frac{1}{\theta_2}-\frac{1}{\mathfrak{a}_2}\right)\right.\\ &\quad\left.+I^{\alpha}_{(1/\theta_1+1/\theta_2-1/\mathfrak{a}_2)}(\omega\circ\mathfrak{g})\left(\frac{1}{\theta_1}+\frac{1}{\theta_2}-\frac{1}{\mathfrak{a}_1}\right)\right]. \end{aligned} \tag{52}$$

Thus, the proof of Theorem 11 is complete. □

Remark 7. If we take $\mathfrak{a}_1=\theta_1$ and $\mathfrak{a}_2=\theta_2$ in Theorem 11, we will get Theorem 3.2 in [24].

Remark 8. Under the assumptions of Theorem 11 with $\alpha=1$, we have

$$\begin{aligned} &\Omega\left(\frac{1}{(1/\theta_1)+(1/\theta_2)-(\mathfrak{a}_1+\mathfrak{a}_2/2\mathfrak{a}_1\mathfrak{a}_2)}\right)\int_{(1/\theta_1+1/\theta_2-1/\mathfrak{a}_1)}^{(1/\theta_1+1/\theta_2-1/\mathfrak{a}_2)}\frac{\omega(\varkappa)}{\varkappa^2}\mathrm{d}\varkappa\\ &\le\int_{(1/\theta_1+1/\theta_2-1/\mathfrak{a}_1)}^{(1/\theta_1+1/\theta_2-1/\mathfrak{a}_2)}\frac{\Omega(\varkappa)}{\varkappa^2}\omega(\varkappa)d\varkappa\\ &\le\frac{1}{2}\left[\Omega\left(\frac{1}{(1/\theta_1)+(1/\theta_2)-(1/\mathfrak{a}_1)}\right)+\Omega\left(\frac{1}{(1/\theta_1)+(1/\theta_2)-(1/\mathfrak{a}_2)}\right)\right]\int_{(1/\theta_1+1/\theta_2-1/\mathfrak{a}_1)}^{(1/\theta_1+1/\theta_2-1/\mathfrak{a}_2)}\frac{\omega(\varkappa)}{\varkappa^2}\mathrm{d}\varkappa. \end{aligned} \tag{53}$$

Remark 9. If $\alpha = 1$, $\mathfrak{a}_1 = \theta_1$, and $\mathfrak{a}_2 = \theta_2$ in Theorem 11, then we can get Hermite–Hadamard–Fejér inequality (8) for harmonically convex function which was proved by Chen and Wu in [12].

4. Pachpatte–Mercer-Type Inequality for Harmonically Convex Function

Theorem 12. *Let Ω, ω: $[\theta_1, \theta_2] \subseteq (0, \infty) \longrightarrow \mathbb{R}$ be functions such that $\Omega, \omega, \Omega\omega \in L[\theta_1, \theta_2]$. If Ω and ω are harmonically convex on $[\theta_1, \theta_2]$, then*

$$\begin{aligned}
&\frac{\alpha\mathfrak{a}_1\mathfrak{a}_2}{2(\mathfrak{a}_2-\mathfrak{a}_1)}\left[I^{\alpha}_{((1/\theta_1+1/\theta_2-1/\mathfrak{a}_1))}(\Omega\omega\circ\mathfrak{g})\left(\frac{1}{\theta_1}+\frac{1}{\theta_2}-\frac{1}{\mathfrak{a}_2}\right)+I^{\alpha}_{(1/\theta_1+1/\theta_2-1/\mathfrak{a}_2)}(\Omega\omega\circ\mathfrak{g})\left(\frac{1}{\theta_1}+\frac{1}{\theta_2}-\frac{1}{\mathfrak{a}_1}\right)\right]\\
&\quad\le\frac{\rho^2-2\rho+4-\left(\rho^2+2\rho+4\right)\exp(-\rho)}{2\rho^3}M(\theta_1,\theta_2,\mathfrak{a}_1,\mathfrak{a}_2)+\frac{\rho-2+\exp(-\rho)(\rho+2)}{\rho^3}N(\theta_1,\theta_2,\mathfrak{a}_1,\mathfrak{a}_2),
\end{aligned}\tag{54}$$

$$\begin{aligned}
&2\Omega\left(\frac{1}{(1/\theta_1)+(1/\theta_2)-(\mathfrak{a}_1+\mathfrak{a}_2/2\mathfrak{a}_1\mathfrak{a}_2)}\right)\omega\left(\frac{1}{(1/\theta_1)+(1/\theta_2)-(\mathfrak{a}_1+\mathfrak{a}_2/2\mathfrak{a}_1\mathfrak{a}_2)}\right)\\
&\quad\le\frac{1-\alpha}{2[1-\exp(-\rho)]}\left[I^{\alpha}_{(1/\theta_1+1/\theta_2-1/\mathfrak{a}_1)}(\Omega\omega\circ\mathfrak{g})\left(\frac{1}{\theta_1}+\frac{1}{\theta_2}-\frac{1}{\mathfrak{a}_2}\right)+I^{\alpha}_{(1/\theta_1+1/\theta_2-1/\mathfrak{a}_2)}(\Omega\omega\circ\mathfrak{g})\left(\frac{1}{\theta_1}+\frac{1}{\theta_2}-\frac{1}{\mathfrak{a}_1}\right)\right]\\
&\quad+\frac{\rho-2+\exp(-\rho)(\rho+2)}{\rho^2[1-\exp(-\rho)]}M(\theta_1,\theta_2,\mathfrak{a}_1,\mathfrak{a}_2)+\frac{\rho^2-2\rho+4-\left(\rho^2+2\rho+4\right)\exp(-\rho)}{2\rho^2[1-\exp(-\rho)]}N(\theta_1,\theta_2,\mathfrak{a}_1,\mathfrak{a}_2),
\end{aligned}\tag{55}$$

where

$$\begin{aligned}
M(\theta_1,\theta_2,\mathfrak{a}_1,\mathfrak{a}_2)&=\Omega\left(\frac{1}{(1/\theta_1)+(1/\theta_2)-(1/\mathfrak{a}_1)}\right)\omega\left(\frac{1}{(1/\theta_1)+(1/\theta_2)-(1/\mathfrak{a}_1)}\right)\\
&\quad+\Omega\left(\frac{1}{(1/\theta_1)+(1/\theta_2)-(1/\mathfrak{a}_2)}\right)\omega\left(\frac{1}{(1/\theta_1)+(1/\theta_2)-(1/\mathfrak{a}_2)}\right),\\
N(\theta_1,\theta_2,\mathfrak{a}_1,\mathfrak{a}_2)&=\Omega\left(\frac{1}{(1/\theta_1)+(1/\theta_2)-(1/\mathfrak{a}_1)}\right)\omega\left(\frac{1}{(1/\theta_1)+(1/\theta_2)-(1/\mathfrak{a}_2)}\right)\\
&\quad+\Omega\left(\frac{1}{(1/\theta_1)+(1/\theta_2)-(1/\mathfrak{a}_2)}\right)\omega\left(\frac{1}{(1/\theta_1)+(1/\theta_2)-(1/\mathfrak{a}_1)}\right),
\end{aligned}\tag{56}$$

for all $\mathfrak{a}_1, \mathfrak{a}_2 \in [\theta_1, \theta_2]$, $\alpha > 0$, and $\mathfrak{g}(u) = 1/u$, $u \in [1/\theta_2, 1/\theta_1]$.

Proof. Since Ω and ω are harmonically convex on $[\theta_1, \theta_2]$, then for all $\eta \in [0, 1]$, we have

$$\begin{aligned}
&\Omega\left(\frac{1}{(1/\theta_1)+(1/\theta_2)-((\eta/\mathfrak{a}_1)+(1-\eta/\mathfrak{a}_2))}\right)\omega\left(\frac{1}{(1/\theta_1)+(1/\theta_2)-((\eta/\mathfrak{a}_1)+(1-\eta/\mathfrak{a}_2))}\right)\\
&\le\eta^2\Omega\left(\frac{1}{(1/\theta_1)+(1/\theta_2)-(1/\mathfrak{a}_1)}\right)\omega\left(\frac{1}{(1/\theta_1)+(1/\theta_2)-(1/\mathfrak{a}_1)}\right)\\
&\quad+(1-\eta)^2\Omega\left(\frac{1}{(1/\theta_1)+(1/\theta_2)-(1/\mathfrak{a}_2)}\right)\omega\left(\frac{1}{(1/\theta_1)+(1/\theta_2)-(1/\mathfrak{a}_2)}\right)
\end{aligned}$$

$$
\begin{aligned}
&+\eta(1-\eta)\left[\Omega\left(\frac{1}{(1/\theta_1)+(1/\theta_2)-(1/\mathfrak{a}_1)}\right)\omega\left(\frac{1}{(1/\theta_1)+(1/\theta_2)-(1/\mathfrak{a}_2)}\right)\right.\\
&\left.+\Omega\left(\frac{1}{(1/\theta_1)+(1/\theta_2)-(1/\mathfrak{a}_2)}\right)\omega\left(\frac{1}{(1/\theta_1)+(1/\theta_2)-(1/\mathfrak{a}_1)}\right)\right],\\
&\Omega\left(\frac{1}{(1/\theta_1)+(1/\theta_2)-((1-\eta/\mathfrak{a}_1)+(\eta/\mathfrak{a}_2))}\right)\omega\left(\frac{1}{(1/\theta_1)+(1/\theta_2)-((1-\eta/\mathfrak{a}_1)+(\eta/\mathfrak{a}_2))}\right)\\
&\le\eta^2\Omega\left(\frac{1}{(1/\theta_1)+(1/\theta_2)-(1/\mathfrak{a}_2)}\right)\omega\left(\frac{1}{(1/\theta_1)+(1/\theta_2)-(1/\mathfrak{a}_2)}\right)\\
&+(1-\eta)^2\Omega\left(\frac{1}{(1/\theta_1)+(1/\theta_2)-(1/\mathfrak{a}_1)}\right)\omega\left(\frac{1}{(1/\theta_1)+(1/\theta_2)-(1/\mathfrak{a}_1)}\right)\\
&+\eta(1-\eta)\left[\Omega\left(\frac{1}{(1/\theta_1)+(1/\theta_2)-(1/\mathfrak{a}_1)}\right)\omega\left(\frac{1}{(1/\theta_1)+(1/\theta_2)-(1/\mathfrak{a}_2)}\right)\right.\\
&\left.+\Omega\left(\frac{1}{(1/\theta_1)+(1/\theta_2)-(1/\mathfrak{a}_2)}\right)\omega\left(\frac{1}{(1/\theta_1)+(1/\theta_2)-(1/\mathfrak{a}_2)}\right)\right].
\end{aligned}
\tag{57}
$$

Adding these inequalities, we have

$$
\begin{aligned}
&\Omega\left(\frac{1}{(1/\theta_1)+(1/\theta_2)-((\eta/\mathfrak{a}_1)+(1-\eta/\mathfrak{a}_2))}\right)\omega\left(\frac{1}{(1/\theta_1)+(1/\theta_2)-((\eta/\mathfrak{a}_1)+(1-\eta/\mathfrak{a}_2))}\right)\\
&+\Omega\left(\frac{1}{(1/\theta_1)+(1/\theta_2)-((1-\eta/\mathfrak{a}_1)+(\eta/\mathfrak{a}_2))}\right)\omega\left(\frac{1}{(1/\theta_1)+(1/\theta_2)-((1-\eta/\mathfrak{a}_1)+(\eta/\mathfrak{a}_2))}\right)\\
&\le\left(2\eta^2-2\eta+1\right)M(\theta_1,\theta_2,\mathfrak{a}_1,\mathfrak{a}_2)+2\eta(1-\eta)N(\theta_1,\theta_2,\mathfrak{a}_1,\mathfrak{a}_2).
\end{aligned}
\tag{58}
$$

Multiplying by $\exp(-\rho\eta)$ on both sides of (58) and then integrating with respect to $\eta\in[0,1]$, we have

$$
\begin{aligned}
&\int_0^1\exp(-\rho\eta)\Omega\left(\frac{1}{(1/\theta_1)+(1/\theta_2)-((\eta/\mathfrak{a}_1)+(1-\eta/\mathfrak{a}_2))}\right)\omega\left(\frac{1}{(1/\theta_1)+(1/\theta_2)-((\eta/\mathfrak{a}_1)+(1-\eta/\mathfrak{a}_2))}\right)\mathrm{d}\eta\\
&+\int_0^1\exp(-\rho\eta)\Omega\left(\frac{1}{(1/\theta_1)+(1/\theta_2)-((1-\eta/\mathfrak{a}_1)+(\eta/\mathfrak{a}_2))}\right)\omega\left(\frac{1}{(1/\theta_1)+(1/\theta_2)-((1-\eta/\mathfrak{a}_1)+(\eta/\mathfrak{a}_2))}\right)\mathrm{d}\eta\\
&\le M(\theta_1,\theta_2,\mathfrak{a}_1,\mathfrak{a}_2)\int_0^1\exp(-\rho\eta)\left(2\eta^2-2\eta+1\right)\mathrm{d}\eta+N(\theta_1,\theta_2,\mathfrak{a}_1,\mathfrak{a}_2)\int_0^1\exp(-\rho\eta)2\eta(1-\eta)\mathrm{d}\eta\\
&=\frac{\rho^2-2\rho+4-\left(\rho^2+2\rho+4\right)\exp(-\rho)}{\rho^3}M(\theta_1,\theta_2,\mathfrak{a}_1,\mathfrak{a}_2)+2\left(\frac{\rho-2+\exp(-\rho)(\rho+2)}{\rho^3}\right)N(\theta_1,\theta_2,\mathfrak{a}_1,\mathfrak{a}_2).
\end{aligned}
\tag{59}
$$

Thus, we have

$$
\begin{aligned}
&\frac{\alpha\mathfrak{a}_1\mathfrak{a}_2}{2(\mathfrak{a}_2-\mathfrak{a}_1)}\left[I^{\alpha}_{(1/\theta_1+1/\theta_2-1/\mathfrak{a}_1)}(\Omega\omega\circ\mathfrak{g})\left(\frac{1}{\theta_1}+\frac{1}{\theta_2}-\frac{1}{\mathfrak{a}_2}\right)+I^{\alpha}_{(1/\theta_1+1/\theta_2-1/\mathfrak{a}_2)}(\Omega\omega\circ\mathfrak{g})\left(\frac{1}{\theta_1}+\frac{1}{\theta_2}-\frac{1}{\mathfrak{a}_1}\right)\right]\\
&\le\frac{\rho^2-2\rho+4-\left(\rho^2+2\rho+4\right)\exp(-\rho)}{2\rho^3}M(\theta_1,\theta_2,\mathfrak{a}_1,\mathfrak{a}_2)+\frac{\rho-2+\exp(-\rho)(\rho+2)}{\rho^3}N(\theta_1,\theta_2,\mathfrak{a}_1,\mathfrak{a}_2).
\end{aligned}
\tag{60}
$$

Thus, inequality (54) is proved. Now we prove inequality (55). By using harmonic convexity of the function Ω on $[\theta_1, \theta_2]$, we have

$$\begin{aligned}\Omega\left(\frac{2\mathfrak{a}_1\mathfrak{a}_2}{\mathfrak{a}_1+\mathfrak{a}_2}\right)\omega\left(\frac{2\mathfrak{a}_1\mathfrak{a}_2}{\mathfrak{a}_1+\mathfrak{a}_2}\right) &= \Omega\left(\frac{1}{1/2\left(\left(\eta/\mathfrak{a}_1\right)+\left(1-\eta/\mathfrak{a}_2\right)+\left(1-\eta/\mathfrak{a}_1\right)+\left(\eta/\mathfrak{a}_2\right)\right)}\right)\\ &\quad\cdot\omega\left(\frac{1}{1/2\left(\left(\eta/\mathfrak{a}_1\right)+\left(1-\eta/\mathfrak{a}_2\right)+\left(1-\eta/\mathfrak{a}_1\right)+\left(\eta/\mathfrak{a}_2\right)\right)}\right)\\ &\le\frac{1}{2}\left[\Omega\left(\frac{1}{\left(\eta/\mathfrak{a}_1\right)+\left(1-\eta/\mathfrak{a}_2\right)}\right)+\Omega\left(\frac{1}{\left(1-\eta/\mathfrak{a}_1\right)+\left(\eta/\mathfrak{a}_2\right)}\right)\right]\\ &\quad\cdot\frac{1}{2}\left[\omega\left(\frac{1}{\left(\eta/\mathfrak{a}_1\right)+\left(1-\eta/\mathfrak{a}_2\right)}\right)+\omega\left(\frac{1}{\left(1-\eta/\mathfrak{a}_1\right)+\left(\eta/\mathfrak{a}_2\right)}\right)\right].\end{aligned} \tag{61}$$

Replacing $\mathfrak{a}_1$ and $\mathfrak{a}_2$ by $1/(1/\theta_1)+(1/\theta_2)-(1/\mathfrak{a}_1)$ and $1/(1/\theta_1)+(1/\theta_2)-(1/\mathfrak{a}_2)$, respectively, we get

$$\begin{aligned}&\Omega\left(\frac{1}{(1/\theta_1)+(1/\theta_2)-\left(\mathfrak{a}_1+\mathfrak{a}_2/2\mathfrak{a}_1\mathfrak{a}_2\right)}\right)\omega\left(\frac{1}{(1/\theta_1)+(1/\theta_2)-\left(\mathfrak{a}_1+\mathfrak{a}_2/2\mathfrak{a}_1\mathfrak{a}_2\right)}\right)\\ &\le\frac{1}{2}\left[\Omega\left(\frac{1}{(1/\theta_1)+(1/\theta_2)-\left(\left(\eta/\mathfrak{a}_1\right)+\left(1-\eta/\mathfrak{a}_2\right)\right)}\right)+\Omega\left(\frac{1}{(1/\theta_1)+(1/\theta_2)-\left(\left(1-\eta/\mathfrak{a}_1\right)+\left(\eta/\mathfrak{a}_2\right)\right)}\right)\right]\\ &\quad\cdot\frac{1}{2}\left[\omega\left(\frac{1}{(1/\theta_1)+(1/\theta_2)-\left(\left(\eta/\mathfrak{a}_1\right)+\left(1-\eta/\mathfrak{a}_2\right)\right)}\right)\right.\\ &\quad\left.+\omega\left(\frac{1}{(1/\theta_1)+(1/\theta_2)-\left(\left(1-\eta/\mathfrak{a}_1\right)+\left(\eta/\mathfrak{a}_2\right)\right)}\right)\right]\\ &\le\frac{1}{4}\left[\Omega\left(\frac{1}{(1/\theta_1)+(1/\theta_2)-\left(\left(\eta/\mathfrak{a}_1\right)+\left(1-\eta/\mathfrak{a}_2\right)\right)}\right)\omega\left(\frac{1}{(1/\theta_1)+(1/\theta_2)-\left(\left(\eta/\mathfrak{a}_1\right)+\left(1-\eta/\mathfrak{a}_2\right)\right)}\right)\right]\\ &\quad+\frac{1}{4}\left[\Omega\left(\frac{1}{(1/\theta_1)+(1/\theta_2)-\left(\left(1-\eta/\mathfrak{a}_1\right)+\left(\eta/\mathfrak{a}_2\right)\right)}\right)\right.\\ &\quad\left.\cdot\omega\left(\frac{1}{(1/\theta_1)+(1/\theta_2)-\left(\left(1-\eta/\mathfrak{a}_1\right)+\left(\eta/\mathfrak{a}_2\right)\right)}\right)\right]+\frac{\eta(1-\eta)}{2}M\left(\theta_1,\theta_2,\mathfrak{a}_1,\mathfrak{a}_2\right)+\frac{2\eta^2-2\eta+1}{4}N\left(\theta_1,\theta_2,\mathfrak{a}_1,\mathfrak{a}_2\right).\end{aligned} \tag{62}$$

Thus,

$$\begin{aligned}&\Omega\left(\frac{1}{(1/\theta_1)+(1/\theta_2)-\left(\mathfrak{a}_1+\mathfrak{a}_2/2\mathfrak{a}_1\mathfrak{a}_2\right)}\right)\omega\left(\frac{1}{(1/\theta_1)+(1/\theta_2)-\left(\mathfrak{a}_1+\mathfrak{a}_2/2\mathfrak{a}_1\mathfrak{a}_2\right)}\right)\\ &\le\frac{1}{4}\left[\Omega\left(\frac{1}{(1/\theta_1)+(1/\theta_2)-\left(\left(\eta/\mathfrak{a}_1\right)+\left(1-\eta/\mathfrak{a}_2\right)\right)}\right)\omega\left(\frac{1}{(1/\theta_1)+(1/\theta_2)-\left(\left(\eta/\mathfrak{a}_1\right)+\left(1-\eta/\mathfrak{a}_2\right)\right)}\right)\right]\\ &\quad+\frac{1}{4}\left[\Omega\left(\frac{1}{(1/\theta_1)+(1/\theta_2)-\left(\left(1-\eta/\mathfrak{a}_1\right)+\left(\eta/\mathfrak{a}_2\right)\right)}\right)\right.\\ &\quad\left.\cdot\omega\left(\frac{1}{(1/\theta_1)+(1/\theta_2)-\left(\left(1-\eta/\mathfrak{a}_1\right)+\left(\eta/\mathfrak{a}_2\right)\right)}\right)\right]+\frac{\eta(1-\eta)}{2}M\left(\theta_1,\theta_2,\mathfrak{a}_1,\mathfrak{a}_2\right)+\frac{2\eta^2-2\eta+1}{4}N\left(\theta_1,\theta_2,\mathfrak{a}_1,\mathfrak{a}_2\right).\end{aligned} \tag{63}$$

Multiplying by $\exp(-\rho\eta)$ on both sides of (63) and then integrating with respect to $\eta \in [0,1]$, we obtain

$$\begin{aligned}
&\frac{1-\exp(-\rho)}{\rho}\Omega\left(\frac{1}{(1/\theta_1)+(1/\theta_2)-(\mathfrak{a}_1+\mathfrak{a}_2/2\mathfrak{a}_1\mathfrak{a}_2)}\right)\omega\left(\frac{1}{(1/\theta_1)+(1/\theta_2)-(\mathfrak{a}_1+\mathfrak{a}_2/2\mathfrak{a}_1\mathfrak{a}_2)}\right)\\
&\le\frac{1}{4}\int_0^1\exp(-\rho\eta)\left[\Omega\left(\frac{1}{(1/\theta_1)+(1/\theta_2)-((\eta/\mathfrak{a}_1)+(1-\eta/\mathfrak{a}_2))}\right)\omega\left(\frac{1}{(1/\theta_1)+(1/\theta_2)-((\eta/\mathfrak{a}_1)+(1-\eta/\mathfrak{a}_2))}\right)\right]d\eta\\
&\quad+\frac{1}{4}\int_0^1\exp(-\rho\eta)\left[\Omega\left(\frac{1}{(1/\theta_1)+(1/\theta_2)-((1-\eta/\mathfrak{a}_1)+(\eta/\mathfrak{a}_2))}\right)\omega\left(\frac{1}{(1/\theta_1)+(1/\theta_2)-((1-\eta/\mathfrak{a}_1)+(\eta/\mathfrak{a}_2))}\right)\right]d\eta\\
&\quad+M(\theta_1,\theta_2,\mathfrak{a}_1,\mathfrak{a}_2)\int_0^1\exp(-\rho\eta)\frac{\eta(1-\eta)}{2}d\eta+N(\theta_1,\theta_2,\mathfrak{a}_1,\mathfrak{a}_2)\int_0^1\exp(-\rho\eta)\frac{2\eta^2-2\eta+1}{4}d\eta\\
&=\frac{\alpha\mathfrak{a}_1\mathfrak{a}_2}{4(\mathfrak{a}_2-\mathfrak{a}_1)}\left[I^{\alpha}_{(1/\theta_1+1/\theta_2-1/\mathfrak{a}_1)}(\Omega\omega\circ\mathfrak{g})\left(\frac{1}{\theta_1}+\frac{1}{\theta_2}-\frac{1}{\mathfrak{a}_2}\right)+I^{\alpha}_{(1/\theta_1+1/\theta_2-1/\mathfrak{a}_2)}(\Omega\omega\circ\mathfrak{g})\left(\frac{1}{\theta_1}+\frac{1}{\theta_2}-\frac{1}{\mathfrak{a}_1}\right)\right]\\
&\quad+\frac{\rho-2+\exp(-\rho)(\rho+2)}{2\rho^3}M(\theta_1,\theta_2,\mathfrak{a}_1,\mathfrak{a}_2)+\frac{\rho^2-2\rho+4-\left(\rho^2+2\rho+4\right)\exp(-\rho)}{4\rho^3}N(\theta_1,\theta_2,\mathfrak{a}_1,\mathfrak{a}_2).
\end{aligned}\tag{64}$$

Thus,

$$\begin{aligned}
&\Omega\left(\frac{1}{(1/\theta_1)+(1/\theta_2)-(\mathfrak{a}_1+\mathfrak{a}_2/2\mathfrak{a}_1\mathfrak{a}_2)}\right)\omega\left(\frac{1}{(1/\theta_1)+(1/\theta_2)-(\mathfrak{a}_1+\mathfrak{a}_2/2\mathfrak{a}_1\mathfrak{a}_2)}\right)\\
&\le\frac{1-\alpha}{4[1-\exp(-\rho)]}\left[I^{\alpha}_{(1/\theta_1+1/\theta_1-1/\mathfrak{a}_1)}(\Omega\omega\circ\mathfrak{g})\left(\frac{1}{\theta_1}+\frac{1}{\theta_2}-\frac{1}{\mathfrak{a}_2}\right)+I^{\alpha}_{(1/\theta_1+1/\theta_1-1/\mathfrak{a}_2)}(\Omega\omega\circ\mathfrak{g})\left(\frac{1}{\theta_1}+\frac{1}{\theta_2}-\frac{1}{\mathfrak{a}_1}\right)\right]\\
&\quad+\frac{\rho-2+\exp(-\rho)(\rho+2)}{2\rho^2[1-\exp(-\rho)]}M(\theta_1,\theta_2,\mathfrak{a}_1,\mathfrak{a}_2)+\frac{\rho^2-2\rho+4-\left(\rho^2+2\rho+4\right)\exp(-\rho)}{4\rho^2[1-\exp(-\rho)]}N(\theta_1,\theta_2,\mathfrak{a}_1,\mathfrak{a}_2).
\end{aligned}\tag{65}$$

□

Remark 10. If we take $\mathfrak{a}_1=\theta_1$ and $\mathfrak{a}_2=\theta_2$ in Theorem 12, then we get Theorem 12 in [24].

Remark 11. For $\alpha\longrightarrow 1$, we have

$$\begin{aligned}
\lim_{\alpha\longrightarrow 1}\frac{1-\alpha}{2[1-\exp(-\rho)]}&=\frac{\mathfrak{a}_1\mathfrak{a}_2}{2(\mathfrak{a}_2-\mathfrak{a}_1)},\\
\lim_{\alpha\longrightarrow 1}\frac{\rho-2+\exp(-\rho)(\rho+2)}{\rho^3}&=\frac{1}{6},\\
\lim_{\alpha\longrightarrow 1}\frac{\rho^2-2\rho+4-\left(\rho^2+2\rho+4\right)\exp(-\rho)}{2\rho^2[1-\exp(-\rho)]}&=\frac{1}{3}.
\end{aligned}\tag{66}$$

Under the assumptions of Theorem 12 with $\alpha = 1$, we have

$$\frac{\mathfrak{a}_1\mathfrak{a}_2}{\mathfrak{a}_2-\mathfrak{a}_1}\int_{1/\theta_1+1/\theta_2-1/\mathfrak{a}_1}^{1/\theta_1+1/\theta_2-1/\mathfrak{a}_2}\frac{\Omega(\varkappa)}{\varkappa^2}\omega(\varkappa)\mathrm{d}\varkappa \le \frac{M(\theta_1,\theta_2,\mathfrak{a}_1,\mathfrak{a}_2)}{3}+\frac{N(\theta_1,\theta_2,\mathfrak{a}_1,\mathfrak{a}_2)}{6},$$

$$2\Omega\left(\frac{1}{(1/\theta_1)+(1/\theta_2)-(\mathfrak{a}_1+\mathfrak{a}_2/2\mathfrak{a}_1\mathfrak{a}_2)}\right)\omega\left(\frac{1}{(1/\theta_1)+(1/\theta_2)-(\mathfrak{a}_1+\mathfrak{a}_2/2\mathfrak{a}_1\mathfrak{a}_2)}\right) \tag{67}$$

$$\le \frac{\mathfrak{a}_1\mathfrak{a}_2}{\mathfrak{a}_2-\mathfrak{a}_1}\int_{1/\theta_1+1/\theta_2-1/\mathfrak{a}_1}^{1/\theta_1+1/\theta_2-1/\mathfrak{a}_2}\frac{\Omega(\varkappa)}{\varkappa^2}\omega(\varkappa)\mathrm{d}\varkappa+\frac{M(\theta_1,\theta_2,\mathfrak{a}_1,\mathfrak{a}_2)}{6}+\frac{N(\theta_1,\theta_2,\mathfrak{a}_1,\mathfrak{a}_2)}{3}.$$

Remark 12. If $\alpha = 1$, $\mathfrak{a}_1 = \theta_1$, and $\mathfrak{a}_2 = \theta_2$ in Theorem 12, then we obtain inequalities (9) and (10) for harmonically convex functions proved by Chen and Wu in [13].

5. Concluding Remarks and Future Directions

In this study, we introduce for the first time the unified variants of Hermite–Hadamard, Fejér–Hadamard, and Pachpatte–Mercer-type inequalities for harmonically convex functions for fractional integral operators with the exponential kernel. New integral identity involving fractional integral operators with exponential kernel is developed. A compact analysis of newly obtained results and their connections is explained in Remarks 2–12. As special cases, we get Hermite–Hadamard, Fejér–Hadamard, and Pachpatte–Mercer-type inequalities for classical calculus with explicit boundary values. Some particular cases reflect the related existing results. One of the direct impact and utilization of the results extracted in this paper is to obtain inequalities involving following new fractional integral operators containing Mittag-Leffler nonsingular kernels:

$$\mathbb{I}_{\mathfrak{a}_1}^{\alpha}\Omega(\varkappa) = \frac{1}{\alpha}\int_{\mathfrak{a}_1}^{\varkappa} E_{\alpha,1}\left(-\frac{1-\alpha}{\alpha}(\varkappa-u)^{\alpha}\right)\Omega(u)\mathrm{d}u, \quad \varkappa > \mathfrak{a}_1,$$

$$\mathbb{I}_{\mathfrak{a}_2}^{\alpha}\Omega(\varkappa) = \frac{1}{\alpha}\int_{\varkappa}^{\mathfrak{a}_2} E_{\alpha,1}\left(-\frac{1-\alpha}{\alpha}(u-\varkappa)^{\alpha}\right)\Omega(u)\mathrm{d}u, \quad \varkappa < \mathfrak{a}_2, \tag{68}$$

for $\alpha \in (0,1)$ and $\Omega \in L(\mathfrak{a}_1,\mathfrak{a}_2)$, where $E_{\alpha,\nu}(\xi)$ is a Mittag-Leffler-type function:

$$E_{\alpha,\nu}(\xi) = \sum_{\iota=0}^{\infty}\frac{\xi^{\iota}}{\Gamma(\alpha\iota+\nu)}. \tag{69}$$

These integral inequalities may be helpful in the circumstances where upper and lower bounds matter for fractional integral operators involving nonlocal kernels. It is natural to investigate such results for other general convexities like harmonically h−convex functions introduced by Noor et al. in [30]. Also, it is interesting to construct such inequalities over fractal domains where we may get optimal and sharp local fractional integral inequalities involving Mittag-Leffler kernel.

Data Availability

No data were used to support this study.

Conflicts of Interest

The authors declare that they have no conflicts of interest.

Acknowledgments

Abdullah M. Alsharif was supported by Taif University Researchers Supporting Project (TURSP-2020/96), Taif University, Taif, Saudi Arabia.

References

[1] D. S. Mitrinović, J. E. Pečarić, and A. M. Fink, "Classical and new inequalities in analysis," *Mathematics and its Applications (East European Series)*, Kluwer Academic Publishers Group, Dordrecht, Netherlands, 1993.

[2] S. S. Dragomir and C. E. M. Pearce, *Selected Topics on Hermite-Hadamard Inequalities and Applications, RGMIA Monographs*, Victoria University, Melbourne, Australia, 2000.

[3] C. P. Niculescu and L. E. Persson, "Convex functions and their applications: a contemporary approach," *CMS Books in Mathematics/Ouvrages de Math ematiques de la SMC*, Springer, New York, NY, USA, 2nd edition, 2018.

[4] M. Khan, Z. Al-sahwi, and Y.-M. Chu, "New estimations for shannon and zipf-mandelbrot entropies," *Entropy*, vol. 20, no. 8, p. 608, 2018.

[5] S. Khan, M. A. Khan, S. I. Butt, and Y. M. Chu, "A new bound for the Jensen gap pertaining twice differentiable functions with applications," *Advances in Difference Equations*, vol. 2020, p. 333, 2020.

[6] S. I. Butt, L. Horváth, D. Pečarić, and J. Pečarić, "Cyclic improvements of Jensen's inequalities (cyclic inequalities in information theory)," *Monographs in Inequalities*, Element, Zagreb, Croatia, 2020.

[7] A. M. Mercer, "A variant of jensen's inequality," *Journal of Inequalities in Pure and Applied Mathematics*, vol. 4, no. 4, p. 73, 2003.

[8] M. Kian and M. Moslehian, "Refinements of the operator Jensen-Mercer inequality," *The Electronic Journal of Linear Algebra*, vol. 26, pp. 742–753, 2013.

[9] E. Anjidani, "Jensen-Mercer operator inequalities involving superquadratic functions," *Mediterranean Journal of Mathematics*, vol. 15, p. 31, 2018.

[10] H. R. Moradi and S. Furuichi, "Improvement and generalization of some Jensen-Mercer-type inequalities," *Journal of Mathematical Inequalities*, vol. 14, no. 2, pp. 377–383, 2020.

[11] Í. Íşcan, "Hermite-Hadamard type inequalities for harmonically convex functions," *Hacettepe Journal of Mathematics and Statistics*, vol. 43, no. 6, pp. 935–942, 2014.

[12] F. Chen and S. Wu, "Fejer Hermite-Hadamard type inqequalities for harmonically convex functions," *Journal of Applied Mathametics*, vol. 2014, Article ID 386806, 2014.

[13] F. Chen and S. Wu, "Some Hermite-Hadamard type inequalities for harmonically s-convex functions," *The Scientific World Journal*, vol. 2014, Article ID 279158, 2014.

[14] R. Gorenflo, "Fractional calculus," in *Fractals and Fractional Calculus in Continuum Mechanics*, A. Carpinteri and F. Mainardi, Eds., Springer-Verlag, New York, NY, USA, 1997.

[15] A. A. Kilbas, H. M. Srivastava, and J. J. Trujillo, *Theory and Applications of Fractional Differential Equations*, Elservier, Amsterdam, Netherlands, 2006.

[16] S. Rashid, Z. Hammouch, D. Baleanu, and Y.-M. Chu, "New generalizations in the sense of the weighted non-singular fractional integral operator," *Fractals*, vol. 28, no. 8, Article ID 2040003, 2020.

[17] S. I. Butt, S. Yousaf, A. O. Akdemir, and M. A. Dokuyucu, "New Hadamard-type integral inequalities via a general form of fractional integral operators," *Chaos, Solitons & Fractals*, vol. 148, Article ID 111025, 2021.

[18] X. Wu, J. R. Wang, and J. Zhang, "Hermite-Hadamard-type inequalities for convex functions via the fractional integrals with exponential kernel," *Mathematics*, vol. 7, no. 845, pp. 1–12, 2019.

[19] A. O. Akdemir, S. I. Butt, M. Nadeem, and M. A. Ragusa, "New general variants of Chebyshev type inequalities via generalized fractional integral operators," *Mathematics*, vol. 9, no. 2, p. 122, 2021.

[20] Í. Íşcan and S. Wu, "Hermite-Hadamard type inequalities for harmonically convex function via fractional integrals," *Applied Mathametics Computation*, vol. 238, pp. 237–244, 2014.

[21] Í. Íşcan and M. Kunt, "Hermite-Hadamard-Fejér type inequalities for harmonically convex functions via fractional integrals," *RGMIA Research Report Collection*, vol. 18, pp. 1–16, 2015.

[22] K. Mehrez and P. Agarwal, "New Hermite–Hadamard type integral inequalities for convex functions and their applications," *Journal of Computer Applied Mathametics*, vol. 350, pp. 274–285, 2019.

[23] B. Ahmad, A. Alsaed, M. Kirane, and B. T. Torebek, "Hermite-Hadamard, Hermite-Hadamard-Fejér, Dragomir-Agarwal and Pachpatte type inequalities for convex functions via new fractional integrals," *Journal of Computer Applied Mathametics*, vol. 353, pp. 120–129, 2019.

[24] S. Rashid, D. Baleanu, and Y.-M. Chu, "Some new extensions for fractional integral operator having exponential in the kernel and their applications in physical systems," *Open Physics*, vol. 18, no. 1, pp. 478–491, 2020.

[25] H.-H. Chu, S. Rashid, Z. Hammouch, and Y. M. Chu, "New fractional estimates for Hermite-Hadamard-Mercer's type inequalities," *Alexandria Engineering Journal*, vol. 59, no. 5, pp. 3079–3089, 2020.

[26] S. I. Butt, M. Umar, S. Rashid, A. O. Akdemir, and Y. M. Chu, "New Hermite-Mercer type inequalities via k-fractional integrals," *Advances in Differential Equations*, vol. 2020, Article ID 635, 2020.

[27] S. I. Butt, J. Nasir, S. Qaisar, and K. M. Abualnaja, "k-Fractional variants of Hermite-Mercer-type inequalities via s-convexity with applications," *Journal of Function Spaces*, vol. 2021, Article ID 5566360, 2021.

[28] I. A. Baloch, A. A. Mughal, Y.-M. U. Haq, and M. D. L. Sen, "A variant of Jensen-type inequality and related results for harmonic convex functions," *AIMS Mathematics*, vol. 5, no. 6, pp. 6404–6418, 2020.

[29] I. A. Baloch, A. A. Mughal, Y. M. Chu, A. U. Haq, and M. D. L. Sen, "Improvement and generalization of some results related to the class of harmonically convex functions and applications," *Journal of Mathametics Computer Science*, vol. 22, no. 3, pp. 282–294, 2021.

[30] M. A. Noor, K. I. Noor, M. U. Awan, and S. Costache, "Improvement and generalization of some results related to the class of harmonically h-convex functions and applications," *U.P.B. Scientific Bulletin Series A*, vol. 77, no. 1, pp. 1–16, 2015.

Hindawi
Mathematical Problems in Engineering
Volume 2022, Article ID 1707894, 9 pages
https://doi.org/10.1155/2022/1707894

Research Article

Bioconvection Flow of MHD Viscous Nanofluid in the Presence of Chemical Reaction and Activation Energy

Muhammad Imran Asjad,[1] **Muhammad Zahid**,[1] **Fahd Jarad**,[2,3,4] **and Abdullah M. Alsharif**[5]

[1]*Department of Mathematics, University of Management and Technology, Lahore 54770, Pakistan*
[2]*Department of Mathematics, Cankaya University, Etimesgut, Ankara, Turkey*
[3]*Department of Mathematics, King Abdul Aziz University, Jeddah, Saudi Arabia*
[4]*Department of Medical Research, China Medical University Hospital, China Medical University, Taichung, Taiwan*
[5]*Department of Mathematics and Statistics, College of Science, Taif University, Taif 21944, Saudi Arabia*

Correspondence should be addressed to Fahd Jarad; fahd@cankaya.edu.tr

Received 14 October 2021; Revised 22 November 2021; Accepted 31 December 2021; Published 7 February 2022

Academic Editor: Muhammad Irfan

Enhancement of heat transfer due to stretching sheets can be appropriately controlled by the movement of the nanofluids. The concentration and settling of the nanoparticles in the viscous MHD fluid and bioconvection are addressed. In this scenario, the fluid flow occurring in the presence of a normal and uniform magnetic field, thermal radiation, and chemical reaction is taken into account. For the two-dimensional flow with heat and mass transfer, five dependent variables and three independent variables constitute the system of partial differential equations. For this purpose, similarity functions are involved to convert these equations to corresponding ODEs. Then, the Runge–Kutta method with shooting technique is used to evaluate the required findings with the utilization of MATLAB script. The fluid velocity becomes slow against the strength of the magnetic parameter. The temperature rises with the parameter of Brownian motion and thermophoresis. The bioconvection Lewis number diminishes the velocity field. Compared with the existing literature, the results show satisfactory congruences.

1. Introduction

The convoluted and quick process in massive machinery and little gadgets has produced a significant problem of thermal imbalance. Varied extraneous techniques like fins and fans are used; however, their utility is restricted because of their giant size. In 1995, the scientist Choi and Eastman [1] introduced that the nanosized particles mixed in the fluid called nanofluid have more capacity of heat transfer as compared with fluid without nanosized particles. Das et al. [2] explained the recent and future applications of fluid involving nanosized particles. Khan et al. [3] using the shooting method analyzed flow features of Williamson nanofluid influenced by variable viscosity depending on temperature and Lorentz force past an inclined nonlinear extending surface. Koo and Kleinstreuer [4] described influences of convection, conduction, viscous dissipation, and thermal transportation on nanofluid flow in a microchannel. Sui et al. [5] introduced the CattaneoeChristov model with double diffusion to analyze the influence of slip velocity, Brownian motion, and variable viscosity on the transportation of an upper convected Maxwell nanofluid through stretching sheet. Imran et al. [6] determined an unsteady stream of Maxwell fluid through an accelerated exponentially vertical surface with influences of radiation, Newtonian heating, MHD, and slip condition taken into account. Khan et al. [7] investigated the flow of micropolar base nanofluid through stretching sheet with thermal radiation and magnetic dipole. Sheikholeslami and Rokni [8] scrutinized magnetic field impacts on the thermal transport rate in a nanofluid. Seyyedi et al. [9] analyzed the entropy generation for Cu-water nanofluid having a semi-annulus porous wavy cavity in the presence of a magnetic field. Molana et al. [10] discussed the characteristics of heat transfer and natural

convection of nanofluid past a porous cavity with a constant inclined magnetic field. Dogonchi et al. [11] explained the characteristics of natural convection and magnetic field on nanofluid flow through porous medium with effects of Hartmann number, Rayleigh number, and Darcy number taken into account. Shaw et al. [12] scrutinized the impact of nonlinear thermal and entropy generation on Casson nanofluid flow with rotating disk and also described the brain function. Chamkha et al. [13] explained MHD nanofluid flow through cavity using the control-volume-based finite element method with effects of natural convection, thermal radiation, and shape factor of nanoparticles taken into account. Dogonchi et al. [14] numerically introduced the importance of the Cattaneo–Christov theory of heat conduction through triangular semicircular heater with viscosity dependent on the magnetic field. Seyyedi et al. [15] described the entropy generation and natural convection heat transfer of Cu-water nanoliquid through the hexagonal cavity. Sadeghi et al. [16] analyzed the thermal behavior of magnetic buoyancy-driven flow in ferrofluid-filled wavy enclosure furnished with two circular cylinders.

Stretching sheets because of their wide applications like plastic film, metal drawing and spinning, glass fiber, paper processing, and heat moving have become an important topic in the past decades. Recently, some researchers investigated the magnetohydrodynamic flow with the different effects such as viscous dissipation and chemical reaction using stretching sheet (see Ismail et al. [17], Rajput et al. [18], Swain et al. [19], Reddy et al. [20], Jat and Chand [21], Sajid and Hayat [22], Ishak [23], Abd El-Aziz [24], Makinde [25], and Goud et al. [26]).

Bioconvection described the phenomena in which living microorganisms denser than water swim upward in suspensions. These microorganisms pile up in the layer of the upper surface and lower surface becomes less dense. The microorganisims fall down due to unstability of density distribution. Bioconvection has applications in biological systems and biotechnology such as purifying cultures, enzyme biosensors, and separating dead and living cells [27]. Raees et al. [28] examined the unsteady stream of bioconvection mixed nanofluid having gyrostatic motile microorganisms through a horizontal channel. Siddiqa et al. [29] numerically studied the bioconvection flow of nanofluid having mass and thermal transportation along with gyrotactic microorganisms through a curved vertical cone. Abbasi et al. [30] introduced the bioconvection stream of viscoelastic nanofluid because of gyrotactic microorganisms past a rotating extending disk having zero mass flux and convective boundary condition and also described the relatable parameters influences on velocity, temperature, local density, Sherwood number, and Nusselt number in detail. Chu et al. [31] analyzed the stream of bioconvection MHD fluid through extending sheet with the significance of motile microorganisms, activation energy, thermophoresis diffusion, Brownian motion, and chemical reaction taken into account. Henda et al. [32] examined the magnetized bioconvection flow of fluid past an extending cylinder with thermal radiation, activation energy, and heat source. Khan et al. [33] scrutinized bioconvection stream of viscous nanofluid through (cone, wedge, and plate) multiple geometries with effects of heat flux, cross-diffusion, and Cattaneo–Christov.

Inspired by the above literature survey, our interest pertains to extending the results of Goud et al. [26] to investigate a more general problem, including bioconvection of nanofluid transportation with the effects of chemical reaction and radiation to avoid probable settling of nanoentities. The connotation of such meaningful attributes can be a useful extension, and the results can be utilized for desired effective thermal transportation in the heat exchanger of various technological processes.

2. Problem Formulation

Here, we considered steady incompressible magnetohydrodynamic nanofluid flow through exponentially stretching sheet along the x-axis and y-axis taken to be normal with velocity $\tilde{U}_w = a_0 e^{x/l}$ as shown in Figure 1. A magnetic field is applied to the flow region and acts in the y-direction. A mild diffusion of microorganisms and nanoparticles is set in the fluid. Thermal radiation is considered, and bioconvection takes place because of microorganisms' movement. The fluid velocity for two-dimensional flow is $\tilde{u}, \tilde{v}$.

Under the above conditions, the governing equations are as follows [20, 26]. Continuity equation is as follows:

$$\tilde{u}_x + \tilde{v}_y = 0, \tag{1}$$

momentum equation is as follows:

$$\tilde{u}\tilde{u}_x + \tilde{v}\tilde{u}_y = \nu\tilde{u}_{yy} - \frac{\sigma}{\rho}\left(B_0^2\tilde{u}\right) + \frac{1}{\rho}\left[g\beta\rho\left(1-\tilde{C}_\infty\right)\left(\tilde{T}-\tilde{T}_\infty\right) - g\left(\rho_p-\rho_f\right)\left(\tilde{C}-\tilde{C}_\infty\right) - g\gamma\left(\rho_m-\rho_f\right)\left(\tilde{N}-\tilde{N}_\infty\right)\right], \tag{2}$$

energy equation is as follows:

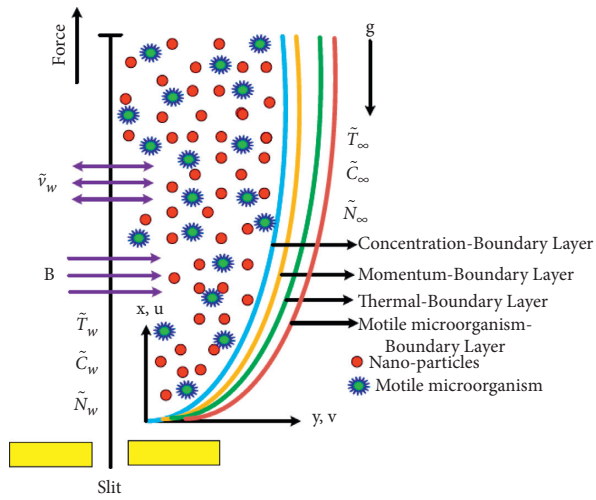

Figure 1: Geometry of the problem.

$$\tilde{u}\tilde{T}_x + \tilde{v}\tilde{T}_y = \alpha\tilde{T}_{yy} - \frac{1}{\rho C_p}\frac{\partial q_r}{\partial y} + \tau\left(D_B\tilde{T}_y\tilde{C}_y + \frac{D_T}{\tilde{T}_\infty}\left(\tilde{T}_y\right)^2\right), \tag{3}$$

concentration equation is as follows:

$$\tilde{u}\tilde{C}_x + \tilde{v}\tilde{C}_y = D\tilde{C}_{yy} - K_r\left(\tilde{C} - \tilde{C}_\infty\right) - K_r^2\left(\tilde{C} - \tilde{C}_\infty\right)\left(\frac{\tilde{T}}{\tilde{T}_\infty}\right)^n \exp\left(\frac{-Ea}{k\tilde{T}}\right) + \frac{D_T}{\tilde{T}_\infty}\tilde{T}_{yy}, \tag{4}$$

bioconvection equation is as follows:

$$\tilde{u}\tilde{N}_x + \tilde{v}\tilde{N}_y + dW_c\frac{\partial}{\partial y}\left(\frac{\tilde{N}}{\Delta\tilde{C}}\tilde{C}_y\right) = \tilde{N}_{yy}D_n, \tag{5}$$

with constraints

$$\begin{aligned}&\tilde{u} = \tilde{U}_w,\ \tilde{v} = 0,\ \tilde{T} = \tilde{T}_w,\ \tilde{C} = \tilde{C}_w,\ \tilde{N} = \tilde{N}_w\ at\ y \longrightarrow 0,\\ &\tilde{u} \longrightarrow 0,\ \tilde{T} \longrightarrow \tilde{T}_\infty,\ \tilde{C} \longrightarrow \tilde{C}_\infty,\ \tilde{N} \longrightarrow \tilde{N}_\infty\ as\ y \longrightarrow \infty.\end{aligned} \tag{6}$$

Now, introducing

$$\tilde{U}_w = a_0e^{x/l},\ \tilde{T}_w = \tilde{T}_\infty + \tilde{T}_0e^{x/2l},\ \tilde{C}_w = \tilde{C}_\infty + \tilde{C}_0e^{x/2l},\ \tilde{N}_w = \tilde{N}_\infty + \tilde{N}_0e^{x/2l}, \tag{7}$$

under the Rosseland approximation q_r [26], equation (3) can be written as

$$\widetilde{u}\widetilde{T}_x + \widetilde{v}\widetilde{T}_y = \widetilde{T}_{yy}\left(\alpha + \frac{16\sigma^* T_\infty^3}{\rho C_p 3k_1}\right) + \tau\left(D_B\widetilde{T}_y\widetilde{C}_y + \frac{D_T}{\widetilde{T}_\infty}\left(\widetilde{T}_y\right)^2\right). \tag{8}$$

Introducing similarity transformation,

$$\begin{aligned}&\eta = y\sqrt{\frac{a_0}{2\nu\ell}}e^{x/2l},\ \widetilde{u} = a_0 e^{x/l} f'(\eta),\ \widetilde{v} = -\sqrt{\frac{a_0\nu}{2\ell}}e^{x/2l}\left[f(\eta) + \eta f'(\eta)\right],\\ &\psi = \sqrt{2\nu L a_0} f(\eta)e^{x/2l}, \widetilde{T} = \widetilde{T}_\infty + \widetilde{T}_0 e^{x/2l},\ \widetilde{C} = \widetilde{C}_\infty + \widetilde{C}_0 e^{x/2l},\ \widetilde{N} = \widetilde{N}_\infty + \widetilde{N}_0 e^{x/2l}.\end{aligned} \tag{9}$$

In view of the above appropriate relations, equation (1) is satisfied identically and equations (2)–(5), respectively, become

$$f''' - Mf' - 2f'^2 + ff'' + \lambda(\theta - Nr\phi - Rb\chi) = 0, \tag{10}$$

$$\left(1 + \frac{4}{3}K\right)\theta'' + \Pr f\theta' - \Pr\theta f' + \theta'\left(Nb\phi' + Nt\theta'\right) = 0, \tag{11}$$

$$\phi'' + \left[f\phi' - Cr\phi - \phi f' - \sigma_m\phi(1+\delta\theta)^n \exp\left(\frac{-E}{1+\delta\theta}\right)\right]Sc + \frac{Nt}{Nb}\theta'' = 0, \tag{12}$$

$$\chi''(\xi) + Lb\Pr f(\xi)\chi'(\xi) - Lb\Pr f'(\xi)\chi(\xi) - Pe\left(\sigma_1\phi''(\xi) + \chi(\xi)\phi''(\xi) + \chi'(\xi)\phi'(\xi)\right) = 0, \tag{13}$$

and the constraints reduce to

$$f'(0) = 1,\ f(0) = 0,\ \phi(0) = 1,\ \theta(0) = 1,\ \chi(0) = 1,\ at\ \eta = 0, \tag{14}$$

$$f'(\infty) \longrightarrow 0,\ \phi(\infty) \longrightarrow 0,\ \theta(\infty) \longrightarrow 0,\ \chi(\infty) \longrightarrow 0.\ as\ \eta \longrightarrow \infty. \tag{15}$$

The associated parameters are

$$M = \frac{2\sigma B_0^2\ell}{\rho\widetilde{U}_w},$$

$$\Pr = \frac{\nu}{\alpha},$$

$$\lambda = \frac{(1 - C_\infty)\beta g(T_w - T_\infty)2\ell}{\widetilde{U}_w^2},$$

$$Nr = \frac{\left(\rho_p - \rho_f\right)(C_w - C_\infty)}{\beta(1 - C_\infty)\rho(T_w - T_\infty)},$$

$$Rb = \frac{\left(\rho_m - \rho_f\right)\gamma(N_w - N_\infty)}{\rho(1 - C_\infty)\beta(T_w - T_\infty)},$$

$$Nt = \frac{\tau D_T(T_w - T_\infty)}{\nu T_\infty},$$

$$Nb = \frac{\tau D_B(C_w - C_\infty)}{\nu},$$

$$\sigma_m = \frac{2K_r^2\ell}{\widetilde{U}_w},$$

$$\delta = \frac{(T_w - T_\infty)}{T_\infty},$$

$$K = \frac{4\sigma^* T_\infty^3}{k^* K},$$

$$\sigma_1 = \frac{N_\infty}{N_w - N_\infty},$$

Table 1: Comparison of $\theta'(0)$ with changed values of K, M, and Pr.

K	M	Pr	Ishak [23]	Goud et al. [26]	Bidin and Nazar [34]	Our results
0.0	0	1.0	0.954 8	0.954 784	0.954 7	0.954 810 6
		2.0	1.471 5	1.471 462	1.471 4	1.471 454 0
		3.0	1.869 1	1.869 073	1.869 1	1.869 068 8
		5.0	2.500 1	2.500 111		2.500 128 0
		10.0	3.660 4	3.660 346		3.660 369 3
	1.0	1.0	0.861 1	0.861 097		0.861 508 6
1.0	0.0		0.531 2	0.531 17	0	0.531 311 2
	1.0		0.450 5	0.450 687	0	0.450 695 5

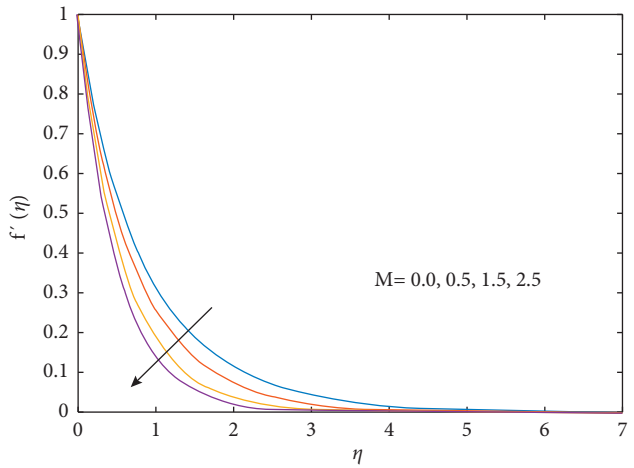

Figure 2: Influences of M on f'.

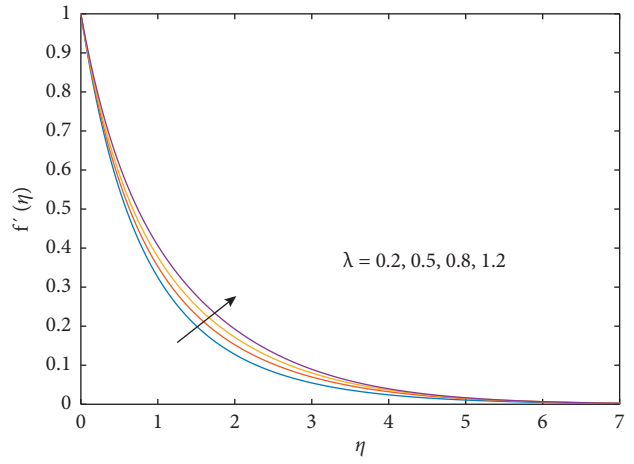

Figure 3: Influences of λ on f'.

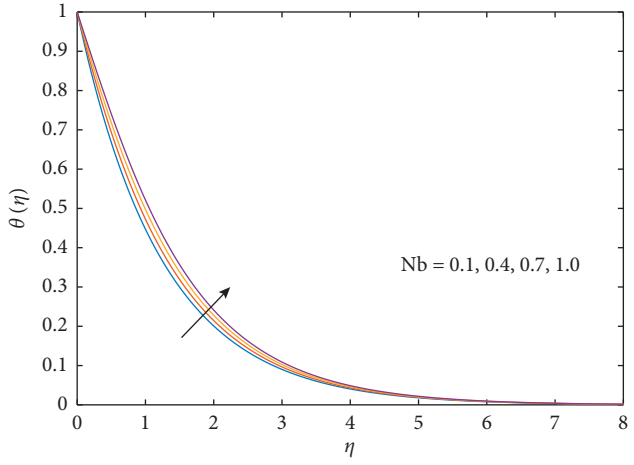

Figure 4: Influences of Nb on θ.

$$E = \frac{Ea}{kT_\infty},$$
$$Sc = \frac{\nu}{D},$$
$$Lb = \frac{\alpha}{D_n},$$
$$Pe = \frac{dW_c}{D_n},$$
$$Cr = \frac{2\ell K_r}{\tilde{U}_w}, \tag{16}$$

where M is the magnetic field parameter, Pr is the Prandtl number, λ is the mixed convection parameter, Nr is the buoyancy ratio number, Rb is the bioconvection Rayleigh number, Nt is the thermopherosis diffusion factor, Nb is the Brownian factor, σ_m denotes the dimensionless reaction rate, δ is used as the temperature distinction parameter, K is the radiation parameter, σ_1 is the bioconvective difference parameter, E means the nondimensional energy activation, Sc is the Schmidt number, Lb is the bioconvection Lewis number, Pe is the peclet number, and Cr is the chemical reaction parameter.

The wall shear stress, thermal flux, and mass flux, respectively, are given as

$$\tau_w - \mu\left(\frac{\partial \tilde{u}}{\partial y}\right)_{y=0} = 0, q_w + k\left(\frac{\partial \tilde{T}}{\partial y}\right)_{y=0} = 0, j_w + D\left(\frac{\partial \tilde{c}}{\partial y}\right)_{y=0} = 0. \tag{17}$$

C_f (skin friction), Nu_x (Nusselt number), and Sh_x (sherwood number) in dimensionless form are

$$C_f = \frac{f''(0)}{\sqrt{2\mathrm{Re}_x}}, \quad Nu_x = -\left(\sqrt{\mathrm{Re}_x}\right)\theta'(0), \quad Sh_x \mathrm{Re}^{-1/2} = -\phi'(0). \tag{18}$$

3. Results and Discussion

Physical meanings of the final nondimensional formulation of time-independent MHD flow of nanofluid due to stretch of an exponential sheet in the presence of chemical reaction along the boundary constraints are solved numerically. Table 1 contains results for $-\theta'(0)$ (Nusselt number). Comparison of the results indicates acceptable agreement to validate this numeric procedure. In Figure 2, the velocity of the flow seems to be reduced significantly when magnetic parameter M $(0.0 \le M \le 2.5)$ is increased because high values of magnetic field parameter improve the contradictory force known as Lorentz force. The improvement of

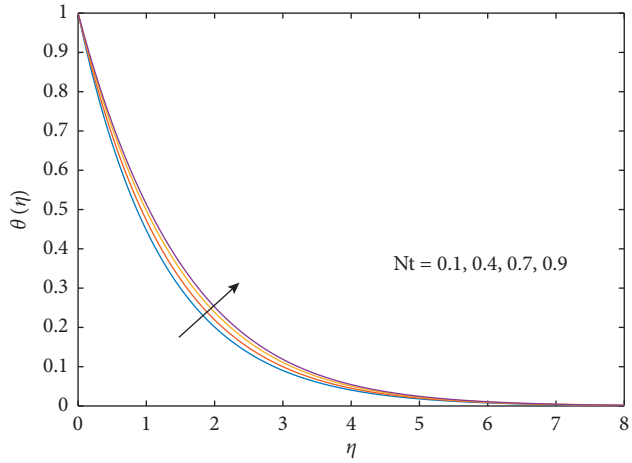

Figure 5: Influence of Nt on ϕ.

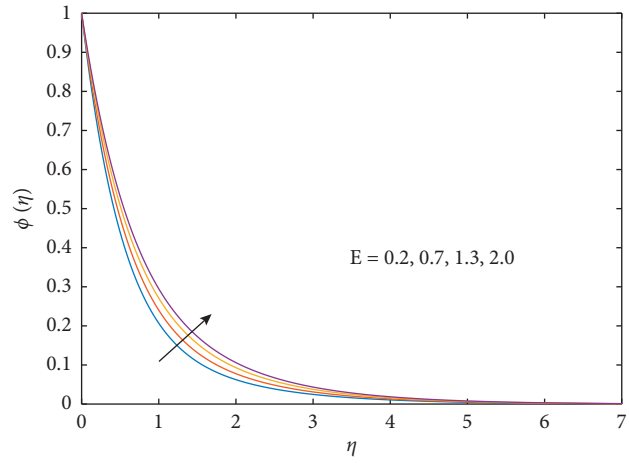

Figure 6: Influences of E on ϕ.

mixed convection parameter λ causes to boost the flow velocity $f'(\eta)$ as shown in Figure 3. From Figures 4 and 5, significant rising behavior of $\theta(\eta)$ is noticed with an enhanced value of Brownian motion parameter Nb and thermophoresis parameter Nt. The fast random motion of nanoparticles characterized by larger Nb is responsible for enhanced heat transfer to raise $\theta(\eta)$. Similarly, the higher Nt means a greater thermophoretic effect which moves the nanoparticles hotter regime to the colder one and increases the thermal distribution. The similarly larger value of E provides strength to $\phi(\eta)$ as depicted in Figure 6. Figure 7 displays the decrement in $\phi(\eta)$ due to the larger value of chemical reaction, and the chemical reaction becomes faster to recede nanoparticles concentration. The bioconvection Rayleigh Rb and parameter are responsible for given direct increment to $\chi(\eta)$ as demonstrated in Figure 8.

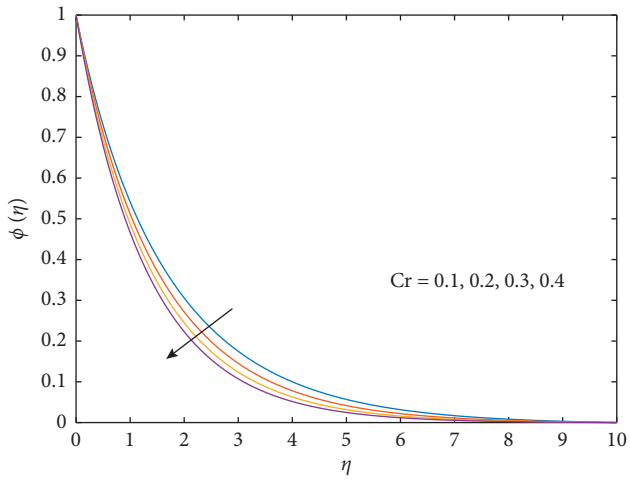

Figure 7: Influences of Cr on ϕ.

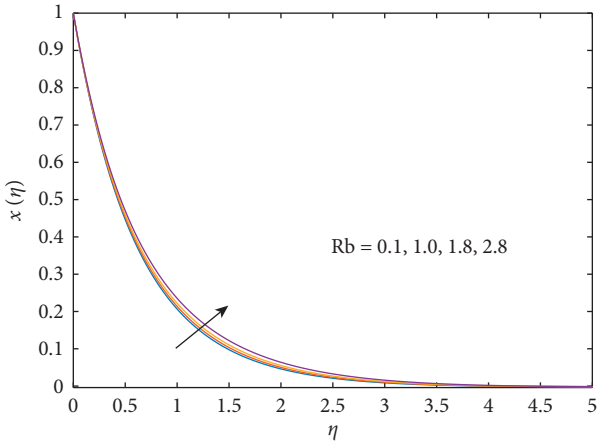

Figure 8: Influences of Rb on χ.

4. Conclusions

Theoretical and numeric analysis for magnetohydrodynamic of nanofluid owing to sudden stretched in an exponential sheet has been made in this communication. Effects of the emerging parameters are enumerated on the physical field, namely, velocity, temperature, and microorganisms distribution. Significant outcomes are summarized as follows:

(i) The velocity reduces with M and boosts with λ

(ii) The conclusion of nanoparticles characterized by parameters Nb and Nt shows an increment in the temperature profile

(iii) Concentration recurses with Cr and is enhanced with E

(iv) Bioconvection parameter is increased with Rb

Nomenclature

B_0: Coefficient of magnetic field
C: Concentration
T: Temperature
N: Concentration of microorganisms
Nt: Thermopherosis parameter
(x, y): Cartesian coordinates
Cr: Chemical reaction parameter
(u, v): Velocity components along (x, y)-axes
τ: Heat capacity ratio
ξ: Similarity variable
D_T: Thermophoretic diffusion coefficient
ϕ: Dimensionless concentration
q_r: Radiative heat flux
ρ: Density
K_r^2: Chemical reaction rate constant
μ: Dynamic viscosity of the fluid
K_r: Rate of chemical reaction
σ: Electrical conductivity
D_B: Brownian diffusivity
ψ: Stream function
K: Radiation parameter
δ: Temperature distinction parameter
Sc: Schmidt number
λ: Mixed convection parameter
U_w: Stretching velocity
ν: Kinematic viscosity
Pr: Prandtl number
θ: Dimensionless temperature
Pe: Peclet number
χ: Dimensionless microorganism factor
M: Magnetic parameter
ρ_f: Density of nanofluid
Nr: Buoyancy ratio number
ρ_m: Density of microorganisms particle
Rb: Bioconvection Rayleigh number
ρ_p: Density of nanoparticles
Nb: Brownian motion parameter
κ: Thermal conductivity
n: Fitted rate constant parameter
α: Thermal diffusivity
g: Gravity
β: Volumetric coefficient of thermal expansion
E: Nondimensional activation energy
γ: Average volume of microorganism
Lb: Bioconvection Lewis number
Sh_x: Local Sherwood Number
W_c: Maximum cell swimming speed
σ_m: Dimensionless reaction rate
D_n: Microorganisms diffusion coefficient
σ_1: Bioconvection diffrrence parameter
σ^*: Stefan Boltzman constant
Nu_x: Local Nusselt number
C_f: Local skin friction number
Re_x: Local Reynolds number.

Data Availability

The data used to support this study are included within this article.

Conflicts of Interest

The authors declare that they have no known personal relationships or conflicts of interest that could have appeared to the work reported in this work.

Authors' Contributions

All authors contributed equally and significantly in writing this paper. All authors read and approved the manuscript.

Acknowledgments

This research was supported by Taif University Researchers Supporting Project Number TURSP-2020/96, Taif University, Taif, Saudi Arabia.

References

[1] S. U. Choi and J. A. Eastman, "Enhancing thermal conductivity of fluids with nanoparticles," Tech. Rep. 96:001707, Argonne National Laboratory, Argonne, IL, USA, 1995.

[2] S. K. Das, S. U. Choi, W. Yu, and T. Pradeep, *Nanofluids: Science and Technology*, John Wiley & Sons, New York, NY, USA, 2007.

[3] M. Khan, M. Y. Malik, T. Salahuddin, and A. Hussian, "Heat and mass transfer of williamson nanofluid flow yield by an inclined lorentz force over a nonlinear stretching sheet," *Results in Physics*, vol. 8, pp. 862–868, 2018.

[4] J. Koo and C. Kleinstreuer, "Laminar nanofluid flow in microheat-sinks," *International Journal of Heat and Mass Transfer*, vol. 48, no. 13, pp. 2652–2661, 2005.

[5] J. Sui, L. Zheng, and X. Zhang, "Boundary layer heat and mass transfer with Cattaneo-Christov double-diffusion in upper-convected Maxwell nanofluid past a stretching sheet with slip velocity," *International Journal of Thermal Sciences*, vol. 104, pp. 461–468, 2016.

[6] M. A. Imran, M. B. Riaz, N. A. Shah, and A. A. Zafar, "Boundary layer flow of mhd generalized Maxwell fluid over an exponentially accelerated infinite vertical surface with slip and Newtonian heating at the boundary," *Results in Physics*, vol. 8, pp. 1061–1067, 2018.

[7] S. A. Khan, B. Ali, C. Eze et al., "Magnetic dipole and thermal radiation impacts on stagnation point flow of micropolar based nanofluids over a vertically stretching sheet: finite element approach," *Processes*, vol. 9, no. 7, p. 1089, 2021.

[8] M. Sheikholeslami and H. B. Rokni, "Simulation of nanofluid heat transfer in presence of magnetic field: a review," *International Journal of Heat and Mass Transfer*, vol. 115, pp. 1203–1233, 2017.

[9] S. M. Seyyedi, A. Dogonchi, R. Nuraei, D. Ganji, and M. Hashemi-Tilehnoee, "Numerical analysis of entropy generation of a nanofluid in a semi-annulus porous enclosure with different nanoparticle shapes in the presence of a magnetic field," *The European Physical Journal Plus*, vol. 134, no. 6, pp. 1–20, 2019.

[10] M. Molana, A. S. Dogonchi, T. Armaghani, A. J. Chamkha, D. D. Ganji, and I. Tlili, "Investigation of hydrothermal behavior of fe3o4-h2o nanofluid natural convection in a novel shape of porous cavity subjected to magnetic field dependent (mfd) viscosity," *Journal of Energy Storage*, vol. 30, p. 101395, 2020.

[11] A. S. Dogonchi, S. M. Seyyedi, M. Hashemi-Tilehnoee, A. J. Chamkha, and D. D. Ganji, "Investigation of natural convection of magnetic nanofluid in an enclosure with a porous medium considering brownian motion," *Case Studies in Thermal Engineering*, vol. 14, p. 100502, 2019.

[12] S. Shaw, A. S. Dogonchi, M. K. Nayak, and O. D. Makinde, "Impact of entropy generation and nonlinear thermal radiation on Darcy-forchheimer flow of MnFe2O4-casson/water nanofluid due to a rotating disk: application to brain dynamics," *Arabian Journal for Science and Engineering*, vol. 45, no. 7, pp. 5471–5490, 2020.

[13] A. Chamkha, A. S. Dogonchi, and D. D. Ganji, "Magneto-hydrodynamic nanofluid natural convection in a cavity under thermal radiation and shape factor of nanoparticles impacts: a numerical study using cvfem," *Applied Sciences*, vol. 8, no. 12, p. 2396, 2018.

[14] A. S. Dogonchi, M. Waqas, M. M. Gulzar, M. Hashemi-Tilehnoee, S. M. Seyyedi, and D. D. Ganji, "Simulation of Fe3O4-H2O nanoliquid in a triangular enclosure subjected to Cattaneo-Christov theory of heat conduction," *International Journal of Numerical Methods for Heat and Fluid Flow*, vol. 29, no. 11, pp. 4430–4444, 2019.

[15] S. M. Seyyedi, A. S. Dogonchi, M. Hashemi-Tilehnoee, D. D. Ganji, and A. J. Chamkha, "Second law analysis of magneto-natural convection in a nanofluid filled wavy-hexagonal porous enclosure," *International Journal of Numerical Methods for Heat and Fluid Flow*, vol. 30, no. 11, pp. 4811–4836, 2020.

[16] M. S. Sadeghi, T. Tayebi, A. S. Dogonchi, M. K. Nayak, and M. Waqas, "Analysis of thermal behavior of magnetic buoyancy-driven flow in ferrofluid-filled wavy enclosure furnished with two circular cylinders," *International Communications in Heat and Mass Transfer*, vol. 120, p. 104951, 2021.

[17] N. S. A. Ismail, A. S. Abd Aziz, M. R. Ilias, and S. K. Soid, "Mhd boundary layer flow in double stratification medium," *Journal of Physics: Conference Series IOP Publishing*, vol. 1770, no. 1, p. 12045, 2021.

[18] G. R. Rajput, B. P. Jadhav, and S. N. Salunkhe, "Magneto-hydrodynamics boundary layer flow and heat transfer in porous medium past an exponentially stretching sheet under the influence of radiation," *Heat Transfer*, vol. 49, no. 5, pp. 2906–2920, 2020.

[19] B. K. Swain, B. C. Parida, S. Kar, and N. Senapati, "Viscous dissipation and joule heating effect on mhd flow and heat transfer past a stretching sheet embedded in a porous medium," *Heliyon*, vol. 6, no. 10, p. e05338, 2020.

[20] N. N. Reddy, V. S. Rao, and B. R. Reddy, "Chemical reaction impact on mhd natural convection flow through porous medium past an exponentially stretching sheet in presence of heat source/sink and viscous dissipation," *Case Studies in Thermal Engineering*, vol. 25, p. 100879, 2021.

[21] R. N. Jat and G. Chand, "Mhd flow and heat transfer over an exponentially stretching sheet with viscous dissipation and radiation effects," *Applied Mathematical Sciences*, vol. 7, no. 4, pp. 167–180, 2013.

[22] M. Sajid and T. Hayat, "Influence of thermal radiation on the boundary layer flow due to an exponentially stretching sheet," *International Communications in Heat and Mass Transfer*, vol. 35, no. 3, pp. 347–356, 2008.

[23] A. Ishak, "Mhd boundary layer flow due to an exponentially stretching sheet with radiation effect," *Sains Malaysiana*, vol. 40, no. 4, pp. 391–395, 2011.

[24] M. Abd El-Aziz, "Viscous dissipation effect on mixed convection flow of a micropolar fluid over an exponentially stretching sheet," *Canadian Journal of Physics*, vol. 87, no. 4, pp. 359–368, 2009.

[25] O. D. Makinde, "Free convection flow with thermal radiation and mass transfer past a moving vertical porous plate," *International Communications in Heat and Mass Transfer*, vol. 32, no. 10, pp. 1411–1419, 2005.

[26] B. Shankar Goud, P. Srilatha, P. Bindu, and Y. Hari Krishna, "Radiation effect on mhd boundary layer flow due to an exponentially stretching sheet," *Advances in Mathematics: Scientific Journal*, vol. 9, no. 12, pp. 10755–10761, 2020.

[27] A. M. Spormann, "Unusual swimming behavior of a magnetotactic bacterium," *FEMS Microbiology Letters*, vol. 45, no. 1, pp. 37–45, 1987.

[28] A. Raees, H. Xu, and S.-J. Liao, "Unsteady mixed nano-bioconvection flow in a horizontal channel with its upper plate expanding or contracting," *International Journal of Heat and Mass Transfer*, vol. 86, pp. 174–182, 2015.

[29] S. Siddiqa, N. Gul-e-Hina, N. Begum, S. Saleem, and M. A. Reddy Gorla, "Numerical solutions of nanofluid bioconvection due to gyrotactic microorganisms along a vertical wavy cone," *International Journal of Heat and Mass Transfer*, vol. 101, pp. 608–613, 2016.

[30] A. Abbasi, F. Mabood, W. Farooq, and M. Batool, "Bioconvective flow of viscoelastic nanofluid over a convective rotating stretching disk," *International Communications in Heat and Mass Transfer*, vol. 119, p. 104921, 2020.

[31] Y.-M. Chu, M. I. Khan, N. B. Khan et al., "Significance of activation energy, bio-convection and magnetohydrodynamic in flow of third grade fluid (non-Newtonian) towards stretched surface: a buongiorno model analysis," *International Communications in Heat and Mass Transfer*, vol. 118, p. 104893, 2020.

[32] M. Ben Henda, H. Waqas, M. Hussain et al., "Applications of activation energy along with thermal and exponential space-based heat source in bioconvection assessment of magnetized third grade nanofluid over stretched cylinder/sheet," *Case Studies in Thermal Engineering*, vol. 26, p. 101043, 2021.

[33] S. A. Khan, H. Waqas, S. M. R. S. Naqvi, M. Alghamdi, and Q. Al-Mdallal, "Cattaneo-christov double diffusions theories with bio-convection in nanofluid flow to enhance the efficiency of nanoparticles diffusion," *Case Studies in Thermal Engineering*, vol. 26, p. 101017, 2021.

[34] B. Bidin and R. Nazar, "Numerical solution of the boundary layer flow over an exponentially stretching sheet with thermal radiation," *European Journal of Scientific Research*, vol. 33, no. 4, pp. 710–717, 2009.

Hindawi
Mathematical Problems in Engineering
Volume 2021, Article ID 2573067, 13 pages
https://doi.org/10.1155/2021/2573067

Research Article

A Novel Homotopy Perturbation Algorithm Using Laplace Transform for Conformable Partial Differential Equations

Sajad Iqbal,[1] **Mohammed K. A. Kaabar**,[2,3] **and Francisco Martínez**[4]

[1]*Department of Mathematics, Zhejiang University, Hangzhou 310027, China*
[2]*Gofa Camp, Near Gofa Industrial College and German Adebabay, Nifas Silk-Lafto 26649, Addis Ababa, Ethiopia*
[3]*Institute of Mathematical Sciences, Faculty of Science, University of Malaya, Kuala Lumpur 50603, Malaysia*
[4]*Department of Applied Mathematics and Statistics, Technological University of Cartagena, Cartagena 30203, Spain*

Correspondence should be addressed to Mohammed K. A. Kaabar; mohammed.kaabar@wsu.edu

Received 16 October 2021; Revised 22 November 2021; Accepted 26 November 2021; Published 14 December 2021

Academic Editor: Muhammad Shoaib Anwar

In this article, the approximate analytical solutions of four different types of conformable partial differential equations are investigated. First, the conformable Laplace transform homotopy perturbation method is reformulated. Then, the approximate analytical solution of four types of conformable partial differential equations is presented via the proposed technique. To check the accuracy of the proposed technique, the numerical and exact solutions are compared with each other. From this comparison, we conclude that the proposed technique is very efficient and easy to apply to various types of conformable partial differential equations.

1. Introduction

The initial idea of fractional derivative in history goes back to the late 17^{th} century, when the French mathematician L'Hopital concerned with the meaning of $(\mathrm{d}^n y/\mathrm{d}x^n)$, when $n = 1/2$. Since then, various definitions of this concept have been formulated from two conceptions: one of a global nature and the other one of a local nature. The global formulation of the fractional derivative is linked to the appearance of the fractional calculus itself, and the Caputo and Riemann–Liouville definitions are the best known [1, 2].

Khalil et al. suggested recently an alternative fractional derivative of local type, named as conformable derivative [3] to solve some issues concerning the challenge of solving fractional differential equations (F-DEs) of nonlocal type. The physical and geometrical interpretations of conformable derivatives have been discussed in [4, 5], respectively.

In several research studies, the methods of homotopy perturbation and Adomian decomposition have been employed to solve various types of F-DEs [6, 7]. Furthermore, a new numerical technique that is relied on the homotopy perturbation method (HPM) and Laplace transform (LT) has been proposed in [8] to solve F-DEs. Madani et al. employed the Laplace transform homotopy perturbation method (LTHPM) to solve one-dimensional in-homogeneous partial differential equations (PDEs) with a variable coefficient [9]. In [10], LTHPM is discussed to obtain the approximate analytical solution of space-fractional and time-fractional Burgers equations.

Fall et al. [11] implemented the homotopy perturbation method to obtain the analytical solution of time-fractional Black–Scholes (T-BSEs) and the generalized fractional BSEs. They have displayed both the solution graphically and discussed the effect of the order ρ of the generalized fractional BSEs in the diffusion processes.

In [12], Yavuz and Ozdemir proposed a novel definition of the Adomian decomposition method (ADM) to get an accurate and quick solution of T-FBSEs and generalized fractional BSEs utilizing initial condition. They obtained an approximate analytical solution to these equations.

Moreover, Ahmed and Elbadri [13] carried out the Sumudu decomposition method (SDM) coupled with the Adomian decomposition method to solve the fractional Newell-Whitehead-Segal equations (F-NWSEs). From their numerical results, they concluded that the proposed technique is straightforward to enforce and provide exact results.

For solving the Newell-Whitehead-Segal equations [14], the authors presented two alternative exponential finite difference methods: implicit exponential finite difference scheme and fully implicit exponential finite difference scheme. Both techniques are demonstrated to be consistent. Furthermore, the local truncation errors are accurate to the first order in time and the second order in space. The approaches described are more accurate than other methods because they are computationally consistent, stable, and convergent.

Yavuz et al. constructed the conformable ADM and HPM, using the aforementioned conformable derivatives to solve various F-DEs such as diffusion equation, Black–Scholes equation (BSEs), and cable equation [15, 16]. In [12], the authors proposed a novel definition of ADM to get an accurate and quick solution of the Black–Scholes equation of time-fractional order (F-BSEs) and the generalized Black–Scholes equation of fractional order (G-FBSEs) utilizing initial condition.

The main purpose of our study is to construct the Laplace transform homotopy perturbation method (LTHPM) for F-DEs using conformable derivatives.

The article is outlined as follows: some fundamental notions of conformable derivatives are revisited in Section 2. Subsequently, HPM is constructed using con-LT in Section 3. Finally, we apply in Section 4 the algorithm which is important to partial derivative equations (F-PDEs). The conclusion of this work is discussed in Section 5.

2. Basic Notions

This section presents some essential concepts of conformable derivatives, which will be necessary in our investigation.

Definition 1. Given $f\colon [0,\infty) \longrightarrow R$ as a function. Then, the α^{th} order conformable derivatives [1] is expressed as

$$\left(T_\alpha f\right)(t) = \lim_{\varepsilon \longrightarrow 0} \frac{f\left(t + \varepsilon t^{1-\alpha}\right) - f(t)}{\varepsilon}, \tag{1}$$

$\forall\, t > 0$, $\alpha \in (0,1]$. If f is α-differentiable (α-DifF) in some $(0,a)$, $a > 0$, and $\left(T_\alpha f\right)(t)$ exists, then it is expressed as

$$\left(T_\alpha f\right)(0) = \lim_{t \longrightarrow 0^+} \left(T_\alpha f\right)(t). \tag{2}$$

Theorem 1 (See [1]). *If a function $f\colon [0,\infty) \longrightarrow R$ is α-DifF at $t_0 > 0$, $\alpha \in (0,1]$, then f is continuous (ContF) at t_0.*

Theorem 2 (See [1]). *Suppose that $\alpha \in (0,1]$, and f, h are α-DifFs at a point $t > 0$. Then, we get*

(i) $T_\alpha(mf + wh) = m\,(T_\alpha f) + w\,(T_\alpha h)$, $\forall m, w \in R$
(ii) $T_\alpha(t^\nu) = \nu t^{\nu-\alpha}$, $\forall\, \nu \in R$
(iii) $T_\alpha(\vartheta) = 0$, $\forall$ *constant function* $f(t) = \vartheta$
(iv) $T_\alpha(fh) = f\,(T_\alpha h) + h\,(T_\alpha f)$
(v) $T_\alpha(f/h) = \left((h\,(T_\alpha f) - f\,(T_\alpha h))/h^2\right)$
(vi) If f is DifF, then $\left(T_\alpha f\right)(t) = t^{1-\alpha}(df/dt)(t)$

From the above definition, the conformable derivatives of some functions are expressed as

(i) $T_\alpha(1) = 0$
(ii) $T_\alpha(\sin\ (at)) = at^{1-\alpha}\cos(at)$
(iii) $T_\alpha(\cos\ (at)) = at^{1-\alpha}\sin(at)$
(iv) $T_\alpha(e^{at}) = ae^{at}$, $a \in R$

In addition, some helpful formulas are expressed as

(i) $T_\alpha((1/\alpha)t^\alpha) = 1$
(ii) $T_\alpha(e^{(1/\alpha)t^\alpha}) = e^{(1/\alpha)t^\alpha}$
(iii) $T_\alpha(\sin\ ((1/\alpha)t^\alpha)) = \cos((1/\alpha)t^\alpha)$
(iv) $T_\alpha(\cos\ ((1/\alpha)t^\alpha)) = -\sin((1/\alpha)t^\alpha)$

Definition 2. The left-conformable derivative beginning from a of function $f\colon [a,\infty) \longrightarrow R$ of order $\alpha \in (0,1]$ is expressed as [2]

$$\left(T_\alpha^a f\right)(t) = \lim_{\varepsilon \longrightarrow 0} \frac{f\left(t + \varepsilon(t-a)^{1-\alpha}\right) - f(t)}{\varepsilon}, \tag{3}$$

when $a = 0$, we have $\left(T_\alpha f\right)(t)$. If f is α-DifF in some (a,b), then we get

$$\left(T_\alpha^a f\right)(a) = \lim_{t \longrightarrow a^+} \left(T_\alpha^a f\right)(t). \tag{4}$$

Theorem 3 (Chain Rule) [2]. *Suppose that $f, h\colon (a,\infty) \longrightarrow R$ be left α-DifFs, where $\alpha \in (0,1]$. Assume that $s(t) = f(h(t))$. $s(t)$ is $\alpha - \text{Dif}\ F\ \forall t \neq a$ and $h(t) \neq 0$. Thus, we obtain*

$$\left(T_\alpha^a s\right)(t) = \left(T_\alpha^a f\right)(h(t)) \cdot \left(T_\alpha^a h\right)(t). \tag{5}$$

If $t = a$, then

$$\left(T_\alpha^a s\right)(a) = \lim_{t \longrightarrow a^+} \left(T_\alpha^a f\right)(h(t)) \cdot \left(T_\alpha^a h\right)(t) \cdot (h(t))^{\alpha-1}. \tag{6}$$

Theorem 4 (See [2]). *Supposed that f is infinitely α-DifF, for some $\alpha \in (0,1]$ at a neighborhood of a point t_0. Then, f has a conformable power series expansion as*

$$f(t) = \sum_{k=0}^{\infty} \frac{\left((k)T_\alpha^{t_0}\right)(t_0)}{\alpha^k k!}(t - t_0)^{k\alpha}, \quad t_0 < t < t_0 + R^{(1/\alpha)}. \tag{7}$$

Hence, $\left((k)T_\alpha^{t_0}\right)(t_0)$ implies the application of conformable derivatives k times.

The α-conformable integral of a function f is beginning from $a \geq 0$.

Definition 3 (See [1]). $I_\alpha^a(f)(t) = \int_a^t (f(x)/x^{1-\alpha}) \cdot \mathrm{d}x$, where this is a usual Riemann improper integral, $\alpha \in (0,1]$.

As a result, we have

Theorem 5. *$T_\alpha^a I_\alpha^a(f)(t) = f(t)$, for $t \geq a$, where f is any ContF in I_α^a's domain.*

Lemma 1. *Suppose that* $f\colon (a,b) \longrightarrow R$ *is DifF and* $\alpha \in (0,1]$. *Then,* $\forall\, a > 0$, *we get [2]*

$$I_\alpha^a T_\alpha^a (f)(t) = f(t) - f(a). \tag{8}$$

Finally, we recall the fractional Laplace transform (F-LT) [2]. In [3], a sufficient condition was accomplished to solve constant coefficient F-DEs via the con-LT method.

Definition 4. Suppose that $\alpha \in (0,1]$ and $f\colon [0,\infty) \longrightarrow R$ are real valued functions. Then, the F-LT of order α beginning from 0 of f is expressed as

$$L_\alpha[f(t)](s) = \int_0^\infty e^{-s(t^\alpha/\alpha)} f(t) \frac{\mathrm{d}t}{t^{1-\alpha}}. \tag{9}$$

Remark 1. The F-LT for the conformable derivatives is expressed as

$$L_\alpha[(T_\alpha f)(t)](s) = sL_\alpha[f(t)](s) - f(0). \tag{10}$$

Thus, we have

Theorem 6. *If* $F_\alpha(s) = L_\alpha[f(t)](s)$ *exists for* $s > 0$, *then*

(i) If c a constant, then

$$L_\alpha[c](s) = \frac{c}{s}. \tag{11}$$

(ii) Let q be a constant:

$$L_\alpha[t^q](s) = \alpha^{(q/\alpha)} \frac{\Gamma(1+(q/\alpha))}{s^{1+(q/\alpha)}}. \tag{12}$$

(iii) If c and q are arbitrary constants,

$$L_\alpha\left[t^q e^{c(t^\alpha/\alpha)}\right](s) = \alpha^{(q/\alpha)} \frac{\Gamma(1+(q/\alpha))}{(s-c)^{1+(q/\alpha)}}. \tag{13}$$

Definition 5. A function f is considered as a conformable exponentially bounded if it satisfies $|f(t)| \le Me^{c(t^\alpha/\alpha)}$, where M and c are the positive real constants and $\alpha \in (0,1]$, $\forall$ sufficiently large t.

3. Conformable Laplace Transform HPM

A conformable version of HPM using LT has been introduced by Madani and Fathizadeh in [17]. In their research work, these authors discuss the effectiveness and ease of this technique to solve ordinary or partial differential equations (PDEs). In our case, a con-PDEs is given as follows:

$$M_\alpha u(x,t) + Nu(x,t) + Ru(x,t) = g(x,t), \tag{14}$$

with the initial condition (I.C):

$$u(x,0) = f(x), \tag{15}$$

where u is the two variables function, $M_\alpha = (\partial^\alpha/\partial t^\alpha)$ is a linear operator (LO) with conformable derivative of order $\alpha \in (0,1]$, R is the LO's other part, N is a nonlinear operator (NLO), and $g(x,t)$ is a nonhomogeneous term. By solving for $M_\alpha u(x,t)$, equation (14) can be written as

$$M_\alpha u(x,t) = g - Nu - Ru. \tag{16}$$

By applying the con-LT to equation (16), we obtain

$$L_\alpha[M_\alpha u(x,t)] = L_\alpha[g - Nu - Ru]. \tag{17}$$

From Remark 1, the above equations can be rewritten as

$$sL_\alpha[u(x,t)](s) - u(x,0) = L_\alpha[g - Nu - Ru]. \tag{18}$$

By substituting I.C, equation (18) can be written as

$$L_\alpha[u(x,t)](s) = \frac{f(x)}{s} + \frac{1}{s}L_\alpha[g] - \frac{1}{s}L_\alpha[Nu] - \frac{1}{s}L_\alpha[Ru]. \tag{19}$$

Furthermore, by applying inverse con-LT to equation (19), we get

$$u(x,t) = G(x,t) - L_\alpha^{-1}\left[\frac{1}{s}L_\alpha[Nu(x,t) + Ru(x,t)]\right], \tag{20}$$

where the term has been arisen from the source term, and the prescribed I.C is denoted by $G(x,t)$.

The HPM suggests the solution $u(x,t)$ to be decomposed into the infinite series of components [18, 19]:

$$u(x,t) = \sum_{n=0}^\infty p^n u_n(x,t), \tag{21}$$

and nonlinear term $Nu(x,t)$ is decomposed to

$$Nu(x,t) = \sum_{n=0}^\infty p^n H_n(u), \tag{22}$$

for some He's polynomials $H_n(u)$ [17, 20] which are given by

$$H_n(u_0,u_1,\ldots,u_n) = \frac{1}{n!}\frac{\partial^n}{\partial p^n}\left[N\left(\sum_{i=0}^\infty p^i u_i\right)\right], \quad n = 0,1,2,3,\ldots. \tag{23}$$

By the substitution of equations (21) and (22) into equation (20), we have

$$\sum_{n=0}^\infty p^n u_n(x,t) = G(x,t) - p\left(L_\alpha^{-1}\left[\frac{1}{s}L_\alpha\left[R\sum_{n=0}^\infty p^n u_n(x,t) + \sum_{n=0}^\infty p^n H_n(u)\right]\right]\right), \tag{24}$$

which is the coupled con-FLT and HPM via He's polynomials. The approximation can be easily obtained by a comparison of all coefficients like powers of p as follows:

$$\begin{aligned}
&p^0 : u_0(x,t) = G(x,t),\\
&p^1 : u_1(x,t) = -L_\alpha^{-1}\left[\frac{1}{s}L_\alpha\left[Ru_0(x,t) + H_0(u)\right]\right],\\
&p^2 : u_2(x,t) = -L_\alpha^{-1}\left[\frac{1}{s}L_\alpha\left[Ru_1(x,t) + H_1(u)\right]\right],\\
&p^3 : u_1(x,t) = -L_\alpha^{-1}\left[\frac{1}{s}L_\alpha\left[Ru_2(x,t) + H_2(u)\right]\right],\\
&\quad\vdots .
\end{aligned} \tag{25}$$

4. Illustrative Examples

The effectiveness of the con-LTHPM is shown in this section through four different problems: the time-fractional nonlinear homogeneous gas dynamics equation (F-GDEs), the time-fractional linear Newell-Whitehead-Segel equation (F-NWSEs), the time-fractional diffusion-convection equation (F-DCEs), and the time-fractional linear Black–Scholes option pricing equation.

Example 1. Consider F-GDEs as follows:

$$\frac{\partial^\alpha v(x,t)}{\partial t^\alpha} + v(x,t)\frac{\partial v(x,t)}{\partial x} - v(x,t)(1 - v(x,t)) = 0, \quad t \geq 0, 0 \leq x \leq 1, 0 < \alpha \leq 1, \tag{26}$$

with I.C: $v(x,0) = ae^{-x}$. If $\alpha = 1$, then equation (26) becomes the classical nonlinear homogeneous GDEs [21].

Remark 2. Note that the mathematical expression of the classical GDEs is based on the physical laws of conservation.

By taking con-LT on equation (26) both sides and from the properties of con-LT, equation (26) reduces to

$$L_\alpha[v(x,t)](s) = \frac{v(x,0)}{s} + \frac{1}{s}L_\alpha\left[v - v^2 - v\frac{\partial v}{\partial x}\right]. \tag{27}$$

Using I.C and inverse con-LT, equation (27) reduces to

$$v(x,t) = ae^{-x} + L_\alpha^{-1}\left[\frac{1}{s}L_\alpha\left[v - v^2 - v\frac{\partial v}{\partial x}\right]\right]. \tag{28}$$

The HPM is applied to obtain

$$\sum_{n=0}^{\infty} p^n v_n(x,t) = ae^{-x} + p\left(L_\alpha^{-1}\left[\frac{1}{s}L_\alpha\left[\sum_{n=0}^{\infty} p^n v_n(x,t) - \sum_{n=0}^{\infty} p^n H_n(v)\right]\right]\right), \tag{29}$$

where $H_n(v)$ represents He's polynomials.

The 1st three parts of $H_n(v)$ are

$$\begin{aligned}
H_0(v) &= v_0^2 + v_0\frac{\partial v_0}{\partial x},\\
H_1(v) &= 2v_0v_1 + v_0\frac{\partial v_1}{\partial x} + v_1\frac{\partial v_0}{\partial x},\\
H_2(v) &= 2v_0v_2 + v_0\frac{\partial v_2}{\partial x} + v_1\frac{\partial v_1}{\partial x} + v_2\frac{\partial v_0}{\partial x} + v_1^2,
\end{aligned} \tag{30}$$

and so on.

The coefficient of power of p is equated in equation (33) to get

$$
\begin{aligned}
&p^0 : v_0(x,t) = ae^{-x},\\
&p^1 : v_1(x,t) = L_\alpha^{-1}\left[\frac{1}{s}L_\alpha\left[v_0 - H_0(v)\right]\right] = L_\alpha^{-1}\left[\frac{1}{s}L_\alpha\left[v_0 - v_0^2 - v_0\frac{\partial v_0}{\partial x}\right]\right] = ae^{-x}\frac{t^\alpha}{\alpha},\\
&p^2 : v_2(x,t) = L_\alpha^{-1}\left[\frac{1}{s}L_\alpha\left[v_1 - H_1(v)\right]\right] = L_\alpha^{-1}\left[\frac{1}{s}L_\alpha\left[v_1 - 2v_0v_1 - v_0\frac{\partial v_1}{\partial x} - v_1\frac{\partial v_0}{\partial x}\right]\right] = ae^{-x}\frac{1}{2!}\left(\frac{t^\alpha}{\alpha}\right)^2,\\
&p^3 : v_3(x,t) = L_\alpha^{-1}\left[\frac{1}{s}L_\alpha\left[v_2 - H_2(v)\right]\right] = L_\alpha^{-1}\left[\frac{1}{s}L_\alpha\left[v_1 - 2v_0v_2 - v_0\frac{\partial v_2}{\partial x} - v_1\frac{\partial v_1}{\partial x} - v_2\frac{\partial v_0}{\partial x} + v_1^2\right]\right] = ae^{-x}\frac{1}{3!}\left(\frac{t^\alpha}{\alpha}\right)^3.
\end{aligned}
\tag{31}
$$

Similarly, the approximations can further be obtained as follows:

and so on.

Substitute the above values in the following equation:

$$
\begin{aligned}
&p^4 : v_4(x,t) = ae^{-x}\frac{1}{4!}\left(\frac{t^\alpha}{\alpha}\right)^4,\\
&p^5 : v_5(x,t) = ae^{-x}\frac{1}{5!}\left(\frac{t^\alpha}{\alpha}\right)^5,
\end{aligned}
\tag{32}
$$

$$
\begin{aligned}
v(x,t) &= v_0(x,t) + v_1(x,t) + v_2(x,t) + v_3(x,t) + \cdots\\
&= a\left(e^{-x} + e^{-x}\frac{t^\alpha}{\alpha} + e^{-x}\frac{1}{2!}\left(\frac{t^\alpha}{\alpha}\right)^2 + e^{-x}\frac{1}{3!}\left(\frac{t^\alpha}{\alpha}\right)^3 + e^{-x}\frac{1}{4!}\left(\frac{t^\alpha}{\alpha}\right)^4 + \cdots\right)\\
&= ae^{-x}\left(1 + \frac{t^\alpha}{\alpha} + \frac{1}{2!}\left(\frac{t^\alpha}{\alpha}\right)^2 + \frac{1}{3!}\left(\frac{t^\alpha}{\alpha}\right)^3 + \frac{1}{4!}\left(\frac{t^\alpha}{\alpha}\right)^4 + \frac{1}{5!}\left(\frac{t^\alpha}{\alpha}\right)^5 + \cdots\right)\\
&= ae^{(t^\alpha/\alpha)-x}.
\end{aligned}
\tag{33}
$$

The equation (26) exact solution with I.C: $v(x,0) = ae^{-x}$ for $\alpha = 1$ as a special case is found as follows:

$$v(x,t) = ae^{t-x}, \tag{34}$$

which is the same solution in [21]. This result is verified graphically in Figure 1.

In Figure 2, the con-LTHPM's solution for various values of α, i.e., $\alpha = 0.7, 0.9$ is represented. The F-GDEs is considered here with parameter $a = 1$.

Example 2. Consider F-NWSEs as follows:

$$\frac{\partial^\alpha v(x,t)}{\partial t^\alpha} = \frac{\partial^2 v(x,t)}{\partial x^2} - 3v(x,t), \tag{35}$$

with I.C: $v(x,0) = e^{2x}$. If $\alpha = 1$, then equation (35) becomes an example of the classical linear NWSEs [22].

Remark 3. This equation has been applied in a wide variety of problems. For example, Faraday instability, nonlinear optics, Rayleigh-Bernard convection, or chemical reactions.

By taking con-LT on equation (45) both sides and from the properties of con-LT, equation (35) reduces to

$$L_\alpha[v(x,t)](s) = \frac{v(x,0)}{s+3} + \frac{1}{s+3}L_\alpha\left[\frac{\partial^2 v(x,t)}{\partial x^2}\right]. \tag{36}$$

Using I.C and inverse con-LT, equation (36) reduces to

$$v(x,t) = e^{2x-3(t^\alpha/\alpha)} + L_\alpha^{-1}\left[\frac{1}{s+3}L_\alpha\left[\frac{\partial^2 v(x,t)}{\partial x^2}\right]\right]. \quad (37)$$

The HPM is applied to obtain

$$\sum_{n=0}^{\infty} p^n v_n(x,t) = e^{2x-3(t^\alpha/\alpha)} + p\left(L_\alpha^{-1}\left[\frac{1}{s+3}L_\alpha\left[\sum_{n=0}^{\infty} p^n \frac{\partial^2 v_n(x,t)}{\partial x^2}\right]\right]\right). \quad (38)$$

The coefficients of the power of p are compared as follows:

$$\begin{aligned}
p^0 &: v_0(x,t) = e^{2x-3(t^\alpha/\alpha)},\\
p^1 &: v_1(x,t) = L_\alpha^{-1}\left[\frac{1}{s+3}L_\alpha\left[\frac{\partial^2 v_0(x,t)}{\partial x^2}\right]\right] = 4\frac{t^\alpha}{\alpha}e^{2x-3(t^\alpha/\alpha)},\\
p^2 &: v_2(x,t) = L_\alpha^{-1}\left[\frac{1}{s+3}L_\alpha\left[\frac{\partial^2 v_1(x,t)}{\partial x^2}\right]\right] = 16\frac{1}{2!}\left(\frac{t^\alpha}{\alpha}\right)^2 e^{2x-3(t^\alpha/\alpha)},\\
p^3 &: v_3(x,t) = L_\alpha^{-1}\left[\frac{1}{s+3}L_\alpha\left[\frac{\partial^2 v_2(x,t)}{\partial x^2}\right]\right] = 64\frac{1}{3!}\left(\frac{t^\alpha}{\alpha}\right)^3 e^{2x-3(t^\alpha/\alpha)}.
\end{aligned} \quad (39)$$

Similarly, approximations can further be obtained as follows:

$$\begin{aligned}
p^4 &: v_4(x,t) = 256\frac{1}{4!}\left(\frac{t^\alpha}{\alpha}\right)^4 e^{2x-3(t^\alpha/\alpha)},\\
p^5 &: v_5(x,t) = 512\frac{1}{5!}\left(\frac{t^\alpha}{\alpha}\right)^5 e^{2x-3(t^\alpha/\alpha)},
\end{aligned} \quad (40)$$

and so on.

Substitute the above values into the following equation:

$$\begin{aligned}
v(x,t) &= v_0(x,t) + v_1(x,t) + v_2(x,t) + v_3(x,t) + \cdots\\
&= e^{2x-3(t^\alpha/\alpha)} + e^{2x-3(t^\alpha/\alpha)}\frac{4t^\alpha}{\alpha} + e^{2x-3(t^\alpha/\alpha)}\frac{1}{2!}\left(\frac{4t^\alpha}{\alpha}\right)^2 + e^{2x-3(t^\alpha/\alpha)}\frac{1}{3!}\left(\frac{4t^\alpha}{\alpha}\right)^3 + e^{2x-3(t^\alpha/\alpha)}\frac{1}{4!}\left(\frac{4t^\alpha}{\alpha}\right)^4 + \cdots\\
&= e^{2x-3(t^\alpha/\alpha)}\left(1 + \frac{4t^\alpha}{\alpha} + \frac{1}{2!}\left(\frac{4t^\alpha}{\alpha}\right)^2 + \frac{1}{3!}\left(\frac{4t^\alpha}{\alpha}\right)^3 + \frac{1}{4!}\left(\frac{4t^\alpha}{\alpha}\right)^4 + \frac{1}{5!}\left(\frac{4t^\alpha}{\alpha}\right)^5 + \cdots\right) = e^{2x+3(t^\alpha/\alpha)}.
\end{aligned} \quad (41)$$

The equation (35) exact solution with $I\,v(x,0) = e^{2x}$, for $\alpha = 1$ as a special case, is found as follows:

$$v(x,t) = e^{2x+t}, \quad (42)$$

which is the same solution in [22]. This result is verified graphically, as shown in Figure 3.

In Figure 4, the con-LTHPM's solution for various values of α, i.e., $\alpha = 0.7, 0.9$ is represented.

Example 3. Consider F-DCEs as follows:

$$\frac{\partial^{\alpha} v(x,t)}{\partial t^{\alpha}} = \frac{\partial^2 v(x,t)}{\partial x^2} + \left(\cos x - \sin^2 x - 1\right) v(x,t), \quad (43)$$

with I.C: $v(x,0) = (1/10)e^{\cos x - 11}$. If $\alpha = 1$, then equation (43) becomes an example of the classical DCEs [23].

Remark 4. The DCEs describe physical phenomena where particles, energy, or other physical quantities are transferred inside a physical system due to two processes: diffusion and convection.

By taking con-LT on equation (43) both sides and from the properties of con-LT, equation (43) reduces to

$$L_{\alpha}[v(x,t)](s) = \frac{v(x,0)}{s} + \frac{1}{s} L_{\alpha}\left[\frac{\partial^2 v(x,t)}{\partial x^2} + \left(\cos x - \sin^2 x - 1\right) v(x,t)\right]. \quad (44)$$

Using I.C and inverse con-LT, equation (44) reduces to

$$v(x,t) = \frac{1}{10} e^{\cos x - 11} + L_{\alpha}^{-1}\left[\frac{1}{s} L_{\alpha}\left[\frac{\partial^2 v(x,t)}{\partial x^2} + \left(\cos x - \sin^2 x - 1\right) v(x,t)\right]\right]. \quad (45)$$

The HPM is applied to obtain

$$\sum_{n=0}^{\infty} p^n v_n(x,t) = \frac{1}{10} e^{\cos x - 11} + p\left(L_{\alpha}^{-1}\left[\frac{1}{s} L_{\alpha}\left[\sum_{n=0}^{\infty} p^n \frac{\partial^2 v_n(x,t)}{\partial x^2} + \left(\cos x - \sin^2 x - 1\right) \sum_{n=0}^{\infty} p^n v_n(x,t)\right]\right]\right). \quad (46)$$

The coefficients of the power of p are compared here as follows:

$$\begin{aligned}
p^0 &: v_0(x,t) = \frac{1}{10} e^{\cos x - 11},\\
p^1 &: v_1(x,t) = L_{\alpha}^{-1}\left[\frac{1}{s} L_{\alpha}\left[\frac{\partial^2 v_0(x,t)}{\partial x^2} + \left(cos\ x - \sin^2 x - 1\right) v_0(x,t)\right]\right] = -\frac{1}{10} e^{\cos x - 11} \frac{t^{\alpha}}{\alpha},\\
p^2 &: v_2(x,t) = L_{\alpha}^{-1}\left[\frac{1}{s} L_{\alpha}\left[\frac{\partial^2 v_1(x,t)}{\partial x^2} + \left(\cos x - \sin^2 x - 1\right) v_1(x,t)\right]\right] = \frac{1}{10} e^{\cos x - 11} \frac{1}{2!}\left(\frac{t^{\alpha}}{\alpha}\right)^2,\\
p^3 &: v_3(x,t) = L_{\alpha}^{-1}\left[\frac{1}{s} L_{\alpha}\left[\frac{\partial^2 v_2(x,t)}{\partial x^2} + \left(\cos x - \sin^2 x - 1\right) v_2(x,t)\right]\right] = -\frac{1}{10} e^{\cos x - 11} \frac{1}{3!}\left(\frac{t^{\alpha}}{\alpha}\right)^3.
\end{aligned} \quad (47)$$

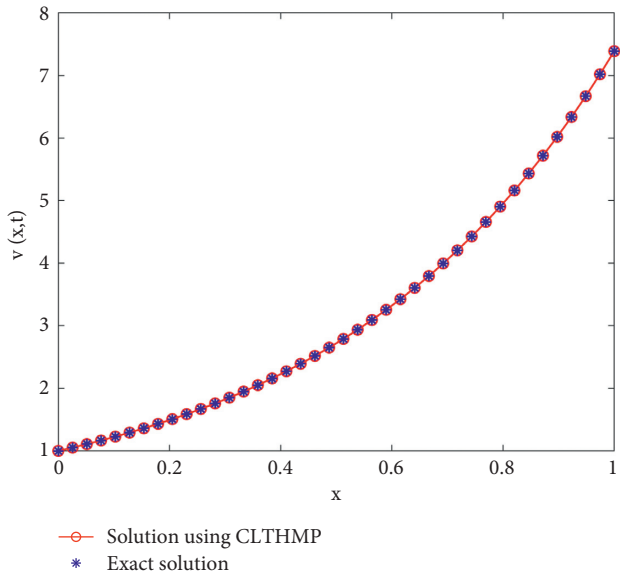

Figure 1: Comparison of the numerical solution and exact solution for $\alpha = 1$.

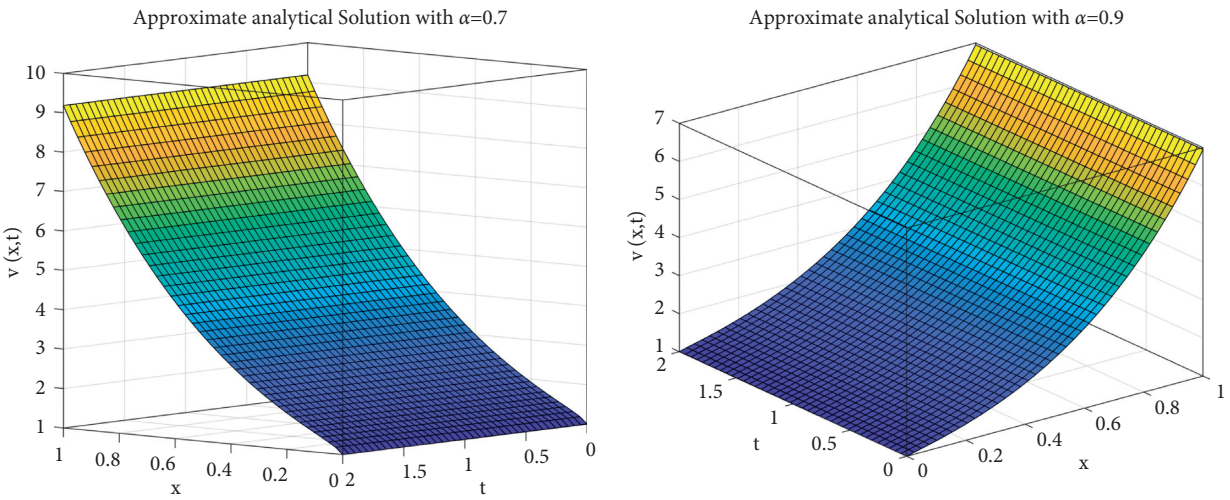

Figure 2: Con-LTHPM's solutions of the F-GDEs.

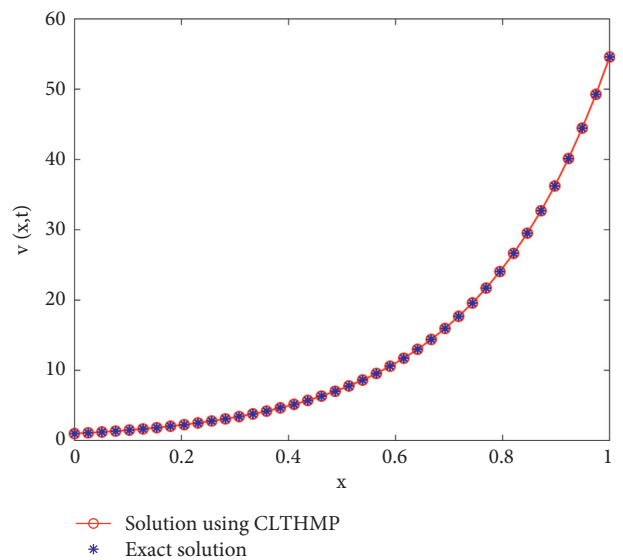

Figure 3: Comparison of the numerical solution and exact solution for $\alpha = 1$.

Similarly, approximations can further be obtained as follows:

$$p^4\colon v_4(x,t) = \frac{1}{10}e^{\cos x-11}\frac{1}{4!}\left(\frac{t^\alpha}{\alpha}\right)^4,$$
$$p^5\colon v_5(x,t) = -\frac{1}{10}e^{\cos x-11}\frac{1}{5!}\left(\frac{t^\alpha}{\alpha}\right)^5, \tag{48}$$

and so on.

Substitute the above values in the following equation:

$$\begin{aligned} v(x,t) &= v_0(x,t) + v_1(x,t) + v_2(x,t) + v_3(x,t) + \cdots \\ &= \frac{1}{10}e^{\cos x-11}\left(1 - \frac{t^\alpha}{\alpha} + \frac{1}{2!}\left(\frac{t^\alpha}{\alpha}\right)^2 - \frac{1}{3!}\left(\frac{t^\alpha}{\alpha}\right)^3 + \frac{1}{4!}\left(\frac{t^\alpha}{\alpha}\right)^4 - \frac{1}{5!}\left(\frac{t^\alpha}{\alpha}\right)^5 + \cdots\right) = \frac{1}{10}e^{\cos x-11-(t^\alpha/\alpha)}. \end{aligned} \tag{49}$$

The equation (43) exact solution with I.C: $v(x,0) = (1/10)e^{\cos x-11}$, for $\alpha = 1$ as a special case, is found as follows:

$$v(x,t) = \frac{1}{10}e^{\cos x-11-t}, \tag{50}$$

which is the same solution with [23]. This result is also verified graphically, as shown in Figure 5.

In Figure 6, the con-LTHPM's solution for various values of α, i.e., $\alpha = 0.7, 0.9$ is represented.

Example 4. Consider the F-BSEs:

$$\frac{\partial^\alpha v(x,t)}{\partial t^\alpha} = \frac{\partial^2 v(x,t)}{\partial x^2} + (k-1)\frac{\partial v(x,t)}{\partial x} - kv(x,t), \quad t > 0, x \in R, 0 < \alpha \le 1, \tag{51}$$

with I.C: $v(x,0) = \max\{e^x - 1, 0\}$. If $\alpha = 1$, then equation (51) becomes the classical linear BSEs [24].

Remark 5. Equation (51) contains only two dimensionless parameters $k = (2r/\sigma^2)$, where k represents the balance between the rates of interest and the variability of the return on stocks and the dimensionless time to expiry $(\sigma^2 T/2)$.

By taking con-LT on equation (51) both sides and from the properties of con-LT, equation (51) reduces to

$$L_\alpha[v(x,t)](s) = \frac{v(x,0)}{s+k} + \frac{1}{s+k}L_\alpha\left[\frac{\partial^2 v(x,t)}{\partial x^2} + (k-1)\frac{\partial v(x,t)}{\partial x}\right]. \tag{52}$$

Using I.C and inverse con-LT, equation (52) reduces to

$$v(x,t) = \max\{e^x - 1, 0\}\, e^{-k(t^\alpha/\alpha)} + L_\alpha^{-1}\left[\frac{1}{s+k}L_\alpha\left[\frac{\partial^2 v(x,t)}{\partial x^2} + (k-1)\frac{\partial v(x,t)}{\partial x}\right]\right]. \tag{53}$$

The HPM is applied to obtain

$$\sum_{n=0}^{\infty} p^n v_n(x,t) = \max\{e^x - 1, 0\}\, e^{-k(t^\alpha/\alpha)} + p\left(L_\alpha^{-1}\left[\frac{1}{s+k}L_\alpha\left[\sum_{n=0}^{\infty} p^n \frac{\partial^2 v_n(x,t)}{\partial x^2} + (k-1)\sum_{n=0}^{\infty} p^n \frac{\partial v_n(x,t)}{\partial x}\right]\right]\right). \tag{54}$$

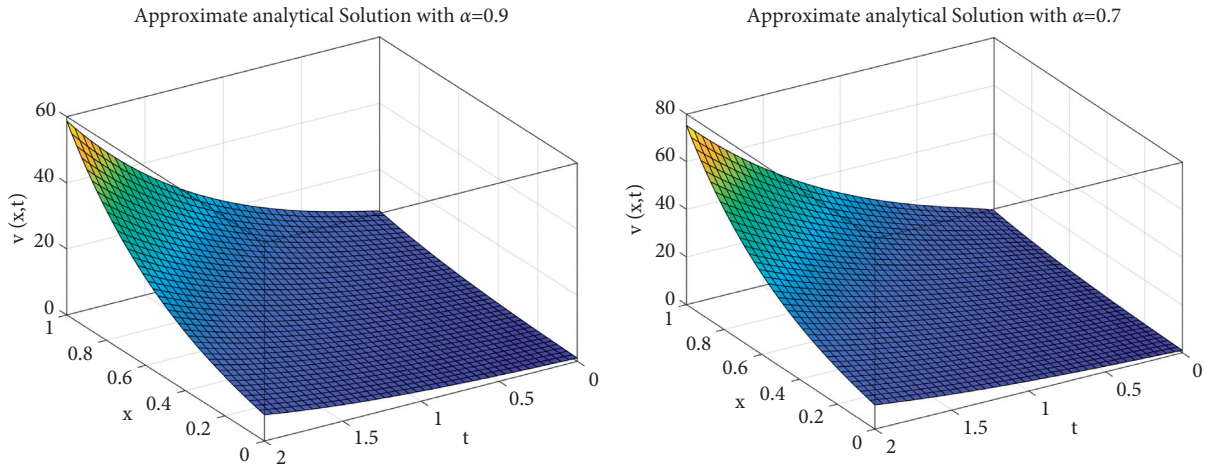

Figure 4: Con-LTHPM's solutions of the F-NWSEs.

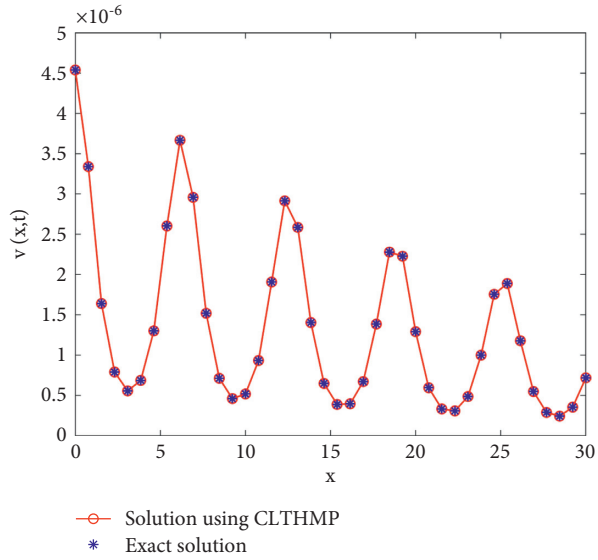

Figure 5: Comparison of the numerical solution and exact solution for $\alpha = 1$.

The coefficients of the power of p are compared to get

$$
\begin{aligned}
p^0 &: v_0(x,t) = \max\{e^x - 1, 0\}\, e^{-k(t^\alpha/\alpha)}, \\
p^1 &: v_1(x,t) = L_\alpha^{-1}\left[\frac{1}{s+k}L_\alpha\left[\frac{\partial^2 v_0(x,t)}{\partial x^2} + (k-1)\frac{\partial v_0(x,t)}{\partial x}\right]\right] = \frac{kt^\alpha}{\alpha}e^{x-k(t^\alpha/\alpha)}, \\
p^2 &: v_2(x,t) = L_\alpha^{-1}\left[\frac{1}{s+k}L_\alpha\left[\frac{\partial^2 v_1(x,t)}{\partial x^2} + (k-1)\frac{\partial v_1(x,t)}{\partial x}\right]\right] = \frac{1}{2!}\left(\frac{Kt^\alpha}{\alpha}\right)^2 e^{x-k(t^\alpha/\alpha)}, \\
p^3 &: v_3(x,t) = L_\alpha^{-1}\left[\frac{1}{s+k}L_\alpha\left[\frac{\partial^2 v_2(x,t)}{\partial x^2} + (k-1)\frac{\partial v_2(x,t)}{\partial x}\right]\right] = \frac{1}{3!}\left(\frac{kt^\alpha}{\alpha}\right)^3 e^{x-k(t^\alpha/\alpha)}.
\end{aligned}
\tag{55}
$$

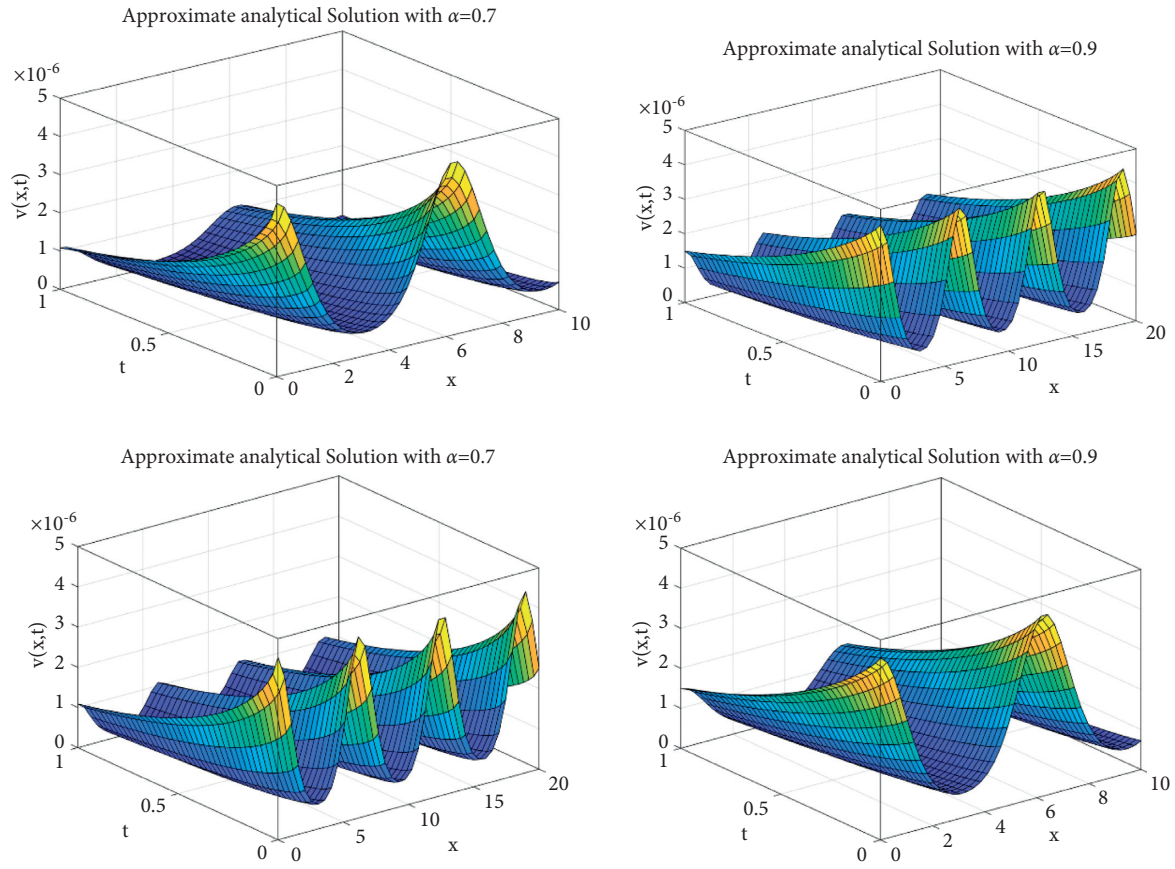

Figure 6: Con-LTHPM's solutions of the F-DCEs.

Similarly, approximations can further be obtained as follows:

$$p^4:\ v_4(x,t) = \frac{1}{4!}\left(\frac{kt^\alpha}{\alpha}\right)^4 e^{x-k(t^\alpha/\alpha)},$$
$$p^5:\ v_5(x,t) = \frac{1}{5!}\left(\frac{kt^\alpha}{\alpha}\right)^5 e^{x-k(t^\alpha/\alpha)}, \tag{56}$$

and so on.

Substitute the above values in the following equation:

$$\begin{aligned} v(x,t) &= v_0(x,t) + v_1(x,t) + v_2(x,t) + v_3(x,t) + \cdots \\ &= \max\{e^x - 1, 0\}\, e^{-k(t^\alpha/\alpha)} + e^{x-k(t^\alpha/\alpha)}\left(\frac{kt^\alpha}{\alpha} + \frac{1}{2!}\left(\frac{kt^\alpha}{\alpha}\right)^2 + \frac{1}{3!}\left(\frac{kt^\alpha}{\alpha}\right)^3 + \frac{1}{4!}\left(\frac{kt^\alpha}{\alpha}\right)^4 + \cdots\right) \\ &= \max\{e^x - 1, 0\}\, e^{-k(t^\alpha/\alpha)} + e^x\left(1 - e^{-k(t^\alpha/\alpha)}\right). \end{aligned} \tag{57}$$

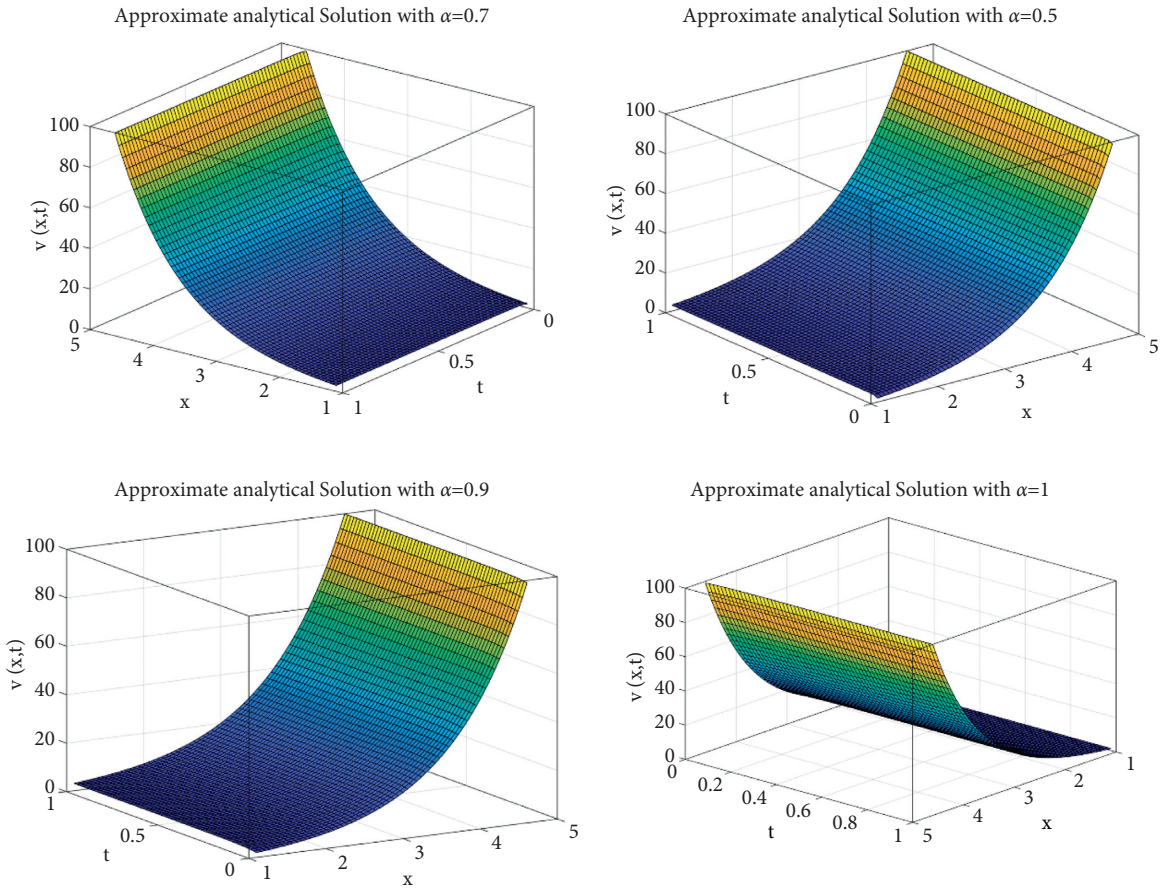

Figure 7: Con-LTHPM's solutions of the F-BSEs.

The equation (35) exact solution with I.C: $v(x,0) = \{e^x - 1, 0\}$, for $\alpha = 1$ as a special case, is found as follows:

$$v(x,t) = \{e^x - 1, 0\}\, e^{-kt} + e^x\left(1 - e^{-kt}\right), \tag{58}$$

which is the same solution in [24].

In Figure 7, the con-LTHPM's solution for various values of α, i.e., $\alpha = 0.5, 0.7, 0.9, 1$ is represented. In this example, F-BSEs is considered for $0 < \alpha \leq 1$.

5. Conclusion

The approximate analytical solutions have been obtained in this work for time F-PDEs, using a numerical method based on the con derivatives, a concept widely used in the field of applications in recent years. We have constructed a con-version of the HPM via LT. This technique's efficiency and approximation have been verified through four important problems. From the illustrative examples, the results using this technique coincide the corresponding exact solution. As a result, our technique can be applicable to many initial-value problems and F-PDEs including linear and nonlinear ones. In fact, future research will focus on studying this conformable methodology of important classic problems such as the in-homogeneous fractional cable equation, the Burgers equation with fractional order of space and time, or the in-homogeneous nonlinear Klein–Gordon equation.

Data Availability

No data were used to support this study.

Conflicts of Interest

The authors declare that they have no conflicts of interest.

Authors' Contributions

Sajad Iqbal involved in actualization, methodology, formal analysis, validation, investigation, and initial draft. Mohammed K. A. Kaabar involved in actualization, methodology, formal analysis, validation, investigation, initial draft, and supervision of the original draft and editing. Francisco Martínez involved in actualization, validation, methodology, formal analysis, investigation, and initial draft. All authors read and approved the final version.

References

[1] A. Kilbas, H. Srivastava, and J. Trujillo, *Theory and Applications of Fractional Differential Equations*, North-Holland, Amsterdam, Netherlands, 2006.

[2] K. S. Miller, *An Introduction to Fractional Calculus and Fractional Differential Equations*, J. Wiley and Sons, Hoboken, NJ, USA, 1993.

[3] R. Khalil, M. Al Horani, A. Yousef, and M. Sababheh, "A new definition of fractional derivative," *Journal of Computational and Applied Mathematics*, vol. 264, pp. 65–70, 2014.

[4] D. Zhao and M. Luo, "General conformable fractional derivative and its physical interpretation," *Calcolo*, vol. 54, no. 3, pp. 903–917, 2017.

[5] R. Khalil, M. Al Horani, and M. Abu Hammad, "Geometric meaning of conformable derivative via fractional cords," *Journal of Mathematics and Computer Science*, vol. 19, no. 4, pp. 241–245, 2019.

[6] N. Bildik and H. Bayramoglu, "The solution of two dimensional nonlinear differential equations by the adomian decomposition method," *Applied Mathematics and Computation*, vol. 163, no. 2, pp. 519–524, 2005.

[7] N. Bildik, A. Konuralp, F. O. Bek, and S. Küçükarslan, "Solution of different type of the partial differential equation by differential transform method and adomian's decomposition method," *Applied Mathematics and Computation*, vol. 172, no. 1, pp. 551–567, 2006.

[8] M. Javidi and B. Ahmad, "Numerical solution of fractional partial differential equations by numerical laplace inversion technique," *Advances in Difference Equations*, vol. 2013, no. 1, 375 pages, 2013.

[9] M. Madani, M. Fathizadeh, Y. Khan, and A. Yildirim, "On the coupling of the homotopy perturbation method and laplace transformation," *Mathematical and Computer Modelling*, vol. 53, no. 9, pp. 1937–1945, 2011.

[10] S. J. Johnston, H. Jafari, S. P. Moshokoa, V. M. Ariyan, and D. Baleanu, "Laplace homotopy perturbation method for burgers equation with space-and time-fractional order," *Open Physics*, vol. 14, no. 1, pp. 247–252, 2016.

[11] A. N. Fall, S. N. Ndiaye, and N. Sene, "Black–scholes option pricing equations described by the caputo generalized fractional derivative," *Chaos, Solitons & Fractals*, vol. 125, pp. 108–118, 2019.

[12] M. Yavuz and N. Özdemir, "A quantitative approach to fractional option pricing problems with decomposition series," *Konuralp Journal of Mathematics*, vol. 6, no. 1, pp. 102–109, 2018.

[13] S. A. Ahmed and M. Elbadri, "Solution of newell-whitehead-segal equation of fractional order by using sumudu decomposition method," *Mathematics and Statistics*, vol. 8, no. 6, pp. 631–636, 2020.

[14] N. Hilal, S. Injrou, and R. Karroum, "Exponential finite difference methods for solving Newell-Whitehead-Segel equation," *Arabian Journal of Mathematics*, vol. 9, no. 2, pp. 367–379, 2020.

[15] M. Yavuz and N. Ozdemir, "A different approach to the European option pricing model with fractional operator," *Mathematical Modelling of Natural Phenomena*, vol. 13, pp. 1–12, 2018.

[16] M. Yavuz, "Novel solution methods for initial boundary value problems of fractional order with conformable differentiation," *An International Journal of Optimization and Control*, vol. 8, no. 1, pp. 1–7, 2018.

[17] M. Madani and M. Fathizadeh, "Homotopy perturbation algorithm using laplace transformation," *Nonlinear Science Letters A*, vol. 1, pp. 263–267, 2010.

[18] Y. Khan and Q. Wu, "Homotopy perturbation transform method for nonlinear equations using he's polynomials," *Computers & Mathematics with Applications*, vol. 61, no. 8, pp. 1963–1967, 2011.

[19] S. T. Mohyud-Din and A. Yildirim, "Homotopy perturbation method for advection problems," *Nonlinear Science Letters A*, vol. 1, pp. 307–312, 2010.

[20] S. T. Mohyud-Din, M. A. Noor, and K. I. Noor, "Traveling wave solutions of seventh-order generalized KdV equation using he's polynomials," *International Journal of Nonlinear Sciences and Numerical Simulation*, vol. 10, no. 2, pp. 227–233, 2009.

[21] P. Kiran, G. Badhane, and V. H. Pradhan, "Application of Laplace transform homotopy perturbation method to gas dynamic equation: a modified approach," *International Journal of Research in Engineering and Technology*, vol. 5, no. 5, pp. 409–411, 2016.

[22] H. K. Jassim, "Homotopy perturbation algorithm using laplace transform for newell-witehead-segel equation," *International Journal of Applied Mathematics and Mechanics*, vol. 2, no. 4, pp. 8–12, 2015.

[23] S. Gupta, D. Kumar, and J. Singh, "Analytical solutions of convection-diffusion problems by combining laplace transform method and homotopy perturbation method," *Alexandria Engineering Journal*, vol. 54, no. 3, pp. 645–651, 2015.

[24] F. Black and M. Scholes, "The pricing of options and corporate liabilities," *Journal of Political Economy*, vol. 81, no. 3, pp. 637–654, 1973.

Hindawi
Mathematical Problems in Engineering
Volume 2021, Article ID 8608447, 7 pages
https://doi.org/10.1155/2021/8608447

Research Article

Stability of Fractional Differential Equations with New Generalized Hattaf Fractional Derivative

Khalid Hattaf

Centre Régional des Métiers de l'Education et de la Formation (CRMEF), 20340 Derb Ghalef, Casablanca, Morocco

Correspondence should be addressed to Khalid Hattaf; k.hattaf@yahoo.fr

Received 2 November 2021; Revised 19 November 2021; Accepted 20 November 2021; Published 2 December 2021

Academic Editor: Muhammad Shoaib Anwar

This paper aims to study the stability of fractional differential equations involving the new generalized Hattaf fractional derivative which includes the most types of fractional derivatives with nonsingular kernels. The stability analysis is obtained by means of the Lyapunov direct method. First, some fundamental results and lemmas are established in order to achieve the goal of this study. Furthermore, the results related to exponential and Mittag–Leffler stability existing in recent studies are extended and generalized. Finally, illustrative examples are presented to show the applicability of our main results in some areas of science and engineering.

1. Introduction

Fractional differential equations (FDEs) are recently developed in order to describe and model the dynamics of systems having memory or hereditary properties. These types of equations have been used and applied in various areas of science and engineering such as epidemiology [1], cancerology [2], viral immunology [3, 4], and viscoelastic fluid flows [5], as well as adaptive control engineering [6].

It is well known that there are two main methods to analyze the stability of ordinary differential equations (ODEs). The first one is called the Lyapunov indirect method that aims to study the local stability by means of the linearization of a system around its steady state (equilibrium point). The second method called the Lyapunov direct method consists to find or construct an appropriate auxiliary function, named a Lyapunov candidate function. Furthermore, the Lyapunov direct method provides a substantial tool for stability analysis of nonlinear systems. It can be used to determine the global dynamical behaviors of these systems without the need to solve explicitly the solutions of ODEs.

The stability of FDEs has attracted the attention of several researchers. In 2010, Li et al. [7] studied the stability of nonlinear systems of FDEs involving the Caputo fractional derivative with singular kernel [8]. They extended the Lyapunov direct method to the case of FDEs. In the same year, Sadati et al. [9] extended the Mittag–Leffler stability theorem for fractional nonlinear systems of FDEs with delay. The stability of a class of nonlinear systems of FDEs involving the Hadamard fractional derivative [10] was investigated in [11] by using a fractional comparison principle.

The theory of the stability of FDEs involving fractional derivatives with nonsingular kernels is new, and it requires an important development in order to study the dynamical behaviors of several systems available in the literature and using such derivatives. For these reasons, the main purpose of this paper is to extend the Lyapunov direct method for systems of FDEs involving the new generalized Hattaf fractional (GHF) derivative [12], which covers the most famous fractional derivatives with nonsingular kernels existing in the literature such as the Caputo–Fabrizio fractional derivative [13], the Atangana–Baleanu fractional derivative [14], and the weighted Atangana–Baleanu fractional derivative [15].

The main advantage of using the GHF derivative is that it is a nonlocal operator and it has a nonsingular kernel formulated by the Mittag–Leffler function with a parameter different to the order of the fractional derivative. Furthermore, this operator is a weighted fractional derivative which can be used to solve various types of integral equations with elegant ways as in [16–18]. On the other hand, the novelties

of this article are the study of the stability of FDEs with the new GHF operator by means of the Lyapunov direct method and the extension and generalization of the results related to exponential and Mittag–Leffler stability presented in [7, 19], as well as the establishment of some interesting properties and inequalities of GHF derivative in order to easily prove the Lyapunov stability theorems and construct Lyapunov candidate functions of quadratic-type, which are frequently used for demonstrating the global stability of many fractional order systems.

The outline of this paper is organized as follows. After an introductory part, Section 2 introduces the basic definitions and provides some lemmas and fundamental properties of the GHF derivative with nonsingular kernel in Caputo sense necessary to achieve the objective of this study. Section 3 is devoted to stability analysis. Finally, Section 4 presents some applications of our main results in the field of epidemiology as well as in the fractional linear systems theory.

2. Fundamental Results

In this section of the paper, we present the definitions and provide some fundamental results related to the GHF derivative with nonsingular kernel.

Definition 1 (see [12]). Let $\alpha \in [0,1)$, $\beta, \gamma > 0$, and $f \in H^1(a,b)$. The GHF derivative of order α in Caputo sense of the function $f(t)$ with respect to the weight function $w(t)$ is defined as follows:

$$ {}^{C}D^{\alpha,\beta,\gamma}_{a,t,w} f(t) = \frac{N(\alpha)}{1-\alpha} \frac{1}{w(t)} \int_a^t E_\beta\left[-\mu_\alpha (t-\tau)^\gamma\right] \frac{\mathrm{d}}{\mathrm{d}\tau} (wf)(\tau)\mathrm{d}\tau, \tag{1} $$

where $w \in C^1(a,b)$, $w, w' > 0$ on $[a, b]$, $N(\alpha)$ is a normalization function obeying $N(0) = N(1) = 1$, $\mu_\alpha = \alpha/(1-\alpha)$, and $E_\beta(t) = \sum_{k=0}^{+\infty} t^k/\Gamma(\beta k + 1)$ is the Mittag–Leffler function of parameter β.

The GHF derivative introduced in the above definition generalizes and extends many special cases available in the literature. For instance, when $w(t) = 1$ and $\beta = \gamma = 1$, (1) reduced to the Caputo–Fabrizio fractional derivative [13] given by

$$ {}^{C}D^{\alpha,1,1}_{a,t,1} f(t) = \frac{N(\alpha)}{1-\alpha} \int_a^t \exp\left[-\mu_\alpha (t-\tau)\right] f'(\tau)\mathrm{d}\tau. \tag{2} $$

When $w(t) = 1$ and $\beta = \gamma = \alpha$, (1) reduced to the Atangana–Baleanu fractional derivative [14] given by

$$ {}^{C}D^{\alpha,\alpha,\alpha}_{a,t,1} f(t) = \frac{N(\alpha)}{1-\alpha} \int_a^t E_\alpha\left[-\mu_\alpha (t-\tau)^\alpha\right] f'(\tau)\mathrm{d}\tau. \tag{3} $$

Furthermore, the weighted Atangana–Baleanu fractional derivative [15], given by

$$ {}^{C}D^{\alpha,\alpha,\alpha}_{a,t,w} f(t) = \frac{N(\alpha)}{1-\alpha} \frac{1}{w(t)} \int_a^t E_\alpha\left[-\mu_\alpha (t-\tau)^\alpha\right] \frac{\mathrm{d}}{\mathrm{d}\tau} (wf)(\tau)\mathrm{d}\tau, \tag{4} $$

is a special case of GHF derivative; it suffices to take $\beta = \gamma = \alpha$.

Considering the importance of weighted fractional derivatives to write and solve many integral equations in an elegant way, the function w has been introduced in equation (1). For instance, we consider the following integral equation:

$$ \lambda \int_0^t e^{-\lambda(t-\tau)} E_\beta\left[-\rho (t-\tau)^\gamma\right] f(\tau)\mathrm{d}\tau + \int_0^t e^{-\lambda(t-\tau)} E_\beta\left[-\rho (t-\tau)^\gamma\right] f'(\tau)\mathrm{d}\tau = \Lambda - \delta f(t), \tag{5} $$

where $\lambda, \rho, \Lambda, \delta > 0$. In terms of the GHF operator, this equation can be written as follows:

$$ {}^{C}D^{\alpha,\beta,\gamma}_{a,t,w} f(t) = A - \mu f(t), \tag{6} $$

where $w(t) = e^{\lambda t}$, $N(\alpha) = 1$, $\alpha = \rho/(1+\rho)$, $A = \Lambda/(1-\alpha)$, and $\mu = \delta/(1-\alpha)$. Similar to the example of HIV infection presented in [12], the solution of the above integral equation when $\gamma = \beta$ is given by

$$ \begin{aligned} f(t) = {} & \frac{A}{\mu} + \frac{N(\alpha) w(0)}{a_\alpha w(t)} \left(f(0) - \frac{A}{\mu} \right) E_\beta\left(-\frac{\alpha\mu}{a_\alpha} t^\beta \right) \\ & - \frac{A N(\alpha)}{\mu a_\alpha w(t)} E_\beta\left(-\frac{\alpha\mu}{a_\alpha} t^\beta \right) * w'(t), \end{aligned} \tag{7} $$

where $a_\alpha = N(\alpha) + \mu(1-\alpha)$.

In various areas of science and engineering, the method of constructing Lyapunov functions is often based on quadratic-type functions. So, we provide the following lemma that estimates the GHF derivative of these types of Lyapunov candidate functions.

Lemma 1. *Let $x(.) \in IR^n$ be a continuously differentiable function and $P \in IR^{n\times n}$ be a symmetric positive definite matrix. Then, for any time $t \geq t_0$, we have*

$$ {}^{C}D^{\alpha,\beta,\gamma}_{t_0,t,1}\left(x(t)^T P x(t) \right) \leq 2x(t)^T P\, {}^{C}D^{\alpha,\beta,\gamma}_{t_0,t,1} x(t). \tag{8} $$

Proof. Similar to [19, 20], we consider the following function:

$$ g(t) = {}^{C}D^{\alpha,\beta,\gamma}_{t_0,t,1}\left(x(t)^T P x(t) \right) - 2x(t)^T P\, {}^{C}D^{\alpha,\beta,\gamma}_{t_0,t,1} x(t). \tag{9} $$

Then,

$$g(t) = \frac{N(\alpha)}{1-\alpha}\int_{t_0}^{t} E_\beta[-\mu_\alpha(t-\tau)^\gamma]\left(2x(\tau)^T P\dot{x}(\tau) - 2x(t)^T P\dot{x}(\tau)\right)\mathrm{d}\tau$$
$$= \frac{N(\alpha)}{1-\alpha}\int_{t_0}^{t} E_\beta[-\mu_\alpha(t-\tau)^\gamma]\left(2y(\tau)^T P\dot{y}(\tau)\right)\mathrm{d}\tau$$
$$= \frac{N(\alpha)}{1-\alpha}\int_{t_0}^{t} E_\beta[-\mu_\alpha(t-\tau)^\gamma]\left(y(\tau)^T Py(\tau)\right)'\mathrm{d}\tau, \tag{10}$$

where $y(\tau) = x(\tau) - x(t)$. Integrating by parts, we obtain

$$g(t) = \frac{N(\alpha)}{1-\alpha}E_\beta[-\mu_\alpha(t-\tau)^\gamma]y(\tau)^T Py(\tau)|_{\tau=t_0}^{\tau=t}$$
$$-\frac{\alpha\gamma N(\alpha)}{(1-\alpha)^2}\int_{t_0}^{t}(t-\tau)^{\gamma-1}E^2_{\beta,\beta+1}[-\mu_\alpha(t-\tau)^\gamma]y(\tau)^T Py(\tau)\mathrm{d}\tau. \tag{11}$$

Since $\lim_{\tau\longrightarrow t}E_\beta[-\mu_\alpha(t-\tau)^\gamma]y(\tau)^T Py(\tau) = y(t)^T Py(t) = 0$, we have

$$g(t) = -\frac{N(\alpha)}{1-\alpha}E_\beta[-\mu_\alpha(t-t_0)^\gamma]y(t_0)^T Py(t_0)$$
$$-\frac{\alpha\gamma N(\alpha)}{(1-\alpha)^2}\int_{t_0}^{t}(t-\tau)^{\gamma-1}E^2_{\beta,\beta+1}[-\mu_\alpha(t-\tau)^\gamma]y(\tau)^T Py(\tau)\mathrm{d}\tau. \tag{12}$$

This follows that $g(t) \le 0$, for all $t \ge t_0$, and the proof is completed. □

Remark 1. It is important to note that the above lemma extends the recent results presented in Lemma 2 of [19] and Corollary 1 of [20]. Moreover, the results presented in Lemma 3.1 of [21] to estimate the Atangana–Baleanu Caputo derivative of quadratic Lyapunov functions is extended to the case of GHF derivative.

For simplicity, denote ${}^{C}D^{\alpha,\beta,\beta}_{a,t,w}$ by $\mathscr{D}^{\alpha,\beta}_{a,w}$. By [12], the generalized fractional integral associated to $\mathscr{D}^{\alpha,\beta}_{a,w}$ is given by the following definition.

Definition 2 (see [12]). The generalized fractional integral operator associated to $\mathscr{D}^{\alpha,\beta}_{a,w}$ is defined by

$$\mathscr{I}^{\alpha,\beta}_{a,w}f(t) = \frac{1-\alpha}{N(\alpha)}f(t) + \frac{\alpha}{N(\alpha)}{}^{RL}\mathscr{I}^{\beta}_{a,w}f(t), \tag{13}$$

where ${}^{RL}\mathscr{I}^{\beta}_{a,w}$ is the standard weighted Riemann–Liouville fractional integral of order β defined

$${}^{RL}\mathscr{I}^{\beta}_{a,w}f(t) = \frac{1}{\Gamma(\beta)}\frac{1}{w(t)}\int_a^t (t-\tau)^{\beta-1}w(\tau)f(\tau)\mathrm{d}x. \tag{14}$$

Remark 2. The Atangana–Baleanu fractional integral operator is a particular case of (7), and it suffices to take $w(t) = 1$ and $\beta = \alpha$.

Now, we recall an important theorem that we will need in the following. This theorem extends the Newton–Leibniz formula introduced in [22, 23].

Theorem 1 (see [20]). *Let $\alpha \in [0,1)$, $\beta > 0$, and $f \in H^1(a,b)$. Then, we have the following properties:*

$$\mathscr{I}^{\alpha,\beta}_{a,w}\left(\mathscr{D}^{\alpha,\beta}_{a,w}f\right)(t) = f(t) - \frac{w(a)f(a)}{w(t)}, \tag{15}$$

$$\mathscr{D}^{\alpha,\beta}_{a,w}\left(\mathscr{I}^{\alpha,\beta}_{a,w}f\right)(t) = f(t) - \frac{w(a)f(a)}{w(t)}. \tag{16}$$

On the contrary, we need the following results.

Lemma 2. *Let $y(.) \in IR^n$. The solution of the following Cauchy problem*

$$\mathscr{D}^{\alpha,\beta}_{0,w}y(t) = \lambda y(t) + u(t), \tag{17}$$

with initial boundary condition $y(0) = y_0$, is given by

$$y(t) = \frac{N(\alpha)w(0)y_0}{a_\alpha w(t)}E_\beta\left(\frac{\alpha\lambda}{a_\alpha}t^\beta\right) + \frac{1-\alpha}{a_\alpha}u(t)$$
$$+\frac{N(\alpha)}{\lambda a_\alpha w(t)}\frac{\mathrm{d}}{\mathrm{d}t}E_\beta\left(\frac{\alpha\lambda}{a_\alpha}t^\beta\right) * (wu)(t), \tag{18}$$

where $a_\alpha = N(\alpha) - \lambda(1-\alpha) \neq 0$ and $\lambda \neq 0$.

Proof. By (11), we have

$$w(t)\mathscr{D}^{\alpha,\beta}_{0,w}y(t) = \lambda w(t)y(t) + w(t)u(t). \tag{19}$$

By applying Laplace transform and using Theorem 2 in [12], we obtain

$$\mathscr{L}\{w(t)y(t)\} = \frac{(1-\alpha)\left(s^\beta + \mu_\alpha\right)}{[N(\alpha) - \lambda(1-\alpha)]s^\beta - \lambda\alpha}\mathscr{L}\{w(t)u(t)\}$$
$$+\frac{N(\alpha)w(0)y(0)s^{\beta-1}}{[N(\alpha) - \lambda(1-\alpha)]s^\beta - \lambda\alpha}. \tag{20}$$

Then,

$$\begin{aligned}\mathscr{L}\{w(t)y(t)\} &= \frac{N(\alpha)w(0)y(0)}{a_\alpha}\frac{s^{\beta-1}}{s^\beta-(\alpha\lambda/a_\alpha)}+\frac{1-\alpha}{a_\alpha}\frac{s^{\beta-1}}{s^\beta-(\alpha\lambda/a_\alpha)}s\mathscr{L}\{w(t)u(t)\}\\&\quad+\frac{\alpha}{a_\alpha}\frac{1}{s^\beta-(\alpha\lambda/a_\alpha)}\mathscr{L}\{w(t)u(t)\}\\&= \frac{N(\alpha)w(0)y(0)}{a_\alpha}\mathscr{L}\left\{E_\beta\left(\frac{\alpha\lambda}{a_\alpha}t^\beta\right)\right\}+\frac{1-\alpha}{a_\alpha}\mathscr{L}\left\{E_\beta\left(\frac{\alpha\lambda}{a_\alpha}t^\beta\right)\right\}\left[\mathscr{L}\{(wu)'(t)\}+w(0)u(0)\right]\\&\quad+\frac{1}{\lambda}\mathscr{L}\left\{\frac{\mathrm{d}}{\mathrm{d}t}E_\beta\left(\frac{\alpha\lambda}{a_\alpha}t^\beta\right)\right\}\mathscr{L}\{w(t)u(t)\}.\end{aligned}\tag{21}$$

The passage to the inverse Laplace gives

$$\begin{aligned}w(t)y(t) &= \frac{N(\alpha)w(0)y(0)}{a_\alpha}E_\beta\left(\frac{\alpha\lambda}{a_\alpha}t^\beta\right)+\frac{1-\alpha}{a_\alpha}w(t)u(t)\\&\quad+\frac{N(\alpha)}{\lambda a_\alpha}\frac{\mathrm{d}}{\mathrm{d}t}E_\beta\left(\frac{\alpha\lambda}{a_\alpha}t^\beta\right)*(wu)(t).\end{aligned}\tag{22}$$

From integration by parts, we have

$$\begin{aligned}\frac{\mathrm{d}}{\mathrm{d}t}E_\beta\left(\frac{\alpha\lambda}{a_\alpha}t^\beta\right)*(wu)(t) &= E_\beta\left(\frac{\alpha\lambda}{a_\alpha}t^\beta\right)(wu)(0)-(wu)(t)\\&\quad+E_\beta\left(\frac{\alpha\lambda}{a_\alpha}t^\beta\right)*(wu)'(t).\end{aligned}\tag{23}$$

Hence,

$$\begin{aligned}y(t) &= \frac{N(\alpha)w(0)y_0}{a_\alpha w(t)}E_\beta\left(\frac{\alpha\lambda}{a_\alpha}t^\beta\right)+\frac{1-\alpha}{a_\alpha}u(t)\\&\quad+\frac{N(\alpha)}{\lambda a_\alpha w(t)}\frac{\mathrm{d}}{\mathrm{d}t}E_\beta\left(\frac{\alpha\lambda}{a_\alpha}t^\beta\right)*(wu)(t).\end{aligned}\tag{24}$$

This completes the proof. □

Remark 3. By using (12), the solution of (11) can be rewritten as follows:

$$\begin{aligned}y(t) &= \frac{(\lambda y_0+u(0))N(\alpha)w(0)}{\lambda a_\alpha w(t)}E_\beta\left(\frac{\alpha\lambda}{a_\alpha}t^\beta\right)-\frac{1}{\lambda}u(t)\\&\quad+\frac{N(\alpha)}{\lambda a_\alpha w(t)}E_\beta\left(\frac{\alpha\lambda}{a_\alpha}t^\beta\right)*(wu)'(t).\end{aligned}\tag{25}$$

Corollary 1. *Let $\lambda>0$ and $f(t)$ be a function satisfying the following inequality:*

$$\mathscr{D}^{\alpha,\beta}_{0,w}f(t)\le-\lambda f(t).\tag{26}$$

Then,

$$f(t)\le f(0)E_\beta\left(\frac{-\alpha\lambda t^\beta}{N(\alpha)+\lambda(1-\alpha)}\right).\tag{27}$$

Proof. From (14), we deduce that there exists a nonnegative function $u(t)$ such that

$$\mathscr{D}^{\alpha,\beta}_{0,w}f(t)=-\lambda f(t)-u(t).\tag{28}$$

By applying Lemma 2, we obtain

$$\begin{aligned}f(t) &= \frac{N(\alpha)w(0)f(0)}{[N(\alpha)+\lambda(1-\alpha)]w(t)}E_\beta\left(\frac{-\alpha\lambda t^\beta}{N(\alpha)+\lambda(1-\alpha)}\right)-\frac{(1-\alpha)u(t)}{N(\alpha)+\lambda(1-\alpha)}\\&\quad+\frac{N(\alpha)}{\lambda[N(\alpha)+\lambda(1-\alpha)]w(t)}\frac{\mathrm{d}}{\mathrm{d}t}E_\beta\left(\frac{-\alpha\lambda t^\beta}{[N(\alpha)+\lambda(1-\alpha)]}\right)*(wu)(t)\\&= \frac{N(\alpha)w(0)f(0)}{[N(\alpha)+\lambda(1-\alpha)]w(t)}E_\beta\left(\frac{-\alpha\lambda t^\beta}{N(\alpha)+\lambda(1-\alpha)}\right)-\frac{(1-\alpha)u(t)}{N(\alpha)+\lambda(1-\alpha)}\\&\quad-\frac{\alpha\beta N(\alpha)}{\lambda[N(\alpha)+\lambda(1-\alpha)]^2w(t)}\left(t^{\beta-1}E^2_{\beta,\beta+1}\left(\frac{-\alpha\lambda t^\beta}{[N(\alpha)+\lambda(1-\alpha)]}\right)*(wu)(t)\right).\end{aligned}\tag{29}$$

Then,

$$f(t) \leq \frac{N(\alpha) w(0) f(0)}{[N(\alpha) + \lambda(1-\alpha)] w(t)} E_{\beta}\left(\frac{-\alpha\lambda t^{\beta}}{N(\alpha) + \lambda(1-\alpha)}\right). \tag{30}$$

Since $N(\alpha) \leq N(\alpha) + \lambda(1-\alpha)$ and $w(0) \leq w(t)$, we easily have (27). □

3. Stability Analysis

In this section, we focus on the stability analysis of the fractional differential equations with the GHF derivative.

Consider the following fractional differential nonautonomous equation:

$$\mathscr{D}_{0,w}^{\alpha,\beta} x(t) = f(t, x(t)), \tag{31}$$

where $x(t) \in IR^n$ is the state variable and $f\colon [0, +\infty) \times \Omega \longrightarrow IR^n$ is a continuous locally Lipschitz function and Ω is a domain of IR^n containing the origin $x = 0$.

System (31) is said to be autonomous if $f(t, x) = f(x)$. In this case, (31) becomes

$$\mathscr{D}_{0,w}^{\alpha,\beta} x(t) = f(x(t)). \tag{32}$$

First, we give some definitions that we will need in the following.

Definition 3. The trivial equilibrium point $x = 0$ of (31) is said to be stable if, for each $\epsilon > 0$, there exists a $\eta > 0$ such that, for any initial condition $x(t_0) = x_0$ satisfying $\|x_0\| < \eta$, the solution $x(t)$ of (31) satisfies $\|x(t)\| < \epsilon$, for all $t \geq t_0$. Furthermore, $x = 0$ is said to be asymptotically stable if it is stable and $\lim_{t \longrightarrow +\infty} x(t) = 0$.

Definition 4. A scalar function $V(x)$ is called a Lyapunov candidate function of autonomous system (32) if it is a positive definite in a neighborhood U of the origin, i.e., $V(0) = 0$ and $V(x) > 0$, for all $x \in U \setminus \{0\}$. In addition, a scalar function $V(t, x)$ is a Lyapunov candidate function of nonautonomous system (31) if it is positive definite, i.e., $V(t, 0) = 0$, for all $t \geq t_0$, and if there is a time-invariant function $V_0(x)$ which is positive definite such that $V(t, x) \geq V_0(x)$, for all $t \geq t_0$.

Also, we introduce the definition of stability in the Mittag–Leffler sense.

Definition 5. The trivial solution of (31) is called Mittag–Leffler stable if

$$\|x(t)\| \leq \left[m(x(t_0)) E_{\beta}\left(-\lambda (t - t_0)^{\beta}\right)\right]^{\nu}, \tag{33}$$

where t_0 is the initial time, $\lambda \geq 0$, $\nu > 0$, $m(0) = 0$, $m(x) \geq 0$, and $m(x)$ is locally Lipschitz on $x \in IR^n$ with the Lipschitz constant m_0.

Remark 4. Mittag–Leffler stability generalizes the exponential stability and it implies asymptotic stability.

Theorem 2. *Let $x = 0$ be an equilibrium point for system (31). Let $V(t, x)\colon [0, +\infty) \times \Omega \longrightarrow IR$ be a continuously differentiable function and locally Lipschitz with respect to x such that*

$$k\|x\|^p \leq V(t, x), \tag{34}$$

$$\mathscr{D}_{0,w}^{\alpha,\beta} V(t, x) \leq -qV(t, x), \tag{35}$$

where $t \geq 0$, $x \in \Omega$, and k, p, and q are arbitrary positive constants. Then, $x = 0$ is Mittag–Leffler stable. If (34) and (35) hold globally on IR^n, then $x = 0$ is globally Mittag–Leffler stable.

Proof. From (35) and according to Corollary 1, we deduce that

$$V(t, x) \leq V(0, x(0)) E_{\beta}\left(\frac{-q\alpha t^{\beta}}{N(\alpha) + q(1-\alpha)}\right). \tag{36}$$

From (34), we obtain

$$k\|x(t)\|^p \leq V(0, x(0)) E_{\beta}\left(\frac{-q\alpha t^{\beta}}{N(\alpha) + q(1-\alpha)}\right), \tag{37}$$

which leads to

$$\|x(t)\| \leq \left[m_1(x(0)) E_{\beta}\left(-\lambda t^{\beta}\right)\right]^{1/p}, \tag{38}$$

where $m_1(x) = V(0, x)/k$ and $\lambda = q\alpha/(N(\alpha) + q(1-\alpha))$. Clearly, $m_1(0) = 0$ and $m_1(x) \geq 0$. Since $V(t, x)$ is locally Lipschitz with respect to x, we deduce that $m_1(x)$ is locally Lipschitz on x. Therefore, the equilibrium $x = 0$ is globally Mittag–Leffler stable. □

Remark 5. Theorem 2 generalizes the result of the exponential stability presented in Theorem 2 of [19]. Indeed, it suffices to take $w(t) = 1$, $\beta = \gamma = 1$, and $k = 1$.

Theorem 3. *Let $x = 0$ be an equilibrium point for system (31). Let $V(t, x)\colon [0, +\infty) \times \Omega \longrightarrow IR$ be a continuously differentiable function and locally Lipschitz with respect to x such that*

$$k_1\|x\|^p \leq V(t, x) \leq k_2\|x\|^{pq}, \tag{39}$$

$$\mathscr{D}_{0,w}^{\alpha,\beta} V(t, x) \leq -k_3\|x\|^{pq}, \tag{40}$$

where $t \geq 0$, $x \in \Omega$, and k_1, k_2, k_3, p, and q are arbitrary positive constants. Then, $x = 0$ is Mittag–Leffler stable. If (39) and (40) hold globally on IR^n, then $x = 0$ is globally Mittag–Leffler stable.

Proof. According to (39) and (40), we have

$$\mathscr{D}_{0,w}^{\alpha,\beta} V(t, x) \leq -\frac{k_3}{k_2} V(t, x). \tag{41}$$

By applying Corollary 1, we have

$$V(t, x) \leq V(0, x(0)) E_{\beta}\left(-\kappa t^{\beta}\right), \tag{42}$$

where $\kappa = k_3\alpha/(k_2N(\alpha) + k_3(1-\alpha))$. By (39), we obtain

$$k_1\|x(t)\|^p \le V(0,x(0))E_\beta\left(-\kappa t^\beta\right), \tag{43}$$

which implies that

$$\|x(t)\| \le \left[m_2(x(0))E_\beta\left(-\kappa t^\beta\right)\right]^{1/p}, \tag{44}$$

where $m_2(x) = V(0,x)/k_1$. This completes the proof. □

Remark 6. Theorem 3 extends the result of the Mittag–Leffler stability presented in Theorem 5.1 of [7] for the GHF derivative with nonsingular kernel. Moreover, the result given in Theorem 4 of [19] for Caputo–Fabrizio fractional derivative is recovered when $w(t) = 1$, $\beta = \gamma = 1$, $p = 2$, and $q = 1$.

4. Applications

In this section, we apply the main results obtained in this paper to investigate the stability of the following examples of fractional systems.

Example 1. Consider the following fractional linear system:

$$\mathscr{D}_{0,w}^{\alpha,\beta}x(t) = Ax(t), \tag{45}$$

where $x(t) \in IR^n$ is the state variable and $A \in IR^{n\times n}$.

To establish the stability of (45), we define the Lyapunov candidate function as follows:

$$V(t,x) = x^TPx, \tag{46}$$

where $P \in IR^{n\times n}$ is a symmetric positive definite matrix. Hence,

$$\lambda_{\min}(P)\|x\|^2 \le V(t,x) \le \lambda_{\max}(P)\|x\|^2, \tag{47}$$

where $\lambda_{\min}(P)$ and $\lambda_{\max}(P)$ are the minimum and the maximum eigenvalues of the matrix P, respectively. Since P is positive definite, we have $\lambda_{\min}(P) > 0$ and $\lambda_{\max}(P) > 0$.

According to Lemma 1, the GHF derivative of the Lyapunov function V along the trajectories of (45) satisfies

$$\begin{aligned}\mathscr{D}_{0,1}^{\alpha,\beta}V(t,x) &\le 2x^TP\mathscr{D}_{0,w}^{\alpha,\beta}x\\ &= x^T\left(A^TP + PA\right)x\\ &= -x^TQx,\end{aligned} \tag{48}$$

where $Q = -(A^TP + PA)$. It is obvious that Q is a symmetric matrix. Assume that Q is a positive definite matrix and let $\lambda_{\min}(Q)$ be the minimum of its positive eigenvalues. Then, we have

$$\mathscr{D}_{0,1}^{\alpha,\beta}V(t,x) \le -\lambda_{\min}(Q)\|x\|^2. \tag{49}$$

By applying Theorem 3, we deduce that the trivial solution of system (45) is globally Mittag–Leffler stable under the condition that Q is positive definite. This condition is satisfied when A is Hurwitz, i.e., all the eigenvalues of A have negative real parts.

Example 2. Consider the following fractional epidemic model:

$$\begin{cases}\mathscr{D}_{0,1}^{\alpha,\beta}S(t) = \mathscr{A} - \nu S(t) - \mathscr{F}(S(t),I(t))I(t),\\ \mathscr{D}_{0,1}^{\alpha,\beta}I(t) = \mathscr{F}(S(t),I(t))I(t) - (\nu + d + r)I(t),\\ \mathscr{D}_{0,1}^{\alpha,\beta}R(t) = rI(t) - \nu R(t),\end{cases} \tag{50}$$

where $S(t)$, $I(t)$, and $R(t)$ are the susceptible, infected, and recovered individuals at time t, respectively. Here, the susceptible individuals are recruited at a constant rate $\mathscr{A}$ and become infected by effective contact with infected individuals at rate $\mathscr{F}(S,I)I$. The natural death rate in all classes is denoted by ν, while d is the death rate due to the disease. Furthermore, r is the recovery rate of the infected individuals.

Obviously, the first two equations of (50) do not depend on the variable R. Then, model (50) can be rewritten by the following system:

$$\begin{cases}\mathscr{D}_{0,1}^{\alpha,\beta}S(t) = \mathscr{A} - \nu S(t) - \mathscr{F}(S(t),I(t))I(t),\\ \mathscr{D}_{0,1}^{\alpha,\beta}I(t) = \mathscr{F}(S(t),I(t))I(t) - (\nu + d + r)I(t).\end{cases} \tag{51}$$

As in [24], we assume that the general incidence $\mathscr{F}$ is continuously differentiable in the interior of IR_+^2 and satisfies the following conditions:

$$\begin{aligned}&(H)\ \mathscr{F}(0,S) = 0,\\ &\frac{\partial\mathscr{F}}{\partial S}(S,I) > 0, \frac{\partial\mathscr{F}}{\partial I}(S,I) \le 0, \quad \text{for all } S,I \ge 0.\end{aligned} \tag{52}$$

It is clear that $\mathscr{E}^0 = (S^0,0)$ is the disease-free equilibrium of (51), where $S^0 = \mathscr{A}/\nu$. Then, the basic reproduction number of (51) is defined as follows:

$$\mathscr{R}_0 = \frac{\mathscr{F}\left(S^0,0\right)}{(\nu + d + r)}, \tag{53}$$

which epidemiologically represents the number of secondary infections produced by a single infected individual throughout the period of infection when all individuals are uninfected. Based on the same technique in [24], we can easily prove that model (51) has another equilibrium when $\mathscr{R}_0 > 1$.

Let $\Omega = \{(S,I) \in IR_+^2 : S \le S^0\}$. Assume that $\mathscr{R}_0 < 1$ and consider the following Lyapunov function:

$$L(S,I) = \varpi\left(S^0 - S\right) + I, \tag{54}$$

where $\varpi = (1-\mathscr{R}_0)/2\mathscr{R}_0$. Obviously, L is a candidate Lyapunov function. Indeed, we have $L(\mathscr{E}^0) = 0$ and $L(S,I) > 0$, for all $(S,I) \in \Omega\setminus\{\mathscr{E}^0\}$. Moreover, we have

$$\begin{aligned}\mathscr{D}_{0,1}^{\alpha,\beta}L(S,I) &= -\varpi\mathscr{D}_{0,1}^{\alpha,\beta}S + \mathscr{D}_{0,1}^{\alpha,\beta}I\\ &\le -\varpi\nu\left(S^0 - S\right) - \frac{\delta\left(1-\mathscr{R}_0\right)}{2}I,\end{aligned} \tag{55}$$

where $\delta = \nu + d + r$. Hence,

$$\mathscr{D}_{0,1}^{\alpha,\beta}L(S,I) \le -\varrho_1L(S,I), \tag{56}$$

where $\varrho_1 = \min\{\nu, \delta(1 - \mathscr{R}_0)/2\}$.

Let $X = (S, I) \in IR^2$ with the norm $\|X\| = |S| + |I|$. Then,

$$\varrho_2 \left\| X - \mathscr{E}^0 \right\| \leq L(S, I), \tag{57}$$

where $\varrho_2 = \min\{\varpi, 1\}$. By applying Theorem 2, we conclude that the disease-free equilibrium $\mathscr{E}^0$ of (51) is Mittag–Leffler stable in Ω when $\mathscr{R}_0 < 1$.

Data Availability

No data were used to support this study.

Conflicts of Interest

The author declares that he has no conflicts of interest.

References

[1] K. R. Cheneke, K. P. Rao, and G. K. Edessa, "Application of a new generalized fractional derivative and rank of control measures on cholera transmission dynamics," *International Journal of Mathematics and Mathematical Sciences*, vol. 2021, Article ID 2104051, 9 pages, 2021.

[2] M. El Younoussi, Z. Hajhouji, K. Hattaf, and N. Yousfi, "A new fractional model for cancer therapy with M1 oncolytic virus," *Complexity*, vol. 2021, Article ID 9934070, 12 pages, 2021.

[3] M. Bachraoui and K. Hattaf, "Noura yousfi, spatiotemporal dynamics of fractional hepatitis B virus infection model with humoral and cellular immunity," in *Proceedings of the International Symposium on Mathematical and Computational Biology*, pp. 293–313, Springer, San Diego, CA, USA, October 2020.

[4] M. Bachraoui, M. A. Ichou, K. Hattaf, and N. Yousfi, "Spatiotemporal dynamics of a fractional model for hepatitis B virus infection with cellular immunity," *Mathematical Modelling of Natural Phenomena*, vol. 16, pp. 1–13, 2021.

[5] A. Rasheed and M. Shoaib Anwar, "Interplay of chemical reacting species in a fractional viscoelastic fluid flow," *Journal of Molecular Liquids*, vol. 273, pp. 576–588, 2019.

[6] S. Ladaci and Y. Bensafia, "Indirect fractional order pole assignment based adaptive control," *Engineering Science and Technology, an International Journal*, vol. 19, no. 1, pp. 518–530, 2016.

[7] Y. Li, Y. Chen, and I. Podlubny, "Stability of fractional-order nonlinear dynamic systems: Lyapunov direct method and generalized Mittag-Leffler stability," *Computers & Mathematics with Applications*, vol. 59, no. 5, pp. 1810–1821, 2010.

[8] I. Podlubny, "Fractional differential equations," *Mathematics in Science and Engineering*, vol. 198, Academic Press, San Diego, CA, USA, 1999.

[9] S. J. Sadati, D. Baleanu, A. Ranjbar, R. Ghaderi, and T. Abdeljawad, "Mittag-leffler stability theorem for fractional nonlinear systems with delay," *Abstract and Applied Analysis*, vol. 2010, Article ID 108651, 7 pages, 2010.

[10] A. A. Kilbas, H. M. Srivastava, and J. J. Trujillo, *Theory and Applications of Fractional Differential Equations*, North-Holland Mathematics Studies, Elsevier, Amsterdam, Netherlands, 2006.

[11] G. Wang, K. Pei, and Y. Chen, "Stability analysis of nonlinear Hadamard fractional differential system," *Journal of the Franklin Institute*, vol. 356, no. 12, pp. 6538–6546, 2019.

[12] K. Hattaf, "A new generalized definition of fractional derivative with non-singular kernel," *Computation*, vol. 8, pp. 1–9, 2020.

[13] A. Caputo and M. Fabrizio, "A new definition of fractional derivative without singular kernel," *Progress in Fractional Differentiation and Applications*, vol. 1, pp. 73–85, 2015.

[14] A. Atangana and D. Baleanu, "New fractional derivatives with nonlocal and non-singular kernel: theory and application to heat transfer model," *Thermal Science*, vol. 20, no. 2, pp. 763–769, 2016.

[15] M. Al-Refai, "On weighted Atangana–Baleanu fractional operators," *Advances in Differential Equations*, vol. 2020, pp. 1–11, 2020.

[16] O. Agrawal, "Some generalized fractional calculus operators and their applications in integral equations," *Fractional Calculus and Applied Analysis*, vol. 15, no. 4, pp. 700–711, 2012.

[17] M. Al-Refai and A. M. Jarrah, "Fundamental results on weighted Caputo-Fabrizio fractional derivative," *Chaos, Solitons & Fractals*, vol. 126, pp. 7–11, 2019.

[18] M. A. Bayrak, A. Demir, and E. Ozbilge, "On solution of fractional partial differential equation by the weighted fractional operator," *Alexandria Engineering Journal*, vol. 59, no. 6, pp. 4805–4819, 2020.

[19] N. Sene, "Stability analysis of the fractional differential equations with the Caputo-Fabrizio fractional derivative," *Journal of Fractional Calculus and Applications*, vol. 11, no. 2, pp. 160–172, 2020.

[20] K. Hattaf, "On some properties of the new generalized fractional derivative with non-singular kernel," *Mathematical Problems in Engineering*, vol. 2021, Article ID 1580396, 6 pages, 2021.

[21] M. A. Taneco-Hernández and C. Vargas-De-León, "Stability and Lyapunov functions for systems with Atangana–Baleanu Caputo derivative: an HIV/AIDS epidemic model," *Chaos, Solitons & Fractals*, vol. 132, Article ID 109586, 2020.

[22] J. D. Djida, A. Atangana, and I. Area, "Numerical computation of a fractional derivative with non-local and non-singular kernel," *Mathematical Modelling of Natural Phenomena*, vol. 12, no. 3, pp. 4–13, 2017.

[23] D. Baleanu and A. Fernandez, "On some new properties of fractional derivatives with Mittag-Leffler kernel," *Communications in Nonlinear Science and Numerical Simulation*, vol. 59, pp. 444–462, 2018.

[24] K. Hattaf, A. A. Lashari, Y. Louartassi, and N. Yousfi, "A delayed SIR epidemic model with a general incidence rate," *Electronic Journal of Qualitative Theory of Differential Equations*, vol. 3, pp. 1–9, 2013.

Hindawi
Mathematical Problems in Engineering
Volume 2021, Article ID 2717507, 8 pages
https://doi.org/10.1155/2021/2717507

Research Article

Numerical Study of Duffing Nonlinearity in the Quantum Dot Embedded Nanomechanical Resonator

Yue Wang[1], **Ghulam Bary**[1], **Riaz Ahmad**[1], **Dameng Yin**[1], **Shiwei Xie**[1], **Qing Lu**[1], **Ilyas Khan**[2], **Nawa Alshammari**[3], **Nawaf N. Hamadneh**[3] and **Mulugeta Andualemb**[4]

[1]*Faculty of Science, Yibin University, Yibin 644000, China*
[2]*Department of Mathematics, College of Science Al-Zulfi, Majmaah University, Al Majmaah 11952, Saudi Arabia*
[3]*Department of Basic Sciences, College of Science and Theoretical Studies, Saudi Electronic University, Riyadh 11673, Saudi Arabia*
[4]*Department of Mathematics, Bonga University, Bonga, Ethiopia*

Correspondence should be addressed to Yue Wang; wy6144@163.com, Ghulam Bary; ghulambary@gmail.com, and Mulugeta Andualemb; mulugetaandualem4@gmail.com

Received 26 September 2021; Accepted 9 November 2021; Published 24 November 2021

Academic Editor: Muhammad Shoaib Anwar

Geometry, electrostatics, and single-electron tunneling contribute to the nonlinearity in the quantum dot embedded nanomechanical resonator, while "Duffing term" is a kind of mathematics describing the third-order nonlinearity of the system as a whole. We study theoretically the influence of a variation of a mathematical parameter Fuffing term on the actual physical effect. The position probability distribution, the average current, and the displacement fluctuation spectrum with the different Duffing parameter and electromechanical coupling are obtained through numerically calculating the Fokker Planck equation. The mechanical bistability has been described by these quantities under different electromechanical coupling and Duffing parameters. We conclude that the nonlinearities of the nanotube resonator contribute to the mechanical bistability, which induces the asymmetry of the position probability distribution, compresses the current, and softens or stiffens the mechanical resonance frequency as the same as the electromechanical coupling to use it in mechanical engineering.

1. Introduction

The linear dynamic description of nanoelectromechanical systems (NEMS) is well understood when the electromechanical coupling is rather weak [1–9]; meanwhile, the existence of the nonlinearities induces too many interesting consequences such as the nonlinear dynamic response in the two-dimensional material membranes, the mechanical bistability in the carbon nanotube (CNT)-based resonator, [10–13], and unusual mechanical response [8, 14–16]. The CNT quantum dot embedded resonators have been widely investigated as ultrasensitive detectors and sensors [17–19]; the experimental research group reported higher record sensitivity in mass and force sensing [20, 21]. Recently, people have found that strong coupling induces strong nonlinear signals in the mechanical resonance frequency and the mechanical noise in the single- or two-level quantum nanomechanical oscillator [22–24]. The strong coupling dominates the quadratic term in the restore force than the geometry, electrostatics, and single-electron tunneling. The nonlinear response of the system contains a mechanical resonator at nanoscale coupled to a transistor of single electron under the external drive which behaves like the Duffing oscillator [25].

The intrinsic nonlinearities of the carbon nanotube have been ignored by most of these research studies. For the given carbon nanotube-based resonators, the nonlinearities come not only from the electromechanical coupling but also from the parent materials themselves. It is significant to consider the intrinsic nonlinearities of the carbon nanotube. In this

work, we pay attention to the term of the Duffing under the force of the restoring with the cubic structure of the considered displacement. We are also interested in the nonlinear CNT-based resonators which will be described by the position probability distribution, the current, and the displacement fluctuations with the different coupling and Duffing parameter [26].

In particular, nonlinearities examine the quantum coherence pure substance which is a pure state of matter that can be quite sensitive. When two identical particles do not overlap, they each have their perfect quantum system described by the quantum oscillator. However, the measured nonlinearities may have been in a miniature form or even stay purest after the quantum mechanical overlapping. It is related to the strength, density, and temperature of the considered system (quantum entanglement). During transition times, when the density concentration is high, bouncing may potentially play a role in quantum wave-particle duality. Hydrodynamics is frequently used to characterize the extremely dense medium formed, which implies local thermodynamic equilibrium and quantum decoherence well above thermal length scale [27].

In this curious and unique research work, we probe the nonlinearities, consequences of average current flow, and intrinsic fluctuations of the probability distributions, as well as the suppression of the displacement under the properties of the considered pioneer quantum system with nanotubes. The creation of a useable source which inflates relativistic interior of the considered field potential about the special oscillator that evaluates over time in the phase of quantum temperature regimes, and we also compute the various parameters for numerous order quantum characteristics by applying the one and two nanotubes for the mentioned phases at distinct temperature and momenta regimes. The nonlinearity of production systems influences the critical parameter significantly under the considered measurements at miscellaneous temperatures' dependence noise which are explored to use in thermal and mechanical applications of engineering.

The study is organized as follows. In Section 2, we introduce our model with the description of the system which consists of the carbon nanotube quantum dot embedded resonator; then, the numerical method is introduced, the Langevin equation are given, and the Fokker Planck equation is discretized to obtain the stationary solution. In Section 3, we study three physical quantities such as the position probability distribution, the average current, and the displacement fluctuations spectrum with the presence of nonlinearity of the CNT and different electromechanical couplings. The mechanical bistability has been described by them. Finally, in Section 4, we present our conclusions.

2. Methods

The Hamiltonian is introduced by William Rowan Hamilton, who created a ground breaking reconceptualization of Newtonian mechanics called as Hamiltonian dynamics, which was substantially vital to the future of quantum physics. Therefore, the Hamiltonian of the quantum dot embedded CNT mechanical resonator (see Figure 1).

We obtain

$$H = H_{re} + H_Q + H_c, \tag{1}$$

where the first term denotes the single-mode mechanical resonator. Specifically, in this study, we consider the influences of the force of restoring under the Duffing term which is cubic within displacement x. The restoring force is illustrated as

$$F_r = -kx - \alpha x^3, \tag{2}$$

where α is the Duffing parameter and then the first term reads:

$$H_{re} = \frac{p^2}{2m} + \frac{m\omega^2}{2}x^2 + \alpha x^4, \tag{3}$$

where the considered mass m, momentum p, and especially the resonating frequency which possess the inverse relation with the mass can be illustrated as $\omega^2 = (k/m)$. In the second term, the Hamiltonian is composed of three parts; two of them are with the specific energy of the quantum dot and electrons, respectively. We consider the CNT as a single-level quantum dot mentioned in [30] with the width of the single level with the dependence of density of the considered states. Such mathematical representations can be manipulated as $\Gamma = \Gamma_l + \Gamma_r$, and the last one is the energy of tunneling [28]. The detail expression of the second term is written as $H_Q = \sum_{\alpha,k}(\varepsilon_{\alpha k} - \mu_\alpha)c^\dagger_{\alpha k}c_{\alpha k} + \epsilon_0 d^\dagger d + \sum_k t_{\alpha k}c^\dagger_{\alpha k}d + H \cdot c$, which possess the factor $\alpha = L(r)$, and $\varepsilon_{\alpha k}$ determines the electrons energy summation in the exaggeration and the energy of chemical potential is μ_α. However, the terms d as well as c represent the dot and destruction operator, respectively. When the tunnel of electron appears at the CNTs, the corresponding rate of tunneling can be mentioned as

$$\Gamma_\alpha = \pi t^2_\alpha \rho_\alpha, \tag{4}$$

where ρ_α represents the density of the considered states. We consider the symmetric system to simplify our findings, and in such techniques, we have to write $\Gamma/2 = \Gamma_l = \Gamma_r$.

The last term that is more crucial and interesting in the nanomechanical systems gives the coupling strength of electromechanical for the aforementioned system, and one can read it as [30]

$$H_c = -F_0 x d^\dagger d. \tag{5}$$

One could find that the coupling strength is the function of the vibration displacement within the CNTs. In such quantum calculations, the factor $n = d^\dagger d$ denotes the numbering of electrons at the average under the tunneling in CNTs, and F_0 represents the active force for the oscillator at that moment when an electron is tunneling just at the top of the CNTs.

In particular, we consider the electron tunnel in the coherent regime under the condition $k_B T \ll \Gamma$. In such circumstances, the factor Γ represents the rate of tunneling, and T measures the strength of the considered temperature. Especially, $\hbar$ as well as k_B denote the Planck and the Boltzmann important constants, respectively. In particular,

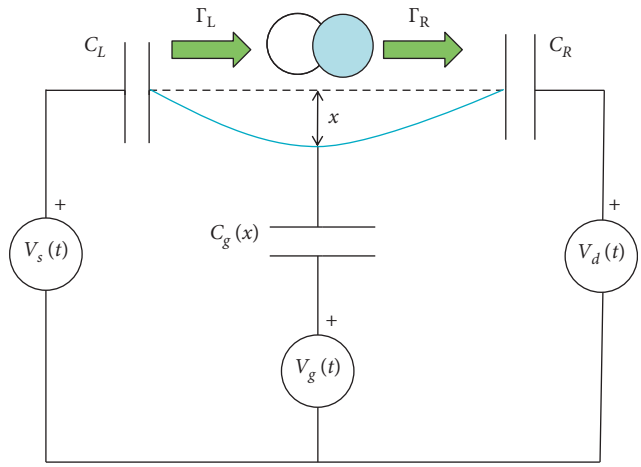

Figure 1: Schematics of the quantum dot embedded nanomechanical resonator. The mentioned CNT is clamped doubly between a drain electrode and source which has been suspended just above the given gate electrode; then, the CNT acts as a quantum dot, and single-electron tunneling is the dominant transport mechanism.

the mechanical mode dynamics with the displacement can be illustrated by a famous equation of Langevin [14]:

$$m\ddot{x} + A(x)\dot{x} + m\omega_0^2 x = eta(t) + F_e(x), \tag{6}$$

where $A(x)$ represents the dissipation and $\eta(t)$ is a force of stochastic that obeys the $\langle \eta(t)\eta(t')\rangle = C(x)\delta(t-t')$. Because the effect of the time interval of the correlations functions can denote Γ^{-1}, in such circumstances, the acquired $\Gamma \gg \omega_0$. So, we approximate the considered calculations by using the function of Dirac delta and the force at an average manipulates as $F_e(x) = F_0 n_d(x)$ and $C(x) = F_0^2 S_{nn}(x, \omega \sim 0)$, and similarly, the expression of $A(x) = -F_0^2(\partial S_{nn}/\partial\omega)(x,\omega)|_{\omega=0}$, within the limit of $n_d = \langle d^\dagger d\rangle$ which examines the mean of the population of our considered dot. m also measures the effectiveness of the mass for the oscillator mode considered. The obvious expressions for n_d, S_{nn}, and A have been derived in detail in the Appendix of [15]. With the equation of Langevin, one can obtain the probability distributions $Q(x,p,t)$ within the framework of the Fokker Planck form:

$$\partial_t Q = \frac{p}{m}\partial_x Q - F\partial_p Q + \frac{A}{m}\partial_p(pQ) + \frac{D}{2}\partial_p^2(Q), \tag{7}$$

where $F(x) = F_r + F_e(x)$.

3. Results and Discussion

The main object of this research is to explore the nature of the nanomechanical system which is originated by quantum mechanical systems at an extraordinary momentum, and it can be feasible by using the system of carbon nanotubes' resonator with numerous cavities and their corresponding mechanical restoring force consistently. Here, we elucidate our model results about nonlinearities of the system, position probability distribution, average current, and displacement fluctuations. We are also interested to examine the characteristics of the position probability, mechanical noise, and average current which behaved meaningful significantly during the considered quantum systems at various energies and momenta, and we presume that the produced sources consist of the debris of frequencies that behave as the nanomechanical system to use in the thermal as well as in mechanical engineering.

3.1. Nonlinearities of the System. In this section, we introduce nonlinearity in our study; the nonlinearity can have various sources. Here, we are interested to explore in the famous and unique sources which are the two within the main unit. One is directly from the electron tunneling, which contributes the F_e in the total force and exhibits from the electromechanical coupling α_{SET}. Another source is from the geometryα_G and electrostatic α_{ES} indirectly. In recent CNT resonator-based experiments [27], one can estimate the Duffing parameter $\alpha = -1/(6m)\mathrm{d}^3F/\mathrm{d}x^3$, when $V_g = 1V$, $\alpha_{SET} = 8 * 10^{31}\mathrm{N}/(\mathrm{kg} * \mathrm{m}^3)$, $\alpha_G = 9.6 * 10^{34}\mathrm{N}/(\mathrm{kg} * \mathrm{m}^3)$, and $\alpha_{ES} = -3.2 * 10^{28}\mathrm{N}/(\mathrm{kg} * \mathrm{m}^3)$. One can write the Duffing term in the restoring force as the nonlinearities. Now, the total resultant force $F(x)$ exerts at the considered oscillator, and such force can be seen in [30]. We also here considered that the vanishing temperature factor which implies $k_B T \ll \Gamma$, as well as the lowest voltages which are bias and demonstrate $eV \ll \Gamma$, could be acquired with the summation of the force restoring factor within the mechanical system and the electronic contribution as mentioned in equation (2). The force due to the electronic contribution refers to [15] and can be illustrated as

$$F_e(x) = f(x, \varepsilon_0, \varepsilon_P). \tag{8}$$

One could see that the Duffing parameter α, the variation of the gate energy ε_0, and coupling ε_P could contribute the nonlinearities for the system.

3.2. Position Probability Distribution. In this section, we discuss the mechanical motion by the position probability distribution of the CNT with the Duffing parameter and the

electromechanical coupling. In order to solve the considered equation of Fokker Planck, we examine and investigate the given equation to solve sophistically and numerically within the linear problem. Defining the operator of the famous Fokker Planck as mentioned $\mathscr{L}$ in the acquired equation,

$$\partial_t Q = \widetilde{\mathscr{L}} Q. \tag{9}$$

For the stationary solution, $\partial_t Q = 0$, we consider the oscillator of quantum mechanical systems in the presence of the symmetry, where the gate energy $\varepsilon_0 = \varepsilon_P/2$ shows the special characteristics, and it also corresponds to adopting the most new point of electron hole symmetry for the aforementioned system [15]. Moreover, the parameters $\omega_0/\Gamma = 10^{-3}$ and $k_B T/\Gamma = 10^{-2}$ also can be useful in the measured calculation. The units of the t, x, p, and α are ω_0^{-1}, $(m\omega_0)^{-1/2}$, $(m\omega_0)^{1/2}$, and $F_0 (m\omega_0)^{3/2}$ in this paper. From Figure 2, the mechanical bistability of this system has been described when Duffing parameter, $\alpha = 0$; these results work well with the conclusions of [15]. We discuss our results from the mechanical view when the Duffing parameter $\alpha = 0$; the total force is

$$F(\widetilde{x}) = -k\widetilde{x} + \frac{F_0}{\pi} \arctan \frac{F_0 \widetilde{x}}{\Gamma}. \tag{10}$$

where $\widetilde{x} = x - x_0$ and $x_0 = F_0/2k$. One can verify that the acquiring force is not symmetric corresponding to the acquiring points of $x_0 = F_0/2k$ and linear with $\widetilde{x}$. The position probability distribution shows that the coupling increases over the critical coupling value $\varepsilon_c = \pi\Gamma$. The position probability distribution displays a strong nonlinear signal which is that merely one curious sharp-peak turns to double peaks which show that the coupling induces strong nonlinear effect and the considered system tilts into the regimes of the bistable $\widetilde{\varepsilon}_p > 1$ which originate from basic single stable regime $\varepsilon_p \leq \varepsilon_c$. For the critical value, our system distribution possess flat and wider sharp peaks. All these interesting consequences could be explained by the potential of the system. One could see that the nonlinear effect from the coupling is dominant in the tunneling process than the Duffing nonlinearity. The position probability distribution with different Duffing parameters shows that the nonlinearity of the nanotube resonator also contributes to the mechanical state's transition; it induces the asymmetric of the position probability distribution with x_0. It could push or slow down the process of electron tunneling.

3.3. The Average Current. Because of its mobility, a quantum particle like an electron generates an electric current. The flow of its likelihood is linked to that current. These currents are determined by the wave function that explains a particle's state. At a higher level, the quantum operator that can operate between states or interact with a density matrix to determine currents even in scenarios such mixed levels of thermodynamic equilibrium which can be found. Here are the concepts and equations which were used to utilize these themes. The current in our model under the coherent tunneling regime shows $k_B T \ll \Gamma$ and under the certain condition implies $V, T \ll \Gamma$ [29]. In such circumstances, the limit of the lower voltage obeys the condition of $eV \ll k_B T$, and it can manipulate as [30]

$$I = \frac{e^2 V}{2\pi} \tau(z), \tag{11}$$

where $\tau = 1/(1 + z^2)$ and $z = (\mu - \epsilon_0 + F_0 x)/\Gamma$. It is easier to commute the average of the current $\omega \ll \Gamma$ with the distribution of the probability P_{st} by integrating x:

$$I = \frac{e^2 V}{2\pi} \int \mathrm{d}x \mathrm{d}p Q(x, p, t) \tau(x). \tag{12}$$

From Figure 3, one could see that the strong electromechanical coupling strongly suppresses the current, which is called the current blockade. The presence of the Duffing nonlinearities could accelerate or slow down the current's declining, especially in the region of the bistable state.

3.4. Displacement Fluctuations. In this section, we investigate the effect of the electromechanical coupling and the Duffing nonlinearity on the system from the displacement fluctuations spectrum. The displacement fluctuations' spectrum is as [13]

$$S_{xx}(\omega) = -2Tr\left[\widehat{\widetilde{x}} \frac{\widehat{\mathscr{L}}}{\omega^2 + \widehat{\mathscr{L}}^2} \widehat{\widetilde{x}} Q_{st}\right]. \tag{13}$$

Here, it is crucial to indicate that the whole terms which acquired a hat in (13) represent the super quantum operators those acting in the regime of the probability space and can be illustrated as $\widehat{\widetilde{x}}(t) = \widehat{x}(t) - \langle x \rangle$.

From Figure 4, one could see that, in the mechanical frequency ω_0 region when the system contains only monostable state, there is appearing unit resonance frequency with the sharpness peak. Once the considering coupling increases over the certain value, the mentioned sharp-peak transference to the extremely low frequency and the corresponding width of mentioned peak becomes broaden and broaden with the softening of an interesting frequency which represents the mechanical phenomena. The Duffing nonlinearity can contribute to the resonance frequency shift under the specific condition that the considered system goes to that regime which is bistable. However, the appearance of the doublet peak originates as the electrons can transform from one identical state to distinct another state. Therefore, the identical fluctuation of displacement spectrum features has also been obtained in [15] and [22]. Both situations appear for a system of nanomechanical within the regime of the semiclassical and the Frank–Condon principle [11]. When the Duffing term α is negative, the resonance frequency shifts to a higher frequency, meaning the stiffening spring behavior. Conversely, within the limit of α which took positive and the corresponding resonance certain peak shifts towards the critical lower frequency, meaning the softening-spring behavior.

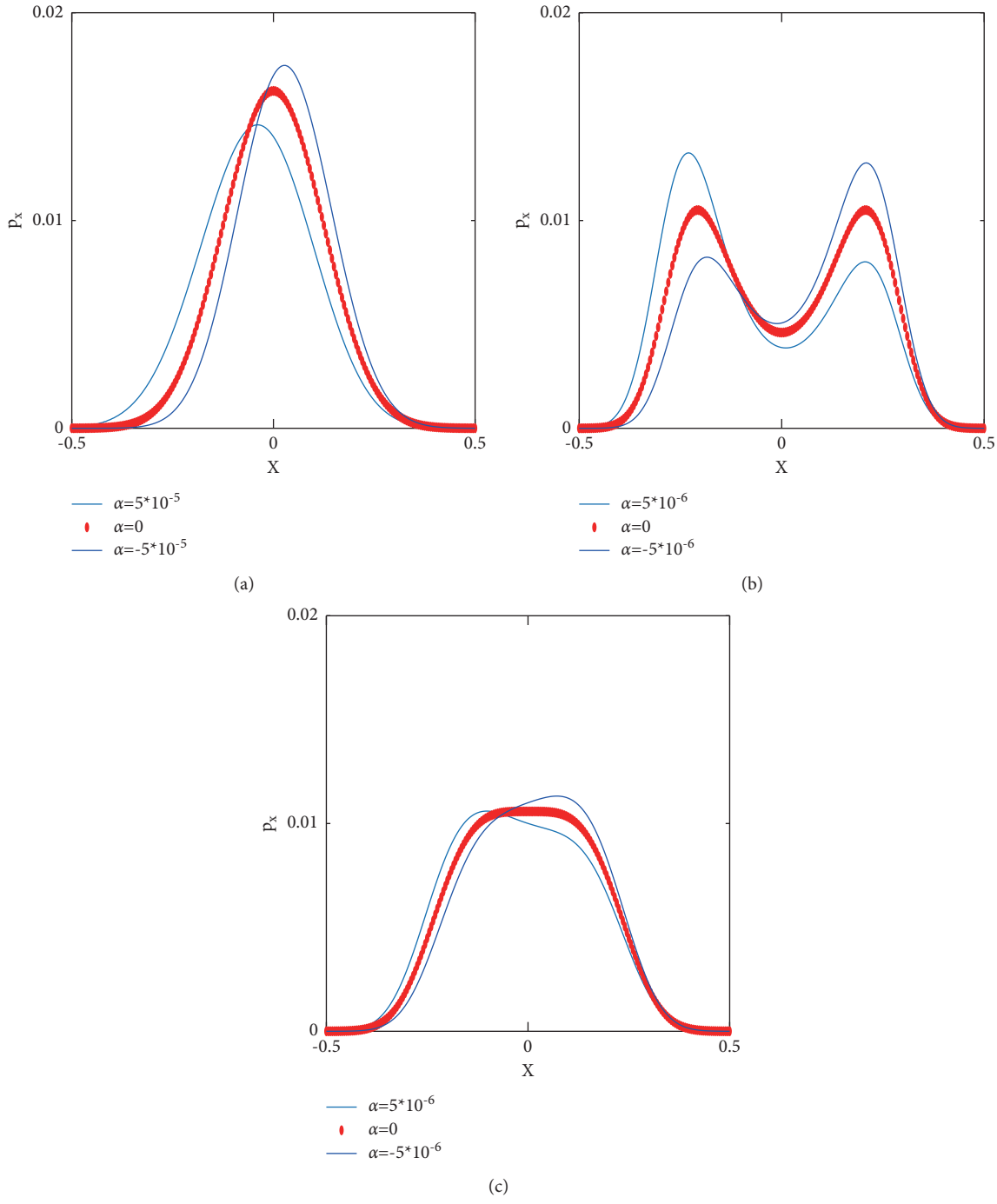

FIGURE 2: The position probability distribution P_x versus displacement with different coupling ($\varepsilon_P = 0.6\pi\Gamma, 1\pi\Gamma, 1.2\pi\Gamma$) and three Duffing parameters ($\alpha = -5 * 10^{-5}, 0, 5 * 10^{-5}$).

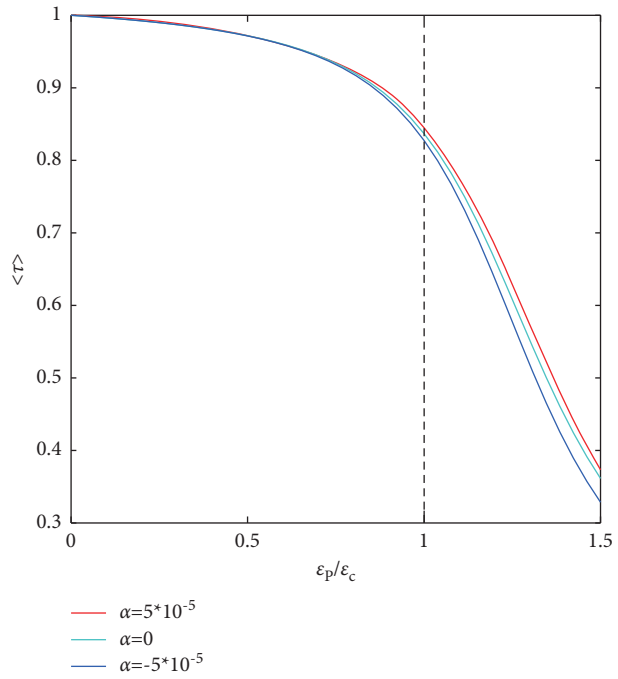

Figure 3: The average current $\langle \tau \rangle$ versus the electromechanical coupling with three Duffing parameters ($\alpha = -5 * 10^{-5}$, 0, $5 * 10^{-5}$).

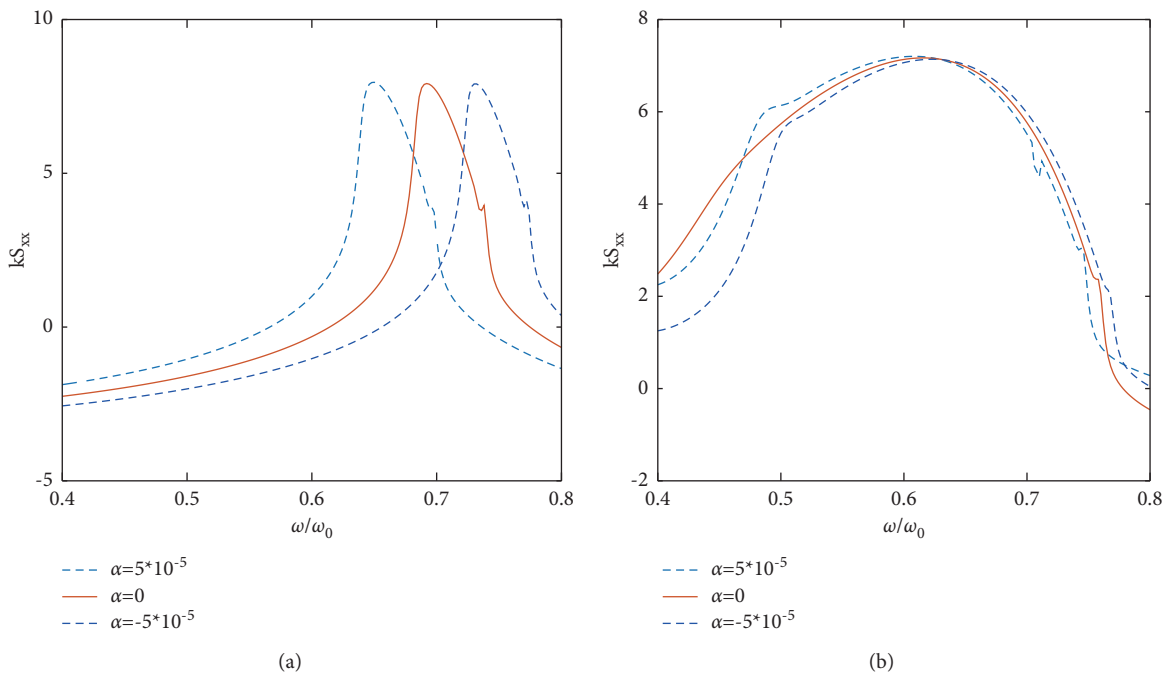

Figure 4: Continued.

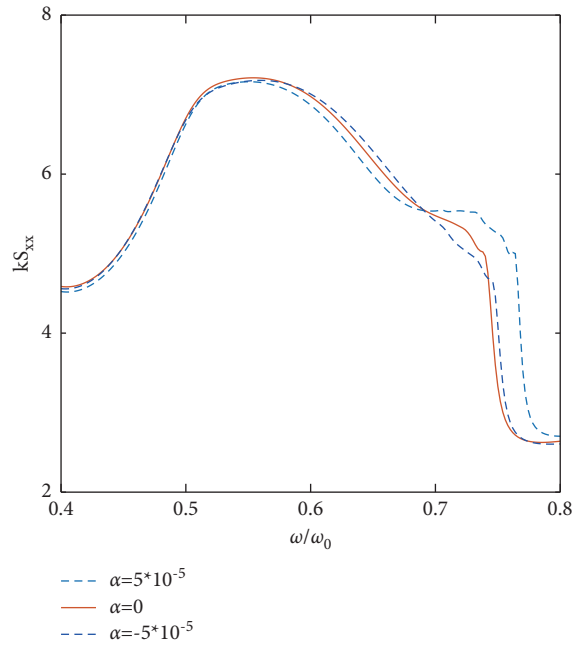

(c)

FIGURE 4: The dimensionless fluctuations of displacement spectrum versus the mechanical distribution of frequency within the various coupling strength ($\epsilon_P = 0.60\pi\Gamma, \pi\Gamma, 1.20\pi\Gamma$) and the three Duffing parameter ($\alpha = -5 * 10^{-5}$, 0, $5 * 10^{-5}$).

4. Conclusions

We afford the research of the nonlinearities in the nanomechanical system of a carbon nanotube resonator strongly coupled to a quantum dot. The two main sources of the nonlinearities are given from the mechanical restoring force; one comes from directly the single-electron tunneling, especially with the presence of the strong electromechanical coupling; another nonlinearity is from geometry, electrostatics, and electron tunneling. The Duffing term is considered that is cubic in displacement included in the restoring force in our paper. The position probability, the average current, and the mechanical noise with different Duffing parameters have been studied. It is found that the Duffing nonlinearities of the CNT-based resonator could induce the asymmetry of the probability distribution of the current blockade, soften, or stiffen the mechanical resonance frequency that is important as the electromechanical coupling in the nanomechanical systems.

We have explored the nonlinearities of the system, position probability distribution, average current, and displacement fluctuations. We have also investigated the characteristics of the position probability, mechanical noise, and average current with various factors which behaved meaningful during the considered quantum systems at distinct energies, momenta in the short, and wide temperature regimes. One persuasive explication of this ramification is that our considered quantum system possessed the asymmetry of the probability distribution.

Data Availability

The data used to support the findings of the study are available within the article.

Disclosure

This paper is new and not submitted to any other journal. All the results included are new and not reported before.

Conflicts of Interest

The authors declare that they have no conflicts of interest or personal relationships that could have appeared to influence the work reported in this paper.

Authors' Contributions

Yue Wang put forward the ideal and wrote the original draft; Ghulam Bary and Riaz Ahmad wrote the manuscript; Dameng Yin and Shiwei Xie performed the calculations; Qing Lu, Ilyas Khan, Nawa Alshammari, Nawaf N. Hamadneh, and Mulugeta Andualemb contributed the check and review of the results and data analysis.

Acknowledgments

This work was supported by the Sailing Plan Project of Yibin University (nos. 2021QH08, 2021QH05, and 2021QH06) and the Open Research Fund of Computational physics Key

Laboratory of Sichuan province, Yibin University (nos. YBXYJSWL-ZD-2020-003 and YBXYJSWL-ZD-2020-004). The authors thank Xulin Peng and Lin Li for careful read and useful suggestions. Yibin University provided the financial support for this study.

References

[1] C. Dutreix, R. Avriller, and B. Lounisand, "Two-level system as topological actuator for nanomechanical modes," *Physical Review Research*, vol. 2, Article ID 023268, 2020.

[2] Q. Schaeverbeke, R. Avriller, T. Frederiksen, and F. Pistolesi, "Single-photon emission mediated by single-electron tunneling in plasmonic nanojunctions," *Physical Review Letters*, vol. 123, no. 24, Article ID 246601, 2019.

[3] R. Avriller, B. Murr, and F. Pistolesi, "Bistability and displacement fluctuations in a quantum nanomechanical oscillator," *Physical Review B*, vol. 97, no. 15, Article ID 155414, 2018.

[4] Y. M. Blanter, O. Usmani, and a. Y. V. Nazarov, "Single-electron tunneling with strong mechanical feedback," *Physical Review Letters*, vol. 93, no. 13, Article ID 136802, 2004.

[5] Ya. M. Blanter, O. Usmani, and E. Nazarov, "Single electron tunneling with strong mechanical feedback," *Physical Review Letters*, vol. 94, Article ID 049904, 2005.

[6] A. D. Armour, M. P. Blencowe, and Y. Zhang, "Classical dynamics of a nanomechanical resonator coupled to a single-electron transistor," *Physical Review B*, vol. 69, no. 12, Article ID 125313, 2004.

[7] C. B. Doiron, W. Belzig, and C. Bruder, "Electrical transport through a single-electron transistor strongly coupled to an oscillator," *Physical Review B*, vol. 74, no. 20, Article ID 205336, 2006.

[8] F. Pistolesi and R. Shekhter, "Tunable spin-polaron state in a singly clamped semiconducting carbon nanotube," *Physical Review B: Condensed Matter*, vol. 92, Article ID 035423, 2015.

[9] R. Ahmad, A. Farooqi, and R. Farooqi, "An analytical approach to study the blood flow over a nonlinear tapering stenosed artery in flow of carreau fluid model measles," *Complexity*, vol. 2021, Article ID 9921642, 11 pages, 2021.

[10] D. Mozyrsky, M. B. Hastings, and I. Martin, "Intermittent polaron dynamics: born-Oppenheimer approximation out of equilibrium," *Physical Review B: Condensed Matter*, vol. 73, Article ID 035104, 2006.

[11] J. Koch and F. von Oppen, "Franck-condon blockade and giant fano factors in transport through single molecules," *Physical Review Letters*, vol. 94, no. 20, Article ID 206804, 2005.

[12] F. Pistolesi and S. Labarthe, "Current blockade in classical single-electron nanomechanical resonator," *Physical Review B*, vol. 76, no. 16, Article ID 165317, 2007.

[13] F. Pistolesi, Y. M. Blanter, and I. Martin, "Self-consistent theory of molecular switching," *Physical Review B: Condensed Matter*, vol. 78, Article ID 085127, 2008.

[14] G. Micchi, R. Avriller, and F. Pistolesi, "Mechanical signatures of the current blockade instability in suspended carbon nanotubes," *Physical Review Letters*, vol. 115, no. 20, Article ID 206802, 2015.

[15] G. Micchi, R. Avriller, and F. Pistolesi, "Electromechanical transition in quantum dots," *Physical Review B*, vol. 94, no. 12, Article ID 125417, 2016.

[16] J. Moser, A. Eichler, J. Güttinger, M. I. Dykman, and A. Bachtold, "Nanotube mechanical resonators with quality factors of up to 5 million," *Nature Nanotechnology*, vol. 9, no. 12, pp. 1007–1011, 2014.

[17] A. Benyamini, A. Hamo, S. V. Kusminskiy, F. von Oppen, and S. Ilani, "Real-space tailoring of the electron-phonon coupling in ultraclean nanotube mechanical resonators," *Nature Physics*, vol. 10, no. 2, pp. 151–156, 2014.

[18] M. Ganzhorn and W. Wernsdorfer, "Dynamics and dissipation induced by single-electron tunneling in carbon nanotube nanoelectromechanical systems," *Physical Review Letters*, vol. 108, no. 17, Article ID 175502, 2012.

[19] K. L. Ekinci, X. M. H. Huang, and M. L. Roukes, "Ultrasensitive nanoelectromechanical mass detection," *Applied Physics Letters*, vol. 84, no. 22, pp. 4469–4471, 2004.

[20] J. Moser, J. Güttinger, A. Eichler et al., "Ultrasensitive force detection with a nanotube mechanical resonator," *Nature Nanotechnology*, vol. 8, no. 7, pp. 493–496, 2013.

[21] B. Lassagne, D. Garcia-Sanchez, A. Aguasca, and A. Bachtold, "Ultrasensitive mass sensing with a nanotube electromechanical resonator," *Nano Letters*, vol. 8, no. 11, pp. 3735–3738, 2008.

[22] R. Avriller, B. Murr, and F. Pistolesi, "Bistability and displacement fluctuations in a quantum nanomechanical oscillator," *Physical Review B*, vol. 97, no. 15, Article ID 155414, 2018.

[23] F. Pistolesi, "Bistability of a slow mechanical oscillator coupled to a laser-driven two-level system," *Physical Review A*, vol. 97, Article ID 063833, 2018.

[24] V. Puller, B. Lounis, and F. Pistolesi, "Single molecule detection of nanomechanical motion," *Physical Review Letters*, vol. 110, no. 12, Article ID 125501, 2013.

[25] P. G. Kirton and A. D. Armour, "Nonlinear dynamics of a driven nanomechanical single-electron transistor," *Physical Review B*, vol. 87, no. 15, Article ID 155407, 2013.

[26] A. A. Clerk, "Quantum-limited position detection and amplification: a linear response perspective," *Physical Review B*, vol. 70, no. 24, Article ID 245306, 2004.

[27] G. Bary, W. Ahmed, M. Sajid et al., "A new analytical approach to study chaos fraction characterization by using intensity interferometry," *Chaos, Solitons & Fractals*, vol. 152, Article ID 111414, 2021.

[28] Y. Wang, F. Liu, and D. Huang, "Electromechanical coupling effect in the detection of nanomechanical motion," *The European Physical Journal B*, vol. 94, no. 5, p. 107, 2021.

[29] Y. M. Blanter and M. Büttiker, "Shot noise in mesoscopic conductors," *Physics Reports*, vol. 336, no. 1-2, pp. 1–166, 2000.

[30] Y. Wang, G. Micchi, and F. Pistolesi, "Sensitivity of the mixing-current technique for the detection of mechanical motion in the coherent tunnelling regime," *Journal of Physics: Condensed Matter*, vol. 29, no. 46, Article ID 465304, 2017.

Hindawi
Mathematical Problems in Engineering
Volume 2021, Article ID 9444803, 9 pages
https://doi.org/10.1155/2021/9444803

Research Article

A Generalized Definition of the Fractional Derivative with Applications

M. Abu-Shady [1] **and Mohammed K. A. Kaabar** [2,3]

[1]*Department of Mathematics and Computer Science, Faculty of Science, Menoufia University, Shibin Al Kawm, Egypt*
[2]*Gofa Camp, Near Gofa Industrial College and German Adebabay, Nifas Silk-Lafto, Addis Ababa 26649, Ethiopia*
[3]*Institute of Mathematical Sciences, Faculty of Science, University of Malaya, Kuala Lumpur 50603, Malaysia*

Correspondence should be addressed to Mohammed K. A. Kaabar; mohammed.kaabar@wsu.edu

Received 27 August 2021; Revised 3 October 2021; Accepted 11 October 2021; Published 23 October 2021

Academic Editor: Muhammad Shoaib Anwar

A generalized fractional derivative (GFD) definition is proposed in this work. For a differentiable function expanded by a Taylor series, we show that $D^{\alpha}D^{\beta}f(t) = D^{\alpha+\beta}f(t); 0 < \alpha \leq 1; 0 < \beta \leq 1$. GFD is applied for some functions to investigate that the GFD coincides with the results from Caputo and Riemann–Liouville fractional derivatives. The solutions of the Riccati fractional differential equation are obtained via the GFD. A comparison with the Bernstein polynomial method (BPM), enhanced homotopy perturbation method (EHPM), and conformable derivative (CD) is also discussed. Our results show that the proposed definition gives a much better accuracy than the well-known definition of the conformable derivative. Therefore, GFD has advantages in comparison with other related definitions. This work provides a new path for a simple tool for obtaining analytical solutions of many problems in the context of fractional calculus.

1. Introduction

Fractional calculus theory is a natural extension of the ordinary derivative which has become an attractive topic of research due to its applications in various fields of science and engineering. The integral inequalities in fractional models play an important role in different fields. Massive attention on the advantages of integral inequalities has been paid for considering economics [1], continuum and statistical mechanics [2], solid mechanics [3], electrochemistry [4], biology [5], and acoustics [6]. Fractional-order derivatives of a given function involve the entire function history where the following state of a fractional-order system is not only dependent on its current state but also all its historical states [7, 8]. Nonlocality plays a very important role in several fractional derivative models [9, 10]. Many studies deal with the discrete versions of this fractional calculus by employing the theory of time scales such as [11, 12]. In the literature, some definitions have been introduced such as Riemann–Liouville, Caputo, Jumarie, Hadamard, and Weyl, but all of these definitions have their advantages and disadvantages. The most commonly used definition is Riemann–Liouville which is defined as follows [13].

For $\alpha \in [n-1, n)$, the α-derivative of $f(t)$ is

$$D^{\mathrm{RL}} f(t) = \frac{1}{\Gamma(n-\alpha)} \frac{d^n}{dx^n} \int_a^{\infty} \frac{f(x)}{(t-x)^{(\alpha-n+1)}} \mathrm{d}x. \tag{1}$$

The Caputo definition is defined as follows.

For $\alpha \in [n-1, n)$, the α-derivative of $f(t)$ is

$$D^{C} f(t) = \frac{1}{\Gamma(n-\alpha)} \int_a^{\infty} \frac{d^n f(x)/dx^n}{(t-x)^{(\alpha-n+1)}} \mathrm{d}x. \tag{2}$$

All definitions including the above (1) and (2) satisfy the linear property of fractional derivatives. These fractional derivatives have several advantages, but they are not suitable for all cases. On the one hand, in the Riemann–Liouville type, when the fractional differential equations are used to describe real-world processes, the Riemann–Liouville derivative has some drawbacks. The Riemann–Liouville derivative of a constant is not zero. Additionally, if an arbitrary

function is a constant at the origin, its fractional derivation has a singularity at the origin for instant exponential and Mittag-Leffler functions. Due to these drawbacks, the applicability range of Riemann–Liouville fractional derivatives is limited. For differentiability, Caputo derivative requires higher regularity conditions: to calculate the fractional derivative of a function in the Caputo type, we should first obtain its derivative. Caputo derivatives are defined only for differentiable functions, while the functions that do not have first-order derivative may have fractional derivatives of all orders less than one in the Riemann–Liouville sense (see [13]).

In [14], a new well-behaved simple fractional derivative, named conformable derivative, was defined by relying only on the basic limit definition of the derivative. The conformable derivative satisfies some important properties that cannot be satisfied in Riemann–Liouville and Caputo definitions. However, in [15], the author proved that the conformable definition in [14] cannot provide good results in comparison with the Caputo definition for some functions.

This work aims to provide a new generalized definition of the fractional derivative that has advantages in comparison with other previous definitions in order to obtain simple solutions of fractional differential equations.

The paper is organized as follows: in Section 2, the basic definitions and tools are introduced. In Section 3, some applications are presented. In Section 4, the conclusion is given.

2. Basic Definitions and Tools

Definition 1. For a function $f\colon (0,\infty) \longrightarrow R$, the generalized fractional derivative of order $0 < \alpha \leq 1$ of $f(t)$ at $t > 0$ is defined as

$$D^{\mathrm{GFD}} f(t) = \lim_{\varepsilon \longrightarrow 0} \frac{f\left(t + \Gamma(\beta)/\Gamma(\beta - \alpha + 1)\varepsilon t^{1-\alpha}\right) - f(t)}{\varepsilon}; \quad \beta > -1, \beta \in R^{+}, \tag{3}$$

and the fractional derivative at 0 is defined as $D^{\mathrm{GFD}} f(0) = \lim_{\varepsilon \longrightarrow 0^{+}} D^{GF\,D} f(t)$.

Theorem 1. *If $f(t)$ is an α–differentiable function, then $D^{GFD} f(t) = \Gamma(\beta)/\Gamma(\beta - \alpha + 1)t^{1-\alpha} df(t)/dt$; $\beta > -1$, $\beta \in R^{+}$.*

Proof. By using the definition in equation (3), we have

$$D^{\mathrm{GFD}} f(t) = \lim_{\varepsilon \longrightarrow 0} \frac{f\left(t + \Gamma(\beta)/\Gamma(\beta - \alpha + 1)\varepsilon t^{1-\alpha}\right) - f(t)}{\varepsilon}; \quad \beta > -1, \beta \in R^{+}, \tag{4}$$

where at $\alpha = \beta = 1$, the classical limit of a derivative function is obtained. Now, let

$$h = \frac{\Gamma(\beta)}{\Gamma(\beta - \alpha + 1)} \varepsilon t^{1-\alpha}, \tag{5}$$

$$\varepsilon = \frac{\Gamma(\beta - \alpha + 1)}{\Gamma(\beta)} h t^{\alpha - 1}. \tag{6}$$

By substituting equation (6) into equation (4), we get

$$D^{\mathrm{GFD}} f(t) = \frac{\Gamma(\beta)}{\Gamma(\beta - \alpha + 1)} t^{1-\alpha} \lim_{h \longrightarrow 0} \frac{f(t+h) - f(t)}{h}. \tag{7}$$

Thus,

$$D^{\mathrm{GFD}} f(t) = \frac{\Gamma(\beta)}{\Gamma(\beta - \alpha + 1)} t^{1-\alpha} \frac{df(t)}{dt}. \tag{8}$$

For a function $f(t) = t^{k}, k > -1, k \in R^{+}$, we prove that

$$D^{\mathrm{GFD}} f(t) = \frac{\Gamma(\beta + 1)}{\Gamma(\beta - \alpha + 1)} t^{\beta - \alpha}. \tag{9}$$

By using equation (8), we obtain

$$\begin{aligned} D^{\mathrm{GFD}} f(t) &= \frac{\Gamma(\beta)}{\Gamma(\beta - \alpha + 1)} t^{1-\alpha} k t^{k-1}, \\ D^{\mathrm{GFD}} f(t) &= \frac{k\Gamma(\beta)}{\Gamma(\beta - \alpha + 1)} t^{k-\alpha}. \end{aligned} \tag{10}$$

By taking $k = \beta$, we get

$$D^{\mathrm{GFD}} t^{\beta} = \frac{\beta\Gamma(\beta)}{\Gamma(\beta - \alpha + 1)} t^{\beta - \alpha}, \tag{11}$$

and then

$$D^{\mathrm{GFD}} t^{\beta} = \frac{\Gamma(\beta + 1)}{\Gamma(\beta - \alpha + 1)} t^{\beta - \alpha}. \tag{12}$$

Equation (12) is compatible with the results of Caputo and Riemann–Liouville derivatives [16]. □

Theorem 2. *For a function derivative of $f(t) = t^{k}$, $k \in R^{+}$, we obtain $D^{\alpha} D^{\beta} t^{k} = D^{\alpha+\beta} t^{k}$.*

Proof. By using equation (12), we get

$$\begin{aligned} D^{\beta} t^{k} &= \frac{\Gamma(k+1)}{\Gamma(k - \beta + 1)} t^{k-\beta}, \\ D^{\alpha} D^{\beta} t^{k} &= \frac{\Gamma(k+1)}{\Gamma(k - \beta + 1)} D^{\alpha} t^{k-\beta}, \\ D^{\alpha} D^{\beta} t^{k} &= \frac{\Gamma(k+1)}{\Gamma(k - \beta + 1)} \frac{\Gamma(k - \beta + 1)}{\Gamma(k - \beta - \alpha + 1)} t^{k-\beta-\alpha}. \end{aligned} \tag{13}$$

$$\mathrm{L.H.S} = D^{\alpha} D^{\beta} t^{k} = \frac{\Gamma(k+1)}{\Gamma(k - \beta - \alpha + 1)} t^{k-\beta-\alpha}. \tag{14}$$

Also, we have

$$\mathrm{R.H.S} = D^{\alpha+\beta} t^{k} = \frac{\Gamma(k+1)}{\Gamma(k - \beta - \alpha + 1)} t^{k-\beta-\alpha}. \tag{15}$$

Thus, by (14) and (15), we get

$$D^{\alpha}D^{\beta}t^{k} = D^{\alpha+\beta}t^{k}. \tag{16}$$

This property is not satisfied in the conformable derivative [14]. □

Theorem 3. *For a differentiable function $f(t)$ that expands about a point such as $f(t) = \sum_{k=0}^{\infty} f^{k}(0)/k!t^{k}$, we have $D^{\alpha}D^{\beta}f(t) = D^{\alpha+\beta}f(t)$.*

Proof. The expanded function by Taylor theory is given by $f(t) = \sum_{k=0}^{\infty} f^{k}(0)/k!t^{k}$,

$$D^{\beta}f(t) = \sum_{k=0}^{\infty}\frac{f^{k}(0)}{k!}D^{\beta}t^{k},$$

$$D^{\beta}f(t) = \sum_{k=0}^{\infty}\frac{f^{k}(0)}{k!}\frac{\Gamma(k+1)}{\Gamma(k-\beta+1)}t^{k-\beta},$$

$$D^{\alpha}D^{\beta}f(t) = \sum_{k=0}^{\infty}\frac{f^{k}(0)}{k!}\frac{\Gamma(k+1)}{\Gamma(k-\beta+1)}D^{\alpha}t^{k-\beta},$$

$$D^{\alpha}D^{\beta}f(t) = \sum_{k=0}^{\infty}\frac{f^{k}(0)}{k!}\frac{\Gamma(k+1)}{\Gamma(k-\beta+1)}\frac{\Gamma(k-\beta+1)}{\Gamma(k-\beta-\alpha+1)}t^{k-\beta-\alpha}, \tag{17}$$

$$\text{L.H.S} = D^{\alpha}D^{\beta}f(t) = \sum_{k=0}^{\infty}\frac{f^{k}(0)}{k!}\frac{\Gamma(k+1)}{\Gamma(k-\beta-\alpha+1)}t^{k-\beta-\alpha}, \tag{18}$$

$$\text{R.H.S} = D^{\alpha+\beta}f(t) = \sum_{k=0}^{\infty}\frac{f^{k}(0)}{k!}D^{\alpha+\beta}t^{k}, \tag{19}$$

$$\text{R.H.S} = D^{\alpha+\beta}f(t) = \sum_{k=0}^{\infty}\frac{f^{k}(0)}{k!}\frac{\Gamma(k+1)}{\Gamma(k-\beta-\alpha+1)}t^{k-\beta-\alpha}. \tag{20}$$

Thus, by equations (18) and (20), we have

$$D^{\alpha}D^{\beta}f(t) = D^{\alpha+\beta}f(t). \tag{21}$$

This property is not satisfied in the conformable derivative [14]. □

Theorem 4. *Let $\alpha \in (0,1]$ and f, g be α–differentiable functions; then,*

$$(i)\ D^{\text{GFD}}(fg) = fD^{\text{GFD}}(g) + gD^{\text{GFD}}(f), \tag{22}$$

$$(ii)\ D^{\text{GFD}}\left(\frac{f}{g}\right) = \frac{gD^{\text{GFD}}(f) - fD^{\text{GFD}}(g)}{g^{2}}. \tag{23}$$

Proof. By using equation (8), we have

$$\text{L.H.S} = D^{\text{GFD}}(fg), \tag{24}$$

$$= \frac{\Gamma(\beta)}{\Gamma(\beta-\alpha+1)}t^{1-\alpha}\frac{d(fg)}{dt}, \tag{25}$$

$$= \frac{\Gamma(\beta)}{\Gamma(\beta-\alpha+1)}t^{1-\alpha}\left[f\frac{dg}{dt} + g\frac{df}{dt}\right], \tag{26}$$

$$= f\frac{\Gamma(\beta)}{\Gamma(\beta-\alpha+1)}t^{1-\alpha}\frac{dg}{dt} + g\frac{\Gamma(\beta)}{\Gamma(\beta-\alpha+1)}t^{1-\alpha}\frac{df}{dt}, \tag{27}$$

$$= \text{FD}^{\text{GFD}}(g) + gD^{\text{GFD}}(f) = \text{R.H.S}. \tag{28}$$

This proves (i).

Now, to prove (ii), we use equation (8) as follows:

$$\begin{aligned}\text{L.H.S} &= D^{\text{GFD}}\left(\frac{f}{g}\right)\\ &= \frac{\Gamma(\beta)}{\Gamma(\beta-\alpha+1)}t^{1-\alpha}\frac{d}{dt}\left(\frac{f}{g}\right),\\ &= \frac{\Gamma(\beta)}{\Gamma(\beta-\alpha+1)}t^{1-\alpha}\left[\frac{gdf/dt - fdg/dt}{g^{2}}\right],\\ &= \frac{g\left[\Gamma(\beta)/\Gamma(\beta-\alpha+1)t^{1-\alpha}df/dt\right] - f\left[\Gamma(\beta)/\Gamma(\beta-\alpha+1)t^{1-\alpha}dg/dt\right]}{g^{2}},\\ &= \frac{gD^{\text{GFD}}(f) - fD^{\text{GFD}}(g)}{g^{2}} = \text{R.H.S}.\end{aligned} \tag{29}$$

Rules (*i*) and (*ii*) are not satisfied in the Caputo and Riemann–Liouville definitions. □

Theorem 5. *(Rolle's theorem for the generalized fractional differential function). Let $a > 0$ and $f\colon [a,b] \longrightarrow R$ be a given function that satisfies the following:*

(i) f is continuous on [a, b]

(ii) f is α–differentiable for some $\alpha \in (0,1]$

(iii) $f(a) = f(b)$

Then, there exists $c \in [a,b]$ such that $f^{(\alpha)}(c) = 0$.

Proof. Since f is continuous on $[a,b]$ and $f(a) = f(b)$, there is $c \in (a,b)$, which is a point of local extrema, and c is assumed to be a point of local minimum. So, we have

$$D^{\mathrm{GFD}} f(c^+) = \lim_{\varepsilon \longrightarrow 0^+} \frac{f\left(c + \Gamma(\beta)/\Gamma(\beta-\alpha+1)\varepsilon c^{1-\alpha}\right) - f(c)}{\varepsilon}; \quad \beta > -1, \beta \in R^+,$$
$$D^{\mathrm{GFD}} f(c^-) = \lim_{\varepsilon \longrightarrow 0^-} \frac{f\left(c + \Gamma(\beta)/\Gamma(\beta-\alpha+1)\varepsilon c^{1-\alpha}\right) - f(c)}{\varepsilon}; \quad \beta > -1, \beta \in R^+. \tag{30}$$

However, $D^{\mathrm{GFD}} f(c^+)$ and $D^{\mathrm{GFD}} f(c^-)$ have opposite signs. Hence, $D^{\mathrm{GFD}} f(c) = 0$. □

Theorem 6. *(mean value theorem for the generalized fractional differential function). Let $a > 0$ and $f\colon [a,b] \longrightarrow R$ be a given function that satisfies the following:*

(i) f is continuous on [a, b]

(ii) f is α–differentiable for some $\alpha \in (0,1)$

Then, there exists $c \in [a,b]$ such that

$$D^{\mathrm{GFD}} f(c) = \left[\frac{f(b) - f(a)}{h\left(b^\alpha - a^\alpha\right)}\right]. \tag{31}$$

Proof. Consider a function such as in [25].

$$g(t) = f(t) - f(a) - \left[\frac{f(b) - f(a)}{h\left(b^\alpha - a^\alpha\right)}\right](ht^\alpha - ha^\alpha), \tag{32}$$

where $h = 1/\Gamma(\alpha)$.

$$D^{\mathrm{GFD}} g(t) = D^{\mathrm{GFD}} f(t) - D^{\mathrm{GFD}} f(a) - \left[\frac{f(b) - f(a)}{h\left(b^\alpha - a^\alpha\right)}\right]\left(hD^{\mathrm{GFD}} t^\alpha - hD^{\mathrm{GFD}} a^\alpha\right). \tag{33}$$

By using equation (8), we get

$$D^{\mathrm{GFD}} g(t) = D^{\mathrm{GFD}} f(t) - \left[\frac{f(b) - f(a)}{h\left(b^\alpha - a^\alpha\right)}\right], \tag{34}$$

at $c \in [a,b]$.

$$D^{\mathrm{GFD}} g(c) = D^{\mathrm{GFD}} f(c) - \left[\frac{f(b) - f(a)}{h\left(b^\alpha - a^\alpha\right)}\right], \tag{35}$$

and the auxiliary function $g(c)$ satisfies all conditions of Theorem 5. Therefore, there exists $c \in [a,b]$ such that $D^{\mathrm{GFD}} g(c) = 0$. Then, we have

$$D^{\mathrm{GFD}} f(c) = \left[\frac{f(b) - f(a)}{h\left(b^\alpha - a^\alpha\right)}\right]. \tag{36}$$

□

Definition 2. $I_\alpha^a(f)(t) = I_1^0(t^{\alpha-1} f(x)) = \Gamma(\beta-\alpha+1)/\Gamma(\beta) \int_0^t f(x)/x^{1-\alpha}\,\mathrm{d}x$ and $\alpha \in (0,1)$.

Theorem 7. *$D^\alpha I_\alpha(f)(t) = f(t)$ for $t \geq 0$ where f is any continuous function in the domain.*

Proof. Since f is continuous, $I_\alpha^a(f)(t)$ is differentiable. Hence,

$$D^\alpha I_\alpha(f)(t) = \frac{\Gamma(\beta)}{\Gamma(\beta-\alpha+1)} t^{1-\alpha} \frac{d}{dt} I_\alpha(f)(t),$$
$$D^\alpha I_\alpha(f)(t) = \frac{\Gamma(\beta)}{\Gamma(\beta-\alpha+1)} t^{1-\alpha} \frac{d}{dt} \frac{\Gamma(\beta-\alpha+1)}{\Gamma(\beta)} \int_0^\infty \frac{f(x)}{x^{1-\alpha}}\,\mathrm{d}x,$$
$$D^\alpha I_\alpha(f)(t) = t^{1-\alpha} \frac{d}{dt} \int_0^t \frac{f(x)}{x^{1-\alpha}}\,\mathrm{d}x,$$
$$D^\alpha I_\alpha(f)(t) = t^{1-\alpha} \frac{f(t)}{t^{1-\alpha}},$$
$$D^\alpha I_\alpha(f)(t) = f(t). \tag{37}$$

□

3. Applications

3.1. Fractional Derivative of the Exponential Function $f(t) = e^{\lambda t}$, $\lambda \in c$.

$$e^{\lambda t} = \sum_{k=0}^{\infty} \frac{\lambda^k}{k!} t^k,$$
$$D^{\mathrm{GFD}} e^{\lambda t} = \sum_{k=0}^{\infty} \frac{\lambda^k}{k!} D^{\mathrm{GFD}} t^k. \tag{38}$$

From equation (12), we get

$$D^{\mathrm{GFD}}t^k = D^C t^k. \tag{39}$$

Let us now write equation (23) as

$$D^{\mathrm{GFD}}e^{\lambda t} = \sum_{k=0}^{\infty}\frac{\lambda^k}{k!}D^C t^k,$$
$$D^{\mathrm{GFD}}e^{\lambda t} = D^C e^{\lambda t}. \tag{40}$$

3.2. Fractional Derivative of Sine and Cosine Functions. For the sine function, we define $f(t) = \sin \omega t$ as

$$\sin \omega t = \frac{1}{2!}\left(e^{i\omega t} - e^{-i\omega t}\right),$$
$$D^{\mathrm{GFD}} \sin \omega t = \frac{1}{2!}\left(D^{\mathrm{GFD}}e^{i\omega t} - D^{\mathrm{GFD}}e^{-i\omega t}\right). \tag{41}$$

From equation (26), we obtain

$$D^{\mathrm{GFD}} \sin \omega t = \frac{1}{2!}\left(D^C e^{i^{\omega t}} - D^C e^{-i^{\omega t}}\right),$$
$${}^{\mathrm{GFD}}D^{\alpha} \sin \omega t = {}^{C}D^{\alpha}\frac{1}{2!}\left(e^{i\omega t} - e^{-i\omega t}\right), \tag{42}$$
$${}^{\mathrm{GFD}}D^{\alpha} \sin \omega t = {}^{C}D^{\alpha} \sin \omega t.$$

Similarly, we can prove the following for $f(t) = \cos \omega t$:

$${}^{\mathrm{GFD}}D^{\alpha} \cos \omega t = {}^{C}D^{\alpha} \cos \omega t. \tag{43}$$

Let us now solve some fractional differential equations in the sense of GFD.

Example 1. $D^{1/2}y(x) = e^{kx}, \quad y(0) = 0.$

Solution 1. Let us find the solution of the above example where $e^{kx} = \sum_{n=0}^{\infty} k^n/k!x^n$.

By using equation (8), we obtain

$$D^{1/2}y(x) = e^{kx},$$
$$\frac{\Gamma(\beta)}{\Gamma(\beta+1/2)}x^{1/2}\frac{dy(x)}{dx} = \sum_{n=0}^{\infty}\frac{k^n}{k!}x^n,$$
$$\frac{dy(x)}{dx} = \frac{\Gamma(\beta+1/2)}{\Gamma(\beta)}\sum_{n=0}^{\infty}\frac{k^n}{n!}x^{n-1/2},$$
$$\int dy(x) = \frac{\Gamma(\beta+1/2)}{\Gamma(\beta)}\sum_{n=0}^{\infty}\frac{k^n}{n!}\int x^{n-1/2}dx,$$
$$y(x) = \frac{\Gamma(\beta+1/2)}{\Gamma(\beta)}\sum_{n=0}^{\infty}\frac{k^n}{n!}\frac{x^{n+1/2}}{n+1/2} + c,$$
$$y(x) = \sum_{n=0}^{\infty}\frac{k^n}{n!}\frac{\Gamma(\beta+1/2)}{\Gamma(\beta)}\frac{x^{n+1/2}}{n+1/2} + c. \tag{44}$$

By taking $\beta = n + 1/2$, we have

$$y(x) = \sum_{n=0}^{\infty}\frac{k^n}{n!}\frac{\Gamma(n+1)}{(n+1/2)\Gamma(n+1/2)}x^{n+1/2} + c,$$
$$y(x) = \sum_{n=0}^{\infty}\frac{k^n}{\Gamma(n+3/2)}x^{n+1/2} + c, \tag{45}$$

since $y(0) = 0$.

$$y(x) = \sum_{n=0}^{\infty}\frac{k^n}{\Gamma(n+3/2)}x^{n+1/2}. \tag{46}$$

This solution is consistent with the Caputo solution.

Example 2. $D^{1/2}y(x) = x^2 \sin x, \quad y(0) = 0.$

Solution 2. Let us find the solution of the above example where $\sin x = \sum_{n=0}^{\infty} x^{2n+1}/(2n+1)!$.

By applying equation (1), we get

$$\frac{\Gamma(\beta)}{\Gamma(\beta+1/2)}x^{1/2}\frac{dy(x)}{dx} = \sum_{n=0}^{\infty}\frac{x^{2n+3}}{(2n+1)!},$$
$$\frac{dy(x)}{dx} = \frac{\Gamma(\beta+1/2)}{\Gamma(\beta)}\sum_{n=0}^{\infty}\frac{x^{2n+5/2}}{(2n+1)!},$$
$$\int dy = \frac{\Gamma(\beta+1/2)}{\Gamma(\beta)}\sum_{n=0}^{\infty}\int\frac{x^{2n+5/2}}{(2n+1)!}\mathrm{d}x,$$
$$y(x) = \sum_{n=0}^{\infty}\frac{\Gamma(\beta+1/2)}{\Gamma(\beta)}\frac{x^{2n+7/2}}{(2n+7/2)(2n+1)!} + c. \tag{47}$$

By taking $\beta = 2n + 7/2$, we get

$$y(x) = \sum_{n=0}^{\infty}\frac{\Gamma(2n+4)}{\Gamma(2n+7/2)}\frac{x^{2n+7/2}}{(2n+7/2)(2n+1)!} + c,$$
$$y(x) = \sum_{n=0}^{\infty}\frac{(2n+3)!}{(2n+7/2)\Gamma(2n+7/2)}\frac{x^{2n+7/2}}{(2n+1)!} + c, \tag{48}$$
$$y(x) = \sum_{n=0}^{\infty}\frac{(2n+3)(2n+2)}{\Gamma(2n+9/2)}x^{2n+7/2} + c,$$

since $y(0) = 0$.

$$y(x) = \sum_{n=0}^{\infty}\frac{(2n+3)(2n+2)}{\Gamma(2n+9/2)}x^{2n+7/2}. \tag{49}$$

This solution is consistent with the Caputo solution.

Example 3. $D^{1/2}y(x) + y(x) = x^2 + 2/\Gamma(2.5)x^{3/2}.$

Solution 3. By applying equation (8), we obtain

$$\frac{\Gamma(\beta)}{\Gamma(\beta+1/2)}x^{1/2}\frac{dy}{dx} + y(x) = x^2 + \frac{2}{\Gamma(2.5)}x^{3/2}. \tag{50}$$

Table 1: Comparison of the results of the GFD with other works at $\alpha = 3/4$.

t	Present work	BPM [17]	EHPM [18]	IABMM [18]	CD [14]
0	0	0	0	0	0
0.2	0.31439	0.30996891	0.3214	0.3117	0.37889
0.4	0.49848	0.48162749	0.5077	0.4855	0.58539
0.6	0.63022	0.59777979	0.6259	0.6045	0.72064
0.8	0.72609	0.67884745	0.7028	0.6880	0.81029
1.0	0.79618	0.73684181	0.7542	0.7478	0.87006

Table 2: Comparison of the results of the GFD with other works at $\alpha = 9/10$.

t	Present work at $\alpha = 9/10$	BPM [17]	MHPM [18]	IABMM [18]	CD [14]
0	0	0	0	0	0
0.2	0.23952	0.23878798	0.2391	0.2393	0.25526
0.4	0.42667	0.42258214	0.4229	0.4234	0.45191
0.6	0.57607	0.56617082	0.5653	0.5679	0.60539
0.8	0.69138	0.67462642	0.6740	0.6774	0.72063
1.0	0.7778	0.75460256	0.7569	0.7584	0.80445

Table 3: Comparison of the results of the GFD with other works at $\alpha = 9/10$ for equation (43).

t	Present work	BPM [17]	FTBM [18]	IABMM [18]	CD [14]
0	0	0	0	0	0
0.2	0.30718	0.31488815	0.31485423	—	0.33295
0.4	0.67131	0.69756771	0.69751826	—	0.73105
0.6	1.0666	1.10789047	0.90364539	—	1.1561
0.8	1.4397	1.47772823	1.47768008	—	1.5422
1.0	1.7485	1.76542008	1.76525852	1.7356	1.8457

The following is a nonlinear differential equation of first order in which we can obtain its solution with the help of Mathematica package.

$$y(x) = \frac{9A^4\sqrt{\pi} - 6A^3(2 + 3\sqrt{\pi}\sqrt{x})\sqrt{\pi}\sqrt{x} - 12A(2 + \sqrt{\pi}\sqrt{x})x + 16x^{3/2} + 6\sqrt{\pi}x^2 + 6A^2(4\sqrt{x} + 3\sqrt{\pi}x)}{6\sqrt{\pi}} + c_1 e^{-2\sqrt{x}/A}. \tag{51}$$

To determine $A = \Gamma(\beta)/(\Gamma(\beta + 1/2))$, we take $\alpha = \beta = 1/2$ as in [19].

Example 4. $d/dx\{(1 - \sqrt{x})(y(x) + 1)\} + \lambda D^{1/2} y(x) = 0$.

Solution 4. By applying equation (8), we obtain

$$\frac{d}{dx}\{(1 - \sqrt{x})(y(x) + 1)\} + \lambda \frac{\Gamma(\beta)}{\Gamma(\beta + 1/2)} x^{1/2} \frac{dy}{dx} = 0. \tag{52}$$

The following is a nonlinear differential equation of first order in which its solution can be obtained using Mathematica package as mentioned in our previous example.

Example 5. Consider the fractional Riccati differential equation [17]:

$$D^{\alpha} y(x) + y^2(x) = 1, y(0) = 0, 0 < \alpha \leq 1. \tag{53}$$

Solution 5. By applying equation (8), we obtain

$$\frac{\Gamma(\beta)}{\Gamma(\beta - \alpha + 1)} x^{1-\alpha} \frac{dy}{dx} + y^2(x) = 1, y(0) = 0, 0 < \alpha \leq 1. \tag{54}$$

To solve this equation at $\alpha = 3/4$ and $\alpha = 9/10$, the package of Mathematica has been used to obtain the following:

$$y(x) = \frac{-1 + e^{8x^{3/4}/sA}}{1 + e^{8x^{3/4}/sA}}, \tag{55}$$

where $A = \Gamma(\beta)/\Gamma(\beta + 1/4)$ and $\beta = \alpha = 3/4$ as in [28].

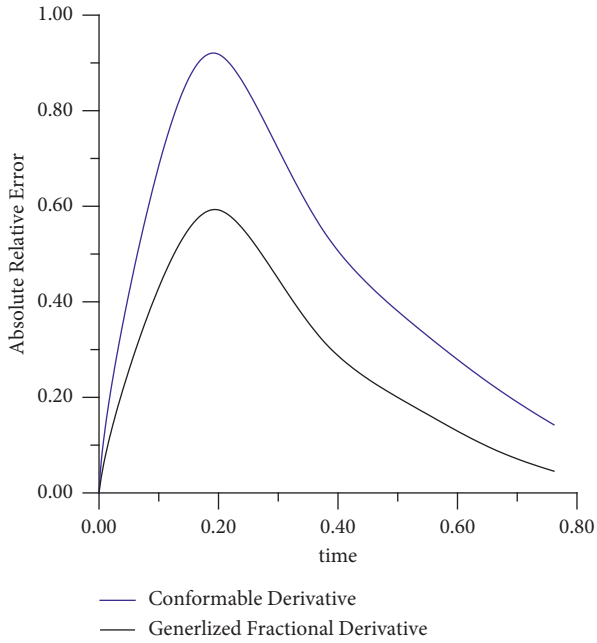

Figure 1: The absolute relative error is plotted for the Riccati fractional differential equation for the conformable derivative and GFD at $\alpha = 0.75$.

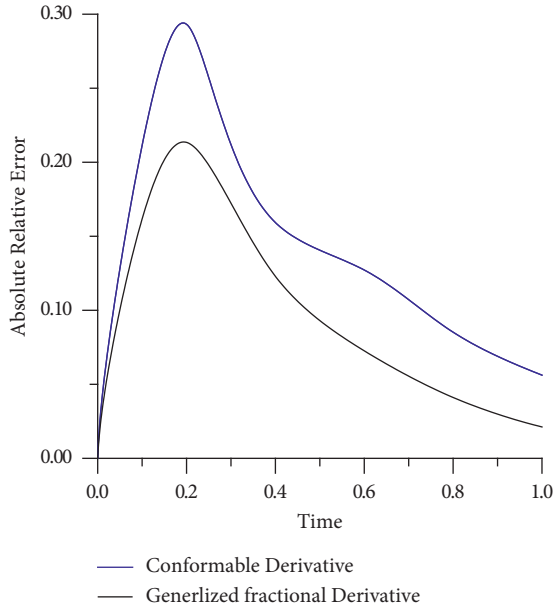

Figure 2: The absolute relative error is plotted for the Riccati fractional differential equation for the conformable derivative and GFD at $\alpha = 0.90$.

$$y(x) = \frac{-1 + e^{20x^{9/10}/9A}}{1 + e^{20x^{9/10}/9A}}, \tag{56}$$

where $A = \Gamma(\beta)/\Gamma(\beta + 1/4)$ and $\beta = \alpha = 9/10$ as in [19].

Example 6. Consider the following Riccati fractional differential equation [17]:

$$D^{\alpha} y(x) = 2y(x) - y^2(x) + 1, y(0) = 0, 0 < \alpha \leq 1. \tag{57}$$

Solution 6. By applying equation (8), we obtain

$$\frac{\Gamma(\beta)}{\Gamma(\beta - \alpha + 1)} x^{1-\alpha} \frac{dy}{dx} = 2y(x) - y^2(x) + 1, y(0) = 0, 0 < \alpha \leq 1. \tag{58}$$

To solve this equation at $\alpha = 9/10$, the package of Mathematica has been used to obtain the following:

$$y(x) = -\left(\frac{-1 - \sqrt{2} - e^S + \sqrt{2}e^S}{1 + e^S}\right), \tag{59}$$

where

$$s = \frac{2\sqrt{2}\left(-10x^{9/10} + 9A \ln(1 + \sqrt{2})/\sqrt{2}\right)}{9A}, \tag{60}$$

$A = \Gamma(\beta)/\Gamma(\beta + 1/4)$ and $\beta = \alpha = 9/10$ as in [19].

4. Discussion of Results

In this section, we show some results for the Riccati fractional differential equation in Tables 1–3 for different values of α, where parameters are taken as $\beta = \alpha$ [19]. As a result, we have obtained a good accuracy in the present calculations, where $\alpha = 3/4$ is taken in Table 1, and $\alpha = 9/10$ is taken in Tables 2 and 3. By comparing our results from the GFD definition with the Bernstein polynomial method (BPM) [17], enhanced homotopy perturbation method (EHPM) [18], IABMM [12], and conformable derivative (CD) [14], it is noticeable that the present results are in good agreement with BPM, EHPM, and IABMM results. In addition, the conformable derivative [14] has been used to solve the fractional Riccati differential equation. However, the results of the conformable derivative do not coincide with other works and our present results. A similar situation is in Table 2, by taking $\alpha = 9/10$, where the present results are compared with the Bernstein polynomial method (BPM) [17], enhanced homotopy perturbation method (EHPM) [18], IABMM [18], and conformable derivative (CD). The obtained results that have been calculated analytically via the GFD are in good agreement with other methods. However, in comparison with the CD, the present results are better than CD results as suggested in [14]. In Figure 1, the absolute relative error shows that the present results of the Riccati fractional differential equation are exactly obtained at $\alpha = 1$ in [17] by comparing it with $\alpha = 3/4$ using the proposed definition and the conformable one. The figure shows a good accuracy for the results of the proposed definition in comparison with the conformable one. A similar situation is provided in Figure 2 at $\alpha = 9/10$.

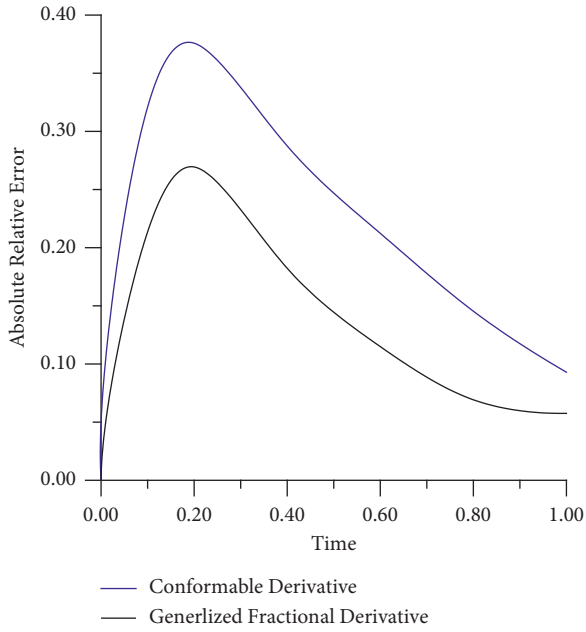

Figure 3: The absolute relative error is plotted for the Riccati fractional differential equation for the conformable derivative and GFD at $\alpha = 0.90$.

In Table 3, one compares the present results obtained from the GFD definition with the Bernstein polynomial method (BPM) [6], fractional Taylor basis method (FTBM) [7], IABMM [8], and conformable derivative (CD) [2]. The results from numerical methods in [6–8] are in agreement with the present results in the context of GFD. In comparison with the conformable derivative results, CD gives more errors than our results that have been obtained in the sense of the GFD. Also, in Figure 3, the results of the GFD give less error in comparison with the conformable derivative definition. Therefore, the present results of the GFD give compatible results with other works.

5. Conclusion

In this work, GFD has been suggested to provide more advantages than other classical Caputo and Riemann–Liouville definitions such as the derivative of two functions, the derivative of the quotient of two functions, Rolle's theorem, and the mean value theorem which have been satisfied in the GFD. The present definition satisfies $D^{\alpha}D^{\beta}f(t) = D^{\alpha+\beta}f(t)$ for a differentiable function $f(t)$ expanded by Taylor series. The fractional integral is introduced. Compatible results with Caputo and Riemann–Liouville results have been obtained for functions that are given in Sections 3.1 and 3.2. Also, a comparison with the conformable derivative is studied.

Some fractional differential equations can be solved analytically in a simple way with the help of our proposed definition which exactly agrees with the classical Caputo and Riemann–Liouville derivatives' results. In comparison with the conformable derivative, less error has been obtained in our GFD results by calculating the absolute relative error as in Figures 1–3 for the given Riccati fractional differential equation. Also, our results from the GFD definition are compared with the Bernstein polynomial method (BPM), enhanced homotopy perturbation method (EHPM), IABMM, and conformable fractional derivative (CD) [14]. The present results are in good agreement with BPM, EHPM, and IABMM.

We conclude that the present definition gives a new direction for solving fractional differential equations in a simple manner in which the results of the Caputo and Riemann–Liouville definitions are exactly deduced. In addition, GFD has advantages in comparison with the conformable derivative definition.

Data Availability

No data were used to support this study.

Conflicts of Interest

The authors declare that they have no conflicts of interest.

References

[1] R. T. Baillie, "Long memory processes and fractional integration in econometrics," *Journal of Econometrics*, vol. 73, no. 1, pp. 5–59, 1996.

[2] F. Mainardi, *Fractional Calculus: Some Basic Problems in Continuum and Statistical Mechanics, Fractals and Fractional Calculus in Continuum Mechanics*, A. Carpinteri and F. Mainardi, Eds., Vienna: Springer-Verlag, Berlin, Germany, pp. 291–348, 1997.

[3] Y. A. Rossikhin and M. V. Shitikova, "Applications of fractional calculus to dynamic problems of linear and nonlinear hereditary mechanics of solids," *Applied Mechanics Reviews*, vol. 50, no. 1, pp. 15–67, 1997.

[4] K. B. Oldham, "Fractional differential equations in electrochemistry," *Advances in Engineering Software*, vol. 41, no. 1, pp. 9–12, 2010.

[5] V. S. Ertürk, Z. M. Odibat, and S. Momani, "An approximate solution of a fractional order differential equation model of human T-cell lymphotropic virus I (HTLV-I) infection of CD4+ T-cells," *Computers and Mathematics with Applications*, vol. 62, no. 3, pp. 996–1002, 2011.

[6] S. A. El-Wakil, E. M. Abulwafa, E. K. El-Shewy, and A. A. Mahmoud, "Ion-acoustic waves in unmagnetized collisionless weakly relativistic plasma of warm-ion and isothermal-electron using time-fractional KdV equation," *Advances in Space Research*, vol. 49, no. 12, pp. 1721–1727, 2012.

[7] R. Gorenflo and F. Mainardi, *Fractals and Fractional Calculus in Continuum Mechanics*, A. Carpinteri and F. Mainardi, Eds., Springer-Verlag, Wien New York, New York, NY, USA, pp. 277–290, 1997.

[8] R. Hilfer, *Applications of Fractional Calculus in Physics*, World Scientific Publishing Company, Singapore, 2000.

[9] A. Atangana and D. Baleanu, "New fractional derivatives with nonlocal and non-singular kernel: theory and application to heat transfer model," *Thermal Science*, vol. 20, no. 2, pp. 763–769, 2016.

[10] R. L. Bagley and P. J. Torvik, "On the fractional calculus model of viscoelastic behavior," *Journal of Rheology*, vol. 30, no. 1, pp. 133–155, 1986.

[11] H. L. Gray and N. F. Zhang, "On a new definition of the fractional difference," *Mathematics of Computation*, vol. 50, no. 182, p. 513, 1988.

[12] K. S. Miller and B. Ross, "Fractional difference calculus," in *Proceedings of the International Symposium on Univalent Functions, Fractional Calculus and Their Applications*, p. 139, Nihon University, Koriyama, Japan, May 1989.

[13] A. Atangana and A. Secer, "A note on fractional order derivatives and table of fractional derivatives of some special functions," *Abstract and Applied Analysis*, vol. 2013, Article ID 279681, 2013.

[14] R. Khalil, M. Al Horani, A. Yousef, and M. Sababheh, "A new definition of fractional derivative," *Journal of Computational and Applied Mathematics*, vol. 264, pp. 65–70, 2014.

[15] A. A. Abdelhakim, "The flaw in the conformable calculus: it is conformable because it is not fractional," *Fractional Calculus and Applied Analysis*, vol. 22, no. 2, pp. 242–254, 2019.

[16] I. Podlubny, *Fractional Differential Equations: An Introduction to Fractional Derivatives, Fractional Differential Equations, to Methods of Their Solution and Some of Their Applications*, Elsevier, Amsterdam, Netherlands, 1998.

[17] S. Yuzbasi, "Numerical solutions of fractional Riccati type differential equations by means of the Bernstein polynomials," *Applied Mathematics and Computation*, vol. 219, p. 6328, 2013.

[18] S. H. Hosseinnia, A. Ranjbar, and S. Momani, "Using an enhanced homotopy perturbation method in fractional differential equations via deforming the linear part," *Computers and Mathematics with Applications*, vol. 56, no. 12, pp. 3138–3149, 2008.

[19] V. S. Krishnasamy, S. Mashayekhi, and M. Razzaghi, "Numerical solutions of fractional differential equations by using fractional Taylor basis," *IEEE/CAA Journal of Automatica Sinica*, vol. 4, no. 1, pp. 98–106, 2017.

Hindawi
Mathematical Problems in Engineering
Volume 2021, Article ID 7594496, 11 pages
https://doi.org/10.1155/2021/7594496

Research Article

An Efficient Mathematical Approach for the Fraction Order Differentiation Based on Future Applications of Chaotic Parameter

Ghulam Bary,[1] **Waqar Ahmed**,[2] **Muhammad Sajid**,[3] **Riaz Ahmad**,[1] **Muhammad Farooq Saleem Khan**,[4] **Md Fayz-Al-Asad**,[5] **Nawaf N. Hamadneh**,[6] **and Ilyas Khan**[7]

[1]*Faculty of Science, Yibin University, Yibin 644000, Sichuan, China*
[2]*Department of Bionanotechnology, Hanyang University, Ansan 155-88, Republic of Korea*
[3]*Faculty of Materials and Chemical Engineering, Yibin University, Yibin 644000, Sichuan, China*
[4]*Faculty of International Applied Technology, Yibin University, Yibin 64400, Sichuan, China*
[5]*Department of Mathematics, Bangladesh University of Engineering and Technology, Dhaka 1000, Bangladesh*
[6]*Department of Basic Sciences, College of Science and Theoretical Studies, Saudi Electronic University, Riyadh 11673, Saudi Arabia*
[7]*Department of Mathematics, College of Science Al-Zulfi, Majmaah University, Al Majmaah 11952, Saudi Arabia*

Correspondence should be addressed to Ghulam Bary; ghulambary@gmail.com

Received 17 August 2021; Accepted 22 September 2021; Published 16 October 2021

Academic Editor: Muhammad Shoaib Anwar

Normalized chaotic parameters examine the characterization of the particle production fluids produced at unusual energies and investigate a remarkable behavior in quantum measurement. The analogous characterization can be analyzed to probe the chaotic systems of boson particles creating sources of extraordinary energy. We observe that the bosons appear to be the appropriate aspirants of chaos fractions, and the normalized chaotic parameters evaluate the presence of such conglomerate phases significantly. The core point of this manuscript is that we calculate and examine the normalized chaotic parameters by differential equations to analyze the characteristics of the chaotic systems and their applications in thermal as well as in mechanical engineering. With such an efficient and distinctive approach, we perceive significant consequences for the correlator at higher temperature regimes.

1. Introduction

The femtoscopy is extensively studied to investigate the characteristics of the chaotic and coherence systems created during the smashing of heavy nuclei at unprecedented energies [1–5]. The chaotic parameter is enormously used to extract the consequences of the hybrid systems under consideration that the boson particles are ejected usually from the partially chaotic sources to analyze the two particles interferometry. Such a unique chaotic parameter possesses the numerical values zero and one for the coherence and chaotic sources, respectively. On the other hand, it approaches unity for the chaotic emissions [1, 2, 6]. Moreover, various factors influence the lower order chaotic parameter like the misidentification of particles, laser emissions as well as the resonances of long-lived [1, 5, 7, 8]. Perpetually, two particles quantum interferences are determined experimentally to investigate the heat chaotic components and the coherence characterization. It is distinguished; if the chaotic fraction is assessed more than fifty percent, then the two particles' chaotic parameter suppresses roughly twenty-five percent ratio. This is the compelling cause to probe the chaotic and coherence properties associated with the produced systems using two particles

interferences alone [9]. Particularly, the quantum correlations for higher ranks interferences contain extra particulars which cannot be probed from the lower order interference. The experimental data about pion correlations investigation have evaluated that the reduction of chaoticity is increased appreciably at third-order correlations than that of the second-order interferences [9–11].

In particular, the femtoscopy at higher order investigates the source chaotic-coherence fractions significantly and also possesses advantages about experimental dominance by the elimination of Fourier phase and resonances decays which appeared long-lived [6, 12–16]. The interferences of third-order measured data results are illustrated experimentally and graphically that the normalized chaotic parameters of third-order correlations report an obvious suppression from the given chaotic limit [15]. Such an obvious suppression of the chaos limit may occur due to the consequences of the coherence at lower temperature and momenta regimes [16]. There are multiple sources of nonchaotic emissions such as coherence of the pions and the pulse radiations which provoke the coherence of the numerous shapes [17–19].

This research work is unique because we have evaluated the chaotic and coherence properties of the thermal system with particles creating a boson gas source. It inflates relativistically by the interior region of the field potential for the special harmonic oscillator that drops out with the specific intervals of time in the hadronic phase temperature regime. Especially, the normalized chaotic parameters for third-order particles interferences are investigated with the applications of the one and two particles density matrices for hadronic phases at disparate temperature regimes. The nonchaotic particulars of production systems influence the chaotic parameter significantly under the considered measurements at miscellaneous temperatures and are explored to use them in thermal engineering [20–22].

This manuscript is organized into 5 sections. We investigate the correlations and chaotic parameters of differential equations in Section 2. In Section 3, we calculate and investigate the normalized chaotic parameter applications. We analyze our model results in Section 4. Finally, in Section 5, we summarize our findings.

2. Correlations and Normalized Chaotic Parameters

2.1. Two and Three Particles Correlation Functions. The two and three particles correlation functions in momentum space can be written in terms of the density matrices [21, 22] as follows:

$$C_2(p_1,p_2)=\frac{\rho^{(2)}(p_1,p_2;p_1,p_2)}{\rho^{(1)}(p_1,p_1)\rho^{(1)}(p_2,p_2)},$$
$$C_3(p_1,p_2,p_3)=\frac{\rho^{(3)}(p_1,p_2,p_3;p_1,p_2,p_3)}{\rho^{(1)}(p_1,p_1)\rho^{(1)}(p_2,p_2)\rho^{(1)}(p_3,p_3)}. \tag{1}$$

Correlations in the experimental analysis of two and three particles are achieved by considering the ratio of all particles correlated and divided by the product of the uncorrelated in the momentum space:

$$C_2(p_1,p_2)=1+\frac{\left|\rho^{(1)}(p_1,p_2)\right|^2-N_{co}^2\left|U_{co}(p_1)\right|^2\left|U_{co}(p_2)\right|^2}{\rho^{1}(p_1,p_1)\rho^{(1)}(p_2,p_2)}. \tag{2}$$

The condensation of Bose–Einstein influences the quantum correlations significantly, and the correlation functions depend crucially on the condensation. However, the effect of higher orders correlations is extensively larger than that of the lower order condensations. The condensation in the case of three particles plays a vital role during the interference of three bosons. In addition, the extraction of coherence from the experimental data possesses the several advantages during the analysis of heat exchange in the thermal and mechanical engineering [22, 23].

$$\begin{aligned}C_3(p_1,p_2,p_3)=1&+\frac{\left|\rho^{(1)}(p_1,p_2)\right|^2-N_{co}^2\left|U_{co}(p_1)\right|^2\left|U_{co}(p_2)\right|^2}{\rho^{1}(p_1,p_1)\rho^{(1)}(p_2,p_2)}\\&+\frac{\left|\rho^{(1)}(p_2,p_3)\right|^2-N_{co}^2\left|U_{co}(p_2)\right|^2\left|U_{co}(p_3)\right|^2}{\rho^{1}(p_2,p_2)\rho^{(1)}(p_3,p_3)}\\&+\frac{\left|\rho^{(1)}(p_1,p_3)\right|^2-N_{co}^2\left|U_{co}(p_1)\right|^2\left|U_{co}(p_3)\right|^2}{\rho^{1}(p_1,p_1)\rho^{(1)}(p_3,p_3)}\\&+\frac{\rho^{(1)}(p_1,p_2)\rho^{(1)}(p_2,p_3)\rho^{(1)}(p_3,p_1)-N_{co}^3\left|U_{co}(p_1)\right|^2\left|U_{co}(p_2)\right|^2\left|U_{co}(p_3)\right|^2}{\rho^{1}(p_1,p_1)\rho^{(1)}(p_3,p_3)\rho^{(1)}(p_2,p_2)}\\&+\frac{\rho^{(1)}(p_2,p_1)\rho^{(1)}(p_3,p_2)\rho^{(1)}(p_1,p_3)-N_{co}^3\left|U_{co}(p_1)\right|^2\left|U_{co}(p_2)\right|^2\left|U_{co}(p_3)\right|^2}{\rho^{1}(p_1,p_1)\rho^{(1)}(p_3,p_3)\rho^{(1)}(p_2,p_2)}.\end{aligned} \tag{3}$$

Here, it is more important to mention that the quantum correlation functions of higher order contained the corresponding correlators which are manipulated for two particles interferences:

$$\Lambda_2(12) = \frac{\left|\rho^{(1)}(p_1,p_2)\right|^2 - N_{co}^2\left|U_{co}(p_1)\right|^2\left|U_{co}(p_2)\right|^2}{\rho^1(p_1,p_1)\rho^{(1)}(p_2,p_2)},$$

$$\Lambda_2(23) = \frac{\left|\rho^{(1)}(p_2,p_3)\right|^2 - N_{co}^2\left|U_{co}(p_2)\right|^2\left|U_{co}(p_3)\right|^2}{\rho^1(p_2,p_3)\rho^{(1)}(p_3,p_2)}, \quad (4)$$

$$\Lambda_2(13) = \frac{\left|\rho^{(1)}(p_1,p_3)\right|^2 - N_{co}^2\left|U_{co}(p_1)\right|^2\left|U_{co}(p_3)\right|^2}{\rho^1(p_1,p_1)\rho^{(1)}(p_3,p_3)},$$

where $\Lambda_2(12)$, $\Lambda_2(23)$, and $\Lambda_2(13)$ are the correlators of the two particles correlations which played the quantum statistical role in three particles interferences. Specifically, the genuine three particles correlator $\Lambda_3(123)$ can be extracted with the subtraction of lower orders correlators like two particles interferences. Thus, the mathematical expression for genuine three particle correlator can be expressed as $\Lambda_3(123) = C_3(123) - \Lambda_2(12) - \Lambda_2(23) - \Lambda_2(13)$.

The genuine three particles correlator possesses the peculiar properties about the behavior of chaos and coherence in the radiated system which has been copiously used in the thermal engineering. Equation (3) can be written for the true three particles correlator in order to show the importance in the field of thermal and mechanical engineering, respectively.

$$\Lambda_3(123) = \frac{\rho^{(1)}(p_1,p_2)\rho^{(1)}(p_2,p_3)\rho^{(1)}(p_3,p_1) - N_{co}^3\left|U_{co}(p_1)\right|^2\left|U_{co}(p_2)\right|^2\left|U_{co}(p_3)\right|^2}{\rho^1(p_1,p_1)\rho^{(1)}(p_3,p_3)\rho^{(1)}(p_2,p_2)} + \frac{\rho^{(1)}(p_2,p_1)\rho^{(1)}(p_3,p_2)\rho^{(1)}(p_1,p_3) - N_{co}^3\left|U_{co}(p_1)\right|^2\left|U_{co}(p_2)\right|^2\left|U_{co}(p_3)\right|^2}{\rho^1(p_1,p_1)\rho^{(1)}(p_3,p_3)\rho^{(1)}(p_2,p_2)}. \quad (5)$$

It is obvious that in the absence of the three particles quantum phases, the normalized chaos correlator $w_3(q_3)$ is numerically measured to 2 at all zero relative momenta. We have been able to proceed and check the model proposed for two as well as three particles correlations [24].

2.2. Normalized Chaotic Parameter with Classical Methods. The condensation of Bose–Einstein has hypercritical effect on the three particles correlations, and the exaction of such coherence from experimental data of three particles has the advantage that the phase as well as the resonance problems can be minimized by using the normalized chaotic parameter. The normalized chaotic parameter of three particle $w_3(q_3) = w_3(p_1,p_2,p_3)$ is obtained by dividing the genuine three particles correlator $\Lambda_3(123)$ with the square root of the product of two particles correlators:

$$w_3(q_3) = \frac{\Lambda_3(q_3)}{\sqrt{\Lambda_2(q_{12})\Lambda_2(q_{23})\Lambda_2(q_{31})}}. \quad (6)$$

In addition, one may also isolate the Fourier phase of three particles by normalizing the genuine three particle correlation with the product of the two particles correlations:

$$w_3(q_3) = \frac{[c_3(q_3) - 1]}{\sqrt{[c_2(q_{12}) - 1][c_2(q_{23}) - 1][c_2(q_{13}) - 1]}}. \quad (7)$$

It has been mentioned that the genuine three particles correlator can be expressed in terms of the momentum-dependent density matrices given as follows:

$$R_3(123) = 2.\rho^{(1)}(p_1,p_2)\rho^{(1)}(p_2,p_3)\rho^{(1)}(p_3,p_1)[1 - g(p_1,p_2,p_3)], \quad (8)$$

where

$$g(p_1,p_2,p_3) = \frac{N_{co}^3\left|U_{co}(p_1)\right|^2\left|U_{co}(p_2)\right|^2\left|U_{co}(p_3)\right|^2}{\rho^{(1)}(p_1,p_1)\rho^{(1)}(p_2,p_2)\rho^{(1)}(p_3,p_3)}. \quad (9)$$

In the aforementioned equations, N_{co} and $U_{co}(p)$ express the particles number and the corresponding wave functions in the ground state. Moreover, the product of the two particles correlators for the quantum statistical interference can be manipulated as

$$\Lambda_2(12)\Lambda_2(23)\Lambda_2(13) = \rho^{(1)}(p_1,p_2)\rho^{(1)}(p_2,p_3)\rho^{(1)}(p_1,p_3) \times P. \quad (10)$$

It is crucial to mention that the multiplier factor P represents the square root of the product of the three particles correlators, and it can be expressed as $\sqrt{[1 - g(p_1,p_2)][1 - g(p_2,p_3)][1 - g(p_1,p_3)]}$. Moreover, the relative coherence probability can be measured by using the partially coherence probability to the total probability during the emissions of particles:

$$g(p_1, p_2) = \frac{N_{co}^2 |U_{co}(p_1)|^2 |U_{co}(p_2)|^2}{\left|\rho^{(1)}(p_1, p_2)\right|^2},$$

$$g(p_2, p_3) = \frac{N_{co}^2 |U_{co}(p_2)|^2 |U_{co}(p_3)|^2}{\left|\rho^{(1)}(p_2, p_3)\right|^2}, \tag{11}$$

$$g(p_1, p_3) = \frac{N_{co}^2 |U_{co}(p_1)|^2 |U_{co}(p_3)|^2}{\left|\rho^{(1)}(p_1, p_3)\right|^2}.$$

In particular, when we substitute the values of equations (8) and (10) into equation (6) under the important assumption that the emissions of three particles possess the identical momenta $p_1 = p_2 = p_3 = p$, then the corresponding results can be written as

$$g(p, p, p) = \frac{N_{co}^3 |U_{co}(p)|^6}{\left|\rho^{(1)}(p)\right|^3} = \frac{|\rho_{co}(p)|^3}{|\rho(p)|^3}, \tag{12}$$

$$g(p, p) = \frac{N_{co}^2 |U_{co}(p)|^4}{\left|\rho^{(1)}(p, p)\right|^2} = \frac{|\rho_{co}(p)|^2}{|\rho(p)|^2}. \tag{13}$$

The genuine three particles correlator in the higher correlations contains the excessive information about the particle ejecting sources, and it acquired the sophisticated form with the substitution of equation (12) into equation (8):

$$\Lambda_3(q_3) = 2.\rho^{(1)}(p, p)\rho^{(1)}(p, p)\rho^{(1)}(p, p)\left[1 - \left[\frac{\rho_{co}(p)}{\rho(p)}\right]^3\right]. \tag{14}$$

In addition, the product of the two particles correlator acquires the fruitful results when we use equation (18) into equation (13) for the three particles ejection. Such useful results can be obtained by using the difference equations, and the application of the analytical techniques become

$$\Lambda_2(12)\Lambda_2(23)\Lambda_2(13) = \rho^{(1)}(p, p)\rho^{(1)}$$
$$(p, p)\rho^{(1)}(p, p)\sqrt{\left[1 - \left[\frac{\rho_{co}(p)}{\rho(p)}\right]^2\right]^3}. \tag{15}$$

Consequently, the results of normalized three particles chaotic parameter possess the sophistical shape after the eradication of some unusual terms, and it can be happen when we substitute the values of equations (14) and (15) into equation (6):

$$w_3(p) = 2\frac{\left[1 - \left[\rho_{co}(p)/\rho^{(p)}\right]^3\right]}{\sqrt{\left[1 - \left[\rho_{co}(p)/\rho^{(p)}\right]^2\right]^3}}. \tag{16}$$

The sensitive parameter of the coherence fraction $D(p) = \rho_{co}(p)/\rho(p)$ and the expression for normalized three particles chaotic parameter can be written in terms of coherence fraction as follows:

$$w_3(p) = 2\frac{\left[1 - [D(p)]^3\right]}{\left[1 - [D(p)]^2\right]^{3/2}}. \tag{17}$$

In particular, the chaotic parameter $w_3(p)$ indicates that the value of correlator becomes 2 for the complete chaotic sources but it reflects to infinity for complete coherence sources. The results of $w_3(p)$ may not explain the experimental data of chaos fraction. Here, the question is that what can we do to explain the experimental data in order to examine the chaos fraction? We can achieve our goal to modify the old model in order to use the new techniques which compelled us to study the higher order quantum correlations in particular direction [24, 25].

3. Characteristics of Normalized Chaotic Parameter

The correlations of two particles are untrammelled about FT phase but it persists in the correlations of three particles considerably. However, such kind of considered phase is potentially isolated by weighing up the cumulant interferences of three particles cumulant to two particles correlations. It is prevailed by the division of three particles correlator under root of computed two particles correlators. Now, we have been able to express the normalized chaotic three particles correlator for aforementioned sources by using the expressions of two as well as three particles correlators. It has been observed that the systems of particles emission behave partially chaotic, and the density matrix for such systems possess the partially coherence as well as partially chaotic components. The mathematical expression for the particle emitted fluid can be illustrated as the sum of the chaotic and coherence components [25–28]:

$$\rho^{(1)}(p_1, p_2) = \rho_{ch}^{(1)}(p_1, p_2) + \rho_{co}^{(1)}(p_1, p_2), \tag{18}$$

where $\rho_{ch}^{(1)}(p_1, p_2)$ represents the density matrix for the chaotic component of the particles ejected sources and $\rho_{co}^{(1)}(p_1, p_2)$ shows the one particle density matrix of the corresponding coherence component. It is more crucial to mention that the density matrices at higher order can be written in terms of two particles density matrices in order to calculate the correlation functions at higher order. We can

expand our mathematical expression of two particles interferences into three particles quantum correlations sophistically given as follows:

$$\begin{aligned}\rho^{(1)}(p_1,p_2)\times\rho^{(1)}(p_2,p_3)\times\rho^{(1)}(p_1,p_3) &= \left[\rho_{ch}^{(1)}(p_1,p_2)+\rho_{co}^{(1)}(p_1,p_2)\right]\\ &\times\left[\rho_{ch}^{(1)}(p_2,p_3)+\rho_{co}^{(1)}(p_2,p_3)\right]\\ &\times\left[\rho_{ch}^{(1)}(p_1,p_3)+\rho_{co}^{(1)}(p_1,p_3)\right].\end{aligned} \tag{19}$$

These density matrices can be multiplied in order to obtain the normalized chaotic parameter, and the adopted methodology of differential equations leads for the multiplication purposes:

$$\begin{aligned}\rho^{(1)}(p_1,p_2)\times\rho^{(1)}(p_2,p_3)\times\rho^{(1)}(p_1,p_3) &= \rho_{ch}^{(1)}(p_1,p_2).\rho_{ch}^{(1)}(p_2,p_3).\rho_{ch}^{(1)}(p_1,p_3)\\ &+\rho_{ch}^{(1)}(p_1,p_2).\rho_{ch}^{(1)}(p_2,p_3).\rho_{co}^{(1)}(p_1,p_3)\\ &+\rho_{ch}^{(1)}(p_1,p_2).\rho_{co}^{(1)}(p_2,p_3).\rho_{ch}^{(1)}(p_1,p_3)\\ &+\rho_{co}^{(1)}(p_1,p_2).\rho_{ch}^{(1)}(p_2,p_3).\rho_{ch}^{(1)}(p_1,p_3)\\ &+\rho_{ch}^{(1)}(p_1,p_2).\rho_{co}^{(1)}(p_2,p_3).\rho_{co}^{(1)}(p_1,p_3)\\ &+\rho_{co}^{(1)}(p_1,p_2).\rho_{ch}^{(1)}(p_2,p_3).\rho_{co}^{(1)}(p_1,p_3)\\ &+\rho_{co}^{(1)}(p_1,p_2).\rho_{co}^{(1)}(p_2,p_3).\rho_{ch}^{(1)}(p_1,p_3)\\ &+\rho_{co}^{(1)}(p_1,p_2).\rho_{co}^{(1)}(p_2,p_3).\rho_{co}^{(1)}(p_1,p_3).\end{aligned} \tag{20}$$

In particular, the possessions of the quantum statistical correlations can be exhibited for the symmetrization of the particles emission points. It has been substantiated that the symmetrization only exists for independently ejected boson particles, and such effect is missing for the coherence particle creations [29, 30]. It has been noted that the productions of bosons from the coherence state behave collectively, and the symmetrization does not occur for pairs of the ejected coherence bosons. Such phenomena can also appear for the mixed pairs of particles from the coherence pool and the other from the chaotic pools of particles production. Thus, the required density matrix can be expressed in terms of the lower energy ground state wave function:

$$\begin{aligned}\rho_{co}^{(1)}(p_1,p_2) &= N_{co}U_{co}(p_1)U_{co}(p_2)\\ \rho_{co}^{(1)}(p_2,p_3) &= N_{co}U_{co}(p_2)U_{co}(p_3)\\ \rho_{co}^{(1)}(p_1,p_3) &= N_{co}U_{co}(p_1)U_{co}(p_3)\\ \rho_{co}^{(1)}(p_1,p_2).\rho_{co}^{(1)}(p_2,p_3) &= N_{co}^2U_{co}(p_1)U_{co}(p_3)\left|U_{co}(p_2)\right|^2\\ \rho_{co}^{(1)}(p_1,p_2).\rho_{co}^{(1)}(p_1,p_3) &= N_{co}^2\left|U_{co}(p_1)\right|^2U_{co}(p_2)U_{co}(p_3)\\ \rho_{co}^{(1)}(p_2,p_3).\rho_{co}^{(1)}(p_1,p_3) &= N_{co}^2U_{co}(p_1)U_{co}(p_2)\left|U_{co}(p_3)\right|^2,\end{aligned} \tag{21}$$

where N_{co} and U_{co} represent the coherence particles number and their associated coherence wave functions, respectively. Here, the above expressions can be manipulated for the further calculations as follows:

$$\begin{aligned}&\rho_{co}^{(1)}(p_1,p_2).\rho_{co}^{(1)}(p_2,p_3).\rho_{co}^{(1)}(p_1,p_3)\\ &=N_{co}^3\left|U_{co}(p_1)U_{co}(p_2)U_{co}(p_3)\right|^2.\end{aligned} \tag{22}$$

Furthermore, the density matrix for the chaotic emissions can be written in the form of the coherence density components as well as the total density matrix by using the following equation:

$$\begin{aligned}\rho_{ch}^{(1)}(p_1,p_2) &= \rho^{(1)}(p_1,p_2)-\rho_{co}^{(1)}(p_1,p_2),\\ \rho_{ch}^{(1)}(p_2,p_3) &= \rho^{(1)}(p_2,p_3)-\rho_{co}^{(1)}(p_2,p_3),\\ \rho_{ch}^{(1)}(p_1,p_3) &= \rho^{(1)}(p_1,p_3)-\rho_{co}^{(1)}(p_1,p_3).\end{aligned} \tag{23}$$

Specifically, the emissions of three particles illustrate in such a way that the two density matrices for coherence emissions and one for the chaotic emission. These results can be expressed in terms of the wave functions:

$$\rho_{ch}^{(1)}(p_1,p_2).\rho_{co}^{(1)}(p_2,p_3).\rho_{co}^{(1)}(p_1,p_3) = \left[\rho^{(1)}(p_1,p_2) - \rho_{co}^{(1)}(p_1,p_2)\right] \times \left[N_{co}^2 U_{co}(p_1)U_{co}(p_2)\left|U_{co}(p_3)\right|^2\right]. \tag{24}$$

The aforementioned equations can be transformed into the symmetrical shape to perform the basic multiplications, and such expression can be expressed in terms of nonchaotic emission:

$$\rho_{ch}^{(1)}(p_1,p_2).\rho_{co}^{(1)}(p_2,p_3).\rho_{co}^{(1)}(p_1,p_3) = \rho^{(1)}(p_1,p_2)N_{co}^2 U_{co}(p_1)U_{co}(p_2)\left|U_{co}(p_3)\right|^2 - N_{co}^3\left|U_{co}(p_1)\right|U_{co}(p_2)U_{co}(p_3)\right|^2. \tag{25}$$

On the other hand, the density matrices for the symmetrization of the other triplet manipulated in the form of nonchaotic emissions are as follows:

$$\rho_{ch}^{(1)}(p_2,p_3).\rho_{co}^{(1)}(p_1,p_2).\rho_{co}^{(1)}(p_1,p_3) = N_{co}^2\rho^{(1)}(p_2,p_3)U_{co}(p_2)U_{co}(p_3)\left|U_{co}(p_1)\right|^2 - N_{co}^3\left|U_{co}(p_1)\right|U_{co}(p_2)U_{co}(p_3)\right|^2. \tag{26}$$

Similarly, the density matrices for the chaotic and coherent particles emissions can also be expressed as follows:

$$\rho_{ch}^{(1)}(p_1,p_3).\rho_{co}^{(1)}(p_1,p_2).\rho_{co}^{(1)}(p_1,p_3) = N_{co}^2\rho^{(1)}(p_1,p_3)U_{co}(p_1)U_{co}(p_3)\left|U_{co}(p_2)\right|^2 - N_{co}^3\left|U_{co}(p_1)\right|U_{co}(p_2)U_{co}(p_3)\right|^2. \tag{27}$$

We are able to generalize the density distributions method to examine the solutions of the chaos fraction by using the differential equations. Different techniques of such fractional differential equations play a vital role in order to probe the types of chaos, coherence, and implicit solutions [31, 32].

In addition, we substitute the mentioned values in equation (20) in order to adopt the proper mathematical expression in sophisticated shape:

$$\begin{aligned}\rho^{(1)}(p_1,p_2).\rho^{(1)}(p_2,p_3).\rho^{(1)}(p_1,p_3) = {} & \rho_{ch}^{(1)}(p_1,p_2).\rho_{ch}^{(1)}(p_2,p_3).\rho_{ch}^{(1)}(p_1,p_3) \\ & + \rho_{ch}^{(1)}(p_1,p_2).\rho_{ch}^{(1)}(p_2,p_3).\rho_{co}^{(1)}(p_1,p_3) \\ & + \rho_{ch}^{(1)}(p_1,p_2).\rho_{co}^{(1)}(p_2,p_3).\rho_{ch}^{(1)}(p_1,p_3) \\ & + \rho_{co}^{(1)}(p_1,p_2).\rho_{ch}^{(1)}(p_2,p_3).\rho_{ch}^{(1)}(p_1,p_3) \\ & + \rho^{(1)}(p_1,p_2)N_{co}^2 U_{co}(p_1)U_{co}(p_2)\left|U_{co}(p_3)\right|^2 \\ & - N_{co}^3\left|U_{co}(p_1)U_{co}(p_2)U_{co}(p_3)\right|^2 \\ & + \rho^{(1)}(p_2,p_3)N_{co}^2 U_{co}(p_2)U_{co}(p_3)\left|U_{co}(p_1)\right|^2 \\ & - N_{co}^3\left|U_{co}(p_1)U_{co}(p_2)U_{co}(p_3)\right|^2\end{aligned}$$

$$
\begin{aligned}
&+\rho^{(1)}(p_1,p_3)N_{co}^2U_{co}(p_1)U_{co}(p_3)\left|U_{co}(p_2)\right|^2\\
&-N_{co}^3\left|U_{co}(p_1)U_{co}(p_2)U_{co}(p_3)\right|^2\\
&+N_{co}^3\left|U_{co}(p_1)U_{co}(p_2)U_{co}(p_3)\right|^2,\\
\rho^{(1)}(p_1,p_2).\rho^{(1)}(p_2,p_3).\rho^{(1)}(p_1,p_3)&=\rho_{ch}^{(1)}(p_1,p_2).\rho_{ch}^{(1)}(p_2,p_3).\rho_{ch}^{(1)}(p_1,p_3)\\
&+\rho_{ch}^{(1)}(p_1,p_2).\rho_{ch}^{(1)}(p_2,p_3).\rho_{co}^{(1)}(p_1,p_3)\\
&+\rho_{ch}^{(1)}(p_1,p_2).\rho_{co}^{(1)}(p_2,p_3).\rho_{ch}^{(1)}(p_1,p_3)\\
&+\rho_{co}^{(1)}(p_1,p_2).\rho_{ch}^{(1)}(p_2,p_3).\rho_{ch}^{(1)}(p_1,p_3)\\
&+\rho^{(1)}(p_1,p_2)N_{co}^2U_{co}(p_1)U_{co}(p_2)\left|U_{co}(p_3)\right|^2\\
&-2N_{co}^3\left|U_{co}(p_1)U_{co}(p_2)U_{co}(p_3)\right|^2\\
&+\rho^{(1)}(p_2,p_3)N_{co}^2U_{co}(p_2)U_{co}(p_3)\left|U_{co}(p_1)\right|^2\\
&+\rho^{(1)}(p_1,p_3)N_{co}^2U_{co}(p_1)U_{co}(p_3)\left|U_{co}(p_2)\right|^2.
\end{aligned}
\tag{28}
$$

The possible terms can be represented for the explanation of the experimental data which play a vital role in the quantum interferences, and these selected components are expressed as follows:

$$
\begin{aligned}
&\rho^{(1)}(p_1,p_2)\rho^{(1)}(p_2,p_3).\rho^{(1)}(p_1,p_3)+2N_{co}^3\left|U_{co}(p_1)U_{co}(p_2)U_{co}(p_3)\right|^2\\
&-\rho^{(1)}(p_1,p_2)N_{co}^2U_{co}(p_1)U_{co}(p_2)\left|U_{co}(p_3)\right|^2\\
&-\rho^{(1)}(p_2,p_3)N_{co}^2U_{co}(p_2)U_{co}(p_3)\left|U_{co}(p_1)\right|^2\\
&-\rho^{(1)}(p_1,p_3)N_{co}^2U_{co}(p_1)U_{co}(p_3)\left|U_{co}(p_2)\right|^2\\
&=\left[\rho_{ch}^{(1)}(p_1,p_2).\rho_{ch}^{(1)}(p_2,p_3).\rho_{ch}^{(1)}(p_1,p_3)\right]\\
&+\rho_{ch}^{(1)}(p_1,p_2).\rho_{ch}^{(1)}(p_2,p_3).\rho_{co}^{(1)}(p_1,p_3)\\
&+\rho_{ch}^{(1)}(p_1,p_2).\rho_{co}^{(1)}(p_2,p_3).\rho_{ch}^{(1)}(p_1,p_3)\\
&+\rho_{co}^{(1)}(p_1,p_2).\rho_{ch}^{(1)}(p_2,p_3).\rho_{ch}^{(1)}(p_1,p_3).
\end{aligned}
\tag{29}
$$

Basically chaotic fluid is utilized to enhance the thermal nature in the corresponding equipment such as heat exchanger, electronic, and nuclear systems. The transfer of energy, momentum, and heat in the partially chaotic fluids has been discussed with the density matrices by several researchers in order to control the aforementioned phenomena [33–35]. It is obvious that the source of ejected particles may be the pure chaotic or partially coherence but this equation plays a versatile role in all considerable cases. We can check the acquired equation for normalized three particles chaotic parameter (correlator) whether it follows the experimental results to examine the chaotic and coherence fractions of the particles ejected sources. Particularly, the three particles correlator can be written in the meaningful way when we use the expression of equations (29) and (5), respectively.

$$\Lambda_3(123) = 2\Big[\rho^{(1)}(p_1,p_2).\rho^{(1)}(p_2,p_3).\rho^{(1)}(p_1,p_3) + 2N_{co}^3\left|U_{co}(p_1)U_{co}(p_2)U_{co}(p_3)\right|^2$$
$$-\rho^{(1)}(p_1,p_2)N_{co}^2U_{co}(p_1)U_{co}(p_2)\left|U_{co}(p_3)\right|^2 - \rho^{(1)}(p_2,p_3)N_{co}^2U_{co}(p_2)U_{co}(p_3)\left|U_{co}(p_1)\right|^2$$
$$-\rho^{(1)}(p_1,p_3)N_{co}^2U_{co}(p_1)U_{co}(p_3)\left|U_{co}(p_2)\right|^2\Big],$$
$$\Lambda_3(123) = 2.\rho^{(1)}(p_1,p_2).\rho^{(1)}(p_2,p_3).\rho^{(1)}(p_3,p_1) \tag{30}$$
$$\cdot\left[1 + 2\frac{N_{co}^3\left|U_{co}(p_1)\right|^2\left|U_{co}(p_2)\right|^2\left|U_{co}(p_3)\right|^2}{\rho^1(p_1,p_1)\rho^{(1)}(p_3,p_3)\rho^{(1)}(p_2,p_2)} - \frac{\rho^{(1)}(p_1,p_2)N_{co}^2U_{co}(p_1)U_{co}(p_2)\left|U_{co}(p_3)\right|^2}{\rho^1(p_1,p_1)\rho^{(1)}(p_3,p_3)\rho^{(1)}(p_2,p_2)}\right.$$
$$\left. - \frac{\rho^{(1)}(p_2,p_3)N_{co}^2U_{co}(p_2)U_{co}(p_3)\left|U_{co}(p_1)\right|^2}{\rho^1(p_1,p_1)\rho^{(1)}(p_3,p_3)\rho^{(1)}(p_2,p_2)} - \frac{\rho^{(1)}(p_1,p_3)N_{co}^2U_{co}(p_1)U_{co}(p_3)\left|U_{co}(p_2)\right|^2}{\rho^1(p_1,p_1)\rho^{(1)}(p_3,p_3)\rho^{(1)}(p_2,p_2)}\right].$$

In particular, the aforementioned expressions indicate that when we substitute the value of $\Lambda_3(123)$ into equation (6), then the corresponding expression acquires the most sophisticated shape under the assumption that the momenta of all emitted particles are identical, i.e., $p_1 = p_2 = p_3 = p$. Therefore, the normalized chaotic parameter can be manipulated as

$$w_3(p) = 2.\frac{\left[1 + 2\left[\rho_{co}(p)/\rho(p)\right]^3 - 3\left[\rho_{co}(p)/\rho(p)\right]^2\right]}{\sqrt{\left[1 - \left[\rho_{co}(p)/\rho(p)\right]^2\right]^3}}. \tag{31}$$

The parameter which measures the chaotic and coherence components is called the chaotic fraction, and we define the chaotic fraction in terms of the coherence and chaotic components in order to write the normalized three particles chaotic parameter:

$$\varepsilon(p) = \frac{\rho_{ch}(p)}{\rho_{co}(p) + \rho_{ch}(p)}, \tag{32}$$

where $\rho_{ch}(p)$ and $\rho_{co}(p)$ represent the chaotic and coherence fractions, respectively. Furthermore, the coherence fraction can be illustrated in terms of the chaos fraction as follows:

$$\frac{\rho_{co}(p)}{\rho_{co}(p) + \rho_{ch}(p)} = \frac{\rho_{co}(p)}{\rho(p)} = 1 - \varepsilon(p). \tag{33}$$

In particular, the special specification of the chaotic parameter can be obtained by substituting the value of equation (33) into equation (31). We can express the mathematical expression for the normalized chaotic parameter of three particles in terms of the chaotic fractions:

$$w_3(p) = 2\frac{\left[1 + 2\left[1 - \varepsilon(p)\right]^3 - 3\left[1 - \varepsilon(p)\right]^2\right]}{\left[1 - \left[1 - \varepsilon(p)\right]^2\right]^{3/2}}. \tag{34}$$

In addition, the normalized chaotic parameter can be simplified by applying some basic algebraic calculations, and it can be written in versatile form as follows:

$$w_3(p) = 2\frac{\sqrt{\varepsilon(p)}\left[3 - 2\varepsilon(p)\right]}{\left[2 - \varepsilon(p)\right]^{3/2}}. \tag{35}$$

From the aforementioned expression, it is obvious that the numerical value of the chaotic fraction $\varepsilon(p) = 1$ for the complete chaotic sources and the normalized chaotic parameter for three particles $w_3(p)$ acquire the chaotic limit 2. Similarly, the chaos fraction for the completely coherence sources is $\varepsilon(p) = 0$, and it means that the value of $w_3(p)$ becomes zero for an ideal condition of the coherence sources but it cannot proceed to infinity in any usual case. This formula can explain the experimental data in very well way for all kind of sources which are studied in thermal as well as in mechanical engineering. We can check the consequences of such unique formula and the model results for two and three bosons which are consistent with the experimental data. The experimental results of the normalized chaos parameter can be proceeded to extract the chaotic and coherence fractions at various temperatures and momenta regimes. The derived formula is correct in all cases: (a) if a source behaves as fully chaotic and (b) the source may be partially coherent or fully coherent. Our mathematical expressions can illustrate the experimental data about two and three particles emission for the partial coherence in order to use it in the artificial intelligence.

In addition, the intercept of the normalized three particles chaotic parameter can be written in terms of the coherence fraction:

$$I_3(p) = w_3(p) = 2\sqrt{1 - f_{co}(p)}\ \frac{\left[1 + 2f_{co}(p)\right]}{\left[1 + f_{co}(p)\right]^{3/2}}. \tag{36}$$

This expression shows that if the source is completely chaotic, i.e., $f_{co} = 0$, then the intercept of w_3 attains its maximum value 2. On the other hand, the corresponding intercept of w_3 appears to be 0 for a complete coherent source $f_{co} = 1$.

4. Results and Discussion

The core point of this research work is to probe the intrinsic properties of the particle production sources created by the impact of nuclei at higher energy. Statistical correlations of three particles and the corresponding normalized chaotic

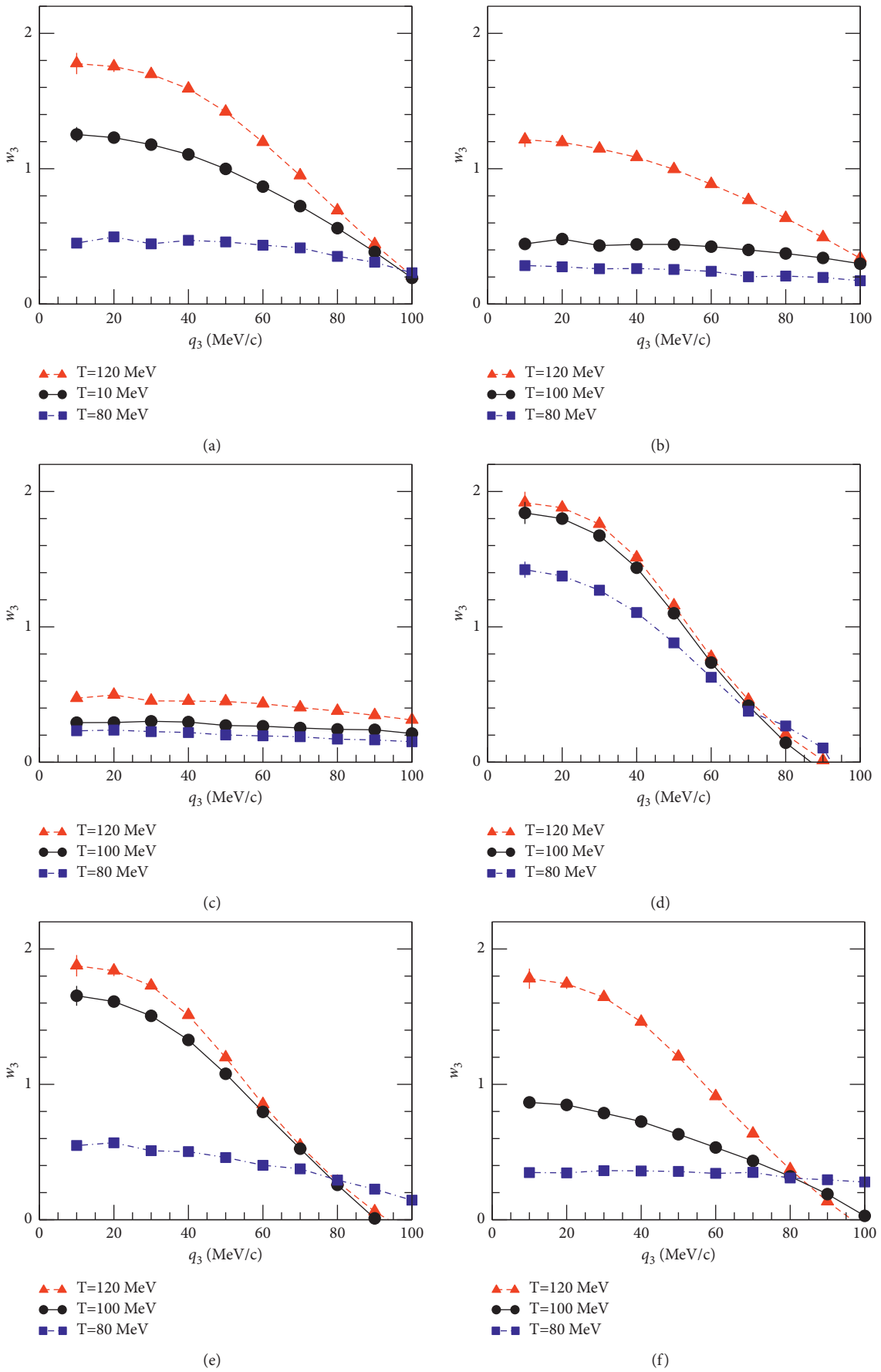

FIGURE 1: Three particles normalized chaotic parameter w_3 versus q_3 at various temperatures with different particles number N_T: (a) $K_s = 0.35$ and $N_T = 600$; (b) $K_s = 0.35$ and $N_T = 800$; (c) $K_s = 0.35$ and $N_T = 1000$; (d) $K_s = 0.40$ and $N_T = 800$; (e) $K_s = 0.40$ and $N_T = 1000$; (f) $K_s = 0.35$ and $N_T = 1200$.

parameters make it feasible consistently to quantify the temperament of the radiation sources by differential equations to use in thermal and mechanical engineering. We explicate our results about the partially chaotic source with temperature dependence characteristics and postulate that the particle ejection sources are comprised of the fluid clusters which act as the chaotic sources at a higher temperature.

Figure 1 illustrates the normalized chaotic parameter w_3 of three particles with relative momenta q_3 for the ejected sources with various temperatures T and the given particles numbers N_T. w_3 for the sources possesses $N_T = 600$, 800, and 1000 for the smaller size sources of parameter $K_s = 0.35$ as shown in Figures 1(a)–1(c). The chaotic parameter of the three particles suppresses considerably by increasing N_T by fixing the temperature T. The reason is obvious because the plenty of particles have the probability to exist the bosons nonchaotically at lower temperature regimes. Such phenomena of temperature reduction with fixed particles N_T reduce considerably the kinetic energy of the particles $K.E \propto T$, and the bosons continue to condensate at the lowest energy level and lead to produce the Bose–Einstein coherence which affects the bosons normalized chaotic parameter consistently. The unique results appear for small sources with $K_s = 0.35$ due to the absence of the quantum interference, and the results approach zero in the presence of large N_T =1000 as illustrated in Figure 1(c). Furthermore, Figures 1(d) and 1(e) represent the changes of w_3 when the particle ejected sources possess excess particles with large size parameter $K_s = 0.40$ which contain $N_T = 800$, 1000, and 1200. The chaotic parameter decreases with increasing N_T because the source with higher particles amount acquired the large coherence effect. Such chaotic parameters increase with increasing the temperature T continuously for fixing N_T due to the reason that at extremely higher temperatures, the particles shifted at higher energy levels and the coherence effect appears negligibly. The normalized chaotic parameter approaches to its chaotic limit 2 at intercepts.

In particular, one can observe that results of w_3 are suppressed notably at the lower temperatures for the fixed N_T under the study of both sources. The chaotic parameter of three particles shows an obvious peak with $K_s = 0.40$ than that for small sources with size $K_s = 0.35$ contains fixed N_T and the temperature T. Such variations happen due to fact that the source with large K_s seems to be large. The corresponding energy levels also seem to narrow which leads to pushing the maximum bosons to shift from lower to high energy states and also possess the large characteristic lengths which suppress the coherence fraction significantly.

5. Summary and Conclusion

The normalization of three particle cumulants to the two particles cumulant is quantified with the normalized chaotic parameter w_3. We find an obvious suppression below the chaotic limit in the measurement of w_3 at lower temperature and momentum, respectively. Such suppression appears to recommend nonchaotic components to particle production to use in thermal and mechanical engineering. It is crucial at lower temperature, and such consideration is qualitatively compatible with the origination of Bose–Einstein coherence which is contemplated to emit coherently at lower energies.

In particular, w_3 is applicable for examining the chaotic and coherence fractions at unusual energies. We evaluated w_3 at various temperatures and momentum regions and explored the consequences of the particle number and source size on the considered chaotic parameter. We have observed that the normalized three particles chaotic parameters are correlated to the chaos thermal limit of the two particle interferences and also delicate to the thermalization of the particle emissions sources.

Specifically, the possession of w_3 at temperature T and the number of particles N_T become sensitive in the high momentum regions, which contemplate the salient features of the particles emission sources from higher energy levels even the sources accompanied a substantial coherence fraction. Although the considered model explained the usual particle ejecting source which enlarged spherically, it produced the characteristics of the chaotic source and coherence fractions in the collisions. In this research work, we analyzed that the considered model confers the normalized chaotic parameter in basic agreement with the experimental applications of the chaos and coherence measurements to use in the field of thermal engineering. We realized that the chaotic parameters are suppressed crucially in the small temperature regimes at small momenta. One plausible reason for this consequence is that the production of particles from the radiated source created in the collision possesses a fraction of coherence which is nonchaotic.

Data Availability

The data are fully available without any restriction and are included within the article.

Conflicts of Interest

The authors declare that they have no conflicts of interest.

Authors' Contributions

GB conceptualized the study and wrote the original draft. WA and MS were responsible for project administration and wrote the original draft. RA and MF were responsible for resources and wrote the original draft. MDF and NH were responsible for resources and revised and edited the manuscript. IK was responsible for literature search and data analysis. Nawaf N. Hamednah and Ilyas Khan contributed equally to this work.

Acknowledgments

The authors would like to thank Prof. Wei-Ning Zhang for invigorating discussions about the consequences of the pion chaotic and coherence fractions. The authors are thankful to the Faculty of Science, Yibin University, Yibin, China, for

support provided for this research and Yibin University for the financial support provided for this study.

References

[1] M. Gyulassy, S. K. Kauffmann, and L. W. Wilson, "Pion interferometry of nuclear collisions. I. Theory," *Physical Review C*, vol. 20, no. 6, pp. 2267–2292, 1979.

[2] U. A. Wienemann and U. Heinz, "Particle interferometry for relativistic heavy-ion collisions," *Physics Reports*, vol. 319, p. 145, 1999.

[3] R. Weiner, "Boson interferometry in high-energy physics," *Physics Reports*, vol. 327, no. 5, pp. 249–346, 2000.

[4] T. Csorgo, "Particle interferometry from 40-MeV to 40-TeV," *Acta Physica Hungarica*, vol. 15, 2002.

[5] M. A. Lisa, S. Pratt, R. Soltz, and U. Wiedemann, "Femtoscopy in relativistic heavy ion collisions: two decades of progress," *Annual Review of Nuclear and Particle Science*, vol. 55, no. 1, pp. 357–402, 2005.

[6] M. M. Aggarwal, "One, two and three particle distributions from 158-A-GeV/c central Pb + Pb collisions," *Physical Review C*, vol. 67, Article ID 014906, 2003.

[7] S. Pratt, "Pion lasers from high-energy collisions," *Physics Letters B*, vol. 301, no. 2-3, pp. 159–164, 1993.

[8] T. Csörgő and J. Zimányi, "Analytic solution of the pion-laser model," *Physical Review Letters*, vol. 80, p. 916, 1998.

[9] D. Gangadharan, "Techniques for multiboson interferometry," *Physical Review C*, vol. 92, 2015.

[10] G. Goldhaber, S. Goldhaber, W. Y. Lee, and A. Pais, "Influence of Bose-Einstein statistics on the anti-proton proton annihilation process," *Physical Review*, vol. 120, 1960.

[11] I. V. Andreev, M. Plumer, and R. M. Weiner, "Quantum statistical approach to Bose-Einstein correlations and its experimental implications," *International Journal of Modern Physics A*, vol. 8, 1993.

[12] H. Boggild, "Three pion correlations in sulphur lead collisions at the CERN SPS," *Physics Letters B*, vol. 455, p. 77, 1999.

[13] J. Adams, "Three pion HBT correlations in relativistic heavy ion collisions from the STAR experiment," *Physical Review Letters*, vol. 91, p. 262301, 2003.

[14] R. Willson, "Measurement of source chaoticity for particle emission in Au+Au collisions at $\sqrt{s_{NN}}$ =130-GeV using three particle HBT correlations," *Nuclear Physics A*, vol. 715, p. 619, 2003.

[15] B. B. Abelev, "Two- and three-pion quantum statistics correlations in Pb-Pb collisions at $\sqrt{s_{NN}}$ =2.76 TeV at the CERN Large Hadron Collider," *Physical Review C*, vol. 89, 2014.

[16] U. W. Heinz and Q. H. Zhang, "What can we learn from three pion interferometry?" *Physical Review C*, vol. 56, 1997.

[17] U. Ornik, M. Plumer, and D. Strottmann, "Bose condensation through resonance decay," *Physics Letters B*, vol. 314, 1993.

[18] J. P. Blaizot, F. Gelis, and J. Liao, "Thermalization and Bose-Einstein condensation in overpopulated glasma," *Nuclear Physics A*, vol. 904-905, 2013.

[19] E. Ikonen, "Chaoticity parameter lamda and multiple coherent components in relativistic heavy-ion collisions," *Physical Review C*, vol. 78, 2008.

[20] C. Y. Wong and W. N. Zhang, "Chaoticity parameter λ in hanbury-Brown–twiss interferometry," *Physical Review C*, vol. 76, Article ID 034905, 2007.

[21] J. Liu, P. Ru, W.-N. Zhang, and C.-Y. Wong, "Chaoticity parameterλin two-pion interferometry in an expanding boson gas model," *Journal of Physics G: Nuclear and Particle Physics*, vol. 41, no. 12, Article ID 125101, 2014.

[22] G. Bary, W.-N. Zhang, P. Ru, and J. Yang, "Analyses of multi-pion Bose-Einstein correlations for granular sources with coherent pion-emission droplets," *Chinese Physics C*, vol. 45, no. 2, Article ID 024106, 2021.

[23] M. I. Jamil, M. Arslan, and Ghani, "Lubna and others, Regio- and stereoselective functionalization of alkenes with emphasis on mechanistic insight and sustainability concerns," *Journal of Saudi Chemical Society*, vol. 20, Article ID 101260, 2021.

[24] C. Y. Wong, W. N. Zhang, J. Liu, and P. Ru, "Chaoticity and coherence in Bose-Einstein condensation and correlations," *Journal of Central European Green Innovation*, vol. 4, pp. 64–79, 2016.

[25] M. Naraschewski and R. J. Glauber, "Spatial coherence and density correlations of trapped Bose gases," *Physical Review A*, vol. 59, no. 6, pp. 4595–4607, 1999.

[26] A. Farooqi, R. Alotaibi, T. A. Nofal, R. Farooqi, and I. Khan, "A comparative epidemiological stability analysis of predictor corrector type non-standard finite difference scheme for the transmissibility of measles," *Results in Physics*, vol. 21, p. 103756, 2021.

[27] B. Jamil, M. S. Anwar, A. Rasheed, and M. Irfan, "MHD Maxwell flow modeled by fractional derivatives with chemical reaction and thermal radiation," *Chinese Journal of Physics*, vol. 67, pp. 512–533, 2020.

[28] A. Khan Zareen and H. Ahmad, "Qualitative properties of solutions of fractional differential and difference equations arising in physical models," *Fractals*, vol. 7, 2021.

[29] Y. Karaca, M. Moonis, and D. Baleanu, "Fractal and multi-fractional-based predictive optimization model for stroke subtypes' classification," *Chaos, Solitons & Fractals*, vol. 136, Article ID 109820, 2020.

[30] A. Abdon and A. Seda İğret, "New concept in calculus: piecewise differential and integral operators," *Chaos, Solitons & Fractals*, vol. 145, Article ID 110638, 2021.

[31] M. S. Hashemi, "A novel approach to find exact solutions of fractional evolution equations with non-singular kernel derivative," *Chaos, Solitons & Fractals*, vol. 152, Article ID 111367, 2021.

[32] M. S. Hashemi, M. Inc, and A. Yusuf, "On three-dimensional variable order time fractional chaotic system with nonsingular kernel," *Chaos, Solitons & Fractals*, vol. 133, Article ID 109628, 2020.

[33] J. Hadi, O. Orozco-López, and M. Pacheco, "Simulation and experimental validation of a non-equilibrium chaotic system," *Chaos, Solitons & Fractals*, vol. 143, p. 110539, 2021.

[34] X. Pei-Ying, J. Hadi, and A. Raúl, "Spectral entropy analysis and synchronization of a multi-stable fractional-order chaotic system using a novel neural network-based chattering-free sliding mode technique," *Chaos, Solitons & Fractals*, vol. 144, Article ID 110576, 2021.

[35] M. S. Anwar, R. T. M. Shahzad, M. Irfan, and M. Z. Ashraf, "Electrified fractional nanofluid flow with suspended carbon nanotubes," *Computers & Mathematics with Applications*, vol. 80, no. 5, pp. 1375–1386, 2020.

Hindawi
Mathematical Problems in Engineering
Volume 2021, Article ID 7285769, 6 pages
https://doi.org/10.1155/2021/7285769

Research Article

Blow-Up of Solutions for Wave Equation Involving the Fractional Laplacian with Nonlinear Source

Y. Bidi,[1] A. Beniani,[2] M. Y. Alnegga,[3] and A. Moumen[4]

[1]*University of Djillali Liabes - B. P. 89, Sidi Bel Abbes 22000, Algeria*
[2]*Department of Mathematics, University of Ain Temouchent, Laboratory of Analysis and Control of Partial Differential Equations, Ain Temouchent 46000, Algeria*
[3]*Department of Mathematics, College of Sciences and Arts, Qassim University, Ar-Rass, Saudi Arabia*
[4]*Department of Mathematics, Faculty of Science, University of Hail, Hail 55425, Saudi Arabia*

Correspondence should be addressed to M. Y. Alnegga; mnkaaa@qu.edu.sa

Received 22 August 2021; Revised 13 September 2021; Accepted 17 September 2021; Published 30 September 2021

Academic Editor: Muhammad Irfan

In this paper, we study the blow-up of solutions for wave equation involving the fractional Laplacian with nonlinear source.

1. Introduction and Brief History of Fractional Integrodifferentiation

Let $\Omega \subset \mathbb{R}^n, n \geq 1$ be an open domain with Lipschitz boundary $\partial\Omega$. In this article, we consider the hyperbolic initial-boundary value problem involving the fractional Laplacian; for $w = w(x,t)$, we consider the wave equation with power nonlinearity:

$$\begin{cases} \partial_t^2 w + (-\Delta)^r w + (-\Delta)^r \partial_t w = w|w|^{p-2}, & x \in \Omega, t > 0, \\ w = 0, & x \in \partial\Omega, t > 0, \\ w(x,0) = w_0(x), \partial_t w(x,0) = w_1(x), & x \in \Omega, \end{cases} \tag{1}$$

where $(-\Delta)^r$ is the fractional Laplacian such that $r \in (0,1)$. The exponent p satisfies

$$2 < p \leq \frac{2n}{n-2r} = 2_r^*, \quad n > 2r. \tag{2}$$

The fractional integrodifferentiation operation is a generalization of the differentiation operations. The idea of fractional differentiation as a generalization of the concept of the derivative to the noninteger value of a arose almost simultaneously with the very concept of differentiation. The first mention of this idea occurs in the correspondence of G. W. Leibniz and Marquis de l'Hospital in 1695 (see [1]). The idea of fractional integrodifferentiation was further developed in the works of L. Euler, who in 1738 noticed that an expression can be given meaning even for noninteger values (see [2]). An explicit calculation formula was given in the treatise by S. Lacroix in 1820 (see [3]). Also in 1812, P.S. Laplace put forward the idea of the possibility of differentiating noninteger order for some functions. The first definition of the derivative of noninteger order was given by J. Fourier in 1822. In its modern form, fractional integrodifferentiation was formed in the works of N.H. Abel and J. Liouville. In 1823, in connection with the problem of tautochrone—a curve, when sliding along which, under the influence of gravitational forces, a body reaches its lowest point in the same time, regardless of its initial position. The idea of considering fractional differentiation as an operation inverse to fractional integration was first proposed by Holmgren in 1865 (see [4–6]). A year later, Grunwald, who was not familiar with Holmgren's work, came to the same idea of Letnikov in 1868 (see [7–13]).

In [14], an efficient novel technique, namely, the q-homotopy analysis transform method (q-HATM), is applied to find the solution for the time-fractional Kaup–Kupershmidt (KK) equation and the study of fractional Emden–Fowler (FEF) equations by utilizing a new

adequate procedure; specifically, the q-homotopy analysis transform method (q-HATM) is considered in [15].

Fractional wave systems with continuous nonlinearities are possessed by a large number of researchers. In [16], the authors considered initial-boundary value problem of degenerate Kirchhoff-type

$$\partial_t^2 w + [w]_r^{2(\theta-1)} (-\Delta)^r w = |w|^{p-1} w, \text{ in } \Omega \times \mathbb{R}_+, \tag{3}$$

where $\Omega \subset \mathbb{R}^n$, $n \geq 1$ is a bounded domain with Lipschitz boundary, $\theta \in [1, 2^*]$, and $[w]_r$ is the Gagliardo seminorm of w defined by

$$[w]_r = \left(\int_\Omega \int_\Omega \frac{|w(x) - w(z)|^2}{|x - z|^{n+2r}} \mathrm{d}x\mathrm{d}z \right)^{1/2}. \tag{4}$$

The authors obtained, under appropriate conditions, the global existence in time and finite blow-up of solutions for (3) owing to the Galerkin method combined with the potential wells. They also showed the global existence of solutions under critical initial conditions. In [17], the authors studied the following damped degenerate Kirchhoff equation:

$$\begin{aligned} \partial_t^2 w + [w]_r^{2(\theta-1)} (-\Delta)^r w + \left|\partial_t w\right|^{\alpha-1} \partial_t w \\ + w = |w|^{p-2} w, \text{ in } \Omega \times \mathbb{R}_+, \end{aligned} \tag{5}$$

where $2 < \alpha < 2\theta < p < 2^* < r$. The global existence, behavior of solutions, and blow-up in time for (4) are obtained, under appropriate assumptions. In [18], the IBVP of Kirchhoff wave equation is considered. Under some sufficient conditions, the blow-up in finite time is shown by using a modified concavity method; for more details, see [19–27].

$$\partial_t^2 w + [w]_r^{2(\theta-1)} (-\Delta)^r w = |w|^{p-2} w, \; in \, \Omega \times \mathbb{R}_+. \tag{6}$$

We highlight here the novelty of the problem:

(1) It is interesting to note that simultaneously with the theoretical developments of classical nonlinear wave operation, practical applications of fractional integrodifferentiation operation can also be found

(2) It is shown that when the nonlinear source dominates the fractional Laplacian in (2), this ensures the global nonexistence in time (blow-up) of solutions

(3) Our results extend many recent results in the literature

2. Auxiliary Results and Function Spaces

The fractional Laplacian $(-\Delta)^r w$ of the function w is given by

$$(-\Delta)^r w(x) = C \int_{\mathbb{R}^n} \frac{w(x) - w(z)}{|x - z|^{n+2r}} dz \, , \quad \forall x \in \mathbb{R}^n, \tag{7}$$

where

$$C^{-1} = \int_{\mathbb{R}^n} \frac{1 - \cos(\zeta_1)}{|\zeta|^{n+2r}} \mathrm{d}\zeta. \tag{8}$$

We define the fractional-order Sobolev space by

$$W^{r,2}(\Omega) = \left\{ v \in L^2(\Omega) : \int_\Omega \int_\Omega \frac{|v(x) - v(z)|^2}{|x - z|^{n+2r}} \mathrm{d}x\mathrm{d}z < \infty \right\}, \tag{9}$$

equipped with the norm

$$\|w\|_{W^{r,2}(\Omega)} = \left(\int_\Omega |w|^2 \mathrm{d}x + \int_\Omega \int_\Omega \frac{|v(x) - v(z)|^2}{|x - z|^{n+2r}} \mathrm{d}x\mathrm{d}z \right)^{1/2}. \tag{10}$$

Let

$$W_0^{r,2}(\Omega) = \left\{ w \in W^{r,2}(\Omega) : w = 0, x \in \partial\Omega \right\}, \tag{11}$$

be a closed linear subspace of $W^{r,2}(\Omega)$, and its norm is given by

$$\|w\|_{W_0^{r,2}(\Omega)} = \left(\int_\Omega \int_\Omega \frac{|v(x) - v(z)|^2}{|x - z|^{n+2r}} \mathrm{d}x\mathrm{d}z \right)^{1/2}. \tag{12}$$

The space $W_0^{r,2}(\Omega)$ is a Hilbert space with inner product

$$\langle w, u \rangle_{W_0^{r,2}(\Omega)} = \int_\Omega \int_\Omega \frac{(w(x) - w(z))(u(x) - u(z))}{|x - z|^{n+2r}} \mathrm{d}x\mathrm{d}z. \tag{13}$$

3. The Potential Wells

For simplicity, in this section, we consider problem (1) in stationary case. In fact, if we replace w in this section by $w(t)$ for any $t \in [0, T)$, all the facts are still valid. We define

$$\mathcal{J}(w) = \frac{1}{2} \|w\|^2_{W_0^{r,2}(\Omega)} - \frac{1}{p} \|w\|_p^p. \tag{14}$$

We denote

$$\mathcal{I}(w) = \|w\|^2_{W_0^{r,2}(\Omega)} - \|w\|_p^p. \tag{15}$$

We introduce now the stable set as follows:

$$\mathcal{W} = \left\{ w \in W_0^{r,2}(\Omega) : \mathcal{I}(w) > 0, \; \mathcal{J}(w) < d \right\} \cup \{0\}, \tag{16}$$

where the mountain pass level d is defined as

$$d = \inf_{w \in W_0^{r,2}(\Omega) \setminus \{0\}} \left\{ \sup_{\mu \geq 0} \mathcal{J}(\mu w) \right\}. \tag{17}$$

We introduce the so-called *Nehari manifold*:

$$\mathcal{N} = \left\{ w \in W_0^{r,2}(\Omega) \setminus \{0\} : \mathcal{I}(w) = 0 \right\}. \tag{18}$$

Then potential depth d is characterized by

$$d = \inf_{w \in \mathcal{N}} \mathcal{J}(w), \tag{19}$$

which implies that

$$\operatorname{dist}(0, \mathcal{N}) = \min_{w \in \mathcal{N}} \|w\|_{W_0^{r,2}(\Omega)}. \tag{20}$$

We will prove the invariance of the set $\mathcal{W}$.

For the reader's convenience, we recall the main embedding results for the fractional Sobolev spaces; see [28] for details.

Lemma 1. *Let Ω be bounded domain. Then*

(1) The embedding $W_0^{r,2}(\Omega) \hookrightarrow L^p(\Omega)$ is compact for any $p \in [1, 2_r^*)$

(2) The embedding $W_0^{r,2}(\Omega) \hookrightarrow L^{2_r^*}(\Omega)$ is continuous

Lemma 2

(1) For any $s \in [1, 2_r^*]$, there exists a positive constant $C_0 = C_0(n, s, r)$ such that for any $u \in W_0^{r,2}(\Omega)$

$$\|w\|_{L^s(\Omega)} \leq C_0 \int_\Omega \int_\Omega \frac{|u(x) - u(z)|^2}{|x - y|^{n+2r}} \mathrm{d}x\mathrm{d}y. \tag{21}$$

(2) For any $s \in [1, 2_r^*]$ and any bounded sequence $(u_j)_j$ in $W_0^{r,2}(\Omega)$, there exists u in $L^s(\mathbb{R}^n)$, with $u = 0$ a.e. in $\mathbb{R}^n - \Omega$, such that up to a subsequence, still denoted by $(u_j)_j$

$$u_j \longrightarrow u \text{ strongly in } L^s(\Omega) as\, j \longrightarrow \infty. \tag{22}$$

Definition 1. A function $w = w(x,t)$ is said to be a global (weak) solution of problem (1), if

$$\begin{aligned} w &\in L^\infty\left(0, \infty, W_0^{r,2}(\Omega)\right), w_t \in L^\infty\left(0, \infty, L^2(\Omega)\right), \\ w_o &\in L^\infty\left(0, \infty, W_0^{r,2}(\Omega)\right), w_t \in L^\infty\left(0, \infty, L^2(\Omega)\right) \\ w_1 &\in L^\infty\left(0, \infty, L^2(\Omega)\right), \end{aligned} \tag{23}$$

and for any $\phi \in L^\infty(0, \infty, W_0^{r,2}(\Omega))$, $t \in \mathbb{R}_+^*$,

$$\begin{aligned} &\left(w_t(.,t), \phi(.,t)\right) + \frac{1}{2}\int_0^t \left(w_t(.,t), \phi(.,t)_{W_0^{r,2}(\Omega)}\right)\mathrm{d}\tau + \int_0^t \left(w_t(.,t), \phi(.,t)_{W_0^{r,2}(\Omega)}\right)\mathrm{d}\tau \\ &= \left(w_1, \phi(.,0)\right) + \int_0^t \left(w(.,\tau)|w(.,\tau)|^{p-2}, \phi(.,\tau)\right)\mathrm{d}\tau. \end{aligned} \tag{24}$$

If a (weak) global solution w belongs to $C(0, \infty; W_0^{r,2}(\Omega))$, we say that u is a strong global solution of problem (1).

The energy $\mathscr{E}$ of solution at time t to (1) is given by

$$\mathscr{E}(t) = \frac{1}{2}\left\|\partial_t w(t)\right\|_2^2 + \mathscr{J}(w). \tag{25}$$

Lemma 3. *Let $w(x,t)$ be a weak solution of problem (1). If $w_0 \in \mathscr{W}$, $w_1 \in L^2(\Omega)$, then $\mathscr{E}(t) \leq \mathscr{E}(0)$.*

4. Blow-Up Result

In this section, we prove the blow-up result to problem (1)

Lemma 4. *Let $w(x,t)$ is the weak solution of problem (1). If $w_0 \in \mathscr{W}$ and $w_1 \in L^2(\Omega)$ satisfying that*

$$\|w\|^2 \geq \frac{2p}{p-2} K\mathscr{E}(0), \tag{26}$$

$$\left(\partial_t w, w\right)_{W_0^{r,2}(\Omega)} < 0, \tag{27}$$

$$w_0 \in \mathscr{M}, \tag{28}$$

$$\int_\Omega w_0 w_1 \mathrm{d}x > 0, \tag{29}$$

then any solution of (1) belongs to $\mathscr{M}$.

Proof. We claim that $w \in \mathscr{M}$ for $t \in [0, T)$; by contradiction, we suppose that $t_0 \in (0, T)$ is the first time such that

$$I\left(w(t_0)\right) = 0, \tag{30}$$

$$\mathscr{J}(w(t)) < 0 \text{ for } t \in [0, t_0). \tag{31}$$

We first introduce an auxiliary function,

$$M(t) = \|w\|^2, \tag{32}$$

and directly

$$M'(t) = \left(\partial_t w, w\right) + \left(w, \partial_t w\right) = 2\left(\partial_t w, w\right), \tag{33}$$

$$M''(t) = 2\left(\partial_t^2 w, w\right) + 2\left\|\partial_t w\right\|^2. \tag{34}$$

Multiplying (1) 1 by w and then by integration over $\mathbb{R}^n$, we have

$$\begin{aligned} &(\partial)t^2 w, w + (w, w)W^{r,2}0(\Omega) + (\partial t)w, wW^{r,2}0(\Omega) \\ &= \int \Omega w^{p-2} w \mathrm{d}x, \end{aligned} \tag{35}$$

so that

$$\left(\partial t^2 w, w\right) = -\|w\|_{W_0^{r,2}(\Omega)} - \left(\partial_t w, w\right)_{W_0^{r,2}(\Omega)} + \int_\Omega w|w|^{p-2} w \mathrm{d}x. \tag{36}$$

Substituting (27) into (36), we obtain

$$M''(t) = 2\left\|\partial_t w\right\|_W^{r,2}0(\Omega) - 2w_{W^{r,2}}0(\Omega) - 2\partial_t w, w)_{W^{r,2}}0(\Omega) + 2\int_\Omega w|w^{p-2}w\mathrm{d}x. \tag{37}$$

By (27), we have

$$M''(t) \geq 2\left\|\partial_t w\right\|^2 - 2.\mathcal{J}(w). \tag{38}$$

By (31), we have $M''(t) > 0$ for any $t \in [0, t_0)$; then, $M'(t)$ is strictly increasing on $[0, t_0)$. Thus

$$M'(t) > M'(0) > 0 \text{ for } t \in [0, t_0). \tag{39}$$

We have $M(t)$ is also strictly increasing on $[0, t_0)$. We have

$$M(t) > M(0) \geq \frac{2p}{p-2} K\mathscr{E}(0) \text{ for all } t \in [0, t_0). \tag{40}$$

From the continuity of w at $t = t_0$, it follows that

$$M(t_0) = \left\|w(t_0)\right\|^2 > 2\frac{p}{p-2} K\mathscr{E}(0). \tag{41}$$

On the other hand,

$$\begin{aligned}\mathscr{E}(0) \geq \mathscr{E}(t) &= \frac{1}{2}\left\|\partial_t w\right\|_2^2 + \frac{1}{2}\|w\|_{W_0^{r,2}(\Omega)}^2 - \frac{1}{p}\|w\|_p^p \\ &= \frac{1}{2}\left\|\partial_t w\right\|_2^2 + \left(\frac{1}{2} - \frac{1}{p}\right)\|w\|_{W_0^{r,2}(\Omega)}^2 + \frac{1}{p}\mathcal{J}(w).\end{aligned} \tag{42}$$

Together with (30) and Lemma 2, we get

$$\begin{aligned}\mathrm{E}(0) &\geq \frac{1}{2}\left\|\partial_t w(., t_0)\right\|_2^2 + \left(\frac{1}{2} - \frac{1}{p}\right)\left\|w(., t_0)\right\|_{W_0^{r,2}(\Omega)}^2 \\ &\geq \frac{1}{2}\left\|\partial_t w(., t_0)\right\|_2^2 + \frac{p-2}{2p}K^{-1}\left\|w(., t_0)\right\|_2^2 \\ &\geq \frac{p-2}{2p}K^{-1}\left\|w(., t_0)\right\|_2^2,\end{aligned} \tag{43}$$

which contradicts (41). This completes the proof. □

We are now ready to prove the finite time blow-up of solution to (1) when $\mathscr{E}(0) > 0$.

Definition 2. We say that the function $w(x,t)$ blows up in finite time if there exists $t^* \in (0, \infty)$ such that

$$\|w(x,t)\|_{L^2(\Omega)} \longrightarrow \infty \, as \, t \longrightarrow t^*. \tag{44}$$

Theorem 1. *Let $w_0 \in W_0^{r,2}(\Omega)$ and $w_1 \in L^2(\Omega)$. Assume that $w_0 \in \mathscr{M}$, $\mathscr{E}(0) > 0$, and $\int_\Omega w_0 w_1 dx > 0$, then any solution of (1) blows-up in finite time.*

Proof. We have $w \in \mathscr{M}$; arguing by contradiction, we suppose that w is weak global solution , for any $t \in [0, \infty)$. From (34) and Cauchy–Schwarts inequality, we get

$$M'^2(t) = 4(w, \partial_t)^2 \leq \|w\|^2\left\|\partial_t w\right\|^2, \quad t \in [0, \infty), \tag{45}$$

which together with (36) implies that

$$\begin{aligned}&M''(t)M(t) - (1+\alpha)(M'(t))^2 \\ &\geq \left(2\left\|\partial_t w\right\|^2 - 2\|w\|_{0}^{r,2}(\Omega)^2 + 2\int_\Omega w|w|^{p-2}wdx\right)M(t) - 4(1+\alpha)(w, \partial_t w)^2 \\ &\geq \left(2\left\|\partial_t w\right\|^2 - 2\|w\|_{0}^{r,2}(\Omega)^2 + 2\int_\Omega w|w|^{p-2}wdx\right)M(t) - 4(1+\alpha)\|w\|^2\left\|\partial_t w\right\|^2 \\ &= \left(-2\|w\|_{0}^{r,2}(\Omega)^2 + 2\int_\Omega w|w|^{p-2}wdx - 2(1+2\alpha)\left\|\partial_t w\right\|^2\right)M(t) = A(t)M(t),\end{aligned} \tag{46}$$

where $\alpha > 0$. We notice that

$$\begin{aligned}A(t) &:= -2\|w\|_{W_0^{r,2}(\Omega)}^2 + 2\|w\|_p^p - 2(1+2\alpha)\left\|\partial_t w\right\|^2 \\ &\geq -2(1+2\alpha)\left\|\partial_t w\right\|^2 - 2\|w\|_{W_0^{r,2}(\Omega)}^2 + p\left\|\partial_t w\right\|^2 + p\|w\|_{W_0^{r,2}(\Omega)}^2 - 2p\mathrm{E}(0) \\ &= -(4\alpha - p + 2)\left\|\partial_t w\right\|^2 + (p-2)\|w\|_{W_0^{r,2}(\Omega)}^2 - 2p\mathrm{E}(0) \\ &\geq -(4\alpha - p + 2)\left\|\partial_t w\right\|^2 + (p-2)K^{-1}\|w\|_2^2 - 2p\mathrm{E}(0),\end{aligned} \tag{47}$$

for $t \in [t, \infty)$. Set $\alpha = (p-2)/4 > 0$, and then $(4\alpha - p + 2)\|\partial_t w\|^2 = 0$. So from (47), we get

$$A(t) \geq K^{-1}(p-2)\|w\|^2 - 2p\mathscr{E}(0) \geq 0. \tag{48}$$

At this point, by (33)–(48), we obtain

$$M''(t)M(t) - (1+\alpha)\left(M'(t)\right)^2 > 0, \quad t \in [0, \infty), \tag{49}$$

where $\alpha > 0$. This implies that

$$\left(M^{-\alpha}\right)' = -\alpha M^{-\alpha-1}M'(t) < 0, \tag{50}$$

$$\left(M^{-\alpha}\right)'' = -\alpha M^{-\alpha-2}\left(M''(t)M(t) - (1+\alpha)\left(M'(t)\right)^2\right) < 0, \tag{51}$$

for all $t \in [0, \infty)$, which means that the function $M^{-\alpha}$ is concave. Obviously, $M(0) > 0$; then, there must exist a $T > 0$ such that

$$\lim_{t \longrightarrow TM^{-a}} (t) = 0, \tag{52}$$

so that

$$\lim_{t \longrightarrow T^-} M(t) = \infty \quad i.e., \quad \lim_{t \longrightarrow T^-} \|w\|^2 = \infty. \tag{53}$$

Thus, the proof is completed. □

Data Availability

No data were used in this study.

Conflicts of Interest

The authors declare that they have no conflicts of interest.

Authors' Contributions

The authors contributed equally and significantly in writing this paper. All authors read and approved the final manuscript.

References

[1] G. H. Pertz and C. J. Gerhardt, Eds., *Dritte Folge Mathematik (Erster Band). A. Asher & Comp., Briefwechsel zwischen Leibniz*, pp. 301-302, Hugens van Zulichem und dem Marquis de l'Hospital, 1849.

[2] L. Euler, "De progressionibus transcendendibus seu quarum termini generales algebraicae Dari nequent," *Commentarii Academiae Scientiarum Imperialis Petropolitanae*, 1730.

[3] S. F. Lacroix, *Traite Du Calcul Differential et du Calcul Integral*, Courcier, vol. 3, pp. 409-410, Paris, 2nd. edition, 1819.

[4] A. A. Kilbas, H. M. Srivastava, and J. J. Trujillo, "Theory and applications of fractional differential equations," Edited by J. V. Mill, Ed., Elsevier, Amsterdam, Netherlands, 2006.

[5] K. S. Miller and B. Ross, *An Introduction to the Fractional Calculus and Fractional Deferential Equations*, John Wiley & Sons, New York, NY, USA, 1993.

[6] K. B. Oldham and J. Spanier, *The Fractional Calculus*, Academic Press, New York, NY, USA, 1974.

[7] L. M. Del Pezzo and J. D. Rossi, "Traces for fractional Sobolev spaces with variable exponents," *Advances in Operator Theory*, vol. 2, pp. 435–446, 2017.

[8] Y. Fu and P. Pucci, "On solutions of space-fractional diffusion equations by means of potential wells," *Electronic Journal of Qualitative Theory of Differential Equations*, vol. 70, 2016.

[9] Q. Li and L. He, "General decay and blow-up of solutions for a nonlinear viscoelastic wave equation with strong damping," *Boundary Value Problems*, vol. 153, 2018.

[10] M. Nakao, "Asymptotic stability of the bounded or almost periodic solution of the wave equation with nonlinear dissipative term," *Journal of Mathematical Analysis and Applications*, vol. 58, no. 2, pp. 336–343, 1977.

[11] D. G. Prakasha, N. S. Malagi, and P. Veeresha, "New approach for fractional schrödinger-boussinesq equations with mittag-leffler kernel," *Mathematical Methods in the Applied Sciences*, vol. 43, no. 17, pp. 9654–9670, 2020.

[12] R. Servadei, E. Valdinoci, and E. Valdinoci, "Variational methods for non-local operators of elliptic type," *Discrete & Continuous Dynamical Systems - A*, vol. 33, no. 5, pp. 2105–2137, 2013.

[13] J. L. Shomberg, "Well-posedness of semilinear strongly damped wave equations with fractional diffusion operators and C^0 potentials on arbitrary bounded domains," *Rocky Mountain Journal of Mathematics*, vol. 49, no. 4, pp. 1307–1334, 2019.

[14] D. G. Prakasha, N. S. Malagi, P. Veeresha, and B. C. Prasannakumara, "An efficient computational technique for time-fractional Kaup-Kupershmidt equation," *Numerical Methods for Partial Differential Equations*, vol. 37, no. 2, pp. 1299–1316, 2021.

[15] N. S. Malagi, P. Veeresha, B. C. Prasannakumara, G. D. Prasanna, and D. G. Prakasha, "A new computational technique for the analytic treatment of time-fractional Emden-Fowler equations," *Mathematics and Computers in Simulation*, vol. 190, pp. 362–376, 2021.

[16] N. Pan, P. Pucci, and B. Zhang, "Degenerate Kirchhoff-type hyperbolic problems involving the fractional Laplacian," *Journal of Evolution Equations*, vol. 18, no. 2, pp. 385–409, 2018.

[17] N. Pan, P. Pucci, R. Xu, and B. Zhang, "Degenerate Kirchhoff-type wave problems involving the fractional Laplacian with nonlinear damping and source terms," *Journal of Evolution Equations*, vol. 19, no. 3, pp. 615–643, 2019.

[18] Q. Lin, X. T. Tian, X. Xu, and M. Zhang, "Blow up and blow up time for degenerate Kirchhoff-type wave problems involving the fractional Laplacian with arbitrary positive initial energy," *Discrete & Continuous Dynamical Systems - S*, vol. 13, no. 7, pp. 2095–2107, 2020.

[19] E. Azroul, A. Benkirane, and M. Shimi, "Eigenvalue problem involving the fractional p-Laplacian operator," *Advances in Operator Theory*, vol. 4-2, pp. 539–555, 2009.

[20] A. Benaissa, D. Ouchenane, and Kh. Zennir, "Blow up of positive initial-energy solutions to systems of nonlinear wave equations with degenerate damping and source terms," *Nonclinical Studies, (J. I)*, vol. 19, no. 4, pp. 523–535, 2012.

[21] A. Braik, Y. Miloudi, and K. Zennir, "A finite-time Blow-up result for a class of solutions with positive initial energy for coupled system of heat equations with memories," *Mathematical Methods in the Applied Sciences*, vol. 41, no. 4, pp. 1674–1682, 2018.

[22] U. Kaufmann, J. D. Rossi, and R. Vida, "Fractional Sobolev spaces with variables exponent and fractional $p(x)$-Laplacian, Electron," *Journal of Qualitative Theory of Differential Equations*, vol. 76, pp. 1–17, 2017.

[23] N. I. Karachalios and N. M. Stavrakakis, "Global existence and blow-up results for some nonlinear wave equations on $\mathbb{R}^N$," *Advances in Difference Equations*, vol. 6, pp. 155–174, 2001.

[24] G. Liu and S. Xia, "Global existence and finite time blow up for a class of semilinear wave equations on RN," *Computers & Mathematics with Applications*, vol. 70, no. 6, pp. 1345–1356, 2015.

[25] K. zennir, "Growth of solutions with positive initial energy to system of degeneratly damped wave equations with memory," *Lobachevskii Journal of Mathematics*, vol. 35, no. 2, pp. 147–156, 2014.

[26] kh. zennir, "Global nonexistence of solutions to system of nonlinear viscoelastic wave equations with degenerate damping and source terms," *Ukrainian Mathematical Journal*, vol. 65, no. 7, pp. 723–739, 2013.

[27] K. zennir and T. Miyasita, "Lifespan of solutions for a class of pseudo-parabolic equation with weak-memory," *Alexandria Engineering Journal*, vol. 59, no. 2, pp. 957–964, 2020.

[28] E. Di Nezza, G. Palatucci, and E. Valdinoci, "Hitchhiker's guide to the fractional Sobolev spaces," *Bulletin des Sciences Mathematiques*, vol. 136, no. 5, pp. 521–573, 2012.